Surface and Deep Water Variability On The Agulhas Plateau Over The Past 170 ka

Elizabeth Grace Molyneux

Submitted for the Degree of Doctor of Philosophy

Cardiff University
School of Earth, Ocean and Planetary Sciences

November 2007

ProQuest LLC
789 East Eisenhower Parkway
P.O. Box 1346
Ann Arbor, MI 48106-1346

This work has not previously been accepted in substance for any degree and is not concurrently submitted in candidature for any degree.

Signed ..... (candidate) Date 22/11/07

STATEMENT 1

This thesis is being submitted in partial fulfillment of the requirements for the degree of .....PhD.....(insert MCh, MD, MPhil, PhD etc, as appropriate)

Signed ..... (candidate) Date 22/11/07

STATEMENT 2

This thesis is the result of my own independent work/investigation, except where otherwise stated.
Other sources are acknowledged by explicit references.

Signed ..... (candidate) Date 22/11/07

STATEMENT 3

I hereby give consent for my thesis, if accepted, to be available for photocopying and for inter-library loan, and for the title and summary to be made available to outside organisations.

Signed ..... (candidate) Date 22/11/07

Abstract

High resolution multi-proxy analysis was undertaken on core MD02-2589 (41°26.03'S, 25°15.30'E, 2660 m water depth) from the Agulhas Plateau, Indian to Atlantic throughflow region, for the past 170 ka in order to provide a detailed record of both deep and surface ocean-climate interactions in the region. Particular focus was on Terminations I and II and Marine Isotope Stage (MIS) 5a-4 transition.

Planktonic foraminifera assemblage counts and inferred sea surface temperature calculations combined with planktonic stable carbon and oxygen isotopes and ice rafted debris counts were used to show that towards the end of glacial periods MIS 6 and 2 there was a pooling of heat and salt in the throughflow region, transported to the area by the Agulhas Current. These waters were unable to be transported into the Atlantic Ocean due to the northwards position of the frontal systems associated with the Antarctic Circumpolar Current (ACC). Wider Southern Ocean warming towards the end of MIS 6, during maximum global ice volume, also shown by the benthic proxies, is seen to release a pulse of the pooled waters through the Agulhas throughflow region, some ~6 ka before a Southern Ocean wide cold reversal linked to the resumption of North Atlantic Deep Water (NADW) convection to interglacial levels. This is significantly longer than ages suggested through modelling for the resumption of the thermohaline circulation interglacial mode following the recommencement of Agulhas leakage. Additional planktonic carbon isotope data from core MD02-2588 (41°19.90'S, 25°49.40'E, 2907 m water depth) show the development of a Carbon Isotope Minima Event during Terminations I and II, probably linked to the breakdown of stratification of the water column following glacial periods.

Benthic stable carbon and oxygen isotope measurements combined with the sortable silt mean grain size sedimentological proxy are used to show the phasing of bottom water changes over terminations, with changes in chemical ventilation being largely decoupled from near-bottom physical flow speeds. Flow speeds record Southern Ocean variability and the chemical ventilation Northern Component Water variability. The results suggest the persistent presence of a high $\delta^{13}C$ water mass, similar to present day NADW, during glacial periods, with a rapid shoaling of NADW in the water column and replacement by Southern Component Water (SCW) over the MIS5a-4 transition.

The benthic $\delta^{13}C$ record of MD02-2589, combined with that of MD95-2042 (*Shackleton et al.*, 2000) from the Iberian Margin, show 8 periods in the past 150 ka

where the mid-depth South Atlantic was bathed by a better ventilated water mass than the mid-depth North Atlantic, corresponding with glacial stages, substages and Heinrich events. The high $\delta^{13}C$ water mass present at MD02-2589 must have originated from outside the North Atlantic. Productivity and air-sea gas exchange overprints on both records cannot explain the full offsets seen with the most likely mechanism being the formation of a separate high $\delta^{13}C$ SCW mass, different to Antarctic Intermediate Water (AAIW) during glacial periods. It is possible that increased depth penetration of AAIW can explain the offset during Heinrich events.

A suite of cores forming a latitudinal and depth transect over the modern day position of the Polar, Subantarctic and Subtropical Fronts (PF, SAF, STF) are investigated for MIS 2, with a chemocline, seen by *Hodell et al.* (2003), being identified. This study however shows the presence of a mid-depth divide north and south of the SAF, with very depleted values south and enriched values north, with deep depths (>3750 m water depth) both north and south of the SAF showing depleted values. This is used to suggest that the high $\delta^{13}C$ SCW mass seen during glacial periods is forming around the SAF in the southeastern Atlantic Ocean due to air-sea gas exchange and upwelling linked to wind forcing and sea ice extent.

This study suggests that previous work using benthic $\delta^{13}C$ data looking at the extent of glacial water masses in the world's oceans may have been over-reconstructing the extent of glacial Northern Component Water as it is likely to have a very similar $\delta^{13}C$ and $\delta^{13}C_{as}$ signature as this SCW mass forming around the SAF and migrating northwards.

Authors Note

Chapter 5 of this thesis has been presented as a paper in an international publication and **Chapter 7** is in preparation for publication. The present status of these publications is summarised as follows:

Chapter 5 of this thesis has been published in *Paleoceanography* as: Molyneux E.G., Hall I.R., Zahn, R. and Diz, P.: (2007): Deep Water Variability On The Southern Agulhas Plateau: Interhemispheric Links Over The Past 170 ka: Volume 22, (PA4209), doi:10.1029/2006PA001407

Chapter 7 is in preparation as: Molyneux E.G. and Martinez-Mendez G.: Glacial to Interglacial Southern Ocean Water Column Structure:

As a consequence of chapters of this thesis being published as individual papers in scientific journals, some repetition of statement could not be avoided.

Declaration of Co-Author Contribution

Chapter 5: Deep Water Variability On The Southern Agulhas Plateau: Interhemispheric Links Over The Past 170 ka

Hall, I.R.	Reviewed several versions of manuscript
Zahn R.	Reviewed several versions of manuscript
Diz, P.	Helped develop the age model and reviewed the final manuscript

Chapter 7: Glacial to Interglacial Southern Ocean Water Column Structure

Martínez-Méndez, G.	Provided insight into glacial mid-depth Southern Ocean water mass: Comments developed as part of this manuscript preparation will be cited as Molyneux and Martínez-Méndez (in prep)
Hall, I.R.	Reviewed several versions of manuscript
Zahn R.	Reviewed several versions of manuscript

Acknowledgements

Firstly I would like to thank my main supervisor Ian Hall for all his support and encouragement during my PhD, along with his patience and understanding. I would also like to thank my second supervisor Rainer Zahn for all his helpful suggestions and comments in developing the ideas and discussion presented in this thesis. A large thank you has to go to Helen Medley, Giancarlo Bianchi and Julia Becker for helping me with all my lab work, teaching how everything works so expertly and running the stable isotope analysis. Thank you also goes to Julia for her endless patience in trying to explain spectral analysis to me, and Helen for all her help with sortable silt analysis and locating samples! Thank you also goes to Ian McMillan for helping me with the long process of foraminifera species identification, Michal Kucera for running the transfer function and Gema Martinez-Mendez for her insight into the Agulhas region.

I would also like to say a really big thank you to my office mates Karin Boessenkool, Paula Diz and Helena Evans who gave me unending practical advice and confidence boosts, as well as being excellent sounding boards and sources of information and inspiration. A big further thanks goes to Rehanna Chaudhri for not only her company and conversation during the long lab work hours but also for being my pub buddy and excellent wine / gossip sharer. Similarly thanks goes to Helen, Helena, Wendy, Christian and many other PhD students for listening to endless rants and traumas over the past 3+ years and especially for the boys, Nick, Cathal, Dan and Mostyn for picking me up towards the end, taking me out and about on exploring adventures, keeping me sane and giving me somewhere to live!

Finally I would like to give a huge thanks to all my friends and family; especially mum, dad, Katherine, Harriet, Phil and Nick for all putting up with me and giving never-ending support, patience, belief and love.

List of Acronyms

AABW	Antarctic Bottom Water
AAIW	Antarctic Intermediate Water
ACC	Antarctic Circumpolar Current
ACR	Antarctic Cold Reversal
ALF	Agulhas Leakage Fauna
AMOC	Atlantic Meridional Overturning Circulation
ANN	Artificial Neural Networks
AR	Agulhas Retroflection
ARC	Agulhas Return Current
CA	Correspondence Analysis
CDW	Circumpolar Deep Water
CH_4	Methane
CLIMAP	Climate: Long-Range Investigation, Mapping, and Prediction
CO_2	Carbon Dioxide
$\delta^{18}O_c$	$\delta^{18}O$ of Foraminiferal Calcite
$\delta^{18}O_{ivc}$	$\delta^{18}O$ Ice Volume Corrected
$\delta^{18}O_{sw}$	$\delta^{18}O$ of Sea Water
DO	Dansgaard–Oeschger
DWBC	Deep Western Boundary Current
EPILOG	Environmental Processes of the Ice Ages, Land, Ocean, Glaciers
GIN	Greenland, Iceland, Norwegian
GNAIW	Glacial North Atlantic Intermediate Water
GRIP	Greenland Ice-Core Project
IKM	Imbrie and Kipp Method
IRD	Ice Rafted Debris
Ka	Thousands Of Years Before Present
LCDW	Lower Circumpolar Deep Water
LGM	Last Glacial Maximum
LSCW	Lower Southern Component Water
MARGO	Multiproxy Approach for the Reconstruction of the Glacial Ocean Surface
MAT	Modern Analog Technique
MD	Marion Dufresne
MIS	Marine Isotope Stage
MIS 5a/4	Marine Isotope Stage 5a to 4 Transition
MOW	Mediterranean Outflow Water

MST	Multi-Sensor Core Logging System
NADW	North Atlantic Deep Water
NCW	Northern Component Water
NERC	Natural Environment Research Council
NSTF	North of the Subtropical Front Only Taxa
OCR	Oceanic Cold Reversal
PF	Polar Front
RAM	Revised Analog Method
$\overline{SS}$	Sortable Silt Mean Grain Size
SAF	Subantarctic Front
SAMW	Subantarctic Mode Water
SAZ	Subantarctic Zone
SCW	Southern Component Water
SPECMAP	Mapping Spectral Variability in Global Climate Project
SSS	Sea Surface Salinity
SST	Sea Surface Temperature
SST_{annual}	Annual Sea Surface Temperature
SST_{summer}	Summer Sea Surface Temperature
SST_{winter}	Winter Sea Surface Temperature
ST/Tr	Subtropical to Transitional Fauna
STF	Subtropical Front
Sv	Sverdrup
THC	Thermohaline Circulation
TI	Termination I
TII	Termination II
TF	Transfer Function
UCDW	Upper Circumpolar Deep Water
USCW	Upper Southern Component Water
VPDB	Vienna Pee Dee Belemnite
VSMOW	Vienna Standard Mean Ocean Water
WBUC	Western Boundary Undercurrent

List of Contents

Chapter 6

Benthic Carbon Isotope Gradients in the Atlantic Ocean and Implications for Meridional Overturning Circulation Variability

Chapter 7

Glacial to Interglacial Southern Ocean Water Column Structure

Chapter 8

Summary Discussion and Conclusions

Chapter 1. Introduction

1.1 Forcing Mechanisms of Climate Change

Palaeoclimatic evidence shows that the ocean and atmosphere have undergone major changes during the Quaternary. In 1973 *Shackleton and Opdyke* published the $\delta^{18}O$ isotope record of marine core V28-238 from the Equatorial Pacific showing variations in Northern Hemisphere ice volume over the past 870,000 years. They showed that glacial to interglacial cycles, previously seen in ice cores from Antarctica (*Johnsen et al.*, 1972), and other ocean cores (e.g. *Broecker and van Donk*, 1970, *Broecker et al.*, 1968), were present in marine cores throughout the World's oceans, not just those close to ice sheets, and could be extended back through 22 glacial and interglacial stages. More recently very high resolution ice core records from Greenland (*Dansgaard et al.*, 1993; *Johnsen et al.*, 1997; *Johnsen et al.*, 2001) have identified intense periods of complex millennial scale variability within both the cold glacial and warm interglacial periods. This has also been shown in extended records from Antarctic ice cores (~430,000 years: *Petit et al.*, 1999; *EPICA Community Members*, 2004).

It has been widely acknowledged that there are external and internal forcing mechanisms that appear to be influencing or driving climate change. The principal known external forcing is that of orbital variations or the astronomical theory of palaeoclimates (Fig. 1.1). Milutin Milankovitch was among the first people to highlight the role that periodic, long-term variations in the Earths orbit and rotation might play in forcing the Earth's climate (*Milankovitch*, 1941). These orbital changes do not affect the amount of solar energy that reaches the planet but cause differences in the distribution of the energy, which in turn

affects the insolation (incident solar radiation) received at a particular location in a particular season (*Berger,* 1992a). Since the pioneering work of Milankovich, insolation has been regarded as the primary forcing of ice ages during the Quaternary. The climatic evolution during the Quaternary shows clear cyclicities of about 19, 23, 41, and 100 ka. These are attributable to rhythmic variations in the orbital constellation of the Earth to the Sun and are clearly seen in various palaeoclimatic records including marine records (e.g. *Pahnke et al.,* 2003), coral reef sequences (e.g. *Chappell et al.,* 1996), pollen records (e.g. *Hooghiemstra et al.,* 1993), loess sequences (e.g. *Kukla,* 1987), ice cores (e.g. *Dansgaard et al.,* 1993) and tropical lake records (e.g. *Kutzback and Street-Perrott,* 1985). This confirms that orbital forcing is the primary driving mechanism in Quaternary climate change.

The longest timescale parameter of the astronomical theory is perturbations in the shape of the Earth's orbit around the sun, known as eccentricity (Fig. 1.1), which ranges from high (elliptic) to low (more circular) and affects the distance of the earth relative to the sun (*Denton and Hughes,* 1983). Whilst the variation between high and low eccentricity is about 7% (i.e. difference from a circle), it only has a very small (~0.1%) effect on insolation (*Berger,* 1989), which is integrated over all latitudes. Eccentricity does however play an important role in modulating the amplitude of the precessional cycle, discussed below. The periodicity of the eccentricity cycle was initially calculated to be ~100 ka (95.8 ka), although *Hays et al.* (1976) were the first to suggest that this 100 ka cycle, present in many palaeo data sets, may be a non-linear climate response to a far longer eccentricity cycle, thought to be ~400 ka (413 ka; *Rial,* 1999).

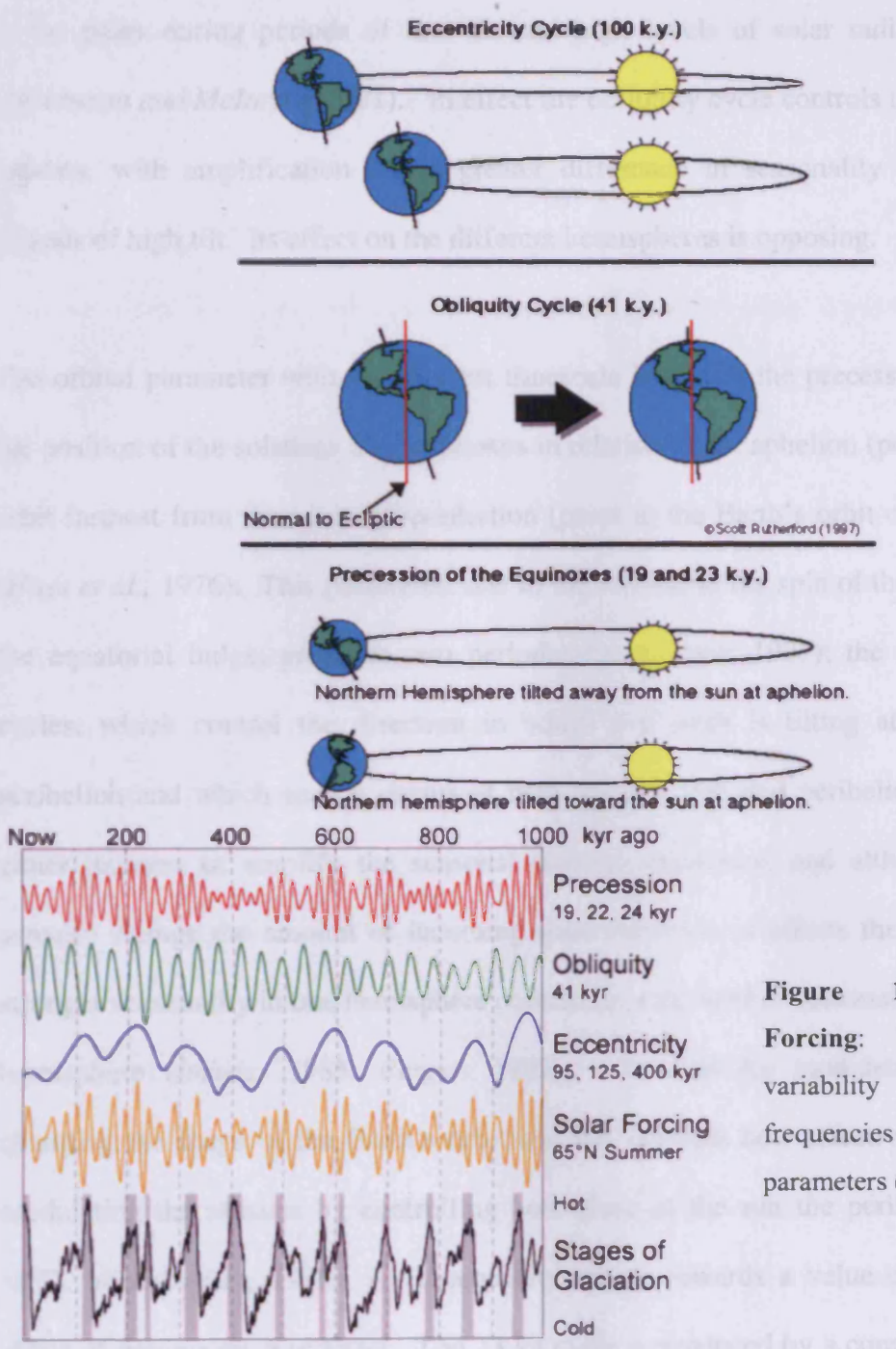

Figure 1.1. Milankovitch Forcing: The three modes of variability and associated frequencies in the Earth's orbital parameters (*Rutherford*, 1997).

The second longest timescale parameter of the astronomical theory is the change in the angle or tilt of the Earth's rotational axis, known as obliquity (Fig. 1.1). The angle of tilt varies from 21.8° – 24.4° (*Denton and Hughes*, 1983) and affects the distribution of incoming radiation on the Earth's surface, producing a 41 ka cycle. This forcing has the greatest effect at high latitudes (poleward of 43°; *Crucifix et al.*, 2006), with less radiation

at the poles during periods of low tilt and high levels of solar radiation at high tilt (*Ruddiman and McIntyre,* 1981). In effect the obliquity cycle controls the strength of the seasons, with amplification and a greater difference in seasonality occurring during periods of high tilt. Its effect on the different hemispheres is opposing.

The orbital parameter with the shortest timescale is that of the precession of equinoxes, the position of the solstices and equinoxes in relation to the aphelion (point in the Earth's orbit farthest from the sun) and perihelion (point in the Earth's orbit closest to the sun) (*Hays et al.,* 1976). This parameter, due to the wobble in the spin of the Earth caused by the equatorial bulge, produces two periodicities (*Berger,* 1977); the 23 ka and 19 ka cycles, which control the direction in which the earth is tilting at the aphelion or perihelion and which season occurs at both the aphelion and perihelion. This acts to either dampen or amplify the seasonal climate variability, and although it does not actually change the amount of incoming solar radiation, it effects the distribution with stronger seasonality in one hemisphere coinciding with weaker seasonality in the opposite hemisphere (*Imbrie,* 1985, *Berger,* 1992a). Eccentricity modulates precession by changing the shape of the Earth's orbit and this controls how effective precession is in modulating the seasons by controlling how close to the sun the perihelion is (*Berger,* 1977, *Milankovitch,* 1930). As eccentricity moves towards a value of 0 (circular) the effect of precession is reduced. The 23 ka cycle is produced by a combination of the 27 ka (axis of rotation of the tilt) and 105 ka (precession of the Earth's orbit) cycles, whilst the 19 ka cycle is a combination of the 27 ka (axis of rotation of the tilt) and the 96 ka (eccentricity) cycles (*Berger,* 1977).

Whilst precession dominates climate variability in most latitudes (*Crucifix et al.*, 2006) its effect is greatest in low latitude regions. Northern hemisphere summer insolation is out of phase with precession so when precession is low, northern hemisphere insolation is high with its hemisphere tilted towards the sun, its summer solstice occurring at the perihelion and its winter solstice at the aphelion (orbital point furthest away from the sun), creating a greater difference in the seasons (*Kim et al.*, 1998). The opposite is true for the southern hemisphere, with its summer solstice occurring at the aphelion and its winter solstice occurring at the perihelion during low precession, which reduces the difference in the seasons and produces low summer insolation. When seasonality is at its greatest in the northern hemisphere (when precession is low) the northern hemisphere land mass plays a greater role in responding to precession, especially in terms of glacial initiation, than the oceans as they cover a larger area and the build up of ice masses on the land causes amplification of the orbital forcing (*Denton and Hughes*, 1983). The opposite is true in the southern hemisphere where a lack of land mass, especially at mid-latitudes means that continental ice fluctuations are low and the hemisphere is mainly dominated by ocean processes.

Calculations of the effect of these cycles on insolation at different latitudes have been produced (e.g. *Berger*, 1992a; *Laskar et al.*, 1993, 1994). Spectral analysis, used to determine the frequency distribution of oscillations within records, has shown that these orbital variations are reflected in numerous proxy records (e.g. *Hays et al.*, 1976; *Imbrie et al.*, 1992, 1993; *Layberie et al.*, 1996; *Roe and Allan*, 1999, *Paillard*, 2001), as are cycles with different periodicities, thought to be non-linear responses of the climate system to the main cycles (*Berger*, 1989).

Variations in atmospheric concentration of greenhouse gasses (*Brook et al.*, 1996) and changes in ocean circulation (e.g. *Boyle*, 2000) are considered the most important internal forcing mechanisms on global climate over the past 170 ka. Variations in concentrations of greenhouse gases in the atmosphere, especially carbon dioxide (CO_2) and methane (CH_4) have been documented in ice core records (*Dansgaard et al.*, 1993; *Petit et al.*, 1999; *EPICA Community Members*, 2004) as changing rapidly in concentration over glacial to interglacial periods. Increased CO_2 and CH_4 levels in the atmosphere increase the greenhouse effect and both are linked with changes in climate (*Bender et al.*, 1997). Whilst the exact cause of glacial to interglacial changes in CO_2 concentration in the atmosphere is still under debate (e.g. *François et al.*, 1997; *Togweiller*, 1999; *Stephens and Keeling*, 2000; *Popova et al.*, 2000; *Watson and Naveira Garbato*, 2006), it is widely accepted that concentrations are linked to the exchange between the surface ocean and the atmosphere, with 99% of the CO_2 in the ocean / atmosphere system residing in the oceans (*Raven and Falkowski*, 1999). Changes in CH_4, whilst being about five times less important than changes in CO_2 (*Lorius et al.*, 1990), do generally reflect variability in the extent of low-latitude wetlands due to increased precipitation and perhaps climate (*Bender et al.*, 1997). Records have shown that changes in greenhouse gas concentrations often slightly lag climate change (*Petit et al.*, 1999) and therefore they are thought to be enhancers of change rather than a primary forcing mechanism. In fact a study on the Dome C Antarctic ice core (*Wolff et al.*, 2006) suggested that dust flux, representative of Patagonian climate conditions, changed at the last eight glacial terminations before both CO_2 concentrations and sea ice suggesting that several mechanisms may be responsible for CO_2 changes on glacial to interglacial scales.

The World's ocean affects climate through its high heat capacity relative to land, linked to its size (71 % of the Earth's surface) and its ability to redistribute this heat from one latitude to another before it is released to the atmosphere or radiated back into space (*Clark et al.*, 2002; *Rahmstorf*, 2002). Whilst changes in ocean circulation and its effects are complex and are discussed further in the following sections, both proxy data and models have shown that certainly some abrupt global climate events originated through changes in the ocean thermohaline circulation (THC) in response to small changes in the hydrological cycle (*Stocker and Wright*, 1991; *Fanning and Weaver*, 1997; *Boyle*, 2000; *Clark et al.*, 2002; *Hemming*, 2004). Ocean circulation changes are possibly a response to other forcing factors so cannot necessarily be classed as a primary forcing mechanism but are known to be a very important factor in climate change.

It has become apparent that climate change is actually caused by a coupled internal-external system where for example, changes in insolation at high latitudes of the Northern Hemisphere, steered by Milankovitch-type variations, act as a global pacemaker, driving or regulating the complex non-linear internal variations within the climate system. Such internal variations may include the growth and decay of ice sheets, changes in vertical ocean circulation and productivity, or CO_2 feedback (e.g. *Brook et al.*, 1996; *Rühlemann et al.*, 1999; *Alley et al.*, 2003). These climate non-linearities are often associated with feedback mechanisms that amplify or dampen climate change relative to the forcing. A prime example of this occurs in cold regions where cooling increases surface coverage of snow and ice. This in turn increases the albedo of the area and therefore reflection of radiation, causing further cooling as a consequence (*Alley et al.*, 2003).

1.2 Rapid Climate Change and Millennial Scale Variability

In addition to the orbital-scale glacial to interglacial variations, ice core records from Greenland (*Dansgaard et al.*, 1993; *Grootes and Stuiver*, 1997) show that these cycles were punctuated on sub-orbital millennial timescales by extreme climate swings, which may for example, alter global mean temperatures by 5 – 6 °C or alter local conditions by 8 – 16 °C over periods as little as a decade or less (*Alley et al.*, 2003). An abrupt climate change event is thought to occur when *'the climate system is forced to cross some threshold, triggering a transition to a new state at a rate determined by the climate system itself and faster than the cause'* (*NRC*, 2004).

These millennial-scale or Dansgaard-Oeschger oscillations have a saw-toothed appearance in the Greenland ice cores, characterised by rapid transitions between cold stadials and warm Dansgaard–Oeschger (DO) interstadials (*Dansgaard et al.*, 1993), and increased meltwater and ice rafted detritus (IRD) influx into the North Atlantic originating from the Iceland and East Greenland ice sheets (*Bond and Lotti*, 1995). They have a cyclicity of 1470 ±532 years (*Bond et al.*, 1997). Despite intensive research efforts, the origin of the glacial DO-type climate variability remains controversial. Suggested hypotheses include internal oscillations of the ocean–atmosphere system (*Broecker and Denton*, 1990; *Schulz et al.*, 2002; *Timmermann et al.*, 2003; *Sarnthein et al.*, 1994; *Ganapolski and Rahmstorf*, 2001; *Clark et al.*, 2002), periodic calving of the Greenland ice sheet (*van Kreveld et al.*, 2000) and external forcing mechanisms (*Ganopolski and Rahmstorf*, 2001). Marine records from the North Atlantic also reveal prominent IRD layers which represent a higher frequency of iceberg discharge on a periodicity of every 7,000 – 10,000 yrs (*Bond and Lotti*, 1995) corresponding to stadials

within the Greenland air temperature record from 60 - 10 ka (*Bond et al.*, 1993). These so called 'Heinrich events' represent the most extreme glacial conditions around the North Atlantic with negative $\delta^{18}O$ excursions of increasingly polar-dominated planktonic foraminifera assemblages (e.g. *Bond et al.*, 1992; *Maslin et al.*, 1995; *Cortijo et al.*, 1997). Heinrich events represent a collapse of the Laurentide Ice Sheet and an increase in iceberg production, mainly through the Hudson Strait, that is estimated to have reduced sea surface temperatures (SST) by 1 – 2 °C and surface salinity by up to 4 ‰ (*Maslin et al.*, 1995) and pushed the Polar Front as far south as 40 °N on at least 10 separate occasions during the last glacial-interglacial cycle (*Chapman et al.*, 2000). Climate oscillations coeval to Heinrich events have been seen in terrestrial and marine records in South America (*Lowell et al.*, 1995), the North Pacific (*Kotilainen and Shackleton*, 1995), the Santa Barbara Basin (*Behl and Kennett*, 1996), the Arabian Sea (*Schulz et al.*, 1998), mid-latitude Indian Ocean (*Sicre et al.*, 2005), mainland China (*Porter and An*, 1995) and the Asian monsoon record from the South China Sea (*Wang et al.*, 1999) suggesting that the influence of these meltwater pulses into the North Atlantic is translated globally either through the oceans or atmosphere.

Millennial-scale activity is also recorded in the Antarctic ice cores (*Blunier et al.*, 1998; *Blunier and Brook*, 2001; *EPICA Community Members*, 2004), with 7 warming events identified preceding Dansgaard-Oeschger (D-O) events in Greenland by 1.5 – 3 ka, and one to one coupling of Antarctic warm events and D-O events (*EPICA Community Members*, 2006). There is also evidence for millennial-scale instability of the Antarctic ice sheet in IRD fluxes found in cores taken across the Southern Ocean Polar Front (41 - 53 °S) (*Kanfoush et al.*, 2000). Between 10 and 60 ka they identified 5 - 6 IRD events with a spacing of 6 - 10 ka (similar to Heinrich events) that followed low planktonic $\delta^{18}O$

values, suggesting reduced salinity and increased temperature of the Antarctic surface waters. These IRD events appeared to be occurring during the strongest interstadials in Greenland and are associated with an increase in benthic $\delta^{13}C$ values, suggesting strong North Atlantic Deep Water (NADW) production and warming in the North Atlantic. There is also evidence in alkenone palaeotemperature reconstructions from the Cape Basin, southeast Atlantic, of millennial-scale temperature excursions of 1 - 3 °C during Marine Isotope Stage 3 (MIS 3: *Sachs et al.*, 2001). The deuterium records of the Dome C ice core record in Antarctica show a 1.5 °C cooling, also seen in the Byrd and Vostok records, known as the Antarctic Cold Reversal (ACR) (*Stenni et al.*, 2001; *Blunier et al*, 1998; *Petit et al*, 1999) at 14 - 12.5 ka., which is matched by a Southern Ocean Oceanic Cold Reversal (OCR), 800 yrs after the start of the ACR. This is due to the slower response time of the oceans (*Stenni et al.*, 2001).

1.3 Thermohaline Circulation

Circulation in the global ocean is forced by density variations where cold, dense water sinks near the poles and warmer water upwells near the Equator, moving poleward to replace the cold. The deep water mass formed in the North Atlantic (NADW) does so by convection of northwards flowing surface waters in the Greenland-Iceland-Norwegian (GIN) and Labrador Seas. After formation NADW travels southwards in the Atlantic as the Western Boundary Undercurrent (WBUC) at a depth of 2000 – 3000 m, until it meets the Antarctic Circumpolar Current (ACC) in the southern South Atlantic, where it mixes with Southern Component Waters (SCW) and is transported through the world's ocean basins (*Warren*, 1981; *Ninnemann and Charles*, 2002). Deep water formation also occurs in the Weddell and Ross Seas around the Antarctic coast (Antarctic Bottom Water

(AABW)), where brine rejection under the ice shelves (*Mackensen*, 2001), combined with super-cooling of the upwelled surface waters in polynyas (*Martinson et al.*, 1981) and intense evaporation (*Kilworth*, 1983) produces very dense waters, which ventilate the worlds ocean abyss below NADW (*Adkins et al.*, 2002). Recent estimates of the rate of deep-water formation is 15 ±2 Sv (1 Sv = 10^6 m^3 s^{-1}) for NADW and 21 ±6 Sv for AABW (*Ganachaud and Wunsch*, 2000).

The sinking of surface waters to form deep water masses in the North Atlantic and around Antarctica is compensated by the warming and rising of deep waters to the surface in the Pacific and Indian oceans, which flow back to the North Atlantic in shallower, surface currents to complete the THC. The surface flow routes through the Drake Passage ('cold water' return route) and the Agulhas Retroflection region ('warm water' return route) are thought to be the main courses by which upper layer water in the Atlantic is replenished and the return route of the THC completed (*Winter and Martin*, 1990).

Whilst the North Atlantic is the only ocean to produce deep water in the Northern Hemisphere, the existence of a circumpolar flow around Antarctica, due to the Drake Passage, makes the THC more complex (e.g. *Saenko et al.*,, 2003). Figure 1.2 shows a schematic map of the ACC and other major surface currents in the Southern Hemisphere. The interaction of NADW with SCW masses in the ACC region produces several deep and intermediate water masses, discussed further below, which influence the deep waters of both the Pacific, Atlantic and Indian Oceans.

The current understanding of Southern Ocean water formation processes and their effects on the THC is limited due to the lack of high resolution data sets from within the

Southern Ocean. Some longer high resolution records (e.g. MD97-2120, *Pahnke et al.*, 2003) exist from the Pacific sector of the Southern Ocean and a few, mainly deep cores, from the Atlantic sector (e.g. RC11-83, *Charles et al.*, 1996; TN057-21, *Ninnemann and Charles*, 2002). However much is still not understood in regards to the response of this large, important region to both glacial to interglacial cycles and millennial-scale variability.

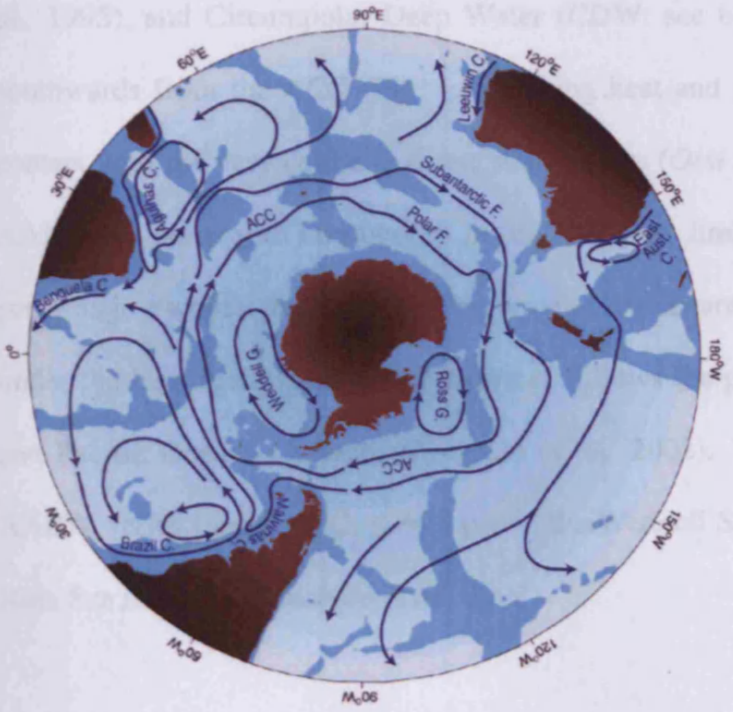

Figure 1.2. Schematic map of the major surface currents in the Southern Hemisphere oceans south of 20 °S. Depths shallower than 3500 m are shaded. The two major cores of the Antarctic Circumpolar Current (ACC) encircling Antarctica are shown: Subantarctic Front and Polar Front. F = front, C = current, G = gyre (*Rintoul et al.*, 2001)

1.4 Southern Ocean Circulation

1.4.1 Deep Water Masses

Water masses are identified by their conservative characteristics, such as potential temperature, salinity and density that are preserved by a water parcel until it mixes with other water. Water at the surface, absorbs gases from the atmosphere such as oxygen or

carbon dioxide which can be used to identify water masses and their pathways, and to calculate how long ago they were ventilated, exposed to the atmosphere, at the surface.

About 60 – 70 % of AABW (*Orsi et al.*, 1999; *Carmack*, 1977) currently forms in the western Weddell Sea (9.7 ±3.7 Sv: *Naveira Garabato et al.*, 2002), by the mixing of Ice Shelf Water, which is highly saline due to salt gain during sea ice freezing, Weddell Deep Water, which is very cold due to super-cooling during polynya formation (*Fahrbach et al.*, 1995), and Circumpolar Deep Water (CDW: see below) which has been entrained southwards from the ACC (Fig. 1.3) loosing heat and gaining density as it comes into contact with the very cold and dense shelf waters (*Orsi et al.*, 1993). The newly formed AABW is conveyed northwards in the western limb of the Weddell Gyre and a percentage escapes the Weddell Sea moving northwards into the Northern Hemisphere under the less dense NADW, whilst some follows the path of ACC into both the Indian and Pacific Oceans (*Naveira Garabato et al.*, 2002). The temperature and salinity of AABW varies from $\leq$-1 °C, $\leq$ 34.6 psu in the Weddell Sea to $\leq$-0.3 °C, $\leq$ 34.72 psu in the Ross Sea (*Naveira Garabato et al.*, 2002).

Circumpolar Deep Water (CDW) is a mixture of NADW, AABW and Antarctic Intermediate Water (AAIW) (Fig. 1.3) as well as some re-circulated deep waters from the Indian and Pacific Oceans (*Georgi*, 1981; *Mantyla and Reid*, 1983; *Sloyan and Rintoul*, 2001). It forms when southwards flowing NADW enters the ACC in the South Atlantic and is mixed with less dense deep waters from the Indian and Pacific basins, as well as colder AABW from below (*Orsi et al.*, 1995). It is entrained in the ACC and travels into the Indian and Pacific Oceans, with a salinity signature of 34.78 psu at the tip of South Africa, decreasing to 34.7 psu in the Pacific (*Mantyla and Reid*, 1995; *Reid*, 1986). At

~45 °S the southwards flowing NADW, which has a temperature and salinity signature of 2 - 3 °C, 34.85 psu between 2000 – 3000 m water depth at 40 °S in the southwestern Atlantic (*Tsuchiya et al.*, 1994), splits CDW (Fig. 1.3) into a lower and upper branch (Lower Circumpolar Deep Water (LCDW) and Upper Circumpolar Deep Water (UCDW)), which are defined by low oxygen and high nutrients in UCDW and a salinity maximum in LCDW (*Orsi et al.*, 1995). UCDW are LCDW are further transformed into lighter AAIW and denser AABW respectively (Fig. 1.3: *Sloyan and Rintoul*, 2001).

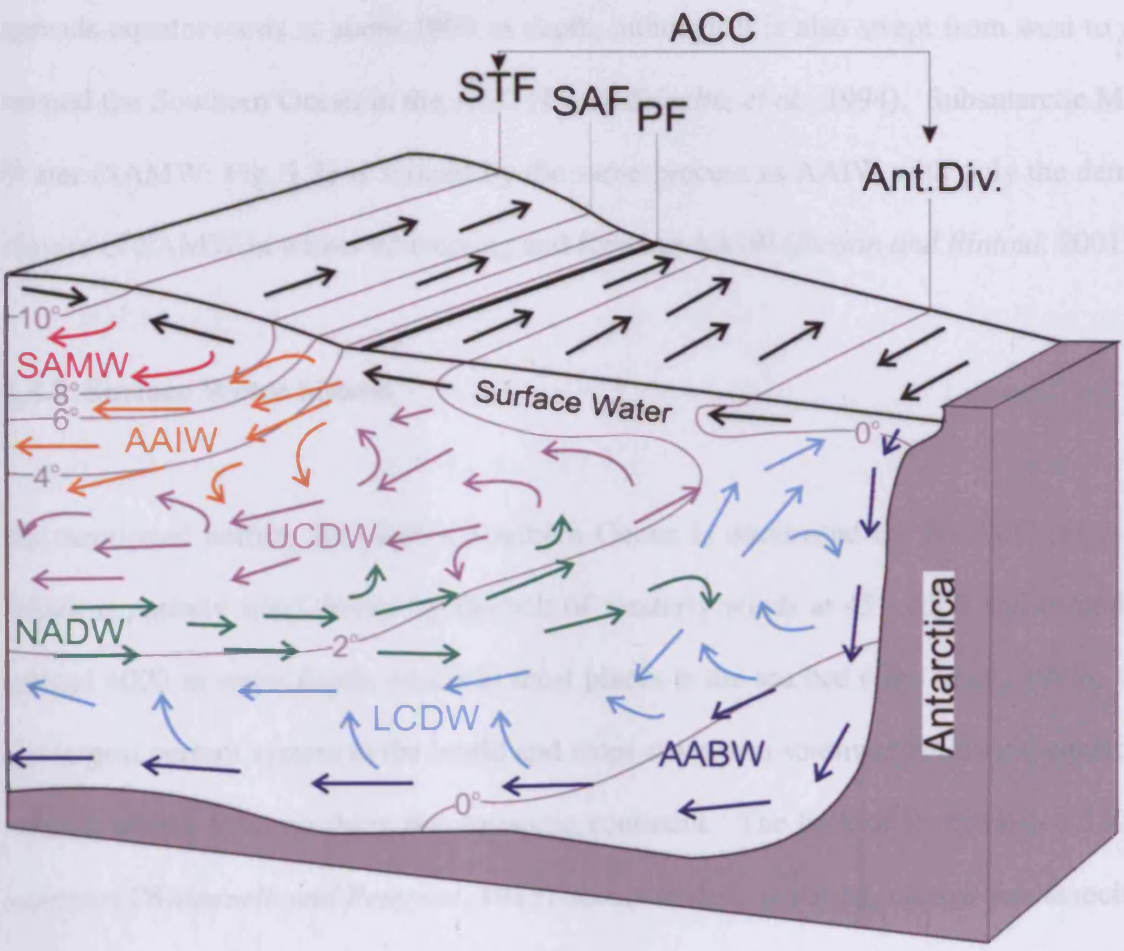

Figure 1.3. Schematic depth-latitude diagram showing the major circulation and water masses of the Southern Ocean: AABW; Antarctic Bottom Water, LCDW; Lower Circumpolar Deep Water, NADW; North Atlantic Deep Water, UCDW; Upper Circumpolar Deep Water, AAIW; Antarctic Intermediate Water, SAMW; Subantarctic Mode Water, STF; Subtropical Front, SAF; Subantarctic Front, PF; Polar Front, Ant. Div.; Antarctic Divergence, ACC; Antarctic Circumpolar Current (After *England et al.*, 2007; *Sugden*, 1982)

AAIW results from the mixing along a density surface at the Polar Front (Fig. 1.3) of cool, fresh Antarctic surface waters with warm, salty surface waters from the southeastern Pacific, Drake Passage, Falkland Current loop and the North Indian Ocean (*Molinelli,* 1978, 1981; *Talley,* 1996). The injection of fresh, cool Antarctic surface waters occurs primarily in the southeast Pacific and southwest Atlantic due to the physical constriction of the ACC flow by the Drake Passage (*Molinelli,* 1978; *Sloyan and Rintoul,* 2001). AAIW is characterised by a fairly low salinity tongue (34.4 psu: *Levitus,* 1983) which spreads equatorwards at about 1000 m depth, although it is also swept from west to east around the Southern Ocean in the ACC (*Lynch-Stieglitz et al.,* 1994). Subantarctic Mode Water (SAMW: Fig. 1.3) is formed by the same process as AAIW with only the densest classes of SAMW in winter convecting and forming AAIW (*Sloyan and Rintoul,* 2001).

1.4.2 Surface Water Masses

As mentioned before, the surface Southern Ocean is dominated by the ACC (Fig. 1.2) which is entirely wind driven by the belt of westerly winds at 45 - 55°S and extends to around 4000 m water depth, which in most places is the sea bed (*Orsi et al.,* 1995). It is the largest current system in the world and stops any warm southwards flowing equatorial surface waters from reaching the Antarctic continent. The bulk of its estimated 130 Sv transport (*Whitworth and Peterson,* 1985) occurs in deep reaching, narrow jets associated with the Polar (PF) and Subantarctic Fronts ((SAF) *Nowlin and Klinck,* 1986; *Gille,* 1994), with transport estimates of 53 Sv ±10 Sv at the SAF and 57.5 ±5.7 Sv at the PF through the Drake Passage (*Cunningham et al.,* 2003) and 42% and 28% of the total transport at the SAF and PF respectively south of South Africa (*Legeais et al.,* 2005). The estimate of 137 ±8 Sv for the transport of the ACC through the Drake Passage

(*Cunningham et al.*, 2003), is about 20 Sv less than that estimated for 35 °W, (157 Sv: *Heywood and King*, 2002) and is probably due to the injection of NADW into the ACC in the western boundary region of the South Atlantic (*Legeais et al.*, 2005), similarly the decrease from 157 Sv at 35 °W to 145 Sv at 0 °E also probably reflects the northward loss of CDW (*Legeais et al.*, 2005).

Associated with the ACC are a series of fronts, which are circumpolar bands of large horizontal density gradients, superimposed on the southward rise of isopycnals associated with the eastwards flow of the ACC (*Orsi et al.*, 1995). The Polar Front or Antarctic convergence (Fig. 1.3) separates Antarctic surface water (2 °C) from Subantarctic surface water (4 °C) and diffuse upwelling in the Antarctic zone from sinking of surface waters to form AAIW in the Subantarctic zone (*Orsi et al.*, 1995). The Subantarctic Front marks the boundary between the Subantarctic surface water (4 °C) and Transitional surface waters (8 °C), with rapid northwards sinking of the salinity minimum associated with AAIW from near the surface at the PF (*Orsi et al.*, 1995). These fronts meander where there is no constraining bed topography (*Moore et al.*, 1999), producing mesoscale eddies and rings (*Gouretski and Danilov*, 1994), although they are continuous around Antarctica. Other fronts, such as the Subtropical Front (STF), are not continuous around the continent although this particular front separating warm, salty Subtropical waters (>11.5 °C) from the cooler, fresher Transitional waters, can be identified by the large temperature gradient of 4 – 5 °C associated with it (*Deacon*, 1982).

1.5 Southern Ocean Glacial Circulation

Numerous studies from the North Atlantic suggest that NADW production was significantly reduced during the last glacial period (e.g. *Boyle and Keigwin*, 1987; *Duplessy et al.*, 1988; *Sarnthein et al.*, 1994; *Curry and Oppo*, 2005). Northern Component Waters (NCW) sank only to intermediate depth (<2000 m) forming Glacial North Atlantic Intermediate Water (GNAIW), and extending from 45 °N – 15 °S. In contrast, it appears the production of water masses from the ACC (i.e. Southern Component Waters) was either comparable or increased with enhanced northwards spreading, ventilating the deep North Atlantic below GNAIW (*Oppo and Fairbanks*, 1987; *Boyle and Keigwin*, 1987; *Marchitto and Broecker*, 2006).

Palaeoceanographic reconstructions of deep ocean variability in the South Atlantic have provided contrasting information on the relative influence of NADW and AABW during the last glacial-interglacial cycle. The suggestion of reduced production and southwards spread of NADW during glacial periods has been concluded by studies using Nd isotope ratios (e.g. *Rutberg et al.*, 2000, *Piotrowski et al.*, 2004, 2005), $^{231}Pa/^{230}Th$ ratios in sediments (*McManus et al.*, 2004; *Gherardi et al.*, 2005), benthic $\delta^{13}C$ records (*Streeter and Shackleton*, 1979; *Sigman and Boyle*, 2000) and clay-mineral tracers (*Diekmann et al.*, 1996) which found that NCW extended no further south than 40 °S at the height of the last glacial period. In contrast, early studies using $^{231}Pa/^{230}Th$ ratios (*Yu et al.*, 1996) suggest that export of NCW to the Southern Ocean continued at a comparable rate to the Holocene during the last glacial maximum (LGM), although probably at a reduced depth, a contention that also seems to be corroborated by Cd/Ca (*Boyle*, 1992; *Lea*, 1995) and foraminiferal isotope measurements in the southeast Pacific and Atlantic (*Matsumoto et*

al., 2001; *Matsumoto and Lynch-Stieglitz,* 1999). Uncertainty is added to the picture by the indication of an expansion of SCW in two branches (USCW and LSCW) that compensated for the suppression of NADW (*Henrich et al.*, 2003; *Curry and Oppo*, 2005) and a suggested presence of GNAIW in the Southern Ocean as a replacement for NADW (*Volbers and Henrich*, 2004). While, *Bickert and Mackensen* (2003) suggest that instead of GNAIW taking over from NADW, Mediterranean Outflow Water (MOW) is more likely to have compensated but at a shallower depth and only certainly as far south as 30 °S.

Surface reconstructions have shown that during glacial periods the flow of the ACC was stronger (*Pudsey and Howe,* 1998), with a northwards shift in the associated frontal systems and sea ice extent (e.g. *Crosta et al.*, 2004; *Stuut et al.*, 2004; *Gersonde et al.*, 2003, 2005; *Wolff et al.*, 2006) in response to increased ice mass on Antarctica. A northwards movement of the fronts has been linked to reduced leakage of warm, salty Indian Ocean water through the Agulhas Retroflection region into the South Atlantic (e.g. *Berger and Wefer,* 1996; *Goldstein et al.*, 1999; *Flores et al.*, 1999; *Rau et al.*, 2002; *Peeters et al.*, 2004).

1.6 Interhemispheric Timing of Rapid Climate Change

The interhemispheric linkage of oceanic change has been the target of conceptual and numerical modelling (*Ganopolski and Rahmstorf*, 2001; *Seidov et al.*, 2001; *Weijer et al.*, 2002; *Knorr and Lohmann*, 2003; *Stocker and Johnsen,* 2003; *Weaver et al.*, 2003; *Knutti et al.*, 2004), while ice-core synchronization exercises, using methane records (*Blunier et al.*, 1998), added insight from interhemispheric atmospheric palaeodata comparisons that

suggest an out-of-phase pattern between the hemispheres (*Blunier et al.*, 1998; *Blunier and Brook*, 2001; *Brook et al.*, 2005; *EPICA*, 2006). The relationship between the two hemispheres means that the climate system was suggested to act like a seesaw with each hemisphere taking turns to drive the system (*Broecker*, 1998; *Stocker*, 1998). The few high-resolution palaeoceanographic records from the Southern Hemisphere oceans confirm this suggestion (*Charles et al.*, 1996; *Pahnke et al.*, 2003; *Pahnke and Zahn*, 2005), although such records are sparse and do not enable a conclusive picture to be drawn for the wider Southern Hemisphere oceans. The likely mechanism for this 'bipolar seesaw' is linked to variations in the relative amount of deepwater formation in the two hemispheres (*Stocker*, 1998; *Seidov and Maslin*, 2000, *Seidov et al.*, 2001), which results in cross-equatorial heat piracy and the warming of one hemisphere whilst the other cools. During interglacial conditions the North Atlantic steals heat from the Southern Hemisphere which maintains a strong Gulf Stream and prevents ice sheet build up in the Northern Hemisphere. During Heinrich events meltwater is injected into the North Atlantic and heat is transported southwards across the equator as the Gulf Stream weakens. This causes the Southern Hemisphere oceans to warm (*Pahnke and Zahn*, 2005) and the Northern hemisphere oceans to cool (*Bond*, 1995). After the iceberg armada associated with Heinrich events has ceased then NADW formation can recommence at interglacial levels and northward cross-equatorial heat transport resumes. It has been suggested by early studies (*Hays et al., 1976; Imbrie et al., 1989; Howard and Prell, 1992; Labeyrie et al., 1996*) that on orbital timescales Southern Ocean SSTs respond early to changes in the orbital parameters and might actually lead global ice volume (*Charles et al., 1996*). The cause of such a lead is not well understood, as is the phasing of changes between the hemispheres on shorter sub-orbital timescales.

1.7 Agulhas Leakage and Atlantic Meridional Overturning Circulation Variability

As mentioned above, interbasin exchange of the 'warm water route' through the Agulhas Retroflection region (Fig. 1.2), along with the 'cold water route' through the Drake Passage, are the primary sources of the Benguela Current, the source of the warm upper-layer water that flows northwards through the Atlantic in compensation for the colder southward flowing NADW. Source estimations for the Benguela Current suggest that in terms of volume the transport of cold, low salinity AAIW through the Drake Passage into the South Atlantic accounts for around 60 - 70% of the flow (*England and Garcon,* 1994; *Schmitz,* 1995), compared to estimates of 25 - 40% for thermocline and intermediate waters leaked through the Agulhas Current system (*England and Garcon,* 1994; *Schmitz,* 1995; *Garzoli and Gordon,* 1996; *You et al.,* 2003). Whilst the greater volume input to the Benguela Current by Drake Passage waters undoubtedly has a large influence on the overturning circulation of the North Atlantic (*Sijp and England,* 2004), recent studies have suggested that the input of Indian Ocean water through the Agulhas Retroflection provides vital heat and salt fluxes to the density-and-temperature sensitive North Atlantic (*Richardson et al.,* 2003) and may stimulate and stabilise the Atlantic Meridional Overturning Circulation (AMOC) (*Weijer et al.,* 2001).

Infact, other studies have suggested that rather than flowing straight into the Benguela Current system, much of the thermocline and intermediate waters of the South Atlantic current (5 - 6 Sv out of 7 Sv), primarily fed by Drake Passage waters actually flows into the Indian Ocean subtropical gyre by a route immediately south of the Agulhas Retroflection and returns to the Atlantic via the Agulhas Current (*Gordon et al.,* 1992; *Friocourt et al.,* 2005), further underlining the importance of Agulhas leakage. However,

these figures have been disputed by other authors such as such *You et al.* (2003) who suggest that of the 12.9 Sv of Benguela Current transport, 10.3 Sv is contributed by intermediate water from the southwest Atlantic, composed of 8.8 Sv directly fed from the Atlantic and only 1.5 Sv returned after a loop in the Indian Ocean subtropical gyre. Despite these differences both sources are seen as important and as they presumably vary in time, the volume to transport ratio of these competing inter-ocean fluxes is thought to be the important factor expected to influence the thermohaline characteristics of the South Atlantic and ultimately the North Atlantic (*Gordon and Haxby,* 1990).

The inter-ocean volume flux through the Agulhas gateway is difficult to determine due to the intermittent nature of ring, eddy and filament formation, the main methods of exchange at the Agulhas Retroflection region (*Lutjeharms and Cooper,* 1996; *Schmitz,* 1996; *de Ruijter et al.,* 1999; *Arhan et al.,* 2003; *Richardon et al.,* 2003; *Lutjeharms et al.,* 2003; *Esper et al.,* 2004). The estimates postulated so far have generally relied on determining the volume of Agulhas rings and their propagation rate. However, different authors have used different techniques, used different assumptions and even measured the rings at different distances from the retroflection, thus seeing them in different states of decay. Problems have also occurred in counting the number of rings shed every year, with a significant number actually reattaching back to the retroflection after a period of time and periods occurring when none are shed, followed by several forming rapidly in one month (*de Ruijter et al.,* 1999). Their small volumes and rapidly lost thermal signature have also hindered the estimation of filament fluxes, whilst inversion studies have also been used to estimate inter-ocean exchange fluxes, but are thought to use data which is diverse and nonsynoptic and unable to take into account the intermittent character of the Agulhas leakage process.

Despite these problems with flux estimations, recent modelling and proxy studies have focused on the role of Agulhas leakage in the THC stability, with proxy studies showing an increase in leakage through the Agulhas Retroflection during late glacial periods when ice volume was maximal (*Peeters et al.*, 2004). Several modelling studies have showed this leakage to be the 'flywheel' of THC initiating changes from glacial state THC to interglacial or 'on' mode (*Knorr and Lohmann*, 2003, 2004) whilst other studies have suggested the importance of Agulhas leakage in stabilising the THC (*Weijer et al.*, 2001; *Marsh et al.*, 2007). Whilst the modelling studies of *Knorr and Lohmann* (2003, 2004) suggest that the THC responds to northwards propagation of heat and salt leaked through the Agulhas Retroflection, a modelling study by *Weijer et al.* (2002) suggests that the overturning strength of the North Atlantic responds to increased South Atlantic buoyancy sources (within 2 years) before any thermohaline anomaly can reach the convection areas, suggesting that the Agulhas heat and salt sources modify the overturning circulation by influencing the meridional pressure gradients, rather than through the thermohaline increase in salt and heat.

These conflicting hypotheses suggest timing is the key to answering the questions. If dating techniques can be improved so that the timing of the start of climate events can be accurately identified then the issue of time lags between the renewed strong inter-basin exchange and the resumption of NADW formation in the Nordic Seas can be resolved and a mechanism identified.

1.8 Aims of This Study

The primary aim of this thesis is to enhance our understanding of the role played by the Southern Ocean in climate change, both on glacial to interglacial and more rapid timescales over the past 170 ka. Particular emphasis in this study is placed on both the reconstruction of glacial to interglacial and millennial-scale Southern Ocean deep water mass changes and the timing of these changes in relation to North Atlantic water mass variability and climate change. Furthermore, reconstructions of the timing and phasing of Southern Ocean surface water mass change at glacial terminations and inceptions, with specific reference to the fluctuations in the amount of 'leakage' of warm water through the Agulhas Retroflection region, are considered in relation to global climate mechanisms. In achieving these aims the key objectives were as follows:

- To develop a robust age model using radiocarbon dating and graphical tuning of a benthic $\delta^{18}O$ record to existing palaeo-records in order to correlate observations from cores MD02-2589 and MD02-2588 with other marine and ice cores from across the globe.
- To construct high-resolution surface ocean hydrographic records for the Agulhas throughflow region over the last two glacial terminations and the Marine Isotope Stage 5/4 transition using planktonic foraminiferal stable isotopes, foraminiferal assemblage counts, IRD counts and transfer function derived SST from core MD02-2589 and planktonic stable isotopes from core MD02-2588.
- To infer mid-depth hydrography, water mass and near-bottom flow speed changes, using high-resolution benthic foraminifera $\delta^{13}C$, $\delta^{18}O$ and sortable silt mean grain size records from core MD02-2589 positioned in the southwards extension of

NADW at the present day in the Atlantic to Indian throughflow region from glacial to interglacial periods. This aims to clarify the contribution of NCW to the Southern Ocean during glacial periods.

- To use the benthic foraminifera $\delta^{13}C$ record of core MD02-2589, along with a benthic $\delta^{13}C$ record from the North Atlantic to identify the phasing of changes over the past 170 ka and its effect on the Atlantic Meridional Overturning Circulation of the Atlantic Ocean
- To further investigate the glacial water mass structure of the Southern Ocean using the foraminifera benthic $\delta^{13}C$ records of a transect of cores from the Subtropical zone over the Subtropical, Subantarctic and Polar fronts into the Antarctic zone.

1.9 Thesis Layout

The principal scientific findings of this study are structured into four results and discussion chapters (Chapters 4, 5, 6 and 7) addressing the main objectives outlined above. Chapters 2 and 3 summarise the techniques used in this study and detail the development of a robust age model for MD02-2589 and MD02-2588, whilst chapter 8 discusses and concludes the main scientific results of this investigation.

Chapter 2. Material and Methods

2.1 Regional Oceanography, Site Setting and Core Preparation

2.1.1 Present Day Hydrography

The region connecting the Indian and Atlantic oceans (Fig. 2.1) is one of several oceanic gateways guiding the flow of surface and deep waters around the global ocean and distributing heat, salt and nutrients between the oceans (*Sloyan and Rintoul*, 2001; *Boebel et al.*, 2003a). The region is characterised by strong meridional gradients in water properties that are maintained by a suite of ocean fronts. To the north of the Agulhas Plateau, located 500 km off the southern tip of Africa, rising to depths of 2500 - 3000 m, with isolated peaks reaching 500 m (*Boebel et al.*, 2003a), lies the warm saline subtropical Agulhas current system (Fig. 2.1a), and to the south the cool, low salinity subpolar ACC, who's northern boundary is defined by the Subtropical Front (STF) (*Peterson and Stramma*, 1991), currently positioned at 42 °S (*Belkin and Gordon*, 1996; *Orsi et al.*, 1995).

The main surface oceanographic feature of the region is the Agulhas Current, which marks the western boundary of the South Indian subtropical gyre and is thought to be the primary boundary current of the Southern Hemisphere, with a total volume flux of ~ 65 Sv over its upper 1000 m (*Flores et al.*, 1999). South of the Agulhas Bank is a bottle-neck area where three major currents interact: the Antarctic Circumpolar Current (ACC), the South Atlantic Current and the Agulhas Current (Fig. 2.1a). It is here that the Agulhas Current retroflects back eastwards into the Indian Ocean as the Agulhas Return

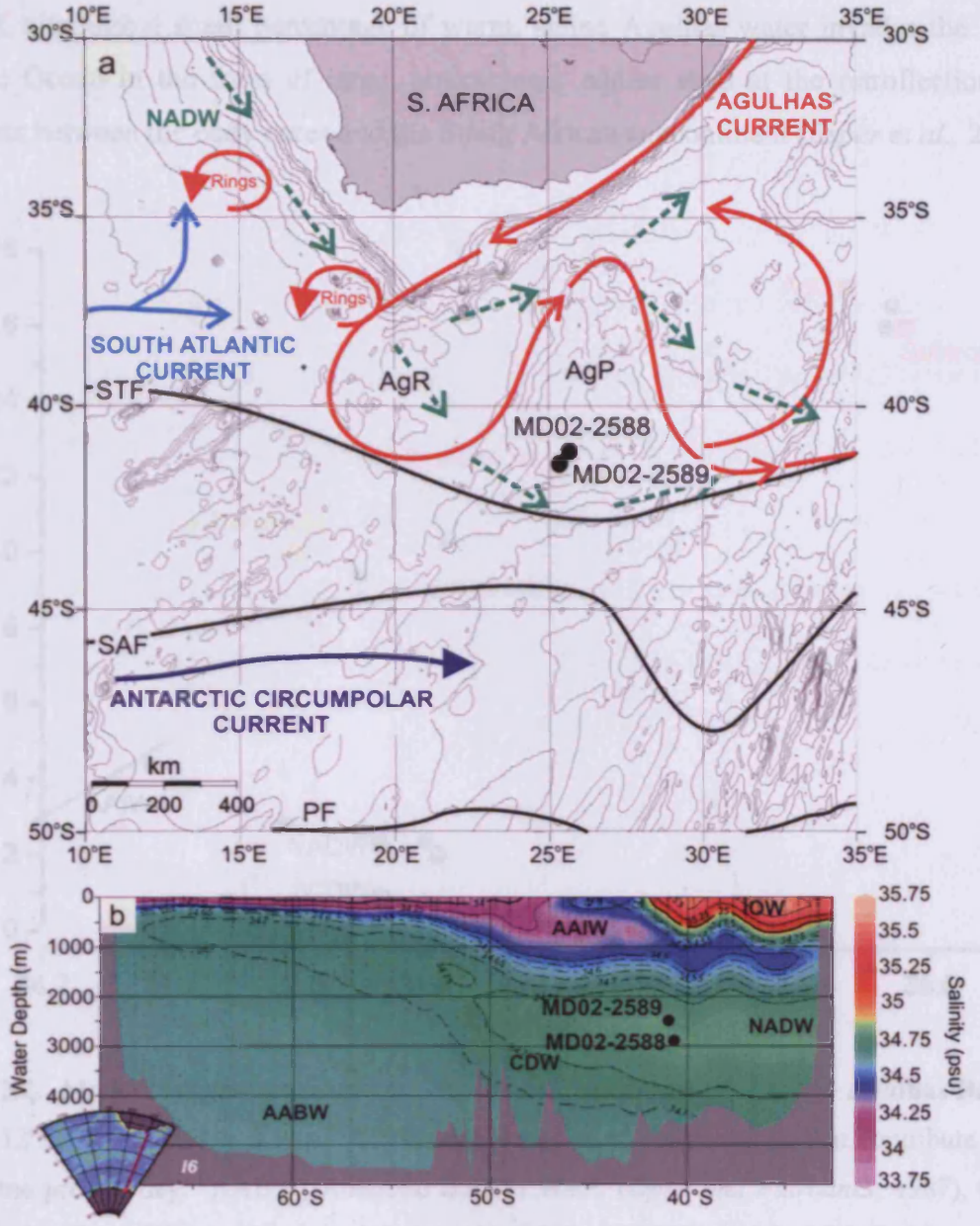

Figure 2.1. (a) Map showing study area and position of cores MD02-2588 and MD02-2589 on the Southern Agulhas Plateau, together with the present day position of the oceanic fronts and generalised ocean circulation (after *Richardson et al.*[2003]). Position of the fronts after *Belkin and Gordon* [1996] and *Orsi et al.* [1995]. Plain arrows = surface water currents, dashed arrows = bottom water currents. Acronyms are NADW = North Atlantic Deep Water; AgP = Agulhas Plateau, AgR = Agulhas Retroflection, STF = Subtropical Front, SAF = Subantarctic Front, PF = Polar Front. **(b) Present day transect of salinity from the coast of South Africa to Antarctica across the Southern Ocean** (modified from *Schlitzer,* 2000) showing the positions of the existing water masses. IOW = Indian Ocean Water, AAIW = Antarctic Intermediate Water, NADW = North Atlantic Deep Water, CDW = Circumpolar Deep Water, AABW = Antarctic Bottom Water.

Current, although a small percentage of warm, saline Agulhas water invades the South Atlantic Ocean in the form of large, anticyclonic eddies shed at the retroflection and filaments between the eddy cores and the South African subcontinent (*Esper et al.*, 2004).

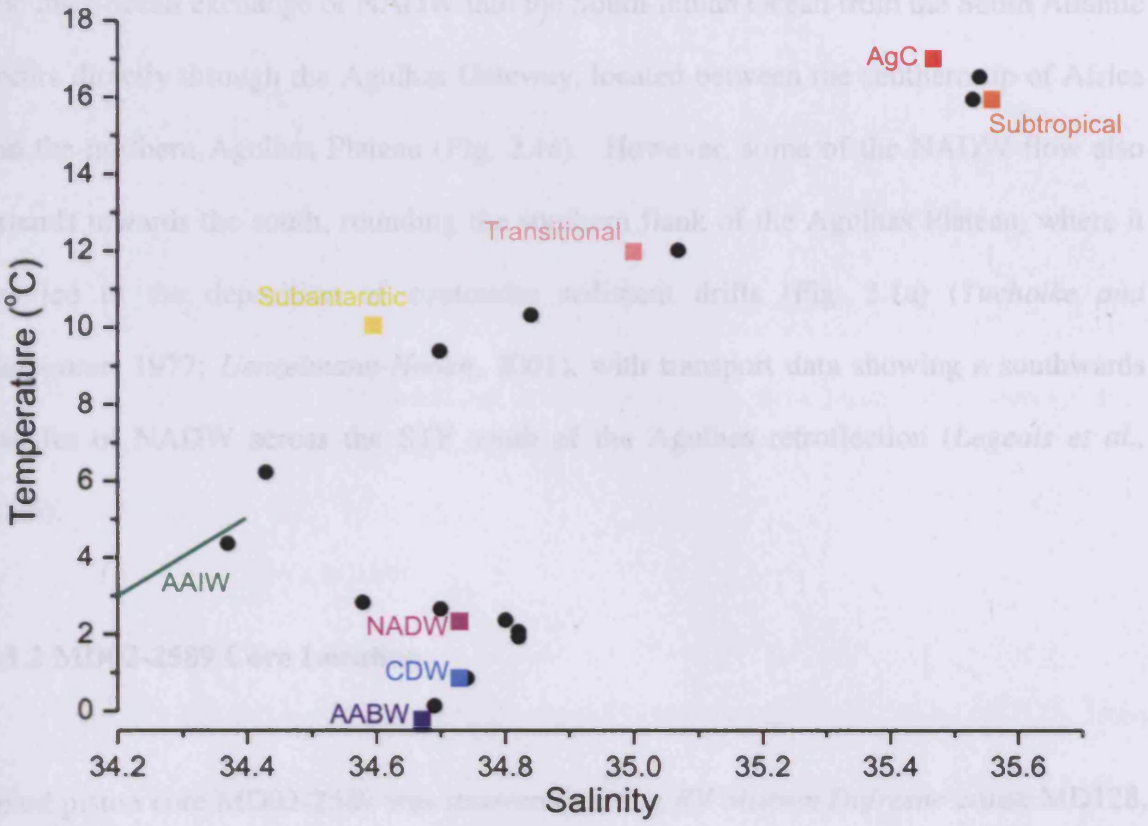

Figure 2.2. Modern annual average temperature vs. salinity profile in the Agulhas Basin at Site 41.12°S, 28.9°E (*Schmidt et al.*, 1999) with water mass end-members that contribute to the area at the present day: AABW; Antarctic Bottom Water (*Oppo and Fairbanks*, 1987), CDW; Circumpolar Deep Water (*Oppo and Fairbanks*, 1987), NADW; North Atlantic Deep Water (*Oppo and Fairbanks*, 1987), AAIW; Antarctic Intermediate Water (*Saenko and England*, 2003), Subantarctic; Subantarctic Surface Waters (*Orsi et al.*, 1995), Transitional; Transitional Surface Waters (*Orsi et al.*, 1995), AgC; Agulhas Current, Subtropical (*Hutson*, 1980); Subtropical Surface Waters (*Hutson*, 1980)

Deep-water circulation in the Agulhas Basin is primarily characterized by the interactions between southward propagating NADW and northward flowing SCW, notably AABW and AAIW (Fig. 2.1b, 2.2; *Reid*, 1989; *Reid*, 2005). The transition between NADW and

LCDW) is at mid-depths sloping upwards to the south (Fig. 2.1b), whilst the deep areas (>5000 m) are filled with AABW (Fig. 2.1b, 2.2; *Orsi et al.*, 1999).

The inter-ocean exchange of NADW into the South Indian Ocean from the South Atlantic occurs directly through the Agulhas Gateway, located between the southern tip of Africa and the northern Agulhas Plateau (Fig. 2.1a). However, some of the NADW flow also extends towards the south, rounding the southern flank of the Agulhas Plateau, where it has led to the deposition of contourite sediment drifts (Fig. 2.1a) (*Tucholke and Carpenter*, 1977; *Uenzelmann-Neben*, 2001), with transport data showing a southwards transfer of NADW across the STF south of the Agulhas retroflection (*Legeais et al.*, 2005).

2.1.2 MD02-2589 Core Location

Giant piston core MD02-2589 was recovered during *RV Marion Dufresne* cruise MD128, 20th September – 14th October 2002, from a contourite drift located on the southern Agulhas Plateau at 41°26.03'S, 25°15.30'E (*Giraudeau et al.*, 2002) (Fig. 2.1a). The site at present is at 2660 m water depth on a sediment drift up to 650 m thick that displays an asymmetric geometry and changes in internal reflector patterns which are indicative of a dynamical circulation pattern in the region back to Oligocene-Miocene times (Fig 2.3; *Uenzelmann-Neben*, 2001). The core recovered 34.55 m of sediment, comprised primarily of foraminiferal ooze (Fig. 2.4), spanning the past ~1.3 Ma (*Giraudeau et al.*, 2002). At this depth the core site at present day lies predominantly in NADW, ~1000 m below Antarctic Intermediate Water (AAIW) and ~1000 m above LCDW (Fig. 2.1b), although there is a substantial LCDW contribution to the site.

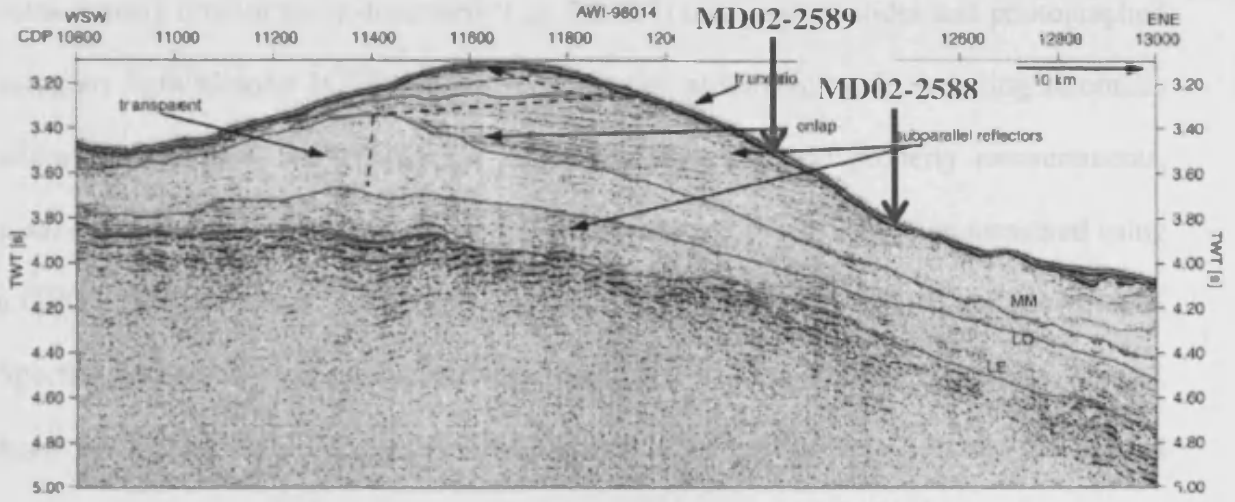

Figure 2.3. Site survey / Multichannel seismic reflection data (after *Uenzelmann-Neben*, 2001): positions of cores identified using a TWT of 1500 m/s

2.1.3 MD02-2588 Core Location

Core MD02-2588 was again recovered during *RV Marion Dufresne* cruise MD128, from the same contourite drift located on the southern Agulhas Plateau as MD02-2589 at 41°19.90' S, 25°49.40' E (*Giraudeau et al.*, 2002) (Fig. 2.1a, 2.3). The site is at present in 2907 m water depth and 10.65 m of primarily light olive silt clay was recovered using a CALYPSO giant pisten core, spanning the past 350 ka (*Giraudeau et al.*, 2002). As with MD02-2589, MD02-2588 lies predominantly in NADW, ~600 m above LCDW and 1300 m below AAIW (Fig. 2.1b).

2.1.4 Core Handling, Shipboard Analysis and Physical Properties

The core liner for core MD02-2589 was extracted from the core barrel onboard the *RV Marion Dufresne* and cut and capped into standard 1.5 m sections. The cores were then

split into 'archive' and 'working' halves using a rotary saw, with the working half subsequently lithologically described (Fig. 2.4, 2.7) using smear slides and photographed using an Agfa/Minolta 3CCD digital camera in full automatic mode including automatic white balance adjustment (Fig. 2.5, 2.6). Sediment physical property measurements, gama-ray density, P-wave velocity and magnetic susceptibility, were then measured using a GEOTEK multi-sensor core logging system (MST) at a resolution of 2 cm down-core. Spectral reflectance measurements were then taken using a Minolta spectrophotometer, again at 2 cm resolution, and summarised using the total reflectance (L*) and the spectral reflectance at 400 and 700 nm. The working halves of MD02-2589 and MD02-2588 were subsequently sub-sampled and processed at i Universitat Autònoma de Barcelona, where the archive halves are stored.

2.1.5 Sample Preparation

The upper 9.8 m of MD02-2589 and 10.6 m of MD02-2588 were sampled every 1 - 2 cm. The samples were first sieved using distilled water through at 63 μm sieve to separate the fine (< 63 μm) and coarse (>63 μm) fractions. Both fractions were then dried at 45 °C and weighed separately and then stored independently awaiting analysis.

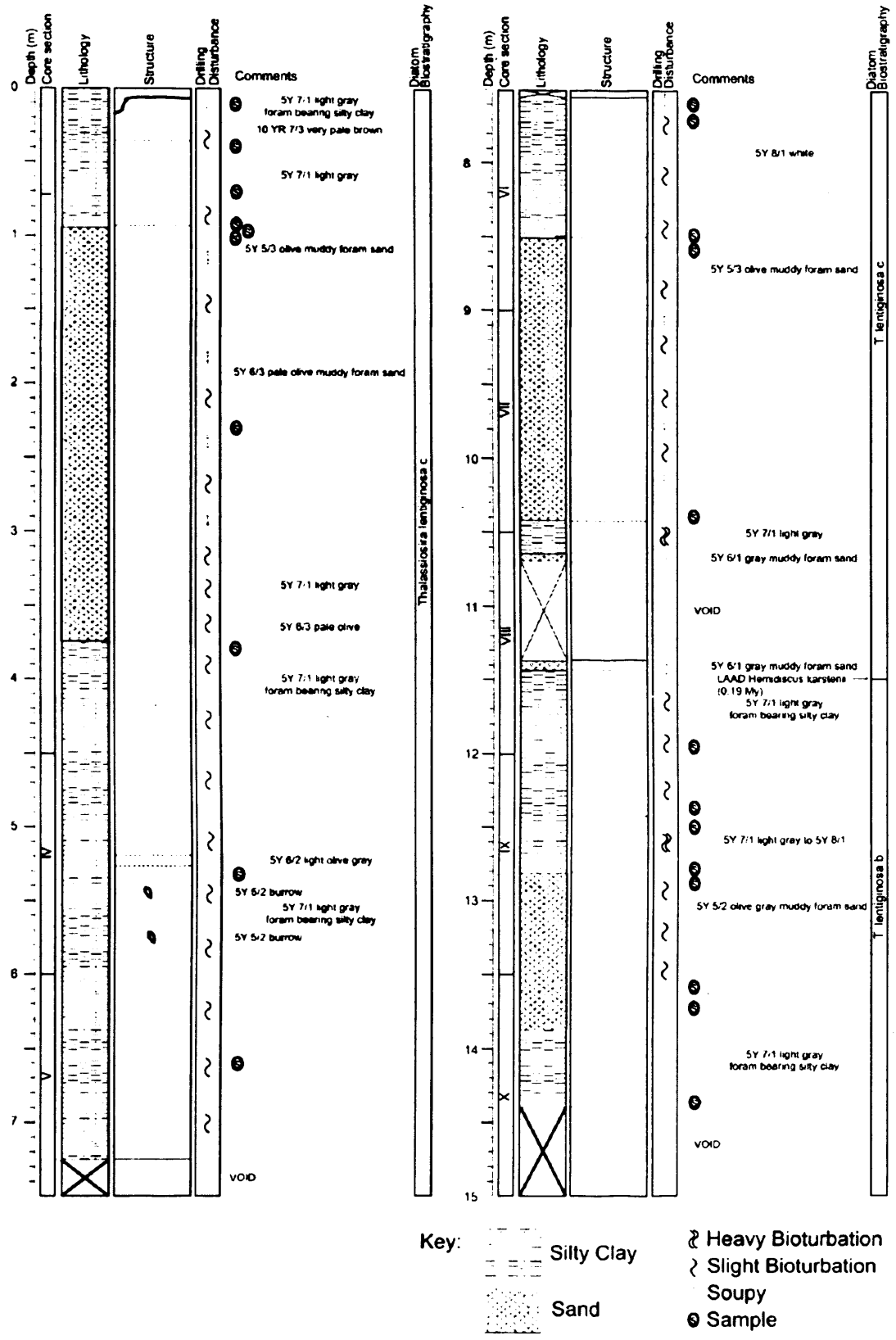

Figure 2.4. Upper 15m lithology of core log MD02-2589 (After *Giraudeau*, 2002)

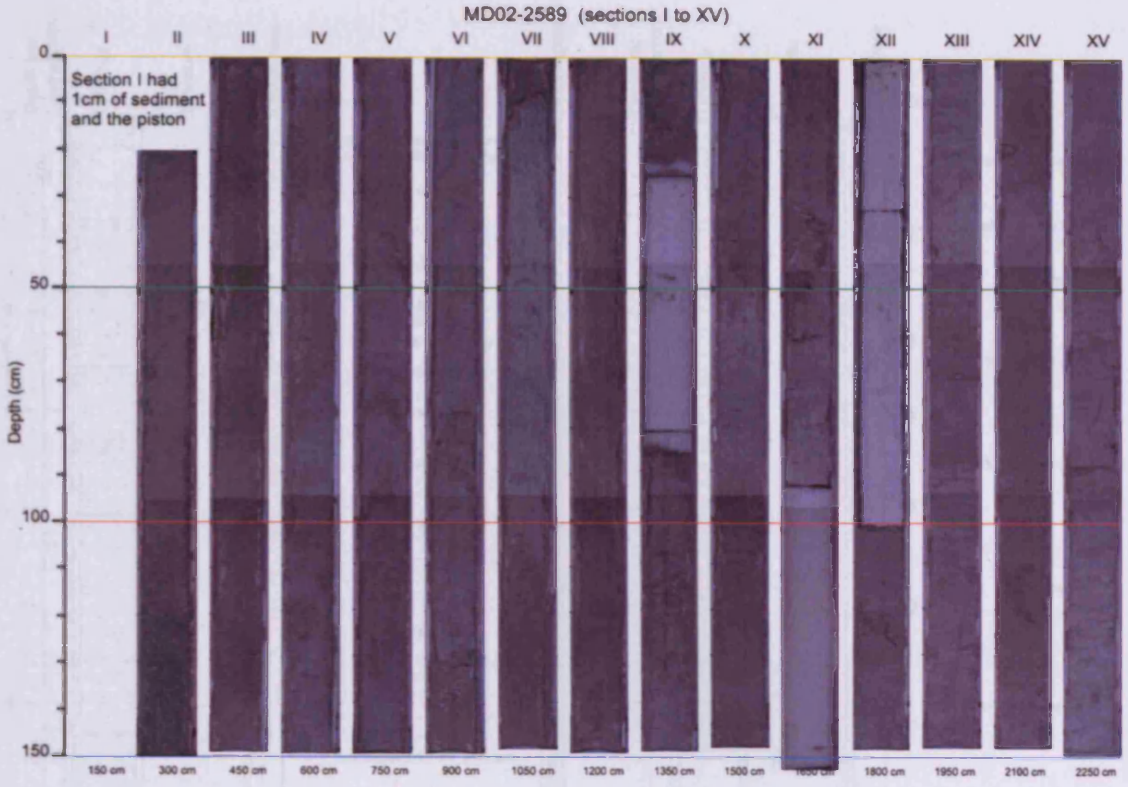

Figure 2.5. Photograph of core MD02-2589. 150cm length sections of the working half

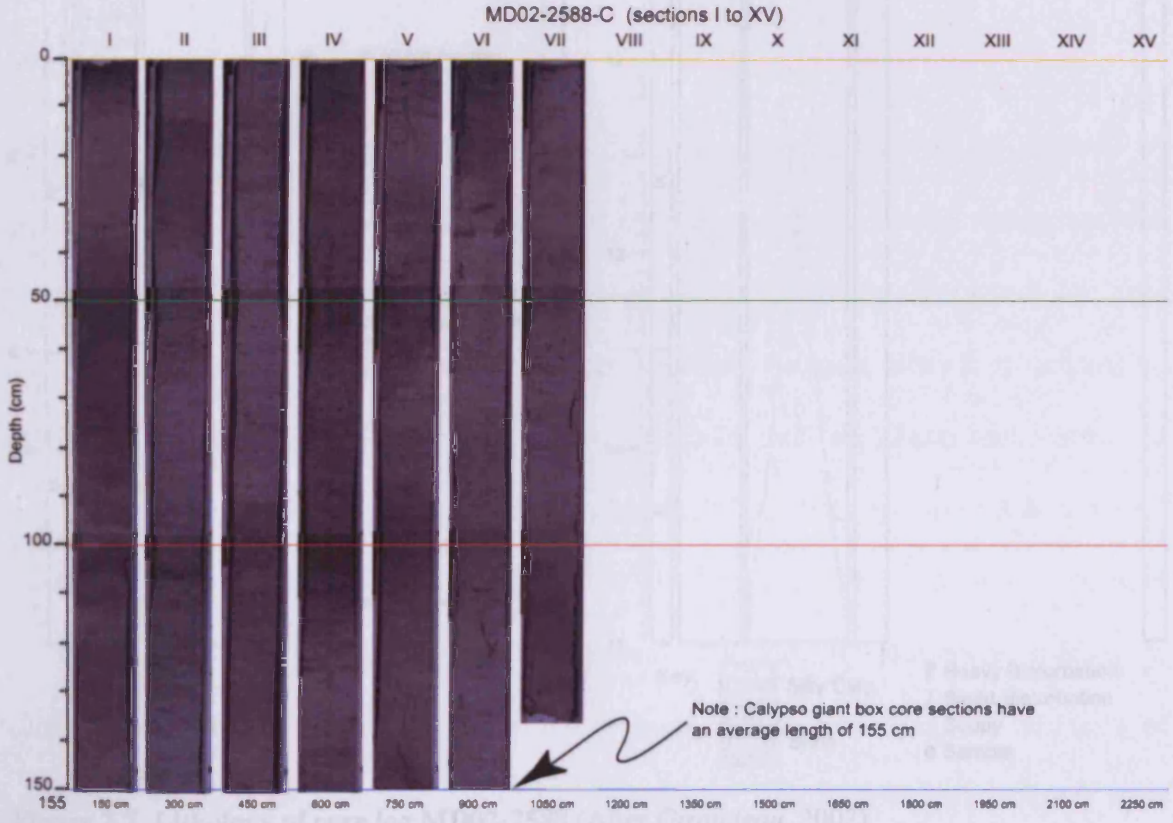

Figure 2.6. Photograph of core MD02-2588. 155cm length sections of the working half

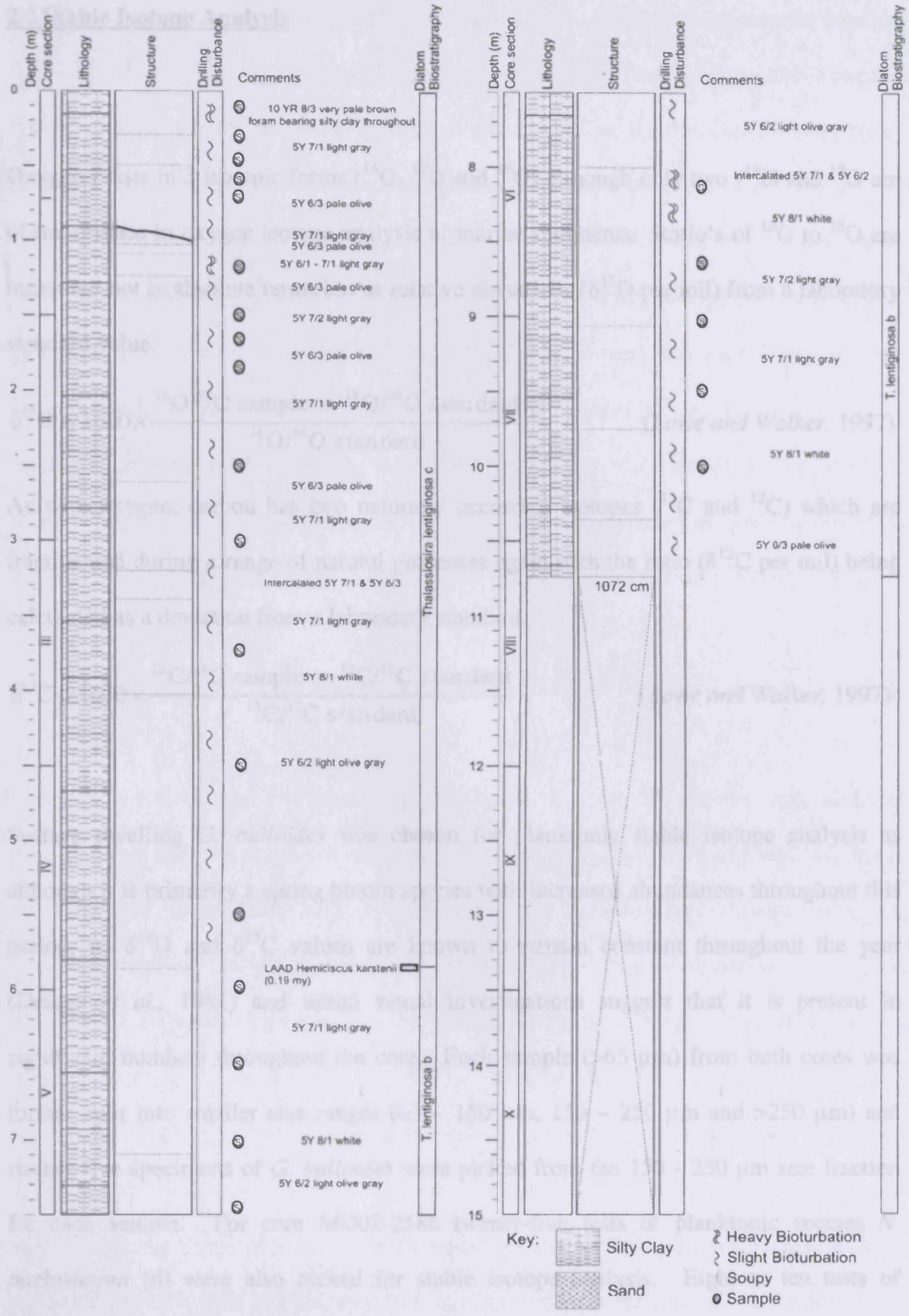

Figure 2.7. Lithology of core log MD02-2588 (After *Giraudeau*, 2002)

2.2 Stable Isotope Analysis

Oxygen exists in 3 isotopic forms (^{16}O, ^{17}O and ^{18}O) although only two (^{16}O and ^{18}O are of importance in oxygen isotope analysis of marine sediments. Ratio's of ^{16}O to ^{18}O are measured not in absolute terms but as relative deviations ($\delta^{18}O$ per mil) from a laboratory standard value:

$$\delta^{18}O = 1000 \times \frac{^{18}O/^{16}O \text{ sample} - {}^{18}O/^{16}O \text{ standard}}{^{18}O/^{16}O \text{ standard}} \qquad \textit{(Lowe and Walker, 1997)}$$

As with oxygen, carbon has two naturally occurring isotopes (^{13}C and ^{12}C) which are fractionated during a range of natural processes again with the ratio ($\delta^{13}C$ per mil) being calculated as a deviation from a laboratory standard:

$$\delta^{13}C = 1000 \times \frac{^{13}C/^{12}C \text{ sample} - {}^{13}C/^{12}C \text{ standard}}{^{13}C/^{12}C \text{ standard}} \qquad \textit{(Lowe and Walker, 1997)}$$

Surface dwelling *G. bulloides* was chosen for planktonic stable isotope analysis as although it is primarily a spring bloom species with increased abundances throughout this period, its $\delta^{18}O$ and $\delta^{13}C$ values are known to remain constant throughout the year (*Deuser et al.*, 1981) and initial visual investigations suggest that it is present in significant numbers throughout the core. Each sample (>65 μm) from both cores was further split into smaller size ranges (63 – 150 μm, 150 – 250 μm and >250 μm) and twenty-five specimens of *G. bulloides* were picked from the 150 - 250 μm size fraction for each sample. For core MD02-2588 twenty-five tests of planktonic species *N. pachyderma* (d) were also picked for stable isotope analysis. Eight to ten tests of epibenthic foraminiferal species *Fontbotia wuellerstorfi* (also commonly referred to as *Cibicidoides wuellerstorfi*), generally known to secrete calcite close to the $\delta^{13}C_{DIC}$ values

of ambient bottom water (*Mackensen et al.*, 2001), were picked for each sample from the 150 - 250 μm size fraction. Both the planktonic and benthic foraminifera were immersed in 3 % hydrogen peroxide for 30 minutes, ultrasonicated in acetone (added to hydrogen peroxide) for 5 seconds, had the excess liquid and residue removed and then dried at 45 °C. The samples were then analysed using a Finnigan MAT 252 mass spectrometer coupled with an automated Kiel-type carbonate preparation device. Long-term analytical precision is 0.06 ‰ for $\delta^{18}O$ and 0.03 ‰ for $\delta^{13}C$. All isotope data are referenced to the Vienna PeeDee Belemnite (VPDB) scale through repeated analysis of NBS 19 international carbonate standard. Oxygen isotopes of the benthic foraminifera *F. wuellerstorfi* have been transferred by +0.64 ‰ to the *Uvigerina* spp. scale as this more closely represents equilibrium with the ambient seawater (*Shackleton and Hall*, 1997).

2.2.1 Use of Benthic $\delta^{13}C$ as a Deep Water Mass Tracer

The carbon isotope ratios of benthic foraminiferal calcite ($\delta^{13}C$) are the traditional tool used to trace deep water masses (*Broecker and Peng*, 1982; *Curry and Lohmann*, 1982; *Duplessy et al.*, 1988; *Kroopnick*, 1985; *Bostock et al.*, 2004), with additional secondary overprints used to study biological productivity changes (e.g. *Mackensen et al.*, 1993; *Mackensen*, 2001; *McCorkle et al.*, 1990) and air-sea gas exchanges (e.g. *Broecker and Mair-Reimer*, 1992; *Zahn and Keir*, 1994). The initial carbon isotopic composition ($\delta^{13}C_{\Sigma CO2}$) of the dissolved inorganic carbon of an ambient water mass, its preformed values, is primarily determined by air-sea gas exchange during its residence in surface waters, with the extent of photosynthesis occurring within the euphotic zone also playing a role (*Kroopnick*, 1985). Photosynthesis in surface waters preferentially utilises ^{12}C and

nutrients (mainly PO_4, NO_3), enriching the waters in ^{13}C and depleting them in nutrients (e.g. *Kroopnick*, 1985; *Rau et al.*, 1991).

The formation of organic matter, enriched in ^{12}C and nutrients, in the surface ocean travels through the water column and eventually settles on the ocean floor and over this time is oxidised, releasing its ^{12}C and nutrients (*Berger and Vincent*, 1986; *Boyle* 1997). Therefore young, nutrient-depleted deep water masses such as those found in the northern North Atlantic (e.g. NADW formation region), have high $\delta^{13}C$ signatures (~1 ‰ at present day), whereas older, nutrient-enriched water masses that have been long isolated from the atmosphere have increasingly negative $\delta^{13}C$ values with increasing age (-0.5 ‰ – 0 ‰ for North Pacific waters (*Charles and Fairbanks*, 1992)) as they gain remineralised low ^{13}C organic carbon from overlying surface productivity during their transit through the ocean basins (*Berger and Vincent*, 1986; *Raymo et al.*, 1990; *Wefer et al.*, 1999). This creates $\delta^{13}C$ gradients along flow paths and partially explains the large-scale variations in $\delta^{13}C$ throughout the World's oceans (*Kroopnick et al.*, 1972; *Kroopnick*, 1980). However it is widely acknowledged that the mixing between water masses with different end-members and distinct isotopic signatures also explains some of this variability (*Rutberg and Peakcock*, 2006).

Dissolved oxygen levels are also associated with the strength of the biological pump, as this controls the amount of oxygen used up in the process of decay. Therefore lower benthic $\delta^{13}C$ levels are typically associated with decreased oxygen levels and increased nutrients as the oxygen is used up in the decay and release of ^{12}C and nutrients into the deep waters (*Kroopnick* 1985).

When interpreting the $\delta^{13}C$ records of benthic foraminifera in terms of deep water circulation changes, however, several additional competing effects need to be considered. The first of these is the rate of air-sea gas exchange, which has a temperature, alkalinity and salinity controlled component related to carbon isotope fractionation (*Wefer et al.*, 1999; *Broecker and Maier-Reimer*, 1992; *Zahn and Keir*, 1994). The $\delta^{13}C$ in the atmosphere is on average 9 ‰ lower that that in the surface ocean and the extent of fractionation is a function of temperature, with higher $\delta^{13}C$ and gas exchange occurring at lower temperatures due to increased CO_2 solubility (e.g. *Broecker and Maier-Reimer*, 1992; *Zahn and Keir*, 1994; *Lynch-Stieglitz and Fairbanks*, 1994; *Raven and Falkowski*, 1999; *Rutberg and Peacock*, 2006). Although this thermodynamic overprint is generally thought not to be very strong due to slow isotopic equilibrium (*Broecker and Peng*, 1982), *Charles and Fairbanks* (1990) have shown that if there is sufficient time for gas exchange, a significant signal is produced. In the Southern Ocean the effect is strong, with the Agulhas Plateau being close to the maximum Southern Ocean air-sea gas exchange region south of the Polar Front (PF) and therefore it is thought that even partial equilibrium may have a significant effect on $\delta^{13}C$ values in the region.

The second consideration is changes in the global terrestrial carbon reservoir; storage of carbon enriched in ^{12}C in the trees and soils on the continent, which on glacial to interglacial timescales is known to have a substantial effect on the global mean ocean $\delta^{13}C$ (*Shackleton*, 1977; *Keigwin and Boyle*, 1985; *Matsumoto and Lynch-Stieglitz*, 1999). The transfer of ^{12}C-rich carbon from the continents to the ocean by the reduction of terrestrial biomass due to expanding glacial ice masses and changes in water balances is thought to reduce the global mean deep ocean $\delta^{13}C$ values during the last glacial

maximum (LGM) by between 0.32 ‰ (*Duplessy et al., 1988*) and 0.46 ‰ (*Curry et al., 1988*).

A third consideration is the effect of changes in productivity, with three main factors having a significant effect on benthic $\delta^{13}C$ values. Upwelled nutrient-rich deep waters encourage increased biological activity in the surface waters which results in an increased organic carbon flux low in ^{13}C to the seafloor, which alters the local $\delta^{13}C$ signal of the deep waters. The strength of upwelling of cooler, nutrient-rich deep waters to the surface is closely linked with wind patterns (*Arrhenius,* 1952; *Schott,* 1983; *Fiúza,* 1983; *Orsi et al.,* 1995; *Little et al.,* 1997; *Smetacek et al.,* 1997; *Wefer et al.,* 1999; *Abrantes,* 2000; *Helber and Weisberg,* 2001; *Peeters et al.,* 2002; *Naidu,* 2004; *Zeldis,* 2004; *Barker and Thomas,* 2004; *Romero,* 2006). The nonconservative 'phytodetritus or Mackensen effect' (*Mackensen et al.,* 1993; *Mackensen and Bickert,* 1999; *Bickert and Mackensen,* 2003), mainly effects epibenthic foraminifera (e.g. *F. wuellerstorfi* which live on top of the sediment) which grow and reproduce during periods of peak seasonal organic matter fluxes to the sea floor. In areas of strong seasonal productivity (e.g. Antarctic PF, coastal upwelling regions) particulate organic matter, with $\delta^{13}C$ values 3 - 4 ‰ lower than the surface sediment organic carbon (*Mackensen and Bickert,* 1999), is rapidly deposited in a phytodetritus layer on the sea floor. This food supply is thought to trigger the chamber building and reproduction of the epibenthic species with the $\delta^{13}C$ values of their shells, formed during the remineralization of this phytodetritus layer, recording $\delta^{13}C$ values that are 0.3 - 0.4 ‰ lower than the ambient bottom waters found throughout the rest of the year (*Sarnthein et al.,* 1988; *Mackensen et al.,* 1993). Thirdly variation in the flux of organic matter to the seafloor is also known to affect foraminifera in different microhabitats (*Urey,* 1947; *Zahn et al.,* 1986). Species that live endobenthically or

infaunally (within the sediment e.g. *Globobulimina* spp. (*Mackensen and Douglas,* 1989*; McCorkle et al.,* 1990)) record the $\delta^{13}C$ of the pore water, which is consistently lower than bottom water $\delta^{13}C_{\Sigma CO2}$ as organic matter decomposition in the sediments releases ^{12}C-enriched CO_2 to the pore water (*McCorkle et al.,* 1985, *Mackensen et al.,* 1993) and therefore have $\delta^{13}C$ values that are depleted relative to ambient bottom water $\delta^{13}C$ (*Mackensen and Douglas,* 1989*; McCorkle et al.,* 1990*; Mackensen et al.,* 1993). Epibenthic species (on top of or in elevated positions above the seafloor (*Lutze and Thiel,* 1989)) are therefore often used for reconstructions of the $\delta^{13}C$ of former deep ocean and bottom water masses because they are thought to secrete calcite, not in isotopic equilibrium with the ambient bottom-water $\delta^{13}C_{\Sigma CO2}$, but in a constant 1:1 relationship (*Woodruff et al.,* 1980*; Belanger et al.,* 1981*; Graham et al.,* 1981*; Zahn et al.,* 1986).

It is also known that different foraminifera size fractions produce different $\delta^{13}C$ signatures and although this is an issue that should be considered mainly when interpreting planktonic foraminifera isotope records it has also been linked to benthic foraminifera (*Mackensen et al.,* 1993). These isotopic offsets probably reflect the different physiologies and feeding habits of foraminifera during their life cycle (*Bostock et al.,* 2004) with individuals living at the environmental limits of its species having slow growth, low metabolic activity and an isotopic fractionation factor that is different to those specimens growing in more favourable conditions (*Hemleben et al.,* 1989). Therefore in paleoceanographic studies it is important to use similar size fractions, preferably the largest adult tests which give a representative signal of a complete life cycle. As a result both benthic and planktonic foraminifera used for isotopic analysis in this study were picked out of the 150 – 250 μm fraction, with the largest tests within that fraction chosen.

2.2.2 Benthic $\Delta\delta^{13}C$ Estimation

The benthic $\delta^{13}C$ records of cores MD02-2589 and MD95-2042 (37° 48'N, 10° 10'W: 3146 m water depth (*Shackleton et al.*, 2000)) were sampled for the same time interval (from 9.7 – 149.79 ka) using linear interpolation at the spacing of the lower resolution MD95-2042 core. The $\Delta\delta^{13}C$ (MD95-2042 – MD02-2589) was then calculated by subtracting the benthic $\delta^{13}C$ values of MD02-2589 from MD95-2042.

2.2.3 Spectral Analysis of Benthic $\delta^{13}C$ Data

The benthic $\delta^{13}C$ data of core MD02-2589 and MD95-2042 (*Shackleton et al.*, 2000) were analysed for their dominant frequencies using spectral analysis. Whilst individual parameters will be further discussed within Chapter 6, all spectral analysis was undertaken using the Blackman-Tukey method (*Jenkins and Watts,* 1968), with a Welch window (*Welch,* 1967) using the *Analyseries* software (*Paillard et al.*, 1996). The Blackman-Tukey spectral analysis algorithm is an autocorrelation derived from the one used in Brown University within the SPECMAP program (*Imbrie,* 1985; *Imbrie et al.*, 1989). The algorithm computes the autcovariance of the data by comparing the time series with itself once it has been offset or lagged by various amounts, then it applies a window and finally Fourier transforms the data to compute the spectrum (*Weedon,* 2003). All spectral analysis was calculated to 95 % confidence intervals unless stated. Significance of spectral peaks was estimated using upper and lower powers calculated by *Analyseries* at the confidence level chosen. A peak within a spectral plot is significant if

both its lower and upper powers are higher than the calculated values for that confidence interval.

Cross-spectral analysis was also undertaken using the *Analyseries* software (*Paillard et al.*, 1996), Blackman-Tukey method and Welch window. Cross-spectral analysis calculates the coherency, the similarity of the amplitude variations in two time series, and the phase difference, the average difference in phase between two time series at different frequencies (*Weedon*, 2003). The coherency is calculated by multiplying together two time series at different lags to obtain a cross-correlation sequence, then applying a window to the cross-covariance and then using the Fourier transform function. The uncertainty in the phase depends on the coherency and variance of the spectral window and can be very large at low coherency meaning that phase estimates of medium or low coherency are of limited use (*Weedon*, 2003). All of the cross-spectral analysis was undertaken at 95 % confidence intervals.

In order to test spectral results and to trace non-stationary signals, Wavelet analysis (Matlab verison 6.5, wavelet toolbox) was carried out by following the protocol of *Torrence and Campo* (1998). This routine applies a simple Morlet waveform on the normalised equally-spaced (linearly interpolated) data. The 95 % confidence interval is indicated by values over 1.5 and orange and red colours in the resulting plot. For filtering in the time domain, we applied band-pass filters (AnalySeries, *Paillard et al.* (1996)), using a Gaussian filter with central frequency.

2.3 Mean Sortable Silt (10 - 63 μm) Grain Size as a Near Bottom Flow Speed Proxy

Grain size analysis of the sortable silt mean grain size (heareafter $\overline{SS}$) palaeocurrent indicator, uses the fraction of the sediment (i.e. the terrigenous 10 - 63 μm component) whose size sorting varies in response to hydrodynamic processes to infer relative changes in near-bottom current speed (*McCave et al.*, 1995a; *McCave and Hall*, 2006). The fine end of the silt fraction (<10 μm) are discarded from the size spectra because material in this fraction is increasingly dominated by clay minerals. Clay minerals, as shown by *McCave et al.* (1995a), behave in a cohesive fashion, as a result of charge imbalances and adhesion from van der Waals forces (*Russel*, 1980; *Weaver*, 1989) and therefore are mainly deposited as aggregates or flocs which are unrelated to the depositional fluid shear environment. Size sorting occurs in the 10 - 63 μm fraction during resuspension and deposition, by aggregate break-up and particle selection according to settling velocity and fluid shear stress, with the controlling variables being: critical erosion stress (τ_e), critical suspension stress (τ_s) and critical deposition stress (τ_d), below which particles of a particular settling velocity will be deposited whilst those with smaller settling velocities will be ejected from the viscous sub-layer (*McCave and Hall,* 2006). Typically, for non-cohesive material, that is the 10 - 63 μm fraction, $\tau_d < \tau_e < \tau_s$. As hydrodynamic processes of sorting in the viscous sub-layer tend to act on particles > 10 μm, under stronger flow this material is size-sorted according to its primary grain size, suggesting that the $\overline{SS}$ can be used as an index of flow speed of the depositing current (*McCave and Hall,* 2006). This proxy has been used successfully in paleocurrent studies in the North Atlantic (e.g. *Manighetti and McCave,* 1995; *Hall et al.*, 1998; *Bianchi and McCave,* 1999; Ellison et al. 2006), South Atlantic (e.g. *Kuhn and Diekmann,* 2002), Indian (e.g. *McCave et al.*, 2005) and Pacific Oceans (e.g. *Hall et al.*, 2001).

The analysis of $\overline{SS}$ was undertaken using a Coulter Counter (see below), which is a residence pulse counter, based on the principal that a particle passing through an electric field maintained in an electrolyte solution (Isoton) will cause a voltage change proportional to its volume (*Bianchi et al.,* 1999). The voltage pulses are related to spherical particle volume by calibration experiments (*Milligan and Kranck,* 1991), with quartz density assumed for all grains in order to convert settling velocity to size and volume to mass.

The <63 μm separated size fraction is used for $\overline{SS}$ analysis. To run $\overline{SS}$ analysis, 2.5 g of the fine terrigenous sub-fraction in a sample needs to be retained after the removal of all carbonates and biogenic silicates (*McCave et al.,* 1995a). To estimate the amount of carbonate in a sample, a small amount of each sample was weighted and burnt in an oven at 400 °C for 3 hours to remove all organic carbon and then analysed using a Perkin-Elmer 2400 CHN machine. The resultant % of inorganic carbon was calculated from the CHN data and the amount of sediment required to maintain 2.5 g of the fine terrigenous sub-fraction after carbonate removal was calculated. The resultant calculated sub-samples were then put into 500 ml jars and decarbonised with two acid rinses of 2M acetic acid for 48 hours to remove the inorganic carbonate. The liquid was drained off once the sediment had settled and the sediment then treated with a two molar solution of sodium carbonate (Na_2CO_3) to remove the biogenic silicates. The sodium carbonate and sediment mix was then placed in a pre-heated water bath at 85 °C for 8 hours and mixed vigorously with a glass rod every 2 hours to re-suspend the sediment. Samples were then rinsed twice using de-ionised water, leaving the sediment to settle before decanting each time. Finally the samples were transferred to 60 ml bottles and filled with 0.2 % sodium

hexametaphosphate (calgon) solution to prevent coagulation of the particles. All the samples were homogenised on a rotating spinner and sonified for 1 minute before analysis, with a 300 µl sub-sample being added to Isoton for analysis using a standardised procedure.

$\overline{SS}$ grain size measurements were undertaken using a Coulter Multisizer III as detailed in *Bianchi et al.* (1999) to a preset particle count of 70,000, with a 140 µm aperture size giving a sensed range of 2.8 – 70 µm due to the fact that the detection window is 2 - 50% of the diameter of the orifice through which the particles are sucked and sensed (*McCave and Hall,* 2006). The Coulter Counter cannot detect the total clay fraction < 2 µm and therefore only the mean sortable silt size, the $\overline{SS}$, can be estimated using this method, rather than the abundance of the SS component (SS%), which is the percentage of the <63 µm fraction that is 10 - 63 µm or the silt/clay ratio. Average $\overline{SS}$ abundance of the 10 - 63 µm fraction in the samples is 8 - 10% enabling the determination of the $\overline{SS}$ index with an error of ±2 % (*Bianchi et al.*, 1999).

2.4 Surface Water Proxy Reconstructions

2.4.1 Planktonic Foraminifera Faunal Assemblages

A total of 112 planktic foraminifera faunal assemblage counts were undertaken for three time periods over the past 170 ka: Termination I (11.6 – 26.5 ka), Termination II (115.5 – 149.5 ka) and interglacial to glacial transition Marine Isotope Stage 5a/4 (64.7 – 77.6 ka). The faunal analysis was based on the >150 µm size fraction, with each sample being quantitatively subsampled using a microsplitter until approximately 300 specimens were

left for microscopic identification. The >150 μm size fraction was chosen as previous studies have shown that most species have reached the adult stage of ontogeny in this fraction and therefore it provides a representative fraction for standard faunal assemblage counts (*Peeters et al.*, 1999). Statistical examination of assemblages using different specimen numbers suggest that to accurately identify a characteristic assemblage >300 individual whole specimens need to be counted (*Lord*, 1980). A total of 28 species were identified under a binocular microscope following the taxonomic concepts of *Bé and Tolderlund* (1971), *Bé* (1977), *Kennett and Srinivasan* (1983) and *Hemleben et al.* (1989) and counts of these species were converted to percentage relative abundance (percentage of species within the total counted).

The dextral and sinistral forms of *Neogloboquadrina pachyderma* were counted separately and those individuals identified in the *Pachyderma:Dutetrei* intergrade (P:D intergrade) category (*Kipp, 1976*) were included in the *N. pachyderma* (d/s) groups of respective coiling direction as there is no evidence that this is a separate species. *N. pachyderma* and *Neogloboquadrina dutetrei* diverged 10 million years ago (*Darling et al., 2004*) and therefore it is not possible for there to be an intergrade between them.

No distinction was made between the different coiling directions of *Globorotalia truncatulinoides* and both individuals of *Globigerinoides sacculifer* with and without sacs were combined as they were present in such low numbers.

As most of the taxa that live predominantly or exclusively north of the STF in the Subtropical Zone (Fig. 2.8) are only present in very small to small percentages, all of these species were separated into one of three groups (detailed below) based on the

modern day distribution of species by *Bé and Tolderlund* (1971), *Niebler and Gersonde* (1998), *Peeters et al.*, (2004) and *Rau et al.*, (2006). Some of the species are present in more than one group.

(i) Taxa that have their maximum abundances north of the STF but also extend southwards into the transitional zone (ST/Tr): *Globigerinita glutinata, Globorotalia truncatulinoides, Globorotalia crassformis, Globigerinella calida, Globorotalia hirsuta, Globorotalia scitula* and *Orbulina universa.*

(ii) Taxa only found north of the STF (NSTF): *Globigerina falconensis, Globigerinoides ruber, Globigerinella siphonifera, Neogloboquadrina dutetrei, Globorotalia menardii, Globigerinoides conglobatus and Globigerinoides sacculifer.*

(iii) Taxa believed to be indicative of the Agulhas Current (Agulhas Leakage Fauna (ALF)) and Indian Ocean subtropical waters (*Peeters et al.*, 2004): *Globigerinita glutinata, Globorotalia scitula, Globigerinoides sacculifer, Globigerinella siphonifera, Pulleniatina obliquiloculata, Globorotaloides hexagona, Globorotalia menardii, Globigerinoides ruber* and *Orbulina universa.*

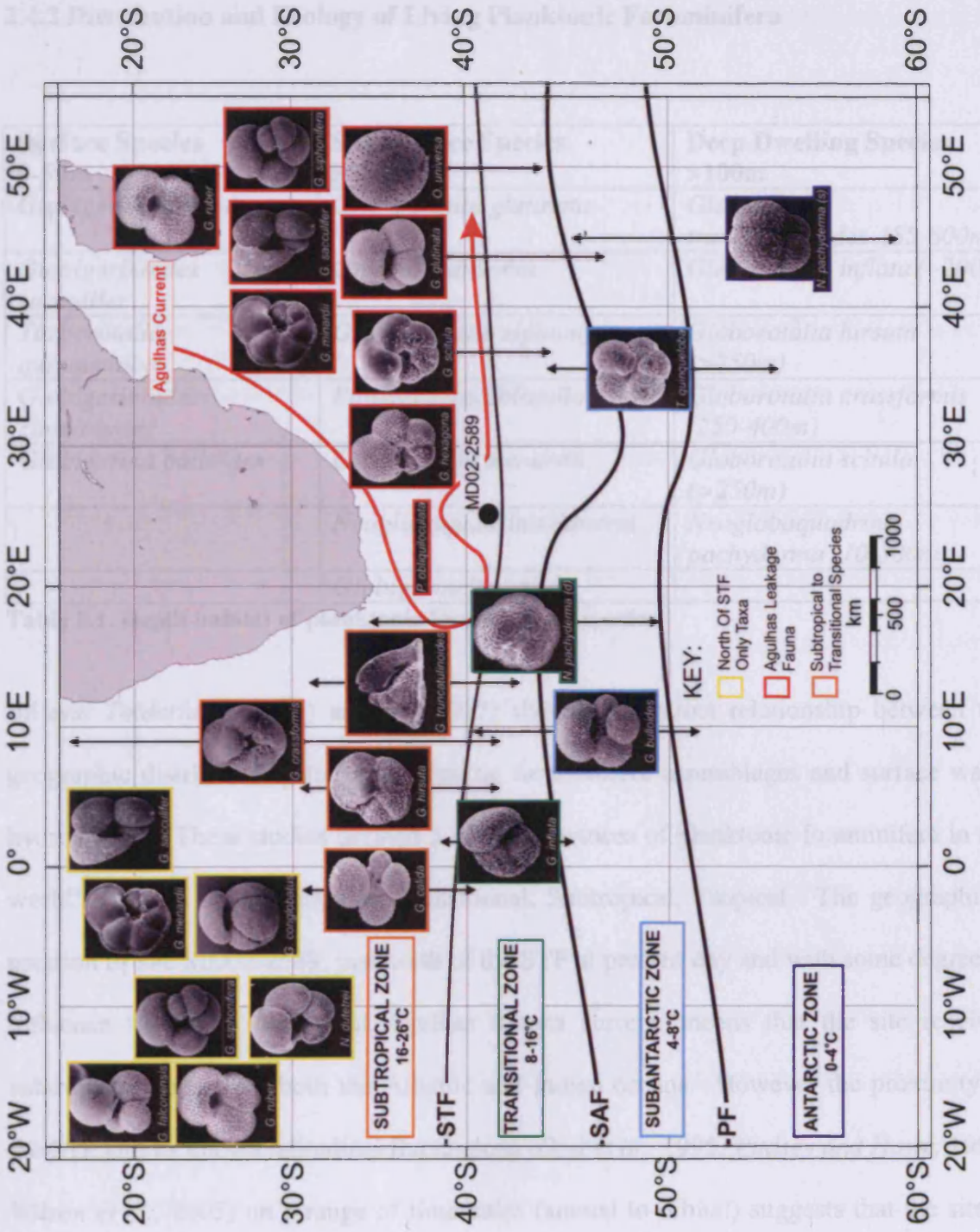

Figure 2.8. Modern day distribution and groupings of planktonic foraminiferal species used in both the sea surface temperature calculation and assemblage discussions (after *Bé and Tolderlund,* 1971; *Niebler and Gersonde,* 1998; *Peeters et al.,* 2004; *Rau et al.,* 2006): Pictures of foraminifera from *EMIDAS* (2007)

2.4.2 Distribution and Ecology of Living Planktonic Foraminifera

Surface Species 0-50m	Sub-surface Species 50-100m	Deep Dwelling Species >100m
Globigerinoides ruber	*Globigerinita glutinata*	*Globorotalia truncatulinoides (85-800m)*
Globigerinoides sacculifer	*Orbulina universa*	*Globorotalia inflata (~200m)*
Turborotalia quinqueloba	*Globigerinella siphonifera*	*Globorotalia hirsuta (>250m)*
Globigerinoides conglobatus	*Pullentiatina obliquiloculata*	*Globorotalia crassformis (250-400m)*
Globigerina bulloides	*Globorotalia menardii*	*Globorotalia scitula (>250m)*
	Neogloboquadrina dutetrei	*Neogloboquadrina pachyderma (10-300m)*
	Globigerinella calida	

Table 2.1. Depth habitat of planktonic foraminiferal species

Bé and Tolderlund (1971) and *Bé* (1977) showed a distinct relationship between the geographic distribution patterns of planktic foraminifera assemblages and surface water hydrography. These studies defined 5 faunal provinces of planktonic foraminifera in the world's oceans: Polar, Subpolar, Transitional, Subtropical, Tropical. The geographical position of site MD02-2589, just north of the STF at present day and with some degree of influence from the subtropical Agulhas Return current, means that the site receives subtropical fauna from both the Atlantic and Indian oceans. However the proximity of the STF and its known latitudinal fluctuations (*Orsi et al.*, 1995; *Pudsey and Howe*, 1998; *Wilson et al.*, 2005) on a range of timescales (annual to orbital) suggests that the site is also influenced by transitional and colder subantarctic faunas, making the Agulhas Plateau an ideal place to study these frontal movements and relative changes in current strengths and positions over a wide range of temperature regimes. In the following discussion *Bé and Tolderlund* (1971), *Bé* (1977), *Niebler and Gersonde* (1998), *Peeters et*

al. (2004) *and Rau et al.* (2006) are used as the general references for the environmental characteristics of the foraminifera species (Fig. 2.8, Table 2.1).

Neogloboquadrina pachyderma (sinistral) is the most dominant species in polar waters comprising 90 % of the total assemblage in waters south of the PF and 50 - 80 % in the Subantarctic Zone. The abundance decreases to 25 % around the SAF and 10 % around the STF, with insignificant numbers in subtropical waters with temperatures >15 °C, although it is found in areas of coastal upwelling off southwest Africa. It is the dominant species in sea ice, with its distribution being very temperature dependant and lives in the temperature range of 0 - 9 °C, although it is most abundant at temperatures below 4 °C. Juvenile forms are known to live in near surface waters (10 - 100 m) and migrate down the water column with increasing size, with adult forms dwelling at deep depths (100 - 300 m).

Turborotalia quinqueloba is also a species that occurs in large numbers in the Antarctic and Subantarctic Zone. It is a small sized surface dwelling species (0 - 10 m water depth), with abundances up to 16 % around the PF and Subantarctic Zone with upper limits being the Transitional Zone, although it is found in small numbers in the Agulhas and Benguela Currents. It is found in a surface temperature range of 1 – 21 °C, although it is most abundant in waters of 1 - 5 °C.

Neogloboquadrina pachyderma (dextral) (*Neogloboquadrina incompta* as suggested by *Darling et al.*, 2006 due to species divergence between *N. pachyderma* sinistral and dextral during the Miocene) is most dominant in Subantarctic and Transitional waters and as with *N. pachyderma* (sinistral) it is found mainly in deep surface waters (>100 m water

depth) although its juvenile forms are found predominantly in upper surface waters. It is found in only trace abundances in Antarctic waters, making up <10 % of the total assemblage at the PF, although its abundances increase up to 20 % at the SAF (~7 °C), with similar values being found in the Transitional Zone up to the STF (up to 20 °C). It is also found in the region between upwelling and subtropical waters along the western coast of South Africa. This species lives in well stratified upper waters, just below the thermocline and in cool, mesotrophic, high nutrient waters of upwelled filaments. As mentioned above individuals identified within the P:D intergrade category were combined with the *N. pachyderma* samples of respective coiling directions. Core top studies in the Southern Ocean (*Hayward, 1983; Schaefer et al., 2005*) suggest that true *N. dutetrei* individuals are rare and *N. pachyderma* (d/s) abundant and therefore P:D intergrade individuals should be combined with the *N. pachyderma* (d) or (s) groups depending on coiling direction.

Globigerina bulloides, discussed in greater detail in section 2.3.6, is the most dominant species in Subantarctic waters, with abundances of over 50 % of the assemblage in this area. It also comprises 80 - 90 % of the assemblage between 40 – 50°S, increasing northwards across the Subantarctic Zone towards the SAF and decreasing to ~40 % at the STF. It has a wide temperature range (4 – 22 °C), although it is most dominant between 10 - 16 °C and is known to increase in abundance in and adjacent to upwelling environments and high-fertility conditions.

Globorotalia inflata is the only species indigenous to the Transitional Zone that separates subpolar and subtropical waters, with a linear peak in abundance between 35 – 45 °S. It comprises values of 15 % in the Subantarctic Zone, rising to 20 % in the Transitional

Zone and peaks (up to 35 %) just north of the STF (16 – 20 °C), decreasing in subtropical waters over 22 °C. This species can tolerate temperatures between 1 – 27 °C and makes up a significant percentage of the assemblage in upwelling areas (Benguela upwelling system) although it is not thought of as a typical upwelling species and has low values in the Agulhas Current. It is a deep dwelling species (up to 200 m water depth) which is reflective of areas of low nutrient content and reduced primary productivity.

Globigerinita glutinata is equally abundant in both cold (10 °C) and warm (28 °C) environments, with a distribution ranging from Antarctic to tropical waters (3 – 30 °C). Despite being a ubiquitous species it is not normally dominant and has abundances of <5 % in most areas, although it has increased abundances in subtropical waters (24 – 27 °C) with a peak of 17 % at 26 °C, making it predominantly a Subtropical species. Its percentage of the total assemblage rises to 5 – 9 % in the Agulhas Return Current and over the area 30 – 40 °E and 35 – 50 °S, with an increase at margins of productivity and upwelling zones associated with a deep-mixed surface layer.

Globorotalia truncatulinoides is a deep dwelling species (85 - 800 m water depth) with a wide distribution zone (4 – 27 °C), although its peak abundance is in the Subtropical Zone (21 – 24 °C). Its abundance is 0 – 5 % in the Transitional Zone increasing to 11 % in the subtropical gyre and is reflective of high salinity deep waters. As the species is deep dwelling it is actually reflective of temperatures at water depths of around 250 m (4 °C at the SAF and 13 – 16 °C in the subtropical gyre).

Globorotalia crassformis is known as a deep dwelling (250 – 400 m water depth) subtropical species although it is known to have low abundances in a wide area from the

PF to the Subtropical Zone with SST of 3 – 24 °C (or 3 – 16 °C at 300 m water depth). Highest occurrences of the taxa (up to 6 %) are found in the northern Transitional Zone and the species is thought to reflect high salinity waters below the thermocline.

Globigerinella calida is a warm subtropical species that is more common in mid to low latitudes and mixed layers with warm water at depth. Although it is characteristic of the Subtropical Zone it is known to occur in small numbers in the Transitional Zone.

Globorotalia hirsuta is a deep dwelling (>250 m water depth) subtropical species which is found in the temperature range of 14 – 26 °C, with peak abundance in 21 – 24 °C waters. It extends into the Transitional Zone, although is rare and not found in large numbers.

Globorotalia scitula again is a deep water species (>250 m water depth) that is widespread but in small numbers. It has maximum abundance in waters of 21 – 24 °C, with a high occurrence in the Agulhas Current and some southwards extension into the Transitional Zone.

Orbulina universa is found in transitional to tropical waters with a temperature range of 10 – 30 °C, with peak abundance in the range of 17 - 23 °C and its lower limits being the southern edge of the transitional zone. High abundances are found on the eastern edges on ocean basins associated with upwelling (up to 41 % in the Benguela Current system) and surface layers of strong current systems (5 – 10 % in the Agulhas Current).

Globigerina falconensis is the warm water version of *G. bulloides* which underlies subtropical waters and is found in the temperature range of 21 – 24 °C where it reaches abundances of 20 %.

Globigerinoides ruber is the most prolific species in equatorial and subtropical waters, reaching abundances of 40 % in temperatures over 23 °C, with a temperature range of 14 – 30 °C and a low salinity tolerance.

Globigerinella siphonifera (previously known as *Globigerinella aequilateralis* (*Brady, 1884*)) is a subtropical species that occurs abundantly in strong currents, transitional waters and upwelling regions. It is common in the Agulhas Current and central Indian Ocean, in temperatures >23 °C, although it has peak abundance in SST's of 19 - 28 °C.

Neogloboquadrina dutetrei is a tropical to subtropical species, living between 50 - 100 m water depth and is common in tropical productive environments and western boundary currents. Its abundance is 5 – 10 % in the Agulhas Current and Agulhas Return Current and has a temperature range of 16 - 24 °C for peak abundance.

Globorotalia menardii is a tropical to subtropical species, which is more abundant in the Indian than Atlantic Oceans, with a peak in tropical, equatorial waters (20 – 25 °C).

Globigerinoides conglobatus is a subtropical surface species, which lives in the photic zone in temperatures >23 °C.

Globigerinoides sacculifer is the most prolific species in tropical waters with a peak abundances occurring at 24 – 30 °C. It is likely to be bought to the site area from the tropics by the Agulhas Current and can tolerate a broad range of salinities.

Of all these species only *Globorotaloides hexagona* is endemic to the Indian Ocean only, being a tropical to subtropical Indo-Pacific species with a temperature range of 25 – 29 °C. Although, as mentioned above, it is likely that any *G. sacculifer* at the site has been transported from the Indian Ocean tropics by the Agulhas Current rather than originating in the tropical Atlantic Ocean. Similarly *Pulleniatina obliquiloculata* has a temperature range of 22 – 24 °C suggesting that its transit from warmer waters is most likely to have occurred via the Agulhas Current.

Three of the species identified by *Peeters et al. (2004)* as ALF taxa are known to primarily be subtropical taxa but with distributions that extend south of the STF into the Transitional Zone: *Globorotalia scitula, Globigerinita glutinata, Orbulina universa* (Fig. 2.8). Of these three species only *G. glutinata* is found in significant numbers in the MD02-2589 record, suggesting that perhaps it is not exclusively related to Agulhas Current flux, although as *Peeters et al.* (2004) noted that it was a main component of the Agulhas Rings investigated in their study it has been included in the ALF results.

Other species that occur in very small numbers (<0.6 % of a sample or <2 out of every 300 individuals and present in less than 3 samples), *Globigerinita uvula, Candeina nitida, Globigerinoides tenellus, Orbulina bilobata, Sphaeroidinella dehiscens, Globorotalia cavernula* and *Globorotalia ungulate*, were not considered in the analysis or groupings.

2.4.3 Relative Abundance of *N. pachyderma* (d) as a SST Proxy

The relative abundance of dextral versus sinistral *Neogloboquadrina pachyderma* has been used as a paleo-indicator of SST (*Tolderlund and Bé,* 1971; *Reynolds and Thunell,* 1986; *Johannessen et al.,* 1994; *Pflaumann et al.,* 2003; *Žarić et al.,* 2005), with sinistral forms dominating assemblages with summer SST <8 °C (*Reynold and Thunell,* 1986). The change in dominance of one coiling direction over the other occurs at 9 °C (*Žarić et al.,* 2005), and studies have shown that the South Atlantic transitional region is dominated by *N. pachyderma* (d) during glacial times (*Rau et al.,* 2002), with SST transfer functions being significantly influenced by its relative abundance. Therefore the percentage ratio of dextral vs. sinistral can be used as a qualitative palaeo-SST indicator.

2.4.4 Relative Position of the Subtropical Front Proxy

Peeters et al., (2004) used the ratio of *Globorotalia truncatulinoides* / (*Neogloboquadrina pachyderma* (d) + *Globorotalia inflata* + *Globorotalia truncatulinoides*) present as a proxy for the distance of the STF from their core site. *G. inflata* and *N. pachyderma* (d) are mainly found in subtropical to subantarctic waters, whilst *G. truncatulinoides* is found in warmer subtropical to transitional waters mainly north of the STF. Whilst this ratio is relative and exact distances cannot be calculated it is used in conjunction with the ST/Tr and NSTF taxa to identify the position of the STF in relation to site MD02-2589.

2.4.5 Sea Surface Temperature Reconstruction Using An Artificial Neural Networks (ANN) Transfer Function

In order to estimate SST using the quantitative planktonic foraminifera assemblages, a 'transfer function', a mathematical analysis of census counts of microfossil assemblages (*Kucera et al.*, 2005a), methodology was adopted. The geographic distribution of living foraminifera in the surface waters is known to be closely linked to surface water temperature and conditions (*Bé and Tolderlund*, 1971; *Bé*, 1977; *Vincent and Berger*, 1981) and therefore fossil assemblages in the geological record are also known to reflect this relationship. There are two approaches to developing a method of quantitative reconstruction of past surface water temperatures from preserved foraminifera assemblages. The first is the transfer function (TF) and the second is the modern analog technique (MAT). Both of these methods rely on the comparison of fossil assemblages with large modern core-top, calibration or reference data sets, which are in turn associated with modern day SST through meteorological data (*Hale and Pflaumann*, 1999). Both of these methods are also based on common assumptions, of constant ecology of the species through the time in question, a systematic relationship between faunal content at the sediment surface and SST, and cross hemisphere similarity of ecological response of the foraminifera used in the study (*Imbrie and Kipp*, 1971; *Pflaumann et al.*, 1996; *Hale and Pflaumann*, 1999).

The development of the transfer function technique by *Imbrie and Kipp* (1971) (Imbrie and Kipp Method (IKM)), based on grouping species by Q-mode factor analysis, has been used in many other studies based on planktonic foraminifera (e.g. *Kipp*, 1976; *Molfino et al.*, 1982; *Howard and Prell*, 1984; *Pflaumann*, 1985; *Mix et al.*, 1986; *Pflaumann et al.*,

1996) the most notable of which is the CLIMAP (Climate: Long-Range Investigations, Mapping and Prediction) project (*CLIMAP Project Members,* 1981), the recently launched EPILOG (Environmental Processes of the Ice Ages, Land, Ocean, Glaciers) initiative (*Mix et al.,* 2001) and MARGO (Multiproxy Approach for the Reconstruction of the Glacial Ocean Surface) effort (*Kucera et al.,* 2005b). The techniques major drawback is that it cannot reliably estimate a SST in cases where the ancient faunal composition differs significantly from modern faunas and no modern analog fit can be made (*Hutson,* 1977; *Pflaumann et al.,* 1996).

In comparison, the modern analog technique (MAT) (*Hutson,* 1980) does not generate a single unique or global calibration formula between assemblage data and physical oceanographic properties (i.e. SST), but instead searches the calibration data set for samples with assemblages that most resemble the fossil assemblage. The physical properties of the best fit data sets, the number of which is predetermined by the size of the calibration data set, are then averaged to compute the SST for the fossil assemblage, (*Prell,* 1985; *Barrows et al.,* 2000, *Kucera et al.,* 2005a). The major drawback of this method is that it is strictly an interpolative method and therefore tends to perform poorly at the extremes of the range of SST, whilst its complete dependence on the size and coverage of the calibration data set means that it is not always able to benefit from the full information in the calibration data set and has limited power to generalise (*Kucera and Darling,* 2002; *Kucera et al.,* 2005a).

It is widely recognised that although there are an extensive range of numerical techniques for calculating SST from foraminifera assemblages (*Birks,* 1995), there is no single mathematical technique that is recommended above the rest, with each individual

technique having advantages and disadvantages. As part of the MARGO project *Kucera et al.* (2005a) employed 4 different SST estimation methods (Modern Analog Technique (MAT), Revised Analog Method (RAM) (*Waelbroeck et al.*, 1998), SIMMAX method (*Pflaumann et al.*, 1996) and the Artificial Neural Networks (ANN) technique (*Malmgren and Nordlund*, 1997; *Malmgren et al.*, 2001; *Kucera et al.*, 2005a)) on core top data-sets from different ocean basins. The South Atlantic database is separated from the North Atlantic, at the zone of minimum seasonality (3° – 8 °N), to avoid the mixing of genetically differentiated populations of foraminifera from the two hemispheres with different SST adaptations (*Darling et al.*, 2004). The South Atlantic is poorly and unevenly sampled (322 core top samples) in comparison to the North Atlantic (862 core top samples), with the majority of the samples being concentrated in the tropical and subtropical areas and only a few samples being available in the polar regions due to carbonate dissolution (with limits of preservation at 56 °S). *Kucera et al.* (2005a) acknowledge that samples particularly from the South Atlantic subtropical gyre had large variations in the SST reconstructions between different methods, with prediction errors larger than those set by the calibration data set. However this is a persistent feature of South Atlantic and Southern Ocean SST reconstructions and *Kucera et al.* (2005a) found that of all the methods used ANN performed best on the South Atlantic data set, probably due to its increased ability above the other techniques to deal with the poor sampling coverage in the southern high latitudes.

The ANN technique (*Malmgren and Nordlund*, 1997; *Malmgren et al.*, 2001; *Kucera et al.*, 2005a) consists of a set of interconnecting processing units (neurons), which map a set of input variables (assemblage counts) onto one or more output variables (environmental parameters). Learning proceeds by adjusting the way each neuron

modifies its input and is based on a procedure that minimises the prediction error for each sample in the calibration data set, with learning stopping when no improvement in prediction error occurs and when the network begins to over fit the data and to learn details of the calibration data set rather than the relationship between assemblage counts and environmental parameters. This technique is very good at generalising, is not dependant on the size of the training set (like MAT) and allows extrapolation. However its major disadvantage is the difficulty in interpreting the resulting network especially in terms of the contribution of individual variables to the resulting SST estimate (*Malmgren et al.*, 2001).

The SST analysis for core MD02-2589 on the southern Agulhas Plateau was performed using ANN on the MARGO South Atlantic core top database (*Kucera et al.*, 2005a; http://www.pangaea.de/Projects/MARGO/), based on the GLAMAP-2000 (Glacial Atlantic Ocean Mapping) compilation (*Pflaumann et al.*, 2003) and Brown University samples (*Trend-Staid and Prell*, 2002), due to the limited number of Indo-Pacific taxa identified in the MD02-2589 assemblages.

For the MD02-2589 ANN SST estimates the maximum number of neurons was set to 16, the maximum number of passes set to 2,500 and the algorithm was set to stop learning when there was no improvement in the predicted error for 40 consecutive passes. The network with the lowest error in the test set was retained, with SST reconstructions being calculated as an average of the outputs of the best 10 networks (*Kucera et al.*, 2005a) for each output variable (summer SST (SST_{summer}), winter SST (SST_{winter}) and annual SST (SST_{annual})), with standard deviation also being calculated.

The reliability of the SST estimates for the ANN method is investigated by *Kucera et al.* (2005a) and they suggest a 1 °C standard deviation value as a threshold between good-analog and poor-analog samples, with a 2 °C standard deviation being the threshold for severe no-analog samples. Based on this criteria 98.2 % of the SST_{summer} estimates, 97.3 % of the SST_{winter} estimates and 100 % of the SST_{annual} estimates are good analogs, with 0 % of all SST estimates using the ANN method being severe no-analog samples. This confirms the suitability of the South Atlantic core top data set over the Indo-Pacific set.

Studies tend to focus on either summer or winter SST in their interpretations with those using the winter SST records for the South Atlantic suggesting that they are characterised by a greater range of variation than summer SST records (*Chen et al.*, 2002) and therefore have been conventionally used for down core estimations in previous studies (*Imbrie and Kipp*, 1971; *Kipp*, 1976). However other studies suggest that summer SST are more useful for paleooceangraphic interpretations as foraminifera flux is strongly focused on the austral summer in the southern high latitudes, as documented by sediment trap experiments (*Becquey and Gersonde*, 2002) and therefore records of summer variations represent a larger proportion of the foraminifera assemblage. In this study SST shown refer to SST_{summer} values unless stated that they are winter or annual values.

2.4.6 $\delta^{18}O$ of Sea Water and Sea Surface Salinity Calculations

The $\delta^{18}O$ of calcite shells ($\delta^{18}O_c$) depends on the temperature and isotopic composition of the ambient water mass ($\delta^{18}O_{sw}$), which in turn is related to salinity and ice volume (*Niebler et al.*, 1999). The relationship between salinity and $\delta^{18}O_{sw}$ occurs as both variables are controlled by the evaporation-precipitation regime of an area, with excess

evaporation over precipitation increasing salinity and $\delta^{18}O_{sw}$ by removing the lighter ^{16}O, leaving the waters more enriched in ^{18}O (*Wolff et al.*, 1999). To calculate the $\delta^{18}O_{sw}$ the SST value from the ANN transfer function was subtracted from the $\delta^{18}O_c$. The $\delta^{18}O_{sw}$, once the global ice volume signature has been removed, can then be converted into an estimate of sea surface salinity (SSS) using the modern day regional $\delta^{18}O_{sw}$ - salinity gradient, which provides an added proxy with which to study the variations in local hydrography and frontal movements. There are however issues with the specific temperature tolerance ranges of individual species (*Duplessy et al.*, 1991), with higher fluxes during times of optimum species temperature and vertical migration of some species through the water column causing bias in the geological record and some discrepancies between computed SST and actual sea surface conditions (*Curry et al.*, 1983; *Mix*, 1987; *Mulitza et al.*, 1998; *Wolff et al.*, 1999).

It is widely recognised that *G. bulloides*, the species used to generate the planktonic $\delta^{18}O$ record of MD02-2589, is abundant in a broad range of temperatures (0 - 27 °C: *Bé and Tolderlund*, 1971; *Mortyn and Charles*, 2003) although an increase in abundance is associated with periods of high productivity and nutrients due to upwelling or phytoplankton bloom conditions (*Deuser et al.*, 1981; *Sauter and Thunell*, 1991; *Ganssen and Kroon*, 2000; *West et al.*, 2004; *Rau et al.*, 2006). Several sediment trap studies have noted that large increases in *G. bulloides* abundances during the spring bloom coincide with the breakdown of thermal stratification, which induces phytoplankton growth and an increase in the availability of food (*Northcoat and Neil*, 2005). Therefore *G. bulloides* is thought to be predominantly a spring bloom species in both hemispheres that in fact records spring SST and $\delta^{18}O$ values and enhanced productivity (*Prell and Curry*, 1981; *Deuser et al.*, 1981; *Ottens*, 1991; *Ganssen and Kroon*, 2000; *Peeters et al.*, 2002;

Mortyn and Charles, 2003; *King and Howard,* 2005), rather than the summer temperatures suggested by *Duplessy et al.* (1991). As a result of this in the $\delta^{18}O_{sw}$ and SSS calculations for MD02-2589 the annual SST was used rather than the summer values so that any productivity effect was minimised. This is further justified by SSS calculations for MD02-2589 done using the summer SST values (not shown) which show values on average 0.65 higher (ranging from 0.27 to 1.05) than those using the annual data and as both values are significantly higher than surrounding core tops, discussed further below, the annual SST values were used in the $\delta^{18}O_{sw}$ and SSS calculations as these produce values closest to the modern day. Regionally it has also been noted that *G. bulloides* production can shift with temperature with a noted change from summer (north of STF) to spring (south of STF) production across the subtropical front east of New Zealand (*King and Howard,* 2005), further underlying the need to use the annual SST values to cover all variability.

Several studies have shown that *G. bulloides* is a surface dweller (0 - 50 m) (*Bé and Tolderlund,* 1971; *Hemleben et al.,* 1989; *Deuser and Ross,* 1989; *Ottens,* 1992; *Niebler et al.,* 1999) associated with the depth of the chlorophyll maximum determined by the presence or absence of upwelling (*Fairbanks et al.,* 1982; *Ortiz et al.,* 1995, *Mortyn and Charles,* 2003; *King and Howard,* 2005), with shallower depths during upwelling conditions (especially during spring and summer (*King and Howard,* 2005)) than during non-upwelling periods. *G. bulloides* reflects these depths with an average calcification temperature of ~1.3 °C lower than the SST (*Peeters et al.,* 2002). This suggests that the species is not calcifying in equilibrium with the surface waters and $\delta^{18}O_c$ values for this disequilibrium, which is thought to remain constant, range from -0.5 ‰ (*Deuser et al.,* 1981), +0.31 ‰ (*Peeters et al.,* 2002), +0.4 ‰ (*King and Howard,* 2005) and +0 - 0.5 ‰

(*Ganssen*, 1983; *Niebler et al.*, 1999). These however are also dependant on the size of the foraminifera used (lighter $\delta^{18}O$ values for juveniles: *Berger et al.*, 1978; *Kandiano and Bauch*, 2002) with laboratory tests suggesting that the $\delta^{18}O_c$ of *G. bulloides* increases by 0.8 ‰ between the smallest and final chambers when temperature and $\delta^{18}O_{sw}$ are kept the same (*Spero and Lea*, 1996). A 0.27 ‰ difference is evident between 250 – 355 μm and 150 - 250 μm size fractions (*Peeters et al.*, 2002) and a 0.34 ‰ difference between 11 (at 24 °C) and 13 (at 15 °C) chambered specimens (*Bemis et al.*, 1998). This had led to the construction of different temperature equations for both different species (residing at different depths) and different size fractions (*Erez and Luz*, 1983; *Bouvier-Soumagnac and Duplessy*, 1985; *Bemis et al.*, 1998).

To calculate the $\delta^{18}O_{sw}$ from the MD02-2589 planktic $\delta^{18}O_c$ record we used the reworked 12-chambered shell palaeotemperature equation for *G. bulloides* (*Bemis et al.*, 1998), which *Bemis et al.* (1998) suggest have temperature estimates within ± 0.5 °C of the 11 and 13 chambered shell equations at 15 °C and negligible differences at 24 °C:

$$\delta^{18}O_{sw} = SST(°C) - 13.2 + 4.89 * \delta^{18}O_c / 4.89$$

The equation calculates $\delta^{18}O_{sw}$ on the VPBD scale, so +0.27 has been added to all $\delta^{18}O_{sw}$ data to convert the values to the standard VSMOW (Vienna Standard Mean Ocean Water) scale (*Hut*, 1987). As $\delta^{18}O_{sw}$ is a combination of ice volume, salinity and local variations, to be able to reconstruct the palaeosalinity of site MD02-2589, the global ice volume signal needs to be removed from the record. The $\delta^{18}O_{sw}$ record of TR163-19 from the Cocos Ridge, East Pacific (*Lea et al.*, 2002) is shown to record sea level changes (associated with ice volume) without any obvious local hydrological component and

shows substantial agreement with other sea level proxies; $\delta^{18}O_{sw}$ reconstructions (*Labeyrie et al.*, 1987; *Shackleton*, 2000) and uplifted and submerged reefs (*Chappell et al.*, 1996; *Fairbanks*, 1989; *Bard et al.*, 1990a; *Gallup et al.*, 1994; *Edwards et al.*, 1997). The chronology of TR163-19 was aligned with MD02-2589 (using the planktonic $\delta^{18}O$ records) to minimise any artefacts arising from temporal offsets and then the $\delta^{18}O_{sw}$ of TR163-19 was subtracted from the $\delta^{18}O_{sw}$ of MD02-2589 to remove the ice volume effect.

To convert the $\delta^{18}O_{ivc}$ (ice volume corrected $\delta^{18}O$) of MD02-2589 to SSS a $\delta^{18}O_{sw}$–salinity relationship for the site needed to be established. This was done using surface ocean salinity and $\delta^{18}O_{sw}$ data from 35 – 45 °S, 24 – 30 °E and 0 – 50 m water depth (Global Seawater Oxygen-18 Database (*Schmidt et al.*, 1999)):

$$\text{Salinity} = 1.6815 * \delta^{18}O_{sw} + 34.679 \qquad (n = 12, r^2 = 0.85)$$

To assess the accuracy of the equation, we can compare the freshwater component ($\delta^{18}O_{sw}$) of the equation, which reflects the surface hydrography (evaporation, precipitation, advection, mixing and river runoff) of the region, with known freshwater endmembers for the area (*Craig and Gordon*, 1965). The endmember suggested by the equation, -20.63 ‰, is very similar to that of -19 ± 4 ‰ measured for the Crozet Basin (*Meredith et al.*, 1999) suggesting that the equation is representative of the region, with no melt water influence from Antarctic ice sheets (values around -50 ‰ *Meredith et al.*, 1999) . If the $\delta^{18}O_{sw}$ – salinity relationship equation is recalculated to have $\delta^{18}O_{sw}$ as the subject then the relationship becomes:

$$\delta^{18}O_{sw} = 0.5064 * \text{salinity} + 17.528 \qquad (n = 12, r^2 = 0.85)$$

This relationship is very similar to that calculated for the mid-latitudes by *Paul et al.*, (1999): $\delta^{18}O_{sw} = 0.497 * \text{salinity} + 17.05$, with any small differences probably being due to the fact that the *Paul et al.* (1999) data represents the mid-latitudes averaged over all the ocean basins. This again provides support that the equation represents the regional $\delta^{18}O_{sw}$ – salinity relationship of the Agulhas region and therefore can be used to provide a first-order reconstruction of palaeosalinities.

As mean ocean salinity changes from glacial to interglacial periods through the extraction of fresh water from the oceans and storage on land during glacial periods, a correction needs to be applied to the SSS calculations. *Adkins et al.* (2002) suggest a mean ocean salinity shift of 0.9 between the LGM and present day. In order to correct the SSS calculations for this shift, the global sea level curve of *Siddall et al.* (2003, 2006b) was re-scaled so that minimum LGM sea level had a SSS value of 0.9 and present day a SSS value of 0 with intermediary values linearly interpolated (Figure 2.9). The resulting sea level derived SSS values were then added to the SSS calculations of MD02-2589.

The errors associated with the SSS calculations were calculated by combining the errors associated with the SST and oxygen isotope measurements for both the $\delta^{18}O$ and $\delta^{18}O_{ivc}$ and propagating them through the $\delta^{18}O_{sw}$ and SSS calculations (*Rohling*, 2007). The resulting errors produce an average standard deviation in the SSS estimate of ± 1.01 (ranging from ± 0.45 - ± 1.54). It should be noted that errors within the regional $\delta^{18}O_{sw}$ – salinity relationship have not been considered as they affect the whole data set uniformly.

The resulting SSS values are higher than surrounding core tops probably due to the higher reconstructed SST (discussed further in Section 4.2.1) and therefore all SSS are shown as a deviation from the modern day at the closest site (41.12 °S, 28.9 °E, 35.54 psu, 54 m water depth) in the *Schmidt et al.* (1999) data.

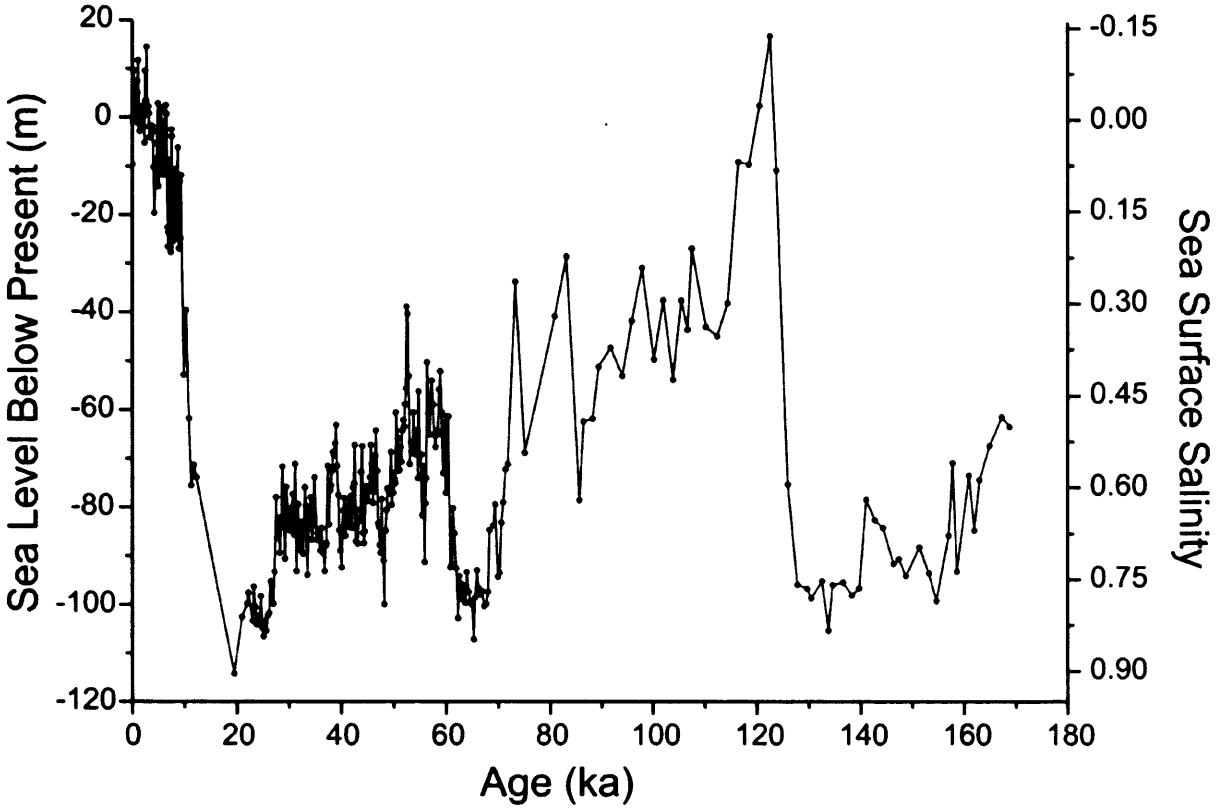

Figure 2.9. Sea level over the past 180 ka rescaled to reflect mean sea surface salinity changes. Sea level curve from *Siddall et al.* (2003, 2006b).

2.4.7 Carbonate Dissolution

The degree of carbonate dissolution was assessed in selected samples using the planktonic foraminiferal fragmentation index (*Williams et al.*, 1985; *Malmgren*, 1987, *Berger et al.*, 1982) described by *Le and Shackleton* (1992). This index contains a devisor relating the number of fragments to the number of tests, so that percentage fragmentation is more likely to respond linearly to dissolution rather than being over sensitive during the early

stages and relatively insensitive during the later stages of dissolution. Samples of the >150 μm size fraction were split as many times as required to obtain approximately 300 whole planktonic foraminifera. All whole planktonic foraminifera were identified and counted whilst all fragments within these splits were also recorded. The percentage fragmentation was calculated using a fragment-devisor of 3 (*Pfuhl and Shackleton,* 2004).

2.4.8 Planktonic Foraminifera Accumulation

The abundance of individual planktonic foraminifera per unit mass has been used as a proxy for production rates linked to productivity (*Schaefer et al.,* 2005) changes. Studies in the Southern Ocean have shown that 97 % of the annual production of foraminifera occurs during the spring bloom conditions (*Northcote and Neil,* 2005) with numbers of individuals relating to the degree of productivity in the surface waters. The number of foraminifera per gram of sediment therefore provides a basic calculation of primary productivity in surface waters, whilst not taking into account taphonomic processes, such as dissolution, sediment focusing or winnowing or sedimentation rates. The fragmentation index however does give a good indication of dissolution. In this study the number of planktonic foraminifera were counted during assemblage identification and multiplied by the number of splits to calculate the number of foraminifera per sample. The number per sample was then divided by the weight of the coarse fraction to obtain the planktonic foraminifera accumulation rate.

2.4.9 Ice Rafted Debris

Lithic grains >150 μm embedded in pelagic sediment are assumed to be ice rafted debris (IRD) and therefore a proxy of iceberg flux to the core site, although this assumption will be further discussed in section 4.3.3. The ≥150 μm size fraction in MD02-2589 was examined under a binocular microscope for the presence of IRD following the methodology of *Allen and Warnke* (1991) and IRD grains counted and classified visually into quartz and lithics. Due to a lack of dry bulk density measurements the IRD is expressed as number of grains per gram of total dry sediment.

Chapter 3. Age Model Construction

3.1 MD02-2589

3.1.1 Initial Stratigraphy and Radiocarbon Dating (0 – 40 ka)

Shipboard spectrophotometry (L*) was used to provide an initial age model for core MD02-2589 (*Giraudeau et al.*, 2002) with the L* record (Fig. 3.1) being tied to Atlantic core ODP 659 (*Tiedermann et al.*, 1994) and Pacific core ODP 1123 (*Hall et al.*, 2001) for the full 34.55 m to create a preliminary chronology from 0 – 1.3 Ma. This initial chronology allowed identification of the 0 - 170 ka time slice, which is the focus of this study, as 0 – 980 cm.

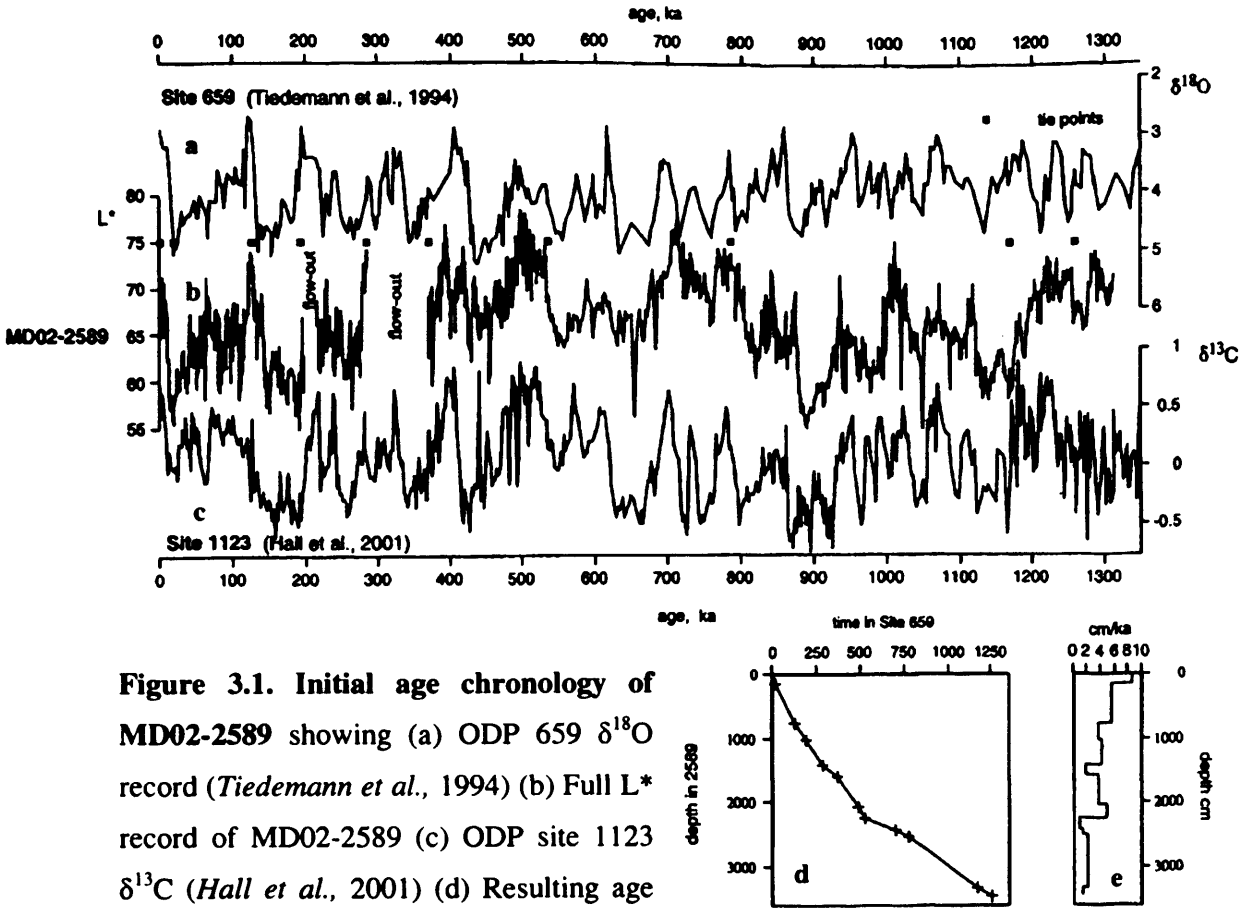

Figure 3.1. Initial age chronology of MD02-2589 showing (a) ODP 659 $\delta^{18}O$ record (*Tiedemann et al.*, 1994) (b) Full L* record of MD02-2589 (c) ODP site 1123 $\delta^{13}C$ (*Hall et al.*, 2001) (d) Resulting age depth relationship of MD02-2589 and (e) Sedimentation rate

Although Fig. 3.1 shows that there are 2 sections that have been affected by flow outs within the core, these are both > 1000 cm and therefore do not impact on this study. The gap discovered in the core between 716 and 735 cm (Fig. 3.2) was attributed to stretching within the core (further discussed in section 3.1.4) rather than any flow out and therefore a composite depth scale was produced.

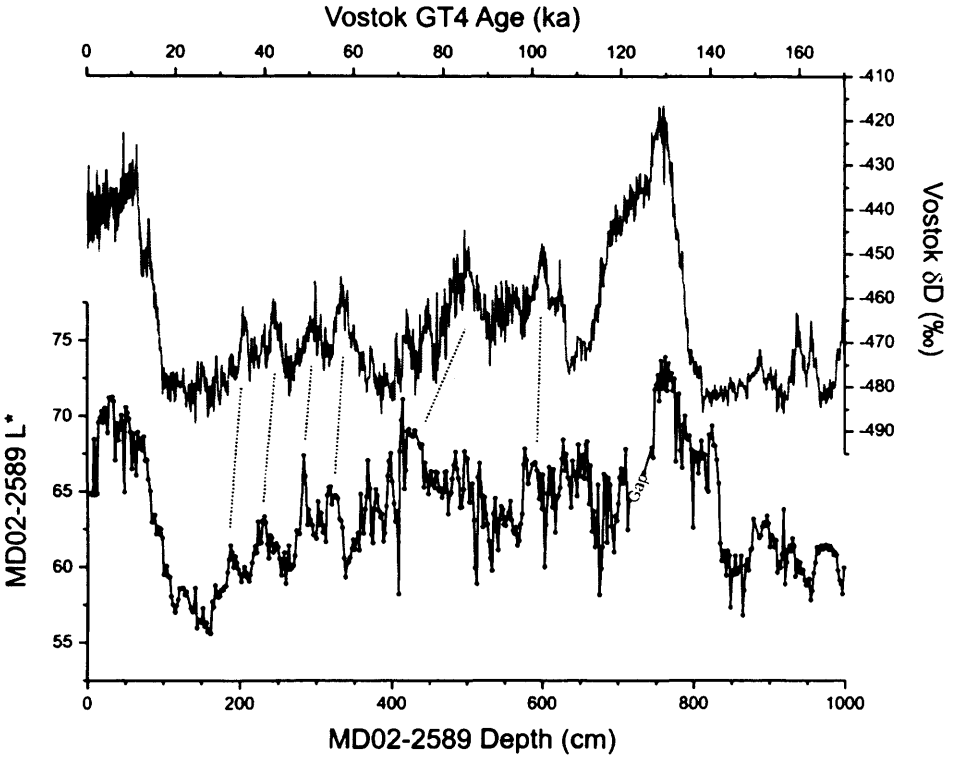

Figure 3.2. L* record (0 – 1000cm) of MD02-2589 with Vostok δD record (0-170 ka *Petit et al.*, 1999) with tie points showing initial visual correlation.

In order to more accurately identify the area of core within the range of radiocarbon dating (0 – 45 ka; *Fairbanks et al.*, 2005), the L* record was graphically correlated to the δD record of Vostok (*Petit et al.*, 1999) and Fig. 3.2 shows that both records have similar features, both on glacial to interglacial and shorter millennial-scale timescales, especially during MIS 3 and 5. As a result, a total of thirteen ^{14}C AMS datings were carried out

within the uppermost 190 cm of core MD02-2589 on monospecific samples containing ~1000 tests of *Globorotalia inflata* (Table 3.1). The depths selected for dating were chosen to represent early, mid and late Holocene, the different stages of deglaciation in the L* record and the first L* positive excursion. The ^{14}C analyses were carried out at the NERC Radiocarbon Laboratory in East Kilbride (Scotland).

Lab Code	Depth (cm)	Species	Conventional ^{14}C Age (yrs)	±1sd (yrs)	Calibrated ^{14}C Age (yrs)	±1sd (yrs)	
SUERC-4667	5-6	*G.Inflata*	13,161	±46	14,367	±159	§†
SUERC-4668	10-11	*G.Inflata*	8,891	±29	9,015	±18	§†
SUERC-4669	20-21	*G.Inflata*	11,731	±39	12,851	±81	§†
SUERC-4670	40-41	*G.Inflata*	10,000	±33	10,341	±70	§†
SUERC-4673	60-61	*G.Inflata*	13,722	±50	15,295	±116	
SUERC-4674	75-76	*G.Inflata*	14,624	±53	16,601	±134	
SUERC-4675	85-86	*G.Inflata*	15,263	±57	17,553	±136	
SUERC-4676	100-101	*G.Inflata*	15,710	±60	18,273	±155	
SUERC-4677	110-111	*G.Inflata*	17,317	±73	19,640	±107	
SUERC-4679	125-126	*G.Inflata*	18,457	±84	21,021	±176	
SUERC-4680	140-141	*G.Inflata*	21,481	±120	24,713	±232	
SUERC-4683	170-171	*G.Inflata*	29,933	±335	34,117	±606	
SUERC-4684	190-191	*G.Inflata*	34,987	±628	39,388	±946	

Table 3.1. ^{14}C AMS ages on planktonic foraminifera and calibrated ages for core MD02-2589: § - Reversal, † - unused

Contamination of samples during the conversion of carbonate to graphite prior to analysis requires 'background' correction. We therefore chose 'blank' samples for sections of the core thought to contain no inherent ^{14}C, in order to calculate the background correction needed. The samples chosen from MIS 4 (330 cm) and MIS 5 (766 cm; Fig. 3.2) had predicted ages of ~58 ka and ~130 ka well beyond the limit of ^{14}C detection. ^{14}C values of 0.38 – 0.46 ±0.01 % of the modern concentration were found within the blank samples, with a value of 0.4 ±0.01 % used for correction. The AMS ^{14}C dates were corrected for the marine reservoir effect using a regional Southern Ocean correction of 800 yrs (*Butzin et al.*, 2005) and subsequently calibrated to calendar years BP using the marine calibration data set of *Fairbanks et al.* (2005) which allows for calibration back to 50 kyr.

The calibrated ages shown in Table 3.1 have 1 standard deviation errors associated with them (±1sd) which are less than 1% of the age estimate for all samples except the two oldest dates, where the errors are <1.7 and 2.5 %.

Two age reversals in the upper 60 cm of the core MD02-2589 led us to discard the four uppermost AMS dates (Table 3.1). Ages for this interval were estimated through extrapolation using a third order polynomial fit of the age/depth relationship of the remaining 9 AMS dates (upper 190 cm: Fig. 3.3).

$$\text{Age} = 0.0022\text{depth}^2 + 0.2473\text{depth}^2 + 19.161\text{depth} + 11613$$

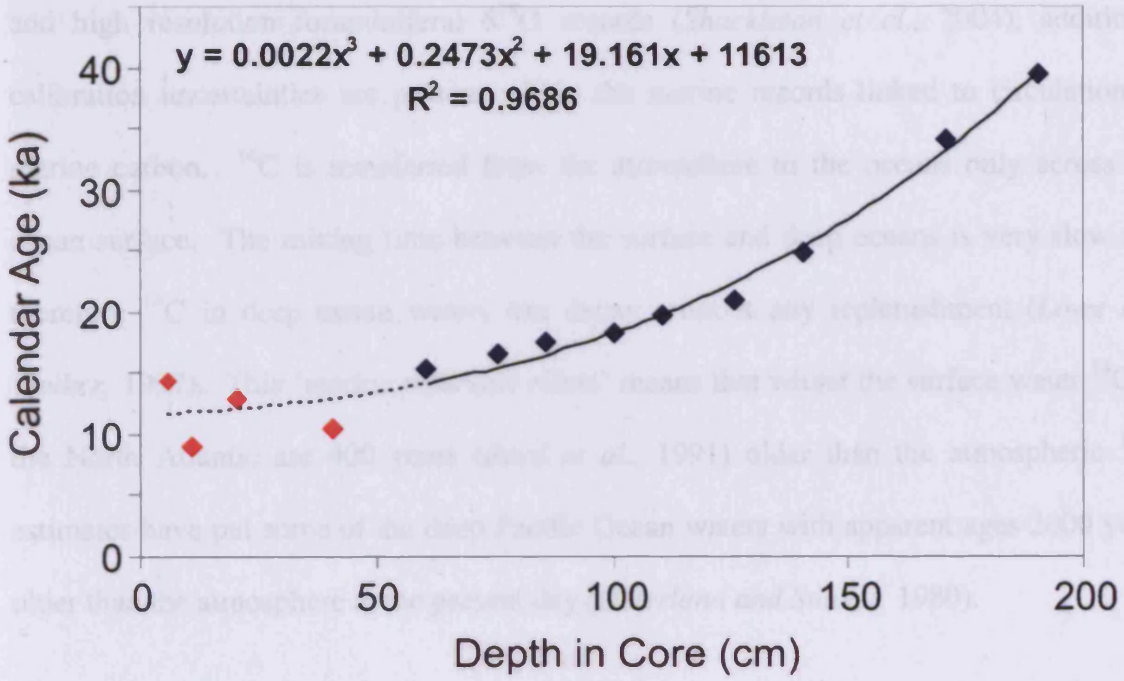

Figure 3.3. Graph showing the polynomial fit used to calculate to age model of the upper 60 cm of MD02-2589: Red diamonds denote discarded calibrated AMS dates, blue diamonds are calibrated AMS dates used in the polynomial fit.

The R^2 value of 0.97 for the polynomial fit suggests that it is accurately predicting the ages.

3.1.2 Possible Limitations of Radiocarbon Dating

The ^{14}C age determined by AMS radiocarbon dating assumes that the concentration of radiocarbon in the atmosphere has remained constant in the past (*Pilcher,* 1991). Studies more than 30 years ago (*de Vries,* 1958) however, showed that the atmospheric levels of ^{14}C have fluctuated markedly, both in production and concentration over the past 50 ka, producing the need for a calibration curve linked to known radiocarbon fluctuations to convert radiocarbon ages to calendar years (*Fairbanks et al.,* 2005). Whilst new and improved versions of the calibration curve are being produced using U-Th dated corals (*Bard et al.,* 1998; *Fairbanks et al.,* 2005), dendrochronology (*Becker and Kromer* 1993) and high resolution foraminiferal $\delta^{18}O$ records (*Shackleton et al.,* 2004), additional calibration uncertainties are present within the marine records linked to circulation of marine carbon. ^{14}C is transferred from the atmosphere to the oceans only across the ocean surface. The mixing time between the surface and deep oceans is very slow and therefore ^{14}C in deep ocean waters can decay without any replenishment (*Lowe and Walker,* 1997). This 'marine reservoir effect' means that whilst the surface water ^{14}C of the North Atlantic are 400 years (*Bard et al.,* 1991) older than the atmospheric ^{14}C, estimates have put some of the deep Pacific Ocean waters with apparent ages 2000 years older than the atmosphere at the present day (*Osterlund and Stuiver,* 1980).

A graphic correlation (Fig. 3.4a, b) of the MD02-2589 benthic $\delta^{18}O$ record on its radiocarbon age-scale with mid-depth Pacific core MD97-2120 (*Pahnke et al.,* 2003) shows that the ^{14}C calibrated ages of MD02-2589 appear typically older than MD97-2120 by ~1 ka in the top 40 ka of the core. Such an offset suggests that the local 800 yr reservoir age that we have adopted for core MD02-2589 may well be an underestimate

and reservoir ages rather are in the range of up to 1800 yrs, similar to those seen in MD97-2120 (*Pahnke et al.*, 2003) and other southwest Pacific Ocean sites (*Sikes et al.*, 2000).

3.1.3 Graphic Correlation (40 – 170 ka)

Within the interval 190 - 982 cm (~40 - 170 ka; Fig. 3.4) 9 age control points were assigned via graphic correlation of the benthic $\delta^{18}O$ record with MD97-2120 (*Pahnke et al.*, 2003). The MD97-2120 age model is based on graphic correlations with both North Atlantic core MD95-2042 and Antarctic ice core, Vostok δD record (*Pahnke et al.*, 2003). MD97-2120 was chosen as a reference to develop the age model for core MD02-2589 because it allowed direct correlation with Antarctic records as well as core MD95-2042 and other Northern Hemisphere climate records. The MD97-2120 benthic $\delta^{18}O$ profile has a similar structure to MD02-2589 especially over the MIS5a/4 transition and in some of the smaller scale features thus facilitating the correlation (Fig. 3.4a, b). Ages between each age control point were estimated by linear interpolation. The resulting age model suggests sedimentation rates vary between ~15 cm/ka during glacials and ~5.5 cm/ka during interglacials (Fig. 3.4c). At our 2 cm sampling resolution this equates to a mean time step along our proxy records of 298 ± 132 yr.

Although core MD97-2120 is in the mid-depth Pacific Ocean in a different water mass to MD02-2589 the tuning of the benthic $\delta^{18}O$ records to create the MD02-2589 age chronology is further supported by the resulting close phase relationship of the planktonic $\delta^{18}O$ records of both cores, which show a high degree of synchronicity (Fig. 3.5).

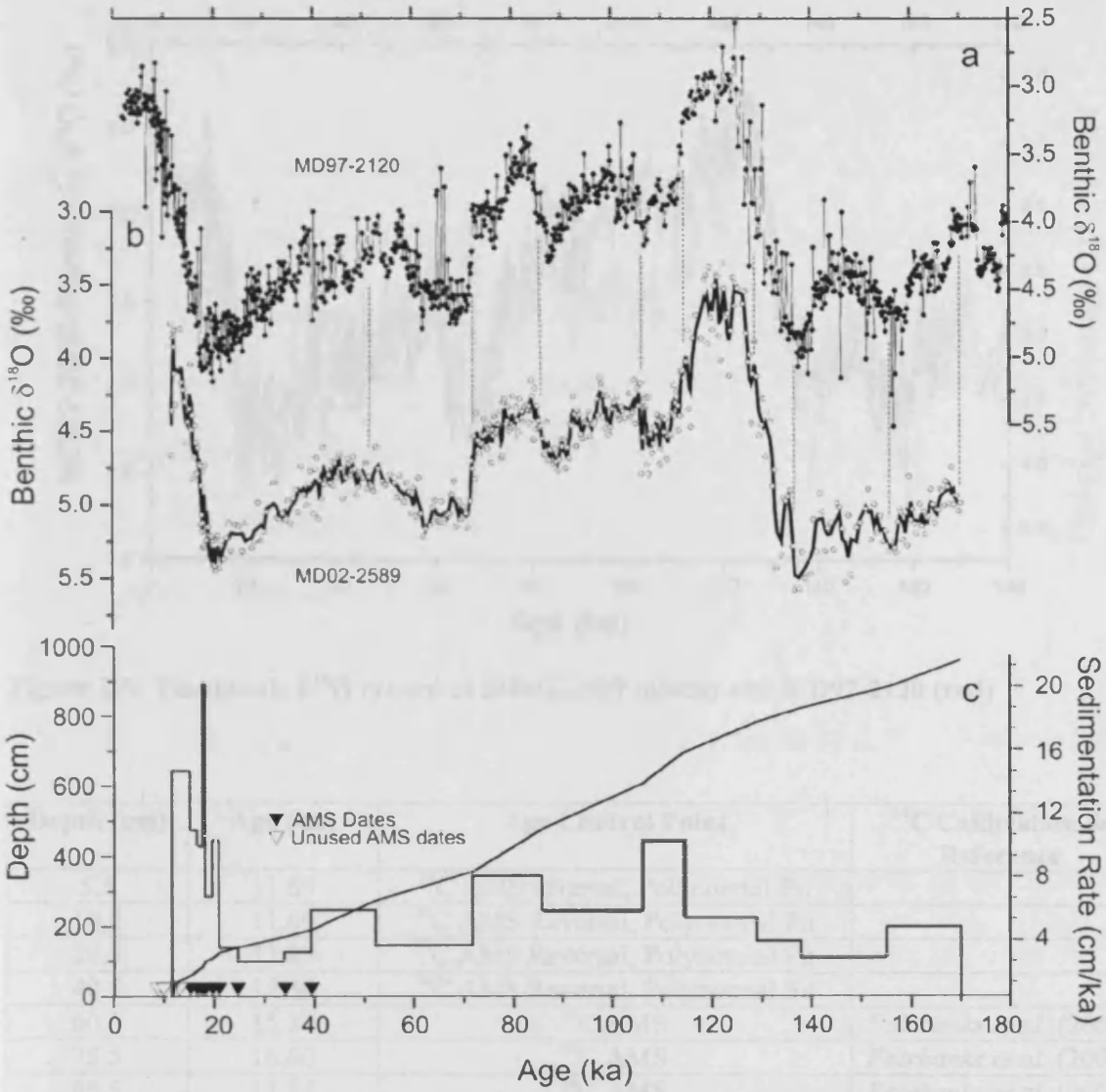

Figure 3.4. Final chronology of core MD02-2589. (a) Benthic $\delta^{18}O$ record of core MD97-2120 (*Pahnke et al.*, 2003) (b) Benthic $\delta^{18}O$ record of MD02-2589, also showing tie points used for correlation and (c) Sedimentation rate and the position of both used and unused radiocarbon dates.

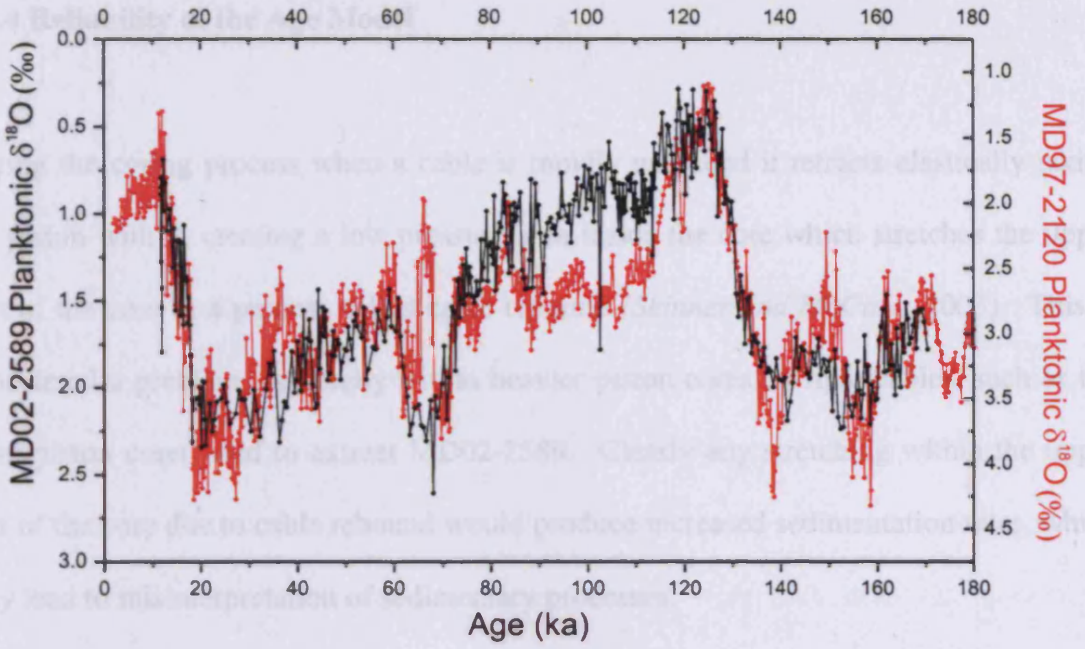

Figure 3.5. Planktonic $\delta^{18}O$ record of MD02-2589 (black) and MD97-2120 (red)

Depth (cm)	Age (ka)	Age Control Point	^{14}C Calibration & Reference
5.5	11.65	^{14}C AMS reversal, Polynomial Fit	
10.5	11.69	^{14}C AMS Reversal, Polynomial Fit	
20.5	11.83	^{14}C AMS Reversal, Polynomial Fit	
40.5	12.36	^{14}C AMS Reversal, Polynomial Fit	
60.5	15.30	^{14}C AMS	*Fairbanks et al.* (2005)
75.5	16.60	^{14}C AMS	*Fairbanks et al.* (2005)
85.5	17.55	^{14}C AMS	*Fairbanks et al.* (2005)
100.5	18.27	^{14}C AMS	*Fairbanks et al.* (2005)
110.5	19.64	^{14}C AMS	*Fairbanks et al.* (2005)
125.5	21.02	^{14}C AMS	*Fairbanks et al.* (2005)
140.5	24.71	^{14}C AMS	*Fairbanks et al,* (2005)
170.5	34.12	^{14}C AMS	*Fairbanks et al.* (2005)
190.5	39.39	^{14}C AMS	*Fairbanks et al.* (2005)
274.5	52.36	$^{18}O_{bn}$ tuned to $^{18}O_{bn}$ of MD97-2120	*Pahnke et al.* (2003)
356.5	71.85	$^{18}O_{bn}$ tuned to $^{18}O_{bn}$ of MD97-2120	*Pahnke et al.* (2003)
478.5	86.01	$^{18}O_{bn}$ tuned to $^{18}O_{bn}$ of MD97-2120	*Pahnke et al.* (2003)
606.5	106.04	$^{18}O_{bn}$ tuned to $^{18}O_{bn}$ of MD97-2120	*Pahnke et al.* (2003)
694.5	114.18	$^{18}O_{bn}$ tuned to $^{18}O_{bn}$ of MD97-2120	*Pahnke et al.* (2003)
782.5	128.95	$^{18}O_{bn}$ tuned to $^{18}O_{bn}$ of MD97-2120	*Pahnke et al.* (2003)
822.5	137.86	$^{18}O_{bn}$ tuned to $^{18}O_{bn}$ of MD97-2120	*Pahnke et al.* (2003)
884.5	155.91	$^{18}O_{bn}$ tuned to $^{18}O_{bn}$ of MD97-2120	*Pahnke et al.* (2003)
960.5	170.00	$^{18}O_{bn}$ tuned to $^{18}O_{bn}$ of MD97-2120	*Pahnke et al.* (2003)

Table 3.2. Age Control Points for Core MD02-2589: $\delta^{18}O_{bn}$ = Benthic $\delta^{18}O$

3.1.4 Reliability of the Age Model

During the coring process when a cable is rapidly unloaded it retracts elastically taking the piston with it, creating a low pressure area inside the core which stretches the upper part of the core in a process called cable rebound (*Skinner and McCave*, 2003). This is considered a problem, especially within heavier piston cores on light cables, such as the giant piston corer used to extract MD02-2589. Clearly any stretching within the upper part of the core due to cable rebound would produce increased sedimentation rates, which may lead to misinterpretation of sedimentary processes.

Both the sedimentation rate of the initial and final chronologies (Fig. 3.1e, 3.4c) show that the sedimentation rate of MD02-2589 does increase towards the top of the core, which suggests that there may be some 'over-sampling' in the upper 19.6 ka of the core in the progressively softer sediments. The 4 age reversals identified in the AMS dates and the lack of full Holocene material in the core (Fig. 3.4b) also suggests that some caution needs to be applied when interpreting Termination I, although both planktonic $\delta^{18}O$ records (Fig. 3.5) of MD02-2589 and MD97-2120 show synchronous shifts over Termination I (20 - 10ka), which is contrary to the ~1ka lead of MD02-2589 seen in the benthic $\delta^{18}O$ records (Fig. 3.4a, b), suggesting that perhaps the reservoir correction applied is more accurate than previously thought. In light of this no further correction has been applied to the MD02-2589 record. However due to this possible stretching uncertainty within the core no proxy records have been converted to flux.

3.2 MD02-2588

The initial chronology for MD02-2588 was produced by correlating the L* record with Vostok δD record (*Petit et al.*, 1999) (Fig. 3.6) and shows that both cores exhibit similar patterns over the past 350 ka. This initial chronology allowed for sixteen samples to be picked within the upper 142 cm for AMS radiocarbon dating, again using ~1000 tests of monospecific species *G. inflata*. The samples were again run at the NERC isotope facility at East Kilbride, Scotland and the resulting ^{14}C ages corrected by 800 years to take the reservoir offset into account. Again the dates were then calibrated to calendar ages using *Fairbanks et al.*, (2005) (Table 3.3).

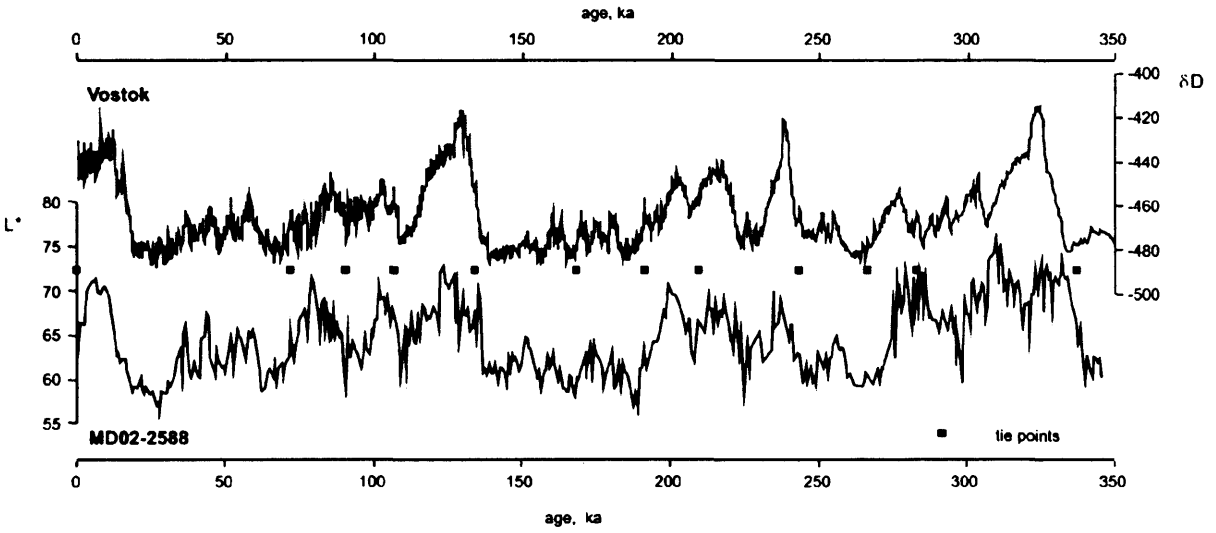

Figure 3.6. Initial chronology of MD02-2588 using L* record and the δD record of Vostok (*Petit et al.*, 1999)

The background sample chosen from MIS 5 (360 cm) had a predicted age of ~120 ka and was indistinguishable from background levels at 44,350 radiocarbon years. The sample from 142 cm (~50 ka) was also indistinguishable from background levels being slightly older than the limits of AMS radiocarbon dating.

Lab Code	Depth (cm)	Species	Conventional ^{14}C Age (yrs)	±1sd (yrs)	Calibrated ^{14}C Age (yrs)	±1sd (yrs)
SUERC-4618	5-6	*G.Inflata*	3,818	25	3,225	43
SUERC-4619	10–11	*G.Inflata*	5,228	25	5,019	72
SUERC-4620	16-17	*G.Inflata*	7,322	25	7,432	14
SUERC-4623	22-23	*G.Inflata*	8,778	29	8,872	89
SUERC-4624	32-33	*G.Inflata*	11,646	38	12,750	44
SUERC-4625	40-41	*G.Inflata*	13,849	48	15,199	111
SUERC-4626	45-46	*G.Inflata*	14,335	52	15,756	123
SUERC-4627	65-66	*G.Inflata*	20,242	102	23,161	198
SUERC-4635	75-76	*G.Inflata*	24,088	164	27,933	232
SUERC-4636	85-86	*G.Inflata*	25,375	191	29,400	276
SUERC-4637	95-96	*G.Inflata*	28,341	277	32,881	333
SUERC-4638	105-106	*G.Inflata*	35,621	680	40,166	671
SUERC-4639	115-116	*G.Inflata*	42,781	1,655	46,464	208
SUERC-4640	120-121	*G.Inflata*	46,049	2,489	49,152	182
SUERC-4643	130-131	*G.Inflata*	47,402	2,942	49,408	50
SUERC-4644	142-143	*G.Inflata*	**	-	-	-

Table 3.3. ^{14}C AMS ages on planktonic foraminifera and calibrated ages for core MD02-2588; ** = Indistinguishable from background signal

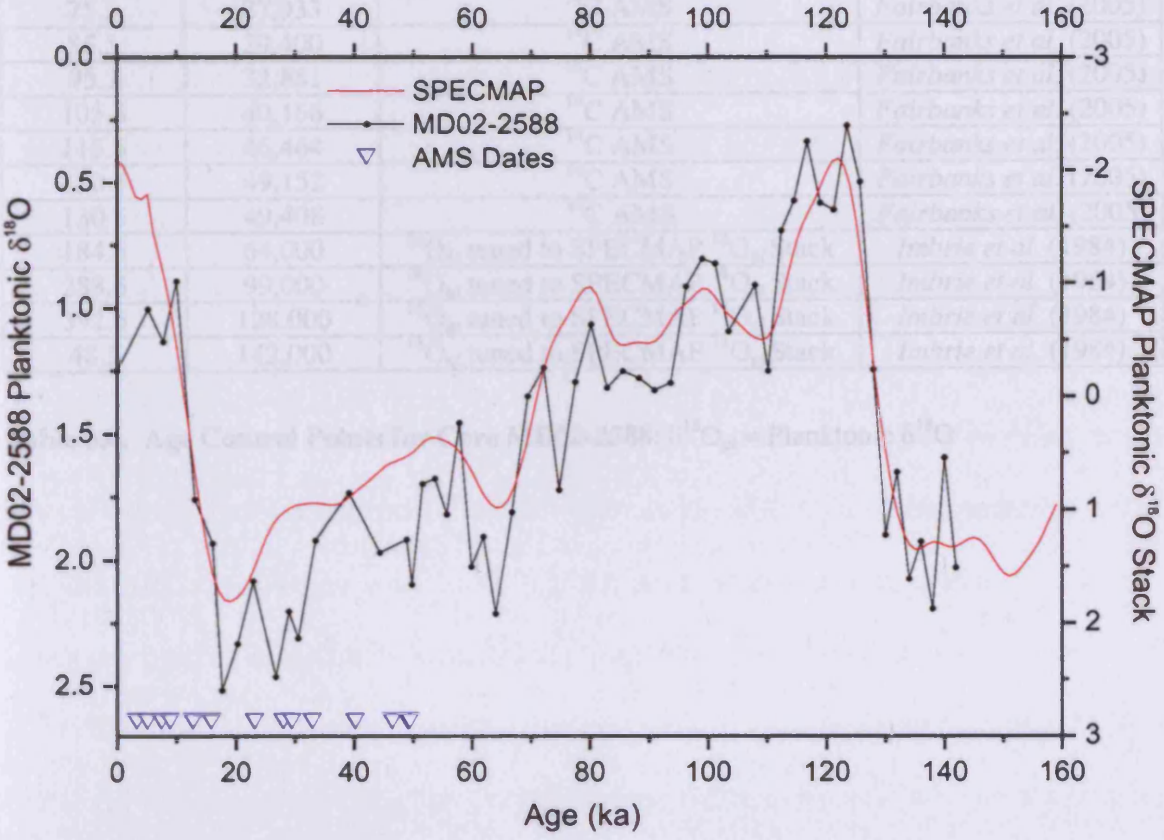

Figure 3.7. Final chronology of MD02-2588 showing the position of the AMS dates and visual correlation with the SPECMAP planktonic δ^{18}O stack record (*Imbrie et al.*, 1984).

For the period 50 - 140 ka (130 - 450 cm) visual tuning of the planktonic $\delta^{18}O$ record (Fig. 3.7) to the SPECMAP planktonic $\delta^{18}O$ stack record (*Imbrie et al.*, 1984) was undertaken. The SPECMAP stack record was chosen as it represents the global signal and can easily be correlated with the low resolution planktonic $\delta^{18}O$ record of MD02-2588. Table 3.4 details the final tie points used to create the chronology.

Depth (cm)	Age (ka)	Age Control Point	^{14}C Calibration & Reference
5.5	3,225	^{14}C AMS	*Fairbanks et al.* (2005)
10.5	5,019	^{14}C AMS	*Fairbanks et al.* (2005)
16.5	7,432	^{14}C AMS	*Fairbanks et al.* (2005)
22.5	8,872	^{14}C AMS	*Fairbanks et al.* (2005)
32.5	12,750	^{14}C AMS	*Fairbanks et al.* (2005)
40.5	15,199	^{14}C AMS	*Fairbanks et al.* (2005)
45.5	15,756	^{14}C AMS	*Fairbanks et al.* (2005)
65.5	23,161	^{14}C AMS	*Fairbanks et al.* (2005)
75.5	27,933	^{14}C AMS	*Fairbanks et al.* (2005)
85.5	29,400	^{14}C AMS	*Fairbanks et al.* (2005)
95.5	32,881	^{14}C AMS	*Fairbanks et al,* (2005)
105.5	40,166	^{14}C AMS	*Fairbanks et al.* (2005)
115.5	46,464	^{14}C AMS	*Fairbanks et al.* (2005)
120.5	49,152	^{14}C AMS	*Fairbanks et al.* (2005)
130.5	49,408	^{14}C AMS	*Fairbanks et al.* (2005)
184.5	64,000	$^{18}O_{pl}$ tuned to SPECMAP $^{18}O_{pl}$ Stack	*Imbrie et al.* (1984)
288.5	99,000	$^{18}O_{pl}$ tuned to SPECMAP $^{18}O_{pl}$ Stack	*Imbrie et al.* (1984)
392.5	128,000	$^{18}O_{pl}$ tuned to SPECMAP $^{18}O_{pl}$ Stack	*Imbrie et al.* (1984)
48.5	142,000	$^{18}O_{pl}$ tuned to SPECMAP $^{18}O_{pl}$ Stack	*Imbrie et al.* (1984)

Table 3.4. Age Control Points for Core MD02-2588: $\delta^{18}O_{pl}$ = Planktonic $\delta^{18}O$

Chapter 4: Phasing and Timing of Surface Oceanographic Changes On the Agulhas Plateau Over Terminations I and II and Glacial Inception MIS5a-4

4.1 Introduction

Core MD02-2589 is on the Southern flank of the Agulhas Plateau (Fig. 2.1) and therefore is in the influence of the Agulhas Retroflection (AR) and Agulhas Return Current (ARC), which contain a mixture of Agulhas Current signature water and Subantarctic waters, which have been transported northwards over the frontal systems, especially during Agulhas ring shedding events (*Gordon et al.*, 1987; 1992). Much of the thermocline and Antarctic Intermediate Water of the South Atlantic Current flows into the Indian Ocean by a route immediately south of the AR promoting heavy mixing between the Agulhas Current and the adjacent water masses (*Gordon et al.*, 1992). Consequentially the Agulhas Current looses up to 22 w/m^2 in heat at the retroflection area, due to intense air-sea exchange, (*Lutjeharms et al.*, 2001) and looses water to interior flow to the subtropical gyre along the ARC. The deeper thermocline water from the Agulhas Current area mixes with South Atlantic Water and enters the retroflection region by being swept in with the anticyclonic circulation of the warm-cored eddies. The 'contamination' of the AR and ARC thermocline with South Atlantic water increases with depth, until density levels are reached at which no contribution from the Indian Ocean is evident (*Gordon et al.*, 1987). It can therefore be expected that any surface Agulhas signal present at MD02-2589 will not mirror true Agulhas Current waters, rather a mixture of these waters with surrounding water masses.

The position of the STF south of Africa has been shown to be determined primarily by the ARC (*Lutjeharms and Valentine,* 1984). *Weeks et al.* (1998) suggest that the ARC as a rule *'follows the STF, enhancing its intensity and only occasionally separating from it between 13 ° and 25 °E to form a double front, comprising the Agulhas Front and the STF'*. Therefore it is not possible to discuss the STF independently from the ARC. The ARC at the present day exhibits three quasi-stationary meanders along its trajectory, the largest and most stable of which coincides with the location of the Agulhas Plateau (*Boebel et al.,* 2003a). The position of this meander has been shown to be seasonally stable at the present day with variations of less than 1 ° longitude over the summer and winter seasons (*Boebel et al.,* 2003a) and although it is probable that the ARC and therefore the STF is topographically locked to the northern edge of the Agulhas Plateau, it is possible that some mobility in its position may occur in response to wind forcing and ACC strength.

This chapter aims to look at the complex interplay between the movement of the Southern Ocean frontal systems and the leakage of warm, salty Agulhas Current water through the retroflection region. Terminations I and II and MIS5/4 transition were chosen so that phasing and timing of changes in Southern Ocean hydrography could be identified over periods of intense and extreme changes in climate and global ocean current patterns. The investigations within this chapter use a combination of planktonic foraminiferal assemblage counts, inferred SST calculations, stable planktonic oxygen and carbon isotopes, IRD counts, $\delta^{18}O$ of sea water and SSS estimations and proxies of planktonic foraminifera abundance and dissolution.

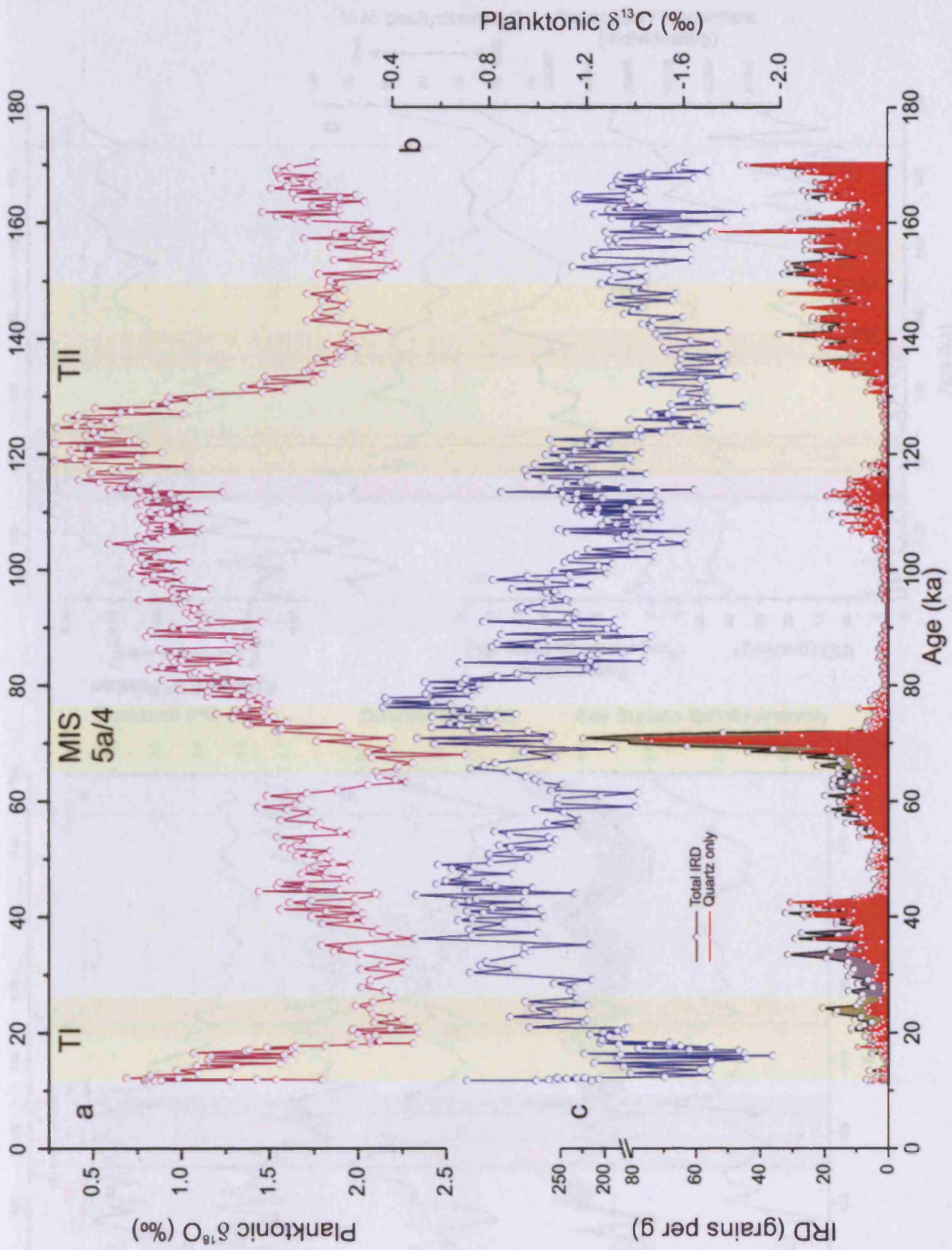

Figure 4.1 Planktonic Isotope Data and IRD Counts of Core MD02-2589 with intervals focused on in this chapter highlighted by yellow shading. (a) planktonic $\delta^{18}O$, (b) planktonic $\delta^{13}C$, (c) IRD counts. TI = Termination I, MIS 5a/4 = MIS 5a to 4 transition, TII = Termination II

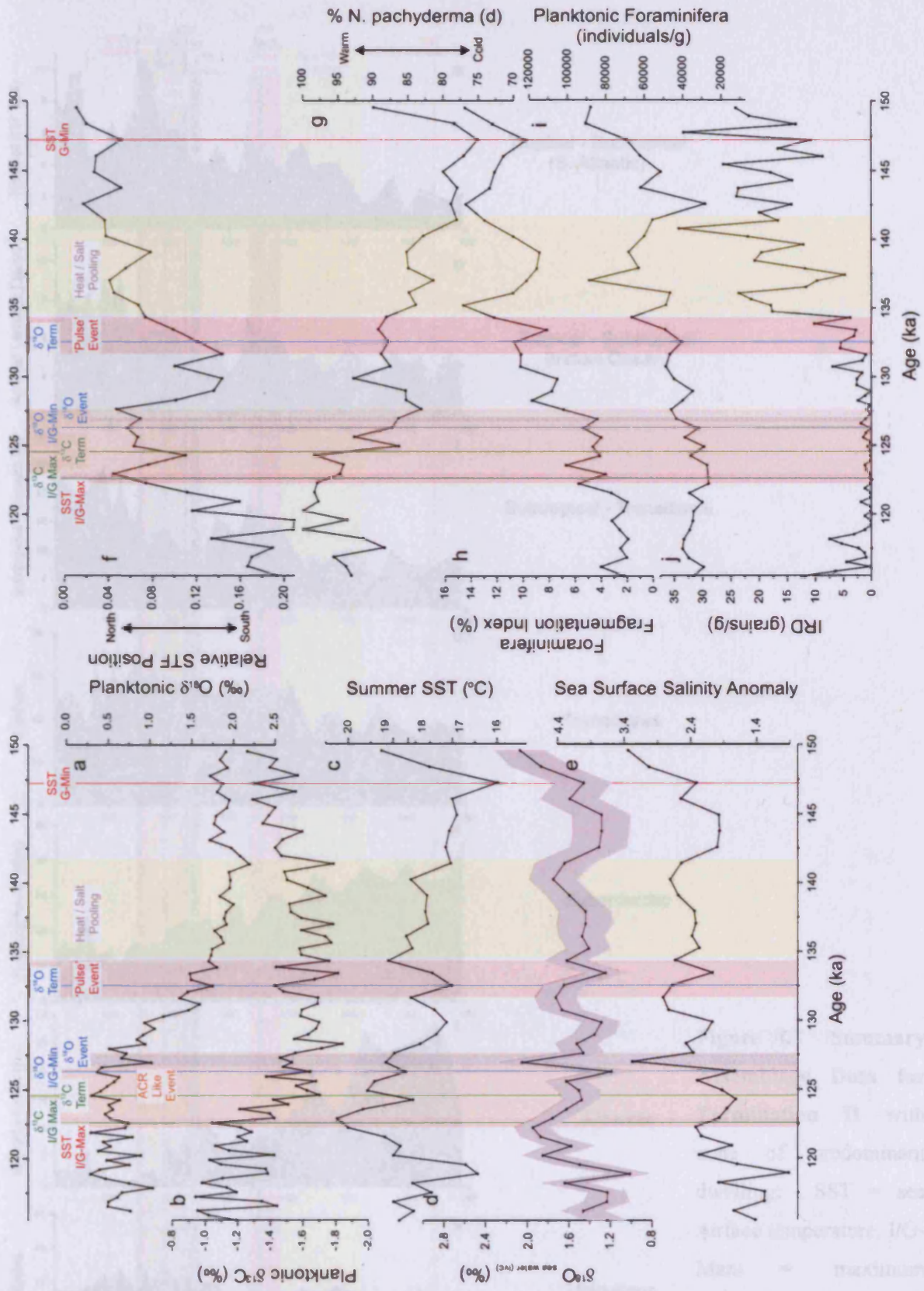

Figure 4.2 Surface proxy data for Termination II (a) planktonic $\delta^{18}O$, (b) planktonic $\delta^{13}C$, (c) Summer SST, (d) $\delta^{18}O$ of sea water ice volume corrected (shading indicates error range), (e) sea surface salinity , (f) relative position of the STF, (g) % *N. pachyderma* (d), (h) foraminifera fragmentation index, (i) number of planktonic foraminifera, (j) IRD counts: SST = sea surface temperature, I/G-Max = maximum interglacial values, Term = termination, G-Min = minimum glacial values

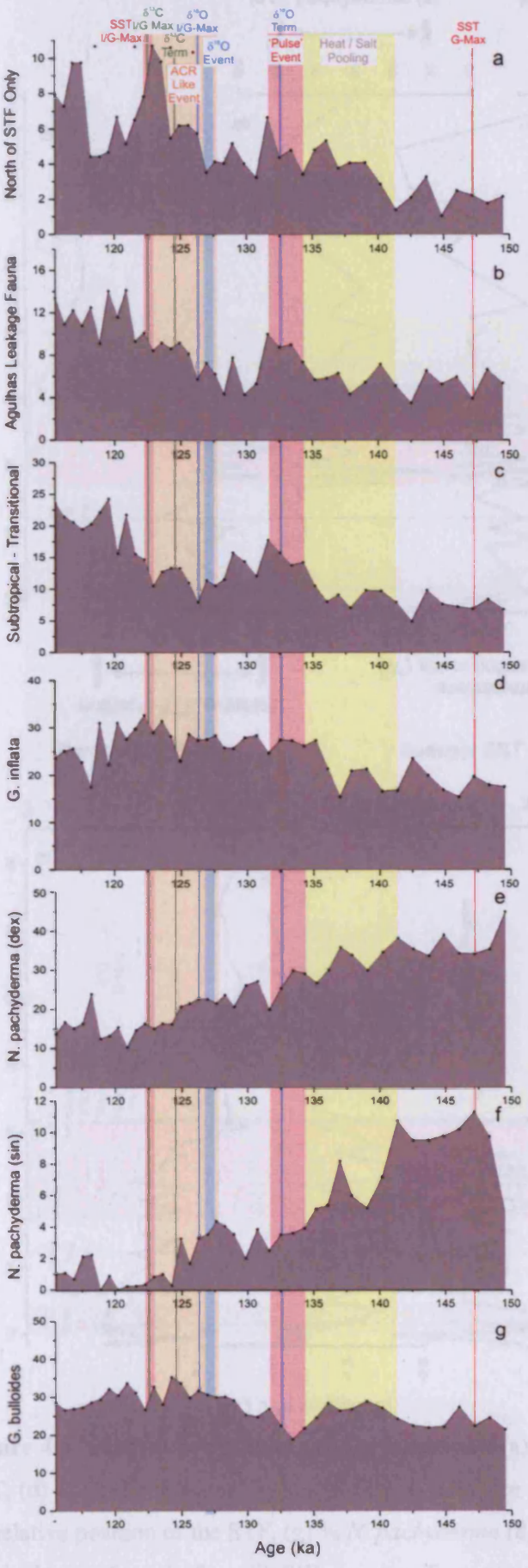

Figure 4.3 Summary Assemblage Data for Termination II with zone of predominant dwelling: SST = sea surface temperature, I/G-Max = maximum interglacial values, Term = termination, G-Max = maximum glacial values

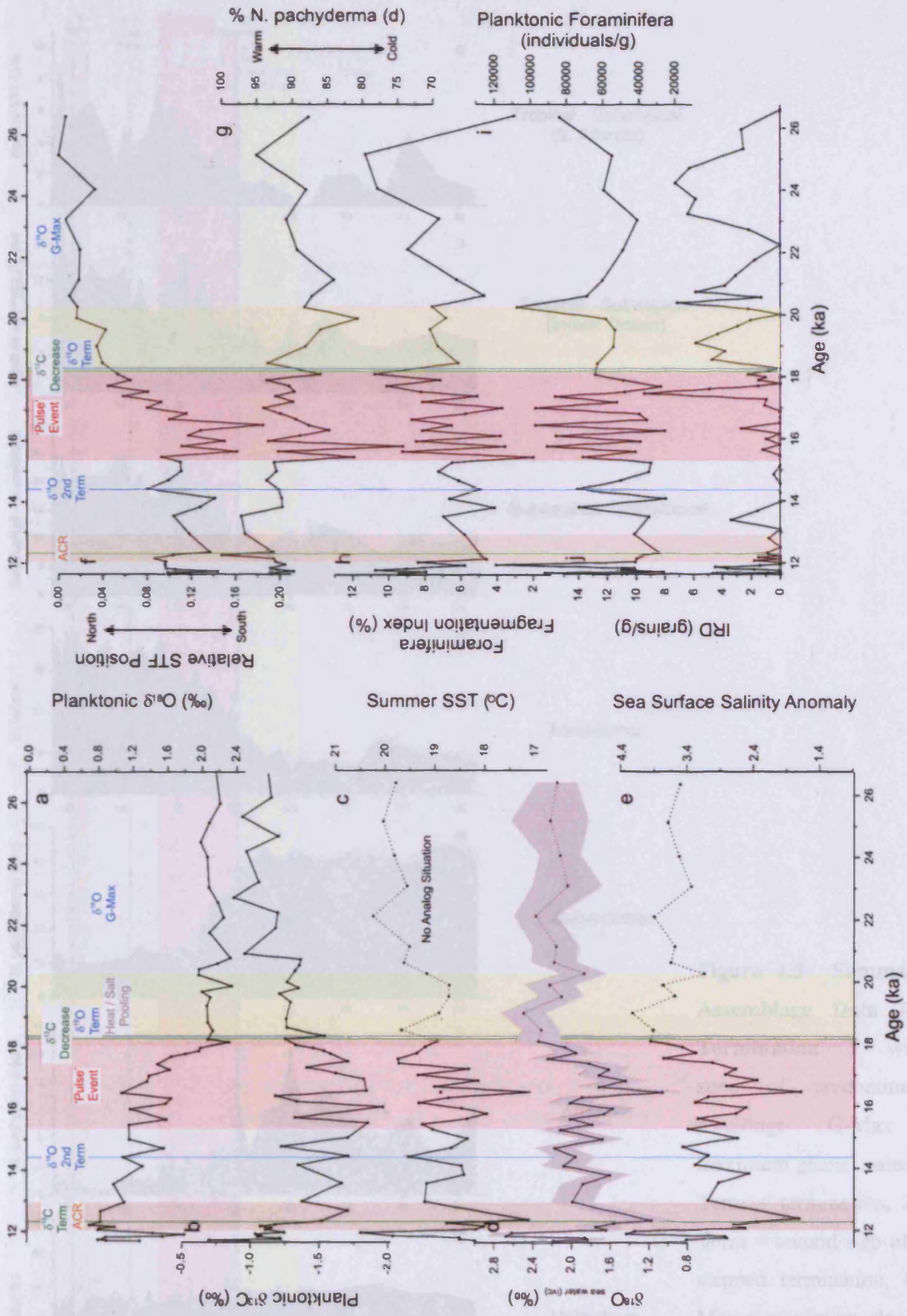

Figure 4.4 Surface proxy data for Termination I (a) planktonic $\delta^{18}O$, (b) planktonic $\delta^{13}C$, (c) Summer SST, (d) $\delta^{18}O$ of sea water, (e) sea surface salinity, ice volume corrected (shading indicates error range) , (f) relative position of the STF, (g) % *N. pachyderma* (d), (h) foraminifera fragmentation index, (i) number of planktonic foraminifera, (j) IRD counts: Term = termination, G-Max = maximum glacial values, 2nd Term = second step of a two stepped termination, ACR = Antarctic Cold Reversal

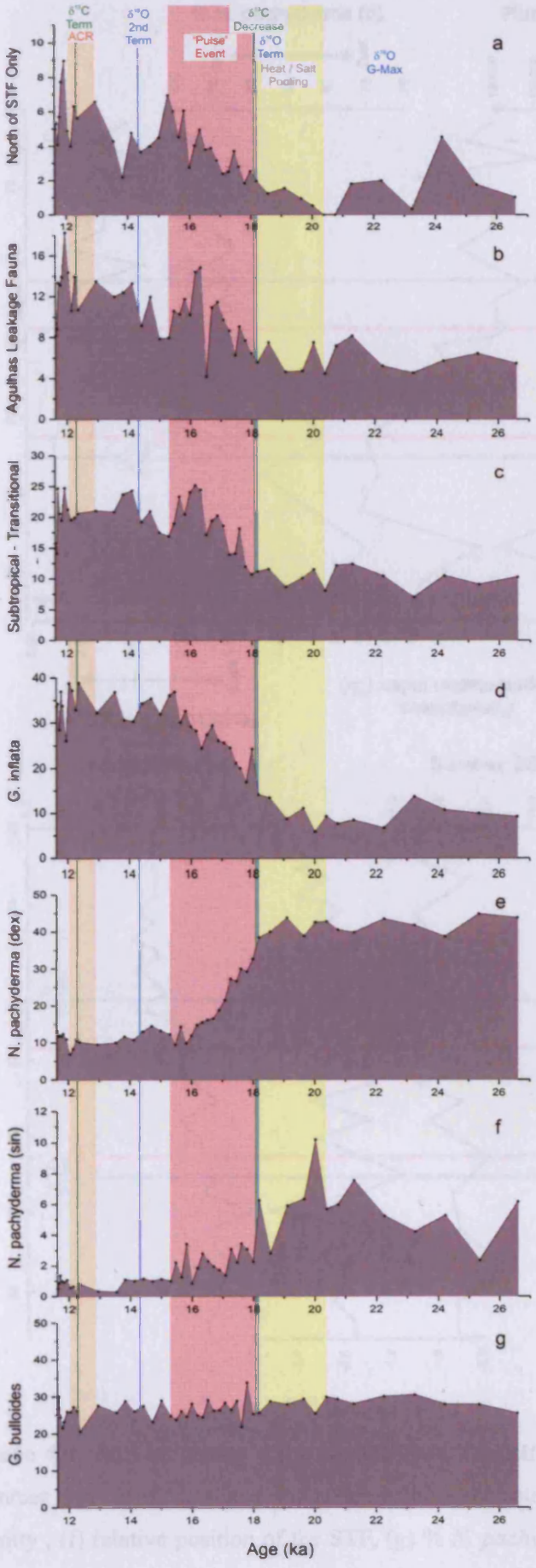

Figure 4.5 Summary Assemblage Data for Termination I with zone of predominant dwelling: G-Max = maximum glacial values, Term = termination, 2nd Term = second step of 2 stepped termination, G-Max = maximum glacial values, ACR = Antarctic Cold Reversal

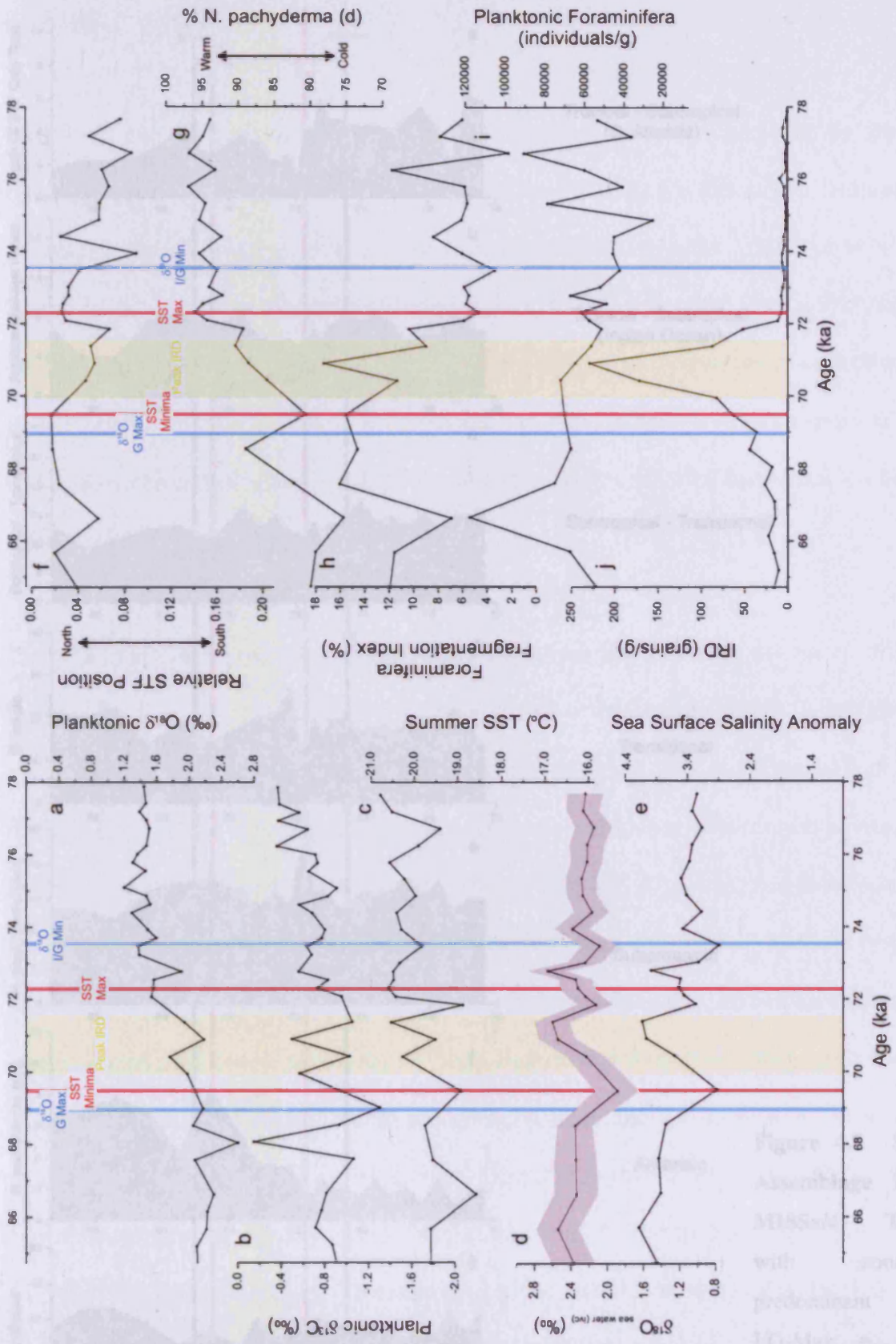

Figure 4.6 Surface proxy data for MIS5a/4 Transition (a) planktonic $\delta^{18}O$, (b) planktonic $\delta^{13}C$, (c) Summer SST, (d) $\delta^{18}O$ of sea water, ice volume corrected (shading represents error range) (e) sea surface salinity , (f) relative position of the STF, (g) % *N. pachyderma* (d), (h) foraminifera fragmentation index, (i) number of planktonic foraminifera, (j) IRD counts: I/G-Max = maximum interglacial values, G-Max = maximum glacial values

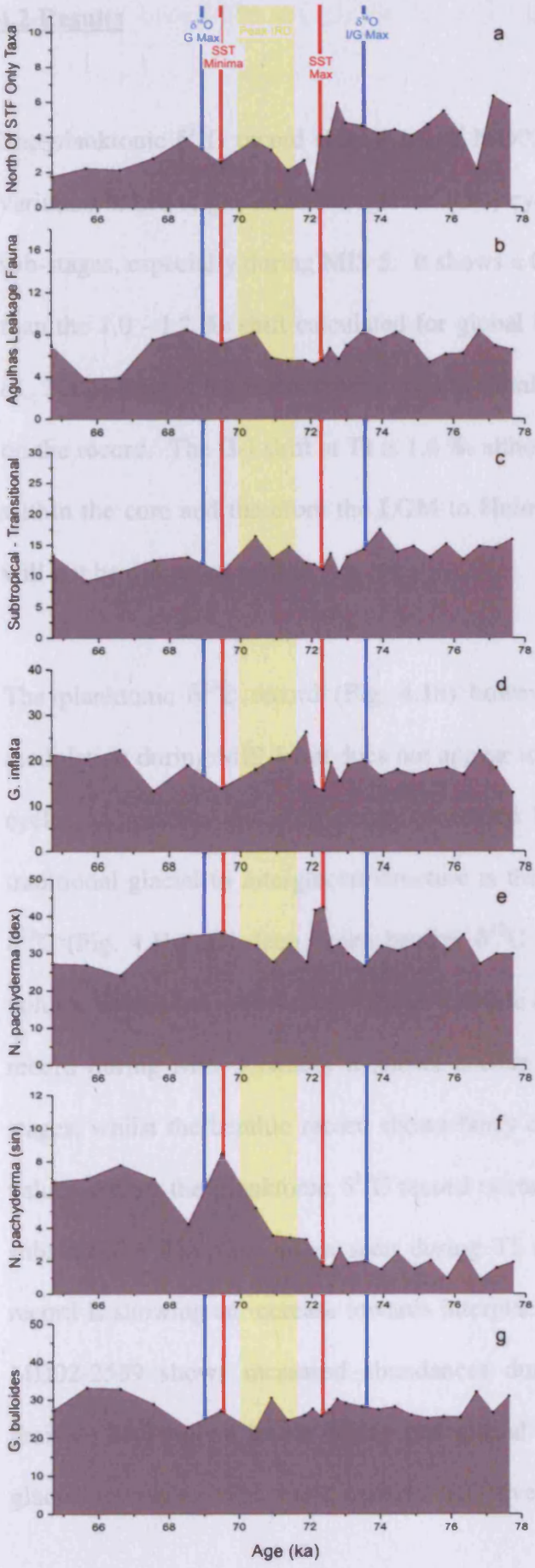

Figure 4.7 Summary Assemblage Data for MIS5a/4 Transition with zone of predominant dwelling: I/G-Max = maximum interglacial values, G-Max = maximum glacial values

4.2 Results

The planktonic $\delta^{18}O$ record (Fig. 4.1a) of MD02-2589 is primarily controlled by orbital variation linked to glacial to interglacial (G-I) cycles, although it is difficult to distinguish sub-stages, especially during MIS 5. It shows a G-I shift of 1.8 ‰ for TII, which is larger than the 1.0 - 1.2 ‰ shift calculated for global ice volume associated change (*Schrag et al.*, 2002), suggesting that temperature and salinity changes at the site had some influence on the record. The G-I shift at TI is 1.6 ‰ although full Holocene conditions are not met within the core and therefore the LGM to Holocene shift cannot be fully quantified and will not be discussed further.

The planktonic $\delta^{13}C$ record (Fig. 4.1b) however does show a high degree of orbital modulation during MIS 5 but does not appear to follow the broader glacial to interglacial cycles, suggesting that it is being controlled by additional factors. This lack of the traditional glacial to interglacial structure is the main difference between the planktonic $\delta^{13}C$ (Fig. 4.1b) and deep ocean benthic $\delta^{13}C$ record (Fig. 5.1), which shows clear ice volume associated modulation. The planktonic $\delta^{13}C$ record also deviates from the benthic record during MIS 5, where it shows a clear structure, possibly associated with sub-stages, whilst the benthic record shows fairly consistent values throughout. The lowest values within the planktonic $\delta^{13}C$ record occur at stage and sub-stage transitions, with substantially depleted values seen during TI and TII, periods when the benthic $\delta^{13}C$ record is showing an increase towards interglacial values. The IRD record (Fig. 4.1c) of MD02-2589 shows increased abundances during glacial periods, rising from 0 - 1 grains/g background levels during interglacial periods to values of ~20 grains/g during glacial intervals. The most marked IRD event occurs coincident with the MIS 5a/4

transition in which IRD abundances reach a maximum of ~200 grains/g. Based on our age model this event spans some 4 ka, although given the age uncertainty in our record this event may have been of a much shorter duration.

The number of planktonic foraminifera (Figs. 4.2i, 4.4i, 4.6i: 70 - 80 k planktonic foraminifera during glacial periods and 40 – 50 k during interglacial periods) and the foraminifera fragmentation index (Figs. 4.2h, 4.4h, 4.6h: 12 % fragmentation during glacial periods and 4 – 6 % during interglacial periods) suggests that both productivity and dissolution were generally higher in glacial periods, with the exception of late TI. Fragmentation index values however remain relatively low overall (<12 %) and are insufficient to suggest that carbonate dissolution has had any significant impact on the faunal composition and SST estimates of MD02-2589.

4.2.1 SST Transfer Function

Initial observations of the estimated SST's for TI and TII (Fig 4.2c, 4.4c) show some striking differences. TII shows lower (~17.5 °C) SST's during the end of glacial stage MIS 6 (141.3 – 147.1 ka) and a general increase over the ice volume defined termination to peak SST's of 20.5 °C at ~130 ka. TI, however, is characterised by complex variability, with high SST's (~20 °C) during the LGM (20.7 - 26.5 ka), highly variable but slightly decreasing temperatures during the termination (14.7 - 18.5 °C) and a large temperature spike near the end of the transition (at ~12 ka).

At TII the SST does not peak until 3.4 ka after the planktonic $\delta^{18}O$ has reached interglacial levels (Fig. 4.2a, c), however at TI full Holocene interglacial levels are not

reached in the core (Fig. 4.1a) and therefore it cannot be deduced if the SST over the transition shows the same pattern. As a result in the following section only differences between the SST values and patterns at MIS 2 (18.1 - 26.5 ka) and 6 (134.2 – 149.5 ka) will be discussed in detail.

Both the TI and TII records show that the dominant taxa are *Globigerina bulloides, Globorotalia inflata and Neogloboquadrina pachyderma* (d) (Fig. 4.3, 4.5) making up 63 - 85 % of the assemblages. The glacial periods are characterised by high percentages of *N. pachyderma* (d) (41.5 % average at TI and 34.3 % average at TII) and low percentages of *G. inflata* (9.9 % average at TI and 9.7 % average at TII), with the interglacial periods being the opposite (TI = 32.7 % *G. inflata*, 11.7 % *N. pachyderma* (d); TII = 28.4 % *G. inflata*, 19.1 % *N. pachyderma* (d)). *G. bulloides* remains persistent at the site over both glacial and interglacial periods, fluctuating between 21.4 and 32.1 % at TII and 20.6 and 33.8 % at TI.

Whilst MIS 2 and 6 are both dominated by *Neogloboquadrina pachyderma* (d), as stated earlier they have very different SST reconstructions. Principal components analysis (PCA) of all MD02-2589 species and samples was run (using statistical analysis program PAST: *Hammer et al.*, 2001) to identify which species are driving the different temperature reconstructions for MIS 2 and 6. Figure 4.8 shows that the MIS 2 sample set (18.1 - 26.5 ka in red) is characterised by high levels of species D, which is *N. pachyderma* (d) and species A (*Globigerina bulloides*), whilst the MIS 6 sample cluster (134.2 – 149.5 ka in blue) is predominantly characterised by high levels of species C, which is *N. pachyderma* (s), and species B (*Globorotalia inflata*). Eigenvalues greater than 0.5 are thought to denote good separation of species along an axis (*Jongman et al.*,

1995) and Figure 4.8 therefore shows two separate sample clusters on the component 1 axis, which accounts for 74.6 % of the total variance. No separation between the clusters can be identified in relation to the component 2 axis. Component 1 axis (and therefore the difference between the two sample sets) is primarily determined by *Globorotalia inflata* (Species B: 0.74 loading) and *N. pachyderma* (d) (Species D: 0.6 loading).

The PCA plot shows MIS 6 is characterised by high *G. inflata* levels and low *N. pachyderma* (d) levels, whereas MIS 2 has low *G. inflata* and high *N. pachyderma* (d) abundances. Both of these species are predominantly transitional species and therefore the pattern suggested by the PCA of higher *N. pachyderma* (d) levels coincident with lower *G. inflata* levels and vice versa may suggest that there is an alternative control to SST affecting the assemblages.

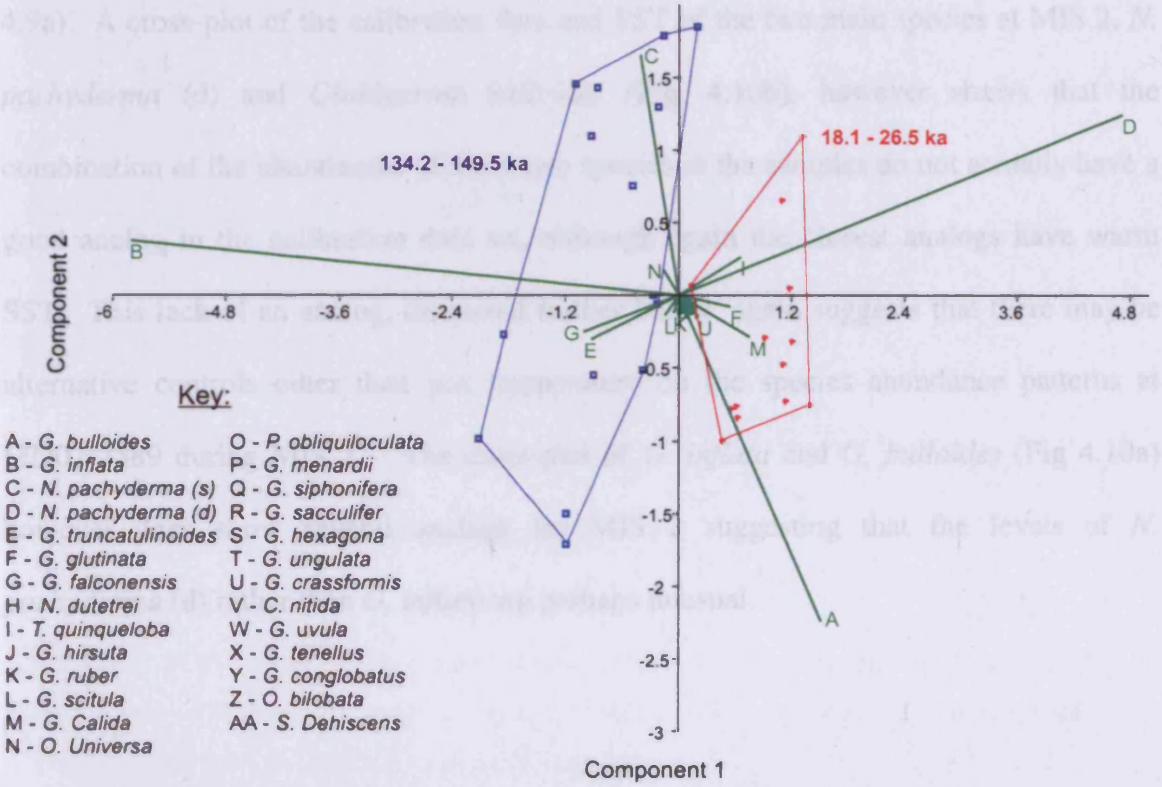

Figure 4.8 Principal Components Analysis of MD02-2589 species and samples for the distinct glacial periods showing which species are characterising each sample and SST estimation (on the Eigenvalue scale).

Figure 4.10c shows that when the abundances of *G. inflata* and *N. pachyderma* (d) are plotted versus each other, the values recorded in MIS 2 appear to have no analog in the MARGO reference dataset, where as the MIS 6 abundances show temperatures around 18 °C. This suggests that perhaps the abundances of these two species seen at MIS 2 rather than MIS 6 are abnormal.

Neogloboquadrina pachyderma (d) has the broadest SST tolerance (10 – 25 °C) of all species in a study on sediment trap observations from 42 sites around the world's oceans (*Žarić et al.*, 2005). However the MARGO dataset used in the transfer function shows that at abundances over 20 % (Fig. 4.9a), *N. pachyderma* (d) is limited to the temperature range of 15 – 22 °C, with a maximum at 21 °C. The percentages of *N. pachyderma* (d) at MIS 2 range from 39 - 45 %, which equates to a temperature range of 18 – 21.5 °C (Fig. 4.9a). A cross-plot of the calibration data and SST of the two main species at MIS 2, *N. pachyderma* (d) and *Globigerina bulloides* (Fig. 4.10b), however shows that the combination of the abundances of these two species in the samples do not actually have a good analog in the calibration data set, although again the closest analogs have warm SST. This lack of an analog, discussed further below, again suggests that there may be alternative controls other than just temperature on the species abundance patterns at MD02-2589 during MIS 2. The cross-plot of *G. inflata* and *G. bulloides* (Fig 4.10a) however does show several analogs for MIS 2 suggesting that the levels of *N. pachyderma* (d) rather than *G. inflata* are perhaps unusual.

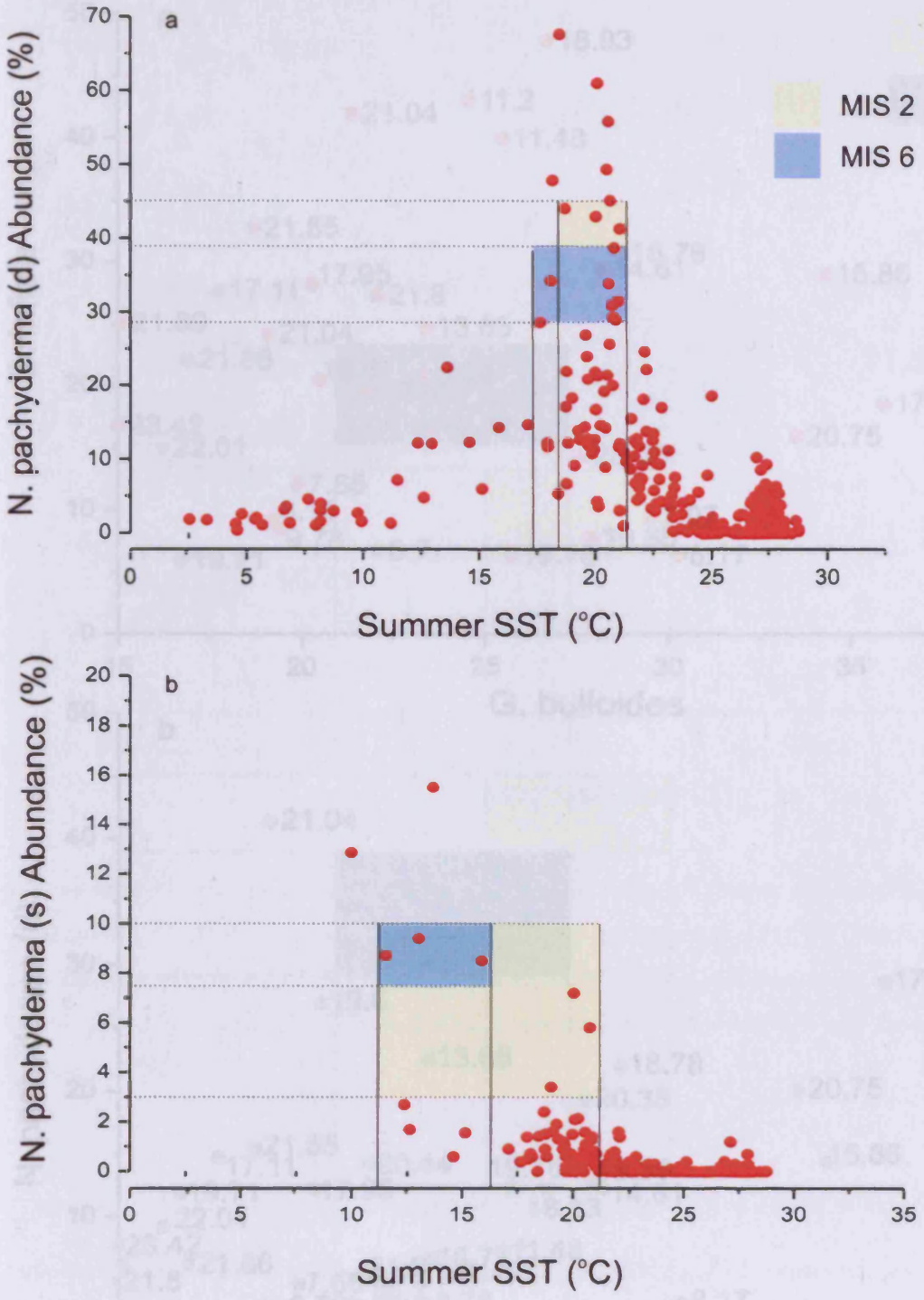

Figure 4.9 Plots showing the temperature range and abundance levels of planktonic foraminifera species: (a) *Neogloboquadrina pachyderma* (s), and (b) *Neogloboquadrina pachyderma* (d) from the MARGO calibration dataset

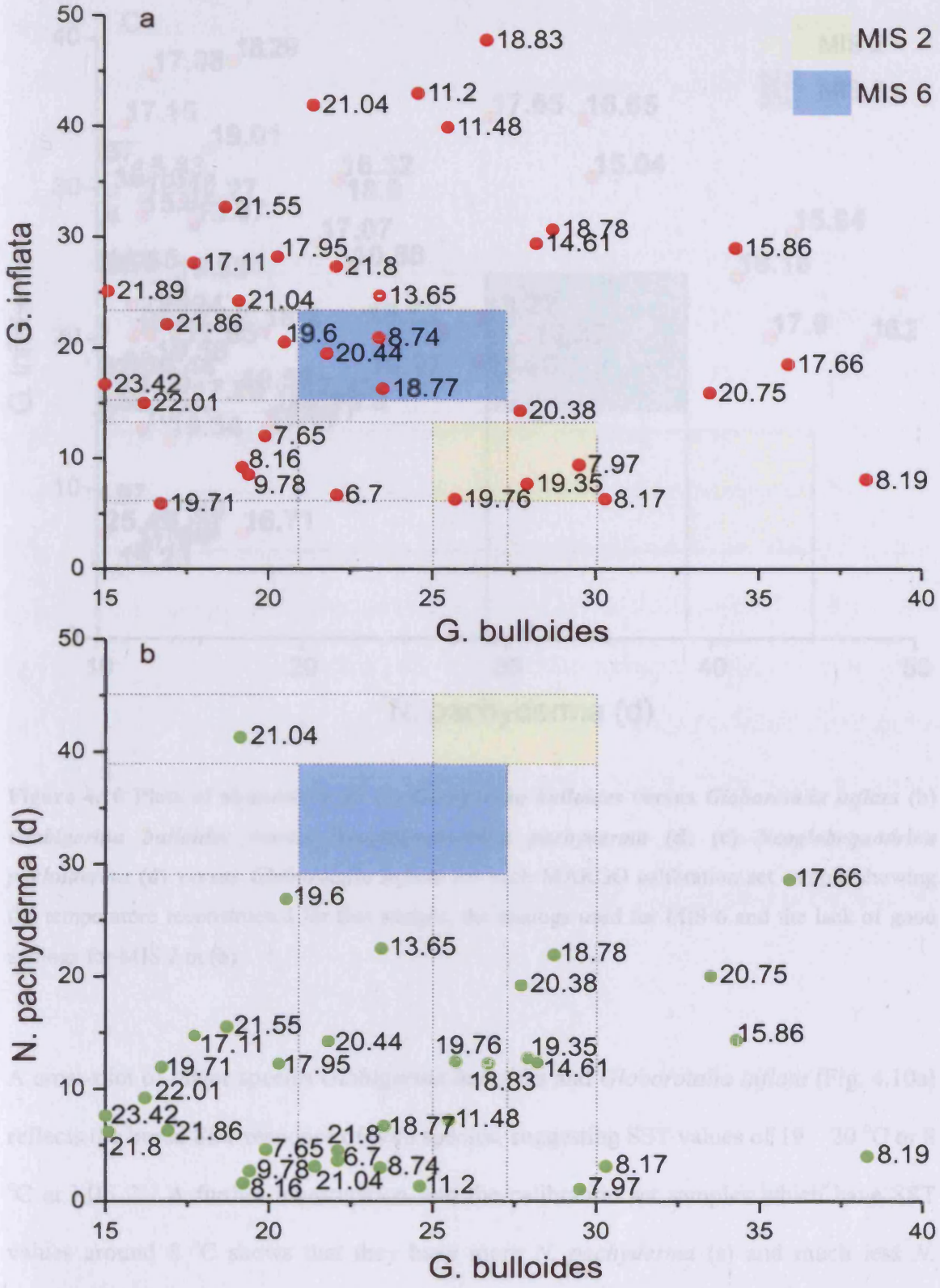
a
MIS 2
MIS 6
G. inflata
G. bulloides
18.83
21.04
11.2
11.48
21.55
18.78
14.61
15.86
17.11
17.95
21.8
21.89
21.04
13.65
21.86
19.6
8.74
20.44
17.66
23.42
18.77
20.75
22.01
20.38
7.65
8.16
7.97
9.78
19.35
8.19
19.71
6.7
19.76
8.17
b
N. pachyderma (d)
G. bulloides
21.04
17.66
19.6
13.65
18.78
20.38
20.75
21.55
15.86
17.11
20.44
19.76
19.35
19.71
17.95
14.61
18.83
22.01
23.42
11.48
18.77
21.86
21.8
7.65
8.19
6.7
8.74
8.17
9.78
21.04
11.2
7.97
8.16

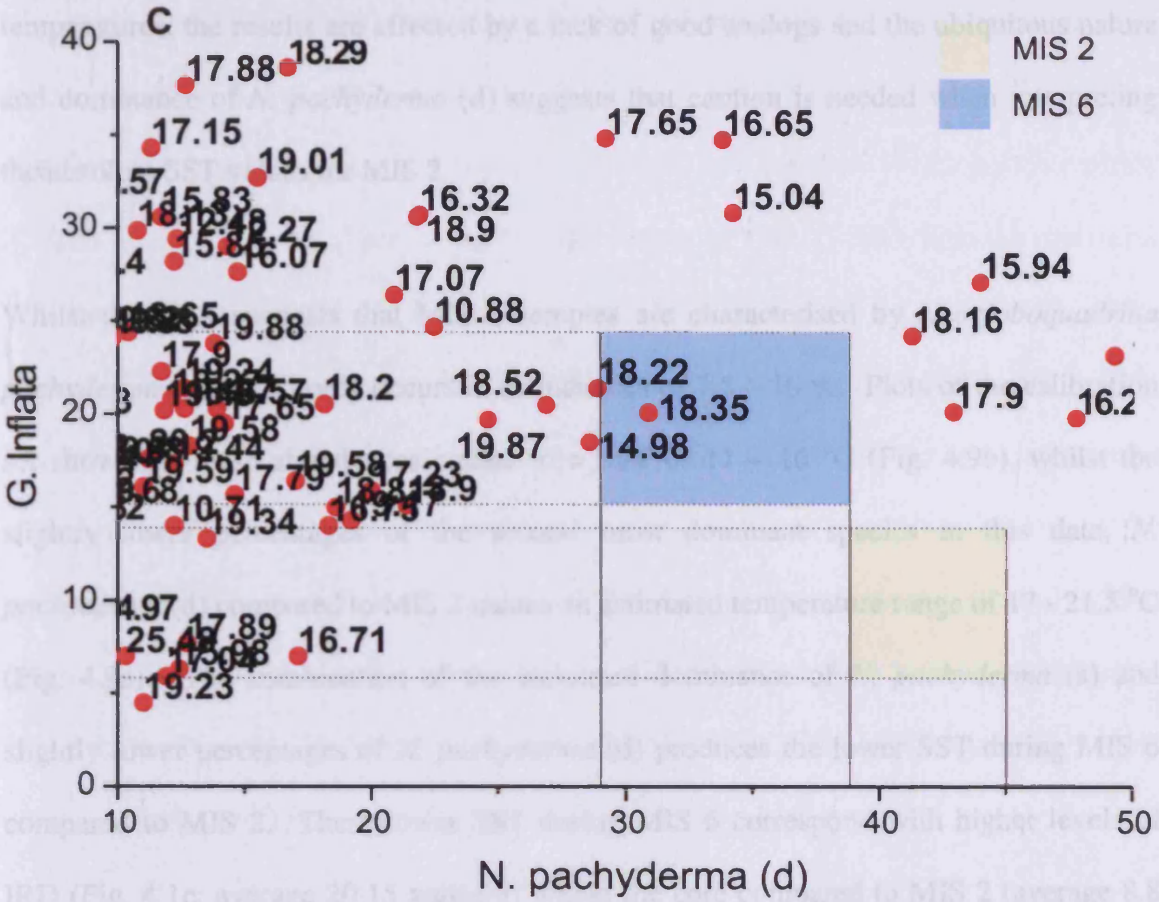

Figure 4.10 Plots of abundance of: (a) *Globigerina bulloides* versus *Globorotalia inflata* (b) *Globigerina bulloides* versus *Neogloboquadrina pachyderma* (d) (c) *Neogloboquadrina pachuderma* (d) versus *Globorotalia inflata* for each MARGO calibration set sample showing the temperature reconstructed for that sample, the analogs used for MIS 6 and the lack of good analogs for MIS 2 in (b)

A cross-plot of major species *Globigerina bulloides* and *Globorotalia inflata* (Fig. 4.10a) reflects the broad SST response of both species, suggesting SST values of 19 – 20 °C or 8 °C at MIS 2. A further investigation into the calibration set samples which have SST values around 8 °C shows that they have more *N. pachyderma* (s) and much less *N. pachyderma* (d) than the MIS 2 samples and none of the warmer species (e.g. *Globigerinoides ruber, Globigerinella calida, Globorotalia menardii*) that can be seen to persist through MIS 2. Although the dominance of *N. pachyderma* (d) suggests warmer

temperatures, the results are affected by a lack of good analogs and the ubiquitous nature and dominance of *N. pachyderma* (d) suggests that caution is needed when interpreting the absolute SST values for MIS 2.

Whilst the PCA suggests that MIS 6 samples are characterised by *Neogloboquadrina pachyderma* (s), it still only occurs in abundances of 7.5 – 10 %. Plots of the calibration set show that these abundances equate to a SST of 11 – 16 °C (Fig. 4.9b), whilst the slightly lower percentages of the second most dominant species in this data, *N. pachyderma* (d) compared to MIS 2 means an estimated temperature range of 17 - 21.5 °C (Fig. 4.9a). The combination of the increased dominance of *N. pachyderma* (s) and slightly lower percentages of *N. pachyderma* (d) produces the lower SST during MIS 6 compared to MIS 2. These lower SST during MIS 6 correspond with higher levels of IRD (Fig. 4.1c: average 20.15 grains/g) within the core compared to MIS 2 (average 8.8 grains/g), suggesting that colder SST were present during MIS 6. This is further reflected in the % *N. pachyderma* (d) record of the two Terminations which shows high percentages and therefore high SST during MIS 2 (85 – 95 %) compared to the lower 75 – 85 % during MIS 6.

Modern day SST_{summer} over the southern edge of the Agulhas Plateau are 17 – 18 °C and SST_{winter} are 13 - 14 °C (*Schlitzer,* 2007). Although Holocene values are not present within the core both summer and winter SST estimates for MIS 5e at MD02-2589 are 2 – 3 °C higher than the modern values. Similarly the modern day value at core site PS2561 (41.5 °S, 28.32 °E; *Gersonde et al.,* 2003), which is geographically close to MD02-2589, is 16.4 °C, again significantly lower than the reconstructed values at our site, whilst LGM reconstructed SST_{summer} for PS2561 show values that are ~4 °C lower than MIS 6 and

LGM values at MD02-2589. The values for PS2561 are based on diatom estimates that are known to be biased towards colder values and generally record values ~2 °C lower than radiolarian temperatures (*Gersonde et al.*, 2003) and therefore if this possible offset is taken into consideration then its modern day values of 16.4 °C fall within the measured values of *Schlitzer* (2007). The SST associated with the STF is 14 °C (*Flores et al.*, 1999; *Rau et al.*, 2002), which is again far lower than the MIS 5e values at MD02-2589, which lies very close to the STF at the present day. However although MIS 5e is an interglacial period, data shows that in austral spring and summer (main bloom seasons) at 40 °S insolation was greater at 120 ka, during MIS 5e, than at the present day (*Laskar*, 1990; *Berger*, 1992b), which may explain the higher SST values for MIS 5e than modern day, although the higher SST estimates for MD02-2589 during the LGM and MIS 6 than previous reconstructions cannot be explained by insolation differences.

Although the SST estimates for MD02-2589 appear consistently higher than either modern day recorded values or reconstructed values, the SST_{annual} change of ~5 °C at TII for MD02-2589 (Fig. 4.2c) (3.6 °C for SST_{summer} and 5.3 °C for SST_{winter}) is in good agreement with other cores from the SAZ, MD96-2085 (SST_{annual} 4 – 6 °C) (*Chang et al., 1999*), PS2821-1 (SST_{summer} 3.2 °C) (*Gersonde et al.*, 2003) and GeoB2019-1 (SST_{summer} 3.8 °C) (*Gersonde et al.*, 2003) suggesting that although the MD02-2589 values may have a consistent positive offset, they still record absolute changes in temperature. Part of this offset may be explained by the 1 °C calculated difference between sea surface temperature and the temperature at the depth *Globoigerina bulloides*, used for the $\delta^{18}O$ estimates, lives at (*Duplessy et al.*, 1991).

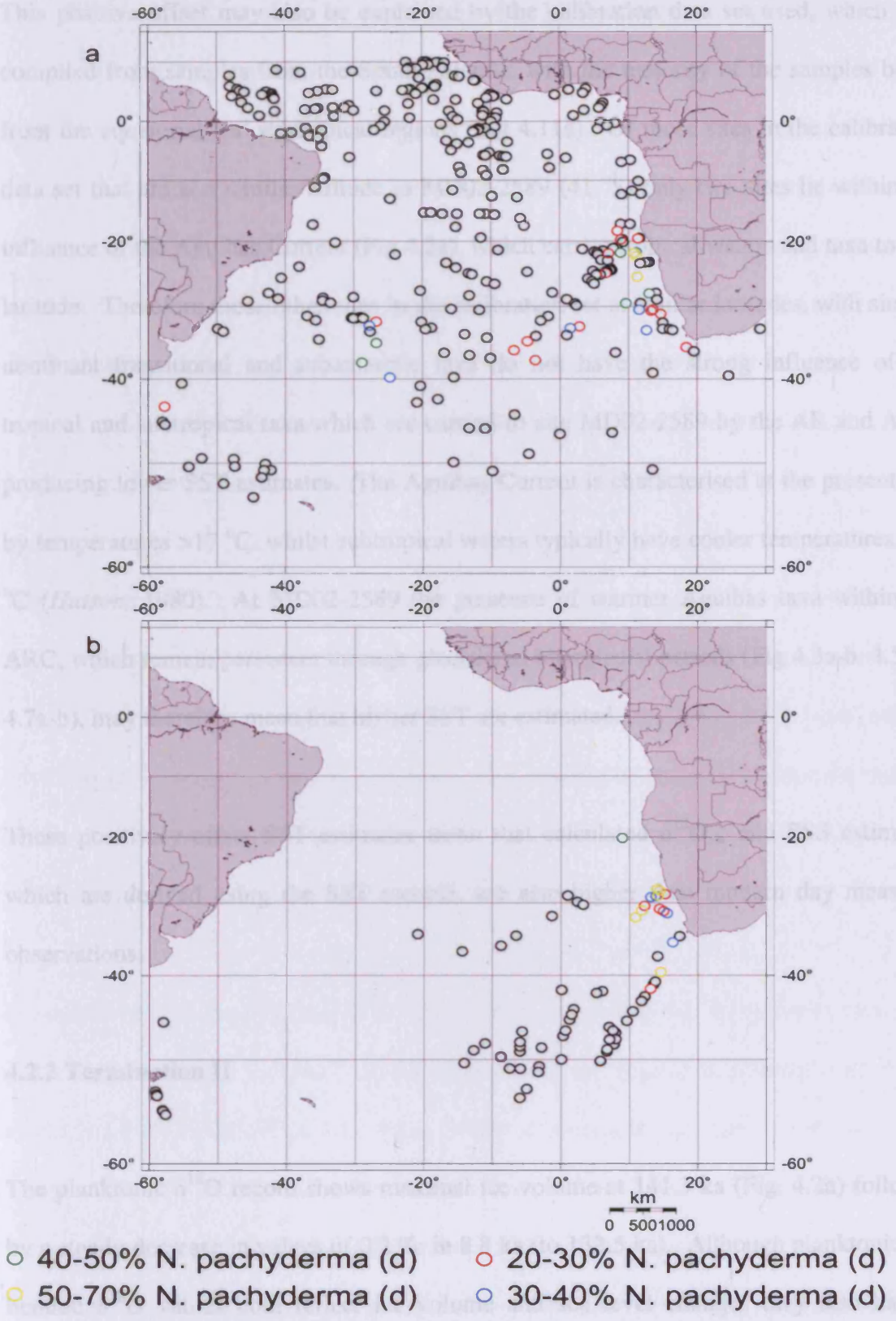

Figure 4.11 Maps showing the sites used in (a) the MARGO South Atlantic transfer function dataset (b) *Niebler and Gersonde*, (1998) with those sites with over 20 % *Neogloboquadrina pachyderma* (d) levels highlighted

This positive offset may also be explained by the calibration data set used, which was compiled from samples from the South Atlantic, with the majority of the samples being from the equatorial and subtropical regions (Fig 4.11a). Of those sites in the calibration data set that are at a similar latitude to MD02-2589 (41 °S) only two sites lie within the influence of the Agulhas Current (Fig 4.2a), which carries tropical waters and taxa to this latitude. Therefore those other sites in the calibration set at similar latitudes, with similar dominant transitional and subantarctic taxa do not have the strong influence of the tropical and subtropical taxa which are carried to site MD02-2589 by the AR and ARC, producing lower SST estimates. The Agulhas Current is characterised at the present day by temperatures >17 °C, whilst subtropical waters typically have cooler temperatures <17 °C (*Hutson,* 1980). At MD02-2589 the presence of warmer Agulhas taxa within the ARC, which remain persistent through glacial and interglacial periods (Fig 4.3a-b, 4.5a-b, 4.7a-b), may therefore mean that higher SST are estimated.

These positively offset SST estimates mean that calculated $\delta^{18}O_{sw}$ and SSS estimates, which are derived using the SST records, are also higher than modern day measured observations.

4.2.2 Termination II

The planktonic $\delta^{18}O$ record shows maximal ice volume at 141.3 ka (Fig. 4.2a) followed by a steady decrease in values of 0.2 ‰ in 8.8 ka (to 132.5 ka). Although planktonic and benthic $\delta^{18}O$ values both reflect ice volume and sea level changes they also have a temperature overprint, which is more significant in the planktonic record, making the benthic $\delta^{18}O$ record better for defining global ice volume levels. The benthic $\delta^{18}O$ record

(Fig. 5.1a) shows that peak ice volume during MIS 6 occurs at 141 ka, which is coincident with that shown in the planktonic record. The planktonic $\delta^{18}O$ record (Fig. 4.2a) then shows a more rapid decrease of 1.4 ‰ in 6.2 ka until full interglacial values of 0.35 ‰ at 126.3 ka. Within this rapid reduction in $\delta^{18}O$ is a short event with more positive values, centred on 126.9 ka, with a 0.5 ‰ increase in $\delta^{18}O$ lasting 1.4 ka. A small reversal event is also seen during TII in the Vostok deuterium record (*Petit et al.*, 1999), although this is dated as 133.2 ka. The $\delta^{18}O$ record then stabilises and remains around 0.4 ‰ with some small scale fluctuations until 118.8 ka, when it has another short event with increased values centred on 117.8 ka.

The planktonic $\delta^{13}C$ record shows slightly greater variability than the planktonic $\delta^{18}O$ record throughout MIS 6 and Termination II (Fig 4.2a, b). Low $\delta^{13}C$ values (around -1.6 – -1.7 ‰) during MIS 6 persist into the ice volume defined termination (Fig. 4.2b) and do not show an increase towards interglacial values until 124.6 ka, 7.9 ka after the start of the rapid reduction in the $\delta^{18}O$ record and 1.7 ka after it reaches interglacial values. The $\delta^{13}C$ record reaches interglacial values of -1.06 ‰ at 122.6 ka.

In contrast to both the $\delta^{13}C$ and $\delta^{18}O$ records the SST record (Fig. 4.2c) shows minimum glacial values at 147.1 ka (16.6 °C), 6 ka before peak ice volume in both the benthic and planktonic $\delta^{18}O$ records (Fig. 5.1a, 4.2a), followed by a steady increase in temperature to a peak of 20.3 °C at 122.9 ka well into ice volume defined MIS5e. There is then a rapid decrease in SST of 2.5 °C in 3.1 ka and a slight recovery to values around 18.9 °C at 116.8 ka. The SST proxy % *Neogloboquadrina pachyderma* (d) (Fig. 4.2g) also shows minimum glacial levels at 147.1 ka, followed by a steady rise to a plateau at 134.2 – 130.7 ka. A decrease in assumed temperature from 129.8 – 125.5 ka is followed by an

increase to interglacial levels at 124.2 ka and a decrease into MIS 5b at 118.8 ka. There seems to be a large degree of coherency between the TF SST record and the % *N. pachyderma* (d) record, again supporting the use of the latter as a SST proxy. However a negative correlation can also be seen between the % *N. pachyderma* (d) record (Fig. 4.2g) and foraminifera fragmentation index (Fig. 4.2h) suggesting that there may be some sort of dissolution overprint on the record which should be taken into consideration. However the slightly elevated values during MIS 6 (~12 %) are well below the ≥33 % level suggested by *Conan et al.* (2002) for the Somali Basin as the limit above which a planktonic foraminiferal assemblage is not palaeoecologically representative, suggesting that any possible dissolution is not having a large effect on the fossil assemblage at MD02-2589.

The $\delta^{18}O_{sw}$ record (Fig. 4.2d) is controlled by salinity variability and local variations and shows fluctuations on shorter timescales than glacial to interglacial cycles, perhaps suggesting a more complex interplay of surface currents with variable salinity signatures.

The IRD record (Fig. 4.2j), whilst showing a high degree of variability during MIS 6, generally shows high values (around 20 grains/g), until 139 ka when there is a decrease to background levels at 131.6 ka. This decrease is interrupted by an increase back up to ~20 grains/g lasting 0.9 ka. The high variability of the IRD record and the general low values of grains per gram is probably related to the distance of the core from PF and the melting zone of icebergs, with only a small number penetrating into the Transitional Zone and as far north as 41 °S.

The foraminifera assemblages are dominated by three species: *Globigerina bulloides, Globorotalia inflata* and *Neogloboquadrina pachyderma* (d) (Fig. 4.3). During MIS 6, as defined by $\delta^{18}O$, the assemblages are dominated by *N. pachyderma* (d) (~37 %), with *G. bulloides* (~23 %), *G. inflata* (~18 %) and *N. pachyderma* (s) (~9 %). At 141.3 ka, the beginning of the initial transition in $\delta^{18}O$, there is both an increase in subtropical taxa (NSTF) and a decrease in *N. pachyderma* (s), but it is not until 136.9 ka that there is a significant, rapid increase in transitional species *G. inflata* (by 12 %), subtropical ALF and ST/Tr fauna and a decrease in IRD levels from 23 grains/g to 3 grains/g coincident with a southwards movement of the STF (Fig. 4.2f). After this initial increase in values, *G. inflata* remains at a stable level until 125 ka, whilst both the ST/Tr and ALF show a peak in values at 131.6 ka followed by a small decrease in values, with the peak being coincident with a reduction in *G. bulloides* (by 10 %), which whilst remaining a dominant species throughout the record shows greater percentages (~32 %) during warmer SST. The STF remains south until 128.9 ka (Fig. 4.2f) when it moves north of the site for 4.7 ka before again moving to its furthest southwards position well into $\delta^{18}O$ defined MIS 5e.

N. pachyderma (s) shows a reduction to background levels as planktonic $\delta^{13}C$ reaches interglacial levels, 1.7 ka after planktonic $\delta^{18}O$, and *N. pachyderma* (d) shows a gradual decrease in values over the termination, with consistent interglacial values (~16 %) being reached at 124.2 ka about 2 ka after the planktonic $\delta^{18}O$ record shows full interglacial values. Whilst the NSTF and ALF show low values (<15 %) throughout the whole record, they both show peak values 2.6 ka and 5.4 ka respectively after $\delta^{18}O$ has reached interglacial levels, with the ALF showing a gradual increase in values throughout the termination and the NSTF taxa showing an abrupt, short lived 5 % increase at 124 ka. The ST/Tr taxa also shows a less gradual increase over the termination with an increase

only occurring after SST have reached their interglacial maximum and peaking at 24 % at 119.5 ka just as the SST show cooler temperatures. All three warm taxa groupings show a distinct peak around 132 ka, followed by a decrease and then increase to interglacial levels.

4.2.3 Termination I

The planktonic $\delta^{18}O$ record shows very little variability during MIS 2, which may in part be due to the lower resolution through this part of the core (32.2 – 18.7 ka: Fig. 4.1a, 4.4a), and although full Holocene levels are not reached within the core it can be seen that the main decrease in planktonic $\delta^{18}O$ occurs in a 3 stepped transition starting with a sharp decrease in values of 1.2 ‰ in 1.7 ka from 18.2 ka to 16.5 ka followed by a plateau, where the $\delta^{18}O$ values stabilise for 2 ka (until 14.4 ka), followed by a less sharp increase of 0.5 ‰ in 2.3 ka to 12.1 ka. There is then a very rapid, short event with increased ice volume (1 ‰ increase) lasting 0.3 ka before a return to values around 0.8 ‰. As in TII the planktonic $\delta^{18}O$ record matches well with the benthic $\delta^{18}O$ record (Fig. 5.1), which better reflects ice volume changes, with the plateau event seen at 16.5 – 14.4 ka in the planktonic $\delta^{18}O$ record seen as a series of two small reversals within a stable period in the benthic $\delta^{18}O$ record (Fig. 5.1).

Similar to TII the planktonic $\delta^{13}C$ record shows low values into the termination (Fig. 4.1b, 4.4b) only showing an increase towards interglacial levels 5.5 ka after the start of the termination in the $\delta^{18}O$ record. The $\delta^{13}C$ values for TI, unlike TII, however actually show reduced values during the termination (average -1.6 ‰ for 17.3 to 12.7 ka) compared to the average MIS 2 values of -1.0 to -1.1 ‰ (Fig. 4.1b).

Whilst the anomalous temperatures during MIS 2 (18 – 27 ka: Fig. 4.4c) have been described above, the SST record for TI shows a high degree of variability especially over the period 17.5 to 13.8 ka. A decreasing trend in SST can be seen over the period 17.4 – 16.5 ka, followed by an increase, plateau and decrease to a low of 17.1 °C at 12.3 ka. A very rapid and short lived SST event with a 2.5 °C warming in ~0.3 ka and subsequent 2 °C cooling in 0.3 ka is coincident with a 1 ‰ increase and rapid decrease in $\delta^{18}O$. The % *N. pachyderma* (d) record (Fig. 4.4g) shows high percentages (95 %) at 25.3 ka indicating of high SST, with a decrease of 15 % in 5 ka, followed by an increase to levels around 93 % at 18.5 ka. The record again shows a period of high variability, with large fluctuations up to 19 % over short time periods (~0.2 ka), although the mean values remains constant through this period. There is then an increase at 13.8 ka to very high levels (~97 %) followed by a slight decrease. Generally the SST record and the % *N. pachyderma* (d) record show a high degree of similarity again further substantiating the SST estimates.

The $\delta^{18}O_{sw}$ and SSS records (Fig. 4.4d, e) for TI show high values during MIS 2, although caution should be extended when interpreting these as they are derived using the SST record, which, as discussed earlier, has higher than expected values during MIS 2. Both records show fairly consistent values until 20.3 ka, when there is an increase in salinity to peak values of +3.3 away from the modern at 19.1 ka. Both records then exhibit a decrease of 2.4 in salinity and 1.4 ‰ in $\delta^{18}O_{sw}$ to a low point at 16.5 ka, concurrent with the furthest southwards position of the STF (Fig. 4.4f). Again both records then show a degree of rapid variability with a slightly increasing and then stabilising trend until 12.9 ka when there is a sharp decrease in salinity of 0.7 followed by a rapid increase of 1.8 in

0.4 ka to a peak which is coincident with the sharp increase seen in the $\delta^{18}O$ (Fig. 4.4a), SST (Fig. 4.4c), and foraminifera accumulation rate (Fig. 4.4i) records.

The transition between the species that are dominant during the glacial periods MIS 2, *Neogloboquadrina pachyderma* (d) and *Neogloboquadrina pachyderma* (s), and those that are dominant during the Holocene, *Globorotalia inflata,* NSTF, ALF and ST/Tr occurs at 19.1 ka in all the above mentioned species (Fig. 4.5) concurrent with a southwards movement of the STF from its northerly glacial position (Fig 4.4f). This is ~ 1ka before the $\delta^{18}O$ defined termination starts and at the same time as peak SSS values before they rapidly decrease into the termination (Fig. 4.4a, e). It is interesting to note that there is such a sharp transition between the colder and warmer indicator species yet the SST record does not reflect this distinct shift in dominance.

Both the NSTF, ALF and ST/Tr species show variability during the period 18 - 15 ka in line with that seen in the other proxies (Fig. 4.5). The warmer taxa (NSTF and ALF) show an increase in values at 12 ka coincident with the event seen in the $\delta^{18}O$, SST, SSS and planktonic accumulation rate.

4.2.4 MIS5a/4 Transition

Planktonic $\delta^{18}O$ (Fig. 4.1a, 4.6a) increases steadily by 1.2 ‰ in 7 ka over the transition, whilst the SST record (Fig. 4.6c) shows consistent values from 75.7 – 72.1 ka of around 20.2 °C followed by a sharp reduction of 1.6 °C and then increase back to 20.5 °C in 0.8 ka. There then follows a general decrease in SST to values of ~19.5 °C, with a short lived cold event with values down to 18.5 °C at 66.6 ka. The % *N. pachyderma* (d) record

shows less variability over the transition with high fairly consistent values around 95 % until a small peak at 72.7 – 72.1 ka followed by a gradual reduction in values to 80.7 % at 69.4 ka. An increase of 9 % followed by a decrease to 75.5 % and then recovery to 79.4 % at 65.6 ka follows.

The $\delta^{18}O_{sw}$ and SSS record (Fig 4.6d, e) show two events with increased salinity of 0.8 centred on 72.7 and 71 ka, with a rapid decrease back to MIS 5a levels from 72.5 – 71.8 ka. Following the second event SSS decreases again back to background MIS 5a levels and then increases slightly into full $\delta^{18}O$ defined MIS 4.

The foraminiferal fragmentation index (Fig. 4.6h) shows a sharp increase in % over the transition from values around 5 % until 72.1 ka to values around 15 % at 70.8 ka, again showing a negative correlation with % *N. pachyderma* (d), which may reflect some dissolution within the record in MIS 4. The IRD record (Fig. 4.6j) shows a large event with increases in IRD from background level to ~250 grains/g from 72.1 – 68 ka and then a reduction to levels similar to glacial stages MIS 6 and 2 (~ 15%).

4.3 Discussion

Previous micropalaeontological studies from the South Atlantic sector of the southern subtropical gyre and Southern Ocean have suggested that the palaeoceanographic history of this area is primarily characterised by the north and south fluctuations of the major oceanic fronts with glacial to interglacial cyclicity (e.g. *Prell et al.*, 1979; *Flores et al.*, 1999). However more recent studies have suggested that the surface hydrological changes and biotic response in this area is much more complex and involves some

millennial scale variability additional to the glacial to interglacial cycles (*Chang et al.*, 1999; *Rau et al.*, 2002). In addition further studies have argued against frontal migration (*Matsumoto et al.*, 2001), with the mean paths of the fronts being closely locked to bottom topography and land-sea configurations, with little variability in their positions (*Moore et al.*, 1999). Instead of latitudinal migration, either the temperature of the isotherms associated with the fronts are suggested to vary on glacial to interglacial timescales (*Gersonde et al.*, 2005) or the temperature gradient across them are thought to intensify during glacial periods (*Schaefer et al.*, 2005).

4.3.1 Termination II

The high abundance of *Neogloboquadrina pachyderma* (d) during MIS 6 suggests an advection of cold, high-nutrient surface subantarctic waters over the site, with the presence of *N. pachyderma* (s) with percentages around 10 – 12 %, *Globorotalia inflata* (18 – 20 %) and *Globigerina bulloides* (23 %) all representative of the modern day transitional zone between the STF and SAF (Fig. 4.3). The relative position of the STF (Fig. 4.2f) suggests that it was north of the site during MIS 6. Studies have suggested that the SAF migrated 3 – 5 ° northwards in the South Atlantic region from its present day position of ~45 °S (*Gersonde et al.*, 2005) during MIS 6, potentially lying close to MD02-2589, although values of *N. pachyderma* (s) and *G. bulloides* are not high enough to suggest that the SAF was very close to the site. This may be due to the fact that the coupling of the ARC and the STF, the position of the retroflection and the possible topographical locking of the STF to the Agulhas Plateau may cause the fronts to act differently in this region to other parts of the South Atlantic.

The continued presence of tropical and subtropical foraminifera throughout MIS 6 (Fig. 4.3a, b), however suggests that the northwards advections of subpolar waters did not cause a significant northwards shift of the STF. This is consistent with previous studies that have suggested that the STF migrated no further northwards than 36 °S (*Rau et al.*, 2002) allowing Agulhas leakage to continue through the Indian-Atlantic throughflow area throughout MIS 6 (*Winter and Martin*, 1990; *Flores et al.*, 1999, *Rau et al.*, 2002, *Gersonde et al.*, 2003; *Esper et al.*, 2004). The present day proximity of MD02-2589 to the STF means that only a small northwards movement of ~2 ° would be required to change the overlying waters from subtropical to transitional. The levels of ALF during MIS 6 are very low (~1 - 2 %: Fig 4.3b) but are consistent with some sort of small continued influence over the site, suggesting that the ARC remained close. However during the LGM *Hutson* (1980) suggested that the Agulhas Current was replaced by cooler subtropical water masses in winter months during glacial periods, with a weak development during summer months and *Prell et al.* (1980) also suggested a cooler, shallower and seasonally variable Agulhas Current with reduced tropical to temperate heat transfer (*Winter and Martin*, 1990). This means that the proportion of the true Agulhas water and Subantarctic water within the ARC would probably have changed over glacial to interglacial periods making the proximity of the AR and ARC difficult to establish using ALF alone. Several studies have suggested that there was probably an eastwards movement of the AR coincident with the slight northwards penetration of the STF (*Flores et al.*, 1999; *Rau et al.*, 2002) during MIS 6. The AR is thought to slowly progress westwards on the time scale of a few months at the present day. When it reaches a critical extension (~15 °E – *Gordon et al.*, 1987) a section of subantarctic water wedges northwards to occlude an Agulhas ring. The warm cored anticyclonic ring then moves off into Cape Basin and the retroflection moves back to its eastern (~21 °E – *Gordon et al.*,

1987) most position (*Boebel et al.*, 2003b). Site MD02-2589 lies at 25.15 °E and therefore any eastwards movement of the retroflection associated with glacial conditions would mean that the site would still remain under the influence of the current, even if it was seasonal.

It is therefore possible that the STF during MIS 6 was still close to the site and fluctuated seasonally producing a weak summer influence of the Agulhas Current over the Agulhas Plateau, although again this is difficult to quantify due to cross frontal water and faunal movements and the mixing between Agulhas Current and Subantarctic waters and assemblages. Previous studies have shown that there are large SST gradients over the STF (*Chang, et al.*, 1999; *Flores et al.*, 1999; *Schaefer et al.*, 2005) which would have increased during glacial periods due to the northwards expansion of the SAF and PF by ~5 ° and the relative small movement of the STF (*Gersonde et al.*, 2003, 2005). It is therefore unlikely that the STF fluctuated seasonally over the actual site as the large temperature differences that this would produce are not recorded, although it is also possible that as the main species driving the SST record are spring bloom species then these fluctuations have not been recorded. Present day surface SST data shows the large degree of variability that occurs in this region over a year and it is therefore possible that as such a large degree of variability in temperatures and surface patterns occurs seasonally any record in the MD02-2589 SST record, which has a sample resolution of ~0.5 ka, would be significantly smoothed.

The initial decrease in planktonic $\delta^{18}O$ values following peak ice volume (Fig. 4.2a) can possibly be explained as being a local temperature signal as the SST record (Fig. 4.2c, g) shows an increase over this period. Both the SST and % *N. pachyderma* (d) record (Fig.

4.2c, g) show that the surface waters started warming at 141.3 ka during peak ice volume in both the benthic and planktonic $\delta^{18}O$ records (Fig. 5.1a, 4.2a), which is consistent with previous studies which have shown early Southern Ocean warming during late MIS 6 (*Labeyrie et al.*, 1996; *Chang et al.*, 1999; *Mashiotta et al.*, 1999; *Bianchi and Gersonde*, 2002). This initial warming however does not seem to be linked to any southward movement of the STF (Fig. 4.2f) or large decrease in IRD levels (Fig. 4.2j) suggesting that possibly it is not linked to changes in Antarctic temperatures, which have a large effect on sea ice distribution and frontal positions. Indeed a southward movement of the STF does not appear to occur until 136 ka (Fig. 4.2f). The studies mentioned above all associate early SST warming with a north-south movement in the location of the fronts, perhaps suggesting that the warming in MD02-2589 from 141.3 ka to 136 ka is not related to the general Southern Ocean warming pattern.

The CLIMAP project (*CLIMAP*, 1981) and other subsequent palaeo-proxy and modelling studies (*Prell*, 1985; *Trend-Staid and Prell*, 2002; *Barrows and Juggins*, 2005) have shown that although the tropical Indian Ocean cooled at the LGM, it cooled to a lesser degree than the high latitudes producing large thermal gradients over the subtropical gyre. The warm, southwards flowing Agulhas Current transporting high salinity, warm Indian Ocean tropical and subtropical waters is thought to still flow during glacial periods but perhaps in a slightly weaker state (*Winter and Martin* 1990, *Hutson* 1980, *Prell et al.*, 1980). Certainly its trajectory to about 35 °S, where it meets the broad continental shelf of the Agulhas Bank, is stabilised by severely inclined shelf gradients (*Lutjeharms et al.*, 2003) which means that the glacial position of the main current is unlikely to have changed substantially (*Winter and Martin*, 1990), with movement in the position of the retroflection being the main variable.

The continued transport of warm, salty Indian Ocean waters to the southern tip of South Africa combined with reduced leakage due to an eastwards movement of the AR in the Indian to Atlantic throughflow region (*Berger and Wefer,* 1996*; deRuijter et al.,* 1999*; Goldstein et al.,* 1999*; Flores et al.,* 1999*; Rau et al.,* 2002*; Kuhn and Diekmann,* 2002*; Peeters et al.,* 2004) suggests that there was possibly a pooling of heat and salt in the area. The increase in SST at MD02-2589 (Fig. 4.2c, g) during MIS 6 may be reflecting this build up of heat over the site due to the persistent activity of the Agulhas Current and reduced Agulhas leakage. The SSS values for the same period (141.3 – 136 ka: Fig. 4.2e), whilst showing some variability, shows high values similar to those in peak MIS 5e, which is not consistent with a reduction in salt over the site associated with the northwards movement of the STF and increased influence of cold, fresher surface ACC waters. As several of the species-related proxies suggest that the STF was north of the site over this period, then the high salinity levels can be again explained by the persistent influence of the Agulhas Current probably seasonally over the site.

The increase in SST associated with heat pooling peaks at 134.3 ka, decreasing rapidly 1.5 °C in 1.8 ka (Fig. 4.2c), concurrent with a rapid southwards movement of the STF (Fig. 4.2f), sharp decrease in SSS (Fig. 4.2e) and IRD values to near background levels (Fig. 4.2j). There is also a rapid increase in ALF, transitional zone dwelling *Globorotalia inflata* and ST/Tr fauna (Fig. 4.3b-d) starting at 135.2 ka, over this period. This can be explained as a rapid southwards movement of the STF, allowing an initial pulse of the pooled Indian Ocean heat and salt through the Agulhas leakage area into the South Atlantic due to a westwards penetration of the AR. This pulse, or collapse of the warm pool, 1.8 ka before the ice volume transition in both planktonic and benthic $\delta^{18}O$, is seen

as an initial short lived temperature and salinity decrease at MD02-2589 due to the loss of pooled heat and salt, with a sharp increase in ALF confirming the increase in inter-ocean exchange. This event may be linked with the previous studies that have identified early SST warming in the Southern Ocean either in late MIS 6 or during TII linked to frontal movements (*Labeyrie et al.*, 1996; *Chang et al.*, 1999; *Mashiotta et al.*, 1999; *Bianchi and Gersonde*, 2002).

At 131.6 ka the SST record shows a slight recovery possibly linked to the end of the pulse with the ALF decreasing rapidly back to almost glacial levels. The *Globorotalia inflata* abundance and position of STF records however suggest that the STF remained in a southerly position until 128.9 ka although the period of lower SST and low ALF abundance does not suggest a greater influence of warm waters. *Bianchi and Gersonde (2002)* note a southwards displacement of the PF by 3 – 5 ° latitude compared to the modern day during late MIS 6, which is consistent with the STF proxy data of MD02-2589 which shows the event lasting 8.5 ka. The dominance of transitional taxa (*G. inflata*, ST/Tr, *Neogloboquadrina pachyderma* (d)) over this period (136.1 – 127.6 ka) and the persistence of colder taxa (*N. pachyderma* (s)) suggests that whilst the STF and SAF migrated southwards the site was still in the Transitional zone, with the STF still north of the site, which would explain the lower SST values during this period.

Several studies have noted a surface cooling in TII (around 129.5 ka) in the Southern Ocean (*CLIMAP*, 1984; *Brathauer and Abelmann*, 1999; *Becquey and Gersonde*, 2002; *Cortese and Abelmann*, 2002; *Bianchi and Gersonde*, 2002) and in marine and terrestrial records from around the world (*Seidenkrantz et al.*, 1996; *Sánchez Goñi et al.*, 1999; *Lototskaya and Ganssen*, 1999; *Heusser*, 2000), although not of the intensity of the ACR

(*Jouzel et al.*, 1995; *Sowers and Bender*, 1995) at TI. The northwards movement of the STF (Fig. 4.2f) from 127.6 – 122.9 ka during TII, reduction in ALF, ST/Tr taxa and decrease in % *N. pachyderma* (d) appear to be consistent with these observations. The occurrence of this cooling and subsequent expansion of the Southern Ocean frontal systems may be linked to the collapse of the warm pool due to a southwards frontal migration, followed rapidly by a northwards frontal rebound, associated with a wider Southern Ocean ACR-like event, which kept the SST low. This may also explain why the SST values at MD02-2589 do not reach peak interglacial levels until well into MIS 5e, although the relationship between position of the fronts and SST can be seen to be non-linear, further confirming the complexity of the area and the influence of the Agulhas Current.

The phasing of SST and planktonic $\delta^{18}O$ over TII at MD02-2589 is very similar to that observed at ODP Site 1089 (40.56 °S, 9.54 °E; *Cortese and Abelmann*, 2002) which is located just south of the STF in the South Atlantic at the present day, suggesting that this may be a robust signal for the wider Southern Ocean STF zone. It may therefore suggest that an ACR-like event during TII, controlled by wider Antarctic climate variables may succeed the collapse of the warm pool in the Agulhas throughflow region. Modelling work by *Knorr and Lohmann* (2003, 2004) has suggested that a switch from a weak glacial to strong interglacial THC mode during deglaciations is due to the northwards propagation of heat and salt leaked through the Agulhas throughflow region. The ACR at TI is thought to occur at the same time as warming in the North Atlantic (*Blunier et al.*, 1997) due to the resumption of NADW production and therefore the phasing at TII in MD02-2589 would support the modelling studies suggestion of a pulse of Agulhas

leakage providing especially salt to the northwards flowing Atlantic Ocean surface currents ~ 6.7 ka before an ACR-like event.

4.3.2 Termination I

MIS 2 and the phasing over TI suggest very different conditions and sequence of events from those seen during MIS 6 and TII.

As discussed in section 4.1.1, the faunal assemblage during MIS 2 is dominated by high levels of *Neogloboquadrina pachyderma* (d), which is the driving force behind the high SST seen during this period. The high levels of *N. pachyderma* (d) may be driven by productivity rather than temperature changes. Dissolution is again a possible driver of the variability within the *% N. pachyderma* (d) record, shown by the negative correlations over TII and MIS5a/4, although again the low values of the fragmentation index suggest that it is not likely to be a very significant factor. *N. pachyderma* (d) is a deep dwelling thermocline species (10 - 300 m) living within or at the base of deep chlorophyll maxima (*Zarić et al.,* 2005), can occur abundantly even at times of very high export productions and indeed appears to increase production during periods of high fertility (*Sauter and Thunell,* 1991). It exhibits a clear preference for mid-temperatures, although it has a very broad SST tolerance range of 10 – 25 °C (*Zarić et al.,* 2005). Studies have suggested that it occurs in high numbers on the edge of the Benguela upwelling system (*Little et al.,* 1997; *Chen et al.,* 2002; *West et al.,* 2004) where it prefers mesotrophic but higher nutrient levels of filaments which have upwelled from shallower depths (*Little et al.,* 1997). Plots of the MARGO reference dataset used in the transfer function (Fig. 4.11a) show that those sites in the South Atlantic with elevated levels of *N. pachyderma* (d)

similar to that seen during MIS 2 (40 – 45 %) at MD02-2589 are only found in and around the Benguela Current upwelling system. Similarly sites forming a transect from 30 – 55 °S in the South Atlantic (Fig. 4.11b: *Niebler and Gersonde,* 1998) again predominantly show elevated levels of *N. pachyderma* (d) in the upwelling area off the Namibian and South African coasts.

The distribution of shallow dwelling (0 - 50 m) species *Globigerina bulloides* is thought to be governed by nutrient levels rather than temperature (*Reynolds and Thunell,* 1985) and has higher abundances associated with periods of enhanced phytoplankton productivity, be that upwelling conditions or spring bloom (*Guptha and Mohan,* 1996; *Zarić et al.,* 2005). During TI the abundance of *G. bulloides* remains fairly stable, with no raised abundances during MIS 2. This therefore suggests that the high levels of *N. pachyderma* (d) seen during MIS 2 are not responding to an increase in surface productivity, or upwelling that reaches the near surface zone.

The strength and position of the ACC is wind-driven with surface convergence and divergence, associated with the easterly and westerly winds in the Southern Ocean (*Toggweiler and Samuels,* 1995; 1998). The surface Ekman drift associated with the zonal winds that drive upwelling of waters from the deep ocean is not dependent on interior diapycnal mixing, and can proceed even if the vertical mixing rate in the interior tends to zero (*Watson and Naveira Garabato,* 2006). Studies have suggested that during glacial periods extended Antarctic sea ice causes an increase of the polar high, expansion of the polar vortex and therefore the northwards shift of the frontal systems and moisture bearing westerly winds (*Sigman and Boyle,* 2000; *Stuut et al.,* 2004). This northwards shift and intensification (*Esper et al.,* 2000) of the westerly wind belts, is thought to

increase the amount of upwelling of intermediate depth waters in the Subantarctic zone (*Sigman and Boyle,* 2000), with reduced upwelling of deep waters in the Antarctic zone (*Toggweiler et al.,* 1999, 2006). As well as this increase in upwelling, the northwards expansion of the PF and SAF and the minor movement of the STF (*Gersonde et al.,* 2003, 2005) causes a steepening of the hydrographic (surface temperature) gradients around the STF and Subantarctic Zone, increasing the velocity of zonal water transport (*Gersonde et al.,* 2003, 2005) and the movement of nutrients from upwelling areas in the Subantarctic zone to the STF region. This increase in upwelling and zonal transport to lower surface waters around the base of thermocline can explain the anomalously high levels of *N. pachyderma* (d) during glacial periods and the apparent consistent levels of *G. bulloides.* This is further confirmed by results of the PCA analysis (Fig. 4.8) which shows that when levels of *N. pachyderma* (d) are high, levels of *Globorotalia inflata* are low. *G. inflata* is though to inhabit areas with low nutrient content and reduced primary productivity (*Niebler and Gersonde,* 1998) and therefore a reduction in abundance, combined with an increase in *N. pachyderma* (d) would again suggest enhanced productivity and nutrient levels.

The planktonic $\delta^{18}O$, SST, position of the STF and the main taxa (Fig. 4.4a, c, f, 4.5) suggest that MIS 2 had very little variability, certainly compared to MIS 6, although this may be an issue of temporal resolution. During MIS 2 the relative position of the STF proxy (Fig. 4.5f, 4.3f) suggests that the STF may be further north than MIS 6, although the IRD levels are significantly lower (Fig. 4.4j) and the main differences in taxa are lower values of transitional taxa *Globorotalia inflata* and higher abundances of *N. pachyderma* (d). Although as discussed earlier caution should be used when discussing the MIS 2 SST record, the higher values may be used to explain the lower IRD levels,

perhaps with changes in the temperature of the isotherms associated with the fronts (*Gersonde et al.*, 2005) or a persistent influence of the Agulhas Current explaining the combination of a northwards extended STF and higher SST. This is consistent with previous studies in the throughflow region (Core GeoB3603-2; 35.07 °S, 17.32 °E) and the STF zone which have shown only a 1 – 2 °C decrease in temperatures in the LGM from the present day due to the continued presence of Agulhas leakage (*Gersonde et al.*, 2003) with substantial SST warming in the Cape Basin area during peak MIS 2 (*Sachs et al.*, 2001).

The increase in salinity and $\delta^{18}O_{sw}$ between 20.3 – 18.1 ka (although again influenced by the no-analog SST estimations), unlike MIS 6, is not associated with a SST increase which suggests that it may not be related to a pooling effect of warm Indian Ocean water at the site. However the slight southwards movement of the STF (Fig. 4.4f) to around MIS 6 levels and slight increase in NSTF fauna over this period might indicate an increased flux and pooling of warmer more saline waters over the site with the SST signal still being obscured by the large levels of *N. pachyderma* (d). Indeed the % *N. pachyderma* (d) record shows an increase at the same time at the SSS increase, potentially suggesting that the SST did increase over this period. Whilst high productivity obviously affects the relative abundances of *N. pachyderma* (d) during MIS 2, it is also likely to affect the abundances of *N. pachyderma* (s). *N. pachyderma (s)* also likes upwelled, nutrient rich waters (*Little et al.*, 1997) and this would therefore mean that the productivity effect on *N. pachyderma* (s) and *N. pachyderma* (d) is cancelled out in the % *N. pachyderma* (d) record. So, as in TII, there appears to be a pooling event associated with a SST and SSS increase and minimal movement of the STF and major taxa before any wider Southern Ocean warming occurs.

The Northern Hemisphere has a far greater ice volume change over glacial to interglacial timescales than the Southern Hemisphere. The initial Southern Ocean warming seen at MD02-2589 at 18.2 ka in the position of the STF and species assemblage records is in line with increasing Northern Hemisphere summer insolation and decreasing Southern Hemisphere summer insolation (*Laskar,* 1990; *Berger,* 1992) and coincides with a rapid decrease in the $\delta^{18}O$ record to a peak (16.5 ka) at the southern most extent of the STF, lowest SSS and SST values. The $\delta^{18}O$ record then remains stable until 14.4 ka when it starts to increase rapidly again. The GRIP ice core dates the start of the TI in the Northern Hemisphere as 14.5 ka (*GRIP members,* 1993) and it can therefore be suggested that the $\delta^{18}O$ record of MD02-2589 is showing rapid early Southern Ocean warming and reduction in Antarctic ice volume, which as it is only a small change in volume happens quickly, stabilising at interglacial levels for ~2 ka before changes in Northern hemisphere ice volume starting at 14.5 ka produce the second decrease in values.

At the start of the ice volume defined termination (18.2 ka) there is a rapid switch from Subantarctic taxa to Subtropical to Transitional taxa, decrease in SSS and a slight decrease in SST, to low values at 16.5 ka consistent with a pulse event similar to that seen at TII. Other studies have shown an increase in Southern Ocean SST at 17 - 18 ka (*Bard et al.,* 1990b; *Cortese and Abelmann,* 2002; *Bianchi and Gersonde,* 2004), coincident with a warming in Antarctic ice cores (*Petit et al.,* 1999; *Jouzel et al.,* 2001) and a rapid decrease in sea ice from 19 – 18 ka to its modern position (*Shemesh et al.,* 2002). This warming probably coincides with Heinrich event 1 in the North Atlantic (18 - 16 ka: *Grousset et al.,* 2001; *Hemming,* 2004) and adds weight to the 'bipolar seesaw'

hypothesis (e.g. *Broecker,* 1998) of warming of the Southern Ocean as the North Atlantic cools and freshens.

This period of Southern Ocean warming is characterised in the MD02-2589 record as a trend towards lower SST and lower SSS, despite an increase in ALF, NST and ST/Tr fauna. Whilst the slight decrease in SST and SSS over this period is probably accentuated by the high LGM values, it is plausible for the same reasons as the decreases seen at 134.3 ka during TII. Although the position of the STF proxy is relative and therefore cannot be translated into a distance, the small increase in values suggests that the STF only moved as far south as its position during the TII event at 134.3 – 128.9 ka rather than full MIS 5e levels and the decrease seems to span about the same time period as the event at TII (2.6 ka for TII, 2.7 ka for TI). This again suggests a pulse or release of the pooled heat and salt in the throughflow region, coincident with a southwards movement of the STF. Higher levels of ALF at the site at this time suggest that there is a greater proportion of Agulhas Current waters within the ARC and AR region compared to Subantarctic waters and this may again signify increased interbasin exchange.

However unlike the smooth warming event at TII, the TI event appears to be punctuated by high variability consistent with latitudinal fluctuations of the STF on periods far shorter than the resolution of the core (Fig. 4.4f), although as previously discussed the number of AMS ^{14}C reversals at the top of the core suggest possible coring disturbance which may be producing these fluctuations. Apart from $\delta^{18}O$, the other main proxies all detail this variability but the phasing is not constant between different proxies probably reflecting the shorter timescales involved (Fig. 4.4). Several studies have shown large temperature and salinity gradients over the STF (*Chang, et al.,* 1999; *Flores et al.,* 1999;

Schaefer et al., 2005), with the front also being associated with elevated surface productivity relative to the surrounding water masses (*Nodder and Northcote,* 2001) which is seasonal, with two to five times greater biomass in the spring than in the winter (*Bradford-Grieve et al.,* 1997). It is therefore plausible that the rapid, large fluctuations, up to 2 °C seen in the SST record, and 1.3 in 200 years, SSS records and in the % *N. pachyderma* (d) record (Fig. 4.4c, e, g) are recording the large temperature and salinity differences either side of the STF, whilst the number of planktonic foraminifera (an indicator of productivity; Fig. 4.4i) is recording the large changes in surface productivity associated with the STF itself and the surrounding waters. However this only remains a possibility as it is difficult to distinguish between changes caused by the fluctuations in the proportion of different source waters within the AR and ARC and those caused by pure frontal movements alone. The position of the STF proxy shows small latitudinal fluctuations within the general southward trend and it may be that these fluctuations also occur in the TII event, but the lower sedimentation rate at that time (Fig. 3.4c) means that the record has been smoothed. If that is the case then it would suggest that the early warming recorded in Southern Ocean records is more complex than initially thought.

The final notable feature of TI is the decreasing SST and SSS (Fig. 4.4c, e) from 12.9 ka to a low point at 12.3 ka followed by a rapid shift in SST, SSS, a 1 ‰ decrease in $\delta^{18}O$ (Fig. 4.4a) lasting ~0.3 ka, northwards shift of the STF, increase in fragmentation and sharp increase in productivity (Fig. 4.4i). Other Southern Ocean marine records see a SST cooling, increase in sea ice and IRD often associated with the ACR (*Shemesh et al.,* 2002; *Cortese and Abelmann,* 2002; *Bianchi and Gersonde,* 2004). The onset of the ACR as defined by the Antarctic ice cores (*Blunier et al.,* 1997; *Morgan et al.,* 2002) is 15 - 14 ka, but the exact timing of this event in marine cores is still open to uncertainty.

The start of the cooling at MD02-2589 1.1 ka later than the youngest estimates for the ice cores possibly reflects the lag of 800 years calculated for the response time of the oceans (Oceanic Cold Reversal: *Stenni et al.*, 2001) to the ACR, although uncertainties surrounding the exact reservoir correction that should be applied for the Southern Ocean could also affect the correlation.

4.3.3 MIS5a/4 Transition

The planktonic $\delta^{18}O$ shift of 1.2 ‰ (Fig. 4.6a) is in line with the 1.0 - 1.2 ‰ shift suggested for interglacial to glacial ice volume changes (*Schrag et al.*, 2002), suggesting that limited temperature and or salinity changes affected the $\delta^{18}O$ record. However although the values of $\delta^{18}O$ during MIS 4 (Fig. 4.1a) are as positive as during glacial stage MIS 2 and 6, the values during MIS5a are higher than would be expected for a full interglacial stage and therefore the magnitude of the $\delta^{18}O$ shift does not represent full interglacial to glacial conditions. The total SST shift of 2 °C (Fig. 4.6c) over the termination is significantly smaller than that seen at TII (3.6 °C) and this may again relate to the fact that MIS 5a is not a full interglacial period. A sea level record from Papua New Guinea and Barbados (*Cutler et al.*, 2003) shows a 57 m sea level drop from 76.2 – 70.8 ka due to rapid Northern Hemisphere ice sheet growth. This sea level drop is about half that seen at TI and TII further suggesting that part of the $\delta^{18}O$ record is being influenced by salinity and or temperature changes, with the SST and % *N. pachyderma* (d) records (Fig. 4.6c, g) suggesting that it is the latter rather than SSS, which shows reasonably consistent values over the transition (Fig. 4.6e).

The period of 73 - 70.8 ka, during the planktonic $\delta^{18}O$ transition, exhibits a high degree of variability, both in the individual species records and the SST, SSS, position of the STF and % *N. pachyderma* (d) records. The position of the STF shows a northwards excursion at 73.4 ka lasting 1.3 ka, coincident with peak SST and % *N. pachyderma* (d). The reduction in warm taxa (ALF, NSTF and ST/Tr) over this period is consistent with a northwards movement of the STF, although the most notable feature of this period is the large and rapid switches in dominance between transitional species *Neogloboquadrina pachyderma* (d) and *Globorotalia inflata* (Fig. 4.7d, e). The abundance of *N. pachyderma* (d) peaks at values similar to MIS 2 and as both of these species are deep dwellers this may be explained by the factors controlling each species. As explained earlier high abundances (>30 %) of *N. pachyderma* (d) are suggested to be associated with high productivity upwelling regions whilst *G. inflata* prefer low nutrient content waters with reduced primary productivity (*Rau et al.*, 2006). Therefore the very rapid increase in dominance of *N. pachyderma* (d) (11 % increase) and decrease in *G. inflata* may be reflecting an upwelling event of nutrient rich waters to the near surface which lasted 0.3 ka, followed by a rapid decrease in nutrients and an associated increase in *G. inflata* of 12 %.

After the SST maximum at 72.3 ka both the SST and % *N. pachyderma (d)* record show a rapid decrease in temperature coincident with a southwards movement of the STF (Fig. 4.6c, f, g). This phasing underlines the complexity of the region, as in other sites a southwards movement of the STF would bring warmer surface waters over the site (*Wilson et al.*, 2005), not colder waters as suggested by the MD02-2589 record. However the southwards movement of the STF is only indicated by a small shift in values which, as it is a relative proxy, may not be large enough to suggest any major movement in the

frontal system, rather some small alternative control on either *Globorotalia truncatulinoides, Globorotalia inflata* or *Neogloboquadrina pachyderma* (d) (used in determining the ratio) may be producing the small change in values.

The most striking feature of the transition is the very large peak in IRD over 6 times greater than the average glacial IRD values (Fig. 4.1c). Interestingly whilst peak IRD is associated with an increase in $\delta^{18}O$ values (Fig. 4.6a), possibly due to a cooling or reduction of salinity in surface waters (planktonic $\delta^{18}O$ has a significant temperature and salinity component) associated with increased fresh water from icebergs, the SST and associated SSS records actually show higher SST and SSS. A study near the STF in the Indian Ocean (*Manthe et al.*, 2003) showed that distinct but low magnitude increases in lithic grain concentrations suggested little-modified surface hydrology with no evidence of significant variation in $\delta^{18}O$ isotopic anomalies. Although the major peak in MD02-2589 is significantly larger than the background glacial IRD for the rest of the core, it only reaches values of 250 grains/g and therefore can still be considered to be a low magnitude event which may not have impacted the surface hydrology.

The provenance of the IRD is uncertain, with the interpretation of IRD in the northern edge of the ACC region difficult to interpret due to surface water temperature over- prints which controls the survival of icebergs, possible rafting of volcanic ashes in sea ice, input from volcanic sources not linked to climate variability and possibility of IRD sources of either the West or East Antarctic ice sheets, which both have very different dynamics (*Diekmann et al.*, 2003). A way to separate out the volcanic factors is to calculate the fluxes of ice-rafted quartz, which are though to be derived from Antarctic sources only

(*Smith et al., 1983; Labeyrie et al.,* 1986*; Kanfoush et al.,* 2000), although caution is needed as the East and West Antarctic sources differ widely.

The IRD peak at the MIS5a/4 transition at MD02-2589 is composed of 40 – 65 % predominantly angular to sub-angular quartz (Fig. 4.12a, b), with the rest being mainly made up of vesicular basaltic or andesitic scoria (Fig. 4.12a, c), with little ash. The Antarctic Peninsula is the main source of quartz to the southern Indian Ocean (*Manthe et al.,* 2000) with some icebergs calving off Antarctica turning northwards and being

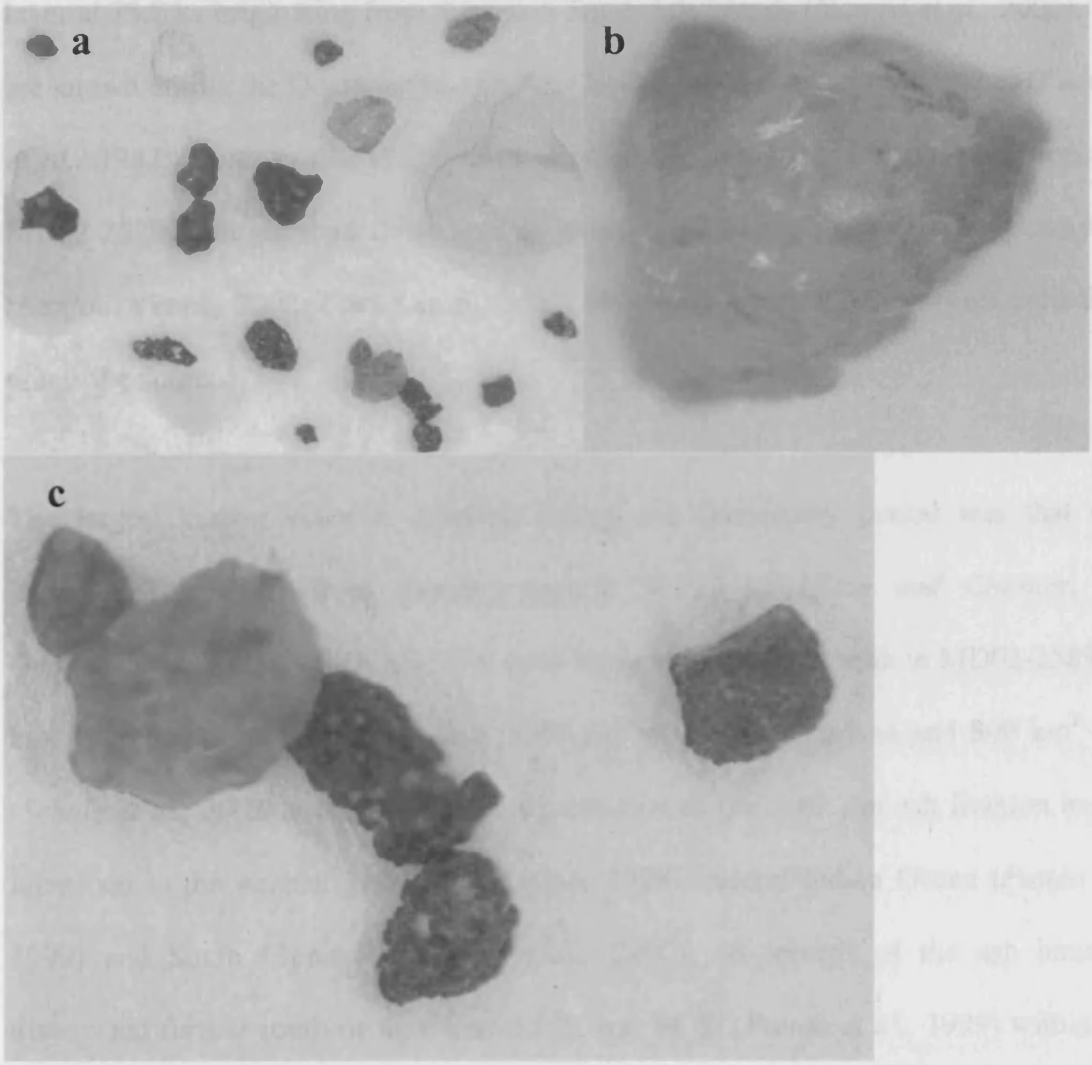

Figure 4.12 Microscope photos of IRD grains from MD02-2589 (a) part of a sample from 70.8 ka showing both quartz and vesicular grains, (b) a typical quartz grain, (c) some typical dark, vesicular basaltic or andesitic scoria

captured by the eastwards flowing ACC (*Tchernia and Jeannin,* 1983). Figure 4.1c shows that although quartz only makes up about half of the main IRD peak, its concentrations are still significantly higher than the MIS 6 and 2 glacial levels suggesting that the peak is originating from ice rafting rather than direct volcanic sources. It is very unlikely that the IRD event coincided with a large volcanic eruption which deposited large amounts or basaltic or andesitic material over the site and therefore this material was transported by the icebergs. The EPICA ice core does record a discrete volcanic ash layer at 73.7 ka originating from the South Sandwich Islands (*Narcisi et al.,* 2005), which are known during the Quaternary to produce both basasltic and andesitic ashes (*Federman et al.,* 1982*; Smith et al.,* 1983*; Hubberten et al.,* 1991) but as the abundance at site MD02-2589 is larger than those seen in many other records from the Southern Ocean (*Kanfoush et al.,* 2002; *Carter et al.*, 2002; *Diekmann et al.,* 2003) it seems unlikely that this is the source.

The largest known volcanic eruption during the Quaternary period was that of the Younger Toba Tuff from Sumatra around 74 ±2 ka (*Rose and Chesner,* 1990; *Oppenheimer,* 2002), which is within error margins of the IRD peak in MD02-2589 (70.8 ka). The eruption produced at least 3000 km^2 of rhyolitic magma and 800 km^2 of ash (*Schulz et al.,* 2002) and although the distribution of the > 63 μm ash fraction has been identified in the Arabian Sea (*Schulz et al.,* 1998), central Indian Ocean (*Pattan et al.,* 1999) and South China Sea (*Song et al.,* 2000), no records of the ash have been discovered further south or west than 15 °S and 64 °E (*Pattan et al.,* 1999) within either the South Atlantic or Southern Oceans. The GISP2 ice core record shows a sulphur peak attributed to the Toba eruption (*Zielinski et al.,* 1996) and several studies have suggested

that a 'volcanic winter', a mean surface temperature drop of 3 – 5 °C (*Sigurdsson,* 1990; *Chesner et al.,* 1991; *Rampino and Self,* 1992; 1993) could have been responsible for the abrupt shift to glacial climates over the MIS 5a/4 transition. However evidence for this Toba-triggered volcanic winter are ambiguous (*Oppenheimer,* 2002; *Schulz et al.,* 2002) and as the IRD peak in MD02-2589 is primarily composed of quartz and scoria, which is probably basaltic in nature, rather than rhyolitic as in the Toba Tuff, it is unlikely that this peak is recording this eruption, although some discrete tephra shards may originate from this eruption.

Whilst IRD fluxes are highest during interglacial stages in the Weddell Sea area (*Ó Cofaigh et al.,* 2001), they are higher during glacial periods towards the northern edge of the ACC, due to SST being the major control on their distribution (*Smith et al.,* 1983; *Labeyrie et al.,* 1986; *Allen and Warnke,* 1991; *Becquey and Gersonde,* 2002). Studies have shown that the northernmost extent of the Southern Ocean IRD layers, around 41 °S, was significantly north of the PF even during the LGM (*Kanfoush et al.,* 2000, 2001; *Carter et al.,* 2002). This has been used to suggest that these IRD events are not simply an artefact of increased iceberg survivability due to decreased SST, as the numbers of icebergs must have been of sufficient size or number to survive the comparatively warm SST up to 41 °S (*Kanfoush et al.,* 2000). It can therefore be suggested that the large peak in MD02-2589 is not necessarily linked to SST. *Grobe and Mackensen* (1992) show that at the transition from interglacial to glacial periods there is intense ice rafting in the Weddell Sea region at the beginning of the transition which decreases at the onset of the glacial maxima. It is plausible that some of this increased rafting could have survived out to 41 °S producing the large IRD spike.

Only core PS2564-3 (46.14 °S 35.90 °E, 3034 m water depth; *Diekmann et al.*, 2003) from the Southern Ocean shows similar IRD abundances at the transition, although core TN057-21 (41.08 °S, 7.49 °E, 4981 m water depth; *Kanfoush et al.*, 2000) also shows a smaller magnitude short lived IRD peak (~75 grains/g) centred at ~74 ka. During the MIS5a/4 transition in the Antarctic ice cores is a warm event A5 (*Blunier and Brook*, 2001) seen in the Vostok δD record (*Petit et al.*, 1999) as well as δD records from the Byrd (*Blunier and Brook*, 2001) and EPICA Dome C ice cores (*Jouzel et al.*, 2004). The IRD peak maximum event in MD02-2589 and PS2564-3 might indeed correlate with this warm event and indicate a localised collapse of an Antarctic ice shelf at the end of the prolonged warm event A5 producing increased iceberg distribution over the Agulhas Plateau sector of the Southern Ocean.

A further comparison of the full IRD record of MD02-2589 with those of *Kanfoush et al.* (2000); TN057-21, TN057-10 (47.06 °S, 5.55 °E, 4390 m water depth) and TN057-13/1094 (53.18 °S, 5.13 °E, 2807 m water depth); shows that certainly though MIS 3 the MD02-2589 record records similar background levels to core TN057-21, which is at a similar latitude, with larger events identified by *Kanfoush et al.* (2002) as South Atlantic IRD events (SA events). These events in MD02-2589 (24.2, 33.4, 36.2 - 37.2, 40.6, 41.8 - 42.7 ka) rising from background levels around 15 grains/g to ~30 grains/g during MIS 3 coincide with SA events 1 – 4, suggesting that these events can be identified over the wider South Atlantic area of the Southern Ocean.

4.3.4 Carbon Isotope Minimum Events

Minima in planktonic $\delta^{13}C$ can be seen in figure 4.1 to occur during TI and TII, significantly after the planktonic $\delta^{18}O$ shows the beginning of the deglaciation. The low values seen in MIS 4 also occur during the transition in the planktonic $\delta^{18}O$ record from MIS4 to 3, rather than in the peak ice volume of the glacial stage. The $\delta^{13}C$ of planktonic foraminifera have been used as to reconstruct the $\delta^{13}C_{DIC}$ of past surface water masses (*Curry and Crowley,* 1987*; Mulitza et al.,* 1999*; Mortyn et al.,* 2002), although the processes controlling the carbon isotope composition are complicated, as carbon incorporated in the shell may be derived from different sources, which are related to different processes (*Peeters et al.,* 2002) and the reconstruction relies on knowing whether the foraminifera species used precipitates its calcite in equilibrium with the ambient seawater or has predictable offsets (*Peeters et al.,* 2002).

The minimum in $\delta^{13}C$ values during deglaciations has been noted in other cores from the Indo-Pacific tropics through to the Southern Ocean (e.g. PS1768-8 (52.35 °S, 4.25 °E, 3270 m water depth) *Mulitza et al.,* 1999; ODP Site 1089 (41.08 °C, 7.49 °E, 4981 m water depth) *Mortyn et al.,* 2002*; Shackleton et al.,* 1983*; Ninnemann and Charles,* 1997*; Spero and Lea,* 2002). Causes of this minimum have been suggested as changes in surface water hydrography, higher carbonate ion contents of Southern Ocean waters or changes in stratification of the water column associated with thermohaline changes, with the origin of the signal in the Subantarctic surface waters being transported through the ocean basins by AAIW (*Lynch-Stieglitz et al.,* 1994*; Ninnemann and Charles,* 1997*; Spero and Lea,* 2002). However *Pahnke and Zahn* (2005) show that the $\delta^{13}C$ values of AAIW during these carbon minima events was actually positive, suggesting that AAIW

cannot be the primary transport route of this signal, rather it is likely to have been transported at SAMW depth.

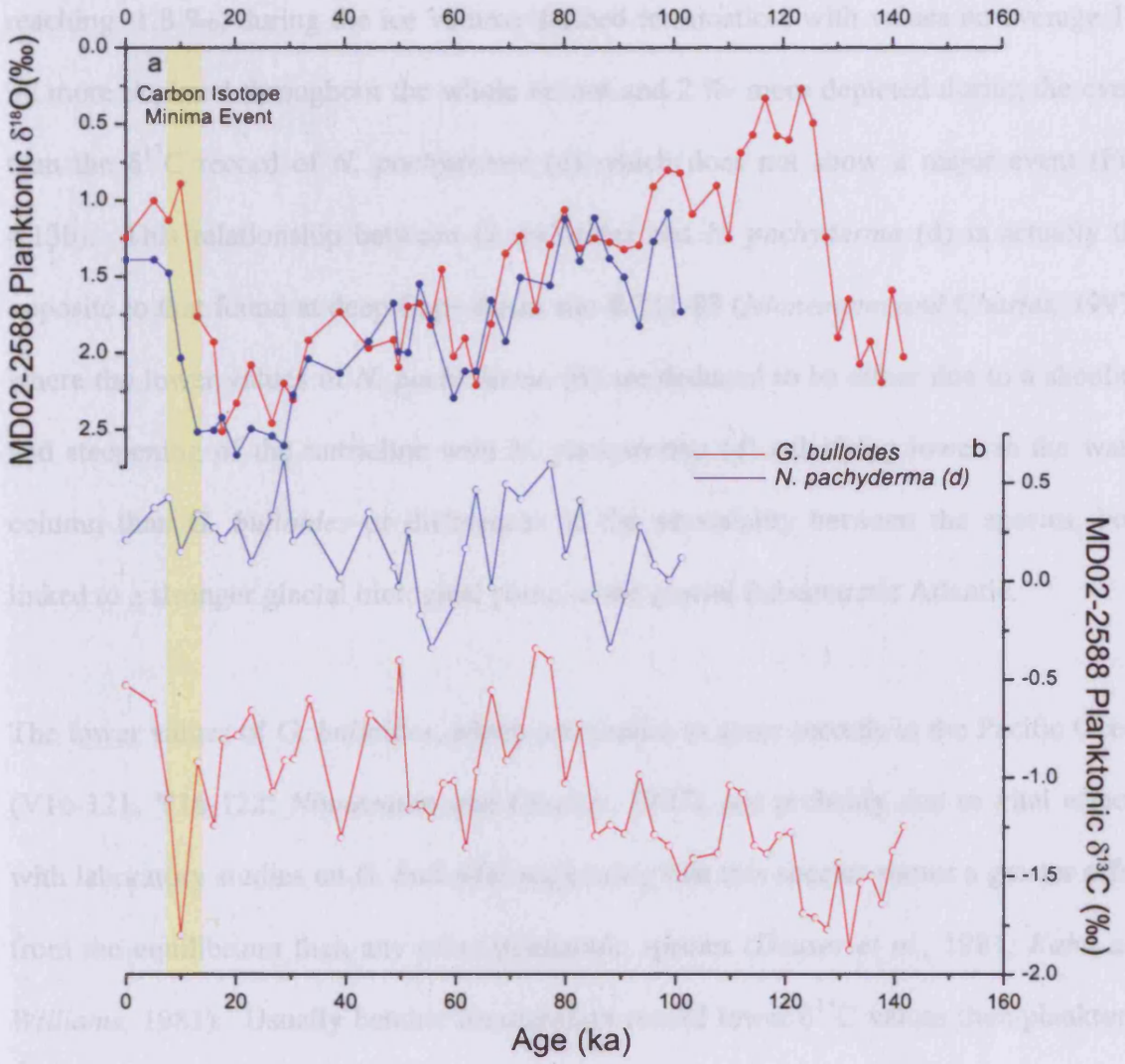

Figure 4.13 Planktonic isotope data of species *G. bulloides* and *N. pachyderma* (d) from core MD02-2588 showing a carbon isotope minima event in the $\delta^{13}C$ of *G. bulloides* but not *N. pachyderma* (d) (b) during Termination I in the $\delta^{18}O$ record (a)

The $\delta^{13}C$ minima at TI reaches values of -1.9 ‰ (Fig. 4.1b), which is significantly lower than $\delta^{13}C$ values recorded for other *Globigerina bulloides* records in the Pacific (-0.5 – 0.0 ‰), Indian (0.4 ‰) or Atlantic (0.0 ‰) Oceans (*Ninnemann and Charles,* 1997). Low resolution planktonic isotopes of *G. bulloides* and *Neogloboquadrina pachyderma*

(d) were run on core MD02-2588 (41.19 °S, 25.49 °E, 2907 m water depth), which is geographically very close to MD02-2589. As in MD02-2589 the $\delta^{13}C$ values of *G. bulloides* from MD02-2588 (Fig. 4.13) show a very negative event at TI (with values reaching -1.8 ‰) during the ice volume defined termination, with values on average 1.2 ‰ more depleted throughout the whole record and 2 ‰ more depleted during the event than the $\delta^{13}C$ record of *N. pachyderma* (d) which does not show a major event (Fig. 4.13b). This relationship between *G. bulloides* and *N. pachyderma* (d) is actually the opposite to that found at deep Cape Basin site RC11-83 (*Ninnemann and Charles,* 1997), where the lower values of *N. pachyderma* (d) are deduced to be either due to a shoaling and steepening of the nutricline with *N. pachyderma* (d) calcifying lower in the water column than *G. bulloides* or differences in the seasonality between the species, both linked to a stronger glacial biological pump in the glacial Subantarctic Atlantic.

The lower values of *G. bulloides*, which are similar to some records in the Pacific Ocean (V16-121, V16-122; *Ninnemann and Charles,* 1997), are probably due to vital effects, with laboratory studies on *G. bulloides* suggesting that this species shows a greater offset from the equilibrium than any other planktonic species (*Deuser et al.,* 1981; *Kahn and Williams,* 1981). Usually benthic foraminifera record lower $\delta^{13}C$ values than planktonic foraminifera due to the enrichment of bottom waters with ^{12}C, but several studies have shown that the planktonic species *G. bulloides* has values that are significantly lower (~1 ‰) than that of benthic foraminifera (*Berger et al.,* 1978; *Naidu and Niitsuma,* 2004), which holds for MD02-2589 (Fig. 4.1b and Fig. 5.1b).

The presence of a carbon isotope minima event at TI in *G. bulloides* and not *N. pachyderma* (d) may relate to the proposed mechanism linked to changes in the

stratification of the water column (*François et al.*, 1997; *Toggweiler*, 1999; *Spero and Lea*, 2002; *Mortyn et al.*, 2002). An increase in the stratification of the interior ocean, reduced vertical mixing and a deep divide whereby the deep and lower intermediate waters (LCDW: *François et al.*, 1997) are isolated from the upper waters and the flux of CO_2 from the deep ocean to the atmosphere is reduced occurred during glacial periods. Mechanisms for this increased stratification include Antarctic sea-ice induced stratification (*Stephens and Keeling*, 2000), northwards shift of the polar easterlies that produce intermediate rather than deep water upwelling (*Sigman and Boyle*, 2000) or changes associated with deep thermohaline circulation mode shifts (*Toggweiler*, 1999). The carbon isotope minimum events during the terminations are considered to be due to the breakdown of this water column stratification associated with upwelling and advection of low $\delta^{13}C$ deep waters to the surface (*Spero and Lea*, 2002). *N. pachyderma* (d) is thought to dwell at deeper depths than *G. bulloides* and therefore it is possible that the glacial stratification of the water column occurred above the dwelling position of *N. pachyderma* (d) and below *G. bulloides*. This would mean that during glacial periods the two species lived in different $\delta^{13}C$ signature water masses, with *N. pachyderma* (d) living in the low $\delta^{13}C$ water mass. As the stratification breaks down the upwelling of these waters to the surface only effects the values of *G. bulloides*, which until then has been living in relatively high $\delta^{13}C$ waters. A further suggestion of topographically-induced upwelling by the Agulhas Plateau of $\delta^{13}C$ depleted deep waters to the mixed layer, whilst explaining the low $\delta^{13}C$ values of *G. bulloides* cannot explain the discrepancy between the two species, especially as *N. pachyderma* (d) is a deeper dwelling species.

The presence of low $\delta^{13}C$ values during TII (Fig. 4.1b, 4.13b) confirms suggestions that this is a persistent feature of glacial Terminations (*Mortyn et al.*, 2002), although the

sharp decrease in values into the event seen at TI is not evident at TII, suggesting that perhaps the breakdown of stratification occurred more gradually.

4.4 Conclusions

Planktonic foraminifera assemblage data combined with SST and SSS salinity estimates for the Southern Agulhas Plateau suggest that there is a pooling of warm, salty waters in the Agulhas throughflow region towards the end of glacial periods MIS 2 and 6 prior to any Southern Ocean warming. The northwards position of the frontal systems associated with the ACC during glacial periods reduces the exchange of waters between the Indian and Atlantic Oceans through the Agulhas retroflection region and therefore warm, salty water transported to the region by the Agulhas Current pools in the region.

Early Southern Ocean-wide warming in late MIS 6 and 2 releases a pulse of the pooled warm, salty water into the Atlantic Ocean through the throughflow region although the early Southern Ocean warming detailed in other studies may be more complex than initially thought with latitudinal movements of the fronts occurring on short timescales. This pulse of heat and salt through the throughflow region occurs ~6.7 ka before an Antarctic Cold Reversal-like event at Termination II which is associated with the resumption of NADW formation in the North Atlantic.

The MIS5a/4 glacial inception is punctuated by a short lived cold event and upwelling of high-nutrient waters to near surface depths. The large pulse of IRD seen at the MIS5a/4 transition may be either related to a local calving event associated with either Antarctic event A5 or increased calving during the transition. The source of the IRD spike is likely

to be Antarctica with the predominance of the quartz in the peak suggesting that it is ice rafted rather than fall out from the Toba mega eruption. IRD peaks within the record correspond with South Atlantic events 1 - 4 (*Kanfoush et al.*, 2002) during MIS 3 suggesting that these are wider Southern Ocean events.

A carbon isotope minima event, identified in other records from the Southern Ocean (*Mulitza et al.*, 1999; *Mortyn et al.*, 2002; *Shackleton et al.*, 1983; *Ninnemann and Charles*, 1997; *Spero and Lea*, 2002), can be seen in the planktonic $\delta^{13}C$ record of MD02-2589 at TI and to some extent TII. Stable planktonic isotope analysis on nearby core MD02-2588 shows that this event is present in the $\delta^{13}C$ record of species *Globigerina bulloides* but not that of *N. pachyderma* (d) suggesting that the mechanism behind the events is possibly linked to a reduction in stratification of the water column at a depth between that of *G. bulloides* and *N. pachyderma* (d).

Chapter 5. Deep Water Variability On The Southern Agulhas Plateau: Interhemispheric Links Over The Past 170 ka

5.1 Introduction

This chapter presents a high-resolution multi-proxy record of deep water variability from sediment core MD02-2589 recovered from the southern flank of the Agulhas Plateau in the southernmost South Atlantic. The location is close to the southern mixing interface between NADW and Southern Source Waters (SSW) in the Southern Ocean enabling the reconstruction of the timing and amplitude of changes in southward advection of NADW and Southern Ocean THC. The site is also strongly influenced by the ACC. The flow of this current extends to depth, often to the sea bed (*Orsi et al.*, 1995) and is wind driven, suggesting that fluctuations in the surface conditions can influence deep-water dynamics. The position of the major frontal systems associated with the ACC can therefore be potentially related to changes in the near bottom flow regime and strength. This chapter concentrates on identifying the phasing between changes in ice volume, the location of surface ocean fronts, deep ventilation and near-bottom flow speeds over the past 170 ka.

5.2 Results

The high resolution benthic $\delta^{18}O$ record of MD02-2589 (Fig. 5.1a) shows that orbital modulation caused by changing ice volume is the dominant control on this record. However, as the glacial-interglacial (G-I) benthic $\delta^{18}O$ amplitudes of the record ($\delta^{18}O$ ~2 ‰) are significantly greater than the shift associated with global ice volume changes ($\delta^{18}O$ 1 - 1.2 ‰ (*Schrag et al.*, 2002)) additional hydrographic changes in regional bottom

water temperature and/or salinity are indicated over these timescales. The Holocene section in MD02-2589 is incomplete thus limiting confidence in the reliability of the LGM to Holocene transition to assess the full G-I $\delta^{18}O$ shift at this location. As a result in the following sections, only TII will be considered in detail. The benthic $\delta^{13}C$ record (Fig. 5.1b) shows a G-I amplitude of ~0.8 ‰ ranging from values of -0.2 – 0 ‰ indicative of low ventilation during glacial stages MIS 6 and LGM, as well as MIS 4, to increased levels during warm stages MIS 5 and 3, with a more steady transition at TII than observed in the benthic $\delta^{18}O$ record. In contrast to the benthic $\delta^{18}O$ the benthic $\delta^{13}C$ values remain fairly consistent throughout MIS 5, with only modest orbital modulation, with minimum benthic $\delta^{13}C$ values occurring 5 - 7 ka after maximum benthic $\delta^{18}O$ associated with each cold substage. Conversely, benthic $\delta^{13}C$ shows clear evidence for millennial-scale variability during MIS 3, which is not as apparent in the $\delta^{18}O$ record (Fig. 5.1).

The modern salinity distribution (Fig. 2.1b) for the Agulhas sector of the Southern Ocean shows that site MD02-2589 lies in the southern extent of NADW close to where it merges with LCDW. Present day NADW $\delta^{13}C$ in the South Atlantic typically has values of ~0.8 ‰ and LCDW is <0.5 ‰ (*Bickert and Wefer*, 1996). A transect of late Holocene benthic $\delta^{13}C$ in the South Atlantic (*Mackensen et al.*, 2001) confirms that MD02-2589 ($\delta^{13}C$ ~0.65 ‰, Fig. 5.1b) is currently positioned near the mixing zone between NADW and LCDW with the admixture of >50 % NADW (e.g. *Bickert and Mackensen,* 2003). Benthic $\delta^{13}C$ values in MIS 5 average 0.65 ‰, which again equates well with predicted $\delta^{13}C$ of NADW in the South Atlantic during interglacial periods (~0.6 - 0.7 ‰ (*Sarnthein et al.*, 1994)).

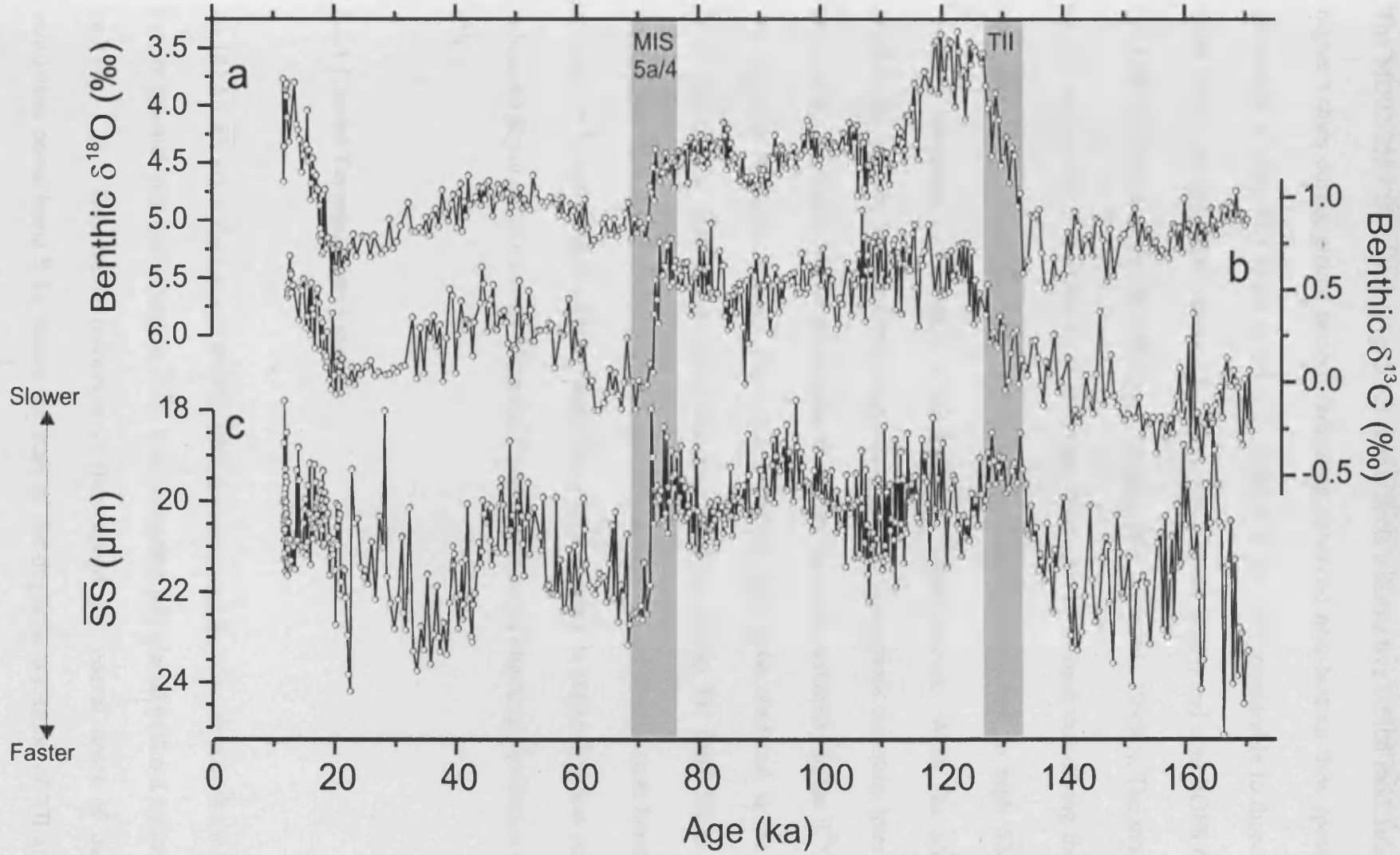

Figure 5.1. Benthic records of core MD02-2589 showing (a) benthic $\delta^{18}O$, (b) benthic $\delta^{13}C$, (c) sortable silt mean grain size. Intervals focused on in this study are highlighted by the shading. MIS5a/4 = Transition between Marine Isotope Stages 5a and 4, TII = Termination II.

The MD02-2589 $\overline{SS}$ record (Fig. 5.1c) also reflects a distinctive orbital modulation, with higher values during glacial periods indicating enhanced near-bottom flow speeds. The amplitude of these G-I shifts in $\overline{SS}$ (G-I shift of 4 μm) are comparable to those seen at ODP Site 1123 in the SW Pacific (3 - 4 μm, (*Hall et al.*, 2001)) and core BOFS 6K from the East Thulean Rise, North Atlantic (3 - 4 μm, (*McCave et al.*, 1995b)). The modulation of $\overline{SS}$ within MIS 5 is offset from that seen in benthic $\delta^{18}O$ such that during the colder substages MIS 5d and 5b flow speeds are in transition from low to high $\overline{SS}$ values reaching maximum values early in the following warm interval. While the $\overline{SS}$ record exhibits the highest degree of millennial-scale variance throughout the entire interval, it is noticeable that within MIS 3 amplitudes of millennial scale variability in the $\delta^{13}C$ record are likewise increased and are substantially greater than those observed in the benthic $\delta^{18}O$ record (Fig 5.1). A complex temporal phasing across TII (and TI) is evident between each of the proxy records but the inferred flow speed changes and benthic $\delta^{13}C$ records are broadly negatively correlated on orbital timescales suggesting that periods of enhanced physical circulation ($\overline{SS}$) went along with reduced chemical ventilation (benthic $\delta^{13}C$).

5.2.1 Glacial Terminations I and II

At 141 ka $\overline{SS}$ grain sizes at site MD02-2589 decrease rapidly coincident with the onset of a more gradual increase in benthic $\delta^{13}C$, both preceding full-glacial MIS 6.2 by some 3 - 4 ka (Fig. 5.2). This initial reduction in flow speed and coeval onset of increasing ventilation occur some 8 ka before the start of the deglacial transition of TII at 133 ka (Fig 5.2d, 5.2f). Although hampered by the lack of Holocene recovery the sequence of

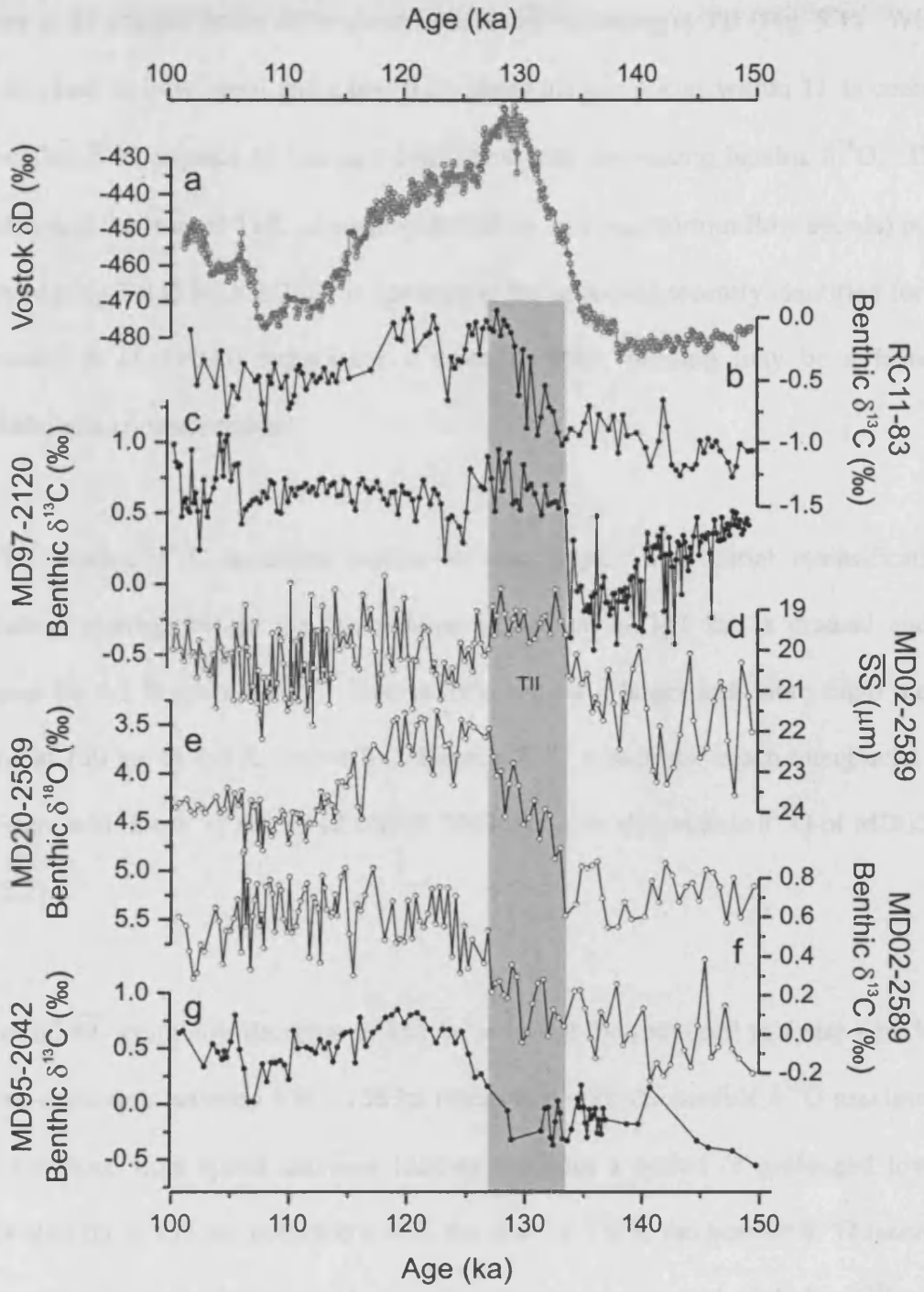

Figure 5.2. Southern hemisphere records for Termination II. (a) Vostok δD (*Petit et al.,* 1999), (b) RC11-83 benthic $\delta^{13}C$ (*Charles et al.,* 1996), (c) MD97-2120 benthic $\delta^{13}C$ (*Pahnke and Zahn*, 2005), (d) MD02-2589 sortable silt mean grain size, (e) MD02-2589 benthic $\delta^{18}O$, (f) MD02-2589 benthic $\delta^{13}C$, (g) MD95-2042 benthic $\delta^{13}C$ (*Shackleton et al.,* 2000). Gray shading shows TII as indicated by MD02-2589 benthic $\delta^{18}O$.

changes at TI suggest some differences from those occurring at TII (Fig. 5.1). While an early decrease in flow speed and a low-flow-speed plateau occurs within TI, in contrast to TII, benthic $\delta^{13}C$ appears to increase coincident with decreasing benthic $\delta^{18}O$. This TI sequence and the lead of THC changes (ventilation and near bottom flow speeds) over ice volume during TII in MD02-2589 is contrary to the sequence recently identified for TI by *Piotrowski et al.* (2005) suggesting a more complex phasing may be a feature of individual glacial terminations.

The TII benthic $\delta^{13}C$ transition occurs in two steps. The initial intensification in ventilation, starting before the ice volume maximum at 141 ka, is gradual and only increases by 0.2 ‰ over 11 ka. This is followed by a larger and more rapid increase, starting at 130 ka, of 0.6 ‰ over 6 ka. Benthic $\delta^{13}C$ values also reach interglacial levels coincident with the $\delta^{13}C$ record of MD95-2042 and after the benthic $\delta^{18}O$ of MD02-2589 (Fig. 5.2).

The initial $\overline{SS}$ grain size decrease at 141 ka is halted by a reversal to faster near bottom currents occurring between 139 - 138 ka coincident with the benthic $\delta^{18}O$ maximum. A more sustained flow speed decrease follows reaching a period of prolonged low flow speeds starting at 133 ka, coincident with the start of TII in the benthic $\delta^{18}O$ record, and lasting some 6 ka. A similar mid-termination feature is seen in the benthic $\delta^{13}C$ records of RC11-83 and MD97-2120 during TII but intriguingly does not appear in the benthic $\delta^{13}C$ record of MD02-2589 (Fig. 5.2).

5.2.2 MIS 5a-4 Transition

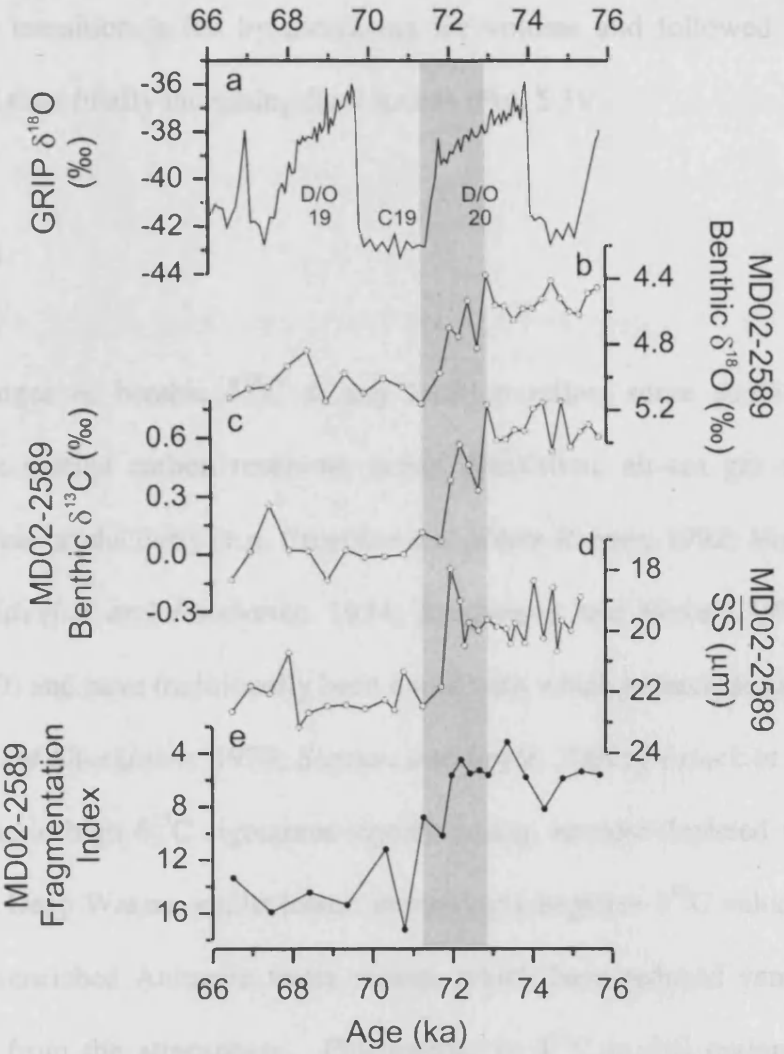

Figure 5.3. Proxy Records of the MIS 5a- 4 Transition. (a) GRIP $\delta^{18}O$ (*Johnsen et al.,* 1997), (b) MD02-2589 benthic $\delta^{18}O$, (c) MD02-2589 benthic $\delta^{13}C$, (d) MD02-2589 sortable silt mean grain size, (e) MD02-2589 fragmentation index. Grey shading shows the transition as defined in the text. Acronyms are D/O = Dansgaard-Oeschgar events, C19 = Greenland event (*McManus et al.*, 1994).

One of the most striking features seen in MD02-2589 records is the rapid transition between MIS 5a and MIS 4 (Fig. 5.1, 5.3). Based on our age model the transition starts at 73 ka from high benthic $\delta^{13}C$ values and low flow speeds. The transition proceeds with a sharp transient increase in benthic $\delta^{18}O$ of 0.45 ‰ and decrease in benthic $\delta^{13}C$ of 0.4 ‰.

Within 700 years of this excursion flow speeds rapidly decrease reaching a minimum at 72 ka. An abrupt transition then occurs in all proxies reaching full MIS 4 conditions at 71.3 ka. The transition is led by increasing ice volume and followed by decreasing ventilation and then finally increasing flow speeds (Fig. 5.3).

5.3 Discussion

Temporal changes in benthic $\delta^{13}C$ at any location reflect some combination of the changes in the marine carbon reservoir, ocean circulation, air-sea gas exchange, and marine biological productivity (e.g. *Broecker and Maier-Reimer,* 1992; *Mackensen et al.*, 1993; *Lynch-Stieglitz and Fairbanks,* 1994; *Mackensen and Bickert* 1999; *Oppo and Horowitz*, 2000) and have traditionally been a tool with which to trace deep water masses. (e.g. *Streeter and Shackleton,* 1979; *Sigman and Boyle,* 2000; *Bostock et al.,* 2004). In the South Atlantic high $\delta^{13}C$ signatures signify young, nutrient-depleted well-ventilated North Atlantic Deep Waters, whilst lower, increasingly negative $\delta^{13}C$ values are linked to older, nutrient-enriched Antarctic water masses which have reduced ventilation due to long isolation from the atmosphere. Fluctuations in $\delta^{13}C$ in this region are linked to variations in the proportion of better ventilated NCW vs lesser ventilated SCW. The mean grain size of the 10 – 63 μm size fraction ($\overline{SS}$) responds linearly to changes in flow conditions 20 – 100 m above the bed (*McCave et al.,* 1995b), with higher grain sizes denoting faster flow and vice versa. The region south of ~40 °S in the Southern Ocean is dominated by the ACC, with changes in $\overline{SS}$ plausibly reflecting variations in the strength of its flow. The ACC flow is driven by surface wind forcing which may affect the whole water column through frictional effects down to deeper depths (*Orsi et al.,* 1995) and is therefore linked into Southern Hemisphere climate change, as is the expansion and

contraction of the surface ocean fronts. However the strengthening and weakening of the ACC can also therefore be possible without frontal movements. These differences in tracer signals allow a decoupling of flow speed and water mass provenance at certain sites, which can be explained by changes in different components of a mixed water mass affecting either provenance or flow speed in different ways.

The export of NCW from the North Atlantic during glacial periods is poorly constrained and has been discussed controversially in the literature (e.g. *Sarnthein et al.*, 1994; *Yu et al.*, 1996; *Matsumoto et al.*, 2001; *Curry and Oppo,* 2005). In order to identify the NCW influence at the MD02-2589 site during glacial periods we compare our data with several existing benthic $\delta^{13}C$ records. For this comparison we have chosen deep South Atlantic cores RC11-83 (*Charles et al.*, 1996) and TN057-21 (Table 1 (*Ninnemann and Charles,* 2002)), which remained strongly influenced by SCW (i.e., AABW) over both glacial and interglacial periods. We also use core MD97-2120 (Table 1 (*Pahnke and Zahn*, 2005)) from the Chatham Rise, Southwest Pacific, as an alternative Southern Ocean record documenting AAIW variability. Finally, core MD95-2042 (Table 1 (*Shackleton et al.*, 2000)) from the Iberian Margin was chosen as a North Atlantic reference as it is high resolution, has a timescale that has been tied to both Vostok and GRIP and reflects changing northern versus southern water sources in the North Atlantic during glacial periods.

Core	Latitude	Longditude	Depth (m)	Reference
MD02-2589	41° 19'S	25° 15'E	2660	*This study*
RC11-83	41° 36'S	9° 48'E	4718	*Charles et al. (1996)*
TN057-21	41° 08'S	7° 49'E	4981	*Ninnemann and Charles (2002)*
MD97-2120	45° 32' S	174° 55' E	1210	*Pahnke and Zahn (2005)*
MD95-2042	37° 48'N	10° 10'W	3146	*Shackleton et al. (2000)*

Table 5.1. Station data for cores used in this chapter

Offsets in amplitude of the benthic $\delta^{18}O$ G-I shifts between MD02-2589 and sites RC11-83, MD97-2120 and MD95-2042 (Fig. 5.4), plausibly reflect differences in *T-S* changes of water masses bathing each site. Average glacial benthic $\delta^{18}O$ values at site MD02-2589 are between 0.3 - 0.7 ‰ heavier than average glacial values in cores from the South Atlantic (core RC11-83), North Atlantic (core MD95-2042) and SW Pacific (core MD97-2120) (fig, 5.4) suggesting that deep water at the Agulhas Plateau during the last two glacial periods was colder or saltier (or a combination of both) than deep waters in the North Atlantic and intermediate water in the southwest Pacific. Assuming that deep-ocean temperature in the glacial ocean was uniformly colder and presumably close to the freezing point of seawater (*Waelbroeck et al.*, 2002; *Adkins and Schrag* 2003) this makes seawater $\delta^{18}O$ and thus, salinity the most plausible candidates to have caused the observed offsets in benthic $\delta^{18}O$, although there was probably a very different salinity – $\delta^{18}O$ relationship during glacial periods to modern day. *Adkins et al.* (2002) and *Adkins and Schrag* (2003) suggest that the Southern Ocean had the saltiest LGM deep water due to increased sea-ice formation. As sea-ice formation offsets seawater $\delta^{18}O$ from its global correlation with salinity, some of the offset in benthic $\delta^{18}O$ seen in Fig. 5.2 may reflect the contribution of these Southern Ocean deep waters to the deeper core sites, namely RC11-83, which at 4600 m water depth and at a location close to the Southern Ocean most likely records modified AABW.

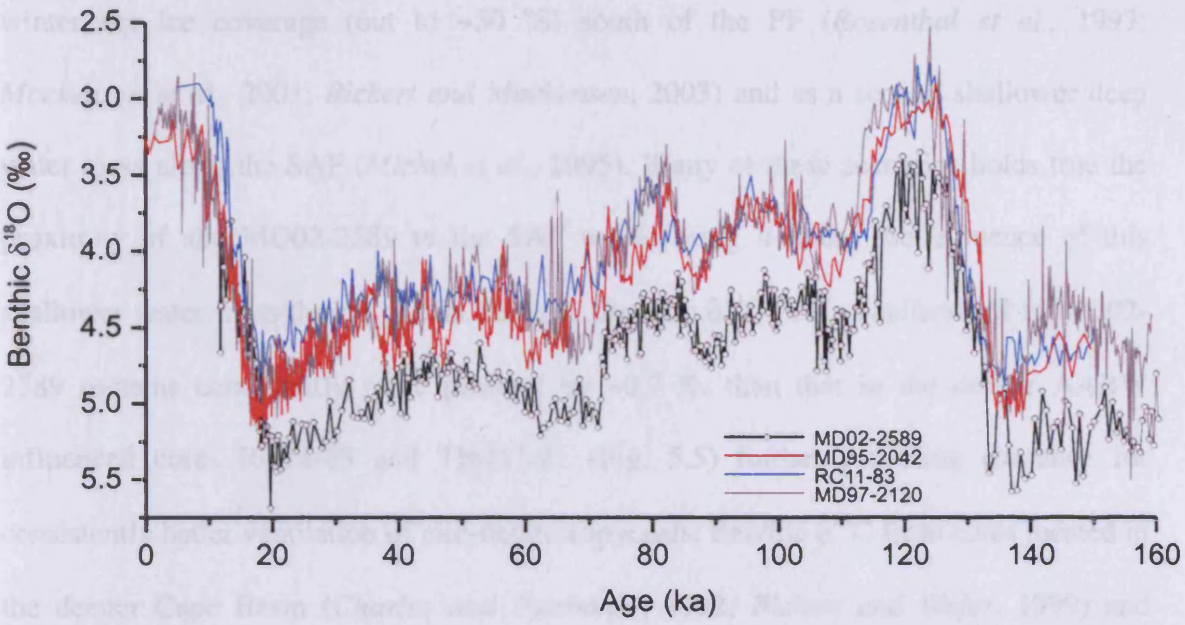

Figure 5.4. Records of benthic $\delta^{18}O$ of *Fontbotia wuellerstorfi* from MD02-2589, RC11-83 (*Charles et al.*, 1996), MD97-2120 (*Pahnke et al.*, 2003) and MD95-2042 (*Shackleton et al.*, 2000). All data are shown on the *Uvigerina* scale.

The mean-ocean shift of $\delta^{13}C$ in seawater ΣCO_2 between the LGM and Holocene has been estimated to between 0.32 ‰ (*Duplessy et al.*, 1988) and 0.46 ‰ (*Curry et al.*, 1988). The benthic $\delta^{13}C$ G-I shift observed in MD02-2589 of 0.8 ‰ (Termination II Fig. 5.1b) suggests an additional 0.3 - 0.4 ‰ variation in $\delta^{13}C$ must be explained by varying water masses, surface productivity changes and/or air-sea exchange processes. This additional 0.3 - 0.4 ‰ $\delta^{13}C$ G-I variation is 20 – 40 % less than the benthic $\delta^{13}C$ shift of 0.5 ‰ predicted for a complete halt of NCW advection to the south (*Charles et al.*, 1996). The reduced $\delta^{13}C$ shift observed in MD02-2489 therefore indicates a persistent contribution of a well-ventilated water mass to the ambient glacial bottom waters with a $\delta^{13}C$ signature similar to present day NCW. This can either be explained as sustained NCW influence at the site over the past 170 ka or the presence of SCW exhibiting a similar $\delta^{13}C$ signature from air-sea gas exchanges. Studies have suggested that during glacial periods enhanced production of deep waters occurred in the zone of extended

winter sea ice coverage (out to ~50 °S) south of the PF (*Rosenthal et al.*, 1997; *Mackensen et al.*, 2001; *Bickert and Mackensen*, 2003) and as a second shallower deep water mass along the SAF (*Michel et al.*, 1995). If any of these scenarios holds true the proximity of site MD02-2589 to the SAF would bring it under the influence of this shallower water mass during glacial periods. Benthic $\delta^{13}C$ of *F. wuellerstorfi* in MD02-2589 remains consistently more positive by ~0.7 ‰ than that in the deeper AABW influenced cores RC11-83 and TN057-21 (Fig. 5.5) further providing evidence for consistently better ventilation of mid-depth isopycnals. Benthic $\delta^{13}C$ from cores located in the deeper Cape Basin (*Charles and Fairbanks*, 1992; *Bickert and Wefer*, 1999) and carbonate dissolution in the Cape and Angola Basins inferred from sand contents (*Bickert and Wefer*, 1996) were used previously to infer reduced NADW advection to the south leading to a reduced contribution to or even complete absence of NCW in the deep glacial Southern Ocean. Based on our data we conclude that this scenario may not hold for the high-latitude South Atlantic as a whole but that a better ventilated water mass must have been present at mid-depth. This is further suggested in a study by *Hodell et al.* (2003) based on a vertical transect of benthic $\delta^{13}C$ at the Agulhas Ridge, which suggests the presence of a well developed chemocline in the South Atlantic at the LGM with a sharp chemical divide between well-ventilated mid-depth waters above 2500 m and less well ventilated deep waters below.

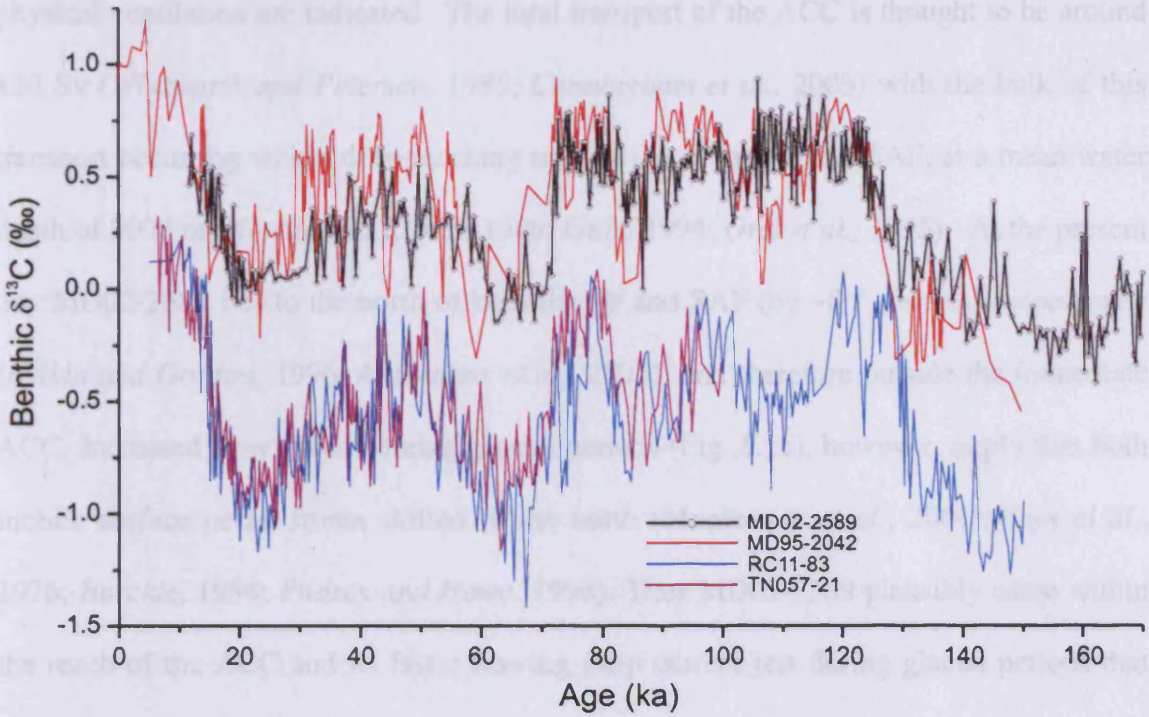

Figure 5.5. Records of benthic $\delta^{13}C$ of *Fontbotia wuellerstorfi* from MD02-2589, RC11-83 (*Charles et al.*, 1996), TN057-21 (*Ninnemann and Charles*, 2002) and MD95-2042 (*Shackleton et al.*, 2000).

Hall et al. (2001) found $\overline{SS}$ grain sizes at ODP Site 1123 in the SW Pacific were coherent with both benthic $\delta^{18}O$ and $\delta^{13}C$ isotopes at each orbital frequency. A clear relationship was also seen between $\overline{SS}$ and the Pacific deep water $\delta^{13}C$ ageing trends ($\Delta\delta^{13}C$ ODP Sites 1123-849) with periods of decreased ageing inferred from isotopes associated with increased DWBC flow speeds (physical ventilation). *Hall et al.* (2001) concluded that such flow changes may be directly related to increased production of AABW during the glacials potentially controlled by Southern Ocean winds or greater annual production of sea-ice leading to water densification through brine rejection. A similar orbital-scale relationship between benthic $\delta^{13}C$ and changing near bottom flow speeds is observed in the MD02-2589 records, with decreased benthic $\delta^{13}C$ and increased near bottom flow speeds during glacial periods. However, given that benthic $\delta^{13}C$ at MD02-2589 suggests better ventilation at mid-depths (compared to bottom water sites) additional controls on

physical ventilation are indicated. The total transport of the ACC is thought to be around 130 Sv (*Whitworth and Peterson,* 1985; *Cunningham et al.,* 2003) with the bulk of this transport occurring within deep-reaching narrow jets at the PF and SAF, at a mean water depth of 3000 m (*Nowlin and Klinck,* 1986; *Gille,* 1994; *Orsi et al.,* 1995). At the present day MD02-2589 lies to the north of both the PF and SAF (by ~8 ° and ~3 ° respectively (*Belkin and Gordon,* 1996; *Anilkumar et al.,* 2005)) and therefore outside the immediate ACC. Increased flow speeds during glacial periods (Fig. 5.1c), however, imply that both mobile surface ocean fronts shifted to the north (*Mackensen et al.*, 2001; *Hays et al.*, 1976; *Burckle*, 1984; *Pudsey and Howe*, 1998). Thus MD02-2589 plausibly came within the reach of the ACC and its faster flowing deep current jets during glacial periods that presumably restricted the southward transports of northern source deep waters deep into the Southern Ocean. Better ventilation of ambient bottom waters at the core site in this case would more clearly support a contribution of a Southern Ocean water mass with a ventilation signature influenced by air-sea gas exchange, similar to that seen in AAIW today.

5.3.1 Glacial Termination

Bianchi and Gersonde (2002) describe a southward displacement of the edge of the winter sea ice and a sea surface temperature warming in the Atlantic and western Indian Antarctic Zone, prior to MIS 5e, during late MIS 6 that was followed by a southward shift of the PF by 3 – 5 ° latitude from its current position during the late termination. The increase in ventilation displayed in the benthic $\delta^{13}C$ record of core RC11-83 and MD97-2120 and the sustained decrease in flow speeds at MD02-2589 starting at ~138 ka (Fig. 5.2) likely correspond to this SST warming. Minimum flow speeds at MD02-2589 and

maximum benthic $\delta^{13}C$ values in RC11-83 and MD97-2120 (Fig. 5.2) coincide with the southward shift of the PF. Evidence for warming within the region during late MIS 6 and a climate optimum within the glacial Termination has recently been shown by faunal records of *Peeters et al.* (2004) from the South African margin which suggest that following the arrival of the STF at its most northerly location during peak MIS 6, it started to move southward well before the start of the Termination allowing increased leakage through the Indian-Atlantic surface through-flow area that reaches a maximum within TII (also seen in modelling evidence of *Knorr and Lohmann* (2003)). Additionally, a sea level record from the Red Sea (*Siddall et al.*, 2006) shows a high stand during TII which lasted several millennia, followed by a reversal of 30 to 40 ± 12 m, coincident with the early warming of the southern latitudes. Correlating the benthic $\delta^{18}O$ shifts and circulation proxy changes in cores MD02-2589 and MD97-2120 (*Pahnke et al.*, 2003) with the Vostok ice core suggests that the prominent δD peak in Vostok that is indicative of peak-maximum air temperatures over Antarctica (*Petit et al.*,1999) (and EPICA Dome C records (*Jouzel et al.*, 2004)) occurred prior to full-interglacial MIS 5e, during mid-TII (Fig. 5.2), although age model constraints don't currently allow us to further address this possibility.

The climate optimum within the transition is followed by a marked cooling at around 128 ka seen in Vostok δD and is coincident with an increase in flow speed at MD02-2589, a decrease in ventilation at RC11-83 and MD97-2120 (fig 5.2), and a southern high latitude-wide SST cooling and expansion of the winter sea ice limit (*Bianchi and Gersonde,* 2002). The cooling of the Antarctic continent evident in the Vostok δD record has been linked with an intensification of Northern Hemisphere deep water to full interglacial levels (*Sarnthein and Tiedemann*, 1990; *Diekmann et al.*, 1996; *Spero and*

Lea, 2002), a suggestion that is supported by the benthic $\delta^{13}C$ record of MD02-2589 which show an increase in ventilation during this event reaching maximum levels at around 124 ka. Given the benthic $\delta^{18}O$ record of MD02-2589 suggests that the onset of MIS 5e occurs at 127 ka (Fig. 5.2) then this period of increased flow speeds and ventilation at Agulhas Plateau and the wider southern hemisphere cooling occurs during the earliest part of the full interglacial.

From the above we conclude that during TII changes in chemical ventilation, related to the southward advection of NCW, are largely decoupled at site MD02-2589 from near bottom physical flow speeds that primarily relate to the expansion and contraction of the ACC in association with meridional movements of the PF and SAF.

5.3.2 MIS 5/4 Transition

The MIS 5a/4 transition starts at 73 ka from benthic $\delta^{13}C$ values indicative of maximum NCW influence and low flow speed values suggestive of weakened ACC flow (Fig. 5.1, 5.3). This supports the suggestion by *Peeters et al.* (2004) for a strong input of NADW to the Southern Ocean associated with an abundance peak in Agulhas leakage fauna, observed in core MD01-2081, before the MIS 5a/4 transition recorded in its associated benthic $\delta^{18}O$ record and plausibly interpreted as a westward propagation of the Agulhas Current and an enhanced Indian-Atlantic surface transport.

The changes observed in $\overline{SS}$ and benthic $\delta^{13}C$ at the transition are similar in magnitude to the opposite trends seen during the TII glacial-interglacial shifts. The MIS 5a/4 benthic $\delta^{13}C$ shift (~0.9 ‰), is also similar in magnitude to those observed in the deep AABW

influenced cores TN057-21 and RC11-83 (~0.95 ‰). Although a significant portion of the MIS 5a/4 benthic $\delta^{13}C$ shift is likely due to a change in the carbon reservoir signal (*Piotrowski et al.*, 2005) as MIS 4 constitutes full glacial conditions for the first time after the prolonged interglacial conditions of MIS 5, these data along with the near-bottom flow speeds, suggest a decrease in NADW influence and an expansion of the SCW over the Agulhas Plateau.

This switch in water mass influence is consistent with a coeval transition in the MD02-2589 record from low fragmentation % indicative of a carbonate-saturated water mass sustaining higher levels of carbonate preservation (e.g. NCW) to high fragmentation % indicative of a carbonate-undersaturated water mass more corrosive to carbonates (e.g. SCW) (*Henrich et al.*, 2003; *Pfuhl and Shackleton*, 2004)) (fig 5.3e). In addition, records from ODP Site 1059 (32.1 °N, 76.4 °W; 2584 m water depth) and Site 1057 (31.40 °N, 75.25 °W; 2985 m water depth) from the Blake Outer Ridge (BOR), North Atlantic (*Evans et al.*, 2007) show a sharp, short-lived, negative excursion in benthic $\delta^{13}C$ over the sites at 73.2 ka and 71.6 ka respectively, during the transition in their associated benthic $\delta^{18}O$ records, which is attributed to an abrupt shoaling (to <2500 m) of the Deep Western Boundary Current at the BOR associated with a reduction in production of NADW, at the MIS 5a/4 transition. The GRIP ice core $\delta^{18}O$ record from Greenland (*Johnsen et al.*, 1997) also exhibits a significant cold event (C19 in contemporaneous marine cores (*McManus et al.*, 1994)) at 71.5 ka (Fig. 5.3). Neodymium isotope analysis on cores RC11-83 and TN057-21 (*Piotrowski et al.*, 2005) also confirm this event, showing a rapid decrease in the proportion of NADW in bottom water over this transition.

5.4 Conclusions

Our high resolution benthic $\delta^{13}C$ record from core MD02-2589 strongly suggests that there was a continued source for enhanced mid-depth ventilation over the southern Agulhas Plateau during glacial periods. While the influence of NCW may have been reduced in the glacial South Atlantic additional well-ventilated waters plausibly have originated in the Southern Ocean. Significantly increased near-bottom flow speeds during glacial periods at MD02-2589 indicate that the vigor of near bottom currents on the Southern Agulhas Plateau is likely influenced by orbital scale meridional expansion and contraction of the ACC and its associated surface fronts.

Ventilation and flow speeds show a late MIS 6 circulation change, associated with the previously documented regional frontal shifts and SST warming in the Southern Ocean, occurring some 8 ka before the start of TII recorded in the benthic $\delta^{18}O$. A mid-TII climate optimum is highlighted in the MD02-2589 record by a transient episode of low flow speeds concurrent with a period of increased ventilation shown in the benthic $\delta^{13}C$ records from other cores from Southern Ocean deep (RC11-83) and intermediate (MD97-2120) sites. This event is not recorded in the benthic $\delta^{13}C$ of MD02-2589.

All of the MD02-2589 records show a rapid, but sequenced, event occurring at the MIS 5a/4 transition, in which changes in flow speed and chemical ventilation were of a similar magnitude (but opposite direction) to those occurring at TII. These changes suggest a switch in the relative influence of northern and southern source waters, together with an increased influence of the ACC, towards MIS 4. This event can be linked to the sudden

shoaling of NADW and reduction in its production possibly related to GRIP cold event C19.

Chapter 6: Benthic Carbon Isotope Gradients in the Atlantic Ocean and Implications for Meridional Overturning Circulation Variability

6.1 Introduction

This chapter compares the $\delta^{13}C$ records of benthic species *F. wuellerstorfi* from core MD02-2589 from the Agulhas Plateau, Indian-Atlantic throughflow region (hereafter termed South Atlantic), with core MD95-2042, from the Iberian Margin (37.48 °N, 10.10 °W, 3146 m water depth), Northeast Atlantic, in order to further investigate the NCW vs SCW interplay at site MD02-2589. Both core sites at the present day lie in NADW (see *Shackleton et al.,* 2000 for MD95-2042 site setting and see Chapter 2.1 for MD02-2589 setting). The bottom water $\delta^{13}C$ value at the present day for site MD95-2042 is ~1 ‰ (*Sarnthein et al.,* 1994; GEOSECS station 23, 60.41 °N, 18.61 °W, 2516 m water depth, 1.1 ‰, GEOSECS station 113, 10.98 °N, 20.51 °W, 3072 m water depth, 0.9 ‰), and ~0.6 ‰ (*Sarnthein et al.,* 1994; GEOSECS station 93, 41.46 °S, 18.27 °E, 2597 m water depth, 0.6 ‰) for waters bathing site MD02-2589. Therefore the expected offset at the present day between the two sites is +0.4 ‰ due to the mixing and ageing of the water mass through the Atlantic Ocean. During glacial stages MIS 2 and 6, MD95-2042 is thought to have been bathed in SCW with MD02-2589 remaining in a high $\delta^{13}C$ water mass (see Chapter 5), similar to present day NCW. Initial observations suggest that the benthic $\delta^{13}C$ records of these 2 cores exhibit similar structure and values over the past 150 ka (Fig. 5.7) and this chapter aims to further investigate these similarities as well as the fluctuations in the $\delta^{13}C$ gradient between the North and South Atlantic and the implications that this has for the variability of the Atlantic Meridional Overturning Circulation (AMOC) and the extent of NCW during glacial periods.

6.2 Age Model Tuning

6.2.1 Graphic Tuning

The synchronisation of the benthic $\delta^{18}O$ records of MD02-2589 and MD95-2042 and subsequent alterations made to the age model of MD02-2589 within this chapter are done so that a detailed comparison of lag times of the response of the benthic $\delta^{13}C$ records of the two cores, and therefore the response time of the oceans, to ice volume changes can be assessed without the possibility of any stratigraphic uncertainties. The resulting MD02-2589 age model used in this chapter should not be considered as an improved version of that detailed in Chapter 3.

In order to allow a detailed comparison of the benthic $\delta^{13}C$ record of MD02-2589 with the Iberian Margin record the MD02-2589 benthic $\delta^{18}O$ record (corrected by +0.64 ‰ to bring it in line with the *Uvigerina* scale (*Shackleton and Opdyke,* 1973)) was initially graphically tuned to the benthic $\delta^{18}O$ record of MD95-2042 (*Uvigerina* corrected *C. wuellerstorfi* only record) using 8 tie-points such that age offsets within the oxygen records were minimised (Fig. 6.1a, b). The AMS dates for MD02-2589 were not used so that the offset at TI resulting from different reservoir correction factors could be minimised. The lack of structure in the benthic $\delta^{18}O$ record of MD02-2589 through MIS 3 resulted in few tie points throughout this period (Fig. 6.1a), and therefore to better correlate the age models, the benthic $\delta^{13}C$ records of both cores were used in MIS 3 (Fig. 6.1c) to fine tune the MD02-2589 age model. The ages between the tie points were estimated using linear interpolation and the resulting MD95-2042 tuned age model suggests that sedimentation rates of MD02-2589 vary from between 12.8 cm/ka during TI to an average of 4.1 cm/ka during glacial periods.

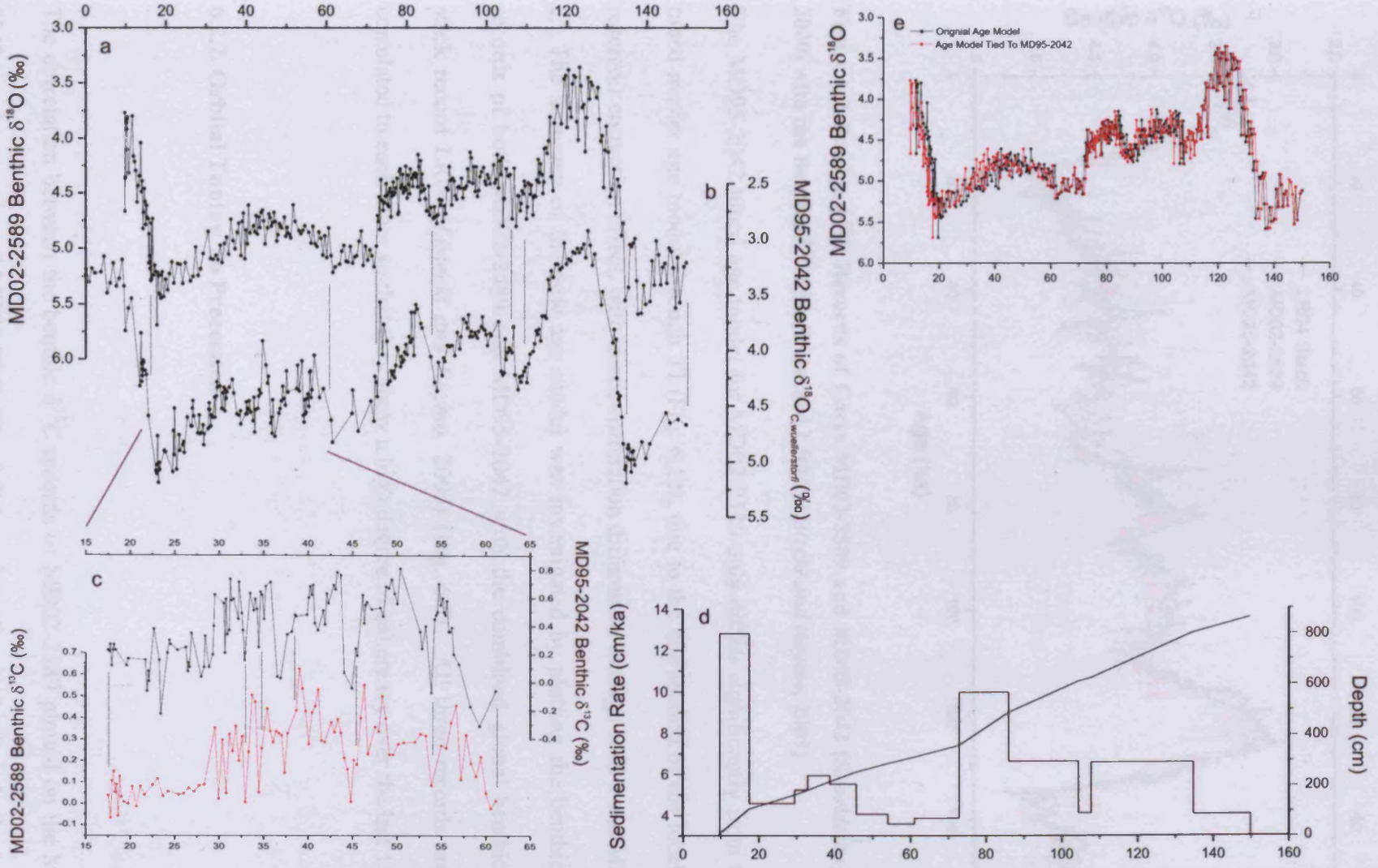

Figure 6.1 Revised Chronology of MD02-2589 (a) Benthic $\delta^{18}O$ of core MD02-2589 and (b) MD95-2042 (*Shackleton et al.,* 2000) showing tie points used for correlation, (c) Benthic $\delta^{13}C$ of core MD02-2589 and MD95-2042 for MIS 3 showing extra tie points used in correlation, (d) Resulting sedimentation rate and (e) MD02-2589 Benthic $\delta^{18}O$ record on both the original age scale (Chapter 3) and the revised MD95-2042 tied age scale

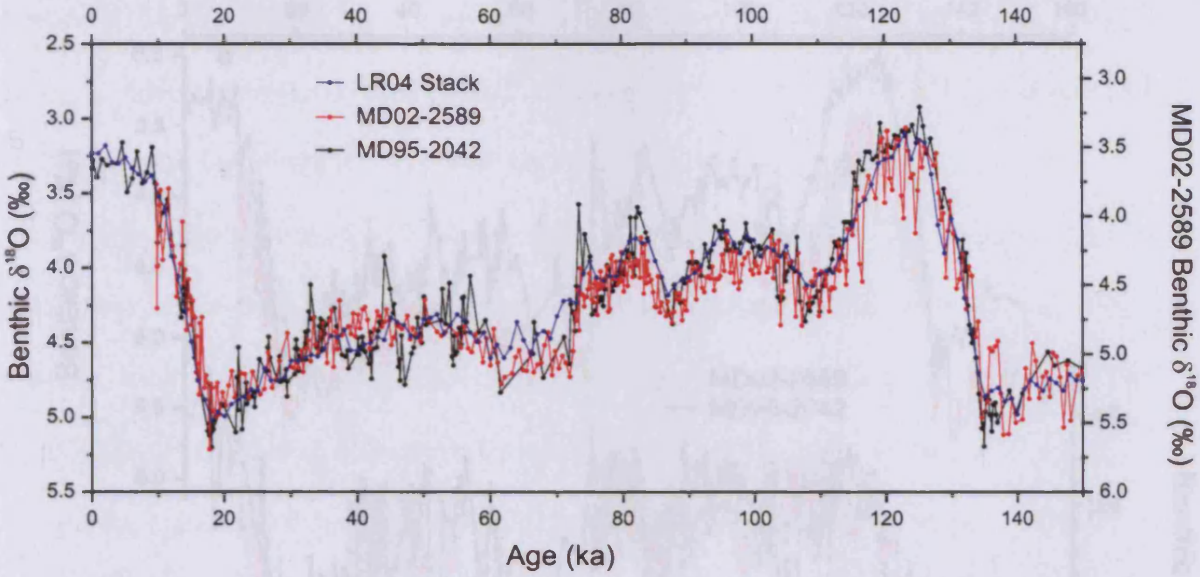

Figure 6.2 Benthic $\delta^{18}O$ Records of Cores MD02-2589 and MD95-2042 (*Shackleton et al.*, 2000) with the Benthic $\delta^{18}O$ Stack Record LR04 (*Lisiecki and Raymo*, 2005)

The MD95-2042 tuned age model for MD02-2589 only differs significantly from the un tuned master age model through TI (Fig. 6.1e), due to the elimination of the local (ΔR) reservoir correction effect, with minor correlation differences through MIS 3 and MIS 5b-c. The accuracy of the new age model was investigated by plotting the benthic $\delta^{18}O$ records of both MD02-2589 and MD95-2042 with the combined global benthic $\delta^{18}O$ stack record LR04 (*Lisiecki and Raymo,* 2005) (Fig. 6.2). All three records are well correlated to each other so that they show a high degree of coherency over the last 150 ka.

6.2.2. Orbital Tuning To Precession

The correlation between the benthic $\delta^{13}C$ records of MD02-2589 plotted on the MD95-2042 tuned age scale and MD95-2042 (Fig. 6.3b) confirms the similarity in both structure and values between the two cores throughout the past 150 ka. The difference between the

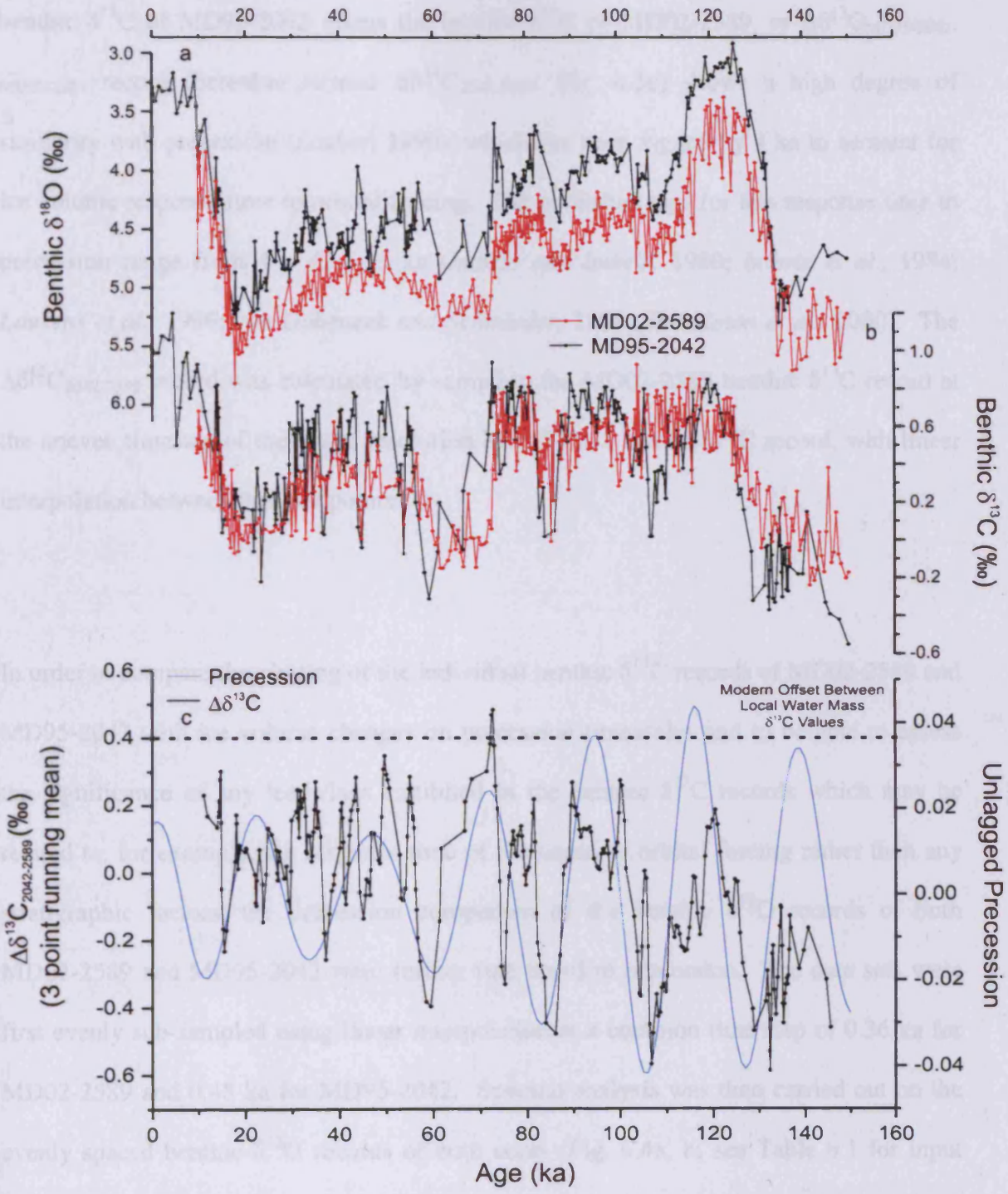

Figure 6.3 Benthic Isotope Records of Cores MD02-2589 and MD95-2042 (*Shackleton et al.*, 2000) with $\Delta\delta^{13}C_{2042\text{-}2589}$ Calculation on MD95-2042 Tied Age Model, (a) Benthic $\delta^{18}O$ records, (b) Benthic $\delta^{13}C$ records, (c) $\Delta\delta^{13}C$ calculation and unlagged precession record (*Laskar*, 1990), showing the modern day $\delta^{13}C$ offset between core sites MD95-2042 and MD02-2589.

benthic $\delta^{13}C$ of MD95-2042 minus the benthic $\delta^{13}C$ of MD02-2589, or $\Delta\delta^{13}C_{MD95\text{-}2042\text{-}MD02\text{-}2589}$ record (hereafter termed $\Delta\delta^{13}C_{2042\text{-}2589}$: Fig. 6.3c) shows a high degree of similarity with precession (*Laskar,* 1990), which has been lagged by 4 ka to account for ice volume response time to orbital forcing. The published lags for this response time to precession range from 4 – 4.2 – 5 ka (*Imbrie and Imbrie,* 1980; *Imbrie et al.,* 1984; *Lourens et al.,* 1996; *von Dobeneck and Schmieder,* 1999; *Shackleton et al.,* 2000). The $\Delta\delta^{13}C_{2042\text{-}2589}$ record was calculated by sampling the MD02-2589 benthic $\delta^{13}C$ record at the uneven timestep of the lower resolution MD95-2042 benthic $\delta^{13}C$ record, with linear interpolation between the data points.

In order to compare the phasing of the individual benthic $\delta^{13}C$ records of MD02-2589 and MD95-2042 with ice volume changes on precession timescales and to be able to assess the significance of any leads/lags exhibited in the benthic $\delta^{13}C$ records which may be related to, for example, the response time of the ocean to orbital forcing rather than any stratigraphic factors, the precession component of the benthic $\delta^{18}O$ records of both MD02-2589 and MD95-2042 were further fine tuned to precession. The data sets were first evenly sub-sampled using linear interpolation at a common time step of 0.36 ka for MD02-2589 and 0.48 ka for MD95-2042. Spectral analysis was then carried out on the evenly spaced benthic $\delta^{18}O$ records of both cores (Fig. 6.4a, b; see Table 6.1 for input parameters). The initial power spectra for both cores (Fig. 6.4a, b) show maximum spectral variance in the eccentricity band, with additional variance significant over 95 % in the obliquity band and at or near the precession band (1/23.8 ka for MD95-2042, 1/26.3 ka for MD02-2589), although both precession bands are being affected by power leakage from the obliquity and eccentricity signals. In order to isolate the precession signal

within the records and determine its central frequency the $\delta^{18}O$ records of both cores were filtered using a band-pass Gaussian filter (Analyseries, *Paillard et al.*, 1996) at the central frequencies of eccentricity and obliquity of the individual time series, shown in Fig. 6.4a, b, and the resulting spectral filters subtracted from the original records. Fig. 6.4c, d show the power spectra of the two $\delta^{18}O$ records with precession and obliquity removed.

Record	Age Model Used	Length of Time Series (ka)	No. of Data Points	Sample Step Original Records (+ / -)	Sampling Step Used (ka)	Band Width	Lags Applied	Nyquist Frequency (ka)
MD02-2589 $\delta^{18}O$	Original	9.69 – 149.79	384	366 yrs (871 / 313)	0.36	0.0146	140	2.47
MD95-2042 $\delta^{18}O$	Original	0.004 – 149.79	310	484 yrs (3536 / 439)	0.48	0.0130	150	8.04
MD02-2589 $\delta^{18}O$	Minus Eccen. and Obliq.	9.69 – 149.79	384	366 yrs (871 / 313)	0.36	0.0146	140	2.47
MD95-2042 $\delta^{18}O$	Minus Eccen. and Obliq.	0.004 – 149.79	310	484 yrs (3536 / 439)	0.48	0.0130	150	8.04
MD02-2589 $\delta^{13}C$, $\delta^{18}O$ X-spectral	Precession Tuned	6 – 147	384	367 yrs (413 / 147)	0.36	0.0295	141	1.56
MD95-2042 $\delta^{13}C$, $\delta^{18}O$ X-spectral	Precession Tuned	0 – 146	310	472 yrs (1528 / 169)	0.48	0.0223	146	4.00
$\Delta\delta^{13}C$	Precession Tuned	7.10 – 142.06	298	458 yrs (1542 / 155)	0.47	0.0136	148	4.00

Table 6.1 Statistics of Performed Spectral Analysis

Both the MD95-2042 and MD02-2589 spectral plots show a high variance centred at 1/24.3 ka (Fig. 6.4c, d), which is significant at the 95 % confidence level. As the records incorporate more than six precession cycles then these are likely to be well-constrained features of each of the records. The central frequencies are different from those identified in the original spectral plots before eccentricity and obliquity were removed as the power leakage to lower frequencies from eccentricity and obliquity were likely affecting the original plots.

Record	Filtered To	Sample Step (ka)	Central Periodicity (ka)	From (ka)	To (ka)
MD02-2589 $\delta^{18}O$	Obliquity[1]	0.36	38.46	30.96	56.46
MD95-2042 $\delta^{18}O$	Obliquity[1]	0.48	38.46	30.76	51.31
MD02-2589 $\delta^{18}O$	Eccentricity[1]	0.36	111.11	61.38	584.62
MD95-2042 $\delta^{18}O$	Eccentricity[1]	0.48	111.11	64.4	401.5
MD02-2589 $\delta^{18}O$	Precession	0.36	24.3	20.71	29.66
MD95-2042 $\delta^{18}O$	Precession	0.48	24.3	21.04	28.99
MD02-2589 $\delta^{18}O$	Eccentricity[2]	0.36	111.1	63.90	425.35
MD95-2042 $\delta^{18}O$	Eccentricity[2]	0.48	100	59.93	301.66
MD02-2589 $\delta^{18}O$	Obliquity[2]	0.36	30.63	38.46	51.67
MD95-2042 $\delta^{18}O$	Obliquity[2]	0.48	37.04	29.68	49.22

Table 6.2 Statistics of Performed Filtering: Eccentricity[1], Obliquity[1] = Eccentricity and obliquity filtering using the original age model for removal of signal from $\delta^{18}O$ record; Eccentricity[2], Obliquity[2] = Eccentricity and obliquity filtering using the precession age model for removal of signal from $\delta^{18}O$ record

In order to extract the precession component of the two benthic $\delta^{18}O$ records the central frequencies were determined and the benthic $\delta^{18}O$ records filtered using band pass Gaussian filtering (*Analyseries; Paillard et al.*, 1996) at the central frequency of the precession. For MD95-2042 the central frequency was defined as 1/24.3 ka, with a band-width of 1/21.04 to 1/28.99 ka, while for MD02-2589 the central frequency used was also 1/24.3 ka but with a band-width of 1/20.71 to 1/29.66 ka.

The filtered precession components of the benthic $\delta^{18}O$ records are both in-phase with the lagged precession (Fig. 6.5a), which is expected as studies have shown that the Northern Hemisphere ice sheets, which dominate the global ice volume record, are sensitive to

precession translated from lower latitudes through the Northern Hemisphere land mass (*Imbrie et al.*, 1992; *Roe and Allen*, 1999; *Clark et al.*, 1999). In general the synchroniety of the precession component of the benthic $\delta^{18}O$ records and (lagged) orbital precession (Fig. 6.5a) confirms that the age model is stratigraphically robust. The small deviations from precession are probably linked to uncertainties within the age model.

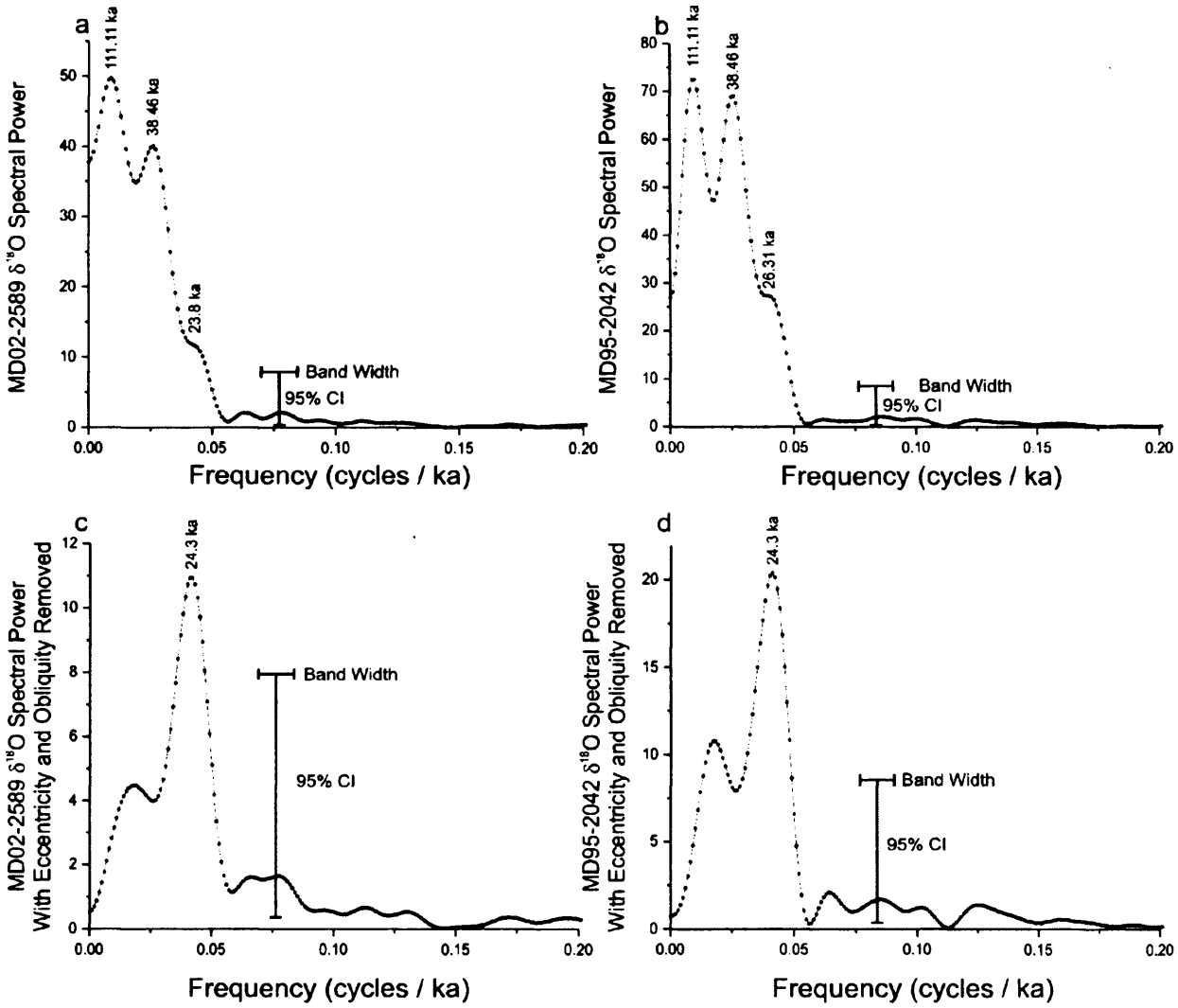

Figure 6.4 Spectral Plots of MD02-2589 and MD95-2042 (*Shackleton et al.*, 2000) Benthic $\delta^{18}O$ Records: Initial spectral plots of (a) MD02-2589 benthic $\delta^{18}O$ record (BW = 0.0146, 95 % CI = 7.95) and (b) MD95-2042 benthic $\delta^{18}O$ record (BW = 0.0130, 95 % CI = 8.55) showing frequencies significant over 95 % confidence levels: Further spectral plots of the benthic $\delta^{18}O$ records of (c) MD02-2589 (BW = 0.0146, 95 % CI = 7.95) and (d) MD95-2042 (BW = 0.013, 95 % CI = 8.55) minus eccentricity and obliquity, with the frequency of the precession peaks labelled

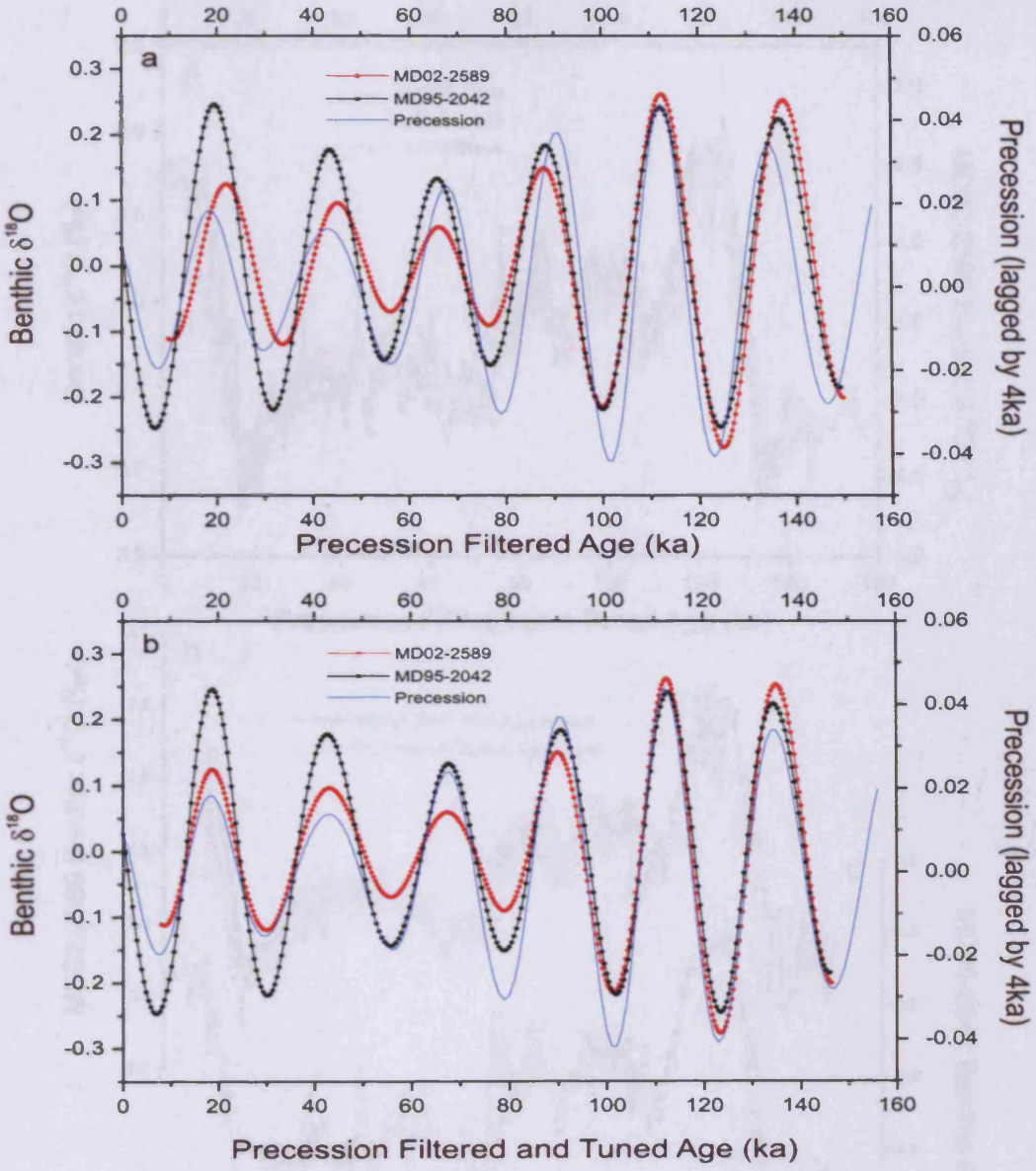

Figure 6.5 Precession Tuning of Benthic $\delta^{18}O$ Records of Cores MD02-2589 and MD95-2042 (*Shackleton et al.*, 2000): (a) Benthic $\delta^{18}O$ records of MD02-2589 and MD95-2042 filtered to precession using frequencies identified in Fig. 6.4 with lagged precession (*Laskar*, 1990; lagged by 4 ka): (b) Benthic $\delta^{18}O$ records of MD02-2589 and MD95-2042 filtered and tied to lagged precession

However in order to remove any minor offsets within the benthic $\delta^{18}O$ records in relation to precession, the precession component of the benthic $\delta^{18}O$ records of both MD02-2589 and MD95-2042 were further fine tuned to precession (Fig. 6.5b).

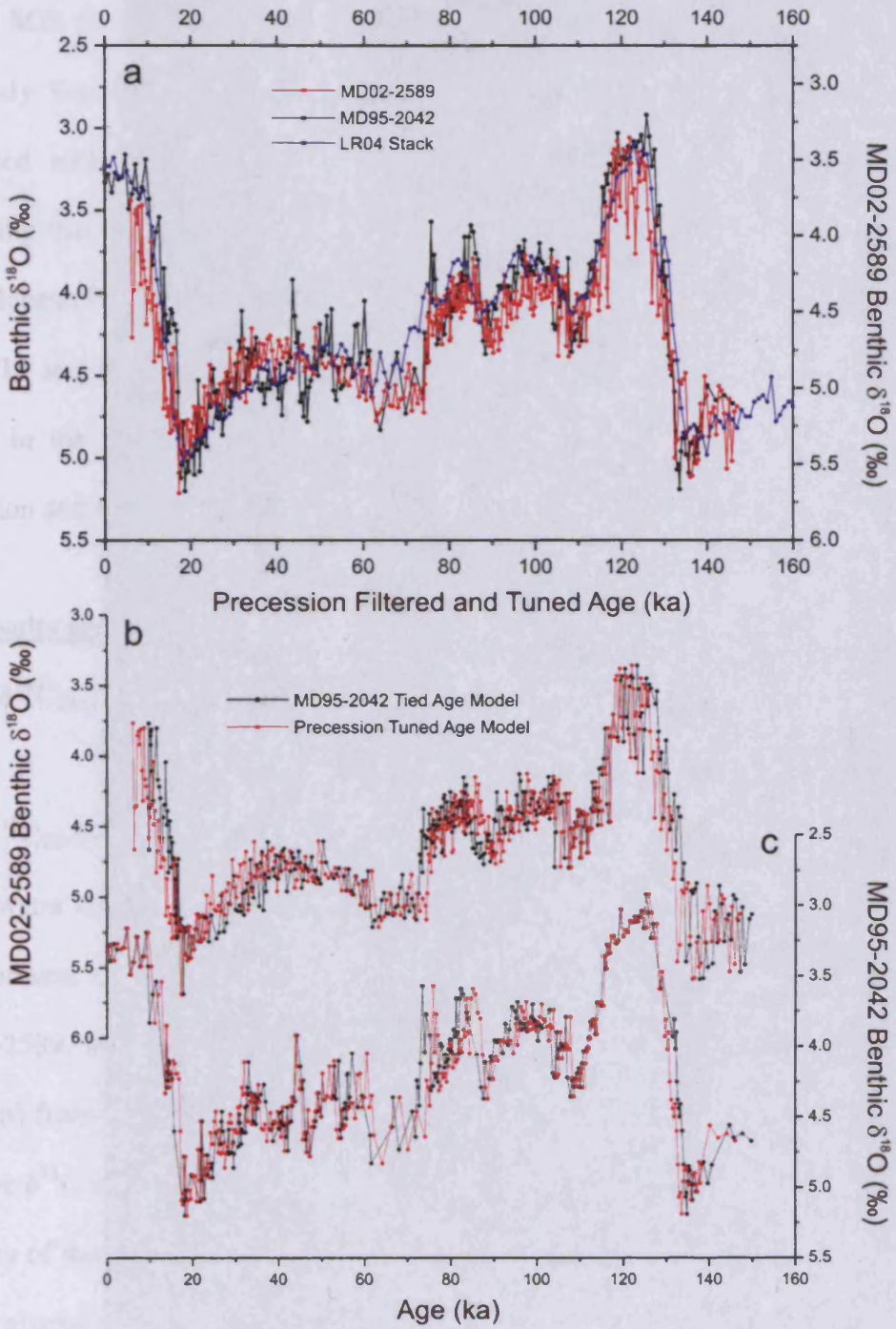

Figure 6.6 Precession Tuned Age Model: (a) Benthic $\delta^{18}O$ records of MD02-2589 and MD95-2042 (*Shackleton et al.,* 2000) on the precession tuned age model with the benthic $\delta^{18}O$ stack LR04 (*Lisiecki and Raymo,* 2005): (b) Benthic $\delta^{18}O$ and (c) Benthic $\delta^{13}C$ records of MD02-2589 and MD95-2042 on both the MD95-2042 tied age model (Fig. 6.1) and precession tuned age model

As the benthic $\delta^{18}O$ records were only slightly offset from precession (Fig. 6.5a) in the un-tuned age model, the precession tuned aged model only differs appreciably over TI,

TII and MIS 5c - 4 for MD02-2589 (Fig. 6.6b) and MD95-2042 (Fig. 6.6c). As noted previously the TI section in MD02-2589 has considerable stratigraphic uncertainty associated with it, with 4 AMS ^{14}C age reversals in the upper 15 ka (Table 3.1), suggesting that there is likely some disturbance in this part of the core. The absence of full Holocene benthic $\delta^{18}O$ values also mean that it is difficult to asses the stratigraphy within TI and this is probably contributing to the wide discrepancies in ages for this section in the three calculated age models (Chapter 3, Fig. 6.1, 6.6b). All further discussion and figures in this chapter are on the precession tuned timescale unless stated.

6.3. Results and Discussion

6.3.1 $\Delta\delta^{13}C_{2042\text{-}2589}$ and Negative Carbon Anomalies

The $\Delta\delta^{13}C_{2042\text{-}2589}$ offset at the present day is around +0.4 ‰ due to the mixing and ageing of the water mass through the Atlantic Ocean. While the $\Delta\delta^{13}C_{2042\text{-}2589}$ offset does not show present day values (Fig.6.7c), due to a lack of material in the upper section of MD02-2589, initial observations show that only at 5 short-lived periods (0.3 – 2.5 ka duration) from MIS 3 to the early Holocene and 1 longer period of 4.7 ka during MIS 4 have the $\delta^{13}C$ records of these two sites shown the modern offset (Fig. 6.7c), although the majority of the record reveals positive offset values. However, it cannot be assumed that during glacial periods, when the hydrography of the Atlantic Ocean is known to be very different to present day, the offset between the two sites remained around +0.4 ‰.

The $\delta^{13}C$ values for the Iberian Margin at 3146 m water depth during the LGM are estimated by *Sarnthein et al.* (1994) to be 0.4 - 0.6 ‰ (Fig. 6.8). The *Sarnthein et al.* (1994) study was based on 95 epibenthic $\delta^{13}C$ records forming a latitudinal transect through the east Atlantic from 60 °N to 50 °S. Several of the cores used have very low

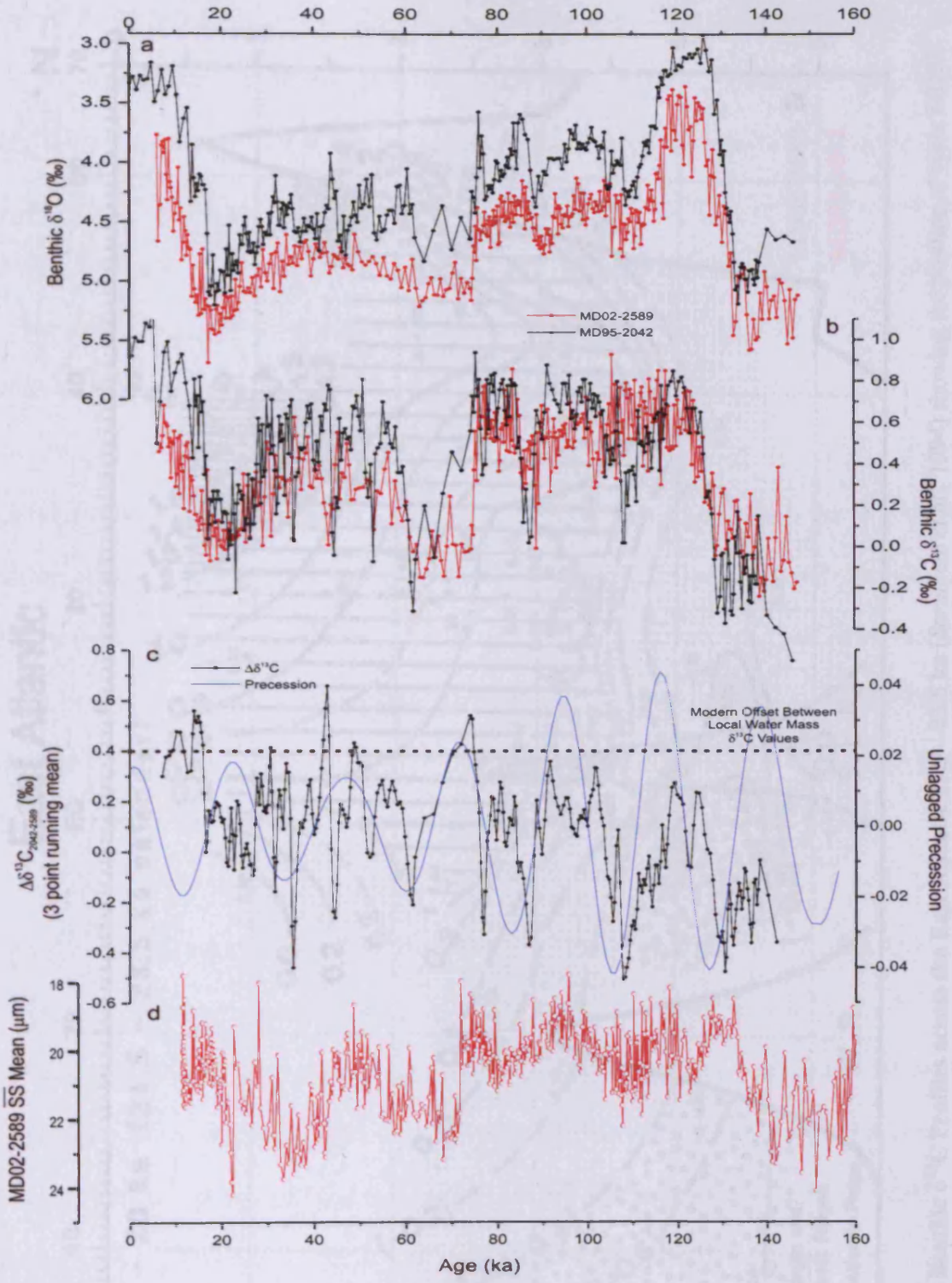

Figure 6.7 Benthic Isotope Records of Cores MD02-2589 and MD95-2042 (*Shackleton et al.*, 2000) with $\Delta\delta^{13}C_{2042\text{-}2589}$ Calculation on Precession Tied Age Model, **(a) Benthic $\delta^{18}O$ records, (b) Benthic $\delta^{13}C$ records, (c) $\Delta\delta^{13}C$ calculation and unlagged precession record (*Laskar*, 1990), showing the modern day $\delta^{13}C$ offset between core sites MD95-2042 and MD02-2589.**

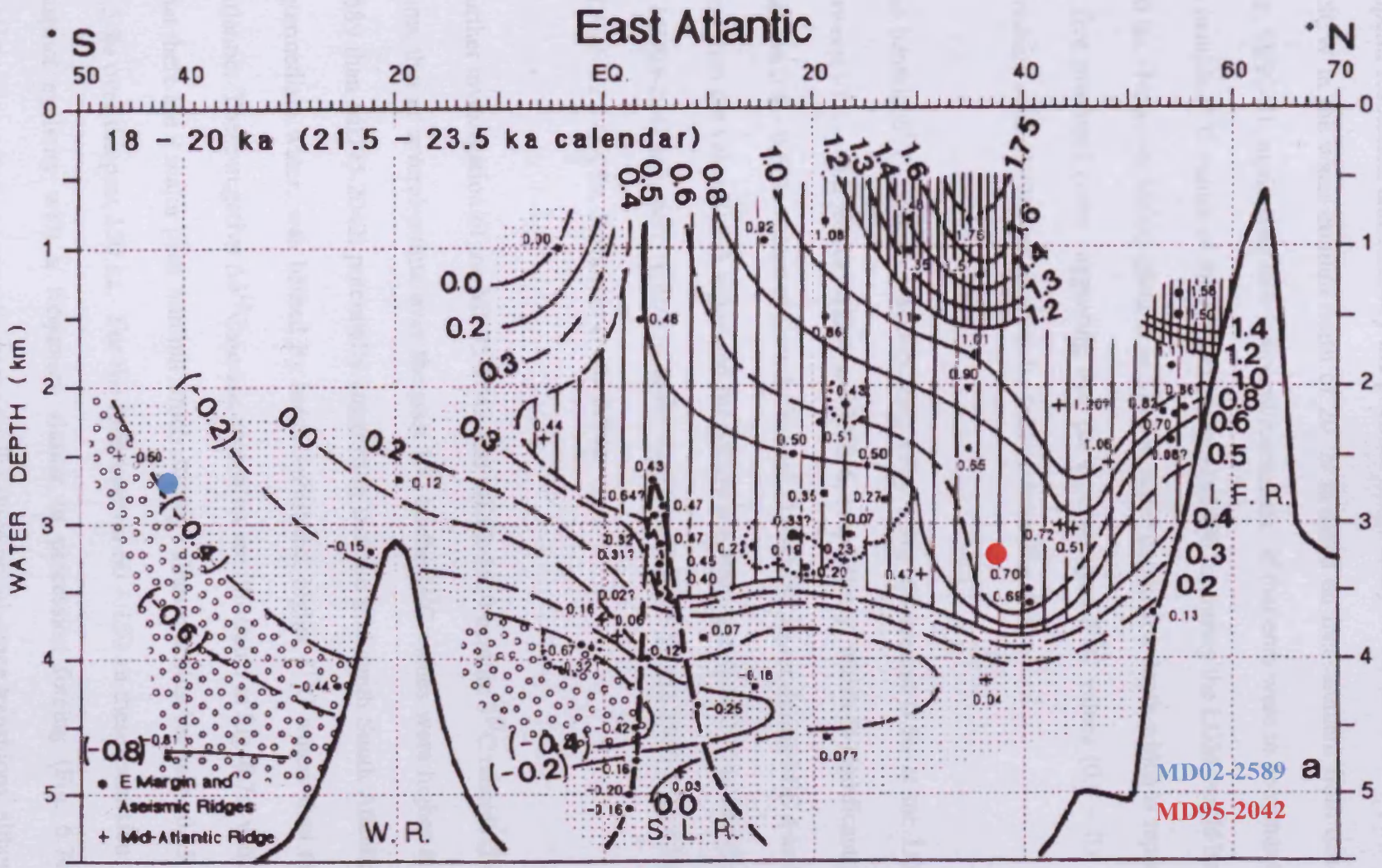

Figure 6.8 Benthic $\delta^{13}C$ Profiles across the East Atlantic 21.5 – 23.5 ka (*Sarnthein et al.,* 1994) showing the position of cores MD95-2042 (Red; *Shackleton et al.,* 2000) and MD02-2589 (Turquoise).

temporal resolution and certainly the position in the study of the northwards propagation of SCW in the water column north of 20 °N is based on measurement from one single core, SU92-21, again with low temporal resolution. If that core were to be removed then the benthic $\delta^{13}C$ values of the Iberian Margin (>3500 m) during the LGM would be closer to 0 ‰. However MD95-2042 is at 3146 m water depth, at a depth which is represented by five proximal cores suggesting that the reconstructed $\delta^{13}C$ values (0.4 – 0.6 ‰) of *Sarnthein et al,* (1994) are likely to be fairly robust (Fig. 6.8).

The benthic $\delta^{13}C$ values of MD95-2042 (Fig. 6.7b) are around 0 ‰ at the LGM and between -0.1 – -0.2 ‰ for MIS 4 and MIS 6, respectively, which is significantly lower than the 0.4 – 0.6 ‰ values of *Sarnthein et al.* (1994) and lower during MIS 4 and MIS 6 even than the value (0 ‰) suggested for northwards propagating SCW. In fact the values at MD95-2042 are more typical of those suggested for site MD02-2589 (Fig. 6.7b) at the LGM (-0.2 - -0.4 ‰, *Sarnthein et al.,* 1994).

Further investigation of the MD95-2042 and MD02-2589 benthic $\delta^{13}C$ records (Fig. 6.7b) show that at several points over the past 150 ka the $\delta^{13}C$ values were higher at MD02-2589 than MD95-2042, potentially suggesting that the mid-depth South Atlantic, below intermediate water, was bathed by better ventilated, higher $\delta^{13}C$ waters than the North Atlantic. These negative $\Delta\delta^{13}C_{2042\text{-}2589}$ anomalies are illustrated in Fig. 6.7c, which shows that there are 8 major peak minima which display values reaching between -0.15 ‰ and -0.5 ‰ over the past 150 ka. For the time interval 60 – 150 ka these excursions, show a distinct cyclicity with a frequency similar to precession forcing (Fig. 6.7c). The $\Delta\delta^{13}C_{2042\text{-}2589}$ minima generally occur during stage or sub-stage transitions, although their magnitude also appears be linked with eccentricity modulation of the precession signal,

such that as the amplitude of the precession signal decreases, a coincident decrease in the $\Delta\delta^{13}C_{2042\text{-}2589}$ record also occurs (Fig. 6.7c). The $\Delta\delta^{13}C_{2042\text{-}2589}$ record also shows a long-term trend towards more positive values with decreasing age and decreasing amplitude of the precession signal. For the time interval 0 – 60 ka the resemblance with orbital precession seems less prominent and fluctuations of shorter duration become more distinct.

It is also noticeable that the benthic $\delta^{13}C$ record of MD95-2042 (Fig. 6.7b) shows greater variability during MIS 5 and 3 than the record of MD02-2589, with the largest negative excursions in $\Delta\delta^{13}C_{2042\text{-}2589}$ being mainly due to the difference in the timing and amplitude of the fluctuations of the two different benthic $\delta^{13}C$ records in response to sub-stage and stage changes. It is therefore probable that the benthic $\delta^{13}C$ record of MD95-2042 is largely driving the $\Delta\delta^{13}C_{2042\text{-}2589}$ record, through its higher amplitude oscillations.

Further evidence of a higher $\delta^{13}C$ mid-depth water mass in the South than North Atlantic during discrete periods, the negative carbon anomalies seen in the $\Delta\delta^{13}C_{2042\text{-}2589}$ record (Fig. 6.7c), can be seen in the percentage NCW vs SCW calculation for the benthic $\delta^{13}C$ records of MD02-2589 and MD95-2042 (Fig. 6.9a - c). The proportion of NCW at a given site relative to SCW (hereafter termed % NCW, *Oppo and Fairbanks,* 1987; *Raymo et al.,* 1990, 1997; *deMenocal et al.,* 1992; *Oppo et al.,* 1995; *Flower et al.,* 2000) uses sites with North Atlantic (ODP Site 980, 55.29 °N, 14.42 °W, 2179 m water depth, *Raymo et al.,* 2004) and Southern Ocean end members (RC11-83, 41.36 °S, 9.48 °E, 4718 m water depth, *Charles et al.,* 1996) for comparison with the benthic $\delta^{13}C$ records of MD02-2589 and MD95-2042. Core RC11-83 lies in the deep Cape Basin, South Atlantic and was chosen as the SCW end member as it is consistently bathed in AABW through both

glacial and interglacial periods, although AABW itself has a NCW component. ODP Site 980 was chosen as the North Atlantic end member as it is the highest resolution record from a shallow site in the North Atlantic over this time period that was available. *Flower et al.,* (2000) however noted that during peak glacial times ODP Site 980 may have been influenced by SCW as it rose to ~2200 m in the water column, although this does not affect variability in MIS 5 and 3.

The benthic $\delta^{18}O$ records of core RC11-83 and ODP Site 980 were graphically correlated to the benthic $\delta^{18}O$ record of MD95-2042 to align the age models and minimise offsets due to age differences. The benthic $\delta^{13}C$ records of cores MD02-2589, MD95-2042 and RC11-83 were then sampled at the time step of core ODP Site 980, which has the lowest resolution of the four records. The % NCW (proportion of NCW relative to SCW) was calculated as follows using MD02-2589 as an example:

$$\% \text{ NCW} = [(\delta^{13}C_{MD02\text{-}2589} - \delta^{13}C_{RC11\text{-}83}) / (\delta^{13}C_{ODP980} - \delta^{13}C_{RC11\text{-}83})] * 100$$

(*Raymo et al.,* 1990)

This % NCW calculates where the benthic $\delta^{13}C$ values of for example MD02-2589 fall relative to the two end members at any one time. High values suggest high levels of NCW over the site (60 % = 60 % NCW contribution to the site), whereas low values suggest little NCW reached the South Atlantic. The difference in the % NCW bathing each site can be calculated by subtracting the MD02-2589 % NCW from the MD95-2042 % NCW record (Δ% NCW), with positive values suggesting more NCW at the Iberian Margin and vice versa.

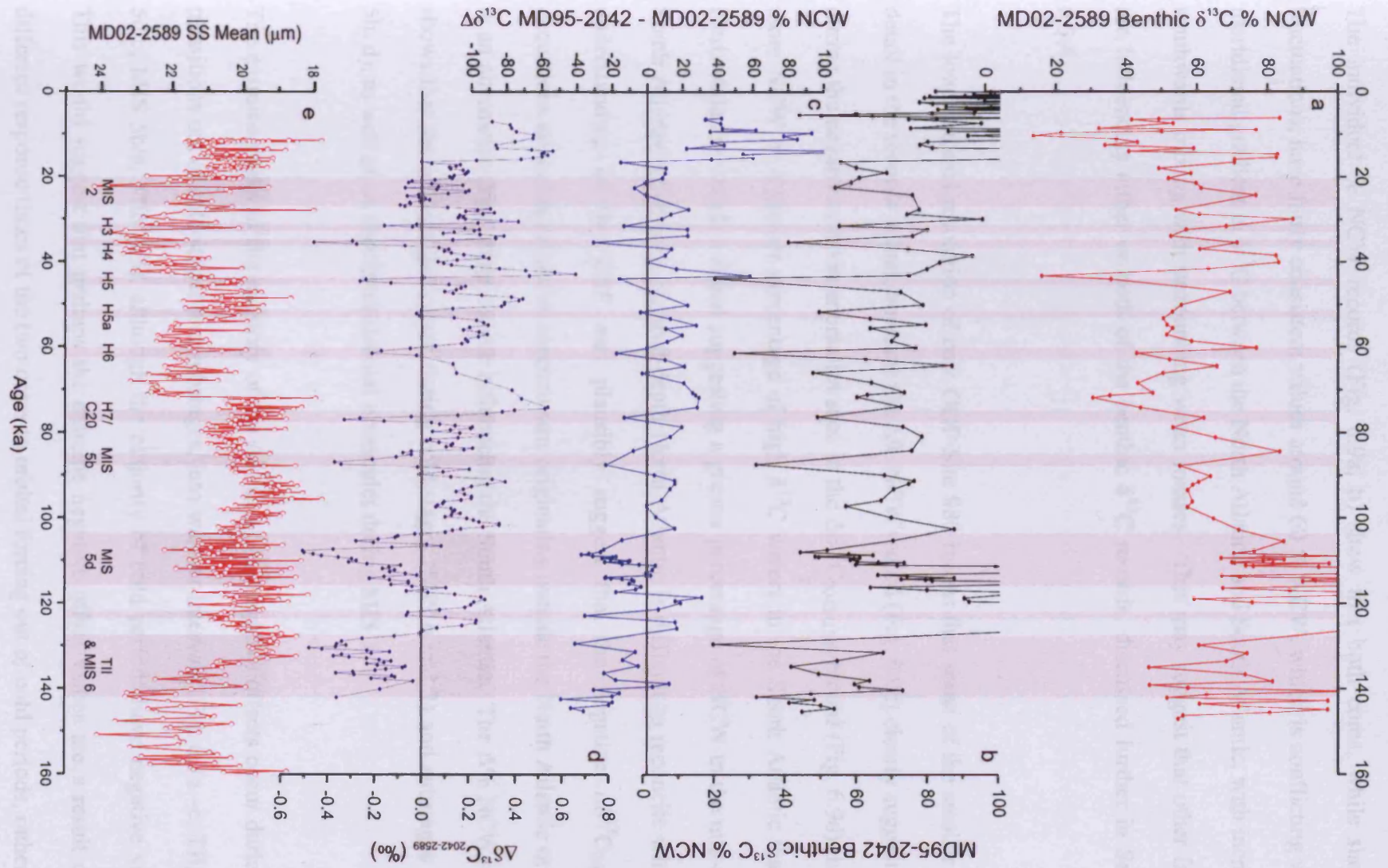

Figure 6.9 % NCW Calculations for Cores MD02-2589 and MD95-2042 (*Shackleton et al.*, 2000): (a) MD02-2589, (b) MD95-2042 benthic $\delta^{13}C$ % NCW calculations, (c) $\Delta\delta^{13}C_{2042\text{-}2589}$ % NCW calculation with negative values below the line indicating more NCW at MD02-2589 than MD95-2042, (d) $\Delta\delta^{13}C$ record with values below the line indicating periods of higher $\delta^{13}C$ at MD02-2589, (e) MD02-2589 mean sortable silt record: Periods with higher $\delta^{13}C$ bottom waters at MD02-2589 compared to MD95-2042 are highlighted in grey: H = Heinrich event, C20 = Atlantic cold event C20 (*Chapman and Shackleton,* 1999)

The individual % NCW records (Fig. 6.9a, b) show that both cores, while showing fluctuations, have fairly consistent values around 60 % NCW, which is conflicting with a meridional gradient in $\delta^{13}C$ between the North Atlantic and South Atlantic, with increased southwards mixing with surrounding water masses. This may suggest that other factors are influencing either or both of the benthic $\delta^{13}C$ records, discussed further in Section 6.3.4.

The low temporal resolution of core ODP Site 980 means that some of the smaller scale detail in the records is lost, however the Δ% NCW record (Fig. 6.9c) clearly suggests that during the negative carbon anomalies seen in the $\Delta\delta^{13}C_{2042\text{-}2589}$ record (Fig. 6.9d) there is more NCW or a greater percentage of high $\delta^{13}C$ waters in the South Atlantic than the North Atlantic. Such a signal suggesting a greater percentage of NCW in the mid-depth South Atlantic relative to the mid-depth North Atlantic is difficult to reconcile with our understanding of the THC and plausibly suggest that the negative $\Delta\delta^{13}C_{2042\text{-}2589}$ excursions are either related to mechanisms originating outside the North Atlantic or there is an alternative deep water source influencing the South Atlantic. The Δ% NCW record shows that these anomalies occur during cold stages (MIS 6 and 2) and substages (MIS 5b, d), as well as on shorter millennial timescales during MIS 3.

The extreme peaks of the majority of the $\Delta\delta^{13}C_{2042\text{-}2589}$ negative offsets occur during the transitions out of cold stages and substages, into warmer intervals (Fig. 6.7a –c; TII, MIS 5d/c, MIS 5b/a, MIS 4/3), although the majority of cold periods have negative values. This would suggest that perhaps the extreme negative offset values are a result of the different response times of the two cores to orbital forcing out of cold periods, rather than the difference between the water masses in the cold period itself. However, the mean

sortable silt record of MD02-2589 also shows higher values at the transitions between substages during MIS 5 and during MIS 3 (Fig. 6.7d), which correlate with many of the negative excursions. Higher mean sortable silt values suggesting more vigorous near bottom flow, have been attributed to the expansion of the ACC linked to Southern Hemisphere cooling suggesting that part of the excursions are likely being forced by Southern Hemisphere factors despite the apparent dominance of the MD95-2042 benthic $\delta^{13}C$ record in the $\Delta\delta^{13}C_{2042\text{-}2589}$ record.

6.3.2 Spectral Analysis, Phasing of Benthic $\delta^{13}C$ Records and Ocean Response To Ice Volume Changes on Precession Timescales

Initial spectral analysis on the individual benthic $\delta^{13}C$ records showed that there was low spectral variance at the precession frequency in the MD02-2589 record, which was not significant at 80 % confidence (Fig. 6.10b). Cross spectral analysis is used to determine the relationship between two different records as a function of frequency and can be used to identify particular frequencies that are present within both records but may not be identifiable in the individual time series of the records. As a result of the unsignificant precession peak in the MD02-2589 benthic $\delta^{13}C$ record, cross spectral analysis was performed for both cores with the benthic $\delta^{18}O$ records (reflecting ice volume) as the target and the benthic $\delta^{13}C$ records as the response (statistics in Table 6.1, 6.2). This was done in order to investigate the mechanisms behind the negative $\Delta\delta^{13}C_{2042\text{-}2589}$ anomalies and therefore the responses of the two benthic $\delta^{13}C$ records to ice volume changes. Cross spectral analysis was undertaken using the Blackman-Tukey method provided by *Analyseries* (*Paillard et al.*, 1996) with a Welch window.

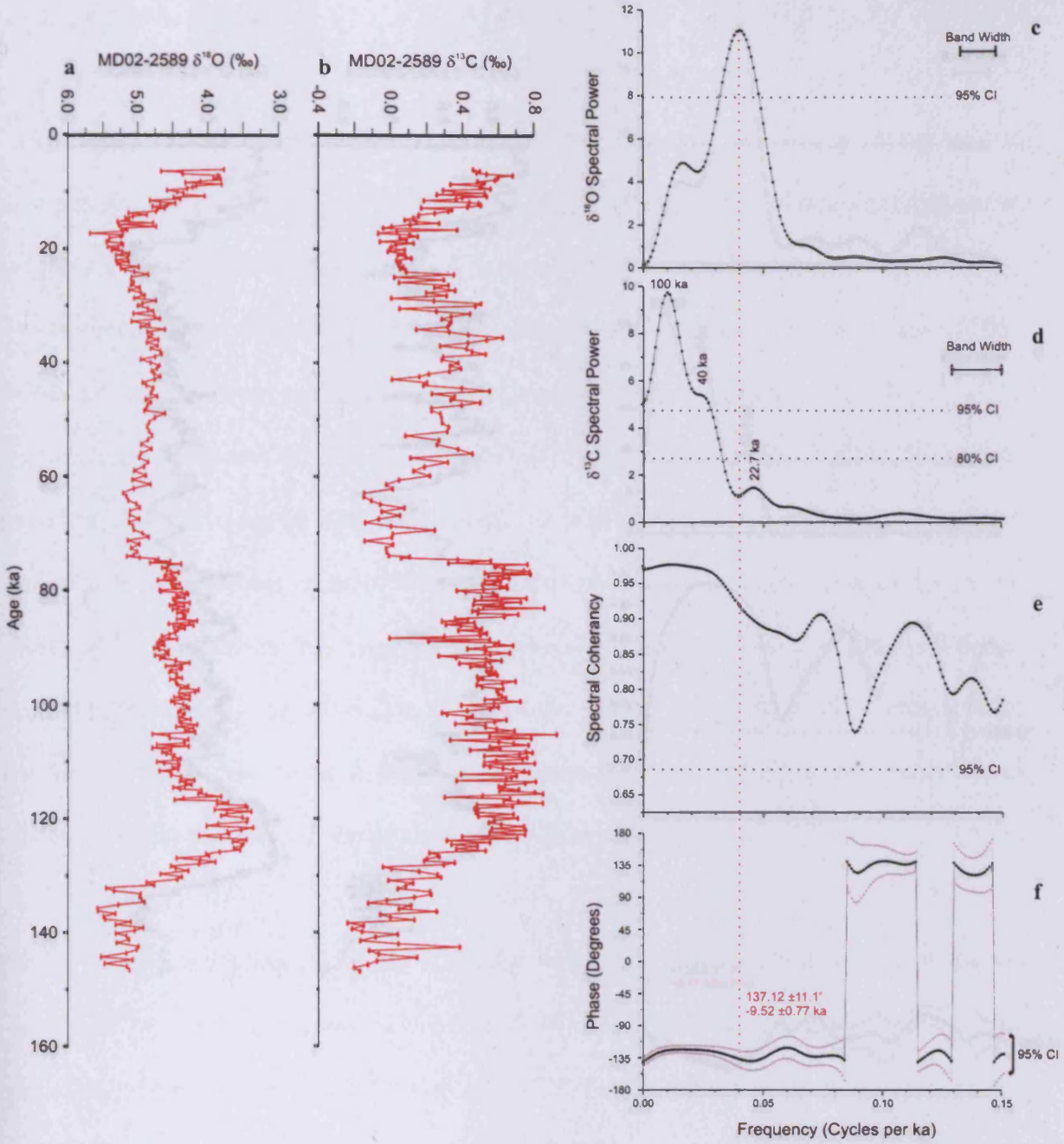

Figure 6.10 Cross Spectral Analysis of MD02-2589 Benthic $\delta^{18}O$ and $\delta^{13}C$ Records: (a) Benthic $\delta^{18}O$ record (target), (b) Benthic $\delta^{13}C$ record (response), (c) Spectral plot of benthic $\delta^{18}O$ record (BW = 0.014, 95 % CI = 7.95), (d) Spectral plot of benthic $\delta^{13}C$ record (BW = 0.029, 95 % CI = 4.84, 80 % CI = 2.79), (e) Spectral coherency of cross spectral analysis (95 % CI = 0.677), (f) Spectral phase showing 95 % confidence interval: Phase angle and lag of the benthic $\delta^{13}C$ record to the benthic $\delta^{18}O$ record (in ka) at the precession frequency defined by the benthic $\delta^{18}O$ spectral plot is shown in red

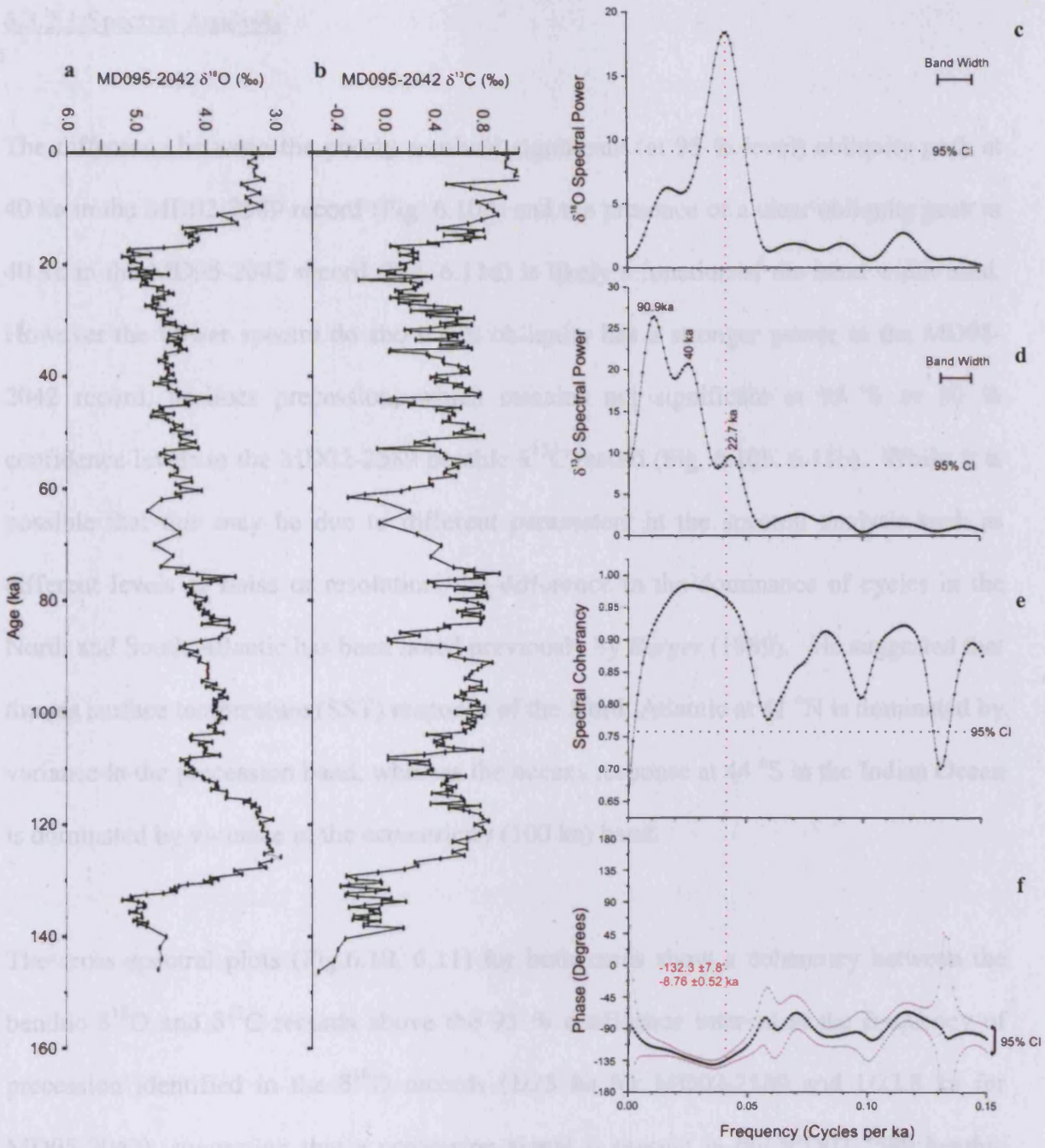

Figure 6.11 Cross Spectral Analysis of MD95-2042 Benthic $\delta^{18}O$ and $\delta^{13}C$ Records: (a) Benthic $\delta^{18}O$ record (target), (b) Benthic $\delta^{13}C$ record (response), (c) Spectral plot of benthic $\delta^{18}O$ record (BW = 0.021, 95 % CI = 8.55), (d) Spectral plot of benthic $\delta^{13}C$ record (BW = 0.013, 95 % CI = 8.53), (e) Spectral coherency of cross spectral analysis (95 % CI = 0.766), (f) Spectral phase showing 95 % confidence interval: Phase angle and lag of the benthic $\delta^{13}C$ record to the benthic $\delta^{18}O$ record (in ka) at the precession frequency defined by the benthic $\delta^{18}O$ spectral plot is shown in red

6.3.2.1 Spectral Analysis

The difference between the poorly resolved significant (at 95 % level) obliquity peak at 40 ka in the MD02-2589 record (Fig. 6.10d) and the presence of a clear obliquity peak at 40 ka in the MD95-2042 record (Fig. 6.11d) is likely a function of the band width used. However the power spectra do show that obliquity has a stronger power in the MD95-2042 record, as does precession, which remains not significant at 95 % or 80 % confidence levels in the MD02-2589 benthic $\delta^{13}C$ record (Fig. 6.10b, 6.11b). Whilst it is possible that this may be due to different parameters in the spectral analysis such as different levels of noise or resolution, the difference in the dominance of cycles in the North and South Atlantic has been noted previously by *Berger* (1989). He suggested that the sea surface temperature (SST) response of the North Atlantic at 41 °N is dominated by variance in the precession band, whereas the oceans response at 44 °S in the Indian Ocean is dominated by variance in the eccentricity (100 ka) band.

The cross spectral plots (Fig.6.10, 6.11) for both cores show a coherency between the benthic $\delta^{18}O$ and $\delta^{13}C$ records above the 95 % confidence interval at the frequency of precession identified in the $\delta^{18}O$ records (1/25 ka for MD02-2589 and 1/23.8 ka for MD95-2042), suggesting that a precession signal is present in the MD02-2589 benthic $\delta^{13}C$ record despite not showing as a significant frequency in the individual power spectra (Fig. 6.10b). Both coherency plots (Fig. 6.10c, 6.11c) show values close to 1, which indicates full coherency. The phase spectra for both cores (Fig. 6.10d, 6.11d) show negative values indicating that the changes in the benthic $\delta^{18}O$ lag changes in the benthic $\delta^{13}C$. As we are investigating the response of the benthic $\delta^{13}C$ record to changes in ice volume (on precession timescales) we can therefore assume that the $\delta^{13}C$ lead of 9.52

±0.77 ka for MD02-2589 and 8.76 ± 0.52 ka for MD95-2042 is in fact a lag from $\delta^{18}O$ of over half a precession cycle (15.48 ka for MD02-2589 and 15.04 ka for MD95-2042). This suggests that both cores are responding to changes in Northern Hemisphere insolation, which is antiphase with precession, rather than Southern Hemisphere insolation, which is in phase with precession. This would however be expected as global ice volume records are dominated by fluctuations in the Northern Hemisphere ice sheets, which respond to Northern Hemisphere insolation changes. However the lag of the benthic $\delta^{13}C$ records to ice volume of 14.7 – 16.25 ka for MD02-2589 and 14.52 – 15.56 ka for MD95-2042 cannot be statistically separated, therefore suggesting a simultaneous response of both cores to ice volume changes on precession timescales.

6.3.2.2 Dominance of Orbital Signals in the North Atlantic

The spectral analysis plots (Fig. 6.10b, 6.11b) show that power within the orbital precession and obliquity bands are far more significant in the benthic $\delta^{13}C$ record of MD95-2042 than MD02-2589. The results of the SPECMAP Atlantic study (*Imbrie et al.*, 1989), based on planktonic $\delta^{18}O$ and SST records, show this sensitivity of the high North Atlantic to all orbital bands compared to the South Atlantic.

Changes in precession dominate the low latitudes (0 - 65° N/S), although an obliquity signal remains as it modulates precession. At high latitudes (65 - 90° N/S) obliquity has relative dominance, although again there is a small precession signal as it modulates obliquity (*Ruddiman and McIntyre,* 1981). Both cores MD02-2589 and MD95-2042 are mid-latitude cores, but in opposing hemispheres and it is known that low latitude palaeoclimatic responses (SST, equatorial upwelling) have a major part of their variability

in the precession band, while proxies which record processes linked with high-latitude climate variability (benthic $\delta^{18}O$, benthic $\delta^{13}C$, Cd/Ca, lysocline depth) have most of their variance in the 100 ka and 41 ka bands (*Imbrie et al.*, 1992, 1993, *Labeyrie et al.*, 1996). It is therefore unexpected that the benthic $\delta^{13}C$ record of mid-latitude MD95-2042 shows such a strong precession signal if circulation changes were only influence on its benthic $\delta^{13}C$ record especially as mid-latitude MD02-2589 benthic $\delta^{13}C$ record shows such an insignificant precession signal.

This may suggest that there are additional factors affecting the benthic $\delta^{13}C$ values at the Iberian Margin, such as changes in the influence of productivity or varying air-sea gas exchange, which are directly forced by low latitude insolation. Nonetheless, studies have shown that Northern Hemisphere high latitude climate, the NADW formation regions, may be forced by climate variability originating from low latitudes and transmitted via the atmosphere (*Cane,* 1998*; Cane and Clement,* 1999*; Wang et al.*, 1999*; Raymo and Nisancioglu,* 2003*; Raymo et al.*, 2004), with a link between global monsoon intensity, forced by precession, and NADW production also being suggested (*Guo et al.*, 1998*; Gupta et al.*, 2003). The Northern Hemisphere ice sheets are sensitive to changes in orbital forcing at each of the orbital frequencies (*Imbrie et al.*, 1992; *Roe and Allen,* 1999; *Clark et al.*, 1999) and have a large influence on deep-water formation in the North Atlantic. Additionally, modelling evidence shows that the Northern Hemisphere land mass may amplify low latitude climatic responses (*Gallée et al.*, 1992*; Crucifix et al.*, 2006) through vegetation, snow and ice feedbacks, while Arctic sea ice, through its influence on radiative feedbacks, nearly doubles the size of the mid-high latitude response to orbital forcing (*Jackson and Broccoli,* 2003).

If indeed the presence of a large land mass in the Northern Hemisphere is amplifying and transmitting the low latitude precession signal to the high latitude deep water formation regions then the lack of land mass in the mid-latitude Southern Hemisphere and the dominance of the oceans may mean that precession remains predominantly a low latitude driver, not greatly affecting the water mass controlling the benthic $\delta^{13}C$ values of MD02-2589. However as MD02-2589 lies at the present day in the southern extension of NADW, close to the divide with LCDW, it is currently bathed by the same water mass as MD95-2042 (although probably not the case during glacials). It is therefore possible that MD95-2042, which lies closer to the source of NADW, is recording small scale fluctuations in the NADW ventilation in response to precession and obliquity, while the NADW signal at MD02-2589 is heavily dampened through mixing with surrounding water masses on its transit to the South Atlantic and therefore records smaller orbital signals. The benthic $\delta^{13}C$ record however suggests it is also possible that MD02-2589 is bathed in SCW during glacial periods (Chapter 5) and therefore the lack of especially precession in the benthic $\delta^{13}C$ record may be due to Southern Ocean variables rather than anything translated through NADW. The possibility of a high $\delta^{13}C$ SCW mass over the site during glacial periods may mean that any precession signal is dampened by a transition between two water masses with similar $\delta^{13}C$ values. The possibility of an air-sea gas exchange effect on the benthic $\delta^{13}C$ record of MD02-2589 (discussed further in Section 6.3.4.2) combined with a dominant influence of SCW over the site may have removed the signal of any NADW related modulation.

The spectral plot of the $\Delta\delta^{13}C_{2042\text{-}2589}$ record (Fig. 6.12) confirms the frequency of the cyclicity visually suggested by Fig. 6.7c as being heavily dominated by precession, with

precession being the only peak within the spectral plot significant at over 85 % confidence level.

6.3.2.3 Response of Southern Hemisphere to Northern Hemisphere Insolation Changes

The relationship between ice volume changes on precession timescales, represented by the $\delta^{18}O$ records, and the benthic $\delta^{13}C$ of MD95-2042 and MD02-2589 (Fig. 6.10, 6.11) is greater than half a precession cycle. This suggests that both the South Atlantic and the North Atlantic are responding simultaneously to Northern Hemisphere insolation changes. *Alley et al.* (2002) suggested that the Northern Hemisphere does lead the south over glacial terminations, although several studies have shown that SST in the southern hemisphere respond quicker to variations in the Earth's orbital parameters and Northern Hemisphere insolation changes than North Atlantic SST (e.g. *Hays et al.*, 1976; *Ruddiman and McIntyre,* 1981; *Howard and Prell,* 1992; *Labeyrie et al.*, 1996; *Brathauer and Abelmann,* 1999). This has been attributed not to variations in NADW flux to the Southern Ocean, but atmospheric circulation changes (*Brathauer and Abelmann,* 1999). While in this case, the mid-depth South Atlantic is not responding quicker than the north, the proposed mechanism of atmospheric teleconnections that influence ocean parameters over long distances can still be applied. Northern Hemisphere summer insolation is suggested to drive the Southern Hemisphere southeastern trade winds (*Schneider et al.*, 1995) and these influence the exchange of energy between the atmosphere, surface ocean and continents within the intertropical region. This in turn affects the surface ocean-atmosphere processes (heat, excess salinity and wind forcing) in the Antarctic Circumpolar frontal zone which through its control on the latitudinal distribution of the major frontal zones affects Southern Ocean SST (*Labeyrie et al.*, 1996)

and can alter intermediate and deep water formation rates significantly (*Saenko and England,* 2003). It may however be possible that the south is rapidly responding to (and in phase with) the response of the Northern Hemisphere to precession. The large ice sheets in the north are likely to dominate any climatic signal world-wide and therefore if they show some response to precession, this signal will most certainly propagate across both hemispheres.

The indistinguishable lead of MD95-2042 $\delta^{13}C$ over MD02-2589 $\delta^{13}C$ with respect to ice volume and importantly Northern Hemisphere insolation can likely be explained by atmospheric versus land processes. The Southern Hemisphere is dominated by oceans and therefore it can respond rapidly to changes in wind forcing (*Labeyrie et al.,* 1996), through atmospheric teleconnections, which affect sea ice extent (*Kim et al.,* 1998, *Shin et al.,* 2003; *Toggweiler et al.,* 2006). Sea ice distribution largely controls air-sea gas exchange, atmospheric CO_2 levels and the ventilation of the southern deep water masses (*Stephens and Keeling,* 2000; *Sigman and Boyle,* 2000; *Keeling and Stephens,* 2001; *Rutberg and Peacock,* 2006; *Toggweiler et al.,* 2006) and therefore productivity and air-sea gas equilibrium of the region.

However the small inertia in the Northern Hemisphere atmospheric, deep and surface oceans are controlled by the lagging response of the ice sheets, which is especially dominant when ice volume is large (*Ruddiman and McIntyre,* 1981; *Imbrie et al.,* 1989; *Ruddiman et al.,* 1989; *Alley et al.,* 2002). Planktonic formamiferal assemblages from the South Atlantic (*Little et al.,* 1997) show that especially during MIS 4 – 2 (< 45 ka) when Northern Hemisphere ice sheets were large, upwelling events in the South Atlantic linked to trade wind intensities lead Heinrich events in the North Atlantic by 3 ka, though

atmospheric teleconnections and wind forcing. A similar interhemsipheric linkage may explain why there is no discernable lag between North and South Atlantic in response to ice volume changes primarily forced by Northern Hemisphere insolation.

6.3.3 Evolution of the $\Delta\delta^{13}C_{2042\text{-}2589}$ Record

The power spectrum of the $\Delta\delta^{13}C_{2042\text{-}2589}$ record (Fig. 6.12) shows that variance at the precession frequency is only significant above the 85 % confidence level. Additional variance is hinted at half precession (1/10.75 ka) and possibly other smaller periodicities. The $\Delta\delta^{13}C_{2042\text{-}2589}$ record itself (Fig. 6.7c) shows that for the time interval 0 – 60 ka fluctuations with a frequency shorter than precession dominate the record. However the longer 60 – 150 ka time interval appears to be dominated by precession. In order to investigate the evolution and control of different frequencies within the $\Delta\delta^{13}C_{2042\text{-}2589}$ record a Wavelet analysis was performed on the record (Fig. 6.13b). The Wavelet technique is a form of Fourier Transform which uses generalised local base functions and flexible windows which narrow when focusing on high-frequency signals and widen when searching for low-frequency signals so that high frequency signals are not overrepresented and low frequency underrepresented as often happens in normal window Fourier transforms (*Lau and Weng,* 1995). The periodicities which are above the 95 % confidence level, are represented by dark orange to dark red colours on the power spectrum (Fig. 6.13b). The lowest theoretical period that can be resolved within a record, the Nyquist frequency (Table 6.1), calculated by two times the maximum sampling period, is 4 ka for the $\Delta\delta^{13}C_{2042\text{-}2589}$ record. While this periodicity is lower than the sub-millennial scale periodicities identified in the $\Delta\delta^{13}C_{2042\text{-}2589}$ power spectra and Wavelet (Fig. 6.12, 6.13b), it has been suggested that as sediment records are not ideal time series

and can be disturbed by for example diagenesis then periodicities lower than 3 - 4 times the sampling rate should be treated with caution (*Grützner et al.*, 2002). In the $\Delta\delta^{13}C_{2042\text{-}2589}$ record this equates to periodicities lower than 6 - 8 ka.

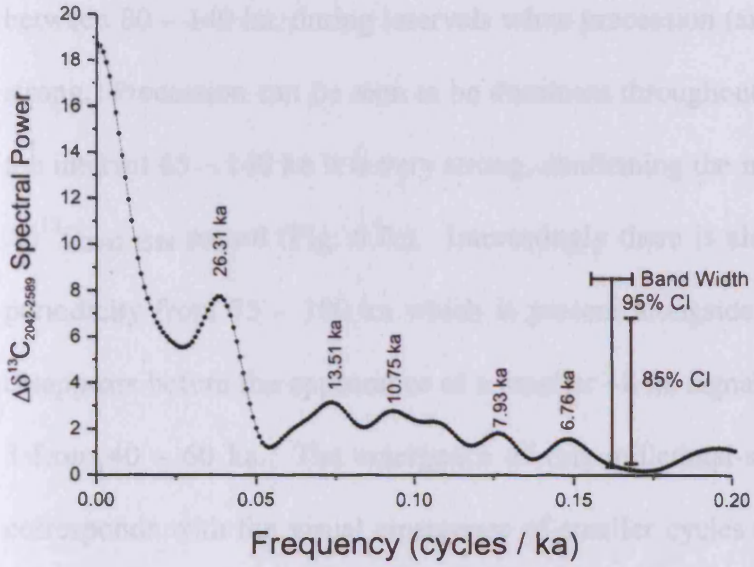

Figure 6.12 Spectral Plot of $\Delta\delta^{13}C_{2042\text{-}2589}$ Record: Showing identifiable lower frequencies than the 95 % CI (8.52) and 85% CI (6.98): BW = 0.013

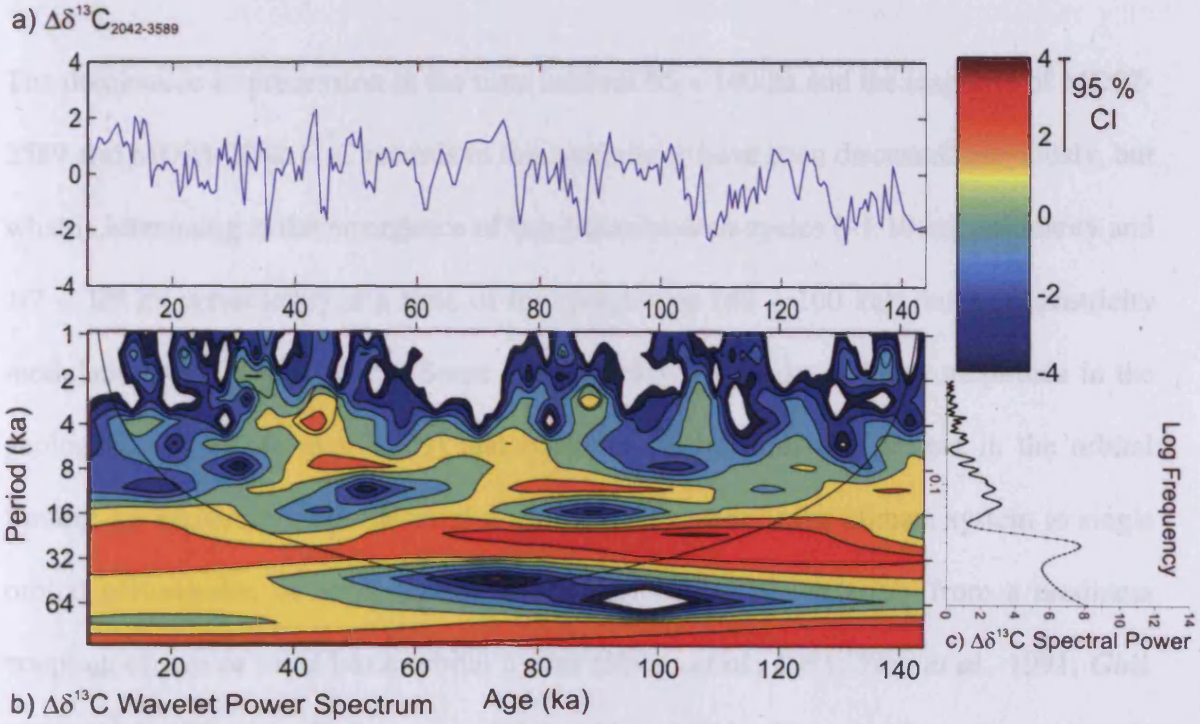

Figure 6.13 Wavelet Analysis of $\Delta\delta^{13}C_{2042\text{-}2589}$ Record: (a) $\Delta\delta^{13}C_{2042\text{-}2589}$ record, (b) Wavelet power spectrum (red and orange colours indicate over 95 % CI), (c) Spectral plot of $\Delta\delta^{13}C_{2042\text{-}2589\ record}$ showing which peaks are represented in the Wavelet spectrum

The wavelet plot shows significant power (>95 % C.I.) at around 90 - 100 ka (eccentricity) throughout the record (Fig. 6.13b), although it is more strongly present between 80 – 140 ka, during intervals when precession (around 26 ka periodicity) is also strong. Precession can be seen to be dominant throughout the whole record although for the interval 65 – 140 ka it is very strong, confirming the initial visual observations of the $\Delta\delta^{13}C_{2042\text{-}2589}$ record (Fig. 6.7c). Interestingly there is also a significant half precession periodicity from 75 – 100 ka which is present alongside the full precession signal and disappears before the appearance of a smaller ~8 ka signal which is present through MIS 3 from 40 – 60 ka. The emergence of this millennial-scale periodicity around 60 ka, corresponds with the visual emergence of smaller cycles in the $\Delta\delta^{13}C_{2042\text{-}2589}$ (Fig. 6.7c) and Δ% NCW records.

The dominance of precession in the time interval 65 – 140 ka and the response of MD02-2589 and MD95-2042 $\delta^{13}C$ records to this periodicity have been discussed previously, but what is interesting is the emergence of sub-Milankovitch cycles (~1/10 ka periodicity and 1/7 – 1/8 ka periodicity) at a time of low precession (40 – 100 ka), due to eccentricity modulation (Fig. 6.13b, 6.7c). Some sub-Milankovitch peaks of lower amplitude in the geological record (*Berger,* 1989) and peaks at periodicities not present in the orbital forcing are known to be products of non-linear responses of the climate system to single orbital periodicities or an 'intermodulation periodicity' which arises from a nonlinear coupling of two or more basic orbital cycles (*Nobes et al.,* 1991; *Yiou et al.,* 1991; *Ghil,* 1994; *Rial,* 1999; *von Dobeneck and Schmeider,* 1999). However the millennial-scale variability seen in the $\delta^{13}C$ record of MD95-2042 and the $\Delta\delta^{13}C$ record can be seen (Fig. 6.14b, c) to correlate with known ages of Heinrich events (H2 – H6 (*Hemming,* 2004;

Rashid et al., 2003) and possibly H7 (*Rasmussen et al.,* 2003) or Atlantic Cold Event C20 (*Chapman and Shackleton,* 1999)) in the North Atlantic.

Heinrich events are known to have a periodicity of 7 – 10 ka (*Bond and Lotti,* 1995), which correlates with the ~8 ka periodicity seen in the $\Delta\delta^{13}C_{2042\text{-}2589}$ record, and are thought to start around 70 ka (*Bond et al.,* 1992), although IRD evidence in cores from the North Atlantic suggest that they may persist into MIS 5 and 6 (*McManus et al.,* 1999; *Rasmussen et al.,* 2003). Heinrich events are defined by a collapse of the Laurentide ice sheet and an increase in iceberg production, mainly through the Hudson Strait, that is estimated to have reduced SST by 1 – 2°C and surface salinity by up to 4 ‰ (*Maslin et al.,* 1995), with a southwards movement of the Polar Front as far as 40 °N on at least 10 separate occasions during the last glacial-interglacial cycle (*Chapman et al.,* 2000). They are associated with poorly ventilated and weakly differentiated deepwater masses, with little if any NADW production and an inflow of SCW into the intermediate and deep Atlantic basin (*Seidov et al.,* 1996; *Vidal et al.,* 1997; *Zahn et al.,* 1997; *Paillard and Cortijo,* 1999; *Elliot et al.,* 2002), with an influence throughout the whole water column and a possible near-collapse of the AMOC, suggested by $^{231}Pa/^{230Th}$ data (*McManus et al.,* 2004; *Hall et al.,* 2006).

The initiation of these sub-Milankovitch frequencies links in with the critical ice sheet mass threshold (*McManus et al.,* 1999; *Schulz et al.,* 2002) shown in modelling and benthic $\delta^{18}O$ records, above which SST oscillations increase and 6 ka frequency events of catastrophic iceberg discharges occur (*McManus et al.,* 1999). The figure of 3.5 ‰ ($\delta^{18}O$) for this threshold (*McManus et al.,* 1999) equates to 4.14 ‰ (as the +0.64 ‰ *Uvigerina* correction used in this study is taken into consideration) in the benthic $\delta^{18}O$

record of core MD95-2042 (Fig. 6.7a) and it can be seen that this threshold is exceeded in MIS 5b, 5d, 5a the MIS 5/4 transition at 72.4 ka and MIS 4 - 2. These critical points at which the threshold is exceeded match the timing of the negative carbon anomalies seen in the $\Delta\delta^{13}C_{2042\text{-}2589}$ record (Fig. 6.14c; controlled by the MD95-2042 benthic $\delta^{13}C$ record), with excursions of higher $\delta^{13}C$ waters in the South Atlantic occurring in MIS 5d, 5b, 5a (as possible H7 / C20) and during MIS 4 – 2 as Heinrich events 2 – 6. The emergence of a half precession cycle during MIS 5 (100 – 75 ka: Fig. 6.13b) rather than the full Heinrich millennial-scale 8 ka cycle seen during MIS 4 – 3 is possibly due to the amount of time the Northern Hemisphere ice sheet mass remained above the critical threshold. The benthic $\delta^{18}O$ record of MD95-2042 (Fig. 6.7a) shows that during MIS 5b, d and a the values remained greater than 4.14 ‰ for only short periods of time (1.8 – 3.3 ka), when precession was strong, compared to the 57 ka period from MIS 4 – 2, when the precession signal was diminished. It is therefore possible that the catastrophic millennial scale events shown by *McManus et al.* (1999) to occur above the benthic $\delta^{18}O$ threshold did not have time to establish in MIS 5d, b, a before ice volume decreased coincident with a warmer period.

Whilst the MD02-2589 benthic $\delta^{13}C$ record during MIS 3 does not show negative carbon excursions of the scale seen in the North Atlantic similar events can still be identified within the record although with far smaller amplitudes (Fig. 6.14a). Some of the events do not appear synchronous with those in MD95-2042 (Fig. 6.14b) and this is possibly an artefact of age model uncertainties through this period although the original age model (Fig. 6.3b, c), whereby the benthic $\delta^{13}C$ anomalies during MIS 3 were synchronised, still shows that negative carbon anomalies ($\Delta\delta^{13}C_{2042\text{-}2589}$ record, Fig. 6.9d) occur during Heinrich events, with higher benthic $\delta^{13}C$ values at site MD02-2589.

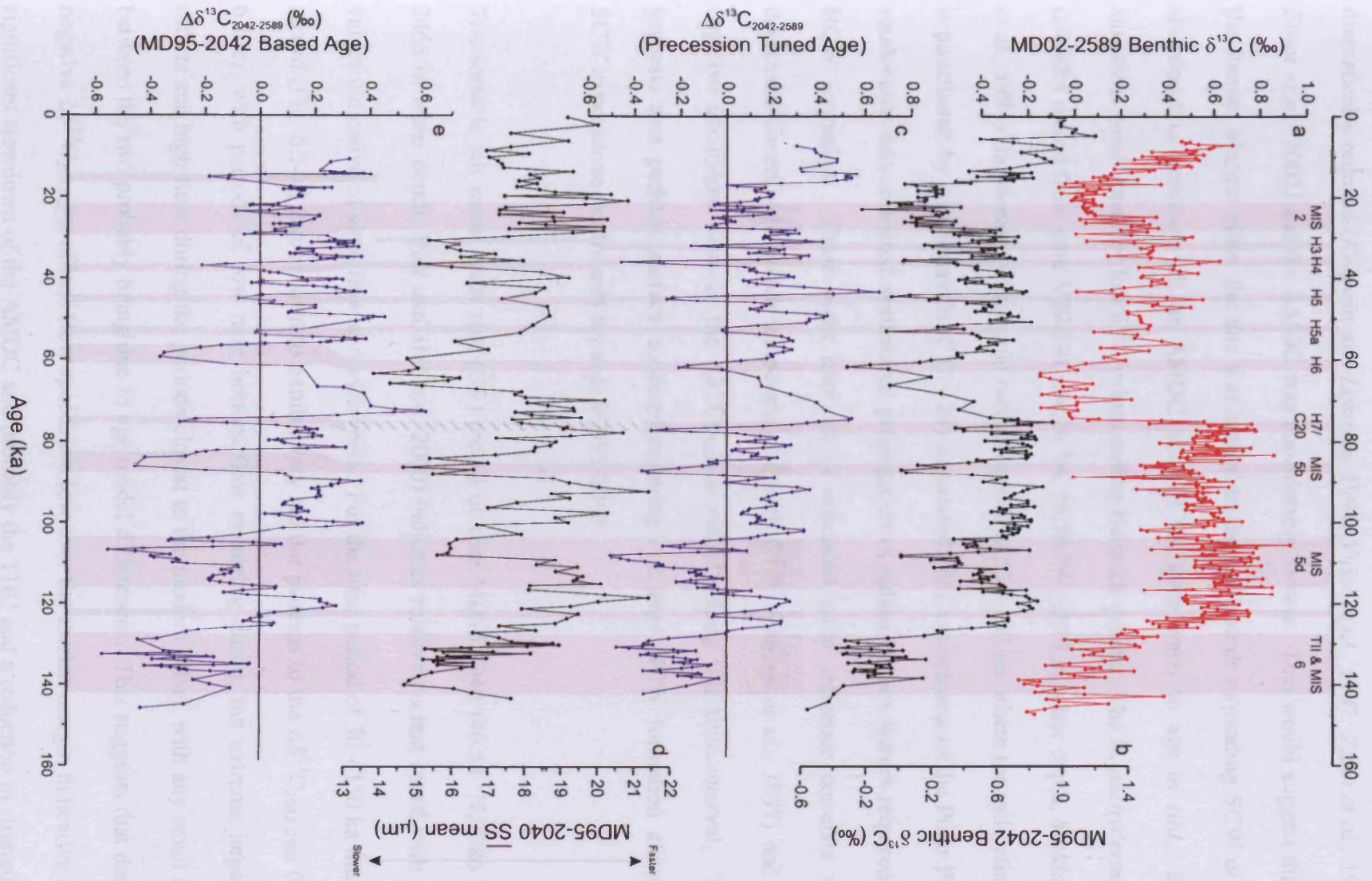

Figure 6.14 Identification of Periods of Negative Carbon Anomalies: (a) MD02-2589 benthic $\delta^{13}C$ record, (b) MD95-2042 benthic $\delta^{13}C$ record, (c) $\Delta\delta^{13}C_{2042\text{-}2589}$ record, (d) MD95-2040 mean sortable silt record (*Hall and McCave,* 2000), (d) $\Delta\delta^{13}C_{2042\text{-}2589}$ record on MD95-2042 tied age model (Fig. 6.1): Grey lines denote negative carbon anomalies

During these Heinrich events it has been well documented that NADW production was dramatically reduced (*Keigwin and Lehman,* 1994*; Vidal et al.,* 1997*; Zahn et al.,* 1997*; Elliot et al.,* 2002*)* and the AMOC was considerably slower. This would suggest that at the Iberian Margin either the site was bathed in the northwards expanding SCW or the slowdown or cessation of the AMOC allowed the deep water to age *in situ.* Both situations would produce low $\delta^{13}C$ values during Heinrich events. The *N. pachyderma %* (NPS%) record from core V29-191 (54.26 °N, 16.78 °W, 2370 m water depth, *McManus et al.,* 1994) shows eight warm-cold oscillations from 55 – 135 ka, where the mild climate is punctuated by cool intervals (C17 - 24) associated with a movement of the Polar Front southwards and restricted northwards propagation of saline surface waters required for NCW formation. These eight intervals of enhanced polar influence correlate with decreased Greenland surface temperatures (GRIP $\delta^{18}O$, *Johnsen et al.,* 1997) and the negative excursions seen in the $\Delta\delta^{13}C_{2042\text{-}2589}$ record during this time interval. This suggests that perhaps surface cooling/freshening restricted NCW formation allowing SCW to penetrate northwards towards MD95-2042.

The sortable silt mean grain size ($\overline{SS}$) record of core MD95-2040 (40.58 °N, 9.86 °W, 2465 m water depth; *Hall and McCave,* 2000) indicates relative current speed with low values indicative of slow flow and vice versa. For the time period of 30 - 150 ka the $\overline{SS}$ record (Fig. 6.14d) can be seen to exhibit very similar patterns to the $\Delta\delta^{13}C_{2042\text{-}2589}$ (Fig. 6.14c), with periods of low near bottom flow occurring during the extreme negative offsets and high flow during the periods closest to the modern offset, with any small lags between the two probably being due to age model differences. This suggests that during negative $\Delta\delta^{13}C_{2042\text{-}2589}$ offsets flow speeds are low over the Iberian margin indicative of a significant slowdown of the AMOC and probably the THC and a reduction in strength of

NCW formation. During these periods there is an increase in influence of SCW over the Iberian Margin producing the low $\delta^{13}C$ values seen at MD95-2042, although it is also possible that during Heinrich events the AMOC slows or stops and the water mass overlying MD95-2042 ages *in situ*, which combined with perhaps enhanced productivity produces very depleted benthic $\delta^{13}C$ values, without any SCW influence over the site. The slowdown of the AMOC and reduction in production of NCW during these negative carbon events, seen in MD95-2042, cannot however conventionally explain how MD02-2589 still retains a high $\delta^{13}C$ water mass (Fig. 6.14a). It can therefore be suggested that either the water mass bathing MD02-2589 during glacial periods and Heinrich events cannot be sourced from the North Atlantic, as it is not present at MD95-2042 or some other factor is affecting the benthic $\delta^{13}C$ values of either or both cores.

6.3.4 Possible Mechanisms for Negative Carbon Anomalies

6.3.4.1 Productivity Effect in the North Atlantic

The negative $\Delta\delta^{13}C_{2042\text{-}2589}$ anomalies, whereby the benthic $\delta^{13}C$ values in the North Atlantic are more negative than the South Atlantic may suggest additional factors, other than circulation, are influencing either benthic $\delta^{13}C$ record. It was noted above that the benthic $\delta^{13}C$ values of MD95-2042 were significantly lower than those estimated for the Iberian Margin by the *Sarnthein et al.* (1994) study, even if the northwards propagating SCW boundary is extended into the region. Upwelling is known to occur seasonally off the Iberian Margin mainly during spring and summer, where under strong northerly winds it can extend 100 – 200 km offshore (*Fiúza,* 1983, *Abrantes,* 2000). This upwelling is controlled by the Azores anticyclonic cell (*Pailler and Bard,* 2002) with intensification of the cell modelled to produce increased upwelling during the LGM (*Hewitt et al.,* 2001),

as well as during Heinrich events (*Little et al.,* 1997). Increased upwelling and its associated increased productivity is known to reduce benthic $\delta^{13}C$ values, due to the increased flux of ^{12}C-rich organic matter to the sea floor (e.g. *Ganssen and Sarnthein,* 1983; *Naidu and Niitsuma,* 2004).

MD95-2042 lies ~100 km offshore and therefore within this zone of extended summer upwelling and increased productivity. This may plausibly explain the anomalously low benthic $\delta^{13}C$ values of core, MD95-2042, as the so called 'Mackensen effect' (*Mackensen et al.,* 1993; *Mackensen and Bickert,* 1999; *Bickert and Mackensen,* 2003) affects epibenthic species, such as *F. wuellerstorfi*, in areas of strong seasonal productivity.

The large precession signal observed in the MD95-2042 benthic $\delta^{13}C$ record is unusual at a deep mid-latitude North Atlantic site which is believed to be responding to changes in bottom water circulation patterns, driven by high latitude production processes. It is well documented that there was higher productivity values during glacial periods on the Iberian margin (*Müller and Erlenkeuser,* 1983; *Abrantes,* 2000; *Pailler and Bard,* 2002) linked to intensified upwelling due to more vigorous atmospheric circulation and intensified trade winds (*CLIMAP,* 1976; *Lautenschlager et al.,* 1992; *Abrantes,* 2000), forced by the low latitude monsoons in response to precession forcing (e.g. *Schott,* 1983; *Clemens et al.,* 1991; *Tuenter et al.,* 2003; *Tian et al.,* 2005; *Ruddiman,* 2006). The presence of Northern Hemisphere ice sheets has also been suggested to intensify the Azores anticyclonic cell through enhanced zonal atmospheric circulation and increased upwelling (*Pailler and Bard,* 2002).

However during the negative carbon anomalies and glacial periods up to a 0.4 - 0.7 ‰ productivity overprint (Fig. 6.7b) would be required to shift the MD95-2042 $\delta^{13}C$ values to the expected offset with MD02-2589 $\delta^{13}C$ values. While values of 0.3 - 0.4 ‰ have been suggested for the Southern Ocean overprint (*Sarnthein et al.,* 1988; *Mackensen et al.,* 1993), productivity levels on the Iberian Margin are considerably smaller than the Southern Ocean.

Fluctuations in productivity both on glacial to interglacial and sub-Milankovitch timescales over the Iberian margin can therefore only be used to explain some of the low benthic $\delta^{13}C$ values and high precession signal recorded within MD95-2042. However if there is an alternative factor affecting the MD02-2589 benthic $\delta^{13}C$ record, making it more positive, then the productivity effect at MD95-2042 may be significant.

6.3.4.2 Air-Sea Gas Exchange in the South Atlantic

The MD02-2589 % NCW record (Fig. 6.9a) suggests that, apart from during MIS 5e and TI, the amount of NCW at the site throughout the record remains fairly consistent at around 60 %. As previously suggested during glacial periods and negative carbon excursions it is unlikely that the MD02-2589 site would have a greater component of NCW than the Iberian Margin and therefore it is possible there is an alternative factor affecting the MD02-2589 record that mimics the high $\delta^{13}C$ values of NCW.

At the present day the region just south of the Antarctic Polar Front has the maximum air-sea gas exchange in the Southern Ocean. Modelling studies (*Sigman and Boyle,* 2000) have shown that air-sea gas exchange increased in the Subantarctic zone during glacial

periods due to the equatorwards shift of the westerly wind belts and increased sea ice in the Antarctic zone (*Togweiller et al.,* 2006). At the present day site MD02-2589 lies just to the north of the Subtropical front, the northern edge of the Subantarctic zone, but in glacial periods the SAF, and therefore the Subantarctic zone, have been reconstructed to have migrated 2 – 3° northwards of their present day position at 45 °S in the South Atlantic (*Prell et al.,* 1980; *Howard and Prell,* 1992; *Belkin and Gordon,* 1996; *Brathauer and Abelman,* 1999) therefore including the MD02-2589 site. It is possible that the $\Delta\delta^{13}C_{2042\text{-}2589}$ offset during these negative excursions may be due to a combination of productivity effects in the North Atlantic, producing anomalously low $\delta^{13}C$ values, and increased air-sea gas exchange in the South Atlantic, producing high $\delta^{13}C$ values.

However if increased air-sea gas exchange was producing high benthic $\delta^{13}C$ values in the mid-latitude South Atlantic, we might expect to see this effect in other cores from similar latitudes in the South Atlantic. Deep Cape Basin cores RC11-83 (41.36 °S, 9.48 °E, 4718 m water depth; *Charles et al.,* 1996) and TN057-21 (41.08 °S, 7.49 °E, 4981 m water depth; *Ninnemann and Charles,* 2002), which are at a very similar latitude to MD02-2589 (41.19 °S, 25.15 °E, 2660 m water depth) do not show similar elevated benthic $\delta^{13}C$, as seen during glacial periods at MD02-2589, but rather show highly negative values (-1 ‰) and possible millennial scale events during MIS 3 (-0.8 ‰). This would argue against an air-sea gas exchange explanation for the high $\delta^{13}C$ values of MD02-2589, although TN057-21 and RC11-83 are from significantly deeper depths than MD02-2589 and previous studies have suggested that they may be affected by alterative mechanisms such as the Mackensen effect (*Mackensen et al.,* 2001).

6.3.4.3 Change in Bottom Water Source

An alternative explanation for negative $\Delta\delta^{13}C_{2042\text{-}2589}$ excursions is the increased influence of a better ventilated mid-depth water mass than currently exists in the South Atlantic in the mid-depth North Atlantic. *Bayon et al.,* (2003) suggest that the strong reduction in NADW influence in the glacial South Atlantic may have been due to an increased flow of CDW rather than any major weakening of NADW itself and variations in the production of deep water around Antarctica rather than changes in NADW or 'conveyor belt strength' have also been suggested as the primary influence on variability in North Atlantic records (*Toggweiler,* 1999*; Keeling and Stephens,* 2001, *Raymo et al.,* 2004).

During Heinrich events and MIS 5b, d the benthic $\delta^{13}C$ gradient from North to South was ~-0.3 ‰ (Fig. 6.7c), which is similar to the gradient at the present day, but in the opposite direction. The present day estimate for transit time within the Atlantic Ocean is ~200 years (*Peacock and Maltrud,* 2006). If the same Southern Hemisphere-sourced water mass was bathing both MD02-2589 and MD95-2042 during especially Heinrich events, you might expect a lag of MD95-2042 benthic $\delta^{13}C$ record to MD02-2589 due to the transit time of the ocean. The cross spectral analysis of the response of the two benthic $\delta^{13}C$ records to ice volume changes (Fig. 6.10, 6.11) show that statistically the response of the two records are indistinguishable. Furthermore a detailed investigation of the raw $\delta^{13}C$ data for both cores (Fig. 6.7c) at shorter timescales actually suggests that in general changes in MD02-2589 lags MD95-2042, especially through MIS 5b, d, MIS 4 – 3, H3 - 6 and TI. This suggests that a full circulation change on the timescales required, although not being totally quantifiable, was unlikely.

6.3.4.4 Southern Ocean High $\delta^{13}C$ Water Mass

If such a circulation change as described above occurred then it would require a relatively high $\delta^{13}C$ mid-depth water mass to be formed in the Southern Ocean. No such water mass exists at mid-depths at the present day. The only high $\delta^{13}C$ Southern Ocean water mass is AAIW, which at the present day forms along the SAF and spreads northwards at ~1000 m water depth (*Lynch-Stielgitz et al.,* 1994). Core MD97-2120 from the Chatham Rise, South Pacific (45.32 °S, 174.55 °E, 1210 m water depth, *Pahnke and Zahn,* 2005) shows positive benthic $\delta^{13}C$ excursions during North Atlantic Heinrich events, linked with increased AAIW formation and higher SST in the Southern Ocean.

Initially AAIW cannot be considered as a mechanism for explaining the high benthic $\delta^{13}C$ values at MD02-2589 during glacial periods, when both hemispheres are known to be colder than present and AAIW less widespread (*Volbers and Henrich,* 2002; *Kameo et al.,* 2004). However modelling work by *Saenko et al.* (2003) suggests that the MOC of the upper 2 - 3 km of the Atlantic is either dominated by an AAIW cell or a NADW cell, with a switch between the two being controlled by densities in both source regions. Similarly, it may be feasible that the high $\delta^{13}C$ water mass during glacial periods is AAIW as studies have suggested that it had increased depth of penetration during glacial periods (*Lohmann and Schwietzer,* 1990; *Bostock et al.,* 2004) and lower $\delta^{13}C$ values than the present day (*Ninnemann and Charles,* 1997; *Spero and Lea,* 2002; *Bostock et al.,* 2004). Despite these suggestions *Saenko et al.* (2003) show that the main dominance of AAIW during 'off' cold modes is still above 1500 m, considerably shallower than the 2660 m water depth of site MD02-2589.

Modelling studies (*Michel et al.,* 1995) have however suggested that during glacial periods a second shallower deep water mass formed around the Subantarctic Front (SAF), an area of increased air-sea gas exchange during glacial periods (*Sigman and Boyle,* 2000). The increased air-sea gas exchange would create a relatively high $\delta^{13}C$ water mass, which would have sunk to mid-depths above the low $\delta^{13}C$ deep waters forming under the extended winter sea ice region south of the Polar Front (*Rosenthal et al.,* 1997; *Mackensen et al.,* 2001; *Bickert and Mackensen,* 2003), but below AAIW.

This suggests that during glacial periods NADW production and the vigour of the AMOC was reduced significantly, while a new mid-depth water mass formed in the Southern Ocean. This water mass was likely only present only during cold periods, when the conventional deep water formation site in the Weddell Sea was blocked due to the grounding of ice sheets (*Rosenthal et al.,* 1997) and the region of intense air-sea gas exchange migrated into the Subantarctic zone due to shifts in the zonal wind patterns and sea ice expansion (*Sigman and Boyle,* 2000). The correlation of periods of high near-bottom flow speeds at MD02-2589, shown by the mean sortable silt record (Fig. 6.7d), with the negative $\Delta\delta^{13}C_{2042\text{-}2589}$ anomalies, especially through MIS 5, further suggests that this water mass forms during cold periods when the ACC has expanded bringing it closer to the site. This mechanism could explain the presence of a better ventilated water mass in the South Atlantic during glacial periods.

Pahnke and Zahn (2005) suggest a bipolar seesaw system (*Broecker,* 1998; *Seidov et al.,* 2001) for Heinrich events, whereby cold events in the North Atlantic and the reduction in NCW production are compensated by warming in the Southern Ocean and increased

AAIW production. If this bipolar seesaw system was operating then it would be expected that during Heinrich events in the north, a high $\delta^{13}C$ mid-depth water mass associated with warming would be forming in the south and extending to mid-depths. At the present day no such water mass exists, MD02-2589 lies around 1000 m below AAIW influence and the high $\delta^{13}C$ glacial SCW mass suggested above probably requires increased air-sea gas exchange linked to sea ice expansion, which would not occur during warm events.

So either this suggests that North Atlantic Heinrich events are not necessarily associated with concurrent warm events in the Southern Ocean, as suggested by authors such as *Blunier et al.,* (1998) or an alternative high $\delta^{13}C$ SCW mass needs to be invoked. Although MD02-2589 lies around 1000 m below AAIW influence at the present day, *Pahnke and Zahn* (2005) do suggest intensified AAIW formation during Heinrich events, with increased depth of penetration (*Lohmann and Schwietzer*, 1990; *Bostock et al.,* 2004). The benthic $\delta^{13}C$ and $\Delta\delta^{13}C_{2042\text{-}2589}$ records (Fig. 6.9a - c) suggest that, as in core MD97-2120 from the South Pacific, during North Atlantic Heinrich events the benthic $\delta^{13}C$ values of MD02-2589 are positive, consistent with a change in influence from NCW to a SCW, and possibly AAIW. Unlike during glacial periods the mean sortable silt record of MD02-2589 does not show increased flow speeds during Heinrich events (Fig. 6.9e) and this may suggest a different mechanism is operating during glacial periods and Heinrich events, perhaps with AAIW being the source during Heinrich events and an alternative SCW mass being the source for glacial periods. Either the formation of a mid-depth water mass with a high $\delta^{13}C$ signature or increased AAIW production would have counteracted the reduction in NCW in the South Atlantic associated with Heinrich events

and would have mixed with any southwards propagating Heinrich event signal, dampening it but not erasing it entirely, as seen in the MD02-2589 $\delta^{13}C$ record.

The presence of a high $\delta^{13}C$ water mass in the South Atlantic during both cold and warm periods may explain the lack of orbital signal within the MD02-2589 record. A switch between two water masses with similar signatures would produce a $\delta^{13}C$ record with little structure, other than that associated with the terrestrial biosphere component, consistent with MD02-2589. This lack of structure in the benthic $\delta^{13}C$ record of MD02-2589 would not mean that precession and obliquity forcing are not strong within the record, but that their influence is being dampened by the changing influence of differing water masses with similar $\delta^{13}C$ signatures, as is the millennial-scale signal of Heinrich events.

6.4 Conclusions

The benthic $\Delta\delta^{13}C_{2042\text{-}2589}$ record of North Atlantic core MD95-2042 minus South Atlantic core MD02-2589 shows that at only five short lived periods and one longer period over the past 150 ka have the two cores shown values similar to the modern offset between the sites due to water mass ageing and mixing. The MD95-2042 benthic $\delta^{13}C$ record suggests that certainly during glacial periods MIS 2, 4 and 6 its values are considerably lower than those reconstructed or expected for the Iberian Margin. Eight negative anomalies are identified in the $\Delta\delta^{13}C_{2042\text{-}2589}$ record whereby the South Atlantic has higher $\delta^{13}C$ values and higher % NCW than the North Atlantic. These events correspond to cold periods MIS 6, 2 5b and 5d and Heinrich events. Several possible mechanisms, including a glacial productivity overprint at MD95-2042 and increased air-sea gas exchange, linked to an equator-ward shift in the westerly wind belts, influencing

site MD02-2589, identified to explain these negative $\Delta\delta^{13}C_{2042\text{-}2589}$ anomalies, while plausible, are unlikely to explain the full difference between the benthic $\delta^{13}C$ values of the two cores.

The $\Delta\delta^{13}C_{2042\text{-}2589}$ record shows that precession is dominant from 140 – 65 ka, although a near half precession and millennial-scale periodicities emerge when the precession forcing is diminished by eccentricity modulation, and possibly a critical ice sheet mass threshold, shown by the benthic $\delta^{18}O$ record, is crossed. Spectral analysis of the benthic $\delta^{13}C$ records show that both cores simultaneously respond to Northern Hemisphere insolation on precession timescales. The response of the South Atlantic to Northern Hemisphere forcing is likely through atmospheric teleconnections and wind forcing, which affects the latitudinal position of the Southern Ocean frontal zones, deep water formation regions, air-sea gas exchange and upwelling.

During Heinrich events and glacial periods when NCW production decreases and shoals within the water column, SCW penetrates further into the Atlantic basin and increases its influence at site MD95-2042. The $\Delta\delta^{13}C_{2042\text{-}2589}$ and individual benthic $\delta^{13}C$ records suggest that during these periods the South Atlantic remains bathed in a well-ventilated and high $\delta^{13}C$ water mass, which is very unlikely therefore to have originated from the North Atlantic. The possibility of a reversal in the flow of water masses in the Atlantic, so a better ventilated mid-depth water mass from the South Atlantic was the source for the mid-depth North Atlantic, is unlikely as the cross spectral analysis suggests that both records respond simultaneously to ice volume changes. It is therefore probable that a Southern Ocean water mass (either AAIW or CDW), with characteristics different from those which exist at the present day, was forming during both glacial periods and

Heinrich events. During glacial periods and cold substages during MIS 5 this water mass is linked with increased flow speeds at MD02-2589 indicative of colder surface conditions and an expanded ACC. This is not detectable during Heinrich events presenting the possibility that two different mechanisms operate for glacial periods and millennial-scale events.

It appears most likely that the MD95-2042 benthic $\delta^{13}C$ record, which dominates the $\Delta\delta^{13}C_{2042\text{-}2589}$ record, is reflecting the strength of NCW formation. The MD02-2589 benthic $\delta^{13}C$ record however reflects changes in the water masses bathing the site but with similar $\delta^{13}C$ signatures suggesting that orbital and millennial-scale signals are dampened within the record, making transitions between the two water masses difficult to identify.

Chapter 7: Glacial to Interglacial Southern Ocean Water Column Structure

7.1. Introduction

Both the benthic $\delta^{13}C$ record of MD02-2589 investigated in Chapter 5 and the $\Delta\delta^{13}C$ offset investigated in Chapter 6 suggest that the benthic $\delta^{13}C$ values of the mid-depth South Atlantic were better ventilated that those in the North Atlantic during glacial periods. Both chapters conclude that during glacial periods and Heinrich events there is a water mass present at mid-depths in the South Atlantic with $\delta^{13}C$ values similar to present day NCW. Conclusions drawn from the $\Delta\delta^{13}C$ record however suggest that the source of this high $\delta^{13}C$ glacial water mass was not the North Atlantic, but more likely originated from the Southern Ocean, although its exact formation location and characteristics are unknown.

In order to investigate further this glacial Southern Ocean high $\delta^{13}C$ water mass a suite of cores were used to assess the glacial water column structure of the southeastern Atlantic sector of the Southern Ocean. The cores form both a latitudinal transect from 25.5° – 51.5 °S over the present day and glacial positions of the Polar, Subantarctic and Subtropical Fronts (*Prell*, 1980; *Belkin and Gordon*, 1996; *Howard and Prell*, 1992; *Brathauer and Abelmann*, 1999) and a depth transect from 1330 – 4980 m water depth. Due to the restricted number of cores with $\delta^{13}C$ records stretching back past MIS 5, the glacial reconstruction was based on LGM (defined by the EPILOG study as 23 - 19 ka; *Mix et al.*, 2001) values as an indication of previous glacial periods.

Comparing benthic $\delta^{13}C$ records from cores forming a depth transect between 1300 – 5000 m water depths between the LGM and Holocene *Hodell et al.* (2003) and *Ninnemann and Charles* (2002) suggest the presence of a well-developed chemocline in the South Atlantic at the LGM and most glacial periods back to 1.1 Ma (Fig. 7.1b: all values are measured on species *F. wuellerstorfi*). They suggest that there was a sharp chemical divide between well-ventilated mid-depth waters above 2500 m and less well-ventilated deep waters below, resulting from a strong pycnocline that caused limited vertical mixing, which produces very depleted $\delta^{13}C$ bottom waters. A compilation of benthic $\delta^{13}C$ and Cd/Ca data (*Curry and Oppo,* 2005; *Marchitto and Broecker,* 2006) further indicates enhanced ventilation of shallow isopycnals with the transition to less ventilated depth levels between 2200 and 2700 m. The development of such a chemocline has been suggested to have contributed to the extremely negative glacial $\delta^{13}C$ values recorded in deep South Atlantic cores (RC11-83 (*Charles et al.,* 1996) and TN057-21 (*Ninnemann and Charles,* 2002)), which are lower than values for the Pacific Ocean (*Ninnemann and Charles,* 2002), compared to the mid-depth and shallower Southern Ocean cores (e.g. ODP 1088 (*Hodell et al.,* 2003) MD02-2589 (see Chapter 5)). This evidence was interpreted by *Hodell et al.* (2003) to suggest a reduction in NADW flux at deep levels into the Southern Ocean during glacial periods, as NADW is a well-ventilated water mass which during the Holocene in the South Atlantic produces a well-mixed homogenous water column.

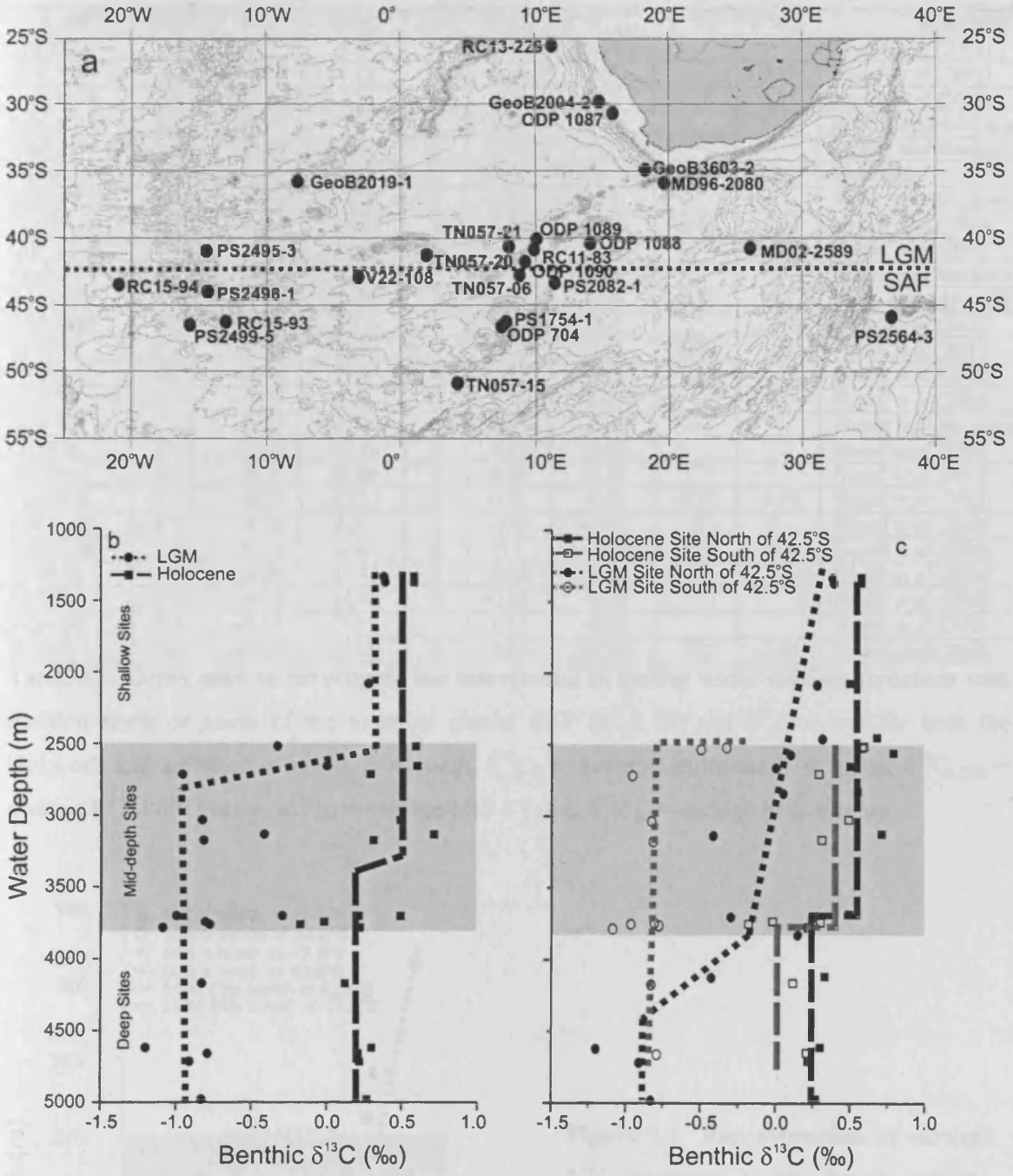

Figure 7.1 Reconstruction of vertical $\delta^{13}C$ gradients in the South Atlantic over the Holocene and LGM a) Map showing the sites used in the data comparison study in Fig. 7.1b and 7.1c (Table 7.1) (*Hodell et al.*, 2003 and *Bickert and Mackensen,* 2003) (b) Vertical carbon gradients in the South Atlantic for the Holocene and LGM taken from *Hodell et al.* (2003) (c) Vertical carbon gradients in the South Atlantic for the Holocene and LGM with the sites divided into those north of 42.5 °S and those south of 42.5 °S.

Core	Depth	Lat.	Long.	N/S	$\delta^{13}C_H$	$\delta^{13}C_{LGM}$	$\delta^{13}C_{S4}$	$\delta^{13}C_{S6}$	Reference
TN057-20	1335	-42.1	0.6	N	0.58	0.38			*Hodell et al (2003)*
ODP 1087	1372	-31.27	15.18	N	0.58	0.39	0.3	0.31	*Hodell et al (2003)*
ODP 1088	2082	-41.8	13.33	N	0.5	0.28	0.16	0.05	*Hodell et al (2003)*
MD96-2080	2488	-36.27	19.47	N	0.65	0.3		0.01	*Martinez-Méndez et al. (2008)*
GeoB2004-2	2569	-30.87	14.54	N	0.79	0.1			*Bickert and Mackensen (2003)*
MD02-2589	2660	-41.26	25.15	N	0.5	0	-0.06	-0.2	*This Study*
GeoB3603-2	2840	-35.13	17.54	N	0.55	0.05			*Bickert and Mackensen (2003)*
PS2495-3	3134	-41.28	-14.49	N	0.71	-0.42	-0.45	-0.35	*Hodell et al (2003)*
ODP 1090	3702	-42.5	8.53	N	0.49	-0.3	-0.44	-0.2	*Hodell et al (2003)*
GeoB2019-1	3825	-36.06	-8.78	N		0.15			*Bickert and Mackensen (2003)*
RC13-229	4191	-25.49	11.30	N	0.30	-0.36	-0.55	-0.7	*Curry and Oppo (1997)*
ODP 1089	4621	-40.56	9.53	N	0.3	-1.2		-1.05	*Hodell et al (2003)*
RC11-83	4718	-41.36	9.48	N	0.22	-0.91	-0.94	-1.1	*Hodell et al (2003)*
TN057-21	4981	-41.08	7.49	N	0.27	-0.83	-1	-1	*Hodell et al (2003)*
PS1754-1	2519	-46.77	7.61	S	0.59	-0.33			*Hodell et al (2003)*
ODP 704	2532	-46.88	7.42	S	0.58	-0.5			*Bickert and Mackensen (2003)*
RC15-93	2714	-46.06	-13.13	S	0.29	-0.96			*Hodell et al (2003)*
PS2564-3	3034	-46.14	35.90	S	0.49	-0.83			*Hodell et al (2003)*
PS2499-5	3175	-46.51	-15.33	S	0.31	-0.82	-0.93	-0.96	*Hodell et al (2003)*
TN057-15	3744	-51.54	4.31	S	-0.02	-0.81			*Hodell et al (2003)*
TN057-06	3751	-42.54	8.58	S	0.3	-0.97	-1.08	-0.8	*Hodell et al (2003)*
RC15-94	3762	-42.59	-20.51	S	-0.18	-0.78			*Hodell et al (2003)*
PS2498-1	3783	-44.15	-14.49	S	0.22	-1.09	-1		*Hodell et al (2003)*
V22-108	4171	-43.11	-3.15	S	0.12	-0.83			*Hodell et al (2003)*
PS2082-1	4661	-43.13	11.45	S	0.21	-0.79	-0.8	-1.05	*Hodell et al (2003)*

Table 7.1. Cores used to investigate the interglacial to glacial water column structure with position north or south of the assumed glacial SAF (42.5 °S) and $\delta^{13}C$ values for both the Holocene and LGM; N = north, S = south, $\delta^{13}C_H$ = average Holocene $\delta^{13}C$ value, $\delta^{13}C_{LGM}$ = average LGM $\delta^{13}C$ value, $\delta^{13}C_{S4}$ = average MIS 4 value, $\delta^{13}C_{S6}$ = average MIS 6 value

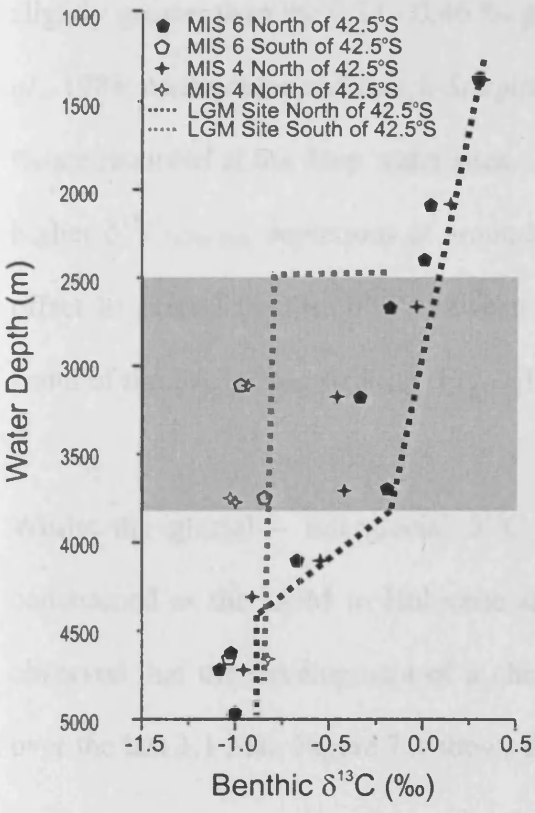

Figure 7.1 Reconstruction of vertical $\delta^{13}C$ gradients in the South Atlantic over MIS 4 and 6 with the sites divided into those north of 42.5 °S and those south of 42.5 °S.

7.2. Interglacial to Glacial Chemocline

The largest amplitude change in benthic $\delta^{13}C$ from the LGM to Holocene (up to 1.3 ‰ VPDB) occurs in the deep cores that are currently located well below the direct influence of NADW (Fig. 7.1b), whilst cores that are currently positioned in modern day NADW display a much smaller change in $\delta^{13}C$ (*Rutberg and Peacock*, 2006). Fig. 7.1c shows the chemocline as proposed by *Hodell et al.* (2003), with additional sites from other studies within the southeastern South Atlantic, while discriminating the spatial distribution of the core sites between those located north (25.5° - 42.5 °S) and south (42.5° - 51.5 °S) of the assumed SAF at the LGM (see also Fig. 7.1a and Table 7.1). This regional separation is based on evidence that suggests that the SAF during the LGM was ~2 - 3°N of its present position at 45 °S (*Belkin and Gordon*, 1996; *Prell*, 1980; *Brathauer and Abelmann*, 1999; *Howard and Prell*, 1992). Sites north of the SAF exhibit a LGM-Holocene benthic $\delta^{13}C$ ($\delta^{13}C_{LGM\text{-}Hol}$) depletion of 0.2 ‰ at shallow to 0.6 ‰ at mid-depth water sites, only slightly greater than the 0.34 - 0.46 ‰ global carbon shift (*Curry et al.*, 1988; *Duplessy et al.*, 1988; *Matsumoto and Lynch-Stieglitz*, 1999), while $\delta^{13}C_{LGM\text{-}Hol}$ depletions of 1.1 – 1.5 ‰ are recorded at the deep water sites. Sites to the south of the SAF display consistently higher $\delta^{13}C_{LGM\text{-}Hol}$ depletions at around 1.2 ‰ from mid-depth to deep waters, with the offset in glacial benthic $\delta^{13}C$ between the mid-depth sites (2500 - 3700 m) north and south of the SAF being striking (Fig. 7.1c).

Whilst the glacial – interglacial $\delta^{13}C$ shift in previous glacial cycles is not as well constrained as the LGM to Holocene shift due to the lack of data, *Hodell et al.* (2003) observed that the development of a chemocline is a persistent feature of glacial periods over the last 1.1 Ma. Figure 7.2 shows the chemocline split presented in figure 7.1 for the

LGM with data for MIS 4 and 6 superimposed on top. The graph clearly shows that whilst the data coverage is not as complete as for MIS 2, there does seem to still be a latitudinal mid-depth split during these two previous glacial periods. Benthic $\delta^{13}C$ data from core MD96-2080 in the Agulhas Bank Slope area (*Martínez-Méndez et al.,* 2008) at 2488 m water depth north of the SAF also imply a persistent presence of well-ventilated waters to at least 2500 m water depth during most of MIS 6 and 8, with strongly reduced presence of NCW at mid depths south of the SAF and increased low $\delta^{13}C$ waters (*Molyneux and Martínez-Méndez,* in prep). On the basis of paired benthic $\delta^{13}C$ and Cd/Ca data *Martínez-Méndez et al.* (2008) suggest that the well-ventilated water mass in the early glacial phases is northern sourced while in late glacial phases such NCW is replaced by USCW. The negative carbon anomalies identified in Chapter 6 tend to occur late in glacial stages and during the transitions from cold to warm periods, which would fit with suggestion of *Martínez-Méndez et al.* (2008) of a separate SCW mass during late glacial periods (different to AAIW).

The presence of high $\delta^{13}C$ waters at glacial mid-depths north of the SAF supports the findings of Chapters 5 and 6, based solely on the MD02-2589 benthic $\delta^{13}C$ record. This chapter aims to identify both the mechanisms behind the high $\delta^{13}C$ mid-depth water mass and the cause of the sharp mid-depth divide north and south of the SAF. While initially the cause is not clear, it can be suggested that it is unlikely to be a reflection of mixing between two different end member water masses as these sites are located too close together. Rather, an increased glacial biological productivity influence on benthic $\delta^{13}C$ values south of the SAF may be indicated or the glacial presence of either some sort of barrier to mixing leading to a strong chemical divide north and south of the ACC, with $\delta^{13}C$ depleted waters only occurring north of the SAF at water depths below ~ 4000 m or

the presence of a different high $\delta^{13}C$ water mass forming around the SAF and only spreading northwards at mid-depths.

7.3. Discussion

7.3.1 Glacial Biological Productivity Effect

One of the possible causes of the low mid-depth to deep $\delta^{13}C$ values south of the SAF may be the 'phytodetritus effect' or 'Mackensen effect' (*Mackensen et al.,* 1993; *Mackensen and Bickert,* 1999; *Bickert and Mackensen,* 2003), which causes benthic foraminifera to record $\delta^{13}C$ values 0.3 - 0.4 ‰ lower than the ambient bottom waters due to the decay of isotopically light organic material at the sediment water interface. *Mackensen et al.* (1993) suggest that sites south of 37 °S may have experienced changes in primary productivity and plankton assemblages during glacial periods in conjunction with meridional shifts of the PF. It is therefore possible that benthic $\delta^{13}C$ values at these sites (those south of the SAF during glacial periods) are considerably overprinted with negative $\delta^{13}C$ signatures from glacially-enhanced productivity due to the increased influence of the PF.

Martinez-Mendez et al. (in review) however show that the $\delta^{13}C_{as}$ ($\delta^{13}C$ air-sea exchange) values of core RC13-229, from the deep Cape Basin (4191 m water depth; *Oppo et al.,* 1990; *Oppo and Rosenthal,* 1994; *Lea,* 1995), do not converge or even increase during glacial periods to similar values to those seen at MD96-2080 (Agulhas Bank; 2488m water depth; *Martinez-Mendez et al.,* in review), which represents the mid-depth high $\delta^{13}C$ sites north of the SAF. This suggests that the phytodetritus effect is either not driving the discrepancy between mid-depth sites north and south of the SAF or is only

part of the explanation. Furthermore, the chemocline has also been observed in the Indian Ocean (*Kallel et al.*, 1988), which is not known to have strongly depleted deep benthic $\delta^{13}C$ values due to the Mackensen effect, again suggesting that the phytodetritus effect is unlikely to be the whole cause of the mid-depth divide.

7.3.2 Physical Barrier To Mixing

A further possible mechanism for the glacial mid-depth gradient in benthic $\delta^{13}C$ north and south of the assumed SAF (Fig. 7.1c) relates to the movement of bottom water formation areas during the LGM and continued southwards propagation of NCW. AABW currently forms in the Weddell Sea, by mixing of Ice Shelf water which is highly saline due to salt gain during sea ice freezing and Weddell deep water which is very cold due to super-cooling during polynya formation (*Fahrbach et al.*, 1995). A change in mode of AABW formation during glacial periods has been widely suggested (e.g. *Kuhn and Diekmann*, 2002; *Pudsey and Howe*, 1998 and *Mackensen et al.*, 2001). The expansion and grounding of ice shelves in the Weddell Sea is believed to reduce or halt brine formation in this area during glacial periods (*Rosenthal et al.*, 1997; *Bickert and Mackensen*, 2003) and instead, enhanced production of deep waters is thought to occur in the zone of extended winter sea ice coverage (out to ~50 °S) south of the PF (*Rosenthal et al.*, 1997; *Mackensen et al.*, 2001; *Bickert and Mackensen*, 2003) with a second shallower deep water mass forming along the SAF (*Michel et al.*, 1995). The position of the SAF during glacial periods is known to be ~43 – 41 °S (*Brathauer and Abelmann*, 1999) which suggests that the divide seen in Fig. 7.1c could possibly be related to the movement of Antarctic bottom water formation areas out to the PF and SAF. It is therefore plausible that NCW penetration was restricted in the areas south of the SAF, reflected in depleted

$\delta^{13}C$, by an expanding CDW and bottom water formation in the areas normally more prominently influenced by NCW (*Molyneux and Martínez-Méndez*, in prep). However, a NCW mass still penetrated in some guise as far south as 42.5 °S and to depths of 2500 m, with mixing increasing its influence down to at least 3700 m, as indicated by more positive $\delta^{13}C$ values of the cores north of the SAF and below 3700 m .

The increase in flow speed seen in the MD02-2589 mean sortable silt record (Chapter 5) during glacial periods associated with the ACC is also seen in other cores (*Pugh et al.*, 2006; *Carter et al.*, 2000; *Martinez-Mendez et al.*, in review) and may have contributed to impeding a southwards penetration of NCW. The ACC, is known to extend to depths of 4000 m (*Orsi et al.*, 1995), with the bulk of its estimated transport occurring in deep reaching, narrow jets associated with the PF and SAF (*Nowlin and Klinck*, 1986; *Gille*, 1994). Studies have suggested that 42 % (south of South Africa; *Legeais et al.*, 2005) of the 145 Sv (at 0 °E; *Legeais et al.*, 2005) transport estimate for the ACC as a whole occurs at the SAF at the present day, with suggestions of increased transport estimates during glacial periods (*Pudsey and Howe*, 1998; *Kim et al.*, 2002). The increase in transport volume of these large deep reaching narrow jets associated with the SAF would possibly have reduced any penetration of high $\delta^{13}C$ NCW into the Southern Ocean producing the divide seen at the SAF.

Work by *Lynch-Stieglitz and Fairbanks* (1994) and *Lynch-Stieglitz et al.* (1996) found well-ventilated, nutrient-rich waters with positive $\delta^{13}C_{as}$ values at intermediate depths in the Pacific Ocean and offshore from South Australia during the LGM. They suggest this water mass is GNAIW, which was advected out of the Atlantic Ocean and transported to intermediate depths in the Pacific Ocean. This is further confirmed by $^{231}Pa/^{230}Th$ ratios

which have been used to suggest that GNAIW export from the Atlantic Ocean was as intensive as NADW is at the present day and penetrated into the Pacific Ocean (*Yu et al.*, 1996). Further *Imbrie et al.* (1992) suggested that this GNAIW bypassed the Southern Ocean, leaving an isolated CDW, which would fit with the mechanism of a southwards penetrating high $\delta^{13}C$ NCW mass not mixing with the low $\delta^{13}C$ Southern Ocean origin water mass. This proposed mechanism supports modelling results by *Michel et al.* (1995) who suggest that glacial intermediate and upper mid-depth waters of the Southern Ocean were northern sourced, with lower mid-depth, SAMW, forming at the SAF during the LGM.

However the $\Delta\delta^{13}C$ record shown in Chapter 6 suggests that the high glacial $\delta^{13}C$ water mass seen at MD02-2589 was not sourced from the North Atlantic, although it is possible that core MD95-2042 lies too deep to be influenced by GNAIW. Similarly the benthic $\delta^{13}C$ and Cd/Ca data from core MD96-2080 (*Martinez-Mendez,* in review), bathed in NADW at the present day, upstream of the *Lynch-Stieglitz and Fairbanks* (1994) and *Lynch-Stieglitz et al.* (1996) cores in the Pacific Ocean in relation to NCW suggest that at times during glacial periods (i.e. MIS 6 and 8) a source for positive $\delta^{13}C_{as}$ levels different from GNAIW must have existed in the South Atlantic. The proposed mechanisms of NCW bypassing the ACC may not necessarily therefore hold true for the entire last glacial period, nor for previous ones (*Molyneux and Martínez-Méndez*, in prep).

7.3.3 Sea Ice and Air – Sea Gas Exchange

Keeling and Stephen (2001) proposed that expanded sea ice cover during glacial periods would have stopped waters forming around Antarctica in the zone of extended winter sea

ice (*Rosenthal et al.,* 1997; *Mackensen et al.,* 2001; *Bickert and Mackensen,* 2003) from having any contact with the atmosphere, producing waters with very low $\delta^{13}C$ values. They suggested that AAIW would have formed at the edge of the sea ice limits, which presumably would have had higher $\delta^{13}C$ values due to air-sea gas exchange. They also proposed that the glacial Southern Ocean water column was only made up of AABW and AAIW, with AAIW being saltier than at the present day and therefore extending down to 1500 – 2500 m water depths and flowing northwards away from AABW formation regions under the sea ice.

The suggestion of the existence of a glacial intermediate to mid-depth water mass forming in the Subantarctic region north of the winter sea ice limit has been suggested by several other studies (*Michel et al.,* 1995; *Ninemann and Charles,* 1997; *Curry and Oppo,* 2005, *Pahnke and Zahn,* 2005), although the chemical characteristics of such a water mass are not well defined. Whilst this is a valid mechanism for producing a mid-depth divide, the northern most limit of the sea ice cover during glacial periods has been reconstructed to around 47 °S (*Gersonde et al.,* 2003, 2005), which while being reasonably close to the suggested mid-depth divide (42.5 °S), cannot explain the sharp change over the SAF 4.5 ° to the north of the winter sea ice limit.

7.3.4 Wind-Driven Upwelling

A final means to obtain a positive $\delta^{13}C_{\Sigma CO2}$, nutrient-laden, mid-depth SCW mass north of the SAF is offered by *Toggweiler* (1999), *Sigman and Boyle* (2000) and *Toggweiler et al.*

(2006). They propose a physical mechanism to explain the existence of the chemical divide in the Atlantic portion of the Southern Ocean. Atmospheric cooling drives equatorwards migrations of the westerly winds which in turn reduces the wind-driven Ekman upwelling of CDW and causes the development of a low-salinity cap and sea ice expansion which further reduces ventilation. The reduced upwelling decreases the CO_2 out-gassing of deep waters and allows for the accumulation of respired CO_2 at depth, thus making this low ocean layer depleted in $\delta^{13}C_{\Sigma CO2}$ and leaving the upper layer enriched. Additionally, a higher density contrast between the upwelling and the bottom water would prevent respired CO_2 exchange from the lower to the upper layer by mixing. These changes occur without substantial variations in the PO_4^{3-} content of both ocean layers. *Adkins et al.* (2002) show that the glacial Southern Ocean had the saltiest water in the deep oceans probably due to brine rejection by an expanded glacial ice pack. Further studies have shown that highly depleted $\delta^{13}C$ values are also associated with these salty bottom waters, suggesting that they had little, if any, contact with the atmosphere (*Toggweiler et al., 2006*). This, combined with the reduced wind-driven upwelling would suggest that sea ice may have had an effect out as far as the SAF, despite studies suggesting that its winter LGM limit in the South Atlantic was around 47 °S (*Gersonde et al.*, 2003, 2005) in the Polar Frontal Zone between the Polar Front (PF) and the SAF.

The northwards shift and intensification of the westerly wind belts during the last glacial (*Esper et al., 2000*), is thought to have increased the amount of upwelling of intermediate depth waters in the Subantarctic zone (*Sigman and Boyle, 2000*), whilst reducing upwelling of deep waters in the Antarctic zone. This increased upwelling between the PF and SAF would produce $\delta^{13}C_{\Sigma CO2}$ enriched mid-depth to surface waters with positive

estimated $\delta^{13}C_{as}$ levels due to the rapid transferal of respired CO_2 to the atmosphere and high nutrient levels, as organisms do not have it within their power to utilize more than a small proportion of the upwelled nutrients (*Toggweiler et al.*, 2006). It can therefore be suggested that this divide between reduced and enhanced upwelling regions in the Southern Ocean was at the SAF (42.5 °S) during glacial periods, with deep waters north of the SAF being below the intermediate depths of the upwelling.

This mechanism would produce well-ventilated higher mid-depth $\delta^{13}C$ values in the region of enhanced upwelling north of the SAF, with lower $\delta^{13}C$ mid-depth values south of the SAF in the region of reduced glacial upwelling (*Molyneux and Martínez-Méndez,* in prep). The mechanism only invokes the upwelling of intermediate waters and therefore deep waters both north and south of the SAF would remain stratified from the rest of the water column, with reduced $\delta^{13}C$ levels.

7.4. Conclusions

Evidence of a strong mid-depth $\delta^{13}C$ gradient across the SAF during the LGM and previous glacial periods suggests continued better ventilation of mid-depth waters north of the SAF and reduced ventilation of mid-depth waters south of the SAF due to lack of atmospheric contact. The low $\delta^{13}C$ water mass south of the SAF spreads northwards at deep depths invading the abyssal depths. During the LGM this well-ventilated upper chemocline water mass north of the SAF was likely to be SCW, although evidence suggests that in other glacial periods glacial NCW penetration would also have generated

this divide. Further evidence of the chemocline in the Indian Ocean (*Kallel et al.*, 1988) suggests that it may be a feature of the wider ACC region and therefore SCW-linked, rather than due to the penetration of glacial NCW, while Cd/Ca evidence (*Martínez-Méndez et al.*, 2008) from core MD96-2080 on the Agulhas Bank suggests that the water mass in the late LGM is different from GNAIW and probably SCW sourced. This idea of a late glacial SCW mass fits with the identification of the negative carbon anomalies (Chapter 6) during late cold stages and transitions into warmer periods.

The mechanism for this divide and the formation of the high $\delta^{13}C$ mid-depth water mass north of the SAF is likely to be due to a combination of several models proposed. Possibly with a productivity overprint, extensive sea ice and northwards migration of the westerly winds would reduce the ventilation of the deep waters and $\delta^{13}C$ values south of the SAF. A faster flowing ACC and formation of a shallow deep water mass, with high $\delta^{13}C$ values due to increased air-sea gas exchange and upwelling, at the SAF would reduce NCW penetration into the Southern Ocean.

The likely position for the formation of this mid-depth high $\delta^{13}C$ water mass is the SAF region at the LGM (42.5 °S) in the southeast Atlantic and although it exact position during previous glacial periods cannot be assessed, several $\delta^{13}C$ and Cd/Ca records suggest that this mechanism is a persistent feature of at least the past three glacial periods.

Chapter 8: Summary Discussion and Conclusions

8.1 Introduction

High-resolution, multi-proxy analysis from marine sediment core MD02-2589 has provided a detailed record of both deep and surface ocean-climate interactions in the Agulhas throughflow region over the past 170 ka, with particular focus on glacial Terminations I and II and the MIS 5a/4 transition. Planktonic foraminiferal isotope measurements and faunal analysis, SST estimations and an IRD record were used to investigate fluctuations in surface currents and ACC-associated frontal systems over the Agulhas Plateau over glacial Terminations I and II and inception MIS5/4. Benthic foraminiferal isotope data combined with $\overline{SS}$ data was used to infer bottom water mass changes on glacial to interglacial timescales. The benthic $\delta^{13}C$ records of MD02-2589 and MD95-2042, from the Iberian Margin, were used to identify both the response of deep water masses to climate forcing and the southwards penetration of NCW during glacial periods within the Atlantic Ocean. Further investigation of the Southern Ocean glacial water column structure was undertaken using the benthic $\delta^{13}C$ records of a suite of cores forming a latitudinal and depth transect over the STF, SAF and PF. The principal findings are summarised and discussed below, followed by suggestions for further work.

8.2 Summary Discussion:

8.2.1 Surface and Deep Water Links On The Agulhas Plateau Over Terminations I And II And The MIS5a-4 Transition

Both the initial increase in ventilation of the benthic $\delta^{13}C$ record (Fig. 8.1b) and the reduction in flow speed (Fig. 8.1d) seen at 141 ka during peak ice volume, indicated by both the planktonic and benthic $\delta^{18}O$ records (Fig. 8.1a), correspond with the early SST increase seen in both the TF (Fig. 8.1c) and the *% N. pachyderma* (d) records (Fig. 8.1g). Whilst it was concluded in Chapter 4 that this early warming (141 - 136 ka) at MD02-2589 was probably not wider Southern Hemisphere-based due to the lack of movement of the STF, the $\overline{SS}$ record (Fig. 8.1d) linked to the proximity of the ACC to the site, and therefore frontal systems, shows a decrease over this time period linked to southern warming. However further investigation notes that removal of the inversion of the $\overline{SS}$ axis shows that both the $\overline{SS}$ record and position of the STF record exhibit very similar patterns over TII (Fig. 81d, f). This is a good indication that both records are reflecting the proximity of the ACC and associated fronts to the site. Indeed during the suggested 'heat and salt pooling' period until 136.7 ka there is only a small decrease in $\overline{SS}$ values (Fig. 8.1d), similar to the general fluctuations seen during MIS 6, corresponding to a slight southwards movement of the STF (Fig. 8.1f). It is only after 136.7 ka that $\overline{SS}$ values decrease rapidly as the position of the STF moves sharply southwards. This corresponds with the rapid early TII Southern Ocean warming seen in other cores (Fig. 4.2) which starts ~8 ka (*Bianchi and Gersonde,* 2002; *Pahnke and Zahn,* 2005) after the

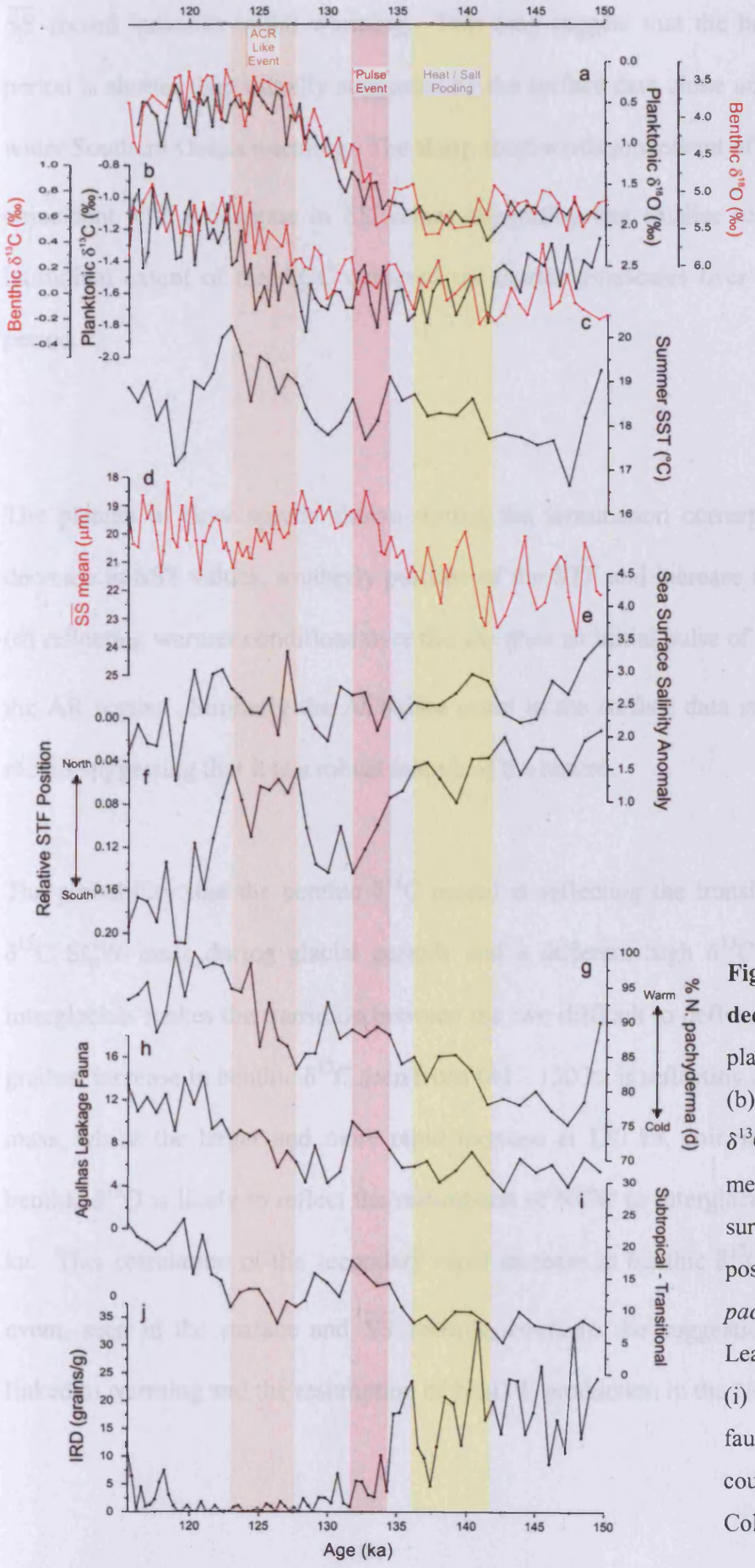

Figure 8.1 Surface and deep proxy data for TII (a) planktonic and benthic $\delta^{18}O$, (b) planktonic and benthic $\delta^{13}C$, (c) summer SST, (d) mean sortable silt, (e) sea surface salinity , (f) relative position of the STF, (g) % *N. pachyderma* (d), (h) Agulhas Leakage Fauna abundance, (i) Subtropical - Transitional fauna abundance, (j) IRD counts: ACR = Antarctic Cold Reversal

$\overline{SS}$ record indicates initial warming. This may suggest that the heat and salt pooling period is shorter than initially suggested by the surface data alone and occurs before any wider Southern Ocean warming. The sharp southwards movement of the STF at 139 ka is coincident with a decrease in $\overline{SS}$ values suggesting that smaller scale variations in the latitudinal extent of the ACC occurred on shorter timescales over the wider transition period.

The plateau in flow speeds shown during the termination corresponds well with the decrease in SST values, southerly position of the STF and increase in *% N. pachyderma* (d) reflecting warmer conditions over the site after an initial pulse of pooled water though the AR region. Similarly the ACR-like event in the surface data is mirrored in the $\overline{SS}$ record suggesting that it is a robust feature of the record.

The probability that the benthic $\delta^{13}C$ record is reflecting the transition between a high $\delta^{13}C$ SCW mass during glacial periods and a different high $\delta^{13}C$ NCW mass during interglacials makes the transition between the two difficult to define. Probably the initial gradual increase in benthic $\delta^{13}C$ seen from 141 - 130 ka is reflecting a change in the SCW mass, whilst the larger and more rapid increase at 130 ka, coincident with decreasing benthic $\delta^{18}O$ is likely to reflect the resumption of NCW to interglacial levels around 124 ka. This correlation of the secondary rapid increase in benthic $\delta^{13}C$ with the ACR like event, seen in the surface and $\overline{SS}$ records, confirms the suggestion that this event is linked to warming and the resumption of NADW production in the North Atlantic.

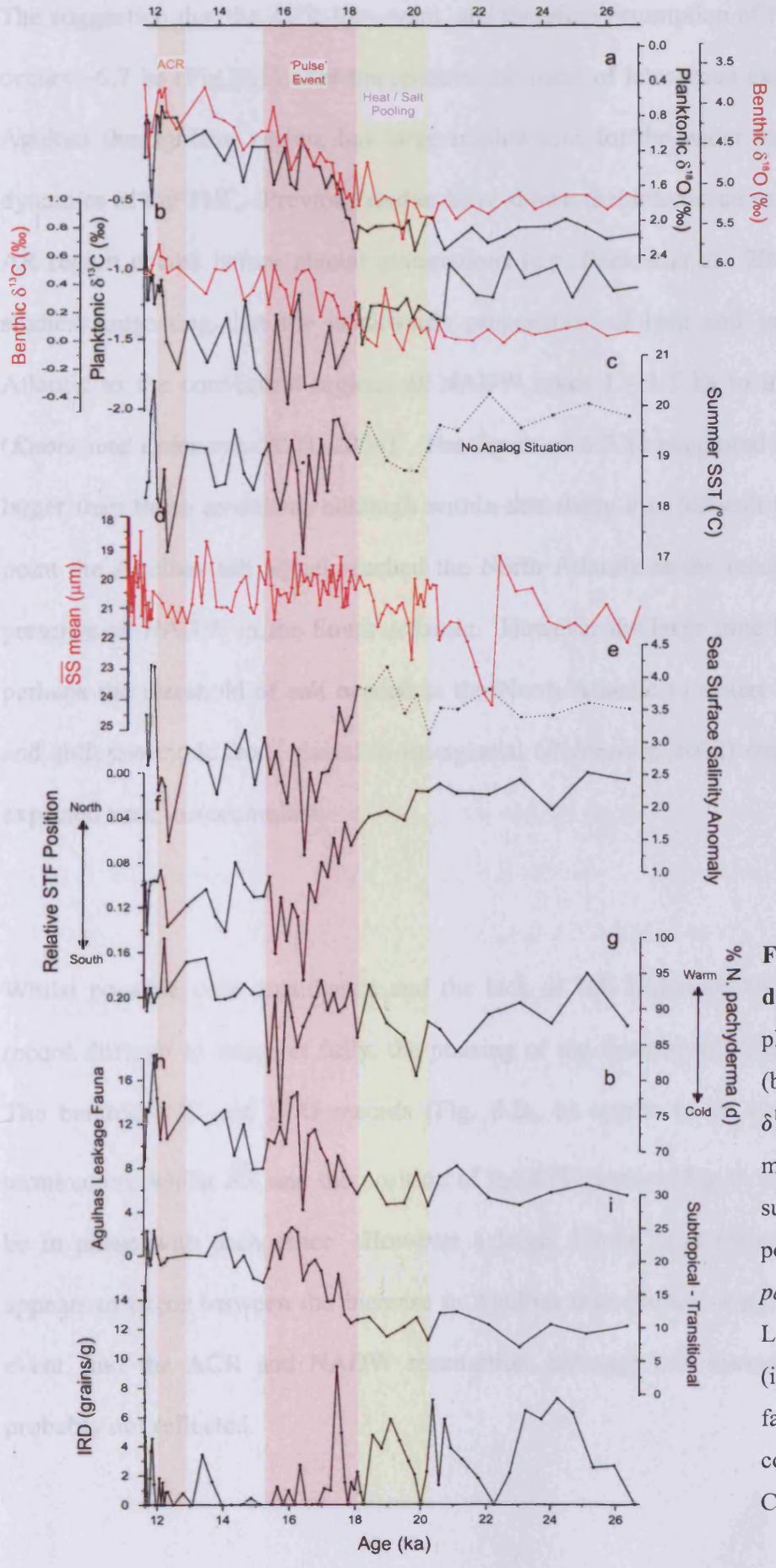

Figure 8.2 Surface and deep proxy data for TI (a) planktonic and benthic $\delta^{18}O$, (b) planktonic and benthic $\delta^{13}C$, (c) summer SST, (d) mean sortable silt, (e) sea surface salinity , (f) relative position of the STF, (g) % *N. pachyderma* (d), (h) Agulhas Leakage Fauna abundance, (i) Subtropical - Transitional fauna abundance, (j) IRD counts: ACR = Antarctic Cold Reversal

The suggestion that the ACR-like event, and therefore resumption of NADW production, occurs ~6.7 ka (Fig. 8.1) after the recommencement of interocean exchange through the Agulhas throughflow region, has large implications for the wider understanding of the dynamics of the THC. Previous studies have shown that interocean exchange through the AR region occurs before glacial terminations (e.g. *Peeters et al.*, 2004) with modelling studies suggesting that the northwards propagation of heat and salt from the South Atlantic to the convection regions of NADW takes 1 - 1.5 ka to intensify convection (*Knorr and Lohmann*, 2003, 2004). The figure of 6.7 ka suggested by this study is far larger than those modelled, although within this study it is difficult to quantify at what point the Agulhas salt signal reached the North Atlantic as the records only reflect the presence of NADW in the South Atlantic. However the large time frame suggests that perhaps the threshold of salt needed in the North Atlantic to restart NADW convection and shift the mode from glacial to interglacial (*Rahmstorf*, 2002) requires a longer than expected time to accumulate.

Whilst possible core disturbance and the lack of full Holocene levels at TI make the record difficult to interpret fully, the phasing of the records are different to that at TII. The benthic $\delta^{13}C$ and $\delta^{18}O$ records (Fig. 8.2a, b) appear to be synchronous over the termination, whilst $\overline{SS}$ and the position of the STF proxies (Fig. 8.2d, f) do not seem to be in phase with each other. However a large, 5.7 ka, time interval (Fig. 8.2) again appears to occur between the increase in Agulhas throughflow, suggested by the 'pulse' event, and the ACR and NADW resumption, although full interglacial circulation is probably not reflected.

The MIS 5a-4 transition is smaller than both TI and TII as although MIS 4 $\delta^{18}O$ record exhibits full glacial values (Fig. 8.3a) MIS 5a can be seen not to be a full interglacial period. Whilst none of the surface proxies show the sharp transition identified in the benthic proxies, a possible upwelling event (seen in the *G. inflata* and *N. pachyderma* (d) records; Fig. 8.3h, i) occurs during the transition in the benthic $\delta^{18}O$ and $\delta^{13}C$ record and the peak minima in flow speeds. The sharp benthic transition is attributed to a shoaling of NADW in the water column and reduction at MD02-2589, with an expansion of SCW over the site in its place. This rapid reorganisation of the deep water masses overlying MD02-2589 may be producing the upwelling event identified in the species abundance records. Chapters 5 - 7 have shown than during glacial periods when NCW production was reduced, a SCW mass forming at the SAF replaced NCW at MD02-2589. This SCW mass forms during cold periods when the ice shelves are grounded in the Weddell Sea region, sea ice extent is expanded, the westerly wind belts have shifted equatorwards and the regions of upwelling and air-sea gas exchange have moved out to the Subantarctic zone. The planktonic $\delta^{18}O$ record (Fig. 8.3a) shows a far more gentle transition over the MIS5a/4 period, with the upwelling event and rapid southwards shift of the ACC, seen in the $\overline{SS}$ record, occurring mid-way through its transition. It may therefore be suggested that the sudden shoaling of NADW in the water column and its subsequent reduction at site MD02-2589 caused a contraction of the ACC as NADW significantly contributes to the formation of all SCW masses. Compensation for this sudden lack of NADW by glacial SCW was not able to occur immediately as the planktonic $\delta^{18}O$ record suggests that the full glacial period had not been reached.

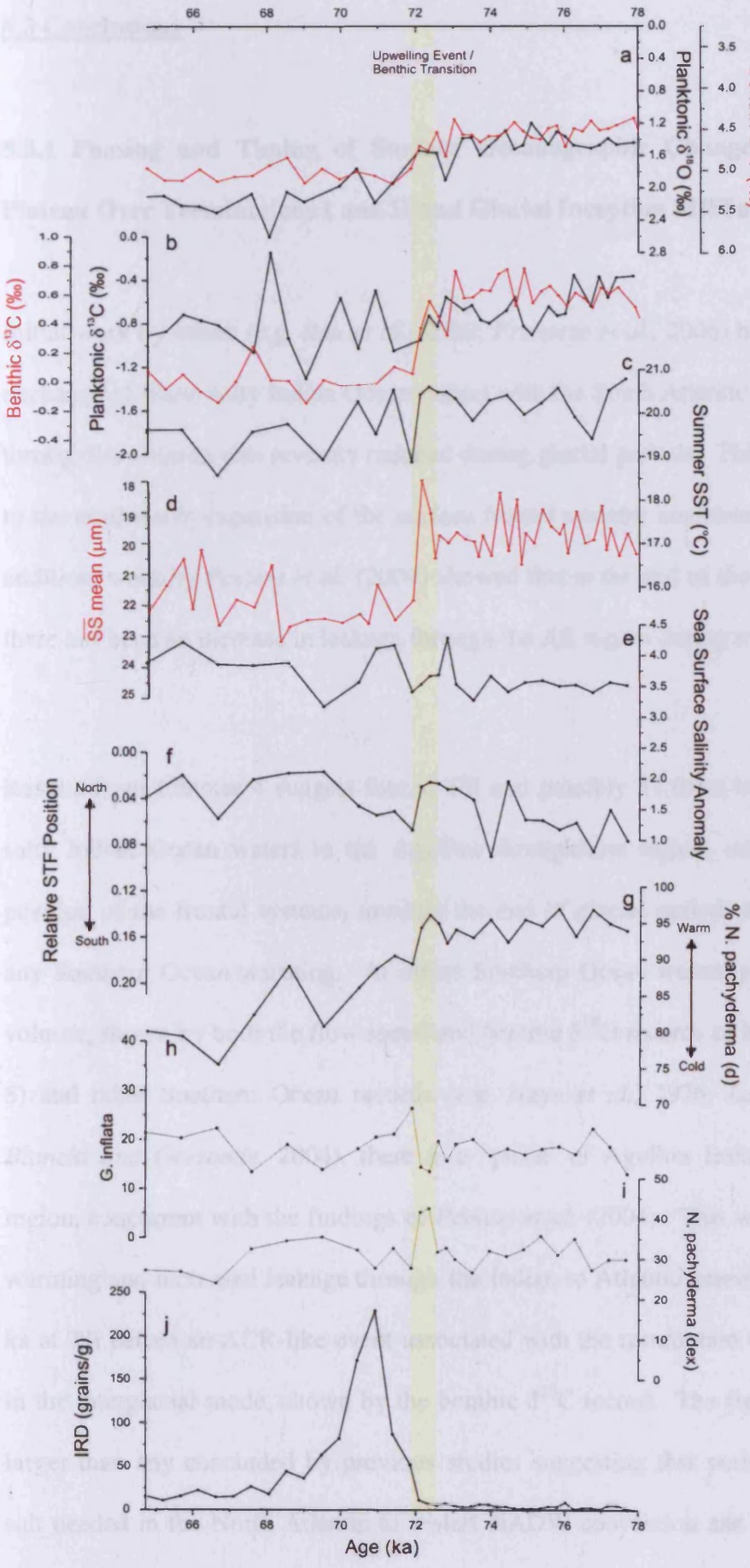

Figure 8.3 Surface and deep proxy data for MIS5a/4 Transition (a) planktonic and benthic $\delta^{18}O$, (b) planktonic and benthic $\delta^{13}C$, (c) summer SST, (d) mean sortable silt, (e) sea surface salinity , (f) relative position of the STF, (g) % *N. pachyderma* (d), (h) *G. inflata* abundance, (i) *N. pachyderma* (d) abundance, (j) IRD counts:

8.3 Conclusions

8.3.1 Phasing and Timing of Surface Oceanographic Changes On the Agulhas Plateau Over Terminations I and II and Glacial Inception MIS5a-4 (Chapter 4)

Initial work by others (e.g. *Rau et al.,* 2002; *Franzese et al.,* 2006) has suggested that the exchange of warm salty Indian Ocean waters with the South Atlantic through the Agulhas throughflow region was severely reduced during glacial periods. This has been attributed to the northwards expansion of the surface frontal systems associated with the ACC. In addition, work by *Peeters et al.* (2004) showed that at the end of the past 5 glacial cycles there has been an increase in leakage through the AR region during maximal ice volume.

Results from Chapter 4 suggest that at TII and possibly TI there is a pooling of warm, salty Indian Ocean waters in the Agulhas throughflow region, due to the northwards position of the frontal systems, towards the end of glacial periods MIS 2 and 6 prior to any Southern Ocean warming. At initial Southern Ocean warming during maximal ice volume, shown by both the flow speed and benthic $\delta^{18}O$ records of MD02-2589 (Chapter 5) and other Southern Ocean records (e.g. *Hays et al.,* 1976; *Layberie et al.,* 1996; *Bianchi and Gersonde,* 2004), there is a 'pulse' of Agulhas leakage through the AR region, concurrent with the findings of *Peeters et al.* (2004). This wider Southern Ocean warming and increased leakage through the Indian to Atlantic gateway occurs some ~6.7 ka at TII before an ACR-like event associated with the resumption of NADW formation in the interglacial mode, shown by the benthic $\delta^{13}C$ record. The figure of ~6.7 ka is far larger than any concluded by previous studies suggesting that perhaps the threshold of salt needed in the North Atlantic to restart NADW convection and shift the mode from

glacial to interglacial (*Rahmstorf,* 2002) requires a longer than expected time to accumulate.

A carbon isotope minima event during TI has been identified in cores from the Southern Ocean (e.g. *Ninnemann and Chalres,* 1997; *Mulitza et al.,* 1999; *Spero and Lea, 2002*). The planktonic $\delta^{13}C$ record of *Globigerina bulloides* at MD02-2589 shows a 1.9 ‰ decrease over TI, which is also seen in the planktonic $\delta^{13}C$ record of nearby core MD02-2588 also using *G. bulloides* (-1.8 ‰) but interestingly not seen in the planktonic $\delta^{13}C$ record of *Neogloboquadrina pachyderma* (d) at the same core site.

The difference between the presence of a carbon isotope minima in *G. bulloides* and an absence in *N. pachyderma* (d) may relate to depth habitats of the two species and changes in the stratification of the water column. Several studies have suggested an increased stratification of the Southern Ocean water column during glacial periods (*François et al.,* 1997; *Toggweiler,* 1999; *Stephens and Keeling,* 2000; *Sigman and Boyle,* 2000), with a breakdown occurring during glacial terminations. This breakdown of stratification advects low $\delta^{13}C$ values from the deeper depths to the surface, reducing the $\delta^{13}C$ of the surface waters. The lack of a distinctive carbon isotope minima signal in the *N. pachyderma* (d) record may signify that during glacial periods it dwelled at deeper depths to *G. bulloides* and therefore was consistently bathed in low $\delta^{13}C$ values, whereas the shallower dwelling *G. bulloides* was bathed in higher $\delta^{13}C$ waters above the stratification. The possible presence of a similar event at TII suggests that this may be a persistent feature of glacial terminations.

8.3.2 Deep Water Variability On The Southern Agulhas Plateau: Interhemispheric Links Over The Past 170 ka (Chapter 5)

MD02-2589 benthic records suggest that during glacial periods (MIS 2 and 6) there was persistent contribution of a well-ventilated water mass within the Atlantic to Indian oceanic gateway, with a $\delta^{13}C$ signature similar to present-day NCW. Several studies have suggested that NCW production was reduced during glacial periods (*e.g. Boyle and Keigwin,* 1987; *Sarnthein et al.,* 1994) and therefore its southwards spread and influence in the Southern Ocean was reduced (e.g. *Piotrowski et al.,* 2004, 2005; *McManus et al.,* 2004; *Sigman and Boyle,* 2000; *Diekmann et al.,* 1996). This suggests that additional well-ventilated waters possibly originated from the Southern Ocean.

The records of chemical ventilation and near-bottom flow vigour reflect changes in the advection of northern source waters and meridional variability in the location of the ACC and its associated fronts. The results suggest that during TII changes in chemical ventilation are largely decoupled from near-bottom physical flow speeds, with the flow speeds recording Southern Ocean variability and the chemical ventilation NCW variability. A mid-TII climate optimum is associated with a low-flow speed plateau at MD02-2589, indicative of a constriction of the ACC frontal systems and previously documented Southern Ocean warming (e.g. *Bianchi and Gersonde,* 2002), concurrent with a period of increased ventilation shown in the benthic $\delta^{13}C$ records of other Southern Ocean cores, RC11-83 (*Charles et al.,* 1996) and MD97-2120 (*Pahnke and Zahn,* 2005) but not that of MD02-2589. The climate optimum is followed by a period of southern cooling around 128 ka coincident with a stronger influence of NCW to interglacial levels at around 124 ka.

All of the proxy records show a near-synchronous and rapid shift during the transition from MIS5a - 4 (73 ka) attributed to a rapid decrease in NADW influence and replacement over the Agulhas Plateau by SCW.

8.3.3 Meridional Benthic Carbon Isotope Gradients in the Atlantic Ocean and Implications for Meridional Overturning Circulation Variability (Chapter 6)

One of the conclusions of Chapter 5 was that there was a persistent influence of a high $\delta^{13}C$, well-ventilated water mass over the Agulhas Plateau during glacial periods. Whilst the source of this water mass could not be identified in Chapter 5, the results of previous studies have suggested that during glacial periods NCW production and southward spread was reduced (e.g. *Boyle and Keigwin,* 1987), signifying that the high $\delta^{13}C$ water mass may be southern sourced.

The benthic $\Delta\delta^{13}C$ record of North Atlantic core MD95-2042 minus MD02-2589 shows that only at 5 discrete time intervals over the past 150 ka has the expected $\delta^{13}C$ offset between the South and North Atlantic been met. In fact at 8 time intervals, named 'negative carbon anomalies', the mid-depth South Atlantic is bathed in a better ventilated water mass than the mid-depth North Atlantic, with the % NCW proxy suggesting that there is more NCW in the South Atlantic than the North.. These events appear to correspond with glacial stages and substages and Heinrich events. As it is unlikely that the South Atlantic had a greater percentage of NCW than the North Atlantic, it is

probable that the source of the high $\delta^{13}C$ water mass seen at MD02-2589 but not MD95-2042 during cold periods is outside the North Atlantic.

Alternative factors affecting both the benthic $\delta^{13}C$ records are investigated and whilst increased glacial productivity over the Iberian Margin and increased air-sea gas exchange at site MD02-2589 may plausibly be affecting both records, they cannot explain all of the offset seen. It is therefore likely that both core sites are influenced by different water masses during glacial periods, with MD95-2042 bathed by very depleted southern component bottom waters and MD02-2589 by a separate SCW mass.

During glacial periods and cold substages during MIS 5 increased flow speeds at MD02-2589 indicate an expanded ACC due to colder conditions. This is not true for Heinrich events, where warmer conditions have been recorded in alternative Southern Ocean cores (e.g. MD97-2120; *Pahnke and Zahn,* 2005) suggesting that the high $\delta^{13}C$ water mass bathing MD02-2589 may form differently during cold periods and Heinrich events, with increased AAIW production and penetration suggested for Heinrich events and a separate SCW mass linked to the air-sea gas exchange, grounding of the Weddell Sea ice shelves and sea ice expansion forming possibly near the SAF postulated for glacial periods.

8.3.4 Glacial to Interglacial Southern Ocean Water Column Structure (Chapter 7)

Conclusions derived from Chapters 5 and 6 suggest that during glacial periods there was a well-ventilated, high $\delta^{13}C$ water mass separate from those present today forming in the Southern Ocean. Spectral analysis work suggests that this water mass is responding to

Northern Hemisphere forcing through atmospheric teleconnections and wind forcing and therefore may be linked to wind forcing, air-sea gas exchange or upwelling.

Hodell et al. (2003) and *Ninnemann and Charles* (2002) suggest the presence of a well-developed chemocline in the South Atlantic at the LGM and most glacial periods back to 1.1 Ma. This chapter uses the *Hodell et al.* (2003) data, with additional sites from the South-Eastern Atlantic Ocean, and spatially discriminates between those sites north and south of the assumed SAF (42.5 °S) at the LGM. It is apparent that there is a mid-depth benthic $\delta^{13}C$ divide north and south of the SAF, with very depleted values south and enriched values north, with deep depths (>3750 m water depth) both north and south of the SAF showing depleted values. This suggests continued better ventilation of mid-depth waters north of the SAF, probably of southern origin and reduced ventilation of mid-depth waters south of the SAF due to lack of atmospheric contact, which spread northwards, invading the abyssal depths.

The results suggest that the formation region of the high $\delta^{13}C$ water mass identified in Chapters 5 and 6 must be around the SAF at 42.5 °S during the LGM, with Cd/Ca and $\delta^{13}C$ data suggesting that it was probably a feature of previous glacial periods and during late glacial periods must be a different water mass to AAIW. The mechanism for this divide and the formation of the high $\delta^{13}C$ mid-depth water mass north of the SAF is likely to be due to a combination of several models proposed. Possibly with a productivity overprint, extensive sea ice and northwards migration of the westerly winds reducing the ventilation of the deep waters and $\delta^{13}C$ values south of the SAF, with a faster flowing ACC and formation of a shallow deep water mass, with high $\delta^{13}C$ values due to increased

air-sea gas exchange and upwelling, at the SAF reducing NCW penetration into the Southern Ocean.

8.3.5 High $\delta^{13}C$ Mid-Depth Southern Ocean Glacial Water Mass: Global Implications

The identification of a high $\delta^{13}C$ mid-depth SCW mass, with a similar $\delta^{13}C$ signature to present day NCW, forming around the SAF during glacial periods and cold substages (different from AAIW) has wider implications for both studies looking at the extent of NCW during glacial periods and the wider Southern Ocean glacial circulation. Whilst the identification of this separate mid-depth water mass confirms suggestions of previous studies (*Hodell et al.,* 2003 *Michel et al.,* 1995; *Ninemann and Charles,* 1997; *Curry and Oppo,* 2005, *Pahnke and Zahn,* 2005), the detection in Chapter 7 of a significant mid-depth divide north and south of the SAF extends these observations and conclusions by suggesting that this water mass was only present at mid-depths north of the SAF. Additional conclusions that this mid-depth divide must mean that the glacial high $\delta^{13}C$ water mass was forming around the SAF and spreading northwards further enhances our knowledge of the glacial Southern Ocean circulation and provides a geographical location for the formation of this water mass, which potentially enables further studies to focus on the exact formation region.

The findings that the glacial high $\delta^{13}C$ water mass was not originating from the North Atlantic, despite exhibiting values very similar to present day NCW, is very important to our understanding of the extent of global glacial water masses. Many studies have used benthic $\delta^{13}C$ records to trace the extent of NCW during glacial periods (e.g. *Streeter and*

Shackleton, 1979; *Sarnthein et al.,* 1994; *Sigman and Boyle,* 2000), often with contradictory results. The presence of a high $\delta^{13}C$ water mass forming around the SAF, extending northwards away from the ACC region, may be the source of the high $\delta^{13}C$ values recorded in the Atlantic, Indian and Pacific Oceans (*Duplessy et al.,* 1988; *Volbers and Henrich,* 2004; *Lynch-Stieglitz and Fairbanks,* 1994; *Lynch-Stieglitz et al.,* 1996; *Oppo and Horowitz,* 2000; *Curry and Oppo,* 2005) which have previously been assumed to be North Atlantic in origin due to high $\delta^{13}C$ and $\delta^{13}C_{as}$ content. This discovery questions certainly the use of $\delta^{13}C$ records alone to investigate the distribution of water masses and the current reconstructions of water patterns in the glacial oceans based on $\delta^{13}C$ values (e.g. *Curry and Oppo*, 2005). Indeed studies looking at the extent of glacial SCW in the world's ocean basins again have possibly been missing this important water mass, as its signature is not typical of SCW masses.

The likely formation mechanism for this water mass involves both increased upwelling of nutrient-rich waters (*Togweiller et al.,* 2006) due to the equatorwards shift of the westerly wind belts and the movement of the region of high air-sea gas exchange from the PF region to the Subantarctic Zone due to extended sea ice (*Sigman and Boyle,* 2000; *Stephens and Keeling,* 2001). Both of these would produce the high $\delta^{13}C$ and $\delta^{13}C_{as}$ signature seen by *Lynch-Stieglitz et al.* (1996) and would also explain the link seen by *Hodell et al.* (2003) between the intermediate to deep carbon gradient and changes in atmospheric pCO_2, through changes in sea ice extent.

Several studies have suggested that sea ice extent in the Southern Ocean may actually drive North Atlantic thermohaline circulation (*Kim et al.,* 1998; *Keeling and Stephens,*

2001; *Shin et al.,* 2003), with changing outflow of SCW, linked to sea ice extent and wind forcing, changing the relative abundance of NCW at any particular site, rather than being controlled by NCW strength itself (*Kim et al.,* 1998; *Togweiller,* 1999; *Bayon et al.,* 2003; *Raymo et al.,* 2004). The possible forcing of the formation of this water mass by Northern Hemisphere insolation, shown in Chapter 6, through atmospheric teleconnections and influence on wind strength and sea ice extent may further imply that this water mass has an important role in forcing global circulation.

8.4 Future Work

Detailed below are some of the issues raised within the study with suggestions of how they may be resolved within future work.

8.4.1 Age Model

The lack of data associated with the values for the Southern Ocean reservoir correction (*CALIB,* 2005), highlighted in Chapter 3, means that large uncertainties exist for the timing of the LGM and TI. The standard regional Southern Ocean correction age of 800 yrs (*Butzin et al.,* 2005), applied to the MD02-2589 AMS ^{14}C dates, cannot accurately reflect the likely variability over the wide Southern Ocean region and indeed can be seen in Chapter 3 to probably be an underestimation for the Agulhas Plateau. Further work into this issue is clearly needed before accurate correlations of Southern Ocean marine cores with others from both the same region and other ocean and terrestrial regions can take place.

8.4.2 Surface Data

The surface data presented in this thesis only focuses on TI, TII and the MIS5a/4 transition. Both TI and TII show small scale variability of the surface frontal systems and currents on shorter timescales within the larger terminations. High resolution planktonic species assemblage data and SST TF should be extended over the whole core in order to understand the variability and timing of mechanisms at stage and sub-stage boundaries

over the past 170 ka. This can then be combined with the existing benthic and $\overline{SS}$ data to identify surface to deep phasing and links.

Chapter 4 shows how the SST record produced using a TF on foraminifera species assemblages can be affected by productivity and vital effects on individual species. As a result an alternative SST proxy, possibly Mg/Ca, independent of foraminifera assemblages should also be produced for the core so that the interpretation of the SST can be furthered.

8.4.3 Timing of Resumption of Agulhas Leakage

Detailed records of the fluctuations of the STF and the ACC are provided within this study. The position of core MD02-2589 within the Agulhas Return Current means that the surface waters are a mix of Agulhas Current signature waters and Subantarctic waters and therefore are not recording true fluctuations in the Agulhas Current. As a result a detailed high-resolution surface record from a core within the Agulhas Retroflection region would provide a better reconstruction of variations in leakage which could be combined with the MD02-2589 data to further investigate the effect of large and small scale frontal movements on leakage in the throughflow region.

8.4.4 Global Implications of Agulhas Leakage

The surface and deep records of MD02-2589 combined appear to suggest that there is a lag of ~6 ka between the resumption of leakage through the Agulhas throughflow region and the resumption of NADW to interglacial levels. This value is far larger than any

previously suggested and may reflect the time needed for enough salt to accumulate in the North Atlantic region to restart convection. Further modelling work needs to be undertaken in order to confirm the transport time of the Agulhas salt signal to the North Atlantic, the probable contribution of the Agulhas salt to the NADW convection regions and therefore the likely amount needed in relation to known leakage to restart NADW production.

8.4.5 Millennial-Scale Activity

Chapter 6 suggests that millennial-scale events are identifiable in the MD02-2589 $\delta^{13}C$ record, although their signal is dampened. Further high resolution benthic $\delta^{13}C$, $\delta^{18}O$ and $\overline{SS}$ records need to be produced over this time period (MIS 3; at 1cm resolution), as well as planktonic proxies to try and further resolve the effect of millennial-scale events on the South Atlantic region. The benthic $\delta^{13}C$ record of MD97-2120 (*Pahnke and Zahn,* 2005) suggests that warming occurs in the intermediate depth Pacific during Heinrich events, whilst MD02-2589 suggests that a well-ventilated high $\delta^{13}C$ water mass existed over the Agulhas Plateau. Further work into whether this mid-depth water mass during Heinrich events is the same as that seen during glacial periods originating from the SAF or expanded AAIW should be carried out.

8.4.6 High $\delta^{13}C$ Glacial Water Mass

Whilst the formation region of the high $\delta^{13}C$ glacial water mass was identified in Chapter 7, as the SAF, further proxy and modelling studies are needed to determine both the

formation mechanism and characteristics of this water mass. Cd/Ca analysis on benthic records should be undertaken to try and identify the characteristics of this water mass and its northwards extent into other ocean basins, as well as the interplay and timing of the exchange between NCW and SCW on glacial inceptions and terminations.

References

Abrantes, F.: (2000): 200 000 yr diatom records from Atlantic upwelling sites reveal maximum productivity during LGM and a shift in phytoplankton community structure at 185 000 yr: *Earth Planet. Sci. Letters*: *176*, 7-16.

Adkins, J. F., K. McIntyre and D. P. Schrag: (2002): The salinity, temperature and $\delta^{18}O$ of the glacial deep ocean: *Science*: *298*, 1769-1773.

Adkins, J. F. and D. P. Schrag: (2003): Reconstructing Last Glacial Maximum bottom water salinities from deep-sea sediment pore fluid profiles: *Earth Planet. Sci. Letters*: *216*,(1-2), 109-123.

Allen, C. P. and D. A. Warnke: (1991): History of ice rafting at Leg 144 sites, Subantarctic/South Atlantic: *Proc. Ocean Drill. Program. Sci. Results*: *114*, 599-607.

Alley, R. B., E. J. Brook and S. Anandakrishnan: (2002): A northern lead in the orbital band: north-south phasing of Ice-Age events: *Quat. Sci. Rev.*: *21*,(1-3), 431-441.

Alley, R. B., J. Marotzke, W. D. Nordhaus, J. T. Overpeck, D. M. Peteet, R. A. Pielke, Jr., R. T. Pierrehumbert, P. B. Rhines, T. F. Stocker, L. D. Talley and J. M. Wallace: (2003): Abrupt climate change: *Science*: *299*,(5615), 2005-2010.

Anilkumar, N., M. K. Dash, A. J. Luis, V. Ramesh Babu, Y. K. Somayajulu, M. Sudhakar and P. C. Pandey: (2005): Oceanic fronts along 45°E across Antarctic Circumpolar Current during austral summer 2004: *Current Science*: *88*,(10), 1669-1673.

Arhan, M., H. Mercier and Y.-H. Park: (2003): On the deep water circulation of the eastern South Atlantic ocean: *Deep Sea Res. Part I*: *50*,(7), 889-916.

Arrhenius, G.: (1952): Sediment cores from the east Pacific: *Reports of the Swedish Deep-Sea Expedition 1947-1948*: *5*, 1-228.

Bard, E., B. Arnold, N. Hamelin, N. Tisnerat-Laborde and G. Cabioch: (1998): Radiocarbon calibration by means of mass- spectrometic Th-230/U-234 and ^{14}C ages of corals: An updated database including samples from Barbados, Mururoa and Tahiti: *Radiocarbon*: *40*, 1085-1092.

Bard, E., M. Arnold and J. C. Duplessy: (1991): Reconciling the sea level record of the last deglaciation with ^{18}O spectra from deep sea cores: Edited by: J. J. Lowe. *Radiocarbon Dating: Recent Applications and Future Potential, Quaternary Proceedings*. Quaternary Research Association, Cambridge *1*: pp. 67-73.

Bard, E., B. Hamelin and R. G. Fairbanks: (1990a): U-Th ages obtained by mass spectrometry in corals from Barbados: sea level during the past 130,000 years: *Nature*: *346*, 456-458.

Bard, E., L. Labeyrie, J. J. Pichon, M. Labracherie, M. Arnold, J. Duprat, J. Moyes and J. C. Duplessy: (1990b): The last deglaciation in the Southern and Northern hemisphere: a comparison based on oxygen isotopes, sea surface temperature estimates and accelerator ^{14}C dating from deep-sea sediments: Edited by: U. Bleil and Thiede, J. *Geological History of the Polar Oceans: Arctic Versus Antarctic, NATO ASI Series*. Kluwer Academic Publishers, Dordrecht *Series C, vol 308*: pp. 405-415.

Barker, P. F. and E. Thomas: (2004): Origin, signature and palaeoclimatic influence of the Antarctic Circumpolar Current: *Earth Sci. Rev.*: *66*,(1-2), 143-162.

Barrows, T. T. and S. Juggins: (2005): Sea-surface temperatures around the Australian margin and Indian Ocean during the Last Glacial Maximum: *Quat. Sci. Rev.*: *24*,(7-9), 1017-1047.

Barrows, T. T., S. Juggins, P. De Deckker, J. Thiede and J. I. Martinez: (2000): Sea-surface temperatures of the southwest Pacific Ocean during the last glacial maximum: *Paleoceanography*: *15*, 95-109.

Bayon, G., C. R. German, R. W. Nesbitt, P. Bertrand and R. R. Schneider: (2003): Increased input of circumpolar deep water-borne detritus to the glacial SE Atlantic Ocean: *Geochem. Geophys. Geosyst.*: *4*,(3), 1-13.

Bé, A. W. H.: (1977): An ecological, zoogeographic and taxonomic review of recent planktonic foraminifera: Edited by: A. T. S. Ramsay. *Oceanic micropaleontology*. Academic Press, New York: pp. 1-100.

Bé, A. W. H. and D. S. Tolderlund: (1971): Distribution and ecology of living planktonic foraminifera in surface waters of the Atlantic and Indian oceans: Edited by: B. M. Funnell and Riedel, W. R. *The Micropaleontology of Oceans*. Cambridge University Press, Cambridge: pp. 105-149.

Becker, B. and B. Kromer: (1993): The continental tree-ring record - absolute chronology ^{14}C calibration and climatic change at 11ka: *Palaeogeogr. Palaeoclimatol. Palaeoecol.*: *103*,(1-2), 67-71.

Becquey, S. and R. Gersonde: (2002): Past hydrographic and climatic changes in the Subantarctic Zone of the South Atlantic - The Pleistocene record from ODP Site 1090: *Palaeogeogr. Palaeoclimatol. Palaeoecol.*: *182*,(3-4), 221-239.

Behl, R. J. and J. P. Kennett: (1996): Brief interstadial events in the Santa Barbara basin, NE Pacific, during the past 60 kyr: *Nature*: *379*, 243-246.

Belanger, P. E., W. B. Curry and R. K. Matthews: (1981): Core-top evaluation of benthic foraminferal isotopic ratios for paleo-oceanographic interpretations: *Palaeogeogr. Palaeoclimatol. Palaeoecol.*: *33*, 205-220.

Belkin, I. M. and A. L. Gordon: (1996): Southern Ocean fronts from the Greenwich meridian to Tasmania: *J. Geophys. Res.*: *101*,(C2), 3675-3696.

Bemis, B. E., H. J. Spero, J. Bijma and D. W. Lea: (1998): Reevaluation of the oxygen isotopic composition of planktonic foraminifera: Experimental results and revised paleotemperature equations: *Paleoceanography*: *13*,(2), 150-160.

Bender, M., T. Sowers and E. J. Brook: (1997): Gases in ice cores: *Proc. Nat. Academy Sci. USA*: *94*, 8343-8349.

Berger, A.: (1977): Long-term variations of the Earth's orbital elements: *Celestial Mechanics*: *15*, 53-74.

Berger, A.: (1989): Pleistocene climatic variability at astronomical frequencies: *Quat. International*: *2*, 1-14.

Berger, A.: (1992a): Astronomical theory of paleoclimates and the last glacial-interglacial cycle: *Quat. Sci. Rev.*: *11*, 571-581.

Berger, A.: (1992b): Orbital Variations and Insolation Database. IGBP PAGES/World Data Center-A for Paleoclimatology Data Contribution Series # 92-007: *NOAA/NGDC Paleoclimatology Program*: http://ftp.ngdc.noaa.gov/paleo/insolation/orbit91.

Berger, A. and G. Wefer: (1996): Expeditions into the past: Paleoceanographic studies in the South Atlantic: Edited by: G. Wefer, Berger, A., Siedler, G. and Webb, D. J. *The South Atlantic: Present and Past Circulation.* Springer-Verlag, Berlin, Heidelberg, New York: pp. 363-410.

Berger, W.H., M.-C. Bonneau, and F.L. Parker: (1982): Foraminifera on the deep-sea floor: lysocline and dissolution rate: *Oceanol. Acta:* 5(2), 249–258.

Berger, W. H., J. S. Killingley and E. Vincent: (1978): Stable isotopes in deep sea carbonates: Box core ERDC-92, west equatorial Pacific: *Oceanological Acta*: *1*, 203-216.

Berger, W. H. and E. Vincent: (1986): Deep-sea carbonates: Reading the carbon-isotope signal: *Geologische Rundschau*: *75*,(1), 249-269.

Bianchi, C. and R. Gersonde: (2002): The Southern Ocean surface between Marine Isotope Stages 6 and 5d: Shape and timing of climate changes: *Palaeogeogr. Palaeoclimatol. Palaeoecol.*: *187*,(1-2), 151-177.

Bianchi, G. G., I. R. Hall, I. N. McCave and L. Joseph: (1999): Measurement of the sortable silt current speed proxy using the Sedigraph 5100 and Coulter Multisizer IIe: precision and accuracy: *Sedimentology*: *46*,(6), 1001-1014.

Bianchi, G. G. and I. N. McCave: (1999): Holocene periodicity in North Atlantic climate and deep-ocean flow south of Iceland: *Nature*: *397*, 515-517.

Bickert, T. and A. Mackensen: (2003): Last glacial to Holocene changes in South Atlantic deep water circulation: Edited by: G. Wefer, Mulitza, S. and Ratmeyer, V. *The South Atlantic in the Late Quaternary: Reconstruction of Material Budgets and*

Current Systems. Springer-Verlag, Berlin, Heidelberg, New York, Tokyo: pp. 671-695.

Bickert, T. and G. Wefer: (1996): Late Quaternary deep water circulation in the South Atlantic: Reconstruction from carbonate dissolution and benthic stable isotopes: Edited by: G. Wefer, Berger, W. H., Siedler, G. and Webb, D. J. *The South Atlantic: Present and Past Circulation*. Springer-Verlag, Berlin Heidelberg: pp. 599-620.

Bickert, T. and G. Wefer: (1999): South Atlantic and benthic foraminifer $\delta^{13}C$ deviations; implications for reconstructing the Late Quaternary deep-water circulation: *Deep Sea Res. Part II*: *46*, 437-452.

Birks, H. J. B.: (1995): Quantitative palaeoenvironmental reconstructions: Edited by: D. Maddy and Brew, J. S. *Statistical Modeling of Quaternary Science Data*. Quaternary Research Association, Cambridge: pp.

Blunier, T. and E. J. Brook: (2001): Timing of millennial-scale climate change in Antarctica and Greenland during the last glacial period: *Science*: *291*,(5501), 109-112.

Blunier, T., J. Chappellaz, J. Schwander, A. Dällenbach, B. Stauffer, T. F. Stocker, D. Raynaud, J. Jouzel, H. B. Clausen, C. U. Hammer and S. J. Johnsen: (1998): Asynchrony of Antarctic and Greenland climate change during the last glacial period: *Nature*: *394*, 739-743.

Blunier, T., J. Schwander, B. Stauffer, T. F. Stocker, A. Dallenbach, A. Indermuhle and J. Tschumi: (1997): Timing of the Antarctic cold reversal and the atmospheric CO_2 increase with respect to the Younger Dryas: *Geophys. Res. Letters*: *24*,(21), 2683-2686.

Boebel, O., T. Rossby, J. Lutjeharms, W. Zenk and C. Barron: (2003a): Path and variability of the Agulhas Return Current: *Deep Sea Res. Part II*: *50*,(1), 35-56.

Boebel, O., J. Lutjeharms, C. Schmid, W. Zenk, T. Rossby and C. Barron: (2003b): The Cape Cauldron: a regime of turbulent inter-ocean exchange: *Deep Sea Res. Part II*: *50*,(1), 57-86.

Bond, G., W. Broecker, S. J. Johnsen, J. McManus, L. Labeyrie, J. Jouzel and G. Bonani: (1993): Correlations between climate records from North Atlantic sediments and Greenland ice: *Nature*: *365*, 143-147.

Bond, G., H. Heinrich, W. Broecker, L. Labeyrie, J. McManus, J. Andrews, S. Huon, R. Jantschik, S. Clasen, C. Simet, K. Tedesco, M. Klas, G. Bonani and S. Ivy: (1992): Evidence for massive discharge of icebergs into the North Atlantic Ocean during the Last Glacial period: *Nature*: *360*, 245-249.

Bond, G. and R. Lotti: (1995): Iceberg discharges into the North Atlantic on millennial time scales during the last glaciation: *Science*: *267*, 1005-1010.

Bond, G., W. Showers, M. Cheseby, R. Lotti, P. Almasi, P. deMenocal, P. Priore, H. Cullen, I. Hajdas and G. Bonani: (1997): A pervasive millennial-scale cycle in North Atlantic Holocene and glacial climates: *Science*: *278*,(5341), 1257-1266.

Bostock, H. C., B. N. Opdyke, M. K. Gagan and L. K. Fifield: (2004): Carbon isotope evidence for changes in Antarctic intermediate water circulation and ocean ventilation in the southwest Pacific during the last deglaciation: *Paleoceanography*: *19*, PA4013, doi:10.1029/2004PA001047

Bouvier-Soumagnca, Y. and J. C. Duplessy: (1985): Carbon and oxygen isotopic composition of planktonic foraminfera from laboratory culture, plankton tows and recent sediments: implications for the reconstruction of paleoclimatic conditions and of the global carbon cycle: *J. Foram. Res.*: *15*, 302-320.

Boyle, E. A.: (1992): Cadmium and $\delta^{13}C$ paleochemical ocean distributions during the Stage 2 glacial maximum: *Annu. Rev. Earth Planet. Sci.*: *20*,(1), 245-287.

Boyle, E. A.: (1997): Characteristics of the deep ocean carbon system during the past 150,000 years: ΣCO_2 distributions, deep water flow patterns, and abrupt climate change: *Proc. Nat. Academy Sci. USA*: *94*, 8300-8307.

Boyle, E. A.: (2000): Is ocean thermohaline circulation linked to abrupt stadial / interstadial transitions?: *Quat. Sci. Rev.*: *19*,(1-5), 255-272.

Boyle, E. A. and L. D. Keigwin: (1987): North Atlantic thermohaline circulation during the past 20,000 years linked to high-latitude surface temperature: *Nature*: *330*, 35-40.

Bradford-Grieve, J. M., F. H. Chang, M. Gall, S. Pickmere and F. Richards: (1997): Size-fractioned phytoplankton standing stocks and primary production during austral winter and spring 1993 in the Subtropical convergence region near New Zealand: *New Zealand J. Marine Freshwater Res.*: *31*, 201-224.

Brathauer, U. and A. Abelmann: (1999): Late Quaternary variations in sea surface temperatures and their relationship to orbital forcing recorded in the Southern Ocean (Atlantic Sector): *Paleoceanography*: *14*,(2), 135-148.

Broecker, W.: (1998): Paleocean circulation during the last deglaciation: A bipolar seesaw?: *Paleoceanography*: *13*,(2), 119-121.

Broecker, W. and E. Maier-Reimer: (1992): The influence of air and sea exchange on the carbon isotope distribution in the sea: *Global Biogeochem. Cycles*: *6*, 315-320.

Broecker, W. and T.-H. Peng: (1982): *Tracers in the Sea*, Eldigio, Palisades, New York:

Broecker, W., D. L. Thurber, Goddard, J., T.-L. Ku, R. K. Matthews and K. J. Mesolella: (1968): Milankovitch hypothesis supported by precise dating of coral reefs and deep-sea sediments: *Science*: *159*, 297-300.

Broecker, W. and J. van Donk: (1970): Insolation changes, ice volume and the $\delta^{18}O$ record in deep-sea cores: *Reviews of Geophysics and Space Physics*: *8*, 169-198.

Broecker, W. S. and G. H. Denton: (1990): The role of ocean-atmosphere reorganizations in glacial cycles: *Quat. Sci. Rev.*: *9*,(4), 305-341.

Brook, E. J., T. Sowers and J. Orchardo: (1996): Rapid variations in atmospheric methane concentration over the past 110,000 years: *Science*: *273*, 1087-1091.

Brook, E. J., J. W. C. White, A. S. M. Schilla, M. L. Bender, B. Barnett, J. P. Severinghaus, K. C. Taylor, R. B. Alley and E. J. Steig: (2005): Timing of millennial-scale climate change at Siple Dome, West Antarctica, during the last glacial period: *Quat. Sci. Rev.*: *24*,(12-13), 1333-1343.

Burckle, L. H.: (1984): Diatom distribution and paleogeographic reconstruction in the Southern Ocean - present and last glacial maximum: *Mar. Micropal.*: *9*, 241-261.

Butzin, M., M. Prange and G. Lohmann: (2005): Radiocarbon simulations for the glacial ocean: the effects of wind stress, Southern Ocean sea ice and Heinrich events: *Earth Planet. Sci. Letters*: *235*, 45-61.

Cane, M.: (1998): A role for the tropical Pacific: *Science*: *282*, 60-61.

Cane, M. and A. Clement: (1999): A role for tropical Pacific coupled ocean-atmosphere system on Milankovitch and millennial timescales: Part II, global impacts: Edited by: P. U. Clark, Webb, R. S. and Keigwin, L. D. *Mechanisms of Global Climate Change at Millennial Time Scales, Geophysical Monograph Series*. AGU, Washington D.C. *112*: pp. 373-383.

Carmack, E. C.: (1977): Water characteristics of the Southern Ocean south of the Polar Front: Edited by: M. Angel. *A Voyage of Discovery, George Deacon 70th Anniversary Volume*. Pergamon Press, Oxford: pp. 15-41.

Carter, L., H. L. Neil and I. N. McCave: (2000): Glacial to interglacial changes in non-carbonate and carbonate accumulation in the SW Pacific Ocean, New Zealand: *Palaeogeogr. Palaeoclimatol. Palaeoecol.*: *162*,(3-4), 333-356.

Carter, L., H. L. Neil and L. Northcote: (2002): Late Quaternary ice-rafting events in the SW Pacific Ocean, off eastern New Zealand: *Mar. Geol.*: *191*,(1-2), 19-35.

Chang, Y.-P., C.-C. Chang, L.-W. Wang, M.-T. Chen, C.-H. Wang and E.-F. Yu: (1999): Planktonic foraminiferal sea surface temperature variations in the Southeast Atlantic Ocean: A high resolution record MD962085 of the past 400,000 years from the IMAGES II - NAUSICAA cruise: *Terrestrial, Atmospheric and Oceanic Sciences*: *10*,(1), 185-200.

Chapman, M. R. and N. J. Shackleton: (1999): Global ice-volume fluctuations, North Atlantic ice-rafting events, and deep-ocean circulation changes between 130 and 70 ka: *Geology*: *27*,(9), 795-798.

Chapman, M. R., N. J. Shackleton and J.-C. Duplessy: (2000): Sea surface temperature variability during the last glacial-interglacial cycle: assessing the magnitude and pattern of climate change in the North Atlantic: *Palaeogeogr. Palaeoclimatol. Palaeoecol.*: *157*,(1-2), 1-25.

Chappell, J., A. Omura, T. Esat, M. McCullock, J. Pandolfi, Y. Ota and B. Pillans: (1996): Reconciliation of late Quaternary sea levels derived from coral terraces at Huon Peninsula with deep sea oxygen isotope records: *Earth Planet. Sci. Letters*: *141*, 227-236.

Charles, C. D. and R. G. Fairbanks: (1990): Glacial to interglacial changes in the isotopic gradients of the Southern Ocean surface water: Edited by: U. Bleil and Thiede, J. *Geological History of the Polar Oceans: Arctic versus Antarctic.* Kluwer, Dortrecht: pp. 519-538.

Charles, C. D. and R. G. Fairbanks: (1992): Evidence from Southern Ocean sediments for the effect of North Atlantic deep-water flux on climate: *Nature*: *355*, 416-419.

Charles, C. D., J. Lynch-Stieglitz, U. S. Ninnemann and R. G. Fairbanks: (1996): Climate connections between the hemisphere revealed by deep sea sediment core/ice core correlations: *Earth Planet. Sci. Letters*: *142*,(1-2), 19-27.

Chen, M.-T., Y.-P. Chang, C.-C. Chang, L.-W. Wang, C.-H. Wang and E.-F. Yu: (2002): Late Quaternary sea-surface temperature variations in the southeast Atlantic: a planktic foraminifer faunal record of the past 6000 000 yr (IMAGES II MD962085): *Mar. Geol.*: *180*, 163-181.

Chesner, C. A., W. I. Rose, A. Deino, R. Drake and J. A. Westgate: (1991): Eruption history of the Earth's largest Quaternary caldera (Toba, Indonesia) clarified: *Geology*: *19*, 200-203.

Clark, P. U., R. B. Alley and D. Pollard: (1999): Northern hemisphere ice-sheet influences on global climate change: *Science*: *286*, 1104-1111.

Clark, P. U., N. G. Pisias, T. F. Stocker and A. J. Weaver: (2002): The role of the thermohaline circulation in abrupt climate change: *Nature*: *415*, 863-869.

Clemens, S., W. L. Prell, D. Murray, G. Schimmield and G. P. Weedon: (1991): Forcing mechanisms of the Indian Ocean monsoon: *Nature*: *353*, 720-725.

CLIMAP Project Members: (1976): The surface of the ice-age Earth: *Science*: *191*, 1131-1137.

CLIMAP Project Members: (1981): Seasonal reconstructions of the Earth's surface at the last glacial maximum: *Geo. Soc. Am, Boulder, CO, Map and Chart Service*: *MC-36*, 18.

CLIMAP Project Members: (1984): The last interglacial ocean: *Quat. Res.*: *21*, 123-224.

Conan, S. M. H., E. M. Ivanova and G. J. A. Brummer: (2002): Quantifying carbonate dissolution and calibration of foraminiferal dissolution indices in the Somali Basin: *Mar. Geol.*: *182*,(3-4), 325-349.

Cortese, G. and A. Abelmann: (2002): Radiolarian-based paleotemperatures during the last 160 kyr at ODP Site 1089 (Southern Ocean, Atlantic sector): *Palaeogeogr. Palaeoclimatol. Palaeoecol.*: *182*, 259-286.

Cortijo, E., L. Labeyrie, L. Vidal, M. Vautravers, M. Chapman, J. C. Duplessy, M. Elliot, M. Arnold, J. L. Turon and G. Auffret: (1997): Changes in sea surface hydrology associated with Heinrich event 4 in the North Atlantic Ocean between 40° and 60° N: *Earth Planet. Sci. Letters*: *146*,(1-2), 29-45.

Craig, H. and L. I. Gordon: (1965): Isotopic oceanography: deuterium and $\delta^{18}O$ variations in the ocean and the marine atmosphere: Edited by: E. Tongiorgi. *Stable Isotopes in Oceanographic Studies and Paleotemperatures*. Spolito: pp. 9-130.

Crosta, X., A. Sturm, L. Armand and J. J. Pichon: (2004): Late Quaternary sea ice history in the Indian sector of the Southern Ocean as recorded by diatom assemblages: *Mar. Micropal.*: *50*, 209-223.

Crucifix, M., M. F. Loutre and A. Berger: (2006): The climate response to the astronomical forcing: *Space Science Reviews*: *125*,(1-4), 213-226.

Cunningham, S., S. Alderson, B. A. King and M. A. Brandon: (2003): Transport and variability of the Antarctic circumpolar current in Drake Passage: *J. Geophys. Res.*: *108*, doi:10.1029/2001JC001147.

Curry, W. B. and T. J. Crowley: (1987): The $\delta^{13}C$ of equatorial Atlantic surface waters: Implications for ice age pCO_2 levels: *Paleoceanography*: *2*, 287-298.

Curry, W. B., J.-C. Duplessy, L. Labeyrie and N. J. Shackleton: (1988): Changes in the distribution of δ13C of deep water ΣCO_2 between the last glaciation and the Holocene: *Paleoceanography*: *3*,(3), 317-341.

Curry, W. B. and G. Lohmann: (1982): Carbon isotope changes in benthic foraminifera from the western South Atlantic: Reconstruction of glacial abyssal circulation patterns: *Quat. Res.*: *18*, 218-235.

Curry, W. B. and D. Oppo: (2005): Glacial water mass geometry and the distribution of $\delta^{13}C$ of CO_2 in the western Atlantic Ocean: *Paleoceanography*: *20*,(PA 1017), doi: 10.1029/2004PA001021.

Curry, W. B., R. C. Thunell and S. Honjo: (1983): Seasonal changes in the isotopic composition of planktonic foraminifera collected in Panama basin sediment traps: *Earth Planet. Sci. Letters*: *64*, 33-43.

Cutler, K. B., R. L. Edwards, F. W. Taylor, H. Cheng, J. Adkins, C. D. Gallup, P. M. Cutler, G. S. Burr and A. L. Bloom: (2003): Rapid sea-level fall and deep-ocean

temperature change since the last interglacial period: *Earth Planet. Sci. Letters*: *206*,(3-4), 253-271.

Dansgaard, W., S. J. Johnsen, H. B. Clausen, D. Dahl-Jensen, N. S. Gundestrup, C. U. Hammer, C. S. Hvidberg, J. P. Steffensen, A. E. Sveinbjörnsdottir, J. Jouzel and G. Bond: (1993): Evidence for general instability of past climate from a 250-kyr ice-core record: *Nature*: *364*, 218-220.

Darling, K., M. Kucera, D. Kroon and C. M. Wade: (2006): A resolution for the coiling direction paradox in *Neogloboquadrina pachyderma*: *Paleoceanography*: *21*, PA2011, doi:10.1029/2005PA001189.

Darling, K., M. Kucera, C. Pudsey and C. M. Wade: (2004): Molecular evidence links cryptic diversification in polar planktonic protists to Quaternary dynamics: *Proc. Nat. Academy Sci. USA*: *101*,(20), 7657-7662.

de Ruijter, W. P. M., A. Biastoch, S. S. Drijfhout, J. R. E. Lutjeharms, R. P. Matano, T. Pichevin, P. J. van Leeuwen and W. Weijer: (1999): Indian-Atlantic interocean exchange: Dynamics, estimation and impact: *J. Geophys. Res.*: *104*,(C9), 20,885-20,910.

de Vries, H.: (1958): Variation in concentration of radiocarbon with time and location on earth: *Koninkijk Nederlandse Akademie von Wetenschappen, Amsterdam, Proc.*: *B61*, 94-102.

Deacon, G. E. R.: (1982): Physical and biological zonation in the Southern Ocean: *Deep Sea Res.*: *29*, 1-15.

deMenocal, P., D. Oppo and W. L. Prell: (1992): Pleistocene $\delta^{13}C$ variability of North Atlantic intermediate waters: *Paleoceanography*: *7*, 229-250.

Denton, G. H. and T. J. Hughes: (1983): Milankovitch theory of ice ages: Hypothesis of ice-sheet linkage between regional insolation and global climate: *Quat. Res.*: *20*, 125-144.

Deuser, W. G. and E. H. Ross: (1989): Seasonally abundant planktonic foraminifera of the Sargasso Sea: Succession, deep-water fluxes, isotopic compositions, paleoceanographic implications: *J. Foram. Res.*: *19*, 268-293.

Deuser, W. G., E. H. Ross, C. Hemleben and M. Spindler: (1981): Seasonal changes in species composition, numbers, mass, size and isotopic composition of planktonic foraminifera settling into the deep Sargasso sea: *Palaeogeogr. Palaeoclimatol. Palaeoecol.*: *33*, 103-127.

Diekmann, B., D. K. Futterer, H. Grobe, C. D. Hillenbrand, G. Kuhn, K. Michels, R. Petschick and M. Pirrung: (2003): Terrigenous sediment supply in the polar to temperate South Atlantic: Land-ocean links of environmental changes during the late Quaternary: Edited by: G. Wefer, Mulitza, S. and Ratmeyer, V. *The South Atlantic in the Late Quaternary: Reconstruction of Material Budgets and Current Systems*. Springer-Verlag, Berlin Heidelberg New York Tokyo: pp. 375-399.

Diekmann, B., R. Petschick, F. X. Gingele, D. K. Futterer, A. Abelmann, U. Brathauer, R. Gersonde and A. Mackensen: (1996): Clay mineral fluctuations in late Quaternary sediments of the southeastern South Atlantic: Implications for past changes in deep water advection: Edited by: G. Wefer, Berger, A., Siedler, G. and Webb, D. J. *The South Atlantic: Present and Past Circulation.* Springer-Verlag, Berlin Heidelberg: pp. 621-644.

Duplessy, J. C., L. Labeyrie, A. Juilletleclerc, F. Maitre, J. Duprat and M. Sarnthein: (1991): Surface salinity reconstruction of the North-Atlantic Ocean during the Last Glacial Maximum: *Oceanologica Acta*: *14*,(4), 311-324.

Duplessy, J.-C., N. J. Shackleton, R. G. Fairbanks, L. Labeyrie, D. Oppo and N. Kallel: (1988): Deepwater source variations during the last climatic cycle and their impact on the global deepwater circulation: *Paleoceanography*: *3*,(3), 343-360.

Edwards, R. L., H. Cheng, M. T. Murrell and S. L. Goldstein: (1997): Pa^{231} dating of carbonates by thermal ionization mass spectrometry: implications for quaternary climate change: *Science*: *276*, 782-786.

Elliot, M. L., L. Labeyrie and J.-C. Duplessy: (2002): Changes in North Atlantic deep-water formation associated with the Dansgaard-Oeschger temperature oscillations (60-10ka): *Quat. Sci. Rev.*: *21*,(10), 1153-1165.

Ellison, C. R. W., M. R. Chapman and I. R. Hall: (2006): Surface and deep ocean interactions during the cold climate event 8200 years ago: *Science*: *312*,(5782), 1929-1932.

EMIDAS (Electronic Microfossil Image Database System): (2007): www.emidas.ethz.ch

England, M., A. Santoso, A. S. Gupta, C. Aiken, R. S. Rintoul and T. Hirst.: (2007): Water mass variability in the Southern Ocean: Separating natural fluctuations from long term change: http://web.maths.unsw.edu.au/~matthew/southern_ocean_variability

England, M. H. and V. C. Garcon: (1994): South-Atlantic Circulation in a World Ocean Model: *Annales Geophysical-Atmospheres Hydrospheres and Space Sciences*: *12*,(9), 812-825.

EPICA Community Members: (2004): Eight glacial cycles from an Antarctic ice core: *Nature*: *429*, 623-628.

EPICA Community Members: (2006): One-to-one hemispheric coupling of millennial polar climate variability during the last glacial: *Nature*: *444*, 195-198.

Erez, J. and B. Luz: (1983): Experimental paleotemperature equation for planktonic foraminifera: *Geochim. Cossmochim. Acta*: *47*, 1025-1031.

Esper, O., G. J. M. Versteegh, K. A. F. Zonneveld and H. Willems: (2004): A palynological reconstruction of the Agulhas Retroflection (South Atlantic Ocean) during the Late Quaternary: *Global Planet. Change*: *41*,(1), 31-62.

Esper, O., K. A. F. Zonneveld, C. Hall, B. Karwath, H. Kuhlmann, R. R. Schneider, A. Vink, I. Weise-Ihlo and H. Willems: (2000): Reconstruction of palaeoceanographic conditions in the South Atlantic Ocean at the last two Terminations based on calcareous dinoflagellate cysts: *Int. Journal Earth Sci.*: *88*,(4), 680-693.

Evans, H. K., I. R. Hall, G. G. Bianchi and D. Oppo: (2007): Intermediate water links to Deep Western Boundary Current variability in the subtropical NW Atlantic during Marine Isotope Stages 5 and 4: *Paleoceanography*: 22,(PA3209), doi:10.1029/2006PA001409.

Fahrbach, E., G. Rohardt, N. Scheele, M. Schroder, V. Strass and A. Wisotzki: (1995): Formation and discharge of deep and bottom water in the northwestern Weddell Sea: *J. Mar. Res.*: *53*,(4), 515-538.

Fairbanks, R. G.: (1989): A 17,000-year glacio-eustatic sea level record: influence of glacial melting rates on the Younger Dryas event and deep-ocean circulation: *Nature*: *342*, 637-642.

Fairbanks, R. G., R. A. Mortlock, T.-C. Chiu, L. Cao, A. Kaplan, T. P. Guilderson, T. W. Fairbanks, A. L. Bloom, P. M. Grootes and M.-J. Nadeau: (2005): Radiocarbon calibration curve spanning 0 to 50,000 years BP based on paired 230Th/234U/238U and 14C dates on pristine corals: *Quat. Sci. Rev.*: *24*,(16-17), 1781-1796.

Fairbanks, R. G., M. Sverdlove, R. Free, P. H. Wiebe and A. W. H. Bé: (1982): Vertical distribution and isotopic fractionation of living planktonic foraminifera from the Paname Basin: *Nature*: *298*, 841-844.

Fanning, A. F. and A. J. Weaver: (1997): Temporal-geographical meltwater influences on the North Atlantic conveyor: Implications for the Younger Dryas: *Paleoceanography*: *12*, 307-320.

Federman, A. N., N. D. Watkins and H. Sigurdsson: (1982): Scoita arc volcanism recorded in abyssal piston cores downwind from the islands: Edited by: C. Craddock. *Antarctic Geoscience*. University of Wisconsin Press, Madison: pp. 223-228.

Fiúza, A. F. G.: (1983): Upwelling patterns off Portugal: Edited by: E. Suess and Thiede, J. *Coastal Upwelling - Its Sediment Record: Part A: Responses of the Sedimentary Regime to Present Coastal Upwelling*. Plenum Press, New York and London: pp. 85-98.

Flores, J.-A., R. Gersonde and F. J. Sierro: (1999): Pleistocene fluctuations in the Agulhas Current Retroflection based on the calcareous plankton record: *Mar. Micropal.*: *37*,(1), 1-22.

Flower, B. P., D. W. Oppo, J. McManus, K. A. Venz, D. A. Hodell and J. L. Cullen: (2000): North Atlantic intermediate to deep water circulation and chemical stratification during the past 1 Myr: *Paleoceanography: 15*,(4), 388-403.

François, R., M. A. Altabet, E. F. Yu, D. M. Sigman, M. P. Bacon, M. Frank, G. Bohrmann, G. Bareille and L. D. Labeyrie: (1997): Contribution of Southern Ocean surface-water stratification to low atmospheric CO2 concentrations during the last glacial period: *Nature*: *389*,(6654), 929-935.

Franzese, A. M., S. R. Hemming, S. L. Goldstein and R. F. Anderson: (2006): Reduced Agulhas Leakage during the Last Glacial Maximum inferred from an integrated provenance and flux study: *Earth and Planetary Science Letters*: *250*, (1-2), 72-88.

Friocourt, Y., S. Drijfhout, B. Blanke and S. Speich: (2005): Water mass export from drake passage to the Atlantic, Indian, and Pacific Oceans: A Lagrangian model analysis: *J. Phys. Ocean.*: *35*,(7), 1206-1222.

Gallée, H., J. P. van Ypersele, T. Fichefet, I. Marsiat, C. Tricot and A. Berger: (1992): Simulation of the last glacial cycle by a coupled, sectorially averaged climate-ice sheet model. Part II: Response to insolation and CO_2 variation: *J. Geophys. Res.*: *97*, 15, 713-715, 740.

Gallup, C. D., R. L. Edwards and R. G. Johnson: (1994): The timing of high sea levels over the past 200,000 years: *Science*: *263*, 796-800.

Ganachaud, A. and C. Wunsch: (2000): Improved estimates of global ocean circulation, heat transport and mixing from hydrographic data: *Nature*: *408*, 453-457.

Ganopolski, A. and S. Rahmstorf: (2001): Rapid changes of glacial climate simulated in a coupled climate model: *Nature*: *409*, 153-158.

Ganssen, G. M. and D. Kroon: (2000): The isotopic signature of planktonic foraminifera from NE Atlantic surface sediments: implications for the reconstruction of past oceanic conditions: *J. Geol. Soc. London*: *157*, 693-699.

Ganssen, G. M.: (1983): Dokumentation von küstennahem Auftrieb anhand stabiler Isotope in rezenten Foraminiferen vor Nordwest-Afrika: *"Meteor" Forsch Ergebn: C37*, 1-46.

Ganssen, G. M. and M. Sarnthein: (1983): Stable-isotope composition of foraminifers: The surface and bottom water record of coastal upwelling: Edited by: E. Suess and Thiede, J. *Coastal Upwelling - Its Sediment Record: Part A: Responses of the Sedimentary Regime to Present Coastal Upwelling*. Plenum Press, New York and London: pp. 99-121.

Garzoli, S. L. and A. L. Gordon: (1996): Origins and variability of the Benguela Current: *J. Geophy Res. Oceans*: *101*,(C1), 897-906.

Georgi, D. T.: (1981): On the relationship between large-scale property variations and fine structure in the Circumpolar Deep Water: *J. Geophys. Res.*: *86*, 6556-6566.

Gersonde, R., A. Abelmann, U. Brathauer, S. Becquey, B. C., G. Cortese, H. Grobe, G. Kuhn, H. S. Niebler, M. Segl, R. Sieger, U. Zielinski and D. K. Futterer: (2003): Last glacial sea surface temperature and sea-ice extent in the southern ocean (Atlantic-Indian sector): a multiproxy approach: *Paleoceanography*: *18*,(3), 1061, doi:10.1029/2002PA000809

Gersonde, R., X. Crosta, A. Abelmann and L. Armand: (2005): Sea-surface temperature and sea ice distribution of the Southern Ocean at the EPILOG Last Glacial Maximum--a circum-Antarctic view based on siliceous microfossil records: *Quat. Sci. Rev.*: *24*,(7-9), 869-896.

Gherardi, J. M., L. Labeyrie, J. F. McManus, R. Francois, L. C. Skinner and E. Cortijo: (2005): Evidence from the Northeastern Atlantic basin for variability in the rate of the meridional overturning circulation through the last deglaciation: *Earth Planet. Sci. Letters*: *240*,(3-4), 710-723.

Ghil, M.: (1994): Cryothermodynaics: the chaotic dynamics of paleoclimate: *Physica D*: *77*, 130-159.

Gille, S. T.: (1994): Mean sea surface height of the Antarctic Circumpolar Current from Geosat data: method and application: *J. Geophys. Res.*: *99*, 18255-18273.

Giraudeau, J., R. Zahn and I. R. Hall: (2002): Agulhas current variability: Calypso long sediment coring off South Africa: *Cruise Report - RV Marion Dufresne cruise MD128.*

Goldstein, S. L., S. R. Hemming, S. Kish and R. L. Rutberg: (1999): Strontium isotopes in South Atlantic detritus: a surface current proxy and tracer of Agulhas Leakage: *Ninth Annual Goldschmidt Conference*: Lunar Planetary Institute, Houston, TX, p. 7537.

Gordon, A. L. and W. F. Haxby: (1990): Agulhas eddies invade the South Atlantic: Evidence from Geosat altimeter and shipboard conductivity-temperature-depth survey: *J. Geophys. Res.*: *95*,(C3), 3117-3125.

Gordon, A. L., J. R. E. Lutjeharms and M. L. Gründlingh: (1987): Stratification and circulation at the Agulhas retroflection: *Deep Sea Res.*: *34*,(4), 565-599.

Gordon, A. L., R. F. Weiss, W. M. Smethie Jr and M. J. Warner: (1992): Thermocline and intermediate water communication between the South Atlantic and Indian oceans: *J. Geophys. Res.*: *97*,(C5), 7223-7240.

Gouretski, V. V. and I. A. Danilov: (1994): Characteristics of warm rings in the African sector of the Antarctic Circumpolar Current: *Deep Sea Res. Part I*: *41*, 1131-1157.

Graham, D. W., B. H. Corliss, M. L. Bender and L. D. Keigwin: (1981): Carbon and oxygen isotopic disequilibria of recent deep-sea benthic foraminifera: *Mar. Micropal.*: *6*, 483-497.

Greenland Ice-core Project (GRIP) Members: (1993): Climate instability during the last interglacial period recorded in the GRIP ice core: *Nature*: *364*, 203-207.

Grobe, H. and A. Mackensen: (1992): Late Quaternary climate cycles as recorded in sediments for the Antarctic continental margin: Edited by: J. P. Kennett and Warnke, D. A. *The Antarctic Paleoenvironment: A perspective on Global Change.* American Geophysical Union, Washington D.C. *56*: pp. 349-376.

Grootes, P. M. and M. Stuiver: (1997): Oxygen 18/16 variability in Greenland snow and ice with 10^3 to 10^5-year time resolution.: *J. Geophys. Res.*: *102*, 26455-26470.

Grousset, F. E., E. Cortijo, S. Huon, L. Herve, T. Richter, D. Burdloff, J. Duprat and O. Weber: (2001): Zooming in on Heinrich layers: *Paleoceanography*: *16*,(3), 240-259.

Grützner, J., L. Giosan, S. O. Franz, R. Tiedemann, E. Cortijo, W. P. Chaisson, R. D. Flood, S. Hagen, L. D. Keigwin, S. Poli, D. Rio and T. Williams: (2002): Astronomical age models for Pleistocene drift sediments from the western North Atlantic (ODP Sites 1055-1063): *Mar. Geol.*: *189*,(1-2), 5-23.

Guo, Z., T. Liu, N. Fedoroff, L. Wei, Z. Ding, N. Wu, H. Lu, W. Jiang and Z. An: (1998): Climate extremes in Loess of China coupled with the strength of deep-water formation in the North Atlantic: *Global Planet. Change*: *18*,(3-4), 113-128.

Gupta, A. K., D. M. Anderson and J. T. Overpeck: (2003): Abrupt changes in the Asian southwest monsoon during the Holocene and their links to the North Atlantic Ocean: *Nature*: *421*,(6921n), 354-357.

Guptha, M. V. S. and R. Mohan: (1996): Seasonal variability of the vertical fluxes of *Globigerina bulloides* (d'Orbigny) in the northern Indian Ocean: *Mitt. Geol.-Palaontol. Inst. Univ. Hamb.*: *79*, 1-17.

Hale, W. and U. Pflaumann: (1999): Sea-surface temperature estimations using a modern analog technique with foraminiferal assemblages from Western Atlantic Quaternary sediments: Edited by: G. Fischer and Wefer, G. *Use of Proxies in Paleoceanography: Examples from the South Atlantic.* Springer-Verlag, Berlin, Heidelberg: pp. 69-90.

Hall, I. R. and I. N. McCave: (2000): Palaeocurrent reconstruction, sediment and thorium focusing on the Iberian margin over the last 140 ka: *Earth Planet. Sci. Letters*: *178*,(1-2), 151-164.

Hall, I. R., I. N. McCave, M. R. Chapman and N. J. Shackleton: (1998): Coherent deep flow variation in the Iceland and American basins during the last interglacial: *Earth Planet. Sci. Letters*: *164*, 15-21.

Hall, I. R., I. N. McCave, N. J. Shackleton, G. P. Weedon and S. E. Harris: (2001): Intensified deep Pacific inflow and ventilation in Pleistocene glacial times: *Nature*: *412*, 809-812.

Hall, I. R., S. B. Moran, R. Zahn, P. C. Knutz, C. C. Shen and R. L. Edwards: (2006): Accelerated drawdown of meridional overturning in the late-glacial Atlantic triggered by transient pre-H event freshwater perturbation: *Geophys. Res. Letters*: *33*,(16) Art. No. L16616

Hammer, Ø., D. A. T. Harper and P. D. Ryan: (2001): PAST: Paleontological Statistics Software Package for Education and Data Analysis: *Palaeontologia Electronica*: *4*,(1), 9.

Hays, J. D., J. Imbrie and N. J. Shackleton: (1976): Variations in the Earth's Orbit: Pacemaker of the Ice Ages: *Science*: *194*,(4270), 1121-1132.

Hayward, B. W.: (1983): Planktic foraminifera (Protozoa) in New Zealand waters: a taxonomic review: *New Zealand J. Zoology*: *10*,(1), 63-74.

Helber, R. W. and R. H. Weisberg: (2001): Equatorial upwelling in the western Pacific warm pool: *J. Geophys. Res.*: *106*,(C5), 8989-9004.

Hemleben, C., M. Spindler and O. R. Anderson: (1989): *Modern Planktonic Foraminifera*, Springer-Verlag, New York

Hemming, S. R.: (2004): Heinrich events: massive late Pleistocene detritus layers of the North Atlantic and their global climate imprint: *Reviews of Geophysics*: *42*, RG1005.

Henrich, R., K.-H. Baumann, S. Gerhardt, M. Gröger and A. N. A. Volbers: (2003): Carbonate preservation in deep and intermediate water masses in the South Atlantic: Evaluation and geological record (a review): Edited by: G. Wefer, Mulitza, S. and Ratmeyer, V. *The South Atlantic in the late Quaternary: Reconstructions of material budgets and current systems*. Springer-Verlag, Berlin Heidelberg New York Tokyo pp. 645-670.

Heusser, L. E.: (2000): Rapid oscillations in western North Atlantic vegetation and climate during oxygen isotope stage 5 inferred from pollen data from Santa Barbara Basin (Hole 893A): *Palaeogeogr. Palaeoclimatol. Palaeoecol.*: *161*, 407-421.

Hewitt, C. D., A. J. Broccoli, J. F. B. Mitchell and R. J. Stouffer: (2001): A coupled model study of the last glacial maximum: Was part of the North Atlantic relatively warm?: *Geophys. Res. Letters*: *28*, 1571-1574.

Heywood, K. J. and B. A. King: (2002): Water masses and baroclinic transports in the South Atlantic and Southern Oceans: *J. Mar. Res.*: *60*, 639-676.

Hodell, D. A., K. A. Venz, C. D. Charles and U. S. Ninnemann: (2003): Pleistocene vertical carbon isotope and carbonate gradients in the south Atlantic sector of the Southern Ocean: *Geochem. Geophys. Geosyst.*: *4*,(1), 1-19.

Hooghiemstra, H., J. L. Melice, A. Berger and N. J. Shackleton: (1993): Frequency sepctra and paleoclimatic variability of the high precision 30-1450 ka Funze 1 pollen record (Eastern Cordillera, Columbia): *Quat. Sci. Rev.*: *12*, 141-156.

Howard, W. R. and W. L. Prell: (1984): A comparison of radiolarian and foraminiferal paleoecology in the southern Indian Ocean: New evidence for the intherhemispheric timing of climatic change: *Quaternary Research*: *21*, 244-263.

Howard, W. R. and W. L. Prell: (1992): Late Quaternary surface circulation of the southern Indian Ocean and its relationship to orbital variations: *Paleoceanography*: *7*,(1), 79-117.

Hubberten, H.-W., W. W. Morche, F. Westall, D. K. Futterer and J. Keller: (1991): Geochemical investigations of volcanic ash layers from southern Atlantic Legs 113 and 114: *Proc. Ocean Drill. Program. Sci. Results*: *114*, 733-749.

Hut, G.: (1987): Consultants group meeting on stable isotope reference samples for geochemical and hydrological investigation: *International Atomic Energy Agency, Vienna*, 1-42.

Hutson, W. H.: (1977): Transfer function under no-analog conditions: Experiments with Indian Ocean planktonic foraminifera: *Quat. Res.*: *8*, 355-367.

Hutson, W. H.: (1980): The Agulhas current during the late Pleistocene: Analysis of modern faunal analogs: *Science*: *207*, 64-66.

Imbrie, J.: (1985): A theoretical framework for the Pleistocene ice ages: *J. Geol. Soc. London*: *142*, 417-432.

Imbrie, J., E. A. Boyle, S. Clemens, A. Duffy, W. R. Howard, G. Kukla, J. E. Kutzbach, D. G. Martinson, A. McIntyre, A. Mix, B. Molfino, J. J. Morley, L. C. Peterson, N. G. Pisias, W. L. Prell, M. E. Raymo, N. J. Shackleton and J. R. Toggweiler: (1992): On the structure and origin of major glaciation cycles: 1. Linear responses to Milankovitch forcing: *Paleoceanography*: *7*,(6), 701-738.

Imbrie, J., J. D. Hays, D. G. Martinson, A. McIntyre, A. Mix, J. J. Morley, N. G. Pisias, W. L. Prell and N. J. Shackleton: (1984): The orbital theory of Pleistocene climate: support from a revised chronology of the marine $\delta^{18}O$ record: Edited by: A. Berger, Imbrie, J., Hays, J. D., Kukla, G. and Saltzman, B. *Milankovitch and Climate: understanding the response to orbital forcing*. Reidel Publishing Company, Dortrecht, Boston, Lancaster: pp. 510.

Imbrie, J. and J. Z. Imbrie: (1980): Modeling the climatic response to orbital variations: *Science*: *207*,(4434), 943-953.

Imbrie, J. and N. J. Kipp: (1971): A new micropaleontological method for quantitative paleoclimatology: Application to a late Pleistocene Caribbean core: Edited by: K. K. Turekian. *The late Cenozoic glacial ages*. Yale University Press, New Haven, Conn.: pp. 71-181.

Imbrie, J., A. McIntyre and A. Mix: (1989): Oceanic response to orbital forcing in the late Quaternary: Observational and experimental strategies: Edited by: A. Berger, Duplessy, J.-C. and Schneider, S. H. *Climate and Geosciences: A Challenge for Science and Society in the 21st Century*, Reiderl, Hingham, MA: pp. 121-164.

Imbrie, J., A. C. Mix and D. G. Martinson: (1993): Milankovitch theory viewed from Devils Hole: *Nature*: *363*,(6429), 531-533.

Jackson, C. S. and A. J. Broccoli: (2003): Orbital forcing of Arctic climate: mechanisms of climate response and implications for continental glaciation: *Climate Dynamics*: *21*, 539-557.

Jenkins, G. M. and D. G. Watts: (1968): *Spectral Analysis and Its Applications*, Holden-Day, Merrifield, Va.

Johannessen, T., E. Jansen, A. Flatøy and A. C. Ravelo: (1994): The relationship between surface water masses, oceanographic fronts and paleoclimatic proxies in surface sediments of Greenland, Iceland, Norwegian Seas: *NATO ASI Series I*: *17*, 61-85.

Johnsen, S. J., H. B. Clausen and et al.: (1997): The $\delta^{18}O$ record along the Greenland Ice Core project deep ice core and the problem of possible Eemian climatic instability: *J. Geophys. Res.*: *102*, 26397-26410.

Johnsen, S. J., D. Dahl-Jensen and et al: (2001): Oxygen isotope and palaeotemperature records from six Greenland ice-core stations: Camp Century, Dye-3, GRIP, GISP2, Renland and NorthGRIP: *Journal of Quaternary Science: 16*, 299-307

Johnsen, S. J., W. Dansgaard, H. B. Clausen and C. C. Langway Jn: (1972): Oxygen isotope profiles through the Antarctic and Greenland ice sheets: *Nature*: *235*, 429-434.

Jongman, R.H.G., C.J.F. ter Braak and O.F.R. van Tongeren: (1995): *Data analysis in community and landscape ecology*: Cambridge University Press, Cambridge.

Jouzel, J., N. Barkov, J. M. Barnola, M. Bender, J. Chappellaz, C. Genthon, V. M. Kotlyakov, V. Lipenkov, C. Loruis, J. R. Petit, D. Raynaud, G. Raisbeck, C. Ritz, T. Sowers, M. Stievenard, F. Yiou and P. Yiou: (1995): Extending the Vostok ice-core record of paleoclimate to the penultimate glacial period: *Nature*: *364*, 407-412.

Jouzel, J. et al.: (2004): EPICA Dome C ice cores deuterium data: *IGBP PAGES/World Data Center for Paleoclimatology Data Contribution Series*: *# 2004-038*, NOAA/NGDC Paleoclimatology Program, Boulder CO, USA.

Jouzel, J., V. Masson, O. Cattani, S. Falourd, M. Stievenard, B. Stenni, A. Longinelli, G. C. Johnsen, J. P. Steffensen, J. R. Petit, J. Schwander, R. Souchez and N. Barkov: (2001): A new 27 ky high resolution East Antarctic climate record: *Geophys. Res. Letters*: *28*, 3199-3202.

Kahn, M. I. and D. F. Williams: (1981): Oxygen and carbon isotopic composition of living planktonic foraminifera from the northeast Pacific Ocean: *Palaeogeogr. Palaeoclimatol. Palaeoecol.*: *33*, 47-69.

Kallel, N., L. D. Labeyrie, A. Juillet-Leclerc and J.-C. Duplessy: (1988): A deep hydrological front between intermediate and deep-water masses in the glacial Indian Ocean: *Nature*: *333*, 651-655.

Kameo, K., M. C. Shearer, A. W. Droxler, I. Mita, R. Watanabe and T. Sato: (2004): Glacial-interglacial surface water variations in the Caribbean Sea during the last 300 ky based on calcareous nannofossil analysis: *Palaeogeogr. Palaeoclimatol. Palaeoecol.*: *212*,(1-2), 65-76.

Kandiano, E. S. and H. A. Bauch: (2002): Implications of planktonic foraminiferal size fractions for the glacial -interglacial paleoceanography of the polar North Atlantic: *J. Foram. Res.*: *32*,(3), 245-251.

Kanfoush, S. L.: (2000): Interpreting iceberg deposits in the deep sea: *Science*: *290*,(5489), 51-52.

Kanfoush, S. L., D. A. Hodell, C. D. Charles, T. P. Guilderson, P. G. Mortyn and U. S. Ninnemann: (2000): Millennial-scale instability of the Antarctic ice sheet during the Last Glaciation: *Science*: *288*,(5472), 1815-1819.

Kanfoush, S. L., D. A. Hodell, C. D. Charles, T. R. Janecek and F. R. Rack: (2002): Comparison of ice-rafted debris and physical properties in ODP Site 1094 (South Atlantic) with the Vostok Ice Core over the last four climatic cycles: *Palaeogeogr. Palaeoclimatol. Palaeoecol.*: *182*,(3-4), 329-349.

Keeling, R. F. and B. B. Stephens: (2001): Antarctic sea ice and the control of Pleistocene climate instability: *Paleoceanography*: *16*,(1), 112-131.

Keigwin, L. D. and E. A. Boyle: (1985): Carbon isotopes in deep-sea foraminifera: precession and changes in low-latitude biomass: Edited by: E. T. Sundquist and Broecker, W. *The Carbon Cycle and Atmospheric C02: Natural Variations Archean to Present*. Geophysical Monographs - American Geophysical Union, *32*: pp. 319-328.

Keigwin, L. D. and S. J. Lehman: (1994): Deep water circulation change linked to Heinrich event 1 and Younger Dryas in a mid-depth North Atlantic core: *Paleoceanography*: *9*,(2), 185-194.

Kennett, J. P. and S. Srinivasan: (1983): *Neogene Planktonic Foraminifera: A Phylogenetic Atlas*, Hutchinson Press, Stroudsburg, PA.

Kilworth, P. D.: (1983): Deep convection of the world ocean: *Review of Geophysical Space Physics*: *21*, 1-26.

Kim, S.-J., T. J. Crowley and A. Stossel: (1998): Local orbital forcing of Antarctic climate change during the last interglacial: *Science*: *280*,(5364), 728-730.

Kim, S. J., G. M. Flato, G. J. Boer and N. A. McFarlane: (2002): A coupled climate model simulation of the Last Glacial Maximum, part 1: transient multi-decadal response: *Climate Dynamics: 19*, (5-6), 515-537

King, A. L. and W. R. Howard: (2005): $\delta^{18}O$ seasonality of planktonic foraminifera from Southern Ocean sediment traps: Latitudinal gradients and implications for paleoclimate reconstructions: *Mar. Micropal.*: *56*, 1-24.

Kipp, N. J.: (1976): New transfer function for estimating past sea-surface conditions from sea bed distribution of planktonic foraminiferal assemblages in the North Atlantic: *Geol. Soc. Am. Members*: *145*, 3-42.

Knorr, G. and G. Lohmann: (2003): Southern ocean origin for the resumption of Atlantic thermohaline circulation during deglaciation: *Nature*: *424*, 532-536.

Knorr, G. and G. Lohmann: (2004): The southern ocean as the flywheel of the oceanic converyor belt circulation: *PAGES News*: *12*,(1), 11-13.

Knutti, R., J. Fluckiger, T. F. Stocker and A. Timmermann: (2004): Strong hemispheric coupling of glacial climate through freshwater discharge and ocean circulation: *Nature*: *430*, 851-856.

Kotilainen, A. T. and N. J. Shackleton: (1995): Rapid climate variability in the North Pacific Ocean during the past 95,000 years: *Nature*: *377*, 323-326.

Kroopnick, P.: (1980): The distribution of $\delta^{13}C$ in the Atlantic Ocean: *Earth and Planetary Science Letters: 49*(2), 469-484.

Kroopnick, P.: (1985): The distribution of ^{13}C in ΣCO_2 in the world oceans: *Deep Sea Res.*: *32*, 57-84.

Kroopnick, P., R. F. Weiss and H. Craig: (1972): Total CO_2, ^{13}C and dissolved oxygen ^{18}O at GEOSECS II in the north Atlantic: *Earth Planet. Sci. Letters*: *16*, 103-110.

Kucera, M. and K. Darling: (2002): Genetic diversity among modern planktonic foraminifer species: its effect on paleoceanographic reconstructions: *Philos. Trans. R. Soc. London A*: *360*, 695-718.

Kucera, M., M. Weinelt, T. Kiefer, U. Pflaumann, A. Hayes, M. Weinelt, M.-T. Chen, A. C. Mix, T. T. Barrows and E. Cortijo: (2005a): Reconstruction of sea-surface temperatures from assemblages of planktonic foraminifera: multi-technique approach based on geographically constrained calibration data sets and its

application to glacial Atlantic and Pacific Oceans: *Quat. Sci. Rev.*: *24*,(7-9), 951-998.

Kucera, M., A. Rosell-Melé, R. R. Schneider, C. Waelbroeck and M. Weinelt: (2005b): Multiproxy approach for the reconstruction of the glacial ocean surface (MARGO): *Quat. Sci. Rev.*: *24*, 813-819.

Kuhn, G. and B. Diekmann: (2002): Late Quaternary variability of ocean circulation in the southeastern South Atlantic inferred from the terrigenous sediment record of a drift deposit in the southern Cape Basin (ODP Site 1089): *Palaeogeogr. Palaeoclimatol. Palaeoecol.*: *182*,(3-4), 287-303.

Kukla, G.: (1987): Loess stratigraphy in central China: *Quat. Sci. Rev.*: *6*, 191-219.

Kutzbach, J. E. and F. Street-Perrott: (1985): Milankovitch forcing of fluctuations in the level of tropical lakes from 18-0 k yr BP: *Nature*: *317*, 1301-1334.

Labeyrie, L., J. C. Duplessy and P. L. Blanc: (1987): Variations in mode of formation and temperature of oceanic deep waters over the past 125,000 years: *Nature*: *327*, 477-482.

Labeyrie, L., M. Labracherie, N. Gorfti, J. J. Pichon, M. Vautravers, M. Arnold, J.-C. Duplessy, M. Paterne, E. Michel, J. Duprat, M. Caralp and J. L. Turon: (1996): Hydrographic changes of the Southern Ocean (southeast Indian sector) over the last 230 kyr: *Paleoceanography*: *11*,(1), 57-76.

Labeyrie, L., J. J. Pichon, M. Labracherie, P. Ippolito, J. Duprat and J. C. Duplessy: (1986): Melting history of Antarctica during the past 60,000 years: *Nature*: *322*, 701-706.

Laskar, J.: (1990): The chaotic motion of the solar system: A numerical estimate of the size of the chaotic zones: *Icarus*: *88*,(2), 266-291.

Laskar, J., F. Joutel and F. Boudin: (1993): Orbital, precessional, and insolation quantities for the Earth from -20 Myr to +10 Myr: *Astronomy and Astrophysics*: *270*,(1-2), 522-533.

Laskar, J., P. Robutel, F. Joutel, M. Gastineau, A. C. M. Correia and B. Levrard: (1994): A long-term numerical solution for the insolation quantities of the Earth: *Astronomy and Astrophysics*: *428*, 261-285.

Lau, K. M. and H. Weng: (1995): Climate signal detection using wavelet transform: How to make a time series sing: *Bull. Am. Metero. Society*: *76*,(12), 2391-2402.

Lautenschlager, M., U. Mikolajewicz, E. Maier-Reimer and C. Heinze: (1992): Application of ocean models for the interpretation of atmospheric general circulation model experiments on the climate of the last glacial maximum: *Paleoceanography*: *7*, 769-782.

Le, J. and N. J. Shackleton: (1992): Carbonate dissolution fluctuations in the western equatorial Pacific during the late Quaternary: *Paleoceanography*: 7,(1), 21-42.

Lea, D. W.: (1995): A trace-metal perspective on the evolution of Antarctic circumpolar deep water chemistry: *Paleoceanography*: *10*, 733-747.

Lea, D. W., P. A. Martin, D. K. Pak and H. J. Spero: (2002): Reconstructing a 350ky history of sea level using planktonic Mg/Ca and oxygen isotope records from a Cocos Ridge core: *Quat. Sci. Rev.*: *21*, 283-293.

Legeais, J.-F., S. Speich, M. Arhan, I. J. Ansorge, E. Fahrbach, S. L. Garzoli and A. Klepikov: (2005): The baroclinic transport of the Antarctic Circumpolar Current south of Africa: *Geophys. Res. Letters*: *32*,(L24602), doi:10.1029/2005GL023271.

Levitus, S.: (1983): *Climatological Atlas of the World Ocean*, Department of Commerce, NOAA Professional Paper 13

Lisiecki, L. E. and M. E. Raymo: (2005): A Pliocene-Pleistocene stack of 57 globally distributed benthic $\delta^{18}O$ records: *Paleoceanography*: *20*, PA1003, doi:10.1029/2004PA001071.

Little, M. G., R. R. Schneider, D. Kroon, B. Price, C. P. Summerhayes and M. Segl: (1997): Trade wind forcing of upwelling, seasonality and Heinrich events as a response to sub-Milankovitch climate variability: *Paleoceanography*: *12*,(4), 568-576.

Lohmann, G. and N. P. Schweitzer: (1990): *Globorotalia truncatulinoides* growth and chemistry as probes of the past thermocline: 1, shell size: *Paleoceanography*: *5*, 55-75.

Lord, A.: (1980): Interpretation of late glacial marine environment of NW Europe by means of foraminifera: Edited by: J. J. Lowe, Gray, J. M. and Robinson, J. E. *Studies in the Lateglacial of North-west Europe*. Pergamon, Oxford: pp. 103-114.

Lorius, C., J. Jouzel, D. Raynaud, J. Hansen and H. L. Treut: (1990): The ice-core record: climate sensitivity and future greenhouse warming: *Nature*: *347*,(6289), 139-145.

Lototskaya, A. and G. M. Ganssen: (1999): The structure of termination II (penultimate deglaciation and Eemian) in the North Atlantic: *Quat. Sci. Rev.*: *18*, 1641-1654.

Lourens, L. J., A. Antonarakou, F. J. Hilgen, A. A. M. Van Hoof, C. Vernaud-Grazzini and W. J. Zachariasse: (1996): Evaluation of the Plio-Pleistocene astronomical timescale: *Paleoceanography*: *11*, 391-413.

Lowe, J. J. and M. J. C. Walker: (1997): *Reconstructing Quaternary Environments*, Longman Group Limited, Harlow, Essex

Lowell, T. V., C. J. Heusser, B. G. Andersen, P. I. Moreno, A. Hauser, L. E. Heusser, C. Schluchter, D. R. Marchant and G. H. Denton: (1995): Interhemispheric correlation of Late Pleistocene glacial events: *Science*: *269*,(5230), 1541-1549.

Lutjeharms, J. R. E. and I. J. Ansorge: (2001): The Agulhas Return Current: *J. Mar. Systems*: *30*,(1-2), 115-138.

Lutjeharms, J. R. E., O. Boebel and H. T. Rossby: (2003): Agulhas cyclones: *Deep Sea Res. Part II*: *50*,(1), 13-34.

Lutjeharms, J. R. E. and J. Cooper: (1996): Interbasin leakage through Agulhas current filaments: *Deep Sea Res. Part I*: *43*,(2), 213-215.

Lutjeharms, J. R. E., P. Penven and C. Roy: (2003): Modelling the shear edge eddies of the southern Agulhas Current: *Continental Shelf Res.*: *23*,(11-13), 1099-1115.

Lutjeharms, J. R. E. and H. R. Valentine: (1984): Southern Ocean thermal fronts south of Africa: *Deep-Sea Res. Part A*: *31*,(12), 1461-1475.

Lutze, G. F. and H. Thiel: (1989): Epibenthic foraminifera from elevated microhabitats: *Cibicidoides wuellerstorfi* and *Planulina ariminensis*: *J. Foram. Res.*: *19*, 153-158.

Lynch-Stieglitz, J. and R. G. Fairbanks: (1994): A conservative tracer for glacial ocean circulation from carbon isotope and paleo-nutrient measurements in benthic foraminifera: *Nature*: *369*, 308-310.

Lynch-Stieglitz, J., R. G. Fairbanks and C. D. Charles: (1994): Glacial-interglacial history of Antarctic intermediate water: Relative strengths of Antarctic versus Indian ocean sources: *Paleoceanography*: *9*,(1), 7-29.

Lynch-Stieglitz, J., A. van Geen and R. G. Fairbanks: (1996): Inter-ocean exchange of Glacial North Atlantic Intermediate Water: Evidence from Subantarctic Cd/Ca and carbon isotope measurements: *Paleoceanography*: *11*, 191-201.

Mackensen, A.: (2001): Oxygen and carbon stable isotope tracers of Weddell Sea water masses: new data and some paleoceanographic implications: *Deep Sea Res. Part I*: *48*,(6), 1401-1422.

Mackensen, A. and T. Bickert: (1999): Stable carbon isotopes in benthic foraminifera: Proxies for deep and bottom water circulation and new production: Edited by: G. Fischer and Wefer, G. *Use of Proxies in Paleoceanography: Examples from the South Atlantic*. Springer-Verlag, Berlin Heidelberg: pp. 229-254.

Mackensen, A. and R. G. Douglas: (1989): Down-core distribution of live and dead deep-water benthic foraminifera in box cores from the Weddell Sea and the California continental borderland: *Deep Sea Res.*: *36*,(6), 879-900.

Mackensen, A., H.-W. Hubberten, T. Bickert, G. Fischer and D. K. Futterer: (1993): The $\delta^{13}C$ in benthic foraminifera tests of *Fontbotia wuellerstorfi* (Schwager) relative to the $\delta^{13}C$ of dissolved inorganic carbon in Southern Ocean deep water: Implications for glacial ocean circulation modes: *Paleoceanography*: *8*,(5), 587-610.

Mackensen, A., M. Rudolph and G. Kuhn: (2001): Late Pleistocene deep-water circulation in the subantarctic eastern Atlantic: *Global Planet. Change*: *30*,(3-4), 197-229.

Malmgren, B.A.: (1987): Differential dissolution of Upper Cretaceous planktonic foraminifera from a temperate region of the South Atlantic Ocean: *Mar. Micropaleontol.:* 11,(4), 251–271.

Malmgren, B. A., M. Kucera, J. Nyberg and C. Waelbroeck: (2001): Comparison of statistical and artificial neural network techniques for estimating past sea-surface temperatures from planktonic foraminifer census data: *Paleoceanography*: *16*, 520-530.

Malmgren, B. A. and U. Nordlund: (1997): Application of artificial neural networks to paleoceanographic data: *Palaeogeogr. Palaeoclimatol. Palaeoecol.*: *136*, 359-373.

Manighetti, B. and I. N. McCave: (1995): Late glacial and Holocene paleocurrents around Rockall Bank, NE Atlantic: *Paleoceanography*: *10*, 611-626.

Manthé, S., G. Bareille, M.-È. Salvignac, M. Labracherie, F. Lemoine and L. Labeyrie: (2000): Variabilité et origine des apports détritiques dans le secteur indien de l'océan Austral au cours des derniers 30 000 ans: *Oceanologica Acta*: *23*,(2), 143-158.

Mantyla, A. W. and J. L. Reid: (1983): Abyssal characteristics of the world's oceans: *Deep Sea Res.*: *30*, 805-833.

Mantyla, A. W. and J. L. Reid: (1995): On the origins of deep and bottom waters in the Indian Ocean: *Journal of Geophysical Research: 100*: 2417-2439

Marchitto, T. M. and W. Broecker: (2006): Deep water mass geometry in the glacial Atlantic Ocean: A review of constraints from the paleonutrient proxy Cd/Ca: *Geochem. Geophys. Geosyst.*: *7*,(Q12003), doi:10.1029/2006GC001323.

Marsh, R., W. Hazeleger, A. Yool and E. J. Rohling: (2007): Stability of the thermohaline circulation under millennial CO2 forcing and two alternative controls on Atlantic salinity: *Geophys. Res. Letters*: *34*,(3).

Martínez-Méndez, G., R. Zahn, I. R. Hall, L. D. Pena and I. Cacho: (2008): 345,000-year-long multi-proxy records off South Africa document variable contributions of Northern versus Southern Component Water to the Deep South Atlantic: *Earth and Planetary Science Letter: 267,* (1-2), 309-321

Martinson, D. G., P. D. Killworth and A. L. Gordon: (1981). A Convective Model for the Weddell Polynya: *Journal of Physical Oceanography: 11*,(4), 466-488.

Mashiotta, T. A., D. W. Lea and H. J. Spero: (1999): Glacial-interglacial changes in Subantarctic sea surface temperature and δ^{18}O-water using foraminiferal Mg: *Earth Planet. Sci. Letters*: *170*,(4), 417-432.

Maslin, M., N. J. Shackleton and U. Pflaumann: (1995): Surface water temperature, salinity and density changes in the northeast Atlantic over the last 45,000 years: Heinrich events, deep water formation and climatic rebounds: *Paleoceanography: 10*,(3), 527-544.

Matsumoto, K. and J. Lynch-Stieglitz: (1999): Similar glacial and Holocene deep water circulation inferred from southeast Pacific benthic foraminiferal carbon isotope composition: *Paleoceanography*: *14*,(2), 149-163.

Matsumoto, K., J. Lynch-Stieglitz and R. F. Anderson: (2001): Similar glacial and Holocene southern ocean hydrography: *Paleoceanography*: *16*,(0), 1-10.

McCave, I. N.: (1995): Sedimentary processes and the creation of the stratigraphic record in the late Quaternary North Atlantic ocean: *Philos. Trans. R. Soc. London B*: *348*, 229-241.

McCave, I. N. and I. R. Hall: (2006): Size sorting in marine muds: Processes, pitfalls and prospects for paleoflow-speed proxies: *Geochem. Geophys. Geosyst.*: *7*,(Q10N05), doi:10.1029/2006GC001284.

McCave, I. N., T. Kiefer, D. J. R. Thornalley and H. Elderfield: (2005): Deep flow in the Madagascar-Mascarene Basin over the last 150 000 years: *Philos. Trans. R. Soc. A*: *363*, 81-99.

McCave, I. N., B. Manighetti and S. G. Robinson: (1995a): Sortable silt and fine sediment size/composition slicing: Parameters for paleocurrent speed and paleoceanography: *Paleoceanography*: *10*,(3), 593-610.

McCave, I. N., B. Manighetti and N. A. S. Berveridge: (1995b): Circulation in the glacial North Atlantic inferred from grain size measurements: *Nature*: *374*, 149-152.

McCorkle, D. C. and S. R. Q. Emerson, P.D.: (1985): Stable carbon isotopes in marine porewaters: *Earth Planet. Sci. Letters*: *74*, 13-26.

McCorkle, D. C., L. D. Keigwin, B. H. Corliss and S. R. Emerson: (1990): The influence of microhabitats on the carbon isotopic composition of deep-sea benthic foraminifera: *Paleoceanography*: *5*,(2), 161-185.

McManus, J., G. Bond, W. Broecker, S. J. Johnsen, L. Labeyrie and S. Higgins: (1994): High resolution climate records from the North Atlantic during the last interglacial: *Nature*: *371*, 326-329.

McManus, J. F., R. Francois, J. M. Gherardi, L. D. Keigwin and S. Brown-Leger: (2004): Collapse and rapid resumption of Atlantic meridional circulation linked to deglacial climate changes: *Nature*: *428*,(6985), 834-837.

McManus, J. F., D. W. Oppo and J. L. Cullen: (1999): A 0.5-million-year record of millennial-scale climate variability in the North Atlantic: *Science*: *283*,(5404), 971-975.

Meredith, M. P., K. J. Heywood, R. D. Frew and P. F. Dennis: (1999): Formation and circulation of the water masses between the southern Indian Ocean and Antarctica: Results from $\delta^{18}O$: *J. Mar. Res.*: *57*, 449-470.

Michel, E., L. Labeyrie, J.-C. Duplessy, N. Gorfti, M. Labracherie and J. L. Turon: (1995): Could the Subantarctic convection feed the world deep basins during the last glacial maximum: *Paleoceanography*: *10*,(5), 927-942.

Milankovitch, M.: (1941): *Kanon der Erdbestrahlung und seine Andwendung auf das Eiszeiten-problem*, Royal Serbian Academy, Belgrade

Milligan, T. G. and K. Kranck: (1991): Electroresistance particle size analyzers: Edited by: J. P. M. Syvitski. *Principals, methods and Application of Particle Size Analysis*. Cambridge University Press, Cambridge: pp. 109-118.

Mix, A.: (1987): The oxygen-isotope record of glaciation: Edited by: W. F. Ruddiman and Wright, H. E. J. *North America and Adjacent Oceans During the Last Deglaciation*. Geological Society of America, Boulder, Colorado: pp. 111-135.

Mix, A., W. F. Ruddiman and A. McIntyre: (1986): Late Quaternary paleoceanography of the tropical Atlantic, 1. Spatial variability of annual mean sea surface temperatures, 0-20.000 years B.P.: *Paleoceanography*: *1*,(1), 43-66.

Mix, A. C., E. Bard and R. Schneider: (2001): Environmental processes of the ice age: land, oceans, glaciers (EPILOG): *Quat. Sci. Rev.*: *20*,(4), 627-657.

Molfino, B., N. J. Kipp and J. J. Morley: (1982): Comparison of foraminiferal, coccolithophorid and radiolarian paleotemperature equations: Assemblage coherency and estimate concordancy: *Quat. Res.*: *17*, 279-313.

Molinelli, E.: (1978): Isohaline thermoclines in southeast Pacific Ocean: *J. Phys. Ocean.*: *8*,(6), 1139-1145.

Molinelli, E. J.: (1981): The Antarctic influence on Antarctic Intermediate Water: *J. Mar. Res.*: *39*,(2), 267-293.

Molyneux, E. G. and G. Martínez-Méndez: (2007): Glacial to interglacial Southern Ocean water column structure: *In prep.*

Moore, J. K., M. R. Abbott and J. G. Richman: (1999): Location and dynamics of the Antarctic Polar Front from satellite sea surface temperature data: *J. Geophys. Res.*: *104*,(C2), 3059-3073.

Morgan, V., M. Delmotte, T. van Ommen, J. Jouzel, J. Chappellaz, S. Woon, V. Masson-Delmotte and D. Raynaud: (2002): Relative timing of deglacial climate events in Antarctica and Greenland: *Science*: *297*, 1862-1864.

Mortyn, P. G. and C. D. Charles: (2003): Planktonic foraminiferal depth habitat and $\delta^{18}O$ calibrations: Plankton tow results from the Atlantic sector of the Southern Ocean: *Paleoceanography: 18*,(2), 1037, doi:10.1029/2001PA000637.

Mortyn, P. G., C. D. Charles and D. A. Hodell: (2002): Southern Ocean upper water column structure over the last 140 kyr with emphasis on the glacial terminations: *Global Planet. Change*: *34*,(3-4), 241-252.

Mortyn, P. G., C. D. Charles, U. S. Ninnemann, K. Ludwig and D. A. Hodell: (2003): Deep sea sedimentary analogs for the Vostok ice core: *Geochem. Geophys. Geosyst.*: *4*,(8), 1-21.

Mulitza, S., H. W. Arz, S. Kemle-von Mücke, C. Moos, H. S. Niebler, J. Patzold and M. Segl: (1999): The South Atlantic carbon isotope record of planktic foraminifera: Edited by: G. Fischer and Wefer, G. *The Use Of Proxies in Paleoceanography: Examples from the South Atlantic*. Springer-Verlag, Berlin, Heidelberg: pp. 427-445.

Mulitza, S., T. Wolff, J. Pätzold, W. Hale and G. Wefer: (1998): Temperature sensitivity of planktonic foraminifera and its influence on the oxygen isotope record: *Mar. Micropal.*: *33*, 223-240.

Müller, P. J. and H. Erlenkeuser: (1983): Glacial-interglacial cycles in oceanic productivity inferred from organic carbon contents in Eastern North Atlantic sediments: Edited by: J. Thiede and Suess, E. *Coastal Upwelling - Its Sediment Record: Part B: Sedimentary Records of Ancient Coastal Upwelling*. Plenum Press, New York and London: pp. 365-398.

Naidu, P. D.: (2004): Isotopic evidences of past upwelling intensity in the Arabian Sea: *Global Planet. Change*: *40*,(3-4), 285-293.

Naidu, P. D. and N. Niitsuma: (2004): Atypical $\delta^{13}C$ signature in Globigerina bulloides at the ODP site 723A (Arabian Sea): implications of environmental changes caused by upwelling: *Mar. Micropal.*: *53*,(1-2), 1-10.

Narcisi, B., J. R. Petit, B. Delmonte, I. Basile-Doelsch and V. Maggi: (2005): Characteristics and sources of tephra layers in the EPICA-Dome C ice record (East Antarctica): Implications for past atmospheric circulation and ice core stratigraphic correlations: *Earth Planet. Sci. Letters*: *239*,(3-4), 253-265.

Naveira Garabato, A. C., E. L. McDonagh, D. P. Stevens, K. J. Heywood and R. J. Sanders: (2002): On the export of Antarctic Bottom Water from the Weddell Sea: *Deep Sea Res. Part II*: *49*,(21), 4715-4742.

Niebler, H. S. and R. Gersonde: (1998): A planktic foraminiferal transfer function for the South Atlantic Ocean: *Mar. Micropal.*: *34*, 213-234.

Niebler, H. S., H.-W. Hubberten and R. Gersonde: (1999): Oxygen isotope values of planktic foraminifera: A tool for the reconstruction of surface water stratification: Edited by: G. Fischer and Wefer, G. *Use of Proxies in Paleoceanography:*

Examples from the South Atlantic. Springer-Verlag, Berlin, Heidelberg: pp. 165-189.

Ninnemann, U. S. and C. D. Charles: (1997): Regional differences in Quaternary Subantarctic nutrient cycling: Links to intermediate and deep water ventilation *Paleoceanography*: *12*,(4), 560-567.

Ninnemann, U. S. and C. D. Charles: (2002): Changes in the mode of Southern Ocean circulation over the last glacial cycle revealed by foraminiferal stable isotopic variability: *Earth Planet. Sci. Letters*: *201*,(2), 383-396.

Nobes, D. C., S. F. Bloomer, J. Mienert and F. Westall: (1991): Milankovitch cycles and non linear response in the Quaternary record in the Atlantic sector of the South oceans: *Proc. Ocean Drill. Program. Sci. Results*: *114*, 551-576.

Nodder, S. D. and L. Northcote: (2001): Episodic particulate fluxes at southern temperate middle latitudes (42-45°S) in the Subtropical Front region, east of New Zealand: *Deep Sea Res. Part I*: *48*, 833-864.

Northcote, L. C. and H. L. Neil: (2005): Seasonal variations in foraminiferal flux in the Southern Ocean, Campbell Plateau, New Zealand: *Mar. Micropal.*: *56*,(3-4), 122-137.

Nowlin, J. W. D. and J. M. Klinck: (1986): The physics of the Antarctic Circumpolar Current: *Reviews of Geophysics*: *24*, 469-491.

NRC (National Research Council): (2004): *Abrupt Climate Change: Inevitable Surprises*: http://books.nap.edu/books/0309074347/html/1.html/#pagetop

Ó Cofaigh, C., J. A. Dowdeswell and C. J. Pudsey: (2001): Late Quaternary iceberg rafting along the Antarctic Peninsula continental rise and in the Weddell and Scotia seas: *Quat. Res.*: *56*, 308-321.

Oppenheimer, C.: (2002): Limited global change due to the large Quaternary eruption, Toba ~74 kyr BP?: *Quat. Sci. Rev.*: *21*,(14-15), 1593-1609.

Oppo, D. and R. G. Fairbanks: (1987): Variability in the deep and intermediate water circulation of the Atlantic Ocean during the past 25,000 years: Northern Hemisphere modulation of the Southern Ocean: *Earth Planet. Sci. Letters*: *86*, 1-15.

Oppo, D., R. G. Fairbanks, A. L. Gordon and N. J. Shackleton: (1990): Late Pleistocene Southern Ocean δ13C variability: *Paleoceanography*: *5*, 43-54.

Oppo, D. and M. Horowitz: (2000): Glacial deep water geometry: South Atlantic benthic foraminiferal Cd/Ca and $\delta^{13}C$ evidence: *Paleoceanography*: *15*,(2), 147-160.

Oppo, D., M. E. Raymo, G. Lohmann, A. Mix, J. D. Wright and W. L. Prell: (1995): A $\delta^{13}C$ record of Upper North Atlantic Deep Water during the past 2.6 million years: *Paleoceanography*: *10*, 373-394.

Oppo, D. W. and Y. Rosenthal: (1994): Cd/Ca changes In a deep Cape Basin core over the past 730,000 years - Response of Circumpolar Deep Water variability to Northern hemisphere ice sheet melting: *Paleoceanography*: *9*,(5), 661-675.

Orsi, A. H., G. C. Johnsen and J. L. Bullister: (1999): Circulation mixing and production of Antarctic bottom water: *Prog. Oceanogr.*: *43*, 55-109.

Orsi, A. H., J. W. D. Nowlin and T. Whitworth I I I: (1993): On the circulation and stratification of the Weddell Gyre: *Deep Sea Res. Part I*: *40*,(1), 169-203.

Orsi, A. H., T. Whitworth III and J. W. D. Nowlin: (1995): On the meridional extent and fronts of the Antarctic Circumpolar Current: *Deep Sea Res. Part I*: *42*,(5), 641-673.

Ortiz, J. D., A. Mix and R. W. Collier: (1995): Environmental control of living symbiotic and symbiotic foraminifera of the California Current: *Paleoceanography*: *10*,(6), 987-1009.

Osterlund, H. G. and M. Stuiver: (1980): GEOSECS Pacific radiocarbon: *Radiocarbon*: *22*, 25-53.

Ottens, J. J.: (1991): Planktonic foraminifera as North Atlantic water mass indicators: *Oceanological Acta*: *14*, 123-140.

Ottens, J. J.: (1992): Spatial dynamics of planktonic foraminifera in the Northeast Atlantic: Edited by: J. J. Ottens. *Planktonic foraminifera as indicators of ocean environments in the Northeastern Atlantic*. Academisch Proefschrift, Vrije Universiteit to Amsterdam, *109-147*: pp.

Pahnke, K. and R. Zahn: (2005): Southern hemisphere water mass conversion linked with North Atlantic climate variability: *Science*: *307*,(5716), 1741-1746.

Pahnke, K., R. Zahn, H. Elderfield and M. Schulz: (2003): 340,000 year centennial-scale marine record of Southern hemisphere climate oscillation: *Science*: *301*, 948-952.

Paillard, D.: (2001): Glacial hiccups: *Nature*: *409*, 147-148.

Paillard, D. and E. Cortijo: (1999): A simulation of the Atlantic meridional circulation during Heinrich event 4 using reconstructed sea surface temperatures and salinities: *Paleoceanography*: *14*,(6), 716-724.

Paillard, D., L. Labeyrie and P. Yiou: (1996): Macintosh program performs time-series analysis: *Eos, Trans. AGU*: *77*, 379.

Pailler, D. and E. Bard: (2002): High frequency paleoceanographic changes during the past 140 000 yr recorded by the organic matter in sediments of the Iberian margin: *Palaeogeogr. Palaeoclimatol. Palaeoecol.*: *181*, 431-452.

Pattan, J. N., P. Shane and V. K. Banakar: (1999): New occurrence of the Youngest Toba Tuff in abyssal sediments of the Central Indian Basin: *Mar. Geol.*: *155*, 243-248.

Paul, A., S. Mulitza, J. Patzold and T. Wolff: (1999): Simulation of oxygen isotopes in a global ocean model: Edited by: G. Fischer and Wefer, G. *Use of Proxies in Paleoceanography: Examples From the South Atlantic*. Springer, Berlin: pp. 655-686.

Peacock, S. and M. Maltrud: (2006): Transit-time distributions in a global ocean model: *J. Phys. Ocean.*: *36*,(3), 474-495.

Peeters, F., E. Ivanova, S. Conan, G.-J. Brummer, G. Ganssen, S. Troelstra and J. van Hinte: (1999): A size analysis of planktonic foraminifera from the Arabian Sea: *Mar. Micropal.*: *36*,(1), 31-63.

Peeters, F. J. C., R. Acheson, G.-J. A. Brummer, W. P. M. De Ruijter, R. R. Schneider, G. M. Ganssen, E. Ufkes and D. Kroon: (2004): Vigorous exchange between the Indian and Atlantic oceans at the end of the past five glacial cycles: *Nature*: *430*, 661-665.

Peeters, F. J. C., G.-J. A. Brummer and G. M. Ganssen: (2002): The effect of upwelling on the distribution and stable isotope composition of *Globigerina bulloides* and *Globigerinoides ruber* (planktonic foraminifera) in modern surface waters of the NW Arabian Sea: *Global Planet. Change*: *34*, 269-291.

Peterson, R. G. and L. Stramma: (1991): Upper-Level Circulation in the South-Atlantic Ocean: *Prog. Oceanogr.*: *26*,(1), 1-73.

Petit, J. R., J. Jouzel, D. Raynaud and et al.: (1999): Climate and atmospheric history of the past 420,000 years from the Vostok ice core, Antarctica: *Nature*: *399*, 429-436.

Pflaumann, U.: (1985): Transfer-function '134/6' a new approach to estimate sea-surface temperatures and salinities of the eastern North Atlantic from the planktonic foraminifers in the sediments: *'Meteor' Forschungsergeb C39*, 37-71.

Pflaumann, U., J. Duprat, C. Pujol and L. Labeyrie: (1996): SIMMAX: A modern analog technique to deduce Atlantic sea surface temperature from planktonic foraminifera in deep-sea sediments: *Paleoceanography*: *11*,(1), 15-35.

Pflaumann, U., M. Sarnthein, M. R. Chapman, L. d'Abreu, B. M. Funnell, M. Huels, T. Kiefer, M. Maslin, H. Schulz, J. Swallow, S. Van Kreveld, M. Vautravers, E. Vogelsang and M. Weinelt: (2003): Glacial North Atlantic: Sea surface conditions reconstructed by GLAMAP 2000: *Paleoceanography*: *18*,(3), doi: 10.1029-2002PA000774.

Pfuhl, H. A. and N. J. Shackleton: (2004): Two proximal, high resolution records of foraminiferal fragmentation and their implications for changes in dissolution: *Deep Sea Res. Part I*: *51*, 809-832.

Pilcher, J. R.: (1991): Radiocarbon dating for the Quaternary scientist: *Quat. Proceedings*: *1*, 27-33.

Piotrowski, A. M., S. L. Goldstein, S. R. Hemming and R. G. Fairbanks: (2004): Intensification and variability of ocean thermohaline circulation through the last deglaciation: *Earth Planet. Sci. Letters*: *225*,(1-2), 205-220.

Piotrowski, A. M., S. L. Goldstein, S. R. Hemming and R. G. Fairbanks: (2005): Temporal Relationships of Carbon Cycling and Ocean Circulation at Glacial Boundaries: *Science*: *307*,(5717), 1933-1938.

Popova, E. E., V. A. Ryabchenko and M. J. R. Fasham: (2000): Biological pump and vertical mixing in the Southern Ocean: Their impact on atmospheric CO_2: *Global Biogeochem. Cycles*: *14*,(1), 477-498.

Porter, S. C. and Z. S. An: (1995): Correlation between climate events in the north Atlantic and China during the last deglaciation: *Nature*: *375*, 305-308.

Prell, W. L.: (1985): The stability of low-latitude sea-surface temperatures: An evaluation of the CLIMAP reconstruction with emphasis on the positive SST anomalies: *US Department of Energy, Carbon Dioxide Research Division Report*: *60*.

Prell, W. L. and W. B. Curry: (1981): Faunal and isotopic indices of monsoonal upwelling, Western Arabian Sea: *Oceanological Acta*: *4*, 91-98.

Prell, W. L., W. H. Hutson and D. F. Williams: (1979): The subtropical convergence and late Quaternary circulation in the Southern Ocean: *Mar. Micropal.*: *4*, 225-234.

Prell, W. L., W. H. Hutson, D. F. Williams, A. W. H. Bé, K. Geitzenauer and B. Molfino: (1980): Surface circulation of the Indian Ocean during the last glacial maximum, approximately 18,000 yr B.P.: *Quat. Res.*: *14*, 309-336.

Pudsey, C. J. and J. A. Howe: (1998): Quaternary history of the Antarctic Circumpolar Current: evidence from the Scotia Sea: *Mar. Geol.*: *148*,(1-2), 83-112.

Pugh, R. S., I. N. McCave, C. Pudsey and C. D. Hillenbrand: (2006): Glacial-interglacial changes in flow vigor of the Antarctic Circumpolar Current in the Scotia Sea: *American Geophysical Union, Fall Meeting*: *PP21D-05*.

Rahmstorf, S.: (2002): Ocean circulation and climate during the past 120,000 years: *Nature*: *419*, 207-214.

Rampino, M. R. and S. Self: (1992): Volcanic winter and accelerated glaciation following the Toba super-eruption: *Nature*: *359*, 50-52.

Rampino, M. R. and S. Self: (1993): Climate-volcanism feedback and the Toba eruption of ~ 74,000 years ago: *Quat. Res.*: *40*, 269-280.

Rashid, H., R. Hesse and D. J. W. Piper: (2003): Evidence for an additional Heinrich event between H5 and H6 in the Labrador Sea: *Paleoceanography*: *18*,(4), 1077, doi:10.1029/2003PA000913

Rasmussen, T. L., D. W. Oppo, E. Thomsen and S. J. Lehman: (2003): Deep sea records from the southeast Labrador Sea: Ocean circulation changes and ice-rafting events during the last 160,000 years: *Paleoceanography*: *18*,(1), 1018, doi:10.1029/2001PA000736

Rau, A., J. Rogers and M.-T. Chen: (2006): Late Quaternary palaeoceanographic record in giant piston cores off South Africa, possibly including evidence of neotectonism: *Quat. International*: *148*,(1), 65-77.

Rau, A. J., J. Rogers, J. R. E. Lutjeharms, J. Giraudeau, J. A. Lee-Thorp, M.-T. Chen and C. Waelbroeck: (2002): A 450-kyr record of hydrological conditions on the western Agulhas Bank Slope, south of Africa: *Mar. Geol.*: *180*,(1-4), 183-201.

Rau, G. H., P. N. Froelich, T. Takahashi and D. J. Des Marais: (1991): Does sedimentary organic $\delta^{13}C$ record variations in the Quaternary ocean [CO_2(aq)]?: *Paleoceanography*: *6*,(335-347).

Raven, J. A. and P. G. Falkowski: (1999): Oceanic sinks for atmospheric CO_2: *Plant, Cell & Environment*: *22*,(6), 741-755.

Raymo, M. E. and K. Nisancioglu: (2003): The 41 kyr world: Milankovitch's other unsolved mystery: *Paleoceanography*: *18*,(1), doi:10.1029/2002PA000791.

Raymo, M. E., D. Oppo and W. B. Curry: (1997): The mid-Pleistocene climate transition: A deep sea carbon isotopic perspective: *Paleoceanography*: *12*, 546-559.

Raymo, M. E., D. W. Oppo, B. P. Flower, D. A. Hodell, J. F. McManus, K. A. Venz, K. F. Kleiven and K. McIntyre: (2004): Stability of North Atlantic water masses in face of pronounced climate variability during the Pleistocene: *Paleoceanography*: *19*, doi:10.1029/2003PA000921.

Raymo, M. E., W. F. Ruddiman, N. J. Shackleton and D. W. Oppo: (1990): Evolution of Atlantic-Pacific $\delta^{13}C$ gradients over the last 2.5 m.y: *Earth Planet. Sci. Letters*: *97*,(3-4), 353-368.

Reid, J. L.: (1986): On the total geostrophic circulation of the South Pacific Ocean: Flow patterns, tracers and transport: *Prog. Oceanogr.*: *16*, 1-61.

Reid, J. L.: (1989): On the Total Geostrophic Circulation of the South-Atlantic Ocean - Flow Patterns, Tracers, and Transports: *Progress in Oceanography*: *23*,(3), 149-244.

Reid, J. L.: (2005): On the world-wide circulation of the deep water from the North Atlantic Ocean: *J. Mar. Res.*: *63*,(1), 187-201.

Reynolds, L. A. and R. C. Thunell: (1985): Seasonal succession of planktonic foraminifera in the subpolar North Pacific: *J. Foram. Res.*: *15*, 282-301.

Rial, J. A.: (1999): Pacemaking the Ice Ages by frequency modulation of Earth's orbital eccentricity: *Science*: *285*, 564-568.

Richardson, P. L., J. R. E. Lutjeharms and O. Boebel: (2003): Introduction to the "Inter-ocean exchange around southern Africa": *Deep Sea Res. Part II*: *50*,(1), 1-12.

Rintoul, R. S., C. Hughes and D. Olbers: (2001): The Antarctic Circumpolar current system: Edited by: G. Siedler, Church, J. and Gould, J. *Ocean Circulation and Climate*. Academic Press, New York: pp. 271-302.

Roe, G. H. and M. R. Allen: (1999): A comparison of competing explanations for the 100,000-yr ice age cycle: *Geophys. Res. Letters*: *26*,(15), 2259-2262.

Rohling, E. J.: (2007): Progress in paleosalinity: Overview and presentation of a new approach: *Paleoceanography: 22,* (PA3215), doi:10.1029/2007PA001437.

Romero, O. E., J. H. Kim and D. Hebbeln: (2006): Paleoproductivity evolution off central Chile from the Last Glacial Maximum to the Early Holocene: *Quat. Res.*: *65*,(3), 519-525.

Rose, W. I. and C. A. Chesner: (1990): Worldwide dispersal of ash and gases from the earth's largest known eruption: Toba, Sumatra, 75ka: *Palaeogeogr. Palaeoclimatol. Palaeoecol.*: *89*, 269-275.

Rosenthal, Y., E. A. Boyle and L. Labeyrie: (1997): Last glacial maximum paleochemistry and deepwater circulation in the Southern Ocean: Evidence from foraminiferal cadmium: *Paleoceanography*: *12*,(6), 787-796.

Ruddiman, W. F.: (2006): What is the timing of orbital-scale monsoon changes?: *Quat. Sci. Rev.*: *25*, 657-658.

Ruddiman, W. F. and A. McIntyre: (1981): Oceanic mechanisms for amplification of the 23,000-year ice-volume cycle: *Science*: *212*, 617-627.

Ruddiman, W. F. and A. McIntyre: (1989): Ice-age thermal response and climatic role of the surface Atlantic Ocean 40°N to 63°N: *Geol. Soc. An. Bull.*: *95*, 381-396.

Ruddiman, W. F., M. E. Raymo, D. G. Martinson, B. M. Clement and J. Backman: (1989): Pleistocene evolution of northern hemisphere climate: *Paleoceanography*: *4*, 353-412.

Rühlemann, C., S. Mulitza, P. J. Müller, G. Wefer and R. Zahn: (1999): Warming of the tropical Atlantic Ocean and slowdown of thermohaline circulation during the last deglaciation: *Nature*: *402*, 511-514.

Russel, W. B.: (1980): Review of the role of colloidal forces in the rheology of suspensions: *Journal of Rheology*: *24*, 287-317.

Rutberg, R. L., S. R. Hemming and S. L. Goldstein: (2000): Reduced North Atlantic deep water flux to the glacial Southern Ocean inferred from neodymium isotope ratios: *Nature*: *405*, 935-938.

Rutberg, R. L. and S. L. Peacock: (2006): High latitude forcing of interior ocean $\delta^{13}C$: *Paleoceanography*: *21*,PA2012, doi: 10.1029/2005PA001226.

Rutherford, S.: (1997): Milankovitch Cycles In Paleoclimate: http://deschutes.gso.uri.edu/~rutherfo/milankovitch.html.

Sachs, J. P., R. F. Anderson and S. J. Lehman: (2001): Glacial Surface Temperatures of the Southeast Atlantic Ocean: *Science*: *293*,(5537), 2077-2079.

Saenko, O. A. and M. England: (2003): On the response of Southern Ocean water-masses to atmospheric meridional moisture advection: *Geophys. Res. Letters*: *30*,(8), 1433.

Saenko, O. A., A. J. Weaver and J. M. Gregory: (2003): On the link between the two modes of the ocean thermohaline circulation and the formation of global-scale water masses: *J. Climate*: *16*,(17), 2797-2801.

Sánchez Goñi, M. F., F. Eynaud, J. L. Turon and N. J. Shackleton: (1999): High resolution palynological record off the Iberian margin: Direct land-sea correlation for the last interglacial complex: *Earth Planet. Sci. Letters*: *171*, 123-137.

Sarnthein, M. and R. Tiedemann: (1990): Younger Dryas-style cooling events at glacial terminations I-VI at ODP site 658: Associated benthic $\delta^{13}C$ anomalies constrain meltwater hypothesis: *Paleoceanography*: *5*, 1041-1055.

Sarnthein, M., K. Winn, J. C. Duplessy and M. R. Fontugne: (1988): Global variations of surface ocean productivity in low and mid latitudes: influence on CO_2 reservoirs of the deep ocean and atmosphere during the last 21 000 years: *Paleoceanography*: *3*,(3), 361-399.

Sarnthein, M., K. Winn, S. J. A. Jung, J.-C. Duplessy, L. Labeyrie, H. Erlenkeuser and G. M. Ganssen: (1994): Changes in east Atlantic deepwater circulation over the last 30,000 years: Eight time slice reconstructions: *Paleoceanography*: *9*,(2), 209-267.

Sauter, L. R. and R. C. Thunell: (1991): Planktonic foraminiferal response to upwelling and seasonal hydrographic conditions: Sediment trap results from San Pedro Basin, Southern California: *J. Foram. Res.*: *21*, 347-363.

Schaefer, G., J. S. Rodger, B. W. Hayward, J. P. Kennett, A. T. Sabaa and G. H. Scott: (2005): Planktonic foraminiferal and sea surface temperature record during the last 1 Myr across the Subtropical Front, Southwest Pacific: *Mar. Micropal.*: *54*, 191-212.

Schlitzer, R.: (2000): Electronic atlas of WOCE hydrographic and tracer data now available: *Eos, Trans. EGU*: *81*,(5), 45.

Schlitzer, R.: (2007): Ocean Data View: http://odv.awi.de.

Schmidt, G. A., G. R. Bigg and E. J. Rohling.: (1999): Global seawater $\delta^{18}O$ database: http://data.giss.nasa.gov/o18data/.

Schmitz Jr, W. J.: (1995): On the interbasin-scale thermohaline circulation: *Reviews of Geophysics*: *33*,(2), 151-173.

Schmitz Jr, W. J.: (1996): On the eddy field in the Agulhas Retroflection, with some global considerations: *J. Geophys. Res.*: *101*,(C7), 16,259-16,271.

Schneider, R. R., P. J. Muller and G. Ruhland: (1995): Late Quaternary surface circulation in the east equatorial South Atlantic: Evidence from alkenone sea surface temperatures: *Paleoceanography*: *10*, 197-219.

Schott, F.: (1983): Monsoon response of the Somali Current and associated upwelling: *Prog. Oceanogr.*: *12*, 357-381.

Schrag, D. P., J. F. Adkins, K. McIntyre, J. L. Alexander, D. A. Hodell, C. D. Charles and J. F. McManus: (2002): The oxygen isotopic composition of seawater during the Last Glacial Maximum: *Quat. Sci. Rev.*: *21*,(1-3), 331-342.

Schulz, H., K.-C. Emeis, H. Erlenkeuser, U. von Rad and C. Rolf: (2002): The Toba volcanic event and interstadial / stadial climates at the marine isotopic stage 5 to 4 transition in the Northern Indian Ocean: *Quat. Res.*: *57*, 22-31.

Schulz, H., U. von Rad and H. Erlenkeuser: (1998): Correlation between Arabian Sea and Greenland climate oscillations of the past 110,000 years: *Nature*: *393*, 54-57.

Schulz, M., A. Paul and A. Timmermann: (2002): Relaxation oscillators in concert: A framework for climate change at millennial timescales during the late Pleistocene: *Geophys. Res. Letters*: *29*,(24).

Seidenkrantz, M.-S., L. Bornmalm, S. J. Johnsen, K. L. Knudsen, A. Kuijpers, S.-E. Lauritzen, S. E. G. Leroy, I. Mergeai, C. Schweger and B. van Viliet-Lanoë: (1996): Two-step deglaciation at the Oxygen Isotope Stage 6/5e transition: The Zeifen-Kattegat climate oscillation: *Quat. Sci. Rev.*: *15*, 63-75.

Seidov, D., B. J. Haupt, E. J. Barron and M. Maslin: (2001): Ocean bi-polar seesaw and climate: Southern versus northern meltwater impacts: *Geophysical Monograph - The Ocean and Rapid Climate Change: Past, Present and Future*: *126*, 147-167.

Seidov, D. and M. Maslin: (2001): Atlantic Ocean heat piracy and the bipolar climate see-saw during Heinrich and Dansgaard-Oeschger events: *Journal of Quaternary Science*: *16*,(4): 321-328

Seidov, D., M. Sarnthein, K. Stattegger, R. Prien and M. Weinelt: (1996): North Atlantic ocean circulation during the last glacial maximum and subsequent meltwater event: A numerical model: *J. Geophys. Res.*: *101*,(C7), 16,305-16,332.

Shackleton, N. J.: (1977): Carbon-13 in Uvigerina: Tropical rainforest history and the equatorial Pacific carbon dissolution cycle: Edited by: N. R. Anderson and Malahoff, A. *Fate of Fossil Fuel CO_2 in the Oceans*. Plenum, New York: pp. 401-427.

Shackleton, N. J.: (2000): The 100,000-year ice-age cycle identified and found to lag temperature, carbon dioxide, and orbital eccentricity: *Science*: *289*,(5486), 1897-1902.

Shackleton, N. J., R. G. Fairbanks, T.-c. Chiu and F. Parrenin: (2004): Absolute calibration of the Greenland time scale: implications for Antarctic time scales and for $\Delta^{14}C$: *Quat. Sci. Rev.*: *23*,(14-15), 1513-1522.

Shackleton, N. J. and M. A. Hall: (1997): The late Miocene stable isotope record, site 926: *Proc. Ocean Drill. Program. Sci. Results*: *154*, 367-373.

Shackleton, N. J., M. A. Hall, J. Line and C. Shuxi: (1983): Carbon isotope data in core V19-30 confirm reduced carbon-dioxide concentration in the ice-age atmosphere: *Nature*: *306*, 319-322.

Shackleton, N. J., M. A. Hall and E. Vincent: (2000): Phase relationships between millennial-scale events 64,000-24,000 years ago: *Paleoceanography*: *15*,(6), 565-569.

Shackleton, N. J. and N. D. Opdyke: (1973): Oxygen isotope and paleomagnetic stratigraphy of equatorial Pacific core V28-238: oxygen isotope temperature and ice volume on a 10^5 year and 10^6 year scale: *Quat. Res.*: *3*, 39-55.

Shemesh, A., D. A. Hodell, X. Crosta, S. L. Kanfoush, C. D. Charles and T. P. Guilderson: (2002): Sequence of events during the last deglaciation in Southern Ocean sediments and Antarctic ice cores: *Paleoceanography*: *17*, (4), 1056, doi:10.1029/2000PA000599

Shin, S.-I., Z. Liu, B. L. Otto-Bliesner, J. E. Kutzbach and S. J. Vavrus: (2003): Southern Ocean sea-ice control of the glacial North Atlantic thermohaline circulation: *Geophys. Res. Letters*: *30*,(2), 1096 doi:10.1029/2002GL015513

Sicre, M. A., L. Labeyrie, U. Ezat, J. Duprat, J. L. Turon, S. Schmidt, E. Michel and A. Mazaud: (2005): Mid-latitude southern Indian ocean response to northern hemisphere Heinrich events: *Earth Planet. Sci. Letters*: *240*, 724-731.

Siddall, M., E. Bard, E. J. Rohling and C. Hemleben: (2006): Sea-level reversal during termination II: *Geology*: *34*,(10), 817-820.

Sidall, M. et al.: (2006b): Red Sea Sea Level Reconstruction: *IGBP PAGES/World Data Center for Paleoclimatology Data Contribution Series # 2006-063*: NOAA/NCDC Paleoclimatology Program, Boulder CO, USA.

Siddall, M., E. J. Rohling, A. Almogi-Labin, C. Hemleben, D. Meishner, I. Schmelzer, D. A. Smeed: (2003): Sea-level fluctuations during the last glacial cycle: *Nature: 423*, 853-858.

Sigman, D. M. and E. A. Boyle: (2000): Glacial/interglacial variations in atmospheric carbon dioxide: *Nature*: *407*,(6806), 859-869.

Sigurdsson, H.: (1990): Evidence of volcanic loading of the atmosphere and climate response: *Palaeogeogr. Palaeoclimatol. Palaeoecol.*: *89*,(3), 277-289.

Sijp, W. P. and M. H. England: (2004): Effect of the Drake Passage throughflow on global climate: *J. Phys. Ocean.*: *34*,(5), 1254-1266.

Sikes, E. L., C. R. Samson, T. P. Guilderson and W. R. Howard: (2000): Old radiocarbon ages in the southwest Pacific Ocean during the last glacial period and deglaciation: *Nature*: *405*,(6786), 555-559.

Skinner, L. C. and I. N. McCave: (2003): Analysis and modelling of gravity and piston coring based on soil mechanics: *Mar. Geol.*: *199*,(1-2), 181-204.

Sloyan, B. M. and R. S. Rintoul: (2001): Circulation, modification and renewal of Antarctic mode and intermediate water: *J. Phys. Ocean.*: *31*, 1005-1030.

Smetacek, V., H. J. W. De Baar, U. V. Bathmann, K. Lochte and M. M. Rutgers Van Der Loeff: (1997): Ecology and biogeochemistry of the Antarctic circumpolar current during austral spring: a summary of southern ocean JGOFS cruise ANT X/6 of R.V. Polarstern: *Deep Sea Res. Part II*: *44*,(1-2), 1-21.

Smith, D. G., M. T. Ledbetter and P. F. Ciesielski: (1983): Ice rafted volcanic ash in the southeast Atlantic sector of the Southern Ocean during the last 1000,000 years: *Mar. Geol.*: *53*, 291-312.

Song, S. R., C. H. Chen, M. Y. Lee, T. F. Yang, Y. Iizuka and K. Y. Wei: (2000): Newly discovered eastern dispersal of the Youngest Toba Tuff: *Mar. Geol.*: *167*, 303-312.

Sowers, T. and M. Bender: (1995): Climate records covering the last deglaciation: *Science*: *269*, 210-214.

Spero, H. J. and D. W. Lea: (1996): Experimental determination of stable isotope variability in *Globigerina bulloides*: Implications for paleoceanographic reconstructions: *Mar. Micropal.*: *28*, 231-246.

Spero, H. J. and D. W. Lea: (2002): The cause of carbon isotope minimum events on glacial terminations: *Science*: *296*,(5567), 522-525.

Stenni, B., V. Masson-Delmotte, S. Johnsen, J. Jouzel, A. Longinelli, E. Monnin, R. Rothlisberger and E. Selmo: (2001): An oceanic cold reversal during the last deglaciation: *Science*: *293*,(5537), 2074-2077.

Stephens, B. B. and R. F. Keeling: (2000): The influence of Antarctic sea ice on glacial-interglacial CO_2 variations: *Nature*: *404*, 171-174.

Stocker, T. F.: (1998): The seesaw effect: *Science*: *282*, 61-62.

Stocker, T. F. and S. J. Johnsen: (2003): A minimum thermodynamic model for the bipolar seesaw: *Paleoceanography*: *18*,(4), 1087.

Stocker, T. F. and D. G. Wright: (1991): Rapid transitions of the oceans deep circulation induced by changes in surface water fluxes: *Nature*: *351*, 729-732.

Streeter, S. S. and N. J. Shackleton: (1979): Paleocirculation of the Deep North Atlantic: 150,000-Year Record of Benthic Foraminifera and $\delta^{18}O$: *Science*: *203*,(4376), 168-171.

Stuut, J.-B. W., X. Crosta, K. van der Borg and R. R. Schneider: (2004): Relationship between Antarctic sea ice and southwest African climate during the late Quaternary: *Geology*: *32*,(10), 909-912.

Sugden, D.: (1982): *Arctic and Antarctic: A Modern Geographical Synthesis*, Barnes and Noble Books, New Jersey

Talley, L. D.: (1996): Antarctic Intermediate water in the South Atlantic: Edited by: G. Wefer, Berger, A., Siedler, G. and Webb, D. J. *The South Atlantic: Present and Past Circulation*. Springer-Verlag, Berlin Heidelberg: pp. 219-238.

Tchernia, P. and P. F. Jeannin: (1983): Quelques aspects de la circulation océanique Antarctique révéles par l'observation de la dérive d'icebergs (1972-1983): Edited by. *Centre National d'Etudes Spatiales, Expedition Polaires Francaises, Museum National d'Histoire Naturelle, Paris*: pp. 99.

Tian, J., P. Wang, X. Cheng, R. Wang and X. Sun: (2005): Forcing mechanism of the Pleistocene east Asian monsoon variations in a phase perspective: *Science in China: Ser. D*: *48*,(10), 1708-1717.

Tiedemann, R., M. Sarnthein and N. J. Shackleton: (1994): Astronomic timescale for the Pliocene Atlantic $\delta^{18}O$ and dust flux records of Ocean Drilling Program Site 659: *Paleoceanography*: *9*, 619-638.

Timmermann, A., H. Gildor, M. Schulz and E. Tziperman: (2003): Coherent resonant millennial-scale climate oscillations triggered by massive meltwater pulses: *J. Climate*: *16*,(15), 2569-2585.

Toggweiler, J. R.: (1999): Variation of atmospheric CO_2 by ventilation of the ocean's deepest water: *Paleoceanography*: *14*, 571-588.

Toggweiler, J. R., J. L. Russell and S. R. Carson: (2006): Midlatitude westerlies, atmospheric CO_2, and climate change during the ice ages: *Paleoceanography*: *21*, PA2005, doi:10.1029/2005PA001154.

Toggweiler, J. R. and B. Samuels: (1995): Effect of drake passage on the global thermohaline circulation: *Deep Sea Res. Part I*: *42*,(4), 477-500.

Toggweiler, J. R. and B. Samuels: (1998): On the ocean's large-scale circulation near the limit of no vertical mixing: *J. Phys. Ocean.*: *28*,(9), 1832-1852.

Tolderlund, D. S. and A. W. H. Bé: (1971): Seasonal distribution of planktonic foraminifera in the western North Atlantic: *Micropaleontology*: *17*, 279-329.

Torrence, C. and G. P. Campo: (1998): A practical guide to wavelet analysis: *Bull. Am. Metero. Society*: *79*, 61-78.

Trend-Staid, M. and W. L. Prell: (2002): Sea surface temperature at the last glacial maximum: a reconstruction using the modern analog technique: *Paleoceanography*: *17*, doi:10.1029/2000PA000506.

Tsuchiya, M., L. D. Talley and M. S. McCartney: (1994): Water mass distribution in the western South Atlantic: A section from South Georgia Island (54S) northwards across the equator: *J. Mar. Res.*: *52*, 55-81.

Tucholke, B. E. and G. B. Carpenter: (1977): Sediment distribution and cenozoic sedimentation patterns on Agulhas Plateau: *Geol. Soc. An. Bull.*: *88*,(9), 1337-1346.

Tuenter, E., S. L. Weber, F. J. Hilgen and L. J. Lourens: (2003): The response of the African summer monsoon to remote and local forcing due to precession and obliquity: *Global Planet. Change*: *36*, 219-235.

Uenzelmann-Neben, G.: (2001): Seismic characteristics of sediment drifts: An example from the Agulhas Plateau, southwest Indian Ocean: *Mar. Geophys. Res.*: *22*, 323-343.

Urey, H. C.: (1947): The thermodynamic properties of isotopic substances: *J. Chemistry*, 562-581.

van Kreveld, S., M. Sarnthein, H. Erlenkeuser, P. Grootes, S. J. A. Jung, M.-J. Nadeau, U. Pflaumann and A. H. L. Voelker: (2000): Potential links between surging ice sheets, circulation changes and the Dansgaard-Oeschger cycles in the Irminger Sea, 60-18 kyr: *Paleoceanography*: *15*,(4), 425-442.

Vidal, L., L. Labeyrie, E. Cortijo, M. Arnold, J.-C. Duplessy, E. Michel, S. Becqué and T. C. E. van Weering: (1997): Evidence for changes in the North Atlantic Deep Water linked to meltwater surges during the Heinrich events: *Earth Planet. Sci. Letters*: *146*, 13-27.

Vincent, E. and A. Berger: (1981): Planktonic foraminifera and their use in paleoceanography: Edited by: C. Emiliani. *The Sea, The Oceanic Lithosphere.* Wiley, New York: pp. 1025-1118.

Volbers, A. N. A. and R. Henrich: (2004): Calcium carbonate corrosiveness in the South Atlantic during the Last Glacial Maximum as inferred from changes in the preservation of *Globigerina bulloides*: A proxy to determine deep-water circulation patterns?: *Mar. Geol.*: *204*, 43-57.

von Dobeneck, T. and F. Schmieder: (1999): Using rock magnetic proxy records for orbital tuning and extended time series analysis into the super- and sub-Milankovitch bands: Edited by: G. Fischer and Wefer, G. *Use of Proxies in Paleoceanography: Examples from the South Atlantic.* Springer-Verlag, Berlin, Heidelberg: pp. 601-633.

Waelbroeck, C., L. Labeyrie, J.-C. Duplessy, J.-C. Guiot, M. Labracherie, H. Leclaire and J. Duprat: (1998): Improving past sea surface temperature estimates based on planktonic fossil faunas: *Paleoceanography*: *13*, 272-283.

Waelbroeck, C., L. Labeyrie, E. Michel, J.-C. Duplessy, J. McManus, K. Lambeck, E. Balbon and M. Labracherie: (2002): Sea-level and deep water temperature changes derived from benthic foraminifera isotopic records: *Quat. Sci. Rev.*: *21*, 295-305.

Wang, L., M. Sarnthein, P. Grootes and H. Erlenkeuser: (1999): Millennial reoccurrence of century-scale abrupt events of East Asian monsoon: A possible heat conveyor for global deglaciation: *Paleoceanography*: *14*, 725-731.

Warren, B. A.: (1981): Deep circulation of the World Ocean: Edited by: B. A. Warren and Wunsch, C. *Evolution of Physical Oceanography.* MIT Press, Cambridge, Ma.: pp.

Watson, A. J. and A. C. Naveira Garabato: (2006): The role of Southern Ocean mixing and upwelling in glacial-interglacial atmospheric CO2 change: *Tellus B*: *58*,(1), 73-87.

Weaver, A. J., O. A. Saenko, P. U. Clark and J. X. Mitrovica: (2003): Meltwater pulse 1A from Antarctica as a trigger of the Bolling-Allerod warm interval: *Science*: *299*,(5613), 1709-1713.

Weaver, C. E.: (1989): *Clays, Muds And Shales*, Elsevier, New York

Weedon, G. P.: (2003): *Time-Series Analysis and Cyclostratigraphy: Examining Stratigraphic Records of Environmental Cycles*, Cambridge Univeristy Press, Cambridge

Weeks, S. J., F. A. Shillington and G. B. Brundrit: (1998): Seasonal and spatial SST variability in the Agulhas retroflection and Agulhas return current: *Deep Sea Res. Part I*: *45*,(10), 1611-1625.

Wefer, G., W. H. Berger, J. Bijma and G. Fischer: (1999): Clues to ocean history: a brief overview of proxies: Edited by: G. Fischer and Wefer, G. *Use of Proxies in Paleoceaonography: Examples from the South Atlantic.* Springer-Verlag, Berlin, Heidelberg: pp. 1-68.

Weijer, W., W. P. M. De Ruijter and H. A. Dijkstra: (2001): Stability of the Atlantic overturning circulation: Competition between Bering Strait freshwater flux and salt sources: *J. Phys. Ocean.*: *31*, 2385-2402.

Weijer, W., W. P. M. De Ruijter, A. Sterl and S. S. Drijfhout: (2002): Response of the Atlantic overturning circulation to South Atlantic sources of buoyancy: *Global Planet. Change*: *34*,(3-4), 293-311.

Welch, P. D.: (1967): The use of fast Fourier transform for the estimation of power spectra: a method based on time averaging over short, modified periodograms: *Audio and Electroacoustics, IEEE Transactions*: *15*,(2), 70-73.

West, S., J. H. F. Jansen and J. B. Stuut: (2004): Surface water conditions in the Northern Benguela Region (SE Atlantic) during the last 450 ky reconstructed from assemblages of planktonic foraminifera: *Mar. Micropal.*: *51*,(3-4), 321-344.

Whitworth III, T. and R. G. Peterson: (1985): Volume transport of the Antarctic Circumpolar Current from bottom pressure measurements: *J. Phys. Ocean.*: *15*, 810-816.

Williams, D.F., N. Healy-Williams, and P. Leschak: (1985) Dissolution and water-mass patterns in the Southeast Indian Ocean. Part I. Evidence from Recent to late Holocene foraminiferal assemblages: *Geol. Soc. Am. Bull.:* 96,(2),176–189

Wilson, K., B. W. Hayward, A. T. Sabaa, G. H. Scott and J. P. Kennett: (2005): A one-million-year history of a north-south segment of the Subtropical front, east of New Zealand: *Paleoceanography*: *20*, doi:10.1029/2004PA001080.

Winter, A. and K. Martin: (1990): Late Quaternary history of the Agulhas current: *Paleoceanography*: *5*,(4), 479-486.

Wolff, E. W., H. Fischer, F. Fundel, U. Ruth, B. Twarloh, G. C. Littot, R. Mulvaney, R. Rathlisberger, M. de Angelis, C. F. Boutron, M. Hansson, U. Jonsell, M. A. Hutterli, F. Lambert, P. Kaufmann, B. Stauffer, T. F. Stocker, J. P. Steffensen, M. Bigler, M. L. Siggaard-Andersen, R. Udisti, S. Becagli, E. Castellano, M. Severi, D. Wagenbach, C. Barbante, P. Gabrielli and V. Gaspari: (2006): Southern Ocean sea-ice extent, productivity and iron flux over the past eight glacial cycles: *Nature*: *440*,(7083), 491-496.

Wolff, T., B. Grieger, W. Hale, A. Dürkoop, S. Mulitza, J. Pätzold and G. Wefer: (1999): On the reconstruction of paleosalinities: Edited by: G. Fischer and Wefer, G. *Use of Proxies in Paleoceanography: Examples from the South Atlantic.* Springer-Verlag, Berlin, Heidelberg: pp. 207-228.

Woodruff, F., S. Savin and R. G. Douglas: (1980): Biological fractionation of oxygen and carbon isotopes by recent benthic foraminifera: *Mar. Micropal.*: *5*, 3-11.

Yiou, P., C. Genthon, M. Ghil, J. Jouzel, H. LeTreut, J. M. Barnola, C. Loruis and Y. N. Korotkevitch: (1991): High frequency paleovariability in climate and CO_2 levels from Vostok ice core records: *J. Geophys. Res.*: *B12*,(96), 20365-20378.

You, Y., J. R. E. Lutjeharms, O. Boebel and W. P. M. de Ruijter: (2003): Quantification of the interocean exchange of intermediate water masses around southern Africa: *Deep Sea Res. Part II*: *50*,(1), 197-228.

Yu, E.-F., R. Francois and M. P. Bacon: (1996): Similar rates of modern and last-glacial ocean thermohaline circulation inferred from radiochemical data: *Nature*: *379*,(6567), 689-694.

Zahn, R. and R. Keir: (1994): Tracer-nutrient correlations in the upper ocean: observational and box model constraints on the use of benthic foraminiferal $\delta^{13}C$ and Cd/Ca as paleo-proxies for the intermediate-depth ocean: Edited by: R. Zahn, Pederson, T. F., Kaminski, M. A. and Labeyrie, L. *Carbon Cycle In The Glacial Oceans: Constraints On The Oceans Role In Global Change.* Springer, Berlin *NATO ASI Series I, Vol 17*: pp. 195-221.

Zahn, R., J. Shönfeld, H.-R. Kudrass, M.-H. Park and H. Erlenkeuser: (1997): Thermohaline instability in the North Atlantic during meltwater events: Stable isotope and ice-rafted detritus records from core SO75-26KL, Portugese Margin: *Paleoceanography*: *12*,(5), 696-710.

Zahn, R., K. Winn and M. Sarnthein: (1986): Benthic foraminiferal $\delta^{13}C$ and accumulation rates of organic carbon: *Uvigerina perigrina* group and *Cibicidoides wuellerstorfi*: *Paleoceanography*: *1*,(1), 27-42.

Žarić, S., B. Donner, G. Fischer, S. Mulitza and G. Wefer: (2005): Sensitivity of planktic foraminifera to sea surface temperature and export production as derived from sediment trap data: *Mar. Micropal.*: *55*,(1-2), 75-105.

Zeldis, J. R., R. A. Walters, M. J. N. Greig and K. Image: (2004): Circulation over the northeastern New Zealand continental slope, shelf and adjacent Hauraki Gulf, during spring and summer: *Continental Shelf Res.*: *24*,(4-5), 543-561.

Zielinski, G. A., P. A. Mayewski, L. D. Meeker, S. Whitlow, M. S. Twickler and K. Taylor: (1996): Potential atmospheric impact of the Toba mega-eruption 71,000 years ago: *Geophys. Res. Letters*: *23*, 837-840.

Appendix A: MD02-2589 Physical Properties

Depth (cm)	Age (ka)	% $CaCO_3$	% >63µm	L*	Mag. Sus.
1	11.61	-	46.63	-	-
2	11.62	-	43.33	-	3
3	11.63	-	40.75	-	-
4	11.64	-	43.80	-	2
5	11.65	-	45.64	64.9	-
6	11.66	-	44.90	-	2
7	11.67	-	41.13	64.76	-
8	11.67	78.08	41.16	-	3
9	11.68	-	42.75	68.47	-
10	11.69	-	39.82	-	2
11	11.71	-	39.36	64.79	-
12	11.72	-	38.80	-	0
13	11.73	-	40.16	64.85	-
14	11.75	-	40.08	-	1
15	11.76	-	41.31	69.59	-
16	11.78	82.42	42.20	-	2
17	11.79	-	38.54	69.89	-
18	11.80	-	39.24	-	3
19	11.82	-	40.52	70.32	-
20	11.83	-	44.23	-	2
21	11.86	-	39.80	69.56	-
22	11.89	-	41.04	-	3
23	11.91	-	41.62	70.53	-
24	11.94	80.50	41.94	-	2
25	11.96	-	41.82	69.97	-
26	11.99	-	41.71	-	2
27	12.02	-	40.09	68.89	-
28	12.04	-	37.92	-	2
29	12.07	-	37.76	71.19	-
30	12.09	-	38.73	-	2
31	12.12	-	38.53	71.19	-
32	12.15	79.33	37.84	-	3
33	12.17	-	38.85	71.27	-
34	12.20	-	36.56	-	2
35	12.23	-	35.02	70.97	-
36	12.25	-	36.44	-	4
37	12.28	-	37.63	67.07	-
38	12.30	-	35.68	-	2
39	12.33	-	37.40	69.5	-
40	12.36	80.08	36.88	-	4
41	12.50	-	36.96	68.39	-
42	12.65	-	36.51	-	2
43	12.80	-	36.74	69.12	-
44	12.94	-	35.96	-	3
45	13.09	-	39.73	70.05	-
46	13.24	-	34.51	-	3
47	13.39	-	37.67	69.55	-
48	13.53	77.58	36.64	-	0
49	13.68	-	34.22	64.95	-
50	13.83	-	37.23	-	3
51	13.97	-	35.18	70.58	-

52	14.12	-	36.05	-	3
53	14.27	-	35.40	70.22	-
54	14.41	-	35.08	-	4
55	14.56	-	35.89	69.81	-
56	14.71	82.33	36.49	-	4
57	14.85	-	36.53	68.93	-
58	15.00	-	36.61	-	1
59	15.15	-	36.35	66.47	-
60	15.30	-	36.46	-	0
61	15.38	-	35.85	68.81	-
62	15.47	-	42.85	-	1
63	15.56	-	40.55	67.87	-
64	15.64	81.25	36.53	-	1
65	15.73	-	37.32	66.07	-
66	15.82	-	34.80	-	2
67	15.90	-	35.21	68.92	-
68	15.99	-	36.47	-	1
69	16.08	-	35.66	67.91	-
70	16.17	-	32.12	-	0
71	16.25	-	35.69	68.47	-
72	16.34	80.33	36.06	-	-1
73	16.43	-	36.91	67.75	-
74	16.51	-	36.84	-	0
75	16.60	-	39.31	68.64	-
76	16.70	-	36.50	-	0
77	16.79	-	38.15	67.05	-
78	16.89	-	38.81	-	1
79	16.98	-	38.50	67.1	-
80	17.08	78.50	41.64	-	0
81	17.17	-	42.50	65.81	-
82	17.27	-	41.91	-	0
83	17.36	-	40.90	65.04	-
84	17.46	-	41.74	-	1
85	17.55	-	40.81	62.96	-
86	17.60	-	41.87	-	0
87	17.65	-	44.07	63.17	-
88	17.70	84.83	43.12	-	-1
89	17.75	-	45.54	63.46	-
90	17.79	-	44.09	-	0
91	17.84	-	43.38	62.19	-
92	17.89	-	45.70	-	0
93	17.94	-	48.44	62.64	-
94	17.99	-	47.48	-	-2
95	18.03	-	47.01	62.2	-
96	18.08	77.50	48.38	-	-1
97	18.13	-	49.40	62.53	-
98	18.18	-	49.66	-	-1
99	18.23	-	51.80	61.91	-
100	18.27	-	52.69	-	-1
101	18.41	-	51.08	59.51	-
102	18.55	-	51.30	-	-1
103	18.68	-	54.19	59.51	-
104	18.82	77.08	54.11	-	-1
105	18.96	-	58.30	60.07	-
106	19.09	-	55.41	-	-1
107	19.23	-	56.08	59.37	-

108	19.37	-	55.87	-	-1
109	19.50	-	55.47	59.36	-
110	19.64	-	55.55	-	-2
111	19.73	-	55.71	58.06	-
112	19.82	77.67	57.82	-	-1
113	19.92	-	58.93	57.51	-
114	20.01	-	56.04	-	-1
115	20.10	-	56.76	-	-
116	20.19	-	57.67	57.01	0
117	20.28	-	56.66	-	-
118	20.38	-	56.57	57.44	-1
119	20.47	-	59.26	-	-
120	20.56	71.75	58.03	57.83	-1
121	20.65	-	55.42	-	-
122	20.74	-	56.56	58.58	0
123	20.84	-	55.75	-	-
124	20.93	-	57.68	58.59	0
125	21.02	-	57.24	-	-
126	21.27	-	53.96	-	-2
127	21.51	-	55.37	58.6	-
128	21.76	72.83	55.08	-	-1
129	22.01	-	54.98	58.17	-
130	22.25	-	55.64	-	-1
131	22.50	-	56.68	58.36	-
132	22.74	-	56.43	-	-1
134	23.24	-	56.55	-	-1
136	23.73	-	54.55	-	0
138	24.22	-	54.24	-	-1
140	24.71	-	52.28	-	0
141	25.03	-	48.17	57.35	-
142	25.34	-	50.00	-	0
144	25.97	72.17	49.94	-	0
146	26.59	-	51.42	-	0
148	27.22	-	51.81	-	0
150	27.85	-	51.89	-	0
151	28.16	-	55.50	56.32	-
152	28.47	70.50	54.92	-	0
156	29.73	-	55.91	-	-1
158	30.36	-	54.16	-	-1
160	30.98	63.92	56.45	-	-1
161	31.30	-	56.44	55.85	-
162	31.61	-	55.59	-	-1
164	32.24	-	56.41	-	-1
166	32.86	-	55.73	-	-1
168	33.49	69.83	58.35	-	-1
170	34.12	-	59.50	-	-1
171	34.38	-	61.51	58.32	-
172	34.64	-	59.30	-	0
174	35.17	-	59.35	-	-1
176	35.70	73.75	59.63	-	-1
178	36.23	-	60.61	-	-1
180	36.75	-	57.29	-	-1
181	37.02	-	60.87	58.68	-
182	37.28	-	60.85	-	0
184	37.81	75.17	59.17	-	-1
186	38.33	-	61.07	-	-1

188	38.86	-	61.37	-	-1
190	39.39	-	57.76	-	-1
191	39.54	-	58.85	60.99	-
192	39.70	75.25	56.02	-	-1
194	40.01	-	58.26	-	-1
196	40.31	-	55.35	-	-2
198	40.62	-	54.58	-	-1
200	40.93	75.00	54.32	-	-2
201	41.09	-	55.52	59.55	-
202	41.24	-	55.35	-	-
204	41.55	-	54.02	-	-1
206	41.86	-	55.70	-	0
208	42.17	74.25	54.33	-	-2
210	42.48	-	51.76	-	-1
211	42.63	-	50.68	59.29	-
212	42.79	-	51.05	-	-2
214	43.09	-	52.46	-	0
216	43.40	75.17	51.12	-	-1
218	43.71	-	49.52	-	0
220	44.02	-	48.88	-	1
221	44.18	-	50.71	61.38	-
222	44.33	-	48.78	-	0
224	44.64	75.25	50.12	-	0
226	44.95	-	47.59	-	-1
228	45.26	-	47.22	-	-1
230	45.57	-	47.71	-	0
231	45.72	-	48.99	63.08	-
232	45.87	79.83	48.95	-	-1
234	46.18	-	48.71	-	0
236	46.49	-	49.00	-	-1
238	46.80	-	48.13	-	-1
240	47.11	77.42	47.60	-	-1
241	47.26	-	48.66	62.11	-
242	47.42	-	48.88	-	-1
244	47.73	-	50.16	-	-1
246	48.04	-	51.49	-	-1
248	48.35	79.33	50.80	-	-1
250	48.65	-	51.34	-	-1
251	48.81	-	51.10	61.31	-
252	48.96	-	51.19	-	1
254	49.27	-	49.40	-	-1
256	49.58	76.25	51.87	-	-1
258	49.89	-	50.15	-	-1
260	50.20	-	52.20	-	-1
261	50.35	-	50.58	58.89	-
262	50.51	-	49.20	-	-1
264	50.82	74.58	50.19	-	0
266	51.13	-	50.26	-	-1
268	51.43	-	51.87	-	-1
270	51.74	-	50.87	-	-1
271	51.90	-	52.34	60.12	-
272	52.05	73.00	50.88	-	-1
274	52.36	-	41.74	-	-2
276	52.84	-	41.88	-	-1
278	53.31	-	41.13	-	0
280	53.79	79.00	41.59	-	-1

281	54.02	-	43.36	-	-
282	54.26	-	45.03	-	0
284	54.74	-	45.91	-	0
286	55.21	-	45.76	-	1
288	55.69	76.83	46.99	-	0
290	56.16	-	48.30	-	-1
291	56.40	-	47.97	63.77	-
292	56.64	-	47.98	-	-1
294	57.11	-	47.71	-	0
296	57.59	75.75	49.40	-	0
298	58.06	-	51.41	-	-1
300	58.54	-	48.77	-	-1
301	58.78	-	48.21	61.88	-
302	59.01	-	48.98	-	-1
304	59.49	78.25	49.06	-	-2
306	59.97	-	48.71	-	-1
308	60.44	-	62.56	-	-2
310	60.92	-	47.27	-	-1
311	61.15	-	48.31	62.7	-
312	61.39	78.08	47.08	-	-1
314	61.87	-	47.43	-	0
316	62.34	-	45.34	-	-1
318	62.82	-	46.11	-	-1
320	63.29	76.67	46.26	-	-1
321	63.53	-	46.02	64.14	-
322	63.77	-	47.44	-	-1
324	64.24	-	47.32	-	0
326	64.72	-	48.91	-	-1
328	65.19	76.50	48.89	-	-1
330	65.67	-	51.68	-	0
331	65.91	-	52.42	63.17	-
332	66.14	-	53.31	-	-1
334	66.62	-	51.80	-	-1
336	67.09	73.67	52.95	-	-1
338	67.57	-	50.67	-	1
340	68.04	-	51.96	-	-1
341	68.28	-	51.65	60.27	-
342	68.52	-	49.31	-	0
344	68.99	71.92	48.84	-	-1
346	69.47	-	57.76	-	-1
348	69.95	-	54.65	-	-1
350	70.42	-	59.63	-	0
351	70.66	-	66.18	61.17	-
352	70.90	72.50	66.81	-	0
354	71.37	-	60.94	-	5
356	71.85	-	55.66	-	-1
358	72.08	-	38.92	-	1
360	72.31	76.08	42.68	-	-1
361	72.43	-	40.06	62.87	-
362	72.54	-	43.98	-	-3
364	72.77	-	42.29	-	-1
366	73.01	-	40.60	-	0
368	73.24	78.17	36.74	-	-2
370	73.47	-	37.99	-	2
371	73.59	-	39.40	65.19	-
372	73.70	-	40.56	-	-1

374	73.94	-	39.38	-	1
376	74.17	79.08	34.93	-	8
378	74.40	-	35.75	-	-4
380	74.63	-	33.90	-	2
381	74.75	-	36.28	64.72	-
382	74.86	-	33.64	-	-1
384	75.10	80.08	31.53	-	0
386	75.33	-	36.07	-	-1
388	75.56	-	34.64	-	-1
390	75.79	-	35.28	-	-4
391	75.91	-	38.56	62.26	-
392	76.03	79.42	37.64	-	11
394	76.26	-	35.81	-	1
396	76.49	-	36.57	-	-2
398	76.72	-	38.26	-	-7
400	76.95	80.17	37.53	-	-1
401	77.07	-	34.53	65.67	-
402	77.19	-	39.46	-	-3
404	77.42	-	38.31	-	1
406	77.65	-	37.07	-	1
408	77.88	81.25	36.44	-	1
410	78.11	-	37.81	-	0
411	78.23	-	39.70	67.65	-
412	78.35	-	38.39	-	0
414	78.58	-	38.76	-	-2
416	78.81	82.08	41.81	-	-4
418	79.04	-	43.13	-	0
420	79.28	-	38.08	-	-1
421	79.39	-	34.43	68.98	-
422	79.51	-	35.45	-	-1
424	79.74	82.83	35.51	-	-1
426	79.97	-	33.67	-	-1
428	80.20	-	30.22		-3
429	80.32	-	33.74	68.67	-
430	80.44	-	36.69	-	-3
432	80.67	85.25	31.91	-	-1
433	80.78	-	38.13	-	-
434	80.90	-	36.70	-	1
436	81.13	-	35.15	-	1
438	81.37	-	37.97	-	-3
440	81.60	82.83	37.67	-	-1
441	81.71	-	37.91	68.12	-
442	81.83	-	34.35	-	-2
444	82.06	-	34.79	-	-2
446	82.29	-	33.38	-	-2
448	82.53	83.17	37.55	-	-11
450	82.76	-	39.63	-	0
451	82.87	-	40.38	65.75	-
452	82.99	-	38.62	-	-3
454	83.22	-	38.70	-	0
456	83.46	79.00	38.68	-	0
458	83.69	-	39.24	-	-1
460	83.92	-	39.45	-	-1
461	84.04	-	39.83	66.27	-
462	84.15	-	39.15	-	0
464	84.38	76.17	40.46	-	0

466	84.62	-	41.16	-	1
468	84.85	-	42.24	-	-1
470	85.08	-	42.22	-	-1
471	85.20	-	42.94	66.29	-
472	85.31	78.50	43.02	-	-1
474	85.54	-	42.86	-	0
476	85.78	-	42.16	-	0
478	86.01	-	40.26	-	-1
480	86.32	79.33	38.64	-	-6
481	86.48	-	38.78	65.84	-
482	86.64	-	40.11	-	-1
484	86.95	-	39.00	-	1
486	87.26	-	38.30	-	-2
488	87.57	78.92	41.61	-	0
490	87.89	-	39.83	-	-1
491	88.04	-	41.43	63.96	-
492	88.20	-	41.38	-	-1
494	88.51	-	41.10	-	0
496	88.83	77.42	39.43	-	2
498	89.14	-	37.67	-	-5
499	89.30	-	39.95	67.25	-
500	89.45	-	39.65	-	3
501	89.61	-	41.15	67.19	-
502	89.77		30.80	-	-1
504	90.08	81.58	37.30	-	4
506	90.39	-	34.37	-	6
508	90.70	-	35.41	-	-4
510	91.02	-	36.67	-	-3
511	91.17	-	40.63	59.91	-
512	91.33	74.67	39.51	-	0
514	91.64	-	41.73	-	-2
516	91.96	-	36.23	-	-1
518	92.27	-	31.41	-	-1
520	92.58	78.00	32.29	-	1
521	92.74	-	31.96	62.64	-
522	92.90	-	32.18	-	0
524	93.21	-	33.11	-	-1
526	93.52	-	29.72	-	0
528	93.83	75.67	37.08	-	-1
530	94.15	-	37.01	-	0
531	94.30	-	37.23	60.57	-
532	94.46	-	38.48	-	-2
534	94.77	-	39.14	-	-1
536	95.09	73.83	38.75	-	0
538	95.40	-	37.70	-	-1
540	95.71	-	39.55	-	0
541	95.87	-	40.72	61.11	-
542	96.03	-	36.03	-	2
544	96.34	78.83	38.51	-	1
546	96.65	-	38.42	-	0
548	96.97	-	38.97	-	-1
550	97.28	-	38.77	-	0
551	97.43	-	41.66	62.73	-
552	97.59	74.42	39.83	-	-2
554	97.90	-	42.40	-	-2
556	98.22	-	39.86	-	0

558	98.53	-	37.77	-	-2
560	98.84	75.67	41.61	-	0
561	99.00	-	39.55	62.38	-
562	99.16	-	41.29	-	-1
564	99.47	-	42.74	-	-5
566	99.78	-	45.80	-	-3
568	100.10	80.83	41.42	-	-1
570	100.41	-	36.78	-	1
571	100.56	-	37.28	62.83	-
572	100.72	-	38.63	-	0
574	101.03	-	35.78	-	-1
576	101.35	77.58	34.10	-	0
578	101.66	-	36.16	-	1
580	101.97	-	37.57	-	0
581	102.13	-	38.22	65.52	-
582	102.29	-	37.95	-	-10
583	102.44		35.82	-	-
584	102.60	78.58	36.92	-	2
586	102.91	-	35.33	-	1
588	103.23	-	38.48	-	0
590	103.54	-	38.37	-	-2
592	103.85	78.67	38.52	-	0
593	104.01	-	41.04	66.4	-
594	104.16	-	40.67	-	-1
596	104.48	-	39.82	-	0
598	104.79	-	43.14	-	1
600	105.10	80.00	41.42	-	-1
602	105.42	-	41.97	-	-1
603	105.57	-	44.05	60.01	-
604	105.73	-	45.48	-	-1
606	106.04	-	45.90	-	-2
608	106.23	78.83	44.41	-	-1
610	106.41	-	47.06	-	-1
612	106.60	-	49.06	-	-2
613	106.69	-	46.70	63.96	-
614	106.78	-	46.03	-	-1
616	106.97	77.83	46.85	-	-2
618	107.15	-	45.50	-	-2
620	107.34	-	45.87	-	0
622	107.52	-	48.02	-	-2
623	107.62	-	47.08	65.26	-
624	107.71	77.83	45.52	-	-2
626	107.89	-	45.29	67.19	0
628	108.08	-	44.78	68.46	0
630	108.26	-	41.37	66.39	-1
632	108.45	77.75	42.46	67.48	-1
633	108.54	-	44.44	-	-
634	108.63	-	40.59	65.93	-3
636	108.82	-	38.11	65.43	1
638	109.00	-	41.91	63.95	-1
640	109.19	77.42	46.45	67.04	-5
642	109.37	-	42.70	66.28	1
643	109.47	-	40.60	-	-
644	109.56	-	40.32	66.04	-1
646	109.74	-	40.03	64.69	-1
648	109.93	78.42	41.47	68.1	0

650	110.11	-	42.14	66	1
652	110.30	-	45.41	67.24	0
653	110.39	-	42.04	-	-
654	110.48	-	38.01	67.42	0
656	110.67	76.67	44.35	65.85	2
658	110.85	-	40.93	68.1	2
660	111.04	-	41.78	68.33	2
662	111.22	-	41.67	64.16	0
663	111.31	-	40.85	-	-
664	111.41	76.83	44.35	66.71	-1
666	111.59	-	43.80	62.37	0
668	111.78	-	42.72	63.69	-3
670	111.96	-	42.12	61.33	0
672	112.15	77.75	41.38	61.7	-1
673	112.24	-	40.45	-	-
674	112.33	-	41.16	65.48	-1
676	112.52	-	41.06	58.16	-2
678	112.70	-	39.01	59.89	0
680	112.89	76.00	39.68	61.33	0
682	113.07	-	37.67	66.18	-1
683	113.16	-	39.19	-	-
684	113.26	-	37.60	66.04	0
686	113.44	-	36.92	61.61	2
688	113.63	79.67	38.82	65.92	0
690	113.81	-	39.33	65.45	-6
692	114.00	-	39.02	62.7	-1
693	114.09	-	36.64	-	-
694	114.18	-	34.32	-	0
696	114.52	76.00	35.04	-	1
698	114.85	-	34.04	-	-1
700	115.19	-	35.68	-	0
702	115.52	-	35.97	-	-2
703	115.69	-	37.41	65.95	-
704	115.86	76.67	38.64	-	0
706	116.20	-	35.99	-	1
708	116.53	-	36.76	-	-1
710	116.87	-	28.95	-	0
712	117.20	81.83	36.41	-	8
713	117.37	-	38.21	62.48	-
714	117.54	-	38.78	-	-1
716	117.87	-	43.60	-	-
718	118.21	-	35.37	-	-3
720	118.55	-	37.86	-	-11
722	118.88	-	31.27	-	-8
724	119.22	-	37.73	-	-3
725	119.39	-	36.13	-	-
726	119.55	76.33	37.04	-	0
728	119.89	-	36.51	-	-13
730	120.22	-	33.33	-	8
732	120.56	-	37.48	-	5
734	120.90	76.75	39.46	-	-4
735	121.06	-	36.23	72.75	-
736	121.23	-	36.51	-	-1
738	121.57	-	33.34	-	1
740	121.90	-	36.43	-	-1
742	122.24	78.08	37.89	-	-2

744	122.57	-	35.33	-	-1
745	122.74	-	38.71	73.95	-
746	122.91	-	33.96	-	4
748	123.25	-	35.71	-	-4
750	123.58	77.92	34.63	-	0
752	123.92	-	36.28	-	-3
754	124.25	-	31.69	-	0
755	124.42	-	36.01	71.67	-
756	124.59	-	34.57	-	0
758	124.92	75.50	33.90	-	-2
760	125.26	-	30.19	-	0
762	125.60	-	28.99	-	-3
764	125.93	-	31.56	-	1
765	126.10	-	31.63	67.7	-
766	126.27	75.33	31.14	-	-
768	126.60	-	32.16	-	-
770	126.94	-	30.42	-	-
772	127.27	-	32.20	-	-
774	127.61	72.33	21.79	-	-
775	127.78	-	46.17	68.45	-
776	127.94	-	29.04		-
778	128.28	-	28.26	-	-
780	128.62	-	30.48	-	-
782	128.95	73.50	29.83	-	0
784	129.40	-	31.80	-	-3
785	129.62	-	34.02	67.05	-
786	129.84	-	33.63	-	4
788	130.29	-	36.79	-	1
790	130.73	72.50	37.26	-	1
792	131.18	-	37.65	-	-1
794	131.62	-	37.30	-	0
795	131.85	-	41.37	67.21	-
796	132.07	-	45.37	-	0
798	132.52	78.33	40.62	-	0
800	132.96	-	37.95	-	1
802	133.41	-	36.66	-	0
804	133.85	-	44.85	-	0
805	134.07	-	45.29	68.58	-
806	134.30	80.08	46.31	-	-7
808	134.74	-	51.23	-	7
810	135.19	-	48.11	-	-13
812	135.63	-	51.47	-	-2
814	136.08	79.67	54.74	-	-2
815	136.30	-	56.10	65.55	-
816	136.52	-	52.72	-	0
818	136.97	-	54.24	-	-1
820	137.41	-	52.47	-	-2
822	137.86	78.83	54.31	-	0
824	138.44	-	55.06	-	-1
825	138.73	-	53.04	59.45	-
826	139.02	-	51.24	-	0
828	139.61	-	57.20	-	-3
830	140.19	76.00	57.81	-	0
832	140.77	-	55.84	-	-3
834	141.35	-	50.35	-	-2
835	141.64	-	52.82	59.49	-

836	141.93	-	54.15	-	0
838	142.52	73.83	56.11	-	-3
840	143.10	-	56.79	-	-1
842	143.68	-	56.81	-	-1
844	144.26	-	55.64	-	-3
845	144.55	-	56.38	60.74	-
846	144.85	73.92	55.54	-	-1
848	145.43	-	53.95	-	-2
850	146.01	-	49.98	-	-1
852	146.59	-	56.94	-	-1
854	147.17	73.08	56.46	-	-1
855	147.46	-	54.20	59.78	
856	147.76	-	54.91	-	-5
858	148.34	-	52.59	-	0
860	148.92	-	53.36	-	-1
862	149.50	75.25	51.10	-	-3
863	149.79	-	51.42	-	-
864	150.08	-	51.91	-	0
866	150.67	-	49.67	-	-1
868	151.25	-	53.31	-	-9
870	151.83	-	50.86	-	10
872	152.41	-	54.09	-	-
874	152.99	-	49.12	-	9
876	153.58	-	49.51	-	-1
878	154.16	-	48.18	-	-1
880	154.74	-	47.94	-	-1
882	155.32	-	51.55	-	-2
884	155.91	-	50.29	-	-1
886	156.28	-	48.74	-	6
888	156.65	-	50.12	-	-3
890	157.02	-	49.32	-	2
892	157.39	-	52.51	-	-3
894	157.76	-	53.45	-	-1
896	158.13	-	47.71	-	-2
898	158.50	-	49.23	-	-
900	158.87	-	48.73	-	-
902	159.24	-	51.05	-	-
904	159.62	-	51.42	-	-
906	159.99	-	52.64	-	-
908	160.36	-	51.50	-	-
910	160.73	-	51.46	-	-
912	161.10	-	54.82	-	-
914	161.47	-	55.27	-	-
916	161.84	-	56.32	-	-
918	162.21	-	56.46	-	-
920	162.58	-	58.61	-	-
922	162.95	-	57.20	-	-
924	163.33	-	54.58	-	-
926	163.70	-	52.95	-	-
928	164.07	-	51.16	-	-
930	164.44	-	49.36	-	-
932	164.81	-	46.47	-	-
934	165.18	-	51.38	-	-
936	165.55	-	51.10	-	-
938	165.92	-	57.59	-	-
940	166.29	-	55.40	-	-

942	166.66	-	56.58	-	-
944	167.04	-	56.34	-	-
946	167.41	-	51.57	-	-
948	167.78	-	53.34	-	-
950	168.15	-	54.68	-	-
952	168.52	-	58.12	-	-
954	168.89	-	57.08	-	-
956	169.26	-	57.35	-	-
958	169.63	-	56.71	-	-
960	170.00	-	54.71	-	-
962	170.37	-	55.56	-	-

Appendix B: MD02-2589 Surface Proxies

Depth (cm)	Age (ka)	Summer SST (°C)	Winter SST (°C)	Mean SST (°C)	Planktonic $\delta^{18}O$	$\delta^{18}O_{sw\ (IVC)}$	$\delta^{18}O_{sw}$ errors (±)	SSS (deviation from closest site)	SSS errors (±)	Frag. Index (%)	Planktonic Accum. Rate
4	11.64	18.25	15.06	16.62	-	-	-	-	-	9.21	47200.39
8	11.67	18.19	14.75	16.41	1.27	2.19	0.10	3.40	1.21	9.73	92397.13
12	11.72	18.49	15.69	17.26	0.79	1.84	0.10	2.80	1.02	8.14	26794.22
16	11.78	18.51	15.54	16.99	0.92	1.86	0.13	2.83	1.03	11.17	49839.61
20	11.83	19.84	16.59	18.24	1.54	2.68	0.11	4.32	1.49	9.29	42754.91
24	11.94	20.49	16.85	18.66	1.43	2.62	0.10	4.19	1.44	5.91	119413.17
28	12.04	18.17	15.65	17.12	0.79	1.65	0.13	2.53	1.00	8.62	42382.49
32	12.15	18.01	15.42	16.93	0.98	1.76	0.13	2.70	1.05	4.65	41753.45
36	12.25	18.75	15.53	17.12	0.78	1.57	0.14	2.35	0.87	4.98	38108.80
40	12.36	17.12	14.70	16.06	0.65	1.18	0.13	1.72	0.69	5.09	29353.83
44	12.94	19.20	16.40	17.94	1.09	1.99	0.13	3.10	1.15	5.92	42949.23
48	13.53	19.16	16.47	18.06	0.97	1.89	0.14	2.93	1.12	7.14	34769.11
50	13.83	18.41	16.03	17.33	0.85	1.61	0.13	2.47	0.93	4.20	73487.69
52	14.12	18.46	16.10	17.50	1.31	2.08	0.14	3.28	1.21	6.77	25440.60
54	14.41	19.53	16.71	18.36	1.08	1.96	0.13	3.09	1.12	5.03	74432.47
56	14.71	18.66	16.07	17.53	1.55	2.18	0.12	3.46	1.26	6.23	50198.53
58	15.00	18.34	15.81	17.22	1.15	1.68	0.14	2.64	0.95	7.42	34774.11
60	15.30	19.04	16.33	17.93	1.49	2.12	0.13	3.39	1.20	6.62	33511.92
62	15.47	19.25	16.41	18.16	1.15	1.79	0.12	2.85	1.04	2.01	71357.07
64	15.64	18.35	16.12	17.40	1.58	2.02	0.12	3.24	1.13	9.52	42216.99
66	15.82	17.95	15.25	16.64	1.43	1.67	0.17	2.66	1.03	3.60	91144.98
68	15.99	18.46	16.26	17.65	1.16	1.58	0.14	2.52	0.98	8.72	39500.98
70	16.17	19.32	16.55	18.05	1.58	2.02	0.13	3.28	1.19	3.86	86128.14
72	16.34	18.72	16.01	17.37	1.64	1.90	0.12	3.09	1.11	8.36	25767.53
74	16.51	17.08	14.85	16.06	1.07	1.06	0.12	1.69	0.57	6.65	97541.47
76	16.70	19.01	16.08	17.56	1.43	1.72	0.13	2.81	0.96	8.98	35862.63
78	16.89	18.13	15.24	16.59	1.36	1.44	0.14	2.35	0.82	5.85	40000.00
80	17.08	19.34	16.47	17.90	1.38	1.72	0.13	2.83	1.00	3.75	97507.96
82	17.27	18.32	14.71	16.28	1.62	1.62	0.13	2.67	0.88	8.36	52396.81
84	17.46	19.72	16.50	18.01	1.48	1.82	0.13	3.02	1.04	5.19	86670.85
86	17.60	19.74	16.45	17.94	1.94	2.25	0.10	3.76	1.23	8.44	48089.23
90	17.79	19.36	15.47	17.17	1.81	1.96	0.11	3.27	1.10	10.46	28060.71
94	17.99	19.20	15.22	16.96	1.98	2.07	0.10	3.48	1.09	7.32	48663.99
98	18.18	18.95	14.95	16.69	2.31	2.35	0.15	3.95	1.40	11.18	64463.86
102	18.55	19.67	15.52	17.45	2.12	2.32	0.11	3.92	1.28	6.25	63270.90
106	19.09	18.92	14.57	16.54	2.49	2.50	0.15	4.23	1.50	7.45	54365.70
110	19.64	18.72	14.81	16.49	2.09	2.11	0.15	3.58	1.30	7.91	53591.26
114	20.01	18.71	14.49	16.26	2.34	2.23	0.18	3.77	1.54	6.97	58473.97
118	20.38	19.16	14.43	16.71	1.96	1.88	0.15	3.15	1.17	7.78	107840.45
122	20.74	19.62	16.02	17.53	2.18	2.18	0.15	3.64	1.36	4.77	69157.96
126	21.27	19.51	15.85	17.40	2.26	2.16	0.16	3.59	1.36	6.34	60374.78
130	22.25	20.24	16.50	18.24	2.25	2.38	0.14	3.90	1.39	9.20	49052.43
134	23.24	19.56	15.08	17.24	2.08	2.05	0.28	3.34	1.17	7.37	41220.34
138	24.22	19.82	16.15	17.75	2.06	2.12	0.13	3.53	1.22	11.00	59781.01
142	25.34	20.04	16.15	17.94	2.08	2.23	0.32	3.70	1.28	11.73	55076.34
146	26.59	19.79	15.98	17.62	2.03	2.16	0.13	3.51	1.29	3.08	84203.89

326	64.72	19.61	15.53	17.42	1.93	2.37	0.16	3.91	1.49	12.42	54882.77
330	65.67	19.62	15.39	17.31	2.22	2.55	0.15	4.20	1.54	12.03	67837.32
334	66.62	18.57	14.44	16.31	2.31	2.34	0.16	3.84	1.47	7.07	118282.45
338	67.57	19.57	15.75	17.40	2.07	2.35	0.15	3.87	1.47	16.94	75540.98
342	68.52	19.75	15.46	17.47	2.05	2.35	0.11	3.76	1.32	15.31	67316.49
346	69.47	18.93	14.50	16.45	1.75	1.89	0.16	2.94	1.22	16.34	70586.41
350	70.42	20.27	16.69	18.31	1.76	2.23	0.13	3.63	1.26	11.75	72492.07
352	70.90	19.52	15.87	17.54	2.18	2.55	0.12	4.08	1.45	18.39	64940.58
354	71.37	20.54	17.00	18.69	1.94	2.61	0.11	4.14	1.46	9.21	56805.84
356	71.85	18.88	15.21	16.85	1.81	2.13	0.11	3.28	1.17	10.68	51666.80
358	72.08	20.43	17.01	18.62	1.53	2.24	0.11	3.47	1.23	5.91	57742.22
360	72.31	20.60	17.24	18.82	1.55	2.33	0.11	3.56	1.24	4.68	62020.62
362	72.54	20.48	17.15	18.76	1.56	2.35	0.10	3.53	1.30	5.73	48979.00
364	72.77	20.49	16.94	18.54	1.90	2.66	0.12	3.99	1.50	5.49	67392.77
366	73.01	20.34	16.95	18.54	1.45	2.24	0.11	3.24	1.22	5.88	52190.79
370	73.47	19.83	16.44	18.03	1.37	2.09	0.11	2.91	1.18	3.32	42455.10
374	73.94	20.30	17.41	18.83	1.49	2.39	0.11	3.49	1.33	6.04	45803.24
378	74.40	20.41	17.03	18.58	1.29	2.17	0.11	3.19	1.20	8.54	45193.30
382	74.86	19.97	16.72	18.23	1.47	2.27	0.09	3.43	1.23	6.12	25470.05
386	75.33	20.23	16.92	18.45	1.44	2.28	0.09	3.52	1.21	5.62	78837.37
390	75.79	20.58	17.15	18.79	1.31	2.22	0.09	3.38	1.18	5.83	40796.29
394	76.26	19.91	16.51	18.03	1.47	2.22	0.11	3.34	1.20	12.15	60015.89
398	76.72	19.41	15.96	17.54	1.51	2.15	0.12	3.18	1.21	2.21	90754.51
402	77.19	20.52	17.07	18.75	1.39	2.27	0.10	3.34	1.23	7.94	36242.70
406	77.65	20.79	17.51	19.03	1.31	2.24	0.12	3.26	1.23	6.03	53394.29
702	115.52	18.86	16.00	17.35	0.42	1.23	0.11	1.43	0.66	2.23	34854.05
706	116.20	18.53	15.42	16.85	0.77	1.47	0.12	1.75	0.79	4.08	29383.25
710	116.87	18.99	15.45	17.04	0.50	1.24	0.14	1.29	0.66	2.04	37221.05
714	117.54	18.13	14.83	16.25	0.66	1.23	0.10	1.28	0.59	2.54	40412.04
736	118.21	18.56	15.27	16.63	0.75	1.64	0.14	1.97	0.95	1.94	39724.14
740	118.88	17.10	14.63	15.72	0.28	1.02	0.11	0.92	0.45	2.60	36735.43
744	119.55	17.37	14.64	15.78	0.75	1.50	0.16	1.70	0.92	3.22	35020.80
748	120.22	18.99	15.15	16.79	0.89	1.85	0.11	2.27	0.97	2.32	34662.48
752	120.90	18.83	15.82	17.16	0.52	1.58	0.15	1.77	0.92	2.02	30046.32
756	121.57	19.18	15.61	17.26	0.79	1.88	0.11	2.23	0.99	3.26	36766.87
760	122.24	20.00	16.57	18.26	0.70	1.95	0.09	2.32	0.99	5.86	26731.97
764	122.91	20.25	16.46	18.41	0.52	1.76	0.09	1.96	0.88	3.70	138240.00
768	123.58	19.67	15.68	17.57	0.55	1.62	0.09	1.85	0.84	6.86	27583.10
772	124.25	18.55	14.71	16.40	0.64	1.48	0.09	1.71	0.72	4.18	36166.73
776	124.92	19.57	16.05	17.59	0.41	1.50	0.13	1.92	0.85	4.72	29122.15
780	125.60	19.41	15.56	17.35	0.57	1.63	0.11	2.30	0.83	4.06	39076.14
784	126.27	18.72	13.96	16.16	0.35	1.19	0.11	1.73	0.55	5.46	31978.16
788	126.94	19.16	15.51	17.11	1.01	2.05	0.13	3.27	1.16	4.35	43584.07
792	127.61	18.97	14.84	16.68	0.72	1.47	0.12	2.36	0.80	7.02	46232.84
796	128.28	18.39	14.73	16.30	0.94	1.53	0.12	2.46	0.84	9.63	40112.90
800	128.95	18.03	14.60	15.99	0.92	1.36	0.12	2.18	0.73	7.98	34953.85
804	129.84	17.80	14.67	15.99	0.93	1.29	0.10	2.07	0.61	7.54	44766.26
808	130.73	18.07	13.93	15.72	1.46	1.67	0.12	2.72	0.91	10.62	49030.51
812	131.62	18.60	15.65	16.90	1.35	1.73	0.12	2.81	0.96	10.53	46935.50
816	132.52	17.69	13.93	15.49	1.75	1.65	0.11	2.67	0.91	11.08	40557.97
820	133.41	18.12	13.85	15.65	1.47	1.25	0.11	2.07	0.64	8.38	49395.73
824	134.30	19.11	15.18	16.96	1.70	1.62	0.12	2.62	0.90	12.71	66796.81
828	135.19	18.57	14.51	16.29	1.74	1.41	0.13	2.27	0.76	15.32	48964.96
832	136.08	18.71	14.02	16.10	1.84	1.48	0.14	2.38	0.80	11.17	46876.44
836	136.97	18.22	13.59	15.60	1.91	1.44	0.19	2.32	0.93	10.06	88970.49
840	137.86	18.28	13.45	15.61	1.91	1.44	0.17	2.34	0.82	9.21	63081.14
844	139.02	18.24	13.99	15.79	1.83	1.60	0.14	2.58	0.89	8.99	68266.67
848	140.19	18.61	14.15	16.09	1.96	1.75	0.15	2.70	1.09	11.14	60134.23

852	141.35	17.71	12.94	14.97	2.19	1.65	0.20	2.54	1.16	13.52	55890.08
856	142.52	17.82	12.42	14.89	1.97	1.31	0.19	2.00	0.87	7.54	28389.11
860	143.68	17.74	13.15	15.10	1.88	1.29	0.19	1.96	0.88	13.07	62036.03
864	144.85	17.57	12.48	14.77	1.79	1.29	0.20	1.97	0.94	12.66	51608.51
868	146.01	17.67	12.28	14.69	1.95	1.60	0.20	2.54	1.14	11.94	62295.40
872	147.17	16.65	11.14	13.58	1.87	1.46	0.19	2.31	1.06	10.07	69577.30
876	148.34	18.18	13.49	15.52	1.92	1.87	0.21	3.02	1.27	12.83	90559.19
880	149.50	19.26	14.65	16.82	1.90	2.07	0.16	3.34	1.13	7.68	87950.92

Appendix C: MD02-2589 Planktonic Foraminifera Assemblage Data

Depth (cm)	Age (ka)	*G. bulloides*	*G. inflata*	*N. pachyderma (sin)*	*N. pachyderma (dex)*	*G. truncatulinoides*	*G. glutinata*	*G. falconensis*	*N. dutetrei*	*T. quinqueloba*	*G. hirsuta*	*G. ruber*	*G. scitula*
4	11.64	26.84	33.68	0.53	13.16	6.32	3.95	2.89	0.79	2.37	0.79	-	2.11
8	11.67	30.09	34.22	0.88	11.80	5.01	5.01	2.65	0.29	2.36	0.29	1.47	1.18
12	11.72	24.43	28.51	1.36	11.99	6.79	6.56	2.71	-	3.17	0.90	0.90	4.98
16	11.78	21.59	36.97	0.99	11.66	5.71	8.19	3.72	0.50	0.50	1.49	0.74	1.49
20	11.83	23.22	33.75	0.93	12.38	4.95	7.74	3.72	1.24	-	0.62	0.93	1.55
24	11.94	25.99	26.16	1.08	10.93	3.94	11.47	4.30	1.08	0.72	1.08	2.15	2.15
28	12.04	25.86	38.79	0.57	6.90	4.89	10.63	2.30	0.86	1.15	0.29	1.44	1.44
32	12.15	27.24	37.21	0.66	8.31	4.32	8.64	1.99	1.33	1.99	1.66	0.33	0.66
36	12.25	26.25	32.89	-	10.63	4.98	8.97	2.66	1.00	1.99	1.66	1.66	1.00
40	12.36	20.64	38.87	0.80	10.19	7.77	8.31	2.95	0.80	2.95	0.27	1.07	-
44	12.94	27.63	32.24	0.33	9.54	5.59	8.55	1.97	0.99	1.32	0.99	1.64	0.66
48	13.53	25.71	36.86	0.29	10.00	5.43	8.86	1.71	0.57	0.57	0.29	0.57	0.86
50	13.83	28.83	30.66	1.09	11.68	6.20	9.12	0.73	0.73	0.73	1.46	0.36	1.82
52	14.12	26.07	30.33	1.00	10.78	6.77	10.53	2.26	1.25	1.75	0.50	0.75	1.00
54	14.41	27.46	34.32	1.14	13.04	4.12	5.49	0.46	1.37	0.92	1.37	1.37	0.92
56	14.71	23.19	35.41	1.00	14.46	5.49	8.98	1.50	1.00	0.50	0.25	0.75	1.50
58	15.00	28.99	31.91	1.12	13.26	5.62	6.07	2.47	1.35	1.80	0.22	0.45	0.67
60	15.30	24.83	36.09	0.99	12.25	5.96	4.64	3.31	1.32	1.32	-	0.66	0.66
62	15.47	23.72	36.86	2.19	9.49	4.74	6.57	2.37	0.73	1.09	0.36	1.46	0.73
64	15.64	26.07	30.08	1.25	14.29	8.52	7.02	2.51	0.50	0.25	1.00	1.25	1.25
66	15.82	24.62	32.58	3.41	9.85	5.30	9.47	2.65	1.52	2.27	0.76	1.14	-
68	15.99	28.09	29.15	0.85	11.91	7.23	8.51	2.13	-	2.55	0.21	0.21	-
70	16.17	25.00	28.19	1.85	14.77	5.70	12.08	1.68	0.67	1.01	0.67	0.34	-
72	16.34	24.46	24.46	2.79	15.48	5.88	10.53	1.86	1.24	1.55	0.93	1.55	1.24
74	16.51	29.09	27.38	2.28	16.16	9.89	1.14	0.76	0.76	3.80	0.38	0.76	0.76
76	16.70	26.21	29.37	1.94	16.50	5.10	6.80	1.94	0.24	2.18	0.49	0.73	1.46
78	16.89	26.34	26.10	1.71	18.78	5.85	9.51	1.95	0.73	2.20	0.24	0.24	1.46
80	17.08	28.33	25.60	1.37	21.50	4.10	8.36	1.71	0.68	0.68	0.34	-	0.68
82	17.27	26.46	24.51	3.06	27.30	5.29	6.13	0.84	-	1.39	-	0.56	0.28
84	17.46	28.89	21.11	2.22	26.67	2.96	4.81	2.22	0.74	1.85	0.74	0.74	-
86	17.60	21.88	20.00	3.44	30.00	4.38	6.25	1.25	-	1.88	1.25	0.31	0.94
90	17.79	33.85	16.92	3.08	29.23	2.15	5.54	1.23	0.31	1.85	0.92	-	0.92
94	17.99	25.35	24.23	2.25	32.68	3.94	4.23	0.56	0.56	0.85	0.56	0.56	0.56
98	18.18	25.66	14.14	6.25	38.49	2.96	3.95	0.99	0.66	0.99	0.66	0.33	0.99
102	18.55	28.75	13.44	2.81	40.00	2.19	5.94	-	0.63	1.25	0.63	0.31	0.94
106	19.09	27.95	8.70	5.90	43.79	1.86	4.35	0.31	0.93	2.80	0.31	0.31	-
110	19.64	29.43	11.08	6.33	38.92	2.22	4.75	0.32	0.63	2.85	0.32	-	-
114	20.01	25.47	5.90	10.19	42.63	0.80	6.97	-	-	3.22	0.54	0.27	-
118	20.38	29.94	9.28	5.69	42.81	0.90	4.19	-	-	3.29	-	-	-
122	20.74	29.36	7.64	5.97	40.57	0.48	6.92	-	-	3.34	-	-	0.24
126	21.27	28.10	8.46	7.55	39.88	0.91	7.55	0.91	0.60	1.21	-	-	-
130	22.25	30.10	6.72	5.22	43.53	1.00	4.48	0.75	0.25	1.00	0.25	0.75	-
134	23.24	30.53	13.68	4.21	41.75	0.35	4.21	0.35	-	2.46	-	-	0.35
138	24.22	27.99	10.77	5.26	38.76	1.67	4.31	3.11	0.24	1.67	0.24	0.96	0.48
142	25.34	27.86	9.97	2.35	44.87	-	5.57	1.17	0.29	3.52	-	-	0.29

146	26.59	25.51	9.25	6.16	43.84	0.34	4.11	1.03	-	3.08	-	-	1.03
326	64.72	27.23	21.35	6.75	27.23	1.96	5.23	1.09	0.22	0.65	0.22	0.44	0.44
330	65.67	33.23	20.25	6.96	26.90	0.95	2.53	1.90	-	0.63	0.95	-	0.95
334	66.62	32.86	22.26	7.77	24.03	2.83	3.53	1.77	0.35	0.35	0.35	-	0.35
338	67.57	28.89	13.33	6.94	32.50	1.11	6.39	2.50	-	1.11	0.28	-	-
342	68.52	22.80	18.89	4.23	34.53	0.98	7.17	3.26	0.33	1.63	0.98	-	0.33
346	69.47	27.04	13.80	8.45	35.49	0.85	6.48	1.97	-	1.97	0.56	-	-
350	70.42	21.86	18.03	5.19	32.24	2.46	6.28	2.19	0.27	1.64	0.55	0.27	0.27
352	70.90	30.48	20.40	3.53	27.71	2.77	4.53	3.02	0.25	1.01	1.01	-	0.25
354	71.37	24.74	21.05	3.42	32.63	2.89	3.68	1.05	0.26	0.26	0.26	0.26	0.79
356	71.85	25.87	26.28	3.29	27.72	3.90	4.72	2.05	-	1.03	0.82	0.21	0.21
358	72.08	27.59	14.29	2.46	41.63	1.72	4.43	0.74	-	1.23	0.25	-	0.49
360	72.31	25.74	13.40	1.70	42.55	1.49	5.11	4.04	-	0.64	-	-	0.43
362	72.54	27.45	19.57	1.67	31.74	1.43	5.97	3.82	-	1.91	-	-	0.48
364	72.77	30.21	15.56	2.75	32.72	1.60	3.66	3.89	0.23	1.83	0.46	0.46	0.23
366	73.01	29.14	18.98	1.87	29.95	1.60	5.08	3.74	0.80	1.07	0.53	-	1.07
370	73.47	28.24	19.93	1.99	26.58	1.99	6.64	2.99	1.00	2.33	0.33	0.33	0.66
374	73.94	27.49	16.62	1.51	32.02	4.83	5.74	2.72	0.60	0.30	-	-	0.91
378	74.40	28.16	18.04	2.53	30.70	1.27	6.01	3.16	0.32	1.27	0.63	0.32	0.95
382	74.86	26.02	16.84	1.53	32.40	3.06	5.87	3.57	0.26	2.55	-	-	1.02
386	75.33	25.17	17.98	2.02	35.73	3.37	3.60	3.82	0.22	0.67	0.67	0.45	1.12
390	75.79	25.57	18.45	0.97	31.07	3.56	3.24	3.56	0.65	1.62	0.97	0.65	0.65
394	76.26	25.42	16.95	2.54	35.03	3.39	3.95	1.98	1.13	1.41	0.85	0.28	-
398	76.72	32.08	22.12	0.88	27.21	4.65	6.19	0.88	-	0.44	0.66	0.22	0.66
402	77.19	26.67	18.41	1.59	29.84	2.54	5.40	5.08	0.63	0.63	0.32	-	0.63
406	77.65	30.96	12.88	1.92	29.86	3.56	4.38	3.29	0.82	1.10	0.82	0.55	0.27
702	115.52	28.54	23.57	0.99	13.65	8.93	7.69	3.72	0.99	0.74	0.50	0.50	1.74
706	116.20	26.61	25.11	1.07	16.74	8.37	6.44	3.86	0.86	0.86	0.86	1.07	1.29
710	116.87	26.92	25.57	0.68	15.16	8.37	4.75	5.20	0.45	0.68	0.23	1.81	0.90
714	117.54	27.33	22.67	2.12	16.31	9.11	4.87	5.93	1.06	0.85	0.85	1.06	1.27
736	118.21	28.61	17.50	2.22	23.89	6.39	6.67	1.94	0.83	2.22	1.11	0.28	2.22
740	118.88	29.43	30.99	-	12.50	11.46	4.17	1.82	0.52	0.26	0.52	1.56	1.82
744	119.55	32.16	22.22	0.88	13.16	9.36	8.48	2.63	0.29	1.46	0.88	1.46	2.34
748	120.22	30.43	31.01	-	15.36	6.09	4.06	2.32	0.87	0.29	0.58	2.32	2.90
752	120.90	33.63	27.58	0.22	10.31	7.17	6.50	2.02	0.67	0.90	-	0.90	3.59
756	121.57	31.16	29.77	0.23	14.65	5.58	4.19	3.95	0.47	0.47	0.70	1.40	1.40
760	122.24	26.71	32.57	0.33	16.29	3.91	4.23	5.21	-	0.33	0.98	0.98	1.63
764	122.91	32.72	29.01	0.82	15.02	2.06	2.47	5.76	1.03	1.03	0.41	2.67	2.26
768	123.58	28.10	31.37	0.98	16.34	3.92	4.90	6.21	0.65	0.33	-	2.61	0.65
772	124.25	35.25	28.20	0.26	16.19	5.48	4.44	2.35	1.04	0.78	0.26	1.04	1.31
776	124.92	33.63	23.01	3.24	20.65	2.95	2.95	3.54	1.18	-	-	0.88	2.95
780	125.60	29.83	28.64	1.67	21.48	3.58	3.10	2.86	0.95	0.48	-	1.67	2.15
784	126.27	31.69	27.32	3.28	22.68	3.01	1.91	3.55	0.55	1.37	-	1.64	1.37
788	126.94	30.64	27.54	3.52	22.57	3.73	2.07	1.86	0.21	0.41	0.21	0.83	3.11
792	127.61	29.96	28.31	4.34	21.49	2.48	2.89	2.89	0.62	0.21	1.03	0.62	1.65
796	128.28	30.12	25.78	4.04	23.60	5.59	1.24	2.48	0.31	0.31	0.31	0.93	0.31
800	128.95	29.11	25.59	3.52	20.66	7.28	3.76	3.05	0.70	-	0.47	-	1.88
804	129.84	25.38	27.89	2.01	26.13	9.05	1.51	2.51	0.50	-	-	0.25	0.75
808	130.73	24.78	28.32	3.83	27.14	6.19	2.65	2.95	-	-	-	-	2.06
812	131.62	26.87	24.65	2.49	19.94	7.48	4.99	3.05	0.83	0.55	-	1.94	1.11
816	132.52	22.45	27.41	3.50	25.36	7.29	5.83	3.21	0.29	0.29	-	0.58	2.04
820	133.41	18.86	27.25	3.59	29.94	6.29	5.09	2.69	-	0.60	-	1.80	0.30
824	134.30	21.76	26.16	3.91	29.10	4.40	4.89	2.93	-	0.49	-	-	1.22
828	135.19	24.62	27.33	5.11	26.73	3.90	4.20	4.20	-	-	-	0.60	0.90
832	136.08	28.40	21.36	5.34	30.10	2.43	3.64	3.88	0.73	0.97	-	0.49	0.97
836	136.97	26.42	15.41	8.18	35.85	2.20	5.35	3.77	-	0.94	-	-	-
840	137.86	26.83	20.87	5.96	33.88	3.25	2.17	2.98	-	1.36	-	0.81	0.27

844	139.02	28.88	21.25	5.18	29.97	4.36	4.09	3.27	-	0.54	-	0.54	-
848	140.19	27.14	16.57	7.14	34.57	2.00	5.14	2.57	-	1.43	-	0.29	1.43
852	141.35	24.24	16.78	10.72	38.23	2.10	3.96	0.93	0.47	0.70	0.23	-	0.23
856	142.52	22.46	23.51	9.47	35.44	1.05	2.81	2.11	-	2.11	-	-	-
860	143.68	21.90	19.93	9.48	33.66	2.94	4.58	2.61	-	1.31	-	0.33	0.33
864	144.85	22.16	16.89	9.76	39.05	1.58	4.75	0.79	0.26	3.17	-	-	-
868	146.01	27.36	15.42	10.20	34.33	1.49	4.48	1.24	0.50	2.74	-	0.25	0.50
872	147.17	22.36	19.66	11.30	34.15	2.95	3.69	1.72	0.49	2.46	-	-	-
876	148.34	24.56	17.92	9.73	35.40	1.11	5.31	1.33	-	1.55	-	0.44	0.22
880	149.50	21.43	17.50	5.00	44.64	0.71	4.29	2.14	-	1.43	-	-	-

Depth (cm)	Age (ka)	*G. Calida*	*O. universa*	*P. Obliquiloculta*	*G. Minardii*	*G. Siphonifera*	*G. Sacculifer*	*G. Hexagona*	*G. Ungulata*	*G. Crassformis*	*C. Nitida*	*G. Uvula*	*G. Tenellus*
4	11.64	2.63	-	0.26	-	1.32	-	0.53	0.26	-	-	-	-
8	11.67	2.36	0.29	-	0.29	0.59	-	-	-	-	-	-	-
12	11.72	4.52	0.45	-	-	0.45	-	-	-	0.45	0.45	-	-
16	11.78	2.73	0.99	0.25	-	0.74	-	0.74	-	-	-	-	-
20	11.83	4.02	0.62	1.24	-	1.86	-	-	-	-	-	-	-
24	11.94	4.66	-	1.08	-	1.43	-	-	-	1.43	-	-	-
28	12.04	3.74	0.29	0.29	-	-	0.29	-	-	-	-	-	-
32	12.15	3.99	0.33	-	0.33	-	-	0.33	-	-	-	-	-
36	12.25	2.99	0.33	1.00	0.33	0.66	-	-	-	-	-	0.33	0.33
40	12.36	4.02	0.27	-	0.27	0.54	-	0.27	-	-	-	-	-
44	12.94	4.93	0.33	-	0.66	0.99	0.33	0.33	-	-	-	-	-
48	13.53	5.14	0.29	-	0.29	1.14	-	-	-	-	-	-	-
50	13.83	4.38	0.73	-	-	0.36	-	-	-	-	-	-	-
52	14.12	5.51	-	0.50	-	0.50	-	-	-	-	-	-	-
54	14.41	6.41	0.92	-	-	0.46	-	-	-	-	-	-	-
56	14.71	4.24	0.50	-	-	0.25	-	-	-	-	-	-	-
58	15.00	4.72	0.22	-	-	0.22	-	0.22	-	-	-	-	-
60	15.30	5.63	-	0.33	-	0.99	0.66	-	-	-	-	-	-
62	15.47	6.57	-	0.73	0.36	0.73	-	-	-	-	-	-	-
64	15.64	5.01	0.50	-	-	0.25	-	-	-	-	-	-	-
66	15.82	4.55	0.38	-	-	0.76	-	-	-	-	-	-	-
68	15.99	7.02	1.06	-	-	0.43	-	-	-	-	-	-	-
70	16.17	6.04	0.67	-	-	1.34	-	-	-	-	-	-	-
72	16.34	4.95	0.93	0.31	0.31	-	-	-	-	-	-	-	-
74	16.51	4.94	-	-	0.38	1.14	-	-	-	-	-	-	-
76	16.70	4.85	0.73	0.24	-	0.97	-	-	-	-	-	-	-
78	16.89	3.17	-	-	0.24	-	-	-	-	-	-	-	-
80	17.08	4.44	0.68	-	-	-	-	-	-	-	-	-	-
82	17.27	1.95	0.28	0.28	0.84	-	0.28	-	-	-	-	-	-
84	17.46	4.81	0.74	-	-	-	-	-	-	-	-	-	-
86	17.60	5.00	0.31	-	0.31	0.94	-	-	-	-	-	-	-
90	17.79	2.15	0.31	0.62	-	0.31	-	-	-	-	-	-	-
94	17.99	1.13	0.28	-	-	0.85	-	-	-	-	-	-	-
98	18.18	1.64	0.33	-	-	-	-	-	-	0.66	-	-	-
102	18.55	0.94	-	-	-	0.31	-	-	-	0.94	-	-	-
106	19.09	1.55	-	-	-	-	-	-	-	0.62	-	-	-
110	19.64	2.53	-	-	-	-	-	-	-	0.32	-	-	-
114	20.01	2.41	-	-	-	0.27	-	-	-	0.80	-	-	-
118	20.38	1.20	0.30	-	-	-	-	-	-	1.50	-	-	-
122	20.74	4.06	-	-	-	-	-	-	-	0.48	-	-	-
126	21.27	3.02	0.30	-	-	0.30	-	-	-	0.60	-	-	-
130	22.25	2.99	-	-	-	-	-	-	-	1.74	-	-	-
134	23.24	1.40	-	-	-	-	-	-	-	0.70	-	-	-
138	24.22	3.35	-	-	-	-	-	-	-	0.48	-	-	-
142	25.34	2.93	0.29	-	-	-	0.29	-	-	-	-	-	-
146	26.59	3.77	0.34	-	-	-	-	-	-	0.68	-	-	-
326	64.72	2.83	0.22	0.65	-	-	-	-	-	2.40	-	-	-
330	65.67	2.22	-	-	-	0.32	-	-	-	1.58	-	-	-
334	66.62	1.77	-	-	-	-	-	-	-	1.77	-	-	-

338	67.57	3.06	0.83	-	-	0.28	-	-	-	0.83	-	-	-
342	68.52	1.63	0.65	-	-	0.33	-	-	-	1.30	-	-	-
346	69.47	1.69	-	-	0.28	0.28	-	-	-	0.85	-	-	-
350	70.42	5.74	-	0.27	0.55	0.55	-	-	-	1.09	-	-	-
352	70.90	3.02	0.50	0.50	-	-	-	-	-	0.76	-	-	-
354	71.37	5.26	-	0.26	0.26	-	0.26	-	-	1.84	-	-	-
356	71.85	2.26	-	-	0.21	0.21	-	-	-	0.21	-	-	-
358	72.08	4.19	-	-	-	0.25	-	-	-	0.74	-	-	-
360	72.31	4.04	-	-	-	-	-	-	-	-	-	-	-
362	72.54	5.49	-	-	0.24	-	-	-	-	0.24	-	-	-
364	72.77	4.35	-	-	0.69	0.69	-	-	-	0.23	-	-	-
366	73.01	4.28	0.53	-	-	0.27	-	-	-	-	-	-	-
370	73.47	4.32	0.33	-	0.33	-	-	-	-	-	-	-	-
374	73.94	6.04	-	-	0.91	-	-	-	-	-	-	-	-
378	74.40	4.75	0.32	-	0.32	0.32	-	-	-	-	-	-	0.63
382	74.86	4.85	-	0.26	0.26	-	-	-	-	-	-	-	-
386	75.33	4.27	-	-	-	0.22	-	-	-	-	-	-	-
390	75.79	5.50	0.65	0.32	-	0.32	0.32	-	-	0.65	-	-	-
394	76.26	3.95	0.56	0.56	0.28	0.28	0.28	-	-	-	-	-	-
398	76.72	1.99	-	0.22	0.88	0.22	-	-	-	0.66	-	-	-
402	77.19	4.44	0.32	-	0.63	-	-	-	-	0.95	-	-	-
406	77.65	6.30	-	0.27	0.55	0.55	-	-	-	0.55	-	-	-
702	115.52	3.23	0.25	0.50	1.74	0.99	-	-	-	1.24	-	-	-
706	116.20	2.36	0.64	-	1.29	0.21	-	-	-	1.50	-	-	-
710	116.87	1.81	2.26	0.23	1.36	0.45	0.45	-	-	2.26	-	-	-
714	117.54	1.91	0.64	1.27	1.06	0.42	0.21	-	-	0.85	-	-	-
736	118.21	2.22	1.39	0.56	0.83	0.56	-	-	-	0.28	-	-	-
740	118.88	1.82	1.04	-	0.26	0.26	-	-	-	1.30	-	-	-
744	119.55	1.75	0.88	0.29	0.29	-	-	0.29	-	0.58	-	-	-
748	120.22	0.58	0.87	0.29	0.58	0.58	-	-	-	0.58	-	-	-
752	120.90	2.24	1.12	0.22	0.22	1.12	0.22	0.22	-	1.12	-	-	-
756	121.57	1.86	0.93	0.47	0.23	0.47	-	0.23	-	0.93	-	0.23	-
760	122.24	3.26	0.65	0.98	0.33	0.98	0.33	-	-	-	-	-	-
764	122.91	2.67	0.21	-	0.41	0.41	-	-	-	0.41	-	-	-
768	123.58	1.63	0.65	-	-	0.33	-	-	-	0.98	-	-	-
772	124.25	0.78	0.78	-	0.26	0.52	0.26	-	-	0.26	-	-	-
776	124.92	2.36	1.77	-	0.29	0.29	-	-	-	0.29	-	-	-
780	125.60	1.67	0.24	-	-	-	0.72	0.24	-	0.24	-	-	-
784	126.27	0.55	0.82	-	-	-	-	-	-	0.27	-	-	-
788	126.94	2.07	0.21	0.41	-	0.62	-	-	-	-	-	-	-
792	127.61	1.24	0.83	0.21	-	-	-	-	-	0.41	-	-	-
796	128.28	1.86	1.55	-	-	0.31	-	-	-	0.62	-	-	-
800	128.95	1.17	0.70	0.23	0.23	0.94	-	-	-	0.47	-	-	-
804	129.84	1.76	1.01	-	-	0.50	0.25	-	-	0.25	-	-	-
808	130.73	0.29	0.29	-	-	0.29	-	-	-	0.59	-	-	-
812	131.62	3.05	1.11	-	-	0.83	-	-	-	-	-	-	-
816	132.52	0.58	-	-	-	0.29	-	-	-	-	0.29	-	-
820	133.41	0.30	1.50	-	-	0.30	-	-	-	0.30	-	-	-
824	134.30	1.47	0.73	-	-	0.49	-	-	-	1.47	-	-	-
828	135.19	1.20	-	-	-	-	-	-	-	0.30	-	-	-
832	136.08	0.49	0.49	-	-	0.24	-	-	-	-	-	-	-
836	136.97	0.63	0.94	-	-	-	-	-	-	-	-	-	-
840	137.86	0.54	0.81	-	-	-	0.27	-	-	-	-	-	-
844	139.02	0.82	0.54	-	-	0.27	-	-	-	-	-	-	-
848	140.19	1.14	-	0.29	-	-	-	-	-	-	-	-	-
852	141.35	0.47	0.93	-	-	-	-	-	-	-	-	-	-
856	142.52	0.35	0.70	-	-	-	-	-	-	-	-	-	-

860	143.68	0.98	0.98	-	0.33	-	-	-	-	-	-	-	-
864	144.85	0.79	0.53	-	-	-	-	-	-	-	-	-	-
868	146.01	0.25	0.25	-	0.25	0.25	-	-	-	0.25	-	-	-
872	147.17	-	0.25	-	-	-	-	-	-	-	-	-	-
876	148.34	1.11	0.66	-	-	-	-	-	-	-	-	-	-
880	149.50	0.71	1.07	-	-	-	-	-	-	-	-	-	-

Depth (cm)	Age (kyr)	*G. conglobatus*	*O. bilobata*	*S. dehiscens*	*G. cavernula*	*Globerigina spp.*	Agulhas Leakage Fauna	North of STF Only Taxa	STF / Tr. Taxa	% N. pachyderma (dex) ratio	Position of STF
4	11.64	-	-	-	-	1.58	8.16	5.00	15.79	96.15	0.12
8	11.67	-	-	-	-	1.18	8.85	5.31	14.16	93.02	0.10
12	11.72	-	-	-	-	1.36	13.35	4.07	24.66	89.83	0.14
16	11.78	-	-	-	-	0.99	13.15	5.71	20.60	92.16	0.11
20	11.83	-	-	-	-	1.24	13.93	7.74	19.50	93.02	0.10
24	11.94	-	-	-	-	0.36	18.28	8.96	24.73	91.04	0.10
28	12.04	-	-	-	-	0.29	14.37	4.89	21.26	92.31	0.10
32	12.15	-	-	-	-	0.66	10.63	3.99	19.60	92.59	0.09
36	12.25	-	-	-	-	0.33	13.95	6.31	19.93	100.00	0.10
40	12.36	-	-	-	-	-	10.72	5.63	20.64	92.68	0.14
44	12.94	-	-	-	-	0.99	13.49	6.58	21.05	96.67	0.12
48	13.53	-	-	-	-	1.43	12.00	4.29	20.86	97.22	0.10
50	13.83	-	-	-	-	1.09	12.41	2.19	23.72	91.43	0.13
52	14.12	-	-	-	-	0.50	13.28	4.76	24.31	91.49	0.14
54	14.41	-	-	-	-	0.23	9.15	3.66	19.22	91.94	0.08
56	14.71	0.50	-	-	-	0.50	11.97	3.99	20.95	93.55	0.10
58	15.00	-	-	-	-	0.67	7.87	4.49	17.53	92.19	0.11
60	15.30	-	-	-	-	0.33	7.95	6.95	16.89	92.50	0.11
62	15.47	0.36	-	-	-	0.91	10.58	6.02	18.98	81.25	0.09
64	15.64	-	-	-	-	0.25	10.28	4.51	23.31	91.94	0.16
66	15.82	-	-	-	-	0.76	11.74	6.06	20.45	74.29	0.11
68	15.99	-	-	-	-	0.64	10.21	2.77	24.04	93.33	0.15
70	16.17	-	-	-	-	-	14.43	4.03	25.17	88.89	0.12
72	16.34	-	-	-	-	1.55	14.86	4.95	24.46	84.75	0.13
74	16.51	-	-	-	-	0.38	4.18	3.80	17.11	87.63	0.19
76	16.70	-	-	-	-	0.24	10.92	3.88	19.42	89.47	0.10
78	16.89	-	-	-	-	1.46	11.46	3.17	20.24	91.67	0.12
80	17.08	-	-	-	-	1.54	9.73	2.39	18.60	94.03	0.08
82	17.27	-	-	-	-	0.56	8.64	2.51	13.93	89.91	0.09
84	17.46	-	-	-	-	1.48	6.30	3.70	14.07	92.31	0.06
86	17.60	-	-	-	-	1.88	9.06	2.81	18.13	89.72	0.08
90	17.79	-	-	-	-	0.62	7.69	1.85	12.00	90.48	0.04
94	17.99	-	-	-	-	1.41	6.48	2.54	10.70	93.55	0.06
98	18.18	-	-	-	-	1.32	5.59	1.97	11.18	86.03	0.05
102	18.55	-	-	-	-	0.94	7.50	1.25	11.56	93.43	0.04
106	19.09	-	-	-	-	0.62	4.66	1.55	8.70	88.13	0.03
110	19.64	-	-	-	-	0.32	4.75	0.95	10.13	86.01	0.04
114	20.01	-	-	-	-	0.54	7.51	0.54	11.53	80.71	0.02
118	20.38	-	-	-	-	0.90	4.49	-	8.08	88.27	0.02
122	20.74	-	-	-	-	0.95	7.16	-	12.17	87.18	0.01
126	21.27	-	-	-	-	0.60	8.16	1.81	12.39	84.08	0.02
130	22.25	0.25	-	-	-	1.00	5.22	1.99	10.45	89.29	0.02
134	23.24	-	-	-	-	-	4.56	0.35	7.02	90.84	0.01
138	24.22	0.24	-	-	-	0.48	5.74	4.55	10.53	88.04	0.03
142	25.34	-	-	-	-	0.59	6.45	1.76	9.09	95.03	-
146	26.59	-	-	-	-	0.86	5.48	1.03	10.27	87.67	0.01
326	64.72	-	-	-	-	1.09	6.97	1.74	13.29	80.13	0.04
330	65.67	-	-	-	-	0.63	3.80	2.22	9.18	79.44	0.02
334	66.62	-	-	-	-	-	3.89	2.12	10.60	75.56	0.06

338	67.57	-	-	-	-	1.94	7.50	2.78	12.50	82.39	0.02
342	68.52	-	-	-	-	0.98	8.47	3.91	13.03	89.08	0.02
346	69.47	-	-	-	-	0.28	7.04	2.54	10.42	80.77	0.02
350	70.42	-	-	-	-	0.55	8.20	3.83	16.39	86.13	0.05
352	70.90	-	-	-	-	0.25	5.79	3.27	12.85	88.71	0.05
354	71.37	-	-	-	-	0.79	5.53	2.11	14.74	90.51	0.05
356	71.85	-	-	-	-	1.03	5.54	2.67	12.11	89.40	0.07
358	72.08	-	-	-	-	-	5.17	0.99	11.82	94.41	0.03
360	72.31	-	-	-	-	0.85	5.53	4.04	11.06	96.15	0.03
362	72.54	-	-	-	-	-	6.68	4.06	13.60	95.00	0.03
364	72.77	-	-	-	-	0.46	5.72	5.95	10.53	92.26	0.03
366	73.01	-	-	-	-	1.07	6.95	4.81	13.10	94.12	0.03
370	73.47	-	-	-	-	1.99	8.31	4.65	14.29	93.02	0.04
374	73.94	-	-	-	-	0.30	7.55	4.23	17.52	95.50	0.09
378	74.40	-	-	-	-	0.32	8.23	4.43	13.92	92.38	0.03
382	74.86	-	-	-	-	1.53	7.40	4.08	14.80	95.49	0.06
386	75.33	-	-	-	-	0.67	5.39	4.72	13.03	94.64	0.06
390	75.79	-	-	-	-	1.29	6.15	5.50	15.21	96.97	0.07
394	76.26	-	-	-	-	1.13	6.21	4.24	12.71	93.23	0.06
398	76.72	-	-	-	-	-	8.41	2.21	14.82	96.85	0.09
402	77.19	-	-	-	-	1.90	6.98	6.35	14.60	94.95	0.05
406	77.65	-	-	-	-	1.37	6.58	5.75	15.89	93.97	0.08
702	115.52	-	-	-	-	0.50	13.40	7.94	23.57	93.22	0.19
706	116.20	-	-	-	-	0.86	10.94	7.30	21.46	93.98	0.17
710	116.87	-	-	-	-	0.45	12.22	9.73	20.59	95.71	0.17
714	117.54	-	-	-	-	0.21	10.81	9.75	19.49	88.51	0.19
736	118.21	-	0.28	-	-	-	12.50	4.44	20.28	91.49	0.13
740	118.88	-	-	-	-	0.26	9.11	4.43	22.14	100.00	0.21
744	119.55	-	-	-	-	0.58	14.04	4.68	24.27	93.75	0.21
748	120.22	-	-	-	-	0.29	11.59	6.67	15.65	100.00	0.12
752	120.90	-	-	-	-	-	14.13	5.16	21.75	97.87	0.16
756	121.57	-	-	-	-	0.70	9.30	6.51	15.58	98.44	0.11
760	122.24	-	-	-	-	0.33	10.10	7.82	14.66	98.04	0.07
764	122.91	0.41	-	0.21	-	-	8.44	10.70	10.49	94.81	0.04
768	123.58	-	-	-	-	0.33	9.15	9.80	12.75	94.34	0.08
772	124.25	-	-	-	-	0.52	8.62	5.48	13.32	98.41	0.11
776	124.92	-	-	-	-	-	9.14	6.19	13.27	86.42	0.06
780	125.60	-	-	-	0.24	0.24	8.11	6.21	10.98	92.78	0.07
784	126.27	-	-	-	-	-	5.74	5.74	7.92	87.37	0.06
788	126.94	-	-	-	-	-	7.25	3.52	11.39	86.51	0.07
792	127.61	-	-	-	-	0.83	6.20	4.13	10.54	83.20	0.05
796	128.28	-	-	-	-	0.62	4.35	4.04	11.49	85.39	0.10
800	128.95	0.23	-	-	-	-	7.75	5.16	15.73	85.44	0.14
804	129.84	-	-	-	-	0.25	4.27	4.02	14.32	92.86	0.14
808	130.73	-	-	-	-	0.59	5.31	3.24	12.09	87.62	0.10
812	131.62	-	-	-	-	1.11	9.97	6.65	17.73	88.89	0.14
816	132.52	-	-	-	-	0.58	8.75	4.37	15.74	87.88	0.12
820	133.41	-	-	-	-	1.20	8.98	4.79	13.77	89.29	0.10
824	134.30	-	-	-	-	0.98	7.33	3.42	14.18	88.15	0.07
828	135.19	-	-	-	-	0.90	5.71	4.80	10.51	83.96	0.07
832	136.08	-	-	-	-	0.49	5.83	5.34	8.01	84.93	0.05
836	136.97	-	-	-	-	0.31	6.29	3.77	9.12	81.43	0.04
840	137.86	-	-	-	-	-	4.34	4.07	7.05	85.03	0.06
844	139.02	-	-	-	-	0.27	5.45	4.09	9.81	85.27	0.08
848	140.19	-	-	-	-	0.29	7.14	2.86	9.71	82.88	0.04
852	141.35	-	-	-	-	-	5.13	1.40	7.93	78.10	0.04
856	142.52	-	-	-	-	-	3.51	2.11	4.91	78.91	0.02

860	143.68	-	-	-	-	0.65	6.54	3.27	9.80	78.03	0.05
864	144.85	-	-	-	-	0.26	5.28	1.06	7.65	80.00	0.03
868	146.01	-	-	-	-	0.25	5.97	2.49	7.21	77.09	0.03
872	147.17	-	-	-	-	0.98	3.93	2.21	6.88	75.14	0.05
876	148.34	-	-	-	-	0.66	6.64	1.77	8.41	78.43	0.02
880	149.50	-	-	-	-	1.07	5.36	2.14	6.79	89.93	0.01

Appendix D: MD02-2589 Stable Isotopes, Mean Sortable Silt and IRD

Depth (cm)	Age (ka)	Benthic $\delta^{18}O$ (Uvigerina corrected) (‰)	Benthic $\delta^{13}C$ (‰)	Planktonic $\delta^{18}O$ (‰)	Planktonic $\delta^{13}C$ (‰)	Mean Sortable Silt (μm)	IRD Quartz (grains/gm)	Total IRD (grains/gm)
1	11.61	-	-	-	-	18.72	-	-
2	11.62	-	-	-	-	20.48	0.00	0.00
3	11.63	-	-	-	-	20.02	-	-
4	11.64	-	-	-	-	20.00	0.00	1.70
5	11.65	-	-	-	-	21.27	-	-
6	11.66	-	-	-	-	20.67	4.70	4.70
7	11.67	-	-	-	-	20.86	-	-
8	11.67	3.77	0.46	1.27	-0.98	17.80	4.38	5.92
9	11.68	-	-	-	-	20.87	-	-
10	11.69	-	-	0.89	-0.70	20.33	0.84	0.84
11	11.71	-	-	-	-	20.62	-	-
12	11.72	-	-	0.79	-1.22	19.96	0.00	0.00
13	11.73	-	-	-	-	21.14	-	-
14	11.75	-	-	0.85	-1.21	20.84	0.00	0.00
15	11.76	-	-	-	-	20.42	-	-
16	11.78	4.67	0.50	-	-	19.83	0.00	0.66
17	11.79	-	-	-	-	21.56	-	-
18	11.80	-	-	0.88	-1.05	20.62	1.79	1.79
19	11.82	-	-	-	-	19.29	-	-
20	11.83	4.37	0.48	1.54	-1.08	19.71	3.66	5.33
21	11.86	-	-	-	-	19.46	-	-
22	11.89	4.36	0.53	1.79	-1.04	20.16	4.52	7.08
23	11.91	-	-	-	-	20.33	-	-
24	11.94	-	-	1.43	-1.24	20.01	1.40	1.40
25	11.96	-	-	-	-	19.58	-	-
26	11.99	-	-	-	-	18.49	0.00	2.98
27	12.02	-	-	-	-	21.27	-	-
28	12.04	-	-	0.79	-1.11	20.27	0.00	0.00
29	12.07	-	-	-	-	21.61	-	-
30	12.09	3.86	0.68	0.81	-1.15	19.58	1.80	1.80
31	12.12	-	-	-	-	20.43	-	-
32	12.15	3.83	0.60	0.98	-1.07	20.91	0.00	0.00
33	12.17	-	-	-	-	21.64	-	-
34	12.20	3.92	0.60	0.69	-1.18	21.29	1.51	3.80
35	12.23	-	-	-	-	20.83	-	-
36	12.25	-	-	-	-	21.37	0.00	0.00
37	12.28	-	-	-	-	21.40	-	-
38	12.30	3.81	0.58	0.82	-1.52	21.05	0.84	0.84
39	12.33	-	-	-	-	21.35	-	-
40	12.36	4.10	0.48	-	-	20.46	0.91	0.91
41	12.50	-	-	-	-	-	-	-
42	12.65	4.32	0.52	0.82	-1.71	20.84	0.00	0.00
43	12.80	-	-	-	-	21.30	-	-
44	12.94	-	-	1.09	-1.37	20.96	0.79	0.79
45	13.09	-	-	-	-	21.48	-	-
46	13.24	-	-	-	-	20.99	0.00	1.52
47	13.39	-	-	-	-	21.50	-	-

48	13.53	3.80	0.33	0.97	-1.66	20.89	3.41	6.00
49	13.68	-	-	-	-	19.32	-	-
50	13.83	4.17	0.51	-	-	20.86	1.56	1.56
51	13.97	-	-	-	-	18.82	-	-
52	14.12	4.21	0.50	1.31	-1.35	19.53	0.00	0.00
53	14.27	-	-	-	-	20.97	-	-
54	14.41	4.30	0.56	1.08	-1.71	20.99	0.00	0.00
55	14.56	-	-	-	-	20.99	-	-
56	14.71	4.58	0.29	1.55	-1.22	21.13	0.00	0.00
57	14.85	-	-	-	-	20.48	-	-
58	15.00	4.43	0.35	1.15	-1.71	20.17	0.45	0.45
59	15.15	-	-	-	-	19.96	-	-
60	15.30	4.35	0.52	-	-	21.00	0.00	0.00
61	15.38	-	-	-	-	21.19	-	-
62	15.47	4.34	0.26	1.15	-1.85	20.89	0.00	0.00
63	15.56	-	-	-	-	19.65	-	-
64	15.64	4.04	0.54	1.58	-1.32	-	1.21	1.57
65	15.73	-	-	-	-	20.24	-	-
66	15.82	4.49	0.40	-	-	19.17	0.00	0.00
67	15.90	-	-	-	-	20.28	-	-
68	15.99	4.39	0.36	1.16	-1.96	21.40	0.96	0.96
69	16.08	-	-	-	-	20.40	-	-
70	16.17	4.82	0.19	1.58	-1.33	20.59	0.00	0.00
71	16.25	-	-	-	-	-	-	-
72	16.34	4.68	0.44	1.64	-1.18	20.52	2.70	5.12
73	16.43	-	-	-	-	20.82	-	-
74	16.51	4.46	0.49	1.07	-1.84	20.35	0.00	0.00
75	16.60	-	-	-	-	19.20	-	-
76	16.70	4.58	0.50	-	-	20.58	0.00	0.99
77	16.79	-	-	-	-	19.57	-	-
78	16.89	4.79	0.43	1.36	-1.82	20.15	0.00	0.00
79	16.98	-	-	-	-	20.02	-	-
80	17.08	4.61	0.17	1.38	-1.62	20.29	1.08	2.25
81	17.17	-	-	-	-	19.89	-	-
82	17.27	4.72	0.34	1.62	-1.40	19.93	0.96	0.96
83	17.36	-	-	-	-	20.92	-	-
84	17.46	4.74	0.32	1.48	-1.71	20.13	9.42	9.42
85	17.55	-	-	-	-	20.46	-	-
86	17.60	5.13	0.25	-	-	20.57	4.92	5.88
87	17.65	-	-	-	-	19.77	-	-
88	17.70	4.87	0.16	1.64	-1.58	20.16	1.52	3.85
89	17.75	-	-	-	-	19.61	-	-
90	17.79	5.07	0.16	1.81	-1.53	-	0.00	0.00
91	17.84	-	-	-	-	20.63	-	-
92	17.89	5.18	0.13	1.96	-1.45	20.10	1.50	1.50
93	17.94	-	-	-	-	19.96	-	-
94	17.99	5.12	0.08	1.98	-1.33	19.33	1.02	3.09
95	18.03	-	-	-	-	20.99	-	-
96	18.08	5.29	0.14	-	-	20.98	2.21	3.43
97	18.13	-	-	-	-	20.36	-	-
98	18.18	4.77	0.27	2.31	-1.25	20.93	0.82	1.50
99	18.23	-	-	-	-	20.15	-	-
100	18.27	5.27	0.11	2.06	-1.54	19.80	0.00	1.36
101	18.41	-	-	-	-	20.42	-	-
102	18.55	4.73	0.01	2.12	-1.26	19.98	4.75	4.75
103	18.68	-	-	-	-	20.31	-	-
104	18.82	5.24	-0.04	2.06	-1.26	20.26	3.81	5.72
105	18.96	-	-	-	-	20.78		

106	19.09	5.15	0.37	-	-	21.63	5.85	5.85
107	19.23	-	-	-	-	21.21	-	-
108	19.37	5.21	0.04	2.06	-1.29	20.91	4.36	7.26
109	19.50	-	-	-	-	21.04	-	-
110	19.64	5.69	-0.07	2.09	-1.21	21.17	2.94	4.42
111	19.73	-	-	-	-	20.94	-	-
112	19.82	5.21	0.11	2.00	-1.35	20.84	2.04	4.08
113	19.92	-	-	-	-	-	-	-
114	20.01	5.25	0.15	2.34	-1.26	21.51	0.00	1.37
115	20.10	-	-	-	-	22.72	-	-
116	20.19	5.41	0.05	-	-	20.05	2.23	2.23
117	20.28	-	-	-	-	20.90	-	-
118	20.38	5.41	0.09	1.96	-1.32	20.57	7.14	11.42
119	20.47	-	-	-	-	20.97	-	-
120	20.56	5.45	-0.06	1.96	-1.35	20.10	1.31	5.24
121	20.65	-	-	-	-	20.39	-	-
122	20.74	5.24	0.13	2.18	-1.36	20.26	5.83	11.67
123	20.84	-	-	-	-	20.28	-	-
124	20.93	5.21	0.03	2.33	-0.96	22.07	3.84	8.97
125	21.02	-	-	-	-	21.77	-	-
126	21.27	5.43	0.01	-	-	21.47	3.08	7.69
127	21.51	-	-	-	-	21.51	-	-
128	21.76	5.28	0.00	2.09	-1.18	22.12	1.76	5.29
129	22.01	-	-	-	-	22.96	-	-
130	22.25	5.37	0.08	2.25	-1.19	23.83	0.00	10.61
131	22.50	-	-	-	-	24.20	-	-
132	22.74	5.23	-0.01	2.18	-0.88	19.29	2.17	8.66
133	22.99	-	-	-	-	-	-	-
134	23.24	5.12	0.08	2.08	-1.06	20.48	6.39	16.61
135	23.48	-	-	-	-	-	-	-
136	23.73	5.31	0.04	-	-	20.38	5.85	16.08
137	23.97	-	-	-	-	-	-	-
138	24.22	-	-	2.06	-0.97	21.46	7.27	20.61
139	24.47	-	-	-	-	-	-	-
140	24.71	5.14	0.09	1.98	-1.20	21.67	6.28	10.05
141	25.03	-	-	-	-	21.51	-	-
142	25.34	5.14	0.12	2.08	-0.94	21.82	2.52	8.83
143	25.65	-	-	-	-	-	-	-
144	25.97	5.31	0.04	2.21	-1.15	20.89	2.68	8.03
145	26.28	-	-	-	-	-	-	-
146	26.59	5.13	0.06	-	-	22.16	0.00	8.11
147	26.91	-	-	-	-	-	-	-
148	27.22	-	-	2.15	-1.12	20.32	1.38	12.44
149	27.53	-	-	-	-	-	-	-
150	27.85	5.29	0.04	2.01	-1.14	21.01	1.26	5.05
151	28.16	-	-	-	-	18.01	-	-
152	28.47	5.25	0.05	2.07	-1.06	21.66	1.38	9.67
153	28.79	-	-	-	-	-	-	-
154	29.10	4.99	0.07	2.07	-1.22	22.24	4.87	6.49
155	29.42	-	-	-	-	-	-	-
156	29.73	5.24	0.06	-	-	22.81	3.74	12.46
157	30.04	-	-	-	-	-	-	-
158	30.36	5.18	0.09	2.25	-0.71	22.15	4.23	11.62
159	30.67	-	-	-	-	-	-	-
160	30.98	5.05	0.09	2.01	-0.89	20.77	3.62	10.86
161	31.30	-	-	-	-	22.45	-	-
162	31.61	-	-	2.13	-0.75	22.84	3.23	12.92
163	31.92	-	-	-	-	-	-	-

164	32.24	4.85	0.35	2.28	-0.78	20.13	6.31	12.62
165	32.55	-	-	-	-	-	-	-
166	32.86	5.09	0.02	-	-	23.31	7.76	19.40
167	33.18	-	-	-	-	-	-	-
168	33.49	5.10	0.30	2.01	-0.93	23.74	12.77	31.35
169	33.80	-	-	-	-	-	-	-
170	34.12	5.06	0.05	1.86	-0.96	22.75	9.00	18.00
171	34.38	-	-	-	-	-	-	-
172	34.64	5.10	0.32	1.92	-0.94	23.28	6.96	12.19
173	34.91	-	-	-	-	-	-	-
174	35.17	4.97	0.24	1.79	-1.21	21.60	10.41	11.71
175	35.43	-	-	-	-	-	-	-
176	35.70	5.13	0.36	-	-	23.59	2.13	8.54
177	35.96	-	-	-	-	-	-	-
178	36.23	4.96	0.20	2.31	-0.49	22.92	23.27	29.09
179	36.49	-	-	-	-	-	-	-
180	36.75	4.90	0.31	2.19	-0.72	21.86	8.41	15.77
181	37.02	-	-	-	-	22.99	-	-
182	37.28	5.05	0.01	2.08	-0.99	23.32	11.39	27.05
183	37.54	-	-	-	-	-	-	-
184	37.81	4.74	0.24	2.11	-0.71	22.67	8.27	10.34
185	38.07	-	-	-	-	-	-	-
186	38.33	4.93	0.51	-	-	23.38	8.48	9.43
187	38.60	-	-	-	-	-	-	-
188	38.86	5.00	0.47	1.79	-0.85	22.22	12.46	16.20
189	39.12	-	-	-	-	-	-	-
190	39.39	4.85	0.05	2.03	-0.66	20.98	12.02	16.03
191	39.54	-	-	-	-	21.38	-	-
192	39.70	4.77	0.26	1.96	-0.72	21.15	11.11	12.35
193	39.85	-	-	-	-	-	-	-
194	40.01	-	-	1.73	-1.02	22.10	23.85	25.84
195	40.16	-	-	-	-	-	-	-
196	40.31	5.06	0.44	-	-	22.80	25.27	26.48
197	40.47	-	-	-	-	-	-	-
198	40.62	4.76	0.34	2.02	-0.76	22.04	24.07	32.09
199	40.78	-	-	-	-	-	-	-
200	40.93	4.68	0.29	1.81	-0.70	21.34	10.86	11.85
201	41.09	-	-	-	-	22.58	-	-
202	41.24	5.09	0.34	1.56	-1.00	22.25	14.13	17.27
203	41.40	-	-	-	-	-	-	-
204	41.55	4.83	0.33	1.97	-0.80	21.26	21.46	22.48
205	41.70	-	-	-	-	-	-	-
206	41.86	4.96	0.32	-	-	20.04	23.45	26.38
207	42.01	-	-	-	-	-	-	-
208	42.17	4.61	0.14	1.71	-0.65	22.11	19.66	20.70
209	42.32	-	-	-	-	-	-	-
210	42.48	4.86	0.33	1.61	-0.93	22.97	30.50	30.50
211	42.63	-	-	-	-	23.10	-	-
212	42.79	-	-	1.73	-0.71	22.26	18.00	18.00
213	42.94	-	-	-	-	-	-	-
214	43.09	-	-	1.98	-0.74	22.01	9.56	10.62
215	43.25	-	-	-	-	-	-	-
216	43.40	4.80	0.43			21.47	7.18	8.21
217	43.56	-	-	-	-	-	-	-
218	43.71	4.85	0.63	2.12	-0.49	20.89	5.47	5.47
219	43.87	-	-	-	-	-	-	-
220	44.02	4.70	0.53	2.09	-1.14	21.35	1.12	1.12
221	44.18	-	-	-	-	21.09	-	-

222	44.33	4.87	0.43	1.44	-0.94	19.96	1.14	2.29
223	44.48	-	-	-	-	-	-	-
224	44.64	4.71	0.28	1.89	-0.69	20.26	1.98	3.95
225	44.79	-	-	-	-	-	-	-
226	44.95	4.81	0.42	1.69	-0.97	20.45	1.83	1.83
227	45.10	-	-	-	-	-	-	-
228	45.26	4.67	0.45	1.54	-0.82	20.06	3.26	3.26
229	45.41	-	-	-	-	-	-	-
230	45.57	4.66	0.53	1.70	-0.57	20.85	1.18	1.18
231	45.72					20.12	-	-
232	45.87	4.75	0.29	1.55	-0.77	21.40	1.97	1.97
233	46.03	-	-	-	-	-	-	-
234	46.18	4.96	0.29	1.96	-0.61	21.05	0.94	0.94
235	46.34	-	-	-	-	-	-	-
236	46.49	-	-	-	-	21.03	2.21	4.42
237	46.65	-	-	-	-	-	-	-
238	46.80	4.81	0.38	1.91	-0.69	21.11	3.00	3.00
239	46.96	-	-	-	-	-	-	-
240	47.11	4.69	0.33	1.81	-0.69	20.05	1.20	2.40
241	47.26	-	-	-	-	-	-	-
242	47.42	4.72	0.39	1.67	-0.89	19.49	1.06	1.06
243	47.57	-	-	-	-	-	-	-
244	47.73	4.80	0.33	1.82	-0.71	20.06	0.00	0.00
245	47.88	-	-	-	-	-	-	-
246	48.04	4.76	0.21	-	-	21.13	0.89	0.89
247	48.19	-	-	-	-	-	-	-
248	48.35	4.67	0.16	1.72	-0.64	20.61	4.53	6.04
249	48.50	-	-	-	-	-	-	-
250	48.65	4.76	0.01	1.75	-0.73	20.74	3.39	4.53
251	48.81	-	-	-	-	-	-	-
252	48.96	4.93	0.20	1.95	-0.58	20.61	1.00	1.00
253	49.12	-	-	-	-	-	-	-
254	49.27	4.88	0.18	1.85	-0.79	20.29	1.90	2.86
255	49.43	-	-	-	-	-	-	-
256	49.58	4.78	0.40	-	-	21.68	4.95	5.77
257	49.74	-	-	-	-	-	-	-
258	49.89	4.80	0.55	1.78	-0.96	19.85	3.60	4.80
259	50.04	-	-	-	-	-	-	-
260	50.20	4.81	0.23	1.78	-0.95	20.10	2.27	2.27
261	50.35	-	-	-	-	20.57	-	-
262	50.51	-	-	1.65	-0.79	19.44	3.83	5.11
263	50.66	-	-	-	-	-	-	-
264	50.82	4.72	0.36	1.72	-0.79	20.30	1.98	2.97
265	50.97	-	-	-	-	20.92	-	-
266	51.13	4.89	0.34	-	-	21.63	0.87	0.87
267	51.28	-	-	-	-	-	-	-
268	51.43	4.81	0.50	1.84	-0.89	20.46	2.13	4.27
269	51.59	-	-	-	-	-	-	-
270	51.74	4.86	0.40	1.62	-1.04	19.57	0.87	0.87
271	51.90					20.31	-	-
272	52.05	4.87	0.23	1.58	-0.88	21.15	0.00	0.00
273	52.21	-	-	-	-	-	-	-
274	52.36	4.91	0.23	1.65	-0.83	-	0.00	0.00
275	52.60	-	-	-	-	-	-	-
276	52.84	4.61	0.28	-	-	20.13	2.88	3.84
277	53.07	-	-	-	-	-	-	-
278	53.31	4.75	0.28	1.71	-1.07	-	0.92	0.92
279	53.55	-	-	-	-	-	-	-

280	53.79	-	-	1.54	-1.04	20.75	8.18	9.09
281	54.02	-	-	-	-	21.07		
282	54.26	4.84	0.29	1.95	-0.88	19.89	2.15	3.23
283	54.50	-	-	-	-	-	-	-
284	54.74	4.87	0.32	1.89	-0.81	21.90	3.86	5.79
285	54.98			-	-	21.82	-	-
286	55.21	4.83	0.32	-	-	21.84	4.89	8.80
287	55.45	-	-	-	-	-	-	-
288	55.69	4.79	0.08	1.76	-1.15	22.02	5.78	5.78
289	55.93	-	-	-	-	-	-	-
290	56.16	-	-	1.78	-1.03	22.02	11.25	13.13
291	56.40	-	-	-	-	19.89	-	-
292	56.64	4.85	0.27	1.56	-1.16	22.06	6.98	7.85
293	56.88	-	-	-	-	-	-	-
294	57.11	4.95	0.26	-	-	21.27	5.93	7.91
295	57.35	-	-	-	-	-	-	-
296	57.59	4.80	0.38	-	-	22.40	8.72	15.69
297	57.83	-	-	-	-	-	-	-
298	58.06	4.96	0.46	1.73	-1.10	22.35	7.83	10.77
299	58.30	-	-	-	-	-	-	-
300	58.54	4.98	0.11	1.59	-0.98	21.04	13.79	18.72
301	58.78					21.83	-	-
302	59.01	4.85	0.32	1.43	-1.40	22.44	8.62	9.58
303	59.25	-	-	-	-	-	-	-
304	59.49	4.91	0.19	1.64	-1.07	20.96	13.98	14.98
305	59.73	-	-	-	-	-	-	-
306	59.97	5.05	0.13	-	-	22.00	13.28	15.17
307	60.20	-	-	-	-	-	-	-
308	60.44	4.88	0.22	1.67	-1.08	21.51	9.62	12.03
309	60.68	-	-	-	-	-	-	-
310	60.92	5.08	0.05	1.48	-1.25	19.92	12.90	19.85
311	61.15	-	-	-	-	20.60	-	-
312	61.39	4.81	-0.02	1.70	-1.40	21.37	6.80	8.50
313	61.63	-	-	-	-	-	-	-
314	61.87	5.06	0.01	1.88	-1.05	21.84	10.07	12.39
315	62.10	-	-	-	-	-	-	-
316	62.34	5.21	-0.15	-	-	21.93	9.52	17.13
317	62.58	-	-	-	-	-	-	-
318	62.82	5.16	-0.15	2.05	-1.09	22.03	12.46	17.45
319	63.05	-	-	-	-	-	-	-
320	63.29	-	-	2.27	-1.00	21.79	6.87	14.72
321	63.53	-	-	-	-	21.58	-	-
322	63.77	5.14	-0.11	2.21	-0.98	21.70	9.38	17.06
323	64.00	-	-	-	-	-	-	-
324	64.24	5.02	-0.06	2.11	-0.94	21.65	4.21	11.78
325	64.48	-	-	-	-	-	-	-
326	64.72	4.97	0.08	-	-	22.20	9.14	15.53
327	64.96	-	-	-	-	-	-	-
328	65.19	5.11	-0.05	2.10	-0.87	21.36	6.19	10.62
329	65.43	-	-	-	-	-	-	-
330	65.67	5.12	0.05	2.22	-0.71	20.50	8.67	15.60
331	65.91	-	-	-	-	22.12	-	-
332	66.14	4.98	-0.06	2.23	-0.77	20.21	10.58	22.22
333	66.38	-	-	-	-	-	-	-
334	66.62	5.13	-0.14	2.31	-0.81	22.65	10.99	14.38
335	66.86	-	-	-	-	-	-	-
336	67.09	5.07	0.00	-	-	21.82	9.24	15.11
337	67.33	-	-	-	-	-	-	-

338	67.57	5.06	0.24	2.07	-1.06	22.06	11.63	26.58
339	67.81	-	-	-	-	-	-	-
340	68.04	4.93	0.01	2.61	-0.15	20.71	10.73	17.88
341	68.28	-	-	-	-	23.17	-	-
342	68.52	4.84	0.01	2.05	-0.93	22.69	27.88	43.93
343	68.76	-	-	-	-	-	-	-
344	68.99	5.15	-0.14	2.17	-1.30	22.47	17.46	36.02
345	69.23	-	-	-	-	-	-	-
346	69.47	4.98	0.01	-	-	22.43	25.12	62.81
347	69.71	-	-	-	-	-	-	-
348	69.95	5.10	-0.02	1.98	-0.56	22.56	46.51	81.86
349	70.18	-	-	-	-	-	-	-
350	70.42	5.01	-0.02	1.76	-1.03	22.28	73.82	171.6
351	70.66	-	-	-	-	22.59	-	-
352	70.90	5.06	-0.01	2.18	-0.49	21.33	76.84	228.8
353	71.13	-	-	-	-	-	-	-
354	71.37	5.16	0.10	1.94	-1.05	22.47	27.05	86.83
355	71.61	-	-	-	-	-	-	-
356	71.85	4.97	0.06	-	-	21.84	33.21	51.67
357	71.96	-	-	-	-	-	-	-
358	72.08	4.70	0.37	1.53	-0.95	17.96	6.92	11.24
359	72.19	-	-	-	-	-	-	-
360	72.31	4.75	0.56	1.55	-0.73	19.02	5.28	7.04
361	72.43	-	-	-	-	20.48	-	-
362	72.54	4.53	0.45	1.56	-0.83	19.73	4.02	5.62
363	72.66	-	-	-	-	-	-	-
364	72.77	4.82	0.32	1.90	-0.55	19.99	5.10	7.13
365	72.89	-	-	-	-	-	-	-
366	73.01	4.38	0.76	-	-	19.63	2.66	5.31
367	73.12	-	-	-	-	-	-	-
368	73.24	4.56	0.58	1.38	-0.67	19.87	2.43	3.24
369	73.36	-	-	-	-	-	-	-
370	73.47	4.57	0.58	1.37	-0.63	19.94	2.46	4.11
371	73.59					20.43	-	-
372	73.70	4.65	0.63	1.59	-0.76	19.74	4.66	6.53
373	73.82	-	-	-	-	-	-	-
374	73.94	4.58	0.63	1.49	-0.79	20.40	6.16	6.16
375	74.05	-	-	-	-	-	-	-
376	74.17	4.58	0.74	-	-	18.35	3.59	3.59
377	74.28	-	-	-	-	-	-	-
378	74.40	4.53	0.78	1.29	-0.68	20.24	4.36	4.36
379	74.52	-	-	-	-	-	-	-
380	74.63	4.41	0.52	1.52	-0.56	18.57	2.16	2.16
381	74.75					20.68	-	-
382	74.86	4.52	0.78	1.47	-0.82	19.66	1.86	1.86
383	74.98	-	-	-	-	-	-	-
384	75.10	4.60	0.54	1.20	-0.90	19.99	0.96	1.93
385	75.21	-	-	-	-	-	-	-
386	75.33	4.62	0.63	-	-	18.89	2.23	2.23
387	75.44	-	-	-	-	-	-	-
388	75.56	4.49	0.66	1.46	-0.64	19.44	4.17	4.17
389	75.68	-	-	-	-	-	-	-
390	75.79	4.45	0.60	1.31	-0.73	19.69	2.80	3.74
391	75.91	-	-	-	-	19.38	-	-
392	76.03	4.71	0.52	1.36	-0.70	20.32	8.82	8.82
393	76.14	-	-	-	-	-	-	-
394	76.26	4.49	0.61	1.47	-0.35	18.96	1.12	1.12
395	76.37	-	-	-	-	-	-	-

396	76.49	4.52	0.58	-	-	19.99	2.61	2.61
397	76.61	-	-	-	-	-	-	-
398	76.72	4.40	0.51	1.51	-0.64	19.89	2.75	2.75
399	76.84	-	-	-	-	-	-	-
400	76.95	4.51	0.65	1.47	-0.37	18.78	0.85	0.85
401	77.07	-	-	-	-	20.21	-	-
402	77.19	4.49	0.61	1.39	-0.56	19.51	3.61	5.41
403	77.30	-	-	-	-	-	-	-
404	77.42	4.45	0.65	1.46	-0.38	20.40	4.66	5.43
405	77.53	-	-	-	-	-	-	-
406	77.65	-	-	-	-	19.67	2.01	2.01
407	77.77	-	-	-	-	-	-	-
408	77.88	4.36	0.52	1.44	-0.36	20.34	0.00	0.00
409	78.00	-	-	-	-	-	-	-
410	78.11	4.69	0.37	1.15	-0.72	20.07	1.46	1.46
411	78.23					20.97		
412	78.35	4.67	0.42	1.38	-0.54	20.23	3.01	4.02
413	78.46	-	-	-	-	-	-	-
414	78.58	4.30	0.57	1.31	-0.53	19.73	2.86	2.86
415	78.70	-	-	-	-	-	-	-
416	78.81	4.28	0.58	-	-	20.74	0.00	0.00
417	78.93	-	-	-	-	-	-	-
418	79.04	4.45	0.59	1.15	-0.70	20.15	0.91	1.82
419	79.16	-	-	-	-	-	-	-
420	79.28	4.43	0.51	0.99	-0.76	21.03	0.00	0.00
421	79.39					18.81		
422	79.51	4.33	0.76	1.39	-0.54	19.11	0.00	0.64
423	79.62	-	-	-	-	-	-	-
424	79.74	4.49	0.62	1.19	-0.67	20.20	0.00	0.00
425	79.86	-	-	-	-	-	-	-
426	79.97	4.48	0.47	-	-	21.17	0.00	0.00
427	80.09	-	-	-	-	-	-	-
428	80.20	4.45	0.73	1.17	-0.75	20.33	0.68	1.02
429	80.32	-	-	-	-	-	-	-
430	80.44	4.26	0.61	1.24	-0.68	20.49	0.45	0.45
431	80.55	-	-	-	-	-	-	-
432	80.67	4.47	0.46	1.29	-0.53	20.38	0.00	0.00
433	80.78	-	-	-	-	20.55	-	-
434	80.90	4.54	0.63	0.90	-0.98	20.96	0.00	0.00
435	81.02	-	-	-	-	-	-	-
436	81.13	4.33	0.52	1.44	-0.70	20.78	1.18	1.18
437	81.25	-	-	-	-	-	-	-
438	81.37	4.42	0.86	-	-	20.59	0.00	0.00
439	81.48	-	-	-	-	-	-	-
440	81.60	4.50	0.49	1.20	-0.82	20.07	0.00	0.00
441	81.71	-	-	-	-	20.61	-	-
442	81.83	4.28	0.45	1.11	-0.92	20.01	1.87	1.87
443	81.95	-	-	-	-	-	-	-
444	82.06	-	-	1.05	-0.91	20.50	1.06	1.06
445	82.18	-	-	-	-	-	-	-
446	82.29	4.36	0.49	1.08	-1.22	20.21	0.00	0.00
447	82.41	-	-	-	-	-	-	-
448	82.53	4.44	0.49	-	-	20.39	0.00	0.00
449	82.64	-	-	-	-	-	-	-
450	82.76	4.33	0.71	0.82	-1.19	20.99	0.00	0.00
451	82.87	-	-	-	-	20.89	-	-
452	82.99	-	-	0.99	-1.19	19.95	1.10	1.10
453	83.11	-	-	-	-	-	-	-

454	83.22	4.32	0.63	0.89	-1.23	20.26	1.77	1.77
455	83.34	-	-	-	-	-	-	-
456	83.46	4.35	0.63	1.17	-1.23	-	0.00	0.00
457	83.57	-	-	-	-	-	-	-
458	83.69	4.32	0.36	-	-	20.10	0.00	0.00
459	83.80	-	-	-	-	-	-	-
460	83.92	4.44	0.43	1.34	-0.67	20.69	0.00	0.00
461	84.04	-	-	-	-	20.38	-	-
462	84.15	4.15	0.29	0.95	-1.43	20.49	0.00	0.00
463	84.27	-	-	-	-	-	-	-
464	84.38	4.26	0.47	1.00	-1.21	20.20	1.02	1.02
465	84.50	-	-	-	-	-	-	-
466	84.62	4.56	0.31	1.30	-1.01	20.02	1.94	2.91
467	84.73	-	-	-	-	-	-	-
468	84.85	4.20	0.39	-	-	20.07	2.19	2.19
469	84.96	-	-	-	-	-	-	-
470	85.08	4.48	0.47	0.94	-1.17	19.24	0.00	2.47
471	85.20	-	-	-	-	20.31	-	-
472	85.31	4.32	0.51	1.04	-1.21	20.74	0.00	0.00
473	85.43	-	-	-	-	-	-	-
474	85.54	4.43	0.38	1.02	-1.24	19.88	0.00	0.00
475	85.66	-	-	-	-	-	-	-
476	85.78	4.47	0.49	0.96	-1.34	19.96	0.91	0.91
477	85.89	-	-	-	-	-	-	-
478	86.01	4.46	0.54	-	-	20.34	0.00	0.00
479	86.17	-	-	-	-	-	-	-
480	86.32	4.55	0.50	0.88	-1.44	19.65	2.86	2.86
481	86.48	-	-	-	-	19.91	-	-
482	86.64	4.66	0.30	1.32	-0.80	20.14	1.10	1.10
483	86.79	-	-	-	-	-	-	-
484	86.95	4.66	-0.01	1.37	-0.99	19.98	0.96	0.96
485	87.10	-	-	-	-	-	-	-
486	87.26	4.43	0.55	1.43	-0.82	19.63	2.06	2.06
487	87.42	-	-	-	-	-	-	-
488	87.57	4.69	0.21	-	-	20.28	0.00	0.00
489	87.73	-	-	-	-	-	-	-
490	87.89	4.62	0.60	1.42	-1.04	18.52	0.83	0.83
491	88.04	-	-	-	-	19.41	-	-
492	88.20	-	-	1.27	-1.24	20.40	0.00	0.00
493	88.36	-	-	-	-	-	-	-
494	88.51	4.72	0.58	0.80	-1.46	20.21	1.05	1.05
495	88.67	-	-	-	-	-	-	-
496	88.83	4.62	0.68	1.42	-0.84	20.22	1.83	1.83
497	88.98	-	-	-	-	-	-	-
498	89.14	4.70	0.52	-	-	20.29	0.85	0.85
499	89.30	-	-	-	-	19.76	-	-
500	89.45	4.77	0.43	0.83	-1.33	19.82	0.92	0.92
501	89.61	-	-	-	-	20.20	-	-
502	89.77	4.69	0.53	1.01	-1.28	19.30	0.00	0.83
503	89.92	-	-	-	-	-	-	-
504	90.08	4.56	0.53	0.95	-1.31	19.30	0.00	0.00
505	90.23	-	-	-	-	-	-	-
506	90.39	4.60	0.66	1.11	-1.14	19.43	1.13	1.13
507	90.55	-	-	-	-	-	-	-
508	90.70	4.56	0.55	-	-	18.98	0.00	0.00
509	90.86	-	-	-	-	-	-	-
510	91.02	4.75	0.27	1.46	-0.77	19.73	0.00	0.00
511	91.17	-	-	-	-	19.82	-	-

512	91.33	4.61	0.36	1.17	-1.31	19.92	0.00	0.00
513	91.49	-	-	-	-	-	-	-
514	91.64	4.68	0.53	1.13	-1.12	19.94	0.00	0.00
515	91.80	-	-	-	-	-	-	-
516	91.96	4.45	0.62	1.05	-1.14	19.19	0.00	0.00
517	92.11	-	-	-	-	18.64	-	-
518	92.27	4.46	0.55	-	-	20.02	0.00	0.00
519	92.43	-	-	-	-	-	-	-
520	92.58	4.26	0.38	1.02	-1.15	18.99	0.00	0.00
521	92.74	-	-	-	-	18.47	-	-
522	92.90	4.38	0.53	1.08	-0.95	19.24	0.00	0.00
523	93.05	-	-	-	-	-	-	-
524	93.21	4.60	0.44	1.07	-0.91	19.32	0.00	0.00
525	93.37	-	-	-	-	-	-	-
526	93.52	4.36	0.56	1.12	-0.92	19.06	0.00	0.00
527	93.68	-	-	-	-	-	-	-
528	93.83	4.39	0.56	-	-	18.71	0.00	0.00
529	93.99	-	-	-	-	-	-	-
530	94.15	4.52	0.53	1.00	-1.02	19.71	0.00	0.00
531	94.30	-	-	-	-	18.31	-	-
532	94.46	4.55	0.58	1.02	-1.13	19.74	0.00	0.00
533	94.62	-	-	-	-	-	-	-
534	94.77	4.44	0.55	0.76	-1.11	18.90	1.05	1.05
535	94.93	-	-	-	-	-	-	-
536	95.09	4.44	0.59	0.95	-1.06	19.19	1.14	1.14
537	95.24	-	-	-	-	-	-	-
538	95.40	4.45	0.48	-	-	19.99	0.00	0.00
539	95.56	-	-	-	-	-	-	-
540	95.71	4.36	0.51	1.01	-1.07	18.62	2.13	2.13
541	95.87	-	-	-	-	17.77	-	-
542	96.03	4.54	0.49	1.05	-1.03	18.78	0.00	0.00
543	96.18	-	-	-	-	-	-	-
544	96.34	4.45	0.70	0.95	-1.06	19.65	0.00	0.00
545	96.50	-	-	-	-	-	-	-
546	96.65	4.45	0.62	1.16	-0.89	18.91	1.86	1.86
547	96.81	-	-	-	-	-	-	-
548	96.97	4.43	0.48	-	-	19.23	0.00	0.92
549	97.12	-	-	-	-	-	-	-
550	97.28	4.28	0.51	0.92	-1.21	20.21	0.89	0.89
551	97.43	-	-	-	-	19.55	-	-
552	97.59	4.39	0.63	0.89	-1.13	19.55	0.00	0.00
553	97.75	-	-	-	-	-	-	-
554	97.90	4.13	0.59	0.80	-1.03	19.61	0.00	0.00
555	98.06	-	-	-	-	-	-	-
556	98.22	4.18	0.60	1.01	-0.81	20.42	1.13	1.13
557	98.37	-	-	-	-	-	-	-
558	98.53	4.41	0.60	-	-	20.62	1.43	1.43
559	98.69	-	-	-	-	-	-	-
560	98.84	4.25	0.62	0.84	-0.95	19.31	0.00	0.00
561	99.00	-	-	-	-	19.81	-	-
562	99.16	4.48	0.64	0.84	-1.12	18.87	0.92	0.92
563	99.31	-	-	-	-	-	-	-
564	99.47	4.26	0.52	0.73	-1.28	19.82	0.00	0.00
565	99.63	-	-	-	-	-	-	-
566	99.78	4.52	0.72	0.97	-1.06	18.95	1.58	1.58
567	99.94	-	-	-	-	-	-	-
568	100.10	4.47	0.58	-	-	19.88	0.00	0.00
569	100.25	-	-	-	-	-	-	-

570	100.41	4.35	0.39	0.74	-1.27	19.98	1.65	1.65
571	100.56	-	-	-	-	19.38	-	-
572	100.72	4.30	0.60	0.92	-1.24	19.53	1.88	1.88
573	100.88	-	-	-	-	-	-	-
574	101.03	-	-	0.79	-1.30	20.00	0.00	0.00
575	101.19	-	-	-	-	-	-	-
576	101.35	4.26	0.55	1.04	-1.11	20.27	0.92	0.92
577	101.50	-	-	-	-	-	-	-
578	101.66	4.39	0.43	-	-	19.32	1.87	1.87
579	101.82	-	-	-	-	-	-	-
580	101.97	4.42	0.29	0.77	-1.13	20.12	0.00	0.00
581	102.13	-	-	-	-	20.05	-	-
582	102.29	4.33	0.31	0.85	-1.48	20.15	0.96	0.96
583	102.44	-	-	-	-	20.68	-	-
584	102.60	4.36	0.46	1.78	-1.15	19.76	0.00	0.88
585	102.76	-	-	-	-	-	-	-
586	102.91	4.41	0.42	0.74	-1.38	20.15	0.00	0.00
587	103.07	-	-	-	-	-	-	-
588	103.23	-	-	-	-	20.48	3.49	3.49
589	103.38	-	-	-	-	-	-	-
590	103.54	-	-	0.96	-1.20	20.62	3.90	3.90
591	103.70	-	-	-	-	-	-	-
592	103.85	4.24	0.65	0.71	-1.38	20.11	2.78	2.78
593	104.01	-	-	-	-	21.43	-	-
594	104.16	4.40	0.58	0.74	-1.47	19.41	0.72	0.72
595	104.32	-	-	-	-	-	-	-
596	104.48	4.37	0.36	0.59	-1.60	19.93	1.83	1.83
597	104.63	-	-	-	-	-	-	-
598	104.79	4.15	0.53	-	-	20.26	1.99	1.99
599	104.95	-	-	-	-	-	-	-
600	105.10	4.45	0.53	0.80	-1.50	20.10	2.59	3.88
601	105.26	-	-	-	-	-	-	-
602	105.42	4.20	0.59	0.88	-1.32	20.07	1.25	1.25
603	105.57	-	-	-	-	21.23	-	-
604	105.73	4.32	0.69	0.76	-1.37	19.38	0.00	0.00
605	105.89	-	-	-	-	-	-	-
606	106.04	4.17	0.42	0.91	-1.35	19.97	2.38	2.38
607	106.14	-	-	-	-	-	-	-
608	106.23	4.79	0.93	-	-	21.22	7.93	7.93
609	106.32	-	-	-	-	-	-	-
610	106.41	4.54	0.55	1.10	-1.11	21.14	7.84	7.84
611	106.51	-	-	-	-	-	-	-
612	106.60	4.54	0.79	0.82	-1.62	18.88	2.52	2.52
613	106.69	-	-	-	-	19.92	-	-
614	106.78	4.27	0.33	0.91	-1.41	20.13	11.29	11.29
615	106.88	-	-	-	-	-	-	-
616	106.97	4.34	0.60	1.12	-1.08	21.26	6.88	6.88
617	107.06	-	-	-	-	-	-	-
618	107.15	4.32	0.69	-	-	20.89	5.28	5.28
619	107.25	-	-	-	-	-	-	-
620	107.34	4.72	0.77	0.83	-1.41	19.30	1.25	1.25
621	107.43	-	-	-	-	-	-	-
622	107.52	4.27	0.55	1.00	-1.38	21.31	5.76	5.76
623	107.62	-	-	-	-	20.50	-	-
624	107.71	4.79	0.61	0.91	-1.26	21.60	8.78	10.24
625	107.80	-	-	-	-	-	-	-
626	107.89	4.52	0.44	0.98	-1.32	22.20	1.57	1.57
627	107.99	-	-	-	-	-	-	-

628	108.08	4.52	0.76	-	-	20.68	14.12	14.12
629	108.17	-	-	-	-	-	-	-
630	108.26	-	-	0.80	-1.38	21.28	4.45	4.45
631	108.36	-	-	-	-	-	-	-
632	108.45	4.65	0.79	0.79	-1.40	21.02	2.12	2.12
633	108.54	-	-	-	-	20.68	-	-
634	108.63	4.59	0.72	0.80	-1.28	20.95	6.97	8.36
635	108.73	-	-	-	-	-	-	-
636	108.82	4.47	0.52	0.86	-1.47	19.58	3.66	3.66
637	108.91	-	-	-	-	-	-	-
638	109.00	-	-	-	-	21.24	2.97	3.96
639	109.10	-	-	-	-	-	-	-
640	109.19	4.50	0.76	0.77	-1.51	20.81	9.26	9.26
641	109.28	-	-	-	-	-	-	-
642	109.37	4.38	0.74	0.97	-1.35	19.50	5.77	5.77
643	109.47	-	-	-	-	19.69	-	-
644	109.56	4.43	0.59	1.01	-1.19	19.77	15.03	17.34
645	109.65	-	-	-	-	-	-	-
646	109.74	-	-	0.89	-1.24	20.33	8.21	8.21
647	109.84	-	-	-	-	-	-	-
648	109.93	4.72	0.52	0.82	-1.50	21.20	7.69	7.69
649	110.02	-	-	-	-	-	-	-
650	110.11	4.62	0.81	1.15	-1.16	21.49	3.34	3.34
651	110.20	-	-	-	-	-	-	-
652	110.30	4.40	0.52	0.92	-1.37	21.31	4.26	4.26
653	110.39	-	-	-	-	18.35	-	-
654	110.48	-	-	1.04	-1.16	20.96	5.86	11.73
655	110.57	-	-	-	-	-	-	-
656	110.67	4.41	0.55	1.05	-1.24	21.16	3.44	3.44
657	110.76	-	-	-	-	-	-	-
658	110.85	4.50	0.63	0.97	-1.35	19.78	6.38	7.29
659	110.94	-	-	-	-	-	-	-
660	111.04	4.42	0.68	1.03	-1.17	21.26	3.84	3.84
661	111.13	-	-	-	-	-	-	-
662	111.22	-	-	0.75	-1.51	19.64	9.40	10.26
663	111.31	-	-	-	-	19.62	-	-
664	111.41	4.69	0.75	0.77	-1.49	20.62	8.12	8.12
665	111.50	-	-	-	-	-	-	-
666	111.59	4.53	0.77	1.04	-1.11	20.36	12.40	12.40
667	111.68	-	-	-	-	-	-	-
668	111.78	4.51	0.39	1.04	-1.41	21.48	11.70	11.70
669	111.87	-	-	-	-	-	-	-
670	111.96	-	-	0.80	-1.48	20.83	6.39	9.58
671	112.05	-	-	-	-	-	-	-
672	112.15	4.52	0.70	0.86	-1.15	18.64	9.55	9.55
673	112.24	-	-	-	-	21.87	-	-
674	112.33	4.37	0.67	0.96	-1.26	20.44	7.58	8.42
675	112.42	-	-	-	-	-	-	-
676	112.52	4.38	0.64	0.99	-1.12	19.52	10.16	11.01
677	112.61	-	-	-	-	-	-	-
678	112.70	4.19	0.37	-	-	19.52	19.10	19.10
679	112.79	-	-	-	-	-	-	-
680	112.89	4.40	0.81	0.86	-1.23	20.79	15.11	15.11
681	112.98	-	-	-	-	-	-	-
682	113.07	4.30	0.75	0.94	-1.09	18.91	8.58	8.58
683	113.16	-	-	-	-	20.48	-	-
684	113.26	4.23	0.64	0.77	-1.15	20.74	6.16	6.16
685	113.35	-	-	-	-	-	-	-

686	113.44	-	-	1.24	-0.84	19.50	16.63	16.63
687	113.53	-	-	-	-	-	-	-
688	113.63	4.32	0.60	0.76	-1.48	21.35	9.49	9.49
689	113.72	-	-	-	-	-	-	-
690	113.81	4.49	0.62	0.59	-1.64	20.60	11.99	11.99
691	113.90	-	-	-	-	-	-	-
692	114.00	4.39	0.72	0.85	-1.06	20.69	7.80	9.11
693	114.09	-	-	-	-	19.65	-	-
694	114.18	4.09	0.61	0.66	-1.34	18.50	8.23	9.25
695	114.35	-	-	-	-	-	-	-
696	114.52	4.08	0.81	0.71	-1.24	19.98	2.85	2.85
697	114.69	-	-	-	-	-	-	-
698	114.85	4.13	0.85	0.72	-1.11	19.61	11.71	11.71
699	115.02	-	-	-	-	-	-	-
700	115.19	4.02	0.51	0.54	-1.17	19.89	3.95	4.94
701	115.36	-	-	-	-	-	-	-
702	115.52	3.81	0.30	0.42	-1.19	19.43	11.66	11.66
703	115.69					19.88	-	-
704	115.86	4.34	0.67	0.75	-1.02	20.35	6.27	6.27
705	116.03	-	-	-	-	-	-	-
706	116.20	4.47	0.63	0.77	-0.95	20.47	0.00	0.00
707	116.36	-	-	-	-	-	-	-
708	116.53	3.86	0.71	0.49	-1.44	18.63	1.71	4.27
709	116.70	-	-	-	-	-	-	-
710	116.87	-	-	0.50	-1.35	19.46	0.76	0.76
711	117.04	-	-	-	-	-	-	-
712	117.20	3.71	0.85	0.61	-0.94	18.99	1.03	1.03
713	117.37	-	-	-	-	19.56	-	-
714	117.54	-	-	0.66	-1.19	20.04	2.08	2.08
715	117.71	-	-	-	-	-	-	-
716	117.87	-	-	1.03	-1.13	21.36	3.41	5.11
717	118.04	-	-	-	-	20.60	-	-
718	118.21	3.87	0.48	0.75	-0.98	-	4.88	7.32
719	118.38	-	-	-	-	18.16	-	-
720	118.55	-	-	0.47	-1.11	-	2.86	2.86
721	118.71	-	-	-	-	20.16	-	-
722	118.88	3.46	0.68	0.28	-1.38	-	0.93	0.93
723	119.05	-	-	-	-	20.47	-	-
724	119.22	3.43	0.47	0.39	-1.37	19.49	0.00	0.00
725	119.39	-	-	-	-	18.99	-	-
726	119.55	3.90	0.49	0.75	-1.10	-	0.00	0.00
727	119.72	-	-	-	-	20.23	-	-
728	119.89	3.38	0.48	0.48	-1.03	-	0.98	0.98
729	120.06	-	-	-	-	18.72	-	-
730	120.22	3.73	0.69	0.89	-1.42	-	0.00	0.00
731	120.39	-	-	-	-	20.23	-	-
732	120.56	3.81	0.49	0.37	-1.15	-	0.00	0.00
733	120.73	-	-	-	-	21.45	-	-
734	120.90	3.51	0.71	0.52	-1.06	20.24	1.66	1.66
735	121.06	-	-	-	-	20.27	-	-
736	121.23	3.43	0.58	0.44	-1.26	-	0.00	0.00
737	121.40	-	-	-	-	19.71	-	-
738	121.57	3.45	0.55	0.79	-1.20	-	0.00	0.00
739	121.73	-	-	-	-	19.43	-	-
740	121.90	3.85	0.62	0.29	-1.29	-	0.95	0.95
741	122.07	-	-	-	-	19.52	-	-
742	122.24	4.01	0.74	0.70	-1.22	-	0.00	0.00
743	122.41	-	-	-	-	20.51	-	-

744	122.57	3.36	0.56	0.74	-1.04	20.31	0.00	0.00
745	122.74	-	-	-	-	20.60	-	-
746	122.91	3.53	0.75	0.52	-1.42	-	0.00	0.00
747	123.08	-	-	-	-	21.21	-	-
748	123.25	3.72	0.55	0.46	-1.40	-	0.69	0.69
749	123.41	-	-	-	-	20.31	-	-
750	123.58	3.70	0.75	0.55	-1.21	-	0.98	0.98
751	123.75	-	-	-	-	20.78	-	-
752	123.92	4.12	0.40	0.50	-1.51	-	0.00	0.00
753	124.08	-	-	-	-	20.45	-	-
754	124.25	3.81	0.71	0.64	-1.42	20.84	0.00	0.00
755	124.42	-	-	-	-	20.87	-	-
756	124.59	3.45	0.31	0.29	-1.70	-	0.00	0.00
757	124.76	-	-	-	-	19.82	-	-
758	124.92	3.64	0.55	0.41	-1.62	-	0.46	0.46
759	125.09	-	-	-	-	20.26	-	-
760	125.26	3.49	0.34	0.48	-1.56	-	0.00	0.00
761	125.43	-	-	-	-	19.96	-	-
762	125.60	3.52	0.48	0.57	-1.68	-	0.42	1.27
763	125.76	-	-	-	-	20.53	-	-
764	125.93	-	-	0.63	-1.37	19.83	0.79	0.79
765	126.10	-	-	-	-	19.04	-	-
766	126.27	-	-	0.35	-1.64	-	0.00	0.00
767	126.43	-	-	-	-	19.83	-	-
768	126.60	3.63	0.37	0.42	-1.48	-	1.70	1.70
769	126.77	-	-	-	-	20.13	-	-
770	126.94	3.54	0.53	1.01	-1.53	-	0.86	0.86
771	127.11	-	-	-	-	19.97	-	-
772	127.27	3.83	0.22	0.66	-1.46	-	0.00	0.00
773	127.44	-	-	-	-	18.91	-	-
774	127.61	4.03	0.26	0.72	-1.55	19.63	0.65	0.65
775	127.78	-	-	-	-	19.15	-	-
776	127.94	3.98	0.27	0.51	-1.71	-	0.00	0.00
777	128.11	-	-	-	-	18.48	-	-
778	128.28	4.44	0.20	0.94	-1.84	-	2.20	2.20
779	128.45	-	-	-	-	19.10	-	-
780	128.62	4.11	0.19	0.84	-1.55	-	0.91	0.91
781	128.78	-	-	-	-	19.61	-	-
782	128.95	3.89	0.36	0.92	-1.63	-	0.00	0.00
783	129.17	-	-	-	-	19.22	-	-
784	129.40	4.12	0.30	1.05	-1.68	19.02	0.80	2.40
785	129.62	-	-	-	-	19.48	-	-
786	129.84	4.52	-0.04	0.93	-1.70	-	1.18	2.36
787	130.07	-	-	-	-	19.04	-	-
788	130.29	4.46	0.01	1.16	-1.58	-	1.43	1.43
789	130.51	-	-	-	-	19.81	-	-
790	130.73	4.28	0.16	1.46	-1.59	-	6.74	6.74
791	130.96	-	-	-	-	19.71	-	-
792	131.18	4.67	0.26	1.59	-1.69	-	1.38	1.38
793	131.40	-	-	-	-	19.33	-	-
794	131.62	4.37	0.28	1.35	-1.69	19.21	0.76	0.76
795	131.85	-	-	-	-	19.15	-	-
796	132.07	4.43	-0.01	1.45	-1.48	-	5.39	5.39
797	132.29	-	-	-	-	19.59	-	-
798	132.52	4.87	0.13	1.75	-1.42	-	5.25	5.25
799	132.74	-	-	-	-	18.49	-	-
800	132.96	4.76	0.09	1.49	-1.67	-	1.93	2.89
801	133.18	-	-	-	-	19.29	-	-

802	133.41	5.46	0.04	1.47	-1.81	-	1.69	2.54
803	133.63	-	-	-	-	19.62	-	-
804	133.85	-	-	1.80	-1.43	20.63	8.74	9.98
805	134.07	-	-	-	-	20.72		
806	134.30	5.34	0.22	1.70	-1.76	-	3.55	3.55
807	134.52	-	-	-	-	20.10	-	-
808	134.74	4.96	0.23	1.73	-1.59	-	15.99	17.44
809	134.96	-	-	-	-	20.82	-	-
810	135.19	4.97	0.13	1.74	-1.58	-	15.48	17.69
811	135.41	-	-	-	-	20.58	-	-
812	135.63	4.94	-0.02	1.88	-1.77	-	18.82	21.18
813	135.86	-	-	-	-	21.53	-	-
814	136.08	4.90	-0.12	1.84	-1.73	21.16	21.41	23.36
815	136.30	-	-	-	-	21.33	-	-
816	136.52	5.28	0.11	1.77	-1.58	-	7.25	11.40
817	136.75	-	-	-	-	21.73	-	-
818	136.97	5.58	0.05	1.91	-1.78	-	9.48	9.48
819	137.19	-	-	-	-	20.48	-	-
820	137.41	-	-	1.89	-1.59	-	4.51	4.51
821	137.64	-	-	-	-	21.31	-	-
822	137.86	5.58	0.26	1.91	-1.52	-	11.60	11.60
823	138.15	-	-	-	-	22.45	-	-
824	138.44	5.32	-0.06	2.00	-1.51	21.07	20.55	20.55
825	138.73	-	-	-	-	21.51	-	-
826	139.02	5.50	0.00	1.83	-1.73	-	16.38	19.36
827	139.32	-	-	-	-	20.46	-	-
828	139.61	-	-	1.95	-1.63	-	10.17	11.86
829	139.90	-	-	-	-	19.91	-	-
830	140.19	5.47	0.13	1.96	-1.50	-	20.17	21.73
831	140.48	-	-	-	-	21.44	-	-
832	140.77	5.10	-0.24	1.94	-1.48	-	28.87	33.97
833	141.06	-	-	-	-	22.96	-	-
834	141.35	5.32	-0.15	2.19	-1.78	23.25	14.35	16.40
835	141.64	-	-	-	-	21.87	-	-
836	141.93	4.92	-0.21	2.08	-1.46	-	16.41	19.69
837	142.23	-	-	-	-	23.30	-	-
838	142.52	5.05	-0.16	1.97	-1.43	-	10.48	13.97
839	142.81	-	-	-	-	22.89	-	-
840	143.10	5.32	0.04	1.71	-1.47	-	21.73	23.70
841	143.39	-	-	-	-	22.09	-	-
842	143.68	5.16	-0.08	1.88	-1.59	-	21.59	23.39
843	143.97	-	-	-	-	-	-	-
844	144.26	5.13	-0.17	1.77	-1.35	20.08	13.88	13.88
845	144.55	-	-	-	-	21.73	-	-
846	144.85	5.31	0.04	1.79	-1.39	-	17.73	17.73
847	145.14	-	-	-	-	22.65	-	-
848	145.43	4.99	0.04	1.92	-1.43	-	26.05	26.05
849	145.72	-	-	-	-	22.42	-	-
850	146.01	5.02	-0.12	1.95	-1.29	-	6.05	8.47
851	146.30	-	-	-	-	21.25	-	-
852	146.59	5.17	-0.07	1.80	-1.55	-	15.14	16.40
853	146.88	-	-	-	-	20.79	-	-
854	147.17	5.53	0.15	1.87	-1.30	20.97	9.05	10.56
855	147.46	-	-	-	-	22.23	-	-
856	147.76	5.07	-0.08	1.71	-1.57	-	32.04	33.07
857	148.05	-	-	-	-	23.58	-	-
858	148.34	5.48	-0.13	1.92	-1.39	-	11.53	13.17
859	148.63	-	-	-	-	20.30	-	-

860	148.92	-	-	1.84	-1.44	-	21.51	21.51
861	149.21	-	-	-	-	21.13	-	-
862	149.50	5.16	-0.20	1.90	-1.26	22.02	23.82	23.82
863	149.79	-	-	-	-	22.15	-	-
864	150.08	5.12	-0.17	1.85	-1.30	-	16.79	19.85
865	150.38	-	-	-	-	-	-	-
866	150.67	-	-	2.13	-1.44	21.22	19.64	21.15
867	150.96	-	-	-	-	-	-	-
868	151.25	5.03	-0.19	1.78	-1.39	24.10	29.06	32.48
869	151.54	-	-	-	-	-	-	-
870	151.83	4.89	-0.08	2.17	-1.31	21.86	19.56	23.47
871	152.12	-	-	-	-	-	-	-
872	152.41	5.24	-0.27	2.24	-1.14	-	25.08	30.46
873	152.70	-	-	-	-	-	-	-
874	152.99	5.00	-0.18	2.22	-1.45	21.65	26.69	31.14
875	153.29	-	-	-	-	-	-	-
876	153.58	5.20	-0.22	1.87	-1.63	21.81	16.99	19.61
877	153.87	-	-	-	-	-	-	-
878	154.16	5.08	-0.19	2.10	-1.19	23.16	6.92	8.30
879	154.45	-	-	-	-	-	-	-
880	154.74	5.25	-0.38	2.16	-1.24	-	16.11	19.34
881	155.03	-	-	-	-	-	-	-
882	155.32	5.18	-0.19	2.10	-1.23	20.92	23.73	25.71
883	155.61	-	-	-	-	-	-	-
884	155.91	5.32	-0.23	1.85	-1.63	20.69	14.60	14.60
885	156.09	-	-	-	-	-	-	-
886	156.28	5.25	-0.29	2.01	-1.30	22.83	15.41	15.41
887	156.46	-	-	-	-	-	-	-
888	156.65	-	-	2.18	-1.33	20.32	23.70	25.68
889	156.83	-	-	-	-	-	-	-
890	157.02	5.29	-0.19	2.04	-1.29	23.00	21.74	23.91
891	157.20	-	-	-	-	-	-	-
892	157.39	5.33	-0.27	1.70	-1.32	21.66	21.54	21.54
893	157.57	-	-	-	-	-	-	-
894	157.76	5.12	-0.16	1.96	-1.69	20.77	20.21	23.32
895	157.95	-	-	-	-	-	-	-
896	158.13	5.03	-0.08	1.88	-1.53	22.59	10.46	10.46
897	158.32	-	-	-	-	-	-	-
898	158.50	5.06	0.08	2.21	-1.28	20.07	53.52	54.89
899	158.69	-	-	-	-	-	-	-
900	158.87	5.24	-0.17	1.98	-1.50	21.45	29.09	32.00
901	159.06	-	-	-	-	-	-	-
902	159.24	5.06	-0.21	-	-	21.37	2.80	2.80
903	159.43	-	-	-	-	-	-	-
904	159.62	5.28	-0.11	2.07	-1.40	18.76	10.68	10.68
905	159.80	-	-	-	-	-	-	-
906	159.99	4.81	0.02	2.06	-1.40	20.52	8.89	8.89
907	160.17	-	-	-	-	-	-	-
908	160.36	5.10	-0.37	1.72	-1.77	19.63	12.39	13.94
909	160.54	-	-	-	-	-	-	-
910	160.73	5.03	0.04	1.65	-1.30	-	25.24	27.18
911	160.91	-	-	-	-	-	-	-
912	161.10	5.13	-0.30	1.55	-1.60	21.13	21.05	21.05
913	161.28	-	-	-	-	-	-	-
914	161.47	5.19	-0.17	1.91	-1.23	21.21	14.95	14.95
915	161.66	-	-	-	-	-	-	-
916	161.84	-	-	1.46	-1.85	20.61	13.49	13.49
917	162.03	-	-	-	-	-	-	-

918	162.21	5.00	-0.42	1.90	-1.29	22.08	6.08	8.10
919	162.40	-	-	-	-	-	-	-
920	162.58	5.15	-0.22	1.87	-1.33	24.16	10.28	10.28
921	162.77	-	-	-	-	-	-	-
922	162.95	5.05	-0.13	1.75	-1.44	23.51	8.01	12.02
923	163.14	-	-	-	-	-	-	-
924	163.33	5.20	-0.26	1.87	-1.38	19.61	7.63	7.63
925	163.51	-	-	-	-	-	-	-
926	163.70	5.09	-0.19	2.04	-1.16	20.72	8.29	8.29
927	163.88	-	-	-	-	-	-	-
928	164.07	5.08	-0.20	1.66	-1.37	20.48	18.52	20.37
929	164.25	-	-	-	-	-	-	-
930	164.44	4.89	-0.12	1.90	-1.15	18.28	16.45	24.68
931	164.62	-	-	-	-	-	-	-
932	164.81	5.00	-0.08	1.99	-1.17	18.87	18.49	18.49
933	164.99	-	-	-	-	-	-	-
934	165.18	5.12	-0.03	1.64	-1.37	19.63	11.03	12.87
935	165.37	-	-	-	-	-	-	-
936	165.55	5.03	-0.19	1.79	-1.44	20.46	24.11	26.30
937	165.74	-	-	-	-	-	-	-
938	165.92	5.04	0.05	1.51	-1.39	20.56	17.72	17.72
939	166.11	-	-	-	-	-	-	-
940	166.29	4.89	0.13	1.60	-1.30	25.17	20.72	20.72
941	166.48	-	-	-	-	-	-	-
942	166.66	4.90	-0.01	1.75	-1.43	21.44	16.46	16.46
943	166.85	-	-	-	-	-	-	-
944	167.04	5.00	-0.02	1.71	-1.42	21.40	22.35	22.35
945	167.22	-	-	-	-	-	-	-
946	167.41	4.84	0.06	1.64	-1.32	20.43	14.87	16.72
947	167.59	-	-	-	-	-	-	-
948	167.78	4.88	0.01	1.56	-1.64	24.04	17.04	17.04
949	167.96	-	-	-	-	-	-	-
950	168.15	5.00	-0.03	1.77	-1.34	21.29	12.63	12.63
951	168.33	-	-	-	-	-	-	-
952	168.52	4.74	-0.30	1.55	-1.45	23.86	25.77	27.76
953	168.70	-	-	-	-	-	-	-
954	168.89	5.00	-0.34	1.55	-1.70	22.79	22.15	22.15
955	169.08	-	-	-	-	-	-	-
956	169.26	4.93	0.02	1.54	-1.56	22.91	22.98	24.75
957	169.45	-	-	-	-	-	-	-
958	169.63	4.94	-0.22	1.62	-1.58	24.49	32.21	34.00
959	169.82	-	-	-	-	-	-	-
960	170.00	5.04	0.06	-	-	23.36	43.59	45.40
961	170.19	-	-	-	-	-	-	-
962	170.37	4.99	-0.26	1.78	-1.61	23.31	28.73	28.73

Appendix E: Spectral Analysis Age Model and Benthic Stable Isotope Data

MD02-2589 Age (MD95-2042 Tied Age Model)	MD02-2589 Age (Precession Tuned Age Model)	MD02-2589 Benthic $\delta^{18}O$	MD02-2589 Benthic $\delta^{13}C$	MD95-2042 Age (Precession Tuned Age Model)	MD95-2042 Benthic $\delta^{18}O$	MD95-2042 Benthic $\delta^{13}C$
9.69	6.00	3.77	0.46	0.00	0.92	3.33
9.80	6.26	4.67	0.50	0.79	1.01	3.28
9.85	6.52	4.37	0.48	1.58	0.99	3.39
9.91	6.78	4.36	0.53	2.37	0.99	3.27
10.12	7.04	3.86	0.68	3.16	1.08	3.31
10.17	7.30	3.83	0.60	3.95	1.06	3.30
10.23	7.56	3.92	0.60	4.74	1.20	3.16
10.33	7.81	3.81	0.58	5.53	0.50	3.49
10.39	8.07	4.10	0.48	6.32	0.70	3.40
10.68	8.33	4.32	0.52	7.11	0.94	3.22
11.58	8.59	3.80	0.33	7.90	0.99	3.43
11.88	8.85	4.17	0.51	8.69	0.75	3.36
12.17	9.11	4.21	0.50	9.48	0.84	3.19
12.47	9.37	4.30	0.56	10.26	0.89	3.43
12.77	9.63	4.58	0.29	11.05	0.93	3.83
13.07	9.89	4.43	0.35	11.84	0.79	3.63
13.37	10.15	4.35	0.52	12.63	0.68	3.54
13.54	10.41	4.34	0.26	13.42	0.43	4.33
13.72	10.67	4.04	0.54	13.74	0.81	3.85
13.90	10.93	4.49	0.40	14.06	0.68	4.13
14.07	11.19	4.39	0.36	14.38	0.73	4.29
14.25	11.44	4.82	0.19	14.71	0.48	4.18
14.43	11.70	4.68	0.44	15.03	0.82	4.24
14.60	11.96	4.46	0.49	15.35	0.65	4.10
14.79	12.22	4.58	0.50	15.67	0.70	4.12
14.98	12.48	4.79	0.43	15.99	0.35	4.19
15.17	12.74	4.61	0.17	16.31	0.44	4.19
15.37	13.00	4.72	0.34	16.63	0.04	4.23
15.56	13.30	4.74	0.32	16.95	0.11	4.60
15.70	13.59	5.13	0.25	17.27	0.23	5.09
15.80	13.89	4.87	0.16	17.59	0.22	5.12
15.90	14.19	5.07	0.16	17.91	0.27	5.04
16.00	14.49	5.18	0.13	18.23	0.12	4.78
16.09	14.78	5.12	0.08	18.55	0.23	5.20
16.19	15.08	5.29	0.14	18.87	0.27	5.09
16.29	15.38	4.77	0.27	19.19	0.23	5.02
16.39	15.68	5.27	0.11	19.51	0.23	5.08
16.66	15.97	4.73	0.01	19.83	0.12	4.91
16.94	16.27	5.24	-0.04	20.15	0.17	4.92
17.22	16.57	5.15	0.37	20.47	0.17	4.92
17.50	16.86	5.21	0.04	20.79	0.16	5.10
17.75	17.16	5.69	-0.07	21.12	-0.06	4.73
17.92	17.46	5.21	0.11	21.44	0.08	4.95
18.09	17.76	5.25	0.15	21.76	0.01	4.53

18.27	18.05	5.41	0.05	22.08	0.38	5.08
18.44	18.35	5.41	0.09	22.40	0.16	4.77
18.61	18.65	5.45	-0.06	22.72	-0.22	4.91
18.78	18.95	5.24	0.13	23.04	0.21	4.86
18.95	19.24	5.21	0.03	23.36	0.30	4.83
19.27	19.54	5.43	0.01	23.68	0.27	4.93
19.73	19.84	5.28	0.00	24.00	0.23	4.61
20.19	20.14	5.37	0.08	24.30	0.25	4.69
20.65	20.43	5.23	-0.01	24.61	0.08	4.69
21.10	20.73	5.12	0.08	24.91	0.14	4.53
21.56	21.03	5.31	0.04	25.21	0.11	4.46
22.48	21.32	5.14	0.09	25.52	0.35	4.60
23.07	21.62	5.14	0.12	25.82	0.04	4.75
23.65	21.92	5.31	0.04	26.12	0.11	4.59
24.24	22.22	5.13	0.06	26.43	0.33	4.76
25.41	22.51	5.29	0.04	26.73	0.11	4.75
25.99	22.81	5.25	0.05	27.03	0.20	4.68
26.58	23.11	4.99	0.07	27.33	0.40	4.86
27.16	23.41	5.24	0.06	27.64	0.62	4.76
27.74	23.70	5.18	0.09	27.94	0.56	4.71
28.33	24.00	5.05	0.09	28.24	0.21	4.54
29.50	24.46	4.85	0.35	28.55	0.59	4.48
29.93	24.92	5.09	0.02	28.85	0.34	4.54
30.35	25.38	5.10	0.30	29.15	0.37	4.69
30.78	25.85	5.06	0.05	29.46	0.73	4.59
31.14	26.31	5.10	0.32	29.76	0.58	4.59
31.50	26.77	4.97	0.24	30.06	0.59	4.61
31.86	27.23	5.13	0.36	30.37	0.45	4.43
32.22	27.69	4.96	0.20	30.67	0.71	4.61
32.58	28.15	4.90	0.31	30.97	0.49	4.42
32.93	28.62	5.05	0.01	31.28	0.37	4.29
33.31	29.08	4.74	0.24	31.58	0.16	4.34
33.69	29.54	4.93	0.51	31.88	0.21	4.11
34.07	30.00	5.00	0.47	32.19	0.63	4.33
34.45	30.46	4.85	0.05	32.49	0.51	4.53
34.77	30.92	4.77	0.26	32.79	0.59	4.53
35.42	31.38	5.06	0.44	33.09	0.52	4.39
35.74	31.85	4.76	0.34	33.40	0.25	4.34
36.07	32.31	4.68	0.29	33.70	0.64	4.55
36.39	32.77	5.09	0.34	34.00	0.62	4.36
36.72	33.23	4.83	0.33	34.31	0.45	4.44
37.04	33.69	4.96	0.32	34.61	0.68	4.38
37.36	34.15	4.61	0.14	34.91	0.71	4.34
37.69	34.62	4.86	0.33	35.22	0.04	4.27
38.66	35.08	4.80	0.43	35.52	0.03	4.39
39.01	35.54	4.85	0.63	35.93	0.34	4.58
39.37	36.00	4.70	0.53	36.35	0.36	4.59
39.72	36.50	4.87	0.43	36.76	0.48	4.55
40.08	37.00	4.71	0.28	37.17	0.47	4.67
40.43	37.50	4.81	0.42	37.59	0.48	4.58
40.79	38.00	4.67	0.45	38.00	0.60	4.47
41.14	38.50	4.66	0.53	38.42	0.68	4.58
41.51	39.00	4.75	0.29	38.83	0.62	4.53
41.87	39.50	4.96	0.29	39.24	0.69	4.54
42.60	40.00	4.81	0.38	39.66	0.42	4.46
42.97	40.50	4.69	0.33	40.07	0.37	4.56
43.33	41.00	4.72	0.39	40.48	0.51	4.64
43.70	41.50	4.80	0.33	40.90	0.41	4.43

44.06	42.00	4.76	0.21	41.31	0.63	4.74
44.43	42.50	4.67	0.16	41.73	0.56	4.54
44.80	43.00	4.76	0.01	42.14	0.69	4.53
45.16	43.50	4.93	0.20	42.55	0.66	4.42
45.53	44.00	4.88	0.18	42.97	0.78	4.36
45.93	44.50	4.78	0.40	43.38	0.76	4.39
46.33	45.00	4.80	0.55	43.79	0.07	3.92
46.73	45.50	4.81	0.23	44.21	-0.04	4.14
47.54	46.00	4.72	0.36	44.62	0.24	4.30
47.94	46.50	4.89	0.34	45.04	0.19	4.24
48.34	47.00	4.81	0.50	45.45	0.62	4.66
48.74	47.50	4.86	0.40	45.86	0.42	4.61
49.14	48.00	4.87	0.23	46.28	0.55	4.75
49.54	48.50	4.91	0.23	46.69	0.57	4.45
50.16	49.00	4.61	0.28	47.10	0.52	4.78
50.78	49.78	4.75	0.28	47.52	0.53	4.57
52.02	50.56	4.84	0.29	47.93	0.47	4.53
52.64	51.34	4.87	0.32	48.35	0.68	4.46
53.25	52.12	4.83	0.32	48.76	0.67	4.33
53.87	52.90	4.79	0.08	49.17	0.73	4.44
54.99	53.68	4.85	0.27	49.59	0.63	4.50
55.54	54.46	4.95	0.26	50.00	0.56	4.19
56.10	55.24	4.80	0.38	50.55	0.81	4.38
56.66	56.02	4.96	0.46	51.09	0.36	4.35
57.21	56.80	4.98	0.11	51.64	0.24	4.14
57.77	57.58	4.85	0.32	52.18	0.40	4.37
58.33	58.36	4.91	0.19	52.73	-0.07	4.10
58.88	59.14	5.05	0.13	53.27	0.45	4.59
59.44	59.92	4.88	0.22	53.82	0.48	4.65
59.99	60.70	5.08	0.05	54.36	0.50	4.45
60.55	61.48	4.81	-0.02	54.91	0.70	4.58
61.11	62.26	5.06	0.01	55.45	0.55	4.56
61.65	63.04	5.21	-0.15	56.00	0.60	4.44
62.19	63.68	5.16	-0.15	56.55	0.50	4.40
63.27	64.33	5.14	-0.11	57.09	0.48	4.40
63.81	64.97	5.02	-0.06	57.64	0.58	4.51
64.35	65.62	4.97	0.08	58.18	0.36	4.20
64.89	66.26	5.11	-0.05	58.73	0.36	4.19
65.43	66.91	5.12	0.05	59.27	0.39	4.43
65.97	67.55	4.98	-0.06	59.82	0.20	4.36
66.51	68.20	5.13	-0.14	60.36	0.13	4.05
67.05	68.84	5.07	0.00	60.91	-0.17	4.43
67.59	69.49	5.06	0.24	61.45	-0.31	4.35
68.13	70.13	4.93	0.01	62.00	-0.06	4.63
68.67	70.78	4.84	0.01	64.00	0.20	4.83
69.20	71.42	5.15	-0.14	66.00	-0.05	4.57
69.74	72.07	4.98	0.01	68.00	0.26	4.36
70.28	72.71	5.10	-0.02	70.00	0.46	4.73
70.82	73.36	5.01	-0.02	72.00	0.37	4.46
71.36	74.00	5.06	-0.01	74.00	0.56	4.64
71.90	74.22	5.16	0.10	74.35	0.73	4.24
72.44	74.44	4.97	0.06	74.71	0.65	4.29
72.71	74.66	4.70	0.37	75.06	0.94	4.42
72.97	74.88	4.75	0.56	75.42	0.73	4.12
73.17	75.10	4.53	0.45	75.77	0.81	3.57
73.36	75.32	4.82	0.32	76.13	0.57	4.04
73.55	75.54	4.38	0.76	76.48	0.35	3.77
73.75	75.76	4.56	0.58	76.84	0.40	3.92

73.94	75.98	4.57	0.58	77.19	0.40	4.31
74.14	76.20	4.65	0.63	77.55	0.81	4.28
74.33	76.42	4.58	0.63	77.90	0.57	4.19
74.53	76.64	4.58	0.74	78.26	0.79	4.22
74.72	76.86	4.53	0.78	78.61	0.83	4.19
74.92	77.08	4.41	0.52	78.97	0.75	4.25
75.11	77.30	4.52	0.78	79.32	0.84	4.14
75.30	77.52	4.60	0.54	79.68	0.53	3.98
75.50	77.74	4.62	0.63	80.03	0.67	4.00
75.69	77.96	4.49	0.66	80.39	0.76	4.15
75.89	78.18	4.45	0.60	80.74	0.79	4.06
76.08	78.40	4.71	0.52	81.10	0.81	4.11
76.28	78.62	4.49	0.61	81.45	0.66	4.09
76.47	78.84	4.52	0.58	81.81	0.59	4.02
76.66	79.06	4.40	0.51	82.16	0.78	3.95
76.86	79.28	4.51	0.65	82.52	0.63	4.04
77.05	79.50	4.49	0.61	82.87	0.81	3.88
77.25	79.72	4.45	0.65	83.23	0.78	3.93
77.64	79.94	4.36	0.52	83.58	0.79	3.66
77.83	80.16	4.69	0.37	83.94	0.78	3.90
78.03	80.38	4.67	0.42	84.29	0.48	4.05
78.22	80.60	4.30	0.57	84.65	0.53	3.66
78.41	80.82	4.28	0.58	85.00	0.43	3.59
78.61	81.04	4.45	0.59	85.59	0.12	3.63
78.80	81.26	4.43	0.51	86.18	0.28	3.76
79.00	81.48	4.33	0.76	86.77	0.02	3.80
79.19	81.70	4.49	0.62	87.36	0.05	4.06
79.39	81.92	4.48	0.47	87.95	0.45	4.29
79.58	82.14	4.45	0.73	88.54	0.66	4.37
79.77	82.36	4.26	0.61	89.14	0.60	4.11
79.97	82.58	4.47	0.46	89.73	0.52	4.23
80.16	82.80	4.54	0.63	90.32	0.65	4.07
80.36	83.02	4.33	0.52	90.91	0.88	4.10
80.55	83.24	4.42	0.86	91.50	0.79	3.96
80.75	83.46	4.50	0.49	92.09	0.76	3.96
80.94	83.68	4.28	0.45	92.68	0.71	3.97
81.33	83.90	4.36	0.49	93.27	0.69	3.96
81.52	84.12	4.44	0.49	93.86	0.65	3.96
81.72	84.34	4.33	0.71	94.45	0.79	4.05
82.11	84.56	4.32	0.63	95.04	0.79	3.84
82.30	84.78	4.35	0.63	95.44	0.69	3.99
82.50	85.00	4.32	0.36	95.84	0.83	3.88
82.69	85.26	4.44	0.43	96.24	0.62	3.72
82.89	85.52	4.15	0.29	96.64	0.66	3.75
83.08	85.79	4.26	0.47	97.04	0.57	3.80
83.27	86.05	4.56	0.31	97.43	0.64	3.68
83.47	86.31	4.20	0.39	97.83	0.75	3.88
83.66	86.57	4.48	0.47	98.23	0.77	3.83
83.86	86.83	4.32	0.51	98.63	0.70	3.88
84.05	87.10	4.43	0.38	99.03	0.81	3.84
84.25	87.36	4.47	0.49	99.43	0.81	3.87
84.44	87.62	4.46	0.54	99.83	0.57	3.89
84.70	87.88	4.55	0.50	100.22	0.71	3.83
84.96	88.14	4.66	0.30	100.62	0.79	3.79
85.23	88.40	4.66	-0.01	101.02	0.67	3.70
85.49	88.67	4.43	0.55	101.42	0.74	3.81
85.75	88.93	4.69	0.21	101.82	0.63	3.82
86.01	89.19	4.62	0.60	102.22	0.73	3.86

86.63	89.45	4.72	0.58	102.62	0.70	3.96
86.94	89.71	4.62	0.68	103.01	0.64	3.85
87.24	89.98	4.70	0.52	103.41	0.66	3.87
87.55	90.24	4.77	0.43	103.81	0.34	3.74
87.86	90.50	4.69	0.53	104.21	0.54	4.19
88.17	90.76	4.56	0.53	104.61	0.47	4.22
88.48	91.02	4.60	0.66	105.01	0.40	4.20
88.78	91.29	4.56	0.55	105.41	0.48	3.90
89.09	91.55	4.75	0.27	105.80	0.42	4.09
89.40	91.81	4.61	0.36	106.20	0.56	4.02
89.71	92.07	4.68	0.53	106.60	0.80	3.98
90.01	92.33	4.45	0.62	107.00	0.49	4.00
90.32	92.60	4.46	0.55	107.38	0.32	4.02
90.63	92.86	4.26	0.38	107.76	0.02	3.79
90.94	93.12	4.38	0.53	108.14	0.02	4.22
91.25	93.38	4.60	0.44	108.52	0.36	4.36
91.55	93.64	4.36	0.56	108.90	0.20	4.24
91.86	93.90	4.39	0.56	109.28	0.37	4.29
92.17	94.17	4.52	0.53	109.66	0.37	4.23
92.48	94.43	4.55	0.58	110.03	0.39	4.19
92.78	94.69	4.44	0.55	110.41	0.35	4.16
93.09	94.95	4.44	0.59	110.79	0.22	4.29
93.40	95.21	4.45	0.48	111.17	0.66	4.12
93.71	95.48	4.36	0.51	111.55	0.50	4.04
94.02	95.74	4.54	0.49	111.93	0.51	4.01
94.32	96.00	4.45	0.70	112.31	0.49	3.94
94.63	96.32	4.45	0.62	112.69	0.46	3.83
94.94	96.65	4.43	0.48	113.07	0.58	3.86
95.25	96.97	4.28	0.51	113.45	0.50	3.81
95.55	97.29	4.39	0.63	113.83	0.55	3.92
95.86	97.62	4.13	0.59	114.21	0.38	3.69
96.17	97.94	4.18	0.60	114.59	0.51	3.69
96.48	98.26	4.41	0.60	114.97	0.62	3.69
96.79	98.59	4.25	0.62	115.34	0.64	3.71
97.09	98.91	4.48	0.64	115.72	0.65	3.36
97.40	99.24	4.26	0.52	116.10	0.37	3.45
97.71	99.56	4.52	0.72	116.48	0.78	3.28
98.02	99.88	4.47	0.58	116.86	0.52	3.34
98.32	100.21	4.35	0.39	117.24	0.64	3.22
98.63	100.53	4.30	0.60	117.62	0.69	3.22
99.25	100.85	4.26	0.55	118.00	0.78	3.27
99.56	101.18	4.39	0.43	118.61	0.80	3.25
99.86	101.50	4.42	0.29	119.22	0.85	3.03
100.17	101.82	4.33	0.31	119.83	0.73	3.22
100.48	102.15	4.36	0.46	120.44	0.80	3.18
100.79	102.47	4.41	0.42	121.05	0.82	3.19
101.71	102.79	4.24	0.65	121.66	0.77	3.11
102.02	103.12	4.40	0.58	122.27	0.67	3.12
102.33	103.44	4.37	0.36	122.88	0.55	3.08
102.63	103.76	4.15	0.53	123.49	0.67	3.12
102.94	104.09	4.45	0.53	124.10	0.67	3.08
103.25	104.41	4.20	0.59	124.71	0.55	3.04
103.56	104.74	4.32	0.69	125.32	0.65	3.16
103.86	105.06	4.17	0.42	125.93	0.45	2.92
104.05	105.38	4.79	0.93	126.54	0.24	3.05
104.23	105.71	4.54	0.55	127.15	0.27	3.23
104.41	106.03	4.54	0.79	127.76	0.16	3.13
104.89	106.35	4.27	0.33	128.37	-0.06	3.59

105.38	106.68	4.34	0.60	128.98	-0.32	3.47
105.86	107.00	4.32	0.69	129.59	-0.24	3.93
106.35	107.27	4.72	0.77	129.90	-0.04	3.81
106.83	107.54	4.27	0.55	130.21	-0.03	4.02
107.32	107.80	4.79	0.61	130.51	-0.30	3.90
107.80	108.07	4.52	0.44	130.82	-0.37	4.25
107.99	108.34	4.52	0.76	131.13	-0.16	4.38
108.38	108.61	4.65	0.79	131.44	0.03	4.44
108.58	108.88	4.59	0.72	131.75	-0.08	4.50
108.77	109.15	4.47	0.52	132.06	-0.31	4.41
109.16	109.41	4.50	0.76	132.37	-0.33	4.60
109.35	109.68	4.38	0.74	132.68	-0.23	4.84
109.55	109.95	4.43	0.59	132.99	0.05	5.07
109.93	110.22	4.72	0.52	133.30	-0.03	5.04
110.13	110.49	4.62	0.81	133.61	0.17	5.19
110.32	110.76	4.40	0.52	133.92	-0.03	4.96
110.71	111.02	4.41	0.55	134.23	-0.17	4.88
110.90	111.29	4.50	0.63	134.54	-0.30	4.85
111.10	111.56	4.42	0.68	134.85	-0.05	4.88
111.49	111.83	4.69	0.75	135.16	-0.13	4.98
111.68	112.10	4.53	0.77	135.47	-0.10	4.98
111.87	112.37	4.51	0.39	135.77	-0.04	5.09
112.26	112.63	4.52	0.70	136.08	-0.26	4.91
112.46	112.90	4.37	0.67	136.39	-0.14	4.91
112.65	113.17	4.38	0.64	136.70	-0.27	4.90
112.84	113.44	4.19	0.37	137.01	-0.04	4.98
113.04	113.71	4.40	0.81	137.32	-0.14	5.03
113.23	113.98	4.30	0.75	137.63	-0.18	4.82
113.43	114.24	4.23	0.64	137.94	-0.18	4.97
113.82	114.51	4.32	0.60	138.25	0.15	4.84
114.01	114.78	4.49	0.62	140.19	-0.33	4.56
114.20	115.05	4.39	0.72	142.13	-0.39	4.65
114.40	115.32	4.09	0.61	144.06	-0.42	4.62
114.75	115.59	4.08	0.81	146.00	-0.55	4.67
115.10	115.85	4.13	0.85	-	-	-
115.45	116.12	4.02	0.51	-	-	-
115.81	116.39	3.81	0.30	-	-	-
116.16	116.66	4.34	0.67	-	-	-
116.51	116.93	4.47	0.63	-	-	-
116.86	117.20	3.86	0.71	-	-	-
117.57	117.46	3.71	0.85	-	-	-
118.62	117.73	3.87	0.48	-	-	-
119.33	118.00	3.46	0.68	-	-	-
119.68	118.35	3.43	0.47	-	-	-
120.03	118.71	3.90	0.49	-	-	-
120.38	119.06	3.38	0.48	-	-	-
120.73	119.42	3.73	0.69	-	-	-
121.09	119.77	3.81	0.49	-	-	-
121.44	120.13	3.51	0.71	-	-	-
121.79	120.48	3.43	0.58	-	-	-
122.14	120.84	3.45	0.55	-	-	-
122.50	121.19	3.85	0.62	-	-	-
122.85	121.55	4.01	0.74	-	-	-
123.20	121.90	3.36	0.56	-	-	-
123.55	122.26	3.53	0.75	-	-	-
123.90	122.61	3.72	0.55	-	-	-
124.26	122.97	3.70	0.75	-	-	-
124.61	123.32	4.12	0.40	-	-	-

124.96	123.68	3.81	0.71	-	-	-
125.31	124.03	3.45	0.31	-	-	-
125.66	124.39	3.64	0.55	-	-	-
126.02	124.74	3.49	0.34	-	-	-
126.37	125.10	3.52	0.48	-	-	-
127.42	125.45	3.63	0.37	-	-	-
127.78	125.81	3.54	0.53	-	-	-
128.13	126.16	3.83	0.22	-	-	-
128.48	126.52	4.03	0.26	-	-	-
128.83	126.87	3.98	0.27	-	-	-
129.18	127.23	4.44	0.20	-	-	-
129.54	127.58	4.11	0.19	-	-	-
129.89	127.94	3.89	0.36	-	-	-
130.36	128.29	4.12	0.30	-	-	-
130.82	128.65	4.52	-0.04	-	-	-
131.29	129.00	4.46	0.01	-	-	-
131.76	129.50	4.28	0.16	-	-	-
132.22	130.00	4.67	0.26	-	-	-
132.69	130.50	4.37	0.28	-	-	-
133.16	131.00	4.43	-0.01	-	-	-
133.63	131.50	4.87	0.13	-	-	-
134.09	132.00	4.76	0.09	-	-	-
134.56	132.50	5.46	0.04	-	-	-
135.37	133.00	5.34	0.22	-	-	-
135.78	133.50	4.96	0.23	-	-	-
136.19	134.00	4.97	0.13	-	-	-
136.59	134.50	4.94	-0.02	-	-	-
137.00	135.00	4.90	-0.12	-	-	-
137.41	135.50	5.28	0.11	-	-	-
137.81	136.00	5.58	0.05	-	-	-
138.63	136.50	5.58	0.26	-	-	-
139.16	137.00	5.32	-0.06	-	-	-
139.69	137.50	5.50	0.00	-	-	-
140.75	138.00	5.47	0.13	-	-	-
141.29	138.50	5.10	-0.24	-	-	-
141.82	139.00	5.32	-0.15	-	-	-
142.35	139.50	4.92	-0.21	-	-	-
142.88	140.00	5.05	-0.16	-	-	-
143.41	140.50	5.32	0.04	-	-	-
143.94	141.00	5.16	-0.08	-	-	-
144.47	141.60	5.13	-0.17	-	-	-
145.01	142.20	5.31	0.04	-	-	-
145.54	142.80	4.99	0.38	-	-	-
146.07	143.40	5.02	-0.12	-	-	-
146.60	144.00	5.17	-0.07	-	-	-
147.13	144.60	5.53	0.15	-	-	-
147.66	145.20	5.07	-0.08	-	-	-
148.20	145.80	5.48	-0.13	-	-	-
149.26	146.40	5.16	-0.20	-	-	-
149.79	147.00	5.12	-0.17	-	-	-

$\Delta\delta^{13}C_{2042\text{-}2589}$ Age (Precession Tuned Age Model)	$\Delta\delta^{13}C_{2042\text{-}2589}$	MD02-2589 Age (Precession Tuned Age Model)	MD02-2589 %NCW	MD095-2042 Age (Precession Tuned Age Model)	MD95-2042 %NCW	$\Delta\delta^{13}C_{2042\text{-}2589}$ Age (Precession Tuned Age Model)	$\Delta\delta^{13}C_{2042\text{-}2589}$ %NCW
6.32	0.21	6.25	83.41	0	81.81	6.25	41.87
7.11	0.28	6.41	49.33	0.15	97.30	6.41	32.81
7.90	0.44	6.56	41.60	0.61	133.35	6.56	32.62
8.69	0.35	7.47	53.32	0.7	92.67	7.47	41.37
9.48	0.39	8.69	32.34	0.76	113.53	8.69	42.38
10.26	0.49	9	76.68	0.85	140.53	9	61.39
11.05	0.55	9.36	50.08	0.92	98.53	9.36	35.27
11.84	0.32	9.72	21.69	1.07	90.17	9.72	92.98
12.63	0.40	10.44	13.76	1.16	80.19	10.44	77.18
13.42	0.14	11.16	37.34	1.22	104.62	11.16	84.69
13.74	0.61	11.88	43.24	1.37	116.56	11.88	36.33
14.06	0.52	12.6	34.04	1.46	93.92	12.6	43.31
14.38	0.59	13.32	58.98	1.53	78.62	13.32	21.93
14.71	0.39	14.04	40.77	1.83	111.45	14.04	129.94
15.03	0.69	14.76	82.70	1.98	114.37	14.76	53.97
15.35	0.39	15.48	82.42	2.23	95.63	15.48	59.78
15.67	0.58	15.91	70.54	2.29	101.16	15.91	36.11
15.99	0.34	16.63	70.51	2.44	116.97	16.63	-15.46
16.31	0.43	18	49.26	2.59	77.26	18	10.22
16.63	-0.26	19.19	58.20	2.9	80.98	19.19	9.80
16.95	0.10	20.33	51.97	3.05	127.92	20.33	8.31
17.27	0.23	21.47	59.70	3.2	227.32	21.47	-1.65
17.59	0.09	22.61	61.16	3.51	130.17	22.61	-7.64
17.91	0.17	24.31	76.61	3.6	84.75	24.31	-1.34
18.23	0.04	27.73	54.13	3.75	97.43	27.73	23.07
18.55	0.24	28.86	60.57	3.81	102.55	28.86	13.13
18.87	0.19	30	87.13	3.91	90.49	30	7.91
19.19	0.18	31.55	68.26	4.12	103.24	31.55	-13.60
19.51	0.22	32.32	57.01	4.27	82.42	32.32	22.49
19.83	0.12	33.87	52.67	4.42	93.07	33.87	22.67
20.15	0.10	35.42	71.31	4.58	116.88	35.42	-30.92
20.47	0.17	36.97	60.69	4.73	100.81	36.97	13.39
20.79	0.09	38.52	82.27	5.03	126.27	38.52	9.87
21.12	-0.12	40.07	83.07	5.13	92.67	40.07	-0.10
21.44	-0.02	41.61	63.15	5.19	80.81	41.61	16.22
21.76	-0.07	43.16	16.26	5.34	59.30	43.16	58.04
22.08	0.33	43.94	35.84	5.43	59.71	43.94	-16.15
22.40	0.11	47.03	69.25	5.64	43.39	47.03	2.78
22.72	-0.27	50.13	55.65	5.8	70.10	50.13	22.62
23.04	0.14	51.68	53.13	5.89	49.58	51.68	-4.10
23.36	0.24	53.23	50.60	5.95	64.00	53.23	12.83
23.68	0.19	54.77	51.58	6.25	125.27	54.77	27.52
24.00	0.14	55.55	53.21	6.41	82.14	55.55	10.18
24.30	-0.01	57.1	51.52	6.56	74.22	57.1	19.55
24.61	-0.17	58.65	58.39	7.47	94.69	58.65	11.02
24.91	0.11	60.19	76.73	8.69	74.72	60.19	-0.51
25.21	-0.09	61.36	43.04	9	138.07	61.36	-17.72
25.52	0.12	62.9	52.33	9.36	85.35	62.9	9.82
25.82	-0.02	64.45	65.57	9.72	114.67	64.45	20.87

26.12	-0.10	66	50.44	10.44	90.94	66	-3.18
26.43	0.03	68.31	43.33	11.16	122.03	68.31	20.45
26.73	-0.14	70.62	47.55	11.88	79.57	70.62	25.44
27.03	-0.11	71.19	35.48	12.6	77.35	71.19	27.11
27.33	0.08	71.77	30.61	13.32	80.91	71.77	29.03
27.64	0.40	74.08	44.10	14.04	170.70	74.08	28.06
27.94	0.30	76.39	61.89	14.76	136.68	76.39	-13.28
28.24	-0.04	78.69	53.26	15.48	142.19	78.69	19.40
28.55	0.54	81	65.15	15.91	106.65	81	12.85
28.85	0.21	84.27	83.34	16.63	55.05	84.27	-8.20
29.15	0.08	87.55	55.20	18	59.48	87.55	-23.79
29.46	0.27	90	63.77	19.19	68.00	90	3.71
29.76	0.09	91.32	60.42	20.33	60.28	91.32	15.38
30.06	0.17	91.99	58.74	21.47	58.05	91.99	15.52
30.37	0.31	93.31	57.36	22.61	53.52	93.31	12.67
30.67	0.57	95.96	58.60	24.31	75.27	95.96	7.89
30.97	0.21	97.28	57.30	27.73	77.20	97.28	-0.79
31.28	-0.03	99.93	64.62	28.86	73.70	99.93	4.73
31.58	-0.24	102.57	71.76	30	95.04	102.57	15.41
31.88	-0.12	105.22	84.47	31.55	54.66	105.22	-14.55
32.19	0.33	107.47	76.11	32.32	79.50	107.47	-24.78
32.49	0.20	108	70.35	33.87	75.35	108	-26.59
32.79	0.25	108.47	90.66	35.42	40.39	108.47	-33.24
33.09	0.19	108.64	101.80	36.97	74.07	108.64	-37.55
33.40	-0.07	108.98	78.91	38.52	92.14	108.98	-30.98
33.70	0.33	109.11	66.79	40.07	82.97	109.11	-17.81
34.00	0.42	109.28	80.36	41.61	79.37	109.28	-19.80
34.31	0.24	109.45	84.60	43.16	74.30	109.45	-25.70
34.61	0.35	109.75	78.71	43.94	19.70	109.75	-20.81
34.91	0.31	110.14	69.85	47.03	72.03	110.14	-9.96
35.22	-0.45	110.26	70.63	50.13	78.27	110.26	-10.83
35.52	-0.59	110.31	81.46	51.68	49.03	110.31	-15.64
35.93	-0.21	110.39	97.32	53.23	63.43	110.39	-24.24
36.35	-0.10	110.9	73.74	54.77	79.10	110.9	-14.33
36.76	0.13	111.03	75.85	55.55	63.39	111.03	-4.72
37.17	0.14	111.2	94.36	57.1	71.07	111.2	4.53
37.59	0.05	112.31	140.63	58.65	69.41	112.31	2.83
38.00	0.15	113.25	67.01	60.19	76.22	113.25	-1.35
38.42	0.16	113.51	72.15	61.36	25.32	113.51	1.76
38.83	0.25	113.94	110.78	62.9	62.15	113.94	-23.58
39.24	0.40	114.11	104.76	64.45	86.44	114.11	-24.05
39.66	0.10	114.23	92.92	66	47.26	114.23	-20.70
40.07	0.00	114.41	93.52	68.31	63.79	114.41	-14.39
40.48	0.18	114.58	89.85	70.62	72.99	114.58	-8.91
40.90	0.03	114.88	125.86	71.19	62.59	114.88	-7.68
41.31	0.28	115.52	115.58	71.77	59.64	115.52	-10.47
41.73	0.28	116.16	67.20	74.08	72.16	116.16	-3.65
42.14	0.49	116.8	86.21	76.39	48.61	116.8	-6.73
42.55	0.52	117.44	127.03	78.69	72.66	117.44	-18.00
42.97	0.76	118.68	59.09	81	77.99	118.68	30.89
43.38	0.60	119.53	75.56	84.27	75.14	119.53	15.76
43.79	-0.12	120	106.02	87.55	31.41	120	18.80
44.21	-0.31	121.5	102.97	90	67.48	121.5	6.32
44.62	-0.20	123	233.23	91.32	75.80	123	-35.51
45.04	-0.34	124.5	124.45	91.99	74.26	124.5	15.71
45.45	0.36	126	104.64	93.31	70.03	126	16.69
45.86	0.10	129.53	60.46	95.96	66.49	129.53	-41.11
46.28	0.20	131.41	74.14	97.28	56.51	131.41	-6.92

46.69	0.17	133.29	68.28	99.93	69.34	133.29	-14.06
47.10	0.04	134.71	46.53	102.57	87.17	134.71	-5.20
47.52	0.14	136.35	73.62	105.22	69.92	136.35	-24.66
47.93	0.22	138	81.34	107.47	51.34	138	-17.98
48.35	0.45	138.82	46.70	108	43.76	138.82	12.34
48.76	0.42	139.55	57.47	108.47	57.41	139.55	2.96
49.17	0.45	140.27	103.19	108.64	64.26	140.27	-30.54
49.59	0.35	141.09	62.71	108.98	47.93	141.09	-15.88
50.00	0.27	141.81	51.59	109.11	48.98	141.81	-20.00
50.55	0.52	142.53	96.94	109.28	60.56	142.53	-49.19
51.09	0.05	143.26	60.63	109.45	58.90	143.26	-19.94
51.64	-0.08	143.87	71.63	109.75	57.90	143.87	-22.07
52.18	0.10	144.6	96.90	110.14	59.89	144.6	-43.50
52.73	-0.21	145.32	80.54	110.26	59.80	145.32	-36.22
53.27	0.28	146.04	56.11	110.31	65.82	-	-
53.82	0.21	146.76	54.74	110.39	73.08	-	-
54.36	0.24	149.54	83.41	110.9	59.42	-	-
54.91	0.37	-	-	111.03	71.13	-	-
55.45	0.15	-	-	111.2	98.89	-	-
56.00	0.15	-	-	112.31	143.47	-	-
56.55	0.28	-	-	113.25	65.65	-	-
57.09	0.29	-	-	113.51	73.90	-	-
57.64	0.27	-	-	113.94	87.19	-	-
58.18	0.14	-	-	114.11	80.71	-	-
58.73	0.20	-	-	114.23	72.22	-	-
59.27	0.25	-	-	114.41	79.13	-	-
59.82	-0.01	-	-	114.58	80.93	-	-
60.36	0.01	-	-	114.88	118.19	-	-
60.91	-0.20	-	-	115.52	105.12	-	-
61.45	-0.29	-	-	116.16	63.55	-	-
62.00	-0.06	-	-	116.8	79.48	-	-
64.00	0.33	-	-	117.44	109.03	-	-
66.00	-0.05	-	-	118.68	89.98	-	-
68.00	0.38	-	-	119.53	91.32	-	-
70.00	0.40	-	-	120	124.82	-	-
72.00	0.37	-	-	121.5	109.29	-	-
74.00	0.57	-	-	123	197.72	-	-
74.35	0.65	-	-	124.5	140.16	-	-
74.71	0.23	-	-	126	121.33	-	-
75.06	0.47	-	-	129.53	19.36	-	-
75.42	0.21	-	-	131.41	67.22	-	-
75.77	0.23	-	-	133.29	54.22	-	-
76.13	-0.05	-	-	134.71	41.33	-	-
76.48	-0.31	-	-	136.35	48.96	-	-
76.84	-0.37	-	-	138	63.35	-	-
77.19	-0.26	-	-	138.82	59.04	-	-
77.55	0.25	-	-	139.55	60.43	-	-
77.90	-0.08	-	-	140.27	72.65	-	-
78.26	0.22	-	-	141.09	46.83	-	-
78.61	0.22	-	-	141.81	31.59	-	-
78.97	0.21	-	-	142.53	47.75	-	-
79.32	0.20	-	-	143.26	40.70	-	-
79.68	-0.11	-	-	143.87	49.56	-	-
80.03	0.22	-	-	144.6	53.40	-	-
80.39	0.34	-	-	145.32	44.32	-	-
80.74	0.22	-	-	-	-	-	-
81.10	0.24	-	-	-	-	-	-
81.45	-0.07	-	-	-	-	-	-

81.81	0.04	-	-	-	-	-	-
82.16	0.06	-	-	-	-	-	-
82.52	0.13	-	-	-	-	-	-
82.87	0.22	-	-	-	-	-	-
83.23	-0.06	-	-	-	-	-	-
83.58	0.32	-	-	-	-	-	-
83.94	0.29	-	-	-	-	-	-
84.29	-0.18	-	-	-	-	-	-
84.65	-0.10	-	-	-	-	-	-
85.00	0.07	-	-	-	-	-	-
85.59	-0.21	-	-	-	-	-	-
86.18	-0.07	-	-	-	-	-	-
86.77	-0.48	-	-	-	-	-	-
87.36	-0.45	-	-	-	-	-	-
87.95	0.01	-	-	-	-	-	-
88.54	0.37	-	-	-	-	-	-
89.14	0.08	-	-	-	-	-	-
89.73	-0.16	-	-	-	-	-	-
90.32	0.19	-	-	-	-	-	-
90.91	0.28	-	-	-	-	-	-
91.50	0.47	-	-	-	-	-	-
92.09	0.22	-	-	-	-	-	-
92.68	0.21	-	-	-	-	-	-
93.27	0.21	-	-	-	-	-	-
93.86	0.09	-	-	-	-	-	-
94.45	0.21	-	-	-	-	-	-
95.04	0.23	-	-	-	-	-	-
95.44	0.18	-	-	-	-	-	-
95.84	0.26	-	-	-	-	-	-
96.24	-0.02	-	-	-	-	-	-
96.64	0.18	-	-	-	-	-	-
97.04	0.04	-	-	-	-	-	-
97.43	0.03	-	-	-	-	-	-
97.83	0.15	-	-	-	-	-	-
98.23	0.17	-	-	-	-	-	-
98.63	0.08	-	-	-	-	-	-
99.03	0.21	-	-	-	-	-	-
99.43	0.17	-	-	-	-	-	-
99.83	-0.03	-	-	-	-	-	-
100.22	0.30	-	-	-	-	-	-
100.62	0.20	-	-	-	-	-	-
101.02	0.18	-	-	-	-	-	-
101.42	0.42	-	-	-	-	-	-
101.82	0.32	-	-	-	-	-	-
102.22	0.28	-	-	-	-	-	-
102.62	0.18	-	-	-	-	-	-
103.01	0.04	-	-	-	-	-	-
103.41	0.28	-	-	-	-	-	-
103.81	-0.19	-	-	-	-	-	-
104.21	-0.01	-	-	-	-	-	-
104.61	-0.18	-	-	-	-	-	-
105.01	-0.06	-	-	-	-	-	-
105.41	-0.42	-	-	-	-	-	-
105.80	-0.20	-	-	-	-	-	-
106.20	0.02	-	-	-	-	-	-
106.60	0.26	-	-	-	-	-	-
107.00	-0.20	-	-	-	-	-	-
107.38	-0.36	-	-	-	-	-	-

107.76	-0.58	-	-	-	-	-	-
108.14	-0.50	-	-	-	-	-	-
108.52	-0.42	-	-	-	-	-	-
108.90	-0.50	-	-	-	-	-	-
109.28	-0.27	-	-	-	-	-	-
109.66	-0.37	-	-	-	-	-	-
110.03	-0.18	-	-	-	-	-	-
110.41	-0.38	-	-	-	-	-	-
110.79	-0.30	-	-	-	-	-	-
111.17	0.07	-	-	-	-	-	-
111.55	-0.18	-	-	-	-	-	-
111.93	-0.25	-	-	-	-	-	-
112.31	0.02	-	-	-	-	-	-
112.69	-0.24	-	-	-	-	-	-
113.07	-0.07	-	-	-	-	-	-
113.45	0.12	-	-	-	-	-	-
113.83	-0.23	-	-	-	-	-	-
114.21	-0.27	-	-	-	-	-	-
114.59	-0.10	-	-	-	-	-	-
114.97	-0.07	-	-	-	-	-	-
115.34	0.01	-	-	-	-	-	-
115.72	-0.18	-	-	-	-	-	-
116.10	-0.17	-	-	-	-	-	-
116.48	0.35	-	-	-	-	-	-
116.86	-0.12	-	-	-	-	-	-
117.24	-0.09	-	-	-	-	-	-
117.62	0.06	-	-	-	-	-	-
118.00	0.10	-	-	-	-	-	-
118.61	0.32	-	-	-	-	-	-
119.22	0.28	-	-	-	-	-	-
119.83	0.21	-	-	-	-	-	-
120.44	0.21	-	-	-	-	-	-
121.05	0.23	-	-	-	-	-	-
121.66	0.08	-	-	-	-	-	-
122.27	-0.08	-	-	-	-	-	-
122.88	-0.15	-	-	-	-	-	-
123.49	0.13	-	-	-	-	-	-
124.10	0.31	-	-	-	-	-	-
124.71	0.19	-	-	-	-	-	-
125.32	0.24	-	-	-	-	-	-
125.93	0.03	-	-	-	-	-	-
126.54	-0.02	-	-	-	-	-	-
127.15	0.05	-	-	-	-	-	-
127.76	-0.11	-	-	-	-	-	-
128.37	-0.28	-	-	-	-	-	-
128.98	-0.32	-	-	-	-	-	-
129.59	-0.42	-	-	-	-	-	-
129.90	-0.28	-	-	-	-	-	-
130.21	-0.30	-	-	-	-	-	-
130.51	-0.57	-	-	-	-	-	-
130.82	-0.46	-	-	-	-	-	-
131.13	-0.19	-	-	-	-	-	-
131.44	-0.08	-	-	-	-	-	-
131.75	-0.18	-	-	-	-	-	-
132.06	-0.39	-	-	-	-	-	-
132.37	-0.38	-	-	-	-	-	-
132.68	-0.34	-	-	-	-	-	-
132.99	-0.17	-	-	-	-	-	-

133.30	-0.25	-	-	-	-	-	-
133.61	-0.04	-	-	-	-	-	-
133.92	-0.18	-	-	-	-	-	-
134.23	-0.23	-	-	-	-	-	-
134.54	-0.27	-	-	-	-	-	-
134.85	0.04	-	-	-	-	-	-
135.16	-0.08	-	-	-	-	-	-
135.47	-0.20	-	-	-	-	-	-
135.77	-0.12	-	-	-	-	-	-
136.08	-0.34	-	-	-	-	-	-
136.39	-0.35	-	-	-	-	-	-
136.70	-0.40	-	-	-	-	-	-
137.01	0.01	-	-	-	-	-	-
137.32	-0.12	-	-	-	-	-	-
137.63	-0.21	-	-	-	-	-	-
137.94	-0.30	-	-	-	-	-	-
138.25	0.20	-	-	-	-	-	-
140.19	-0.25	-	-	-	-	-	-
142.13	-0.41	-	-	-	-	-	-
144.06	-0.38	-	-	-	-	-	-

Appendix F: MD02-2588 Planktonic Stable Isotope Data

Depth (cm)	Age (ka)	*G. bulloides* $\delta^{18}O$	*G. bulloides* $\delta^{13}C$	*N. pachyderma* (d) $\delta^{18}O$	*N. pachyderma* (d) $\delta^{13}C$
0	0.00	1.25	-0.54	1.39	0.20
8	3.88	1.00	-0.63	1.39	0.37
16	7.77	1.13	-1.11	1.48	0.42
24	10.01	0.89	-1.81	2.04	0.14
32	13.06	1.76	-0.93	2.52	0.34
40	16.05	1.93	-1.25	2.51	0.27
48	17.61	2.52	-0.81	2.43	0.21
56	20.27	2.33	-0.79	2.67	0.30
64	22.93	2.08	-0.67	2.50	0.09
72	26.76	2.46	-1.08	2.55	0.33
80	28.95	2.20	-0.92	2.61	0.62
88	30.57	2.31	-0.91	2.28	0.20
96	33.45	1.92	-0.61	2.04	0.29
104	39.16	1.73	-1.31	2.14	0.01
112	44.33	1.97	-0.69	1.93	0.34
120	48.94	1.92	-0.82	1.68	0.06
128	49.80	2.10	-0.41	2.00	-0.04
136	51.57	1.70	-1.17	2.00	0.25
144	53.64	1.68	-1.15	1.55	-0.18
152	55.71	1.82	-1.21	1.78	-0.35
160	57.79	1.46	-1.04	-0.12	1.68
168	59.86	2.03	-1.02	2.30	-0.13
176	61.93	1.91	-1.36	2.12	0.16
184	64.00	2.21	-0.97	2.12	0.46
192	66.69	1.81	-0.57	1.66	-0.04
200	69.38	1.35	-0.92	1.93	0.49
208	72.08	1.24	-0.80	1.51	0.41
216	74.77	1.72	-0.35	0.26	1.45
224	77.46	1.30	-0.41	1.56	0.59
232	80.15	1.07	-1.04	1.13	0.12
240	82.85	1.32	-0.74	1.40	0.40
248	85.54	1.25	-1.30	1.12	-0.07
256	88.23	1.28	-1.25	1.38	-0.35
264	90.92	1.33	-1.29	1.51	-0.08
272	93.62	1.30	-0.99	1.83	0.28
280	96.31	0.91	-1.30	1.27	0.07
288	99.00	0.81	-1.36	1.09	0.00
296	101.55	0.82	-1.52	1.73	0.11
304	104.10	1.09	-1.42		
320	109.19	0.91	-1.39		
328	111.74	1.25	-1.05		
336	114.29	0.69	-1.08		
344	116.84	0.57	-1.35		
352	119.39	0.34	-1.40		
360	121.94	0.58	-1.30		
368	124.49	0.61	-1.29		
376	127.04	0.27	-1.70		

384	129.58	0.50	-1.72		
392	132.13	1.25	-1.78		
400	135.00	1.90	-1.44		
408	136.14	1.65	-1.88		
416	137.29	2.08	-1.54		
424	138.43	1.93	-1.51		
432	139.57	2.19	-1.65		
440	140.71	1.59	-1.38		
448	142.00	2.03	-1.26		

PALEOCEANOGRAPHY, VOL. 22, PA4209, doi:10.1029/2006PA001407, 2007

Deep water variability on the southern Agulhas Plateau: Interhemispheric links over the past 170 ka

Elizabeth G. Molyneux,[1] Ian R. Hall,[1] Rainer Zahn,[2] and Paula Diz[1]

Received 14 December 2006; revised 8 June 2007; accepted 29 June 2007; published 13 November 2007.

[1] Sortable silt mean grain sizes together with oxygen and carbon isotopic data produced on the benthic foraminiferal species *Fontbotia wuellerstorfi* are used to construct high-resolution records of near-bottom flow vigour and deep water ventilation at a core site MD02-2589 located at 2660 m water depth on the southern Agulhas Plateau. The results suggest that during glacial periods (marine oxygen isotope stages 2 and 6, MIS 2 and MIS 6, respectively), there was a persistent contribution of a well-ventilated water mass within the Atlantic to Indian oceanic gateway with a $\delta^{13}C$ signature similar to present-day Northern Component Water (NCW), e.g., North Atlantic Deep Water (NADW). The records of chemical ventilation and near-bottom flow vigor reflect changes in the advection of northern source waters and meridional variability in the location of the Antarctic Circumpolar Current and its associated fronts. We suggest that during Termination II (TII), changes in chemical ventilation are largely decoupled from near-bottom physical flow speeds. A mid-TII climate optimum is associated with a low-flow speed plateau concurrent with a period of increased ventilation shown in the benthic $\delta^{13}C$ of other Southern Ocean records but not in our benthic $\delta^{13}C$ of MD02-2589. The climate optimum is followed by a period of southern cooling around 128 ka coincident with a stronger influence of NCW to interglacial levels at around 124 ka. All proxy records show a near synchronous and rapid shift during the transition from MIS 5a-4 (73 ka). This large event is attributed to a rapid decrease in NADW influence and replacement over the Agulhas Plateau by southern source waters.

Citation: Molyneux, E. G., I. R. Hall, R. Zahn, and P. Diz (2007), Deep water variability on the southern Agulhas Plateau: Interhemispheric links over the past 170 ka, *Paleoceanography, 22*, PA4209, doi:10.1029/2006PA001407.

1. Introduction

[2] A key element of the global ocean thermohaline circulation (THC) is the oceanic connection between the Indian and South Atlantic Oceans off South Africa [*de Ruijter et al.*, 1999; *Sloyan and Rintoul*, 2001] (Figure 1). Variable amounts of warm, salt-enriched South Indian Ocean waters enter the South Atlantic, the so-called "warm water return route" (the "cold water return route" being through the Drake Passage), and provide a source for heat and salt to the Atlantic thermocline that ultimately preconditions the Atlantic meridional overturning circulation for convection in the north, the formation of North Atlantic Deep Water (NADW) [*Richardson et al.*, 2003]. This westward surface return flow is compensated at depth by an eastward setting deep flow into the Indian Ocean that consists of NADW exiting the South Atlantic and the Antarctic Circumpolar Current (ACC) [*Gordon*, 1996; *Lutjeharms*, 1996].

[3] Numerous studies from the North Atlantic suggest that NADW production was significantly reduced during the last glacial period [e.g., *Boyle and Keigwin*, 1987; *Duplessy et al.*, 1988; *Sarnthein et al.*, 1994; *Curry and Oppo*, 2005]. Northern Component Waters (NCW) sank only to intermediate depth (<2000 m) forming Glacial North Atlantic Intermediate Water (GNAIW), extending from 45°N to 15°S. In contrast, it appears the production of water masses from the ACC (i.e., Southern Component Waters (SCW)) was either comparable to present day or increased with enhanced northward spreading, ventilating the deep North Atlantic below GNAIW [*Oppo and Fairbanks*, 1987; *Boyle and Keigwin*, 1987; *Marchitto and Broecker*, 2006].

[4] Paleoceanographic reconstructions of deep ocean variability in the South Atlantic have provided contrasting information on the relative influence of NADW and Antarctic Bottom Water (AABW) during the last glacial-interglacial cycle. Reduced production and southward spread of NADW during glacial periods has been suggested by studies using Nd isotope ratios [e.g., *Rutberg et al.*, 2000; *Piotrowski et al.*, 2004, 2005], $^{231}Pa/^{230}Th$ ratios in sediments [*McManus et al.*, 2004; *Gherardi et al.*, 2005], benthic $\delta^{13}C$ records [*Streeter and Shackleton*, 1979; *Sigman and Boyle*, 2000], and clay-mineral tracers [*Diekmann et al.*, 1996] which found that NCW extended no farther south than 40°S at the height of the last glacial period. In contrast, early studies using $^{231}Pa/^{230}Th$ ratios [*Yu et al.*, 1996] suggest that export of NCW to the Southern Ocean continued at a comparable rate to the Holocene during the Last Glacial Maximum (LGM), although probably at a reduced depth, a contention that also seems to be

[1]School of Earth, Ocean, and Planetary Sciences, Cardiff University, Cardiff, UK.
[2]Institució Catalana de Recerca i Estudis Avançats, Institut de Ciencia i Tecnologia Ambientals, Universitat Autónoma de Barcelona, Bellaterra, Spain.

0883-8305/07/2006PA001407$12.00

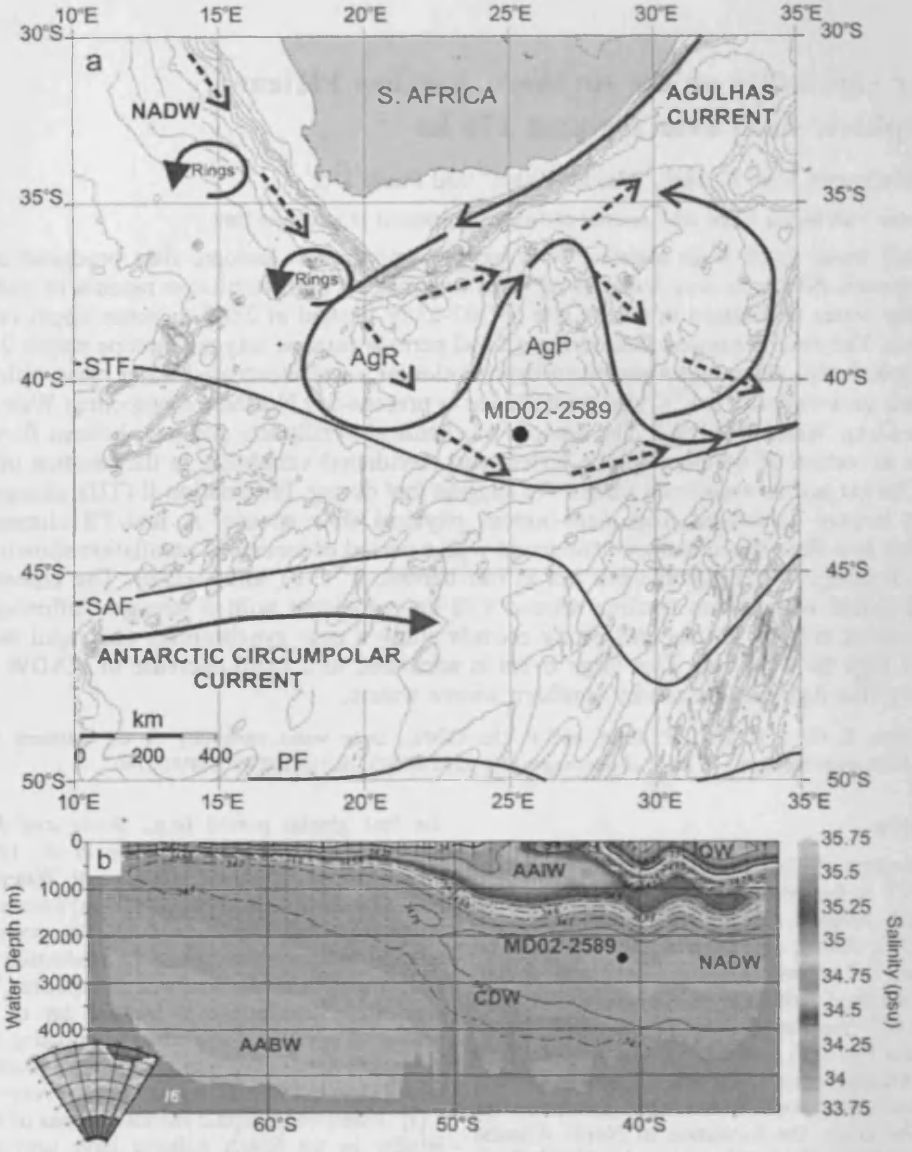

Figure 1. (a) Map showing study area and position of core MD02-2589 on the southern Agulhas Plateau, together with the present-day position of the oceanic fronts and generalised ocean circulation (after *Richardson et al.* [2003]). Position of the fronts after *Belkin and Gordon* [1996] and *Orsi et al.* [1995]. Solid arrows are surface water currents, and dashed arrows are bottom water currents. NADW, North Atlantic Deep Water; AgP, Agulhas Plateau; AgR, Agulhas Retroflection; STF, Subtropical Front; SAF, Subantarctic Front; PF, Polar Front. (b) Present-day transect of salinity from the coast of South Africa to Antarctica across the Southern Ocean (modified from *Schlitzer* [2000]) showing the positions of the existing water masses. IOW, Indian Ocean Water; AAIW, Antarctic Intermediate Water; NADW, North Atlantic Deep Water; CDW, Circumpolar Deep Water; AABW, Antarctic Bottom Water.

corroborated by Cd/Ca [*Boyle*, 1992; *Lea*, 1995] and foraminiferal isotope measurements in the southeast Pacific and Atlantic [*Matsumoto et al.*, 2001; *Matsumoto and Lynch-Stieglitz*, 1999]. Uncertainty is added to the picture by the indication of an expansion of SCW in two branches (Upper Southern Component Water and Lower Southern Component Water) that compensated for the suppression of NADW [*Henrich et al.*, 2003; *Curry and Oppo*, 2005] and a suggested presence of GNAIW in the Southern Ocean as a replacement for NADW [*Volbers and Henrich*, 2004]. *Bickert and*

Mackensen [2003] suggest that instead of GNAIW taking over from NADW, Mediterranean Outflow Water is more likely to have compensated but at a shallower depth and only certainly as far south as 30°S.

[5] The interhemispheric linkage of oceanic change has been the target of conceptual and numerical modeling [*Ganopolski and Rahmstorf*, 2001; *Seidov et al.*, 2001; *Weijer et al.*, 2002; *Knorr and Lohmann*, 2003; *Stocker and Johnsen*, 2003; *Weaver et al.*, 2003; *Knutti et al.*, 2004], while ice core synchronization exercises added insight from interhemispheric atmospheric paleodata comparisons that suggest an out-of-phase pattern between the hemispheres [*Blunier et al.*, 1998; *Blunier and Brook*, 2001; *Brook et al.*, 2005; *EPICA Community Members*, 2006]. The few high-resolution paleoceanographic records from the Southern Hemisphere oceans confirm this suggestion [*Charles et al.*, 1996; *Pahnke et al.*, 2003; *Pahnke and Zahn*, 2005], although such records are sparse and do not allow us to draw a conclusive picture for the wider Southern Hemisphere oceans. It has been suggested by early studies [*Hays et al.*, 1976; *Imbrie et al.*, 1989; *Howard and Prell*, 1992; *Labeyrie et al.*, 1996] that on orbital timescales, Southern Ocean sea surface temperatures (SST) respond early to changes in the orbital parameters and might actually lead global ice volume [*Charles et al.*, 1996]. The cause of such a lead is not well understood, as is the phasing of changes between the hemispheres on shorter suborbital timescales.

[6] Here we present a high-resolution multiproxy record of deep water variability from a sediment core recovered from the southern flank of the Agulhas Plateau in the southernmost South Atlantic. The location is close to the southern mixing interface between NADW and southern source waters in the Southern Ocean, enabling the reconstruction of the timing and amplitude of changes in southward advection of NADW and Southern Ocean THC. The site is also strongly influenced by the ACC. The flow of this current extends to depth, often to the seabed [*Orsi et al.*, 1995], and is wind driven, suggesting that fluctuations in the surface conditions can influence deep water dynamics. The position of the major frontal systems associated with the ACC can therefore be potentially related to changes in the near-bottom flow regime and strength. We concentrate on identifying the phasing between changes in ice volume, the location of surface ocean fronts, deep ventilation, and near-bottom flow speeds over the past 170 ka.

2. Regional Deep Water Oceanography

[7] The region connecting the Indian and Atlantic oceans (Figure 1) is one of several oceanic gateways guiding the flow of surface and deep waters around the global ocean and distributing heat, salt, and nutrients between the oceans [*Sloyan and Rintoul*, 2001; *Boebel et al.*, 2003]. Here deep water circulation is primarily characterized by the interactions between southward propagating NADW and northward flowing SCW, notably AABW and Antarctic Intermediate Water (AAIW) [*Reid*, 1989, 2005]. The transition between NADW and Lower Circumpolar Deep Water (LCDW) is at middepths sloping upward to the south (Figure 1b), while the deep areas (>5000 m) are filled with AABW, a mix of Weddell Sea Deep Water and LCDW [*Orsi et al.*, 1999].

[8] The interocean exchange of NADW into the South Indian Ocean from the South Atlantic occurs directly through the Agulhas Gateway, located between the southern tip of Africa and the northern Agulhas Plateau (Figure 1a). However, some of the NADW flow also extends toward the south, rounding the southern flank of the Agulhas Plateau where it has led to the deposition of contourite sediment drifts (Figure 1a) [*Tucholke and Carpenter*, 1977; *Uenzelmann-Neben*, 2001]. Core MD02-2589 (Figure 1) is positioned in a sediment drift up to 650 m thick that displays an asymmetric geometry and changes in internal reflector patterns which are indicative of a dynamical circulation pattern in the region back to Oligocene-Miocene times [*Uenzelmann-Neben*, 2002]. The core site today is predominantly bathed in NADW with a substantial Circumpolar Deep Water (CDW) contribution. The site thus offers the possibility to monitor past variations in CDW as a member of the Southern Ocean THC and the southward spreading of NADW.

3. Material and Methods

[9] Giant piston core MD02-2589 was recovered during R/V *Marion Dufresne* cruise MD128 from a contourite drift located on the southern Agulhas Plateau (41°26.03′S, 25°15.30′E, 2660 m water depth) (Figure 1a). At this depth the core site lies in NADW, ~1000 m below AAIW and ~1000 m above LCDW (Figure 1b). The core recovered 34.55 m of sediment, composed primarily of foraminiferal ooze, spanning the past ~1.3 Ma [*Giraudeau et al.*, 2002]. Here we focus on the upper 9.8 m of the sediment core, representing the last ~170 ka B.P. We sampled every 2 cm for stable isotope and grain-size analysis.

[10] The samples were first sieved to separate the fine (<63 μm) and coarse (>63 μm) fractions, with the fine fractions being used for grain-size analysis and the coarse fractions for isotope analysis. Epibenthic foraminiferal species *Fontbotia wuellerstorfi* (also commonly referred to as *Cibicidoides wuellerstorfi*), generally known to secrete calcite close to the $\delta^{13}C_{DIC}$ values of ambient bottom water [*Mackensen et al.*, 2001], was picked from the 150–250 μm size fraction. Eight to ten tests for each sample were analysed using a Finnigan MAT 252 mass spectrometer coupled with an automated Kiel III carbonate device. Long-term analytical precision is 0.06‰ for $\delta^{18}O$ and 0.03‰ for $\delta^{13}C$. All isotope data are referenced to the Vienna Peedee belemnite scale through repeated analysis of NBS 19 international carbonate standard. Oxygen isotopes of the benthic foraminifera *F. wuellerstorfi* have been transferred by +0.64‰ to the *Uvigerina spp.* scale as this more closely represents equilibrium with the ambient seawater [*Shackleton and Hall*, 1997].

[11] Grain-size analysis of the so-called sortable silt mean grain-size paleocurrent indicator uses the fraction of the sediment whose size sorting varies in response to hydrodynamic processes (i.e., the terrigenous 10–63 μm component) to infer relative changes in near-bottom current speed [*McCave et al.*, 1995a; *McCave and Hall*, 2006]. This proxy

Table 1. The ^{14}C AMS Ages on Planktonic Foraminifera and Calibrated Ages for Core MD02-2589

Lab Code	Depth, cm	Species[a]	Conventional ^{14}C Age, a	±1SD, a	Calibrated ^{14}C Age, a	±1SD, a
SUERC-4667[b]	5-6	*G. inflata*	13,161	±46	15,061	±102
SUERC-4668[b]	10-11	*G. inflata*	8,891	±29	9,505	±20
SUERC-4669[b]	20-21	*G. inflata*	11,731	±39	13,261	±103
SUERC-4670[b]	40-41	*G. inflata*	10,000	±33	10,954	±111
SUERC-4673	60-61	*G. inflata*	13,722	±50	15,874	±129
SUERC-4674	75-76	*G. inflata*	14,624	±53	17,181	±129
SUERC-4675	85-86	*G. inflata*	15,263	±57	18,230	±178
SUERC-4676	100-101	*G. inflata*	15,710	±60	18,603	±36
SUERC-4677	110-111	*G. inflata*	17,317	±73	20,137	±104
SUERC-4679	125-126	*G. inflata*	18,457	±84	21,538	±132
SUERC-4680	140-141	*G. inflata*	21,481	±120	25,288	±142
SUERC-4683	170-171	*G. inflata*	29,933	±335	34,664	±470
SUERC-4684	190-191	*G. inflata*	34,987	±628	39,927	±889

[a]*G., Globorotalia.*
[b]Reversal and unused.

has been used successfully in paleocurrent studies in the North Atlantic [e.g., *Manighetti and McCave*, 1995; *Hall et al.*, 1998; *Bianchi and McCave*, 1999; *Ellison et al.*, 2006], South Atlantic [e.g., *Kuhn and Diekmann*, 2002], Indian [e.g., *McCave et al.*, 2005], and Pacific oceans [e.g., *Hall et al.*, 2001]. The samples were disaggregated in purified water on a rotating carousel for 24 h before being washed over a 63 μm mesh. Fine fraction residues were dried at 50°C, and carbonate was removed with 2 *M* acetic acid followed by digestion in 0.2% sodium carbonate at 80°C for 8 h to remove the biogenic silicates. Sortable silt mean ($\overline{SS}$) grain-size measurements were undertaken using a Coulter Multisizer III as detailed by *Bianchi et al.* [1999]. Average $\overline{SS}$ abundance in the samples is 8–10% enabling the determination of the $\overline{SS}$ index with an error of ±2% [*Bianchi et al.*, 1999].

[12] The degree of carbonate dissolution was assessed in selected samples using the planktonic foraminiferal fragmentation index described by *Le and Shackleton* [1992]. This index contains a devisor relating the number of fragments to the number of tests, so that percentage fragmentation is more likely to respond linearly to dissolution rather than being over sensitive during the early stages and relatively insensitive during the later stages of dissolution. Samples of the >150 μm size fraction were split as many times as required to obtain approximately 300 whole planktonic foraminifera. All whole planktonic foraminifera were identified and counted, while all fragments within these splits were also recorded. The percentage fragmentation was calculated using a fragment devisor of 3 [*Pfuhl and Shackleton*, 2004].

[13] A total of thirteen ^{14}C accelerator mass spectrometry (AMS) datings were carried out within the uppermost 190 cm of core MD02-2589 on monospecific samples containing ~1000 tests of *Globorotalia inflata* (Table 1). The ^{14}C analyses were carried out at the Natural Environment Research Council Radiocarbon Laboratory in East Kilbride, UK. The ^{14}C dates were corrected for the marine reservoir effect using a regional Southern Ocean correction of 800 years (a) [*Butzin et al.*, 2005] and subsequently calibrated to calendar years B.P. using the marine calibration data set of *Fairbanks et al.* [2005] which allows for calibration back to 50 ka.

4. MD02-2589 Chronology

[14] The age model for MD02-2589 was developed using a combination of AMS radiocarbon dating and graphic tuning of the benthic $\delta^{18}O$ records to core MD97-2120 [*Pahnke et al.*, 2003] (Figure 2) from the Chatham Rise, South Pacific. Two age reversals in the upper 60 cm of the core MD02-2589 led us to discard the four uppermost AMS dates (Table 1). Ages for this interval were estimated through extrapolation using a polynomial fit of the age/depth relationship of the remaining nine AMS dates (upper 190 cm). It should be noted that the ^{14}C calibrated ages appear typically older by ~1 ka from those derived by graphic correlation of the benthic $\delta^{18}O$ records of MD02-2589 and MD97-2120. Such an offset suggests that the local 800 a reservoir age that we have adopted for core MD02-2589 may well be an underestimate and reservoir ages rather are in the range of up to 1800 a, similar to those seen in MD97-2120 [*Pahnke et al.*, 2003] and other southwest Pacific Ocean sites [*Sikes et al.*, 2000]. Within the interval 190-982 cm (~40–170 ka), ages control points were assigned via graphic correlation of the benthic $\delta^{18}O$ with MD97-2120 (Figure 2) [*Pahnke et al.*, 2003]. The tuning of the benthic $\delta^{18}O$ records is further supported by the resulting close phase relationship of the planktonic $\delta^{18}O$ records of both cores, which show a high degree of synchronicity (not shown). The MD97-2120 age model is based on graphic correlations with both North Atlantic core MD95-2042 and Antarctic ice core Vostok δD record [*Pahnke et al.*, 2003]. MD97-2120 chosen as a reference to develop the age model for core MD02-2589 because it allowed direct correlation with Antarctic records as well as core MD95-2042 and other Northern Hemisphere climate records. The MD97-2120 benthic $\delta^{18}O$ profile has a similar structure to MD02-2589 especially over the MIS 5a/4 transition and in some of the smaller scale features thus facilitating the correlation (Figures 2a and 2b). Ages between each age control point were estimated by linear interpolation. The resulting age model suggests sedimenta-

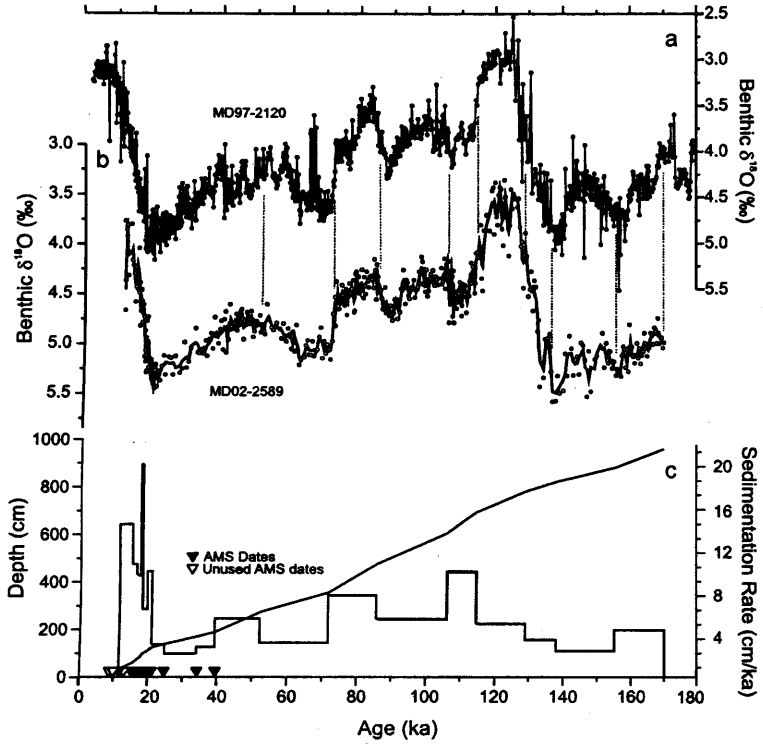

Figure 2. Chronology of core MD02-2589. (a) Benthic $\delta^{18}O$ record of core MD97-2120 [*Pahnke et al.*, 2003] and (b) benthic $\delta^{18}O$ record of MD02-2589, also showing tie points used for correlation, and (c) sedimentation rate and the position of both used and unused radiocarbon dates.

tion rates vary between ~15 cm ka^{-1} during glacials and ~5.5 cm ka^{-1} during interglacials (Figure 2c). At our 2 cm sampling resolution this equates to a mean time step along our proxy records of 298 ± 132 a.

5. Results

[15] The high-resolution benthic $\delta^{18}O$ record of MD02-2589 (Figure 3a) shows that orbital modulation caused by changing ice volume is the dominant control on this record. However, as the glacial-interglacial (G-I) benthic $\delta^{18}O$ amplitudes of the record ($\delta^{18}O$ ~2‰) are significantly greater than the shift associated with global ice volume changes ($\delta^{18}O$ 1–1.2‰ [*Schrag et al.*, 2002]) additional hydrographic changes in regional bottom water temperature and/or salinity are indicated over these timescales. The Holocene section in MD02-2589 is incomplete thus limiting our confidence in the reliability of the LGM to Holocene transition to assess the full G-I $\delta^{18}O$ shift at this location. As a result in the following discussion, only Termination II (TII) will be considered in detail. The benthic $\delta^{13}C$ record (Figure 3b) shows a G-I amplitude of ~0.8‰ ranging from values of −0.2–0‰ indicative of low ventilation during glacial stages MIS 6 and LGM, as well as MIS 4, to increased levels during warm stages MIS 5 and 3, with a more steady transition at TII than observed in the benthic $\delta^{18}O$ record. In contrast to the benthic $\delta^{18}O$ the benthic $\delta^{13}C$ values remain fairly consistent throughout MIS 5, with only modest orbital modulation, with minimum benthic $\delta^{13}C$ values occurring 5–7 ka after maximum benthic $\delta^{18}O$ associated with each cold substage. Conversely, benthic $\delta^{13}C$ shows clear evidence for millennial scale variability during MIS 3, which is not as apparent in the $\delta^{18}O$ record (Figure 3).

[16] The modern salinity distribution (Figure 1b) for the Agulhas sector of the Southern Ocean shows that site MD02-2589 lies in the southern extent of NADW close to where it merges with LCDW. Present-day NADW $\delta^{13}C$ in the South Atlantic typically has values of ~0.8‰ and LCDW is <0.5‰ [*Bickert and Wefer*, 1996]. A transect of late Holocene benthic $\delta^{13}C$ in the South Atlantic [*Mackensen et al.*, 2001] confirms that MD02-2589 ($\delta^{13}C$ ~0.65‰, Figure 3b) is currently positioned near the mixing zone between NADW and LCDW with the admixture of >50% NADW [e.g., *Bickert and Mackensen*, 2003]. Benthic $\delta^{13}C$ values in MIS 5 average 0.65‰ which again equates well with predicted $\delta^{13}C$ of NADW in the South Atlantic during interglacial periods (~0.6 – 0.7‰ [*Sarnthein et al.*, 1994]).

[17] The MD02-2589 $\overline{SS}$ record (Figure 3c) also reflects a distinctive orbital modulation, with higher values during glacial periods indicating enhanced near-bottom flow speeds. The amplitude of these G-I shifts in $\overline{SS}$ (G-I shift of 4 μm) are comparable to those seen at Ocean Drilling

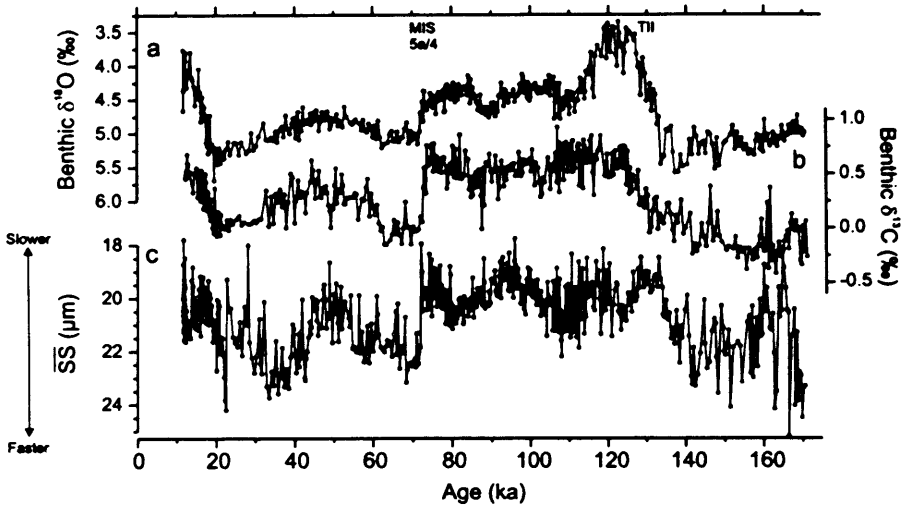

Figure 3. Benthic records of core MD02-2589 showing (a) benthic $\delta^{18}O$, (b) benthic $\delta^{13}C$, and (c) sortable silt mean grain size. Intervals focused on in this study are highlighted by the gray shading. MIS 5a/4, transition between marine oxygen isotope stages 5a and 4; TII, Termination II.

Program (ODP) Site 1123 in the SW Pacific (3–4 μm, [*Hall et al.*, 2001]) and core BOFS 6K from the East Thulean Rise, North Atlantic (3–4 μm, [*McCave et al.*, 1995b]). The modulation of $\overline{SS}$ within MIS 5 is offset from that seen in benthic $\delta^{18}O$ such that during the colder substages, MIS 5d and 5b flow speeds are in transition from low- to high-$\overline{SS}$ values reaching maximum values early in the following warm interval. While the $\overline{SS}$ record exhibits the highest degree of millennial scale variance throughout the entire interval, it is noticeable that within MIS 3, amplitudes of millennial scale variability in the $\delta^{13}C$ record are likewise increased and are substantially greater than those observed in the benthic $\delta^{18}O$ record (Figure 3). A complex temporal phasing across TII (and Termination I (TI)) is evident between each of the proxy records but the inferred flow speed changes and benthic $\delta^{13}C$ records are broadly negatively correlated on orbital timescales suggesting that periods of enhanced physical circulation ($\overline{SS}$) went along with reduced chemical ventilation (benthic $\delta^{13}C$).

5.1. Glacial Terminations I and II

[18] At 141 ka, $\overline{SS}$ grain sizes at site MD02-2589 decrease rapidly coincident with the onset of a more gradual increase in benthic $\delta^{13}C$, both preceding full glacial MIS 6.2 by some 3–4 ka (Figure 4). This initial reduction in flow speed and coeval onset of increasing ventilation occur some 8 ka before the start of the deglacial transition of TII at 133 ka (Figures 4d and 4f). Although hampered by the lack of Holocene recovery, the sequence of changes at TI suggests some differences from those occurring at TII (Figure 3). While an early decrease in flow speed and a low-flow speed plateau occurs within TI, in contrast to TII, benthic $\delta^{13}C$ appears to increase coincident with decreasing benthic $\delta^{18}O$. This TI sequence and the lead of THC changes (ventilation and near-bottom flow speeds) over ice volume during TII in MD02-2589 is contrary to the sequence recently identified for TI by *Piotrowski et al.* [2005] suggesting a more complex phasing may be a feature of individual glacial terminations.

[19] The TII benthic $\delta^{13}C$ transition occurs in two steps. The initial intensification in ventilation, starting before the ice volume maximum at 141 ka, is gradual and only increases by 0.2‰ over 11 ka. This is followed by a larger and more rapid increase, starting at 130 ka, of 0.6‰ over 6 ka. Benthic $\delta^{13}C$ values also reach interglacial levels coincident with the $\delta^{13}C$ record of MD95-2042 and after the benthic $\delta^{18}O$ of MD02-2589 (Figure 4).

[20] The initial $\overline{SS}$ grain size decrease at 141 ka is halted by a reversal to faster near-bottom currents occurring between 139 and 138 ka coincident with the benthic $\delta^{18}O$ maximum. A more sustained flow speed decrease follows, reaching a period of prolonged low-flow speeds starting at 133 ka coincident with the start of TII in the benthic $\delta^{18}O$ record and lasting some 6 ka. A similar midtermination feature is seen in the benthic $\delta^{13}C$ records of RC11-83 and MD97-2120 during TII but intriguingly does not appear in the benthic $\delta^{13}C$ record of MD02-2589 (Figure 4).

5.2. MIS 5/4 Transition

[21] One of the most striking features seen in MD02-2589 records is the rapid transition between MIS 5a and MIS 4 (Figures 3 and 5). On the basis of our age model the transition starts at 73 ka from high benthic $\delta^{13}C$ values and low-flow speeds. The transition proceeds with a sharp transient increase in benthic $\delta^{18}O$ of 0.45‰ and decrease in benthic $\delta^{13}C$ of 0.4‰. Within 700 a of this excursion, flow speeds rapidly decrease reaching a minimum at 72 ka. An abrupt transition then occurs in all proxies reaching full MIS 4 conditions at 71.3 ka. The transition is led by increasing ice volume and followed by decreasing ventilation and then finally increasing flow speeds (Figure 5).

6. Discussion

[22] Temporal changes in benthic $\delta^{13}C$ at any location reflect some combination of the changes in the marine

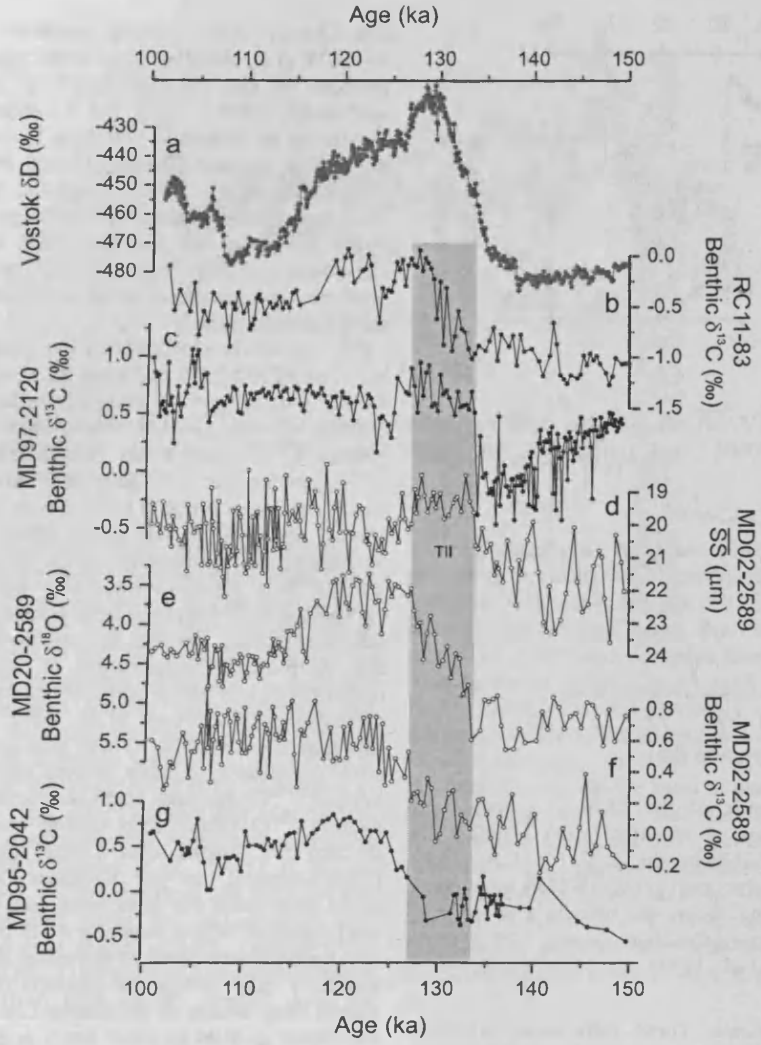

Figure 4. Southern Hemisphere records for Termination II. (a) Vostok δD [*Petit et al.*, 1999], (b) RC11-83 benthic δ^{13}C [*Charles et al.*, 1996], (c) MD97-2120 benthic δ^{13}C [*Pahnke and Zahn*, 2005], (d) MD02-2589 sortable silt mean grain size, (e) MD02-2589 benthic δ^{18}O, (f) MD02-2589 benthic δ^{13}C, and (g) MD95-2042 benthic δ^{13}C [*Shackleton et al.*, 2000]. Gray shading shows TII as indicated by MD02-2589 benthic δ^{18}O.

carbon reservoir, ocean circulation, air-sea gas exchange, and marine biological productivity [e.g., *Broecker and Maier-Reimer*, 1992; *Mackensen et al.*, 1993; *Lynch-Stieglitz and Fairbanks*, 1994; *Mackensen and Bickert*, 1999; *Oppo and Horowitz*, 2000] and have traditionally been a tool with which to trace deep water masses. [e.g., *Streeter and Shackleton*, 1979; *Sigman and Boyle*, 2000; *Bostock et al.*, 2004]. In the South Atlantic, high δ^{13}C signatures signify young, nutrient-depleted, well-ventilated North Atlantic Deep Waters, while lower increasingly negative δ^{13}C values are linked to older, nutrient-enriched Antarctic water masses which have reduced ventilation due to long isolation from the atmosphere. Fluctuations in δ^{13}C in this region are linked to variations in the proportion of better ventilated NCW versus lesser ventilated SCW. The mean grain size of the 10–63 μm size fraction ($\overline{SS}$) responds linearly to changes in flow conditions 20–100 m above the bed [*McCave et al.*, 1995b], with higher grain sizes denoting faster flow and vice versa. The region south of ~40°S in the Southern Ocean is dominated by the ACC, with changes in $\overline{SS}$ plausibly reflecting variations in the strength of its flow. The ACC flow is driven by surface wind forcing which may affect the whole water column through frictional effects down to deeper depths [*Orsi et al.*, 1995] and is therefore linked into Southern Hemisphere climate change, as is the expansion and contraction of the surface ocean fronts. However, the strengthening and weakening of the ACC can also therefore be possible

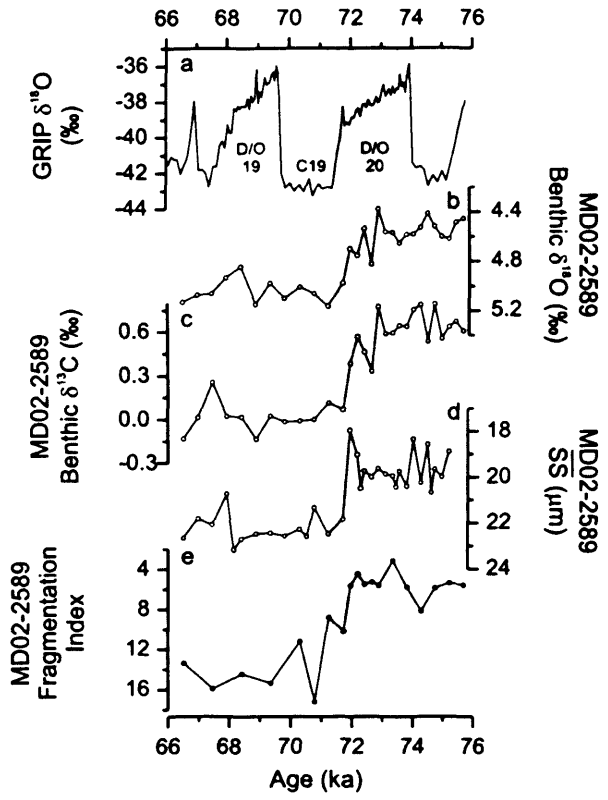

Figure 5. Proxy records of the MIS 5a-4 transition. (a) GRIP $\delta^{18}O$ [*Johnsen et al.*, 1997], (b) MD02-2589 benthic $\delta^{18}O$, (c) MD02-2589 benthic $\delta^{13}C$, (d) MD02-2589 sortable silt mean grain size, and (e) MD02-2589 fragmentation index. Gray shading shows the transition as defined in the text. D/O, Dansgaard-Oeschger events; C19, Greenland event [*McManus et al.*, 1994].

without frontal movements. These differences in tracer signals allow a decoupling of flow speed and water mass provenance at certain sites, which can be explained by changes in different components of a mixed water mass affecting either provenance or flow speed in different ways.

[23] The export of NCW from the North Atlantic during glacial periods is poorly constrained and has been discussed controversially in literature [e.g., *Sarnthein et al.*, 1994; *Yu et al.*, 1996; *Matsumoto et al.*, 2001; *Curry and Oppo*, 2005]. In order to identify the NCW influence at the MD02-2589 site during glacial periods we compare our data with several existing benthic $\delta^{13}C$ records. For this comparison we have chosen deep South Atlantic cores RC11-83 [*Charles et al.*, 1996] and TN057-21 (Table 2 [*Ninnemann and Charles*, 2002]), which remained strongly influenced by SCW (i.e., AABW) over both glacial and interglacial periods. We also use core MD97-2120 (Table 2 [*Pahnke and Zahn*, 2005]) from the Chatham Rise, southwest Pacific, as an alternative Southern Ocean record documenting AAIW variability. Finally, core MD95-2042 (Table 2 [*Shackleton et al.*, 2000]) from the Iberian Margin was chosen as a North Atlantic reference as it is high resolution, has a timescale that has been tied to both Vostok and Greenland Ice Core Project (GRIP) and reflects changing northern versus southern water sources in the North Atlantic during glacial periods.

[24] Offsets in amplitude of the benthic $\delta^{18}O$ G-I shifts between MD02-2589 and sites RC11-83, MD97-2120, and MD95-2042 (Figure 6) plausibly reflect differences in *T-S* changes of water masses bathing each site. Average glacial benthic $\delta^{18}O$ values at site MD02-2589 are between 0.3–0.7‰ heavier than average glacial values in cores from the South Atlantic (core RC11-83), North Atlantic (core MD95-2042), and SW Pacific (core MD97-2120) (Figure 6), suggesting that deep water at the Agulhas Plateau during the last two glacial periods was colder or saltier (or a combination of both) than deep waters in the North Atlantic and intermediate water in the southwest Pacific. Assuming that deep ocean temperature in the glacial ocean was uniformly colder and presumably close to the freezing point of seawater [*Waelbroeck et al.*, 2002; *Adkins et al.*, 2002], this makes seawater $\delta^{18}O$ and thus salinity the most plausible candidates to have caused the observed offsets in benthic $\delta^{18}O$, although there was probably a very different salinity-$\delta^{18}O$ relationship during glacial periods than in modern day. *Adkins et al.* [2002] and *Adkins and Schrag* [2003] suggest that the Southern Ocean had the saltiest LGM deep water due to increased sea-ice formation. As sea-ice formation offsets seawater $\delta^{18}O$ from its global correlation with salinity, some of the offset in benthic $\delta^{18}O$ seen in Figure 4 may reflect the contribution of these Southern Ocean deep waters to the deeper core sites, namely RC11-83, which at 4600 m water depth and at a location close to the Southern Ocean most likely records modified AABW.

[25] The mean ocean shift of $\delta^{13}C$ in seawater ΣCO_2 between the LGM and Holocene has been estimated to be between 0.32‰ [*Duplessy et al.*, 1988] and 0.46‰ [*Curry et al.*, 1988]. The benthic $\delta^{13}C$ G-I shift observed in MD02-2589 of 0.8‰ (Termination II Figure 3b) suggests an additional 0.3–0.4‰ variation in $\delta^{13}C$ must be explained by varying water masses, surface productivity changes, and/or air-sea exchange processes. This additional 0.3–0.4‰ $\delta^{13}C$ G-I variation is 20–40% less than the benthic $\delta^{13}C$ shift of 0.5‰ predicted for a complete halt of NCW advection to the south [*Charles et al.*, 1996]. The reduced

Table 2. Station Data for Cores Used in This Study

Core	Latitude	Longitude	Depth, m	Reference
MD02-2589	41°19′S	25°15′E	2660	This study
RC11-83	41°36′S	9°48′E	4718	*Charles et al.* [1996]
TN057-21	41°08′S	7°49′E	4981	*Ninnemann and Charles* [2002]
MD97-2120	45°32′S	174°55′E	1210	*Pahnke and Zahn* [2005]
MD95-2042	37°48′N	10°10′W	3146	*Shackleton et al.* [2000]

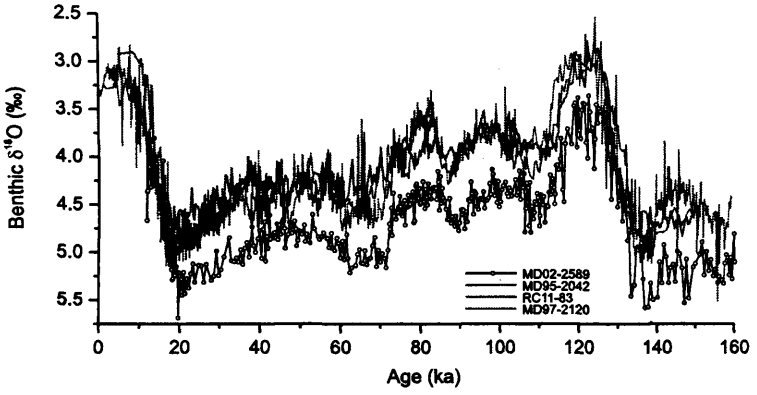

Figure 6. Records of benthic $\delta^{18}O$ of *Fontbotia wuellerstorfi* from MD02-2589, RC11-83 [*Charles et al.*, 1996], MD97-2120 [*Pahnke et al.*, 2003], and MD95-2042 [*Shackleton et al.*, 2000]. All data are shown on the Uvigerina scale.

$\delta^{13}C$ shift observed in MD02-2489 therefore indicates a persistent contribution of a well-ventilated water mass to the ambient glacial bottom waters with a $\delta^{13}C$ signature similar to present-day NCW. This can either be explained as sustained NCW influence at the site over the past 170 ka or the presence of SCW exhibiting a similar $\delta^{13}C$ signature from air-sea gas exchanges. Studies have suggested that during glacial periods, enhanced production of deep waters occurred in the zone of extended winter sea ice coverage (out to ~50°S) south of the Polar Front (PF) [*Rosenthal et al.*, 1997; *Mackensen et al.*, 2001; *Bickert and Mackensen*, 2003] and as a second shallower deep water mass along the Subantarctic Front (SAF) [*Michel et al.*, 1995]. If any of these scenarios holds true, the proximity of site MD02-2589 to the SAF would bring it under the influence of this shallower water mass during glacial periods. Benthic $\delta^{13}C$ of *F. wuellerstorfi* in MD02-2589 remains consistently more positive by ~0.7‰ than that in the deeper AABW-influenced cores RC11-83 and TN057-21(Figure 7) further providing evidence for a consistently better ventilation of middepth isopycnals. Benthic $\delta^{13}C$ from cores located in the deeper Cape Basin [*Charles and Fairbanks*, 1992; *Bickert and Wefer*, 1999] and carbonate dissolution in the Cape and Angola basins inferred from sand contents [*Bickert and Wefer*, 1996] were used previously to infer reduced NADW advection to the south leading to a reduced contribution to or even complete absence of NCW in the deep glacial Southern Ocean. On the basis of our data we conclude that this scenario may not hold for the high-latitude South Atlantic as a whole but that a better ventilated water mass must have been present at middepth. This is further suggested in a study by *Hodell et al.* [2003] based on a vertical transect of benthic $\delta^{13}C$ at the Agulhas Ridge, which suggests the presence of a well-developed chemocline in the South Atlantic at the LGM with a sharp chemical divide

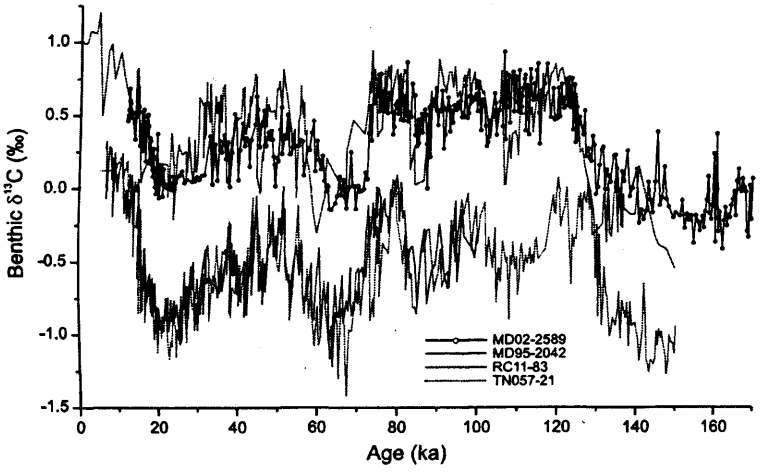

Figure 7. Records of benthic $\delta^{13}C$ of *Fontbotia wuellerstorfi* from MD02-2589, RC11-83 [*Charles et al.*, 1996], TN057-21 [*Ninnemann and Charles*, 2002], and MD95-2042 [*Shackleton et al.*, 2000].

between well-ventilated middepth waters above 2500 m and less well-ventilated deep waters below.

[26] *Hall et al.* [2001] found $\overline{SS}$ grain sizes at ODP Site 1123 in the SW Pacific were coherent with both benthic $\delta^{18}O$ and $\delta^{13}C$ isotopes at each orbital frequency. A clear relationship was also seen between $\overline{SS}$ and the Pacific deep water $\delta^{13}C$ aging trends ($\Delta\delta^{13}C$ ODP Sites 1123–849) with periods of decreased aging inferred from isotopes associated with increased Deep Western Boundary Current (DWBC) flow speeds (physical ventilation). *Hall et al.* [2001] concluded that such flow changes may be directly related to increased production of AABW during the glacials potentially controlled by Southern Ocean winds or greater annual production of sea ice leading to water densification through brine rejection. A similar orbital scale relationship between benthic $\delta^{13}C$ and changing near-bottom flow speeds is observed in the MD02-2589 records, with decreased benthic $\delta^{13}C$ and increased near-bottom flow speeds during glacial periods. However, given that benthic $\delta^{13}C$ at MD02-2589 suggests better ventilation at middepths (compared to bottom water sites), additional controls on physical ventilation are indicated. The total transport of the ACC is thought to be around 130 sverdrup (10^6 m^3 s^{-1}) [*Whitworth and Peterson*, 1985; *Cunningham et al.*, 2003] with the bulk of this transport occurring within deep-reaching narrow jets at the PF and SAF, at a mean water depth of 3000 m [*Nowlin and Klinck*, 1986; *Gille*, 1994; *Orsi et al.*, 1995]. At the present-day, MD02-2589 lies to the north of both the PF and SAF (by ~8° and ~3°, respectively [*Belkin and Gordon*, 1996; *Anilkumar et al.*, 2005]) and therefore outside the immediate ACC. Increased flow speeds during glacial periods (Figure 3c), however, imply that both mobile surface ocean fronts shifted to the north [*Mackensen et al.*, 2001; *Hays et al.*, 1976; *Burckle*, 1984; *Pudsey and Howe*, 1998]. Thus MD02-2589 plausibly came within the reach of the ACC and its faster flowing deep current jets during glacial periods that presumably restricted the southward transports of northern source deep waters deep into the Southern Ocean. Better ventilation of ambient bottom waters at the core site, in this case, would more clearly support a contribution of a Southern Ocean water mass with a ventilation signature influenced by air-sea gas exchange, similar to that seen in AAIW today.

6.1. Glacial Termination

[27] *Bianchi and Gersonde* [2002] describe a southward displacement of the edge of the winter sea ice and a sea surface temperature warming in the Atlantic and western Indian Antarctic Zone, prior to MIS 5e, during late MIS 6 that was followed by a southward shift of the PF by 3–5° latitude from its current position during the late termination. The increase in ventilation displayed in the benthic $\delta^{13}C$ record of core RC11-83 and MD97-2120 and the sustained decrease in flow speeds at MD02-2589 starting at ~138 ka (Figure 4) likely correspond to this SST warming. Minimum flow speeds at MD02-2589 and maximum benthic $\delta^{13}C$ values in RC11-83 and MD97-2120 (Figure 4) coincide with the southward shift of the PF. Evidence for warming within the region during late MIS 6 and a climate optimum within the glacial termination has recently been shown by faunal records of *Peeters et al.* [2004] from the South African margin which suggest that following the arrival of the Subtropical Front at its most northerly location during peak MIS 6, it started to move southward well before the start of the termination allowing increased leakage through the Indian-Atlantic surface throughflow area that reaches a maximum within TII (also seen in modeling evidence of *Knorr and Lohmann* [2003]). Additionally, a sea level record from the Red Sea [*Siddall et al.*, 2006] shows a highstand during TII which lasted several millennia, followed by a reversal of 30 to 40 ± 12 m coincident with the early warming of the southern latitudes. Correlating the benthic $\delta^{18}O$ shifts and circulation proxy changes in cores MD02-2589 and MD97-2120 [*Pahnke et al.*, 2003] with the Vostok ice core, suggests that the prominent δD peak in Vostok that is indicative of peak maximum air temperatures over Antarctica [*Petit et al.*, 1999] (and EPICA Dome C records [*Jouzel et al.*, 2004]) occurred prior to full-interglacial MIS 5e during mid-TII (Figure 4), although age model constraints do not currently allow us to further address this possibility.

[28] The climate optimum within the transition is followed by a marked cooling at around 128 ka, seen in Vostok δD, and is coincident with an increase in flow speed at MD02-2589, a decrease in ventilation at RC11-83 and MD97-2120 (Figure 4), and a southern high-latitude-wide SST cooling and expansion of the winter sea ice limit [*Bianchi and Gersonde*, 2002]. The cooling of the Antarctic continent evident in the Vostok δD record has been linked with an intensification of Northern Hemisphere deep water to full interglacial levels [*Sarnthein and Tiedemann*, 1990; *Diekmann et al.*, 1996; *Spero and Lea*, 2002], a suggestion that is supported by the benthic $\delta^{13}C$ record of MD02-2589 which show an increase in ventilation during this event reaching maximum levels at around 124 ka. Given the benthic $\delta^{18}O$ record of MD02-2589 suggests that the onset of MIS 5e occurs at 127 ka (Figure 4), then this period of increased flow speeds and ventilation at Agulhas Plateau and the wider Southern Hemisphere cooling occurs during the earliest part of the full interglacial.

[29] From the above we conclude that during TII, changes in chemical ventilation, related to the southward advection of NCW, are largely decoupled at site MD02-2589 from near-bottom physical flow speeds that primarily relate to the expansion and contraction of the ACC in association with meridional movements of the PF and SAF.

6.2. MIS 5/4 Transition

[30] The MIS 5a/4 transition starts at 73 ka from benthic $\delta^{13}C$ values indicative of maximum NCW influence and low-flow speed values suggestive of weakened ACC flow (Figures 3 and 5). This supports the suggestion by *Peeters et al.* [2004] for a strong input of NADW to the Southern Ocean associated with an abundance peak in Agulhas leakage fauna, observed in core MD01-2081, before the MIS 5a/4 transition recorded in its associated benthic $\delta^{18}O$ record and plausibly interpreted as a westward propagation of the Agulhas Current and an enhanced Indian-Atlantic surface transport.

[31] The changes observed in $\overline{SS}$ and benthic $\delta^{13}C$ at the transition are similar in magnitude to the opposite trends seen during the TII glacial-interglacial shifts. The MIS 5a/4 benthic $\delta^{13}C$ shift (~0.9‰) is also similar in magnitude to those observed in deep AABW-influenced cores TN057-21 and RC11-83 (~0.95‰). Although a significant portion of the MIS 5a/4 benthic $\delta^{13}C$ shift is likely due to a change in the carbon reservoir signal [*Piotrowski et al.*, 2005], as MIS 4 constitutes full glacial conditions for the first time after the prolonged interglacial conditions of MIS 5, these data along with the near-bottom flow speeds suggest a decrease in NADW influence and an expansion of the SCW over the Agulhas Plateau.

[32] This switch in water mass influence is consistent with a coeval transition in the MD02-2589 record from low fragmentation percentage, indicative of a carbonate saturated water mass sustaining higher levels of carbonate preservation (e.g., NCW), to high fragmentation percentage, indicative of a carbonate undersaturated water mass more corrosive to carbonates (e.g., SCW) [*Henrich et al.*, 2003; *Pfuhl and Shackleton*, 2004]) (Figure 5e). In addition, records from ODP Site 1059 (32.1°N, 76.4°W, 2584 m water depth) and 1057 (31.40°N, 75.25°W, 2985 m water depth) from the Blake Outer Ridge (BOR), North Atlantic [*Evans et al.*, 2007], show a sharp, short-lived, negative excursion in benthic $\delta^{13}C$ over the sites at 73.2 ka and 71.6 ka, respectively, during the transition in their associated benthic $\delta^{18}O$ records, which is attributed to an abrupt shoaling (to <2500 m) of the DWBC at the BOR associated with a reduction in production of NADW, at the MIS 5a/4 transition. The GRIP ice core $\delta^{18}O$ record from Greenland [*Johnsen et al.*, 1997] also exhibits a significant cold event (C19 in contemporaneous marine cores [*McManus et al.*, 1994]) at 71.5 ka (Figure 5). Neodymium isotope analysis on cores RC11-83 and TN057-21 [*Piotrowski et al.*, 2005] also confirm this event, showing a rapid decrease in the proportion of NADW in bottom water over this transition.

7. Conclusions

[33] Our high-resolution benthic $\delta^{13}C$ record from core MD02-2589 strongly suggests that there was a continued source for enhanced middepth ventilation over the southern Agulhas Plateau during glacial periods. While the influence of NCW may have been reduced in the glacial South Atlantic, additional well-ventilated waters plausibly have originated in the Southern Ocean. Significantly increased near-bottom flow speeds during glacial periods at MD02-2589 indicate that the vigor of near-bottom currents on the southern Agulhas Plateau is likely influenced by orbital scale meridional expansion and contraction of the ACC and its associated surface fronts.

[34] Ventilation and flow speeds show a late MIS 6 circulation change, associated with the previously documented [e.g., *Bianchi and Gersonde*, 2002] regional frontal shifts and SST warming in the Southern Ocean, occurring some 8 ka before the start of TII recorded in the benthic $\delta^{18}O$. A mid-TII climate optimum is highlighted in the MD02-2589 record by a transient episode of low-flow speeds concurrent with a period of increased ventilation shown in the benthic $\delta^{13}C$ records from other cores from Southern Ocean deep (RC11-83) and intermediate (MD97-2120) sites. This event is not recorded in the benthic $\delta^{13}C$ of MD02-2589.

[35] All of the MD02-2589 records show a rapid, but sequenced, event occurring at the MIS 5a/4 transition, in which changes in flow speed and chemical ventilation were of a similar magnitude (but opposite direction) to those occurring at TII. These changes suggest a switch in the relative influence of northern and southern source waters, together with an increased influence of the ACC, toward MIS 4. This event can be linked to the sudden shoaling of NADW and reduction in its production possibly related to GRIP 2 cold event C19.

[36] **Acknowledgments.** We are grateful to G.G. Bianchi, J. Becker, and H. Medley for assistance with sample preparation and analysis. E.M. and I.H. acknowledge support by the Natural Environment Research Council (NERC) and the NERC Radiocarbon Laboratory, UK. R.Z. acknowledges support from the Ministerio de Educacion y Ciencias, Spain. We would also like to thank A.M. Piotrowski, E. Michel, B. Diekmann, and an anonymous reviewer for their constructive reviews and comments which greatly improved this manuscript. G. Martinez-Mendez, Universitat Autònoma de Barcelona, provided her insight into the paleoceanography of the Agulhas Corridor region. We thank the Institut Polaire Français Paul Emile Victor for technical support and for making the R/V *Marion Dufresne* available and J. Giraudeau and Y. Balut for their support in recovering this core.

References

Adkins, J. F., and D. P. Schrag (2003), Reconstructing Last Glacial Maximum bottom water salinities from deep-sea sediment pore fluid profiles, *Earth Planet. Sci. Lett.*, *216*, 109–123.

Adkins, J. F., K. McIntyre, and D. P. Schrag (2002), The salinity, temperature, and $\delta^{18}O$ of the glacial deep ocean, *Science*, *298*, 1769–1773.

Anilkumar, N., M. K. Dash, A. J. Luis, V. Ramesh Babu, Y. K. Somayajulu, M. Sudhakar, and P. C. Pandey (2005), Oceanic fronts along 45°E across Antarctic Circumpolar Current during austral summer 2004, *Curr. Sci.*, *88*, 1669–1673.

Belkin, I. M., and A. L. Gordon (1996), Southern Ocean fronts from the Greenwich meridian to Tasmania, *J. Geophys. Res.*, *101*, 3675–3696.

Bianchi, C., and R. Gersonde (2002), The Southern Ocean surface between Marine Isotope Stages 6 and 5d: Shape and timing of climate changes, *Palaeogeogr. Palaeoclimatol. Palaeoecol.*, *187*, 151–177.

Bianchi, G. G., and I. N. McCave (1999), Holocene periodicity in North Atlantic climate and deep-ocean flow south of Iceland, *Nature*, *397*, 515–517.

Bianchi, G. G., I. R. Hall, I. N. McCave, and L. Joseph (1999), Measurement of the sortable silt current speed proxy using the Sedigraph 5100 and Coulter Multisizer IIe: Precision and accuracy, *Sedimentology*, *46*, 1001–1014.

Bickert, T., and A. Mackensen (2003), Last glacial to Holocene changes in South Atlantic deep water circulation, in *The South Atlantic in the Late Quaternary: Reconstruction of Material Budgets and Current Systems*, edited by G. Wefer, S. Mulitza, and V. Ratmeyer, pp. 671–695, Springer-Verlag, Berlin.

Bickert, T., and G. Wefer (1996), Late Quaternary deep water circulation in the South Atlantic: Reconstruction from carbonate dissolution and benthic stable isotopes, in *The South Atlantic: Present and Past Circulation*, edited

by G. Wefer et al., pp. 599–620, Springer-Verlag, Berlin.

Bickert, T., and G. Wefer (1999), South Atlantic and benthic foraminifer $\delta^{13}C$ deviations: Implications for reconstructing the late Quaternary deep-water circulation, *Deep Sea Res. Part II, 46*, 437–452.

Blunier, T., and E. J. Brook (2001), Timing of millennial-scale climate change in Antarctica and Greenland during the last glacial period, *Science, 291*, 109–112.

Blunier, T., et al. (1998), Asynchrony of Antarctic and Greenland climate change during the last glacial period, *Nature, 394*, 739–743.

Boebel, O., J. Lutjeharms, C. Schmid, W. Zenk, T. Rossby, and C. Barron (2003), The Cape Cauldron: A regime of turbulent inter-ocean exchange, *Deep Sea Res. Part II, 50*, 57–86.

Bostock, H. C., B. N. Opdyke, M. K. Gagan, and L. K. Fifield (2004), Carbon isotope evidence for changes in Antarctic Intermediate Water circulation and ocean ventilation in the southwest Pacific during the last deglaciation, *Paleoceanography, 19*, PA4013, doi:10.1029/2004PA001047.

Boyle, E. A. (1992), Cadmium and $\delta^{13}C$ paleochemical ocean distributions during the stage 2 glacial maximum, *Annu. Rev. Earth Planet. Sci., 20*, 245–287.

Boyle, E. A., and L. D. Keigwin (1987), North Atlantic thermohaline circulation during the past 20,000 years linked to high-latitude surface temperature, *Nature, 330*, 35–40.

Broecker, W. S., and E. Maier-Reimer (1992), The influence of air and sea exchange on the carbon isotope distribution in the sea, *Global Biogeochem. Cycles, 6*, 315–320.

Brook, E. J., J. W. C. White, A. S. M. Schilla, M. L. Bender, B. Barnett, J. P. Severinghaus, K. C. Taylor, R. B. Alley, and E. J. Steig (2005), Timing of millennial-scale climate change at Siple Dome, West Antarctica, during the last glacial period, *Quat. Sci. Rev., 24*, 1333–1343.

Burckle, L. H. (1984), Diatom distribution and paleogeographic reconstruction in the Southern Ocean: Present and Last Glacial Maximum, *Mar. Micropaleontol., 9*, 241–261.

Butzin, M., M. Prange, and G. Lohmann (2005), Radiocarbon simulations for the glacial ocean: The effects of wind stress, Southern Ocean sea ice, and Heinrich events, *Earth Planet. Sci. Lett., 235*, 45–61.

Charles, C. D., and R. G. Fairbanks (1992), Evidence from Southern Ocean sediments for the effect of North Atlantic deep-water flux on climate, *Nature, 355*, 416–419.

Charles, C. D., J. Lynch-Stieglitz, U. S. Ninnemann, and R. G. Fairbanks (1996), Climate connections between the hemisphere revealed by deep sea sediment core/ice core correlations, *Earth Planet. Sci. Lett., 142*, 19–27.

Cunningham, S. A., S. G. Alderson, B. A. King, and M. A. Brandon (2003), Transport and variability of the Antarctic Circumpolar Current in Drake Passage, *J. Geophys. Res., 108*(C5), 8084, doi:10.1029/2001JC001147.

Curry, W. B., and D. W. Oppo (2005), Glacial water mass geometry and the distribution of $\delta^{13}C$ of ΣCO_2 in the western Atlantic Ocean, *Paleoceanography, 20*, PA1017, doi:10.1029/2004PA001021.

Curry, W. B., J.-C. Duplessy, L. Labeyrie, and N. J. Shackleton (1988), Changes in the distribution of $\delta^{13}C$ of deep water ΣCO_2 between the last glaciation and the Holocene, *Paleoceanography, 3*, 317–341.

de Ruijter, W. P. M., A. Biastoch, S. S. Drijfhout, J. R. E. Lutjeharms, R. P. Matano, T. Pichevin, P. J. van Leeuwen, and W. Weijer (1999), Indian-Atlantic interocean exchange: Dynamics, estimation and impact, *J. Geophys. Res., 104*, 20,885–20,910.

Diekmann, B., R. Petschick, F. X. Gingele, D. K. Futterer, A. Abelmann, U. Brathauer, R. Gersonde, and A. Mackensen (1996), Clay mineral fluctuations in late Quaternary sediments of the southeastern South Atlantic: Implications for past changes in deep water advection, in *The South Atlantic: Present and Past Circulation*, edited by G. Wefer et al., pp. 621–644, Springer-Verlag, Berlin.

Duplessy, J.-C., N. J. Shackleton, R. G. Fairbanks, L. Labeyrie, D. Oppo, and N. Kallel (1988), Deepwater source variations during the last climatic cycle and their impact on the global deepwater circulation, *Paleoceanography, 3*, 343–360.

Ellison, C. R. W., M. R. Chapman, and I. R. Hall (2006), Surface and deep ocean interactions during the cold climate event 8200 years ago, *Science, 312*, 1929–1932.

EPICA Community Members (2006), One-to-one hemispheric coupling of millennial polar climate variability during the last glacial, *Nature, 444*, 195–198.

Evans, H. K., I. R. Hall, G. G. Bianchi, and D. W. Oppo (2007), Intermediate water links to Deep Western Boundary Current variability in the subtropical NW Atlantic during marine isotope stages 5 and 4, *Paleoceanography, 22*, PA3209, doi:10.1029/2006PA001409.

Fairbanks, R. G., R. A. Mortlock, T.-C. Chiu, L. Cao, A. Kaplan, T. P. Guilderson, T. W. Fairbanks, A. L. Bloom, P. M. Grootes, and M.-J. Nadeau (2005), Radiocarbon calibration curve spanning 0 to 50,000 years BP based on paired 230Th/234U/238U and 14C dates on pristine corals, *Quat. Sci. Rev., 24*, 1781–1796.

Ganopolski, A., and S. Rahmstorf (2001), Rapid changes of glacial climate simulated in a coupled climate model, *Nature, 409*, 153–158.

Gherardi, J. M., L. Labeyrie, J. F. McManus, R. Francois, L. C. Skinner, and E. Cortijo (2005), Evidence from the northeastern Atlantic basin for variability in the rate of the meridional overturning circulation through the last deglaciation, *Earth Planet. Sci. Lett., 240*, 710–723.

Gille, S. T. (1994), Mean sea surface height of the Antarctic Circumpolar Current from Geosat data: Method and application, *J. Geophys. Res., 99*(C9), 18,255–18,273.

Giraudeau, J., R. Zahn, and I. R. Hall (2002), Agulhas current variability: Calypso long sediment coring off South Africa, cruise report R/V Marion Dufresne cruise MD128, Dept. of Geol. and Oceanogr., Univ. of Bordeaux, Talence, France.

Gordon, A. L. (1996), Comment of the South Atlantic's role in the global circulation, in *The South Atlantic: Present and Past Circulation*, edited by G. Wefer et al., pp. 121–124, Springer-Verlag, Berlin.

Hall, I. R., I. N. McCave, M. R. Chapman, and N. J. Shackleton (1998), Coherent deep flow variation in the Iceland and American basins during the last interglacial, *Earth Planet. Sci. Lett., 164*, 15–21.

Hall, I. R., I. N. McCave, N. J. Shackleton, G. P. Weedon, and S. E. Harris (2001), Intensified deep Pacific inflow and ventilation in Pleistocene glacial times, *Nature, 412*, 809–812.

Hays, J. D., J. Imbrie, and N. J. Shackleton (1976), Variations in the Earth's orbit: Pacemaker of the ice ages, *Science, 194*, 1121–1132.

Henrich, R., K.-H. Baumann, S. Gerhardt, M. Gröger, and A. N. A. Volbers (2003), Carbonate preservation in deep and intermediate water masses in the South Atlantic: Evaluation and geological record (a review), in *The South Atlantic in the Late Quaternary: Reconstructions of Material Budgets and Current Systems*, edited by G. Wefer, S. Mulitza, and V. Ratmeyerl, pp. 645–670, Springer, Berlin.

Hodell, D. A., C. D. Charles, J. H. Curtis, P. G. Mortyn, U. S. Ninnemann, and K. A. Venz (2003), Pleistocene vertical carbon isotope and carbonate gradients in the south Atlantic sector of the Southern Ocean, *Geochem. Geophys. Geosyst., 4*(1), 1004, doi:10.1029/2002GC000367.

Howard, W. R., and W. L. Prell (1992), Late Quaternary surface circulation of the southern Indian Ocean and its relationship to orbital variations, *Paleoceanography, 7*, 79–117.

Imbrie, J., A. McIntyre, and A. Mix (1989), Oceanic response to orbital forcing in the late Quaternary: Observational and experimental strategies, in *Climate and Geosciences: A Challenge for Science and Society in the 21st Century*, edited by A. Berger, J.-C. Duplessy, and S. H. Schneider, pp. 121–164, Reidel, Hingham, Mass.

Johnsen, S. J., et al. (1997), The $\delta^{18}O$ record along the Greenland Ice Core Project deep ice core and the problem of possible Eemian climatic instability, *J. Geophys. Res., 102*, 26,397–26,410.

Jouzel, J., et al. (2004), EPICA Dome C ice cores deuterium data, ftp://ftp.ncdc.noaa.gov/pub/data/paleo/icecore/antarctica/epica_domec/edc_dd.txt, Paleoclimatology Program, Natl. Geophys. Data Cent., Boulder, Colo.

Knorr, G., and G. Lohmann (2003), Southern Ocean origin for the resumption of Atlantic thermohaline circulation during deglaciation, *Nature, 424*, 532–536.

Knutti, R., J. Fluckiger, T. F. Stocker, and A. Timmermann (2004), Strong hemispheric coupling of glacial climate through freshwater discharge and ocean circulation, *Nature, 430*, 851–856.

Kuhn, G., and B. Diekmann (2002), Late Quaternary variability of ocean circulation in the southeastern South Atlantic inferred from the terrigenous sediment record of a drift deposit in the southern Cape Basin (ODP Site 1089), *Palaeogeogr. Palaeoclimatol. Palaeoecol., 182*, 287–303.

Labeyrie, L., et al. (1996), Hydrographic changes of the Southern Ocean (southeast Indian sector) over the last 230 kyr, *Paleoceanography, 11*, 57–76.

Le, J., and N. J. Shackleton (1992), Carbonate dissolution fluctuations in the western equatorial Pacific during the late Quaternary, *Paleoceanography, 7*, 21–42.

Lea, D. W. (1995), A trace-metal perspective on the evolution of Antarctic circumpolar deep water chemistry, *Paleoceanography, 10*, 733–747.

Lutjeharms, J. R. E. (1996), The exchange of water between the South Indian and South Atlantic oceans, in *The South Atlantic: Present and Past Circulation*, edited by G. Wefer et al., pp. 125–162, Springer-Verlag, Berlin.

Lynch-Stieglitz, J., and R. G. Fairbanks (1994), A conservative tracer for glacial ocean circulation from carbon isotope and paleonutrient measurements in benthic foraminifer, *Nature, 369*, 308–310.

Mackensen, A., and T. Bickert (1999), Stable carbon isotopes in benthic foraminifera: Proxies for deep and bottom water circulation and new production, in *Use of Proxies in Paleoceanography: Examples From the South Atlantic*, edited by G. Fischer and G. Wefer, pp. 229–254, Springer-Verlag, Berlin.

Mackensen, A., H.-W. Hubberten, T. Bickert, G. Fischer, and D. K. Fütterer (1993), The $\delta^{13}C$ in benthic for a foraminiferal tests of Fontbotia Wuellerstorfi (Schwager) relative to the $\delta^{13}C$ of dissolved inorganic carbon in Southern Ocean deep water: Implications for glacial ocean circulation models, *Paleoceanography, 8*(5), 587–610.

Mackensen, A., M. Rudolph, and G. Kuhn (2001), Late Pleistocene deep-water circulation in the subantarctic eastern Atlantic, *Global Planet. Change, 30*, 197–229.

Manighetti, B., and I. N. McCave (1995), Late glacial and Holocene palaeocurrents around Rockall Bank, NE Atlantic Ocean, *Paleoceanography, 10*, 611–626.

Marchitto, T. M., and W. S. Broecker (2006), Deep water mass geometry in the glacial Atlantic Ocean: A review of constraints from the paleonutrient proxy Cd/Ca, *Geochem. Geophys. Geosyst., 7*, Q12003, doi:10.1029/2006GC001323.

Matsumoto, K., and J. Lynch-Stieglitz (1999), Similar glacial and Holocene deep water circulation inferred from southeast Pacific benthic foraminiferal carbon isotope composition, *Paleoceanography, 14*(2), 149–163.

Matsumoto, K., J. Lynch-Stieglitz, and R. F. Anderson (2001), Similar glacial and Holocene Southern Ocean hydrography, *Paleoceanography, 16*, 445–454.

McCave, I. N., and I. R. Hall (2006), Size sorting in marine muds: Processes, pitfalls, and prospects for paleoflow-speed proxies, *Geochem. Geophys. Geosyst., 7*, Q10N05, doi:10.1029/2006GC001284.

McCave, I. N., B. Manighetti, and N. A. S. Berveridge (1995a), Circulation in the glacial North Atlantic inferred from grain size measurements, *Nature, 374*, 149–152.

McCave, I. N., B. Manighetti, and S. G. Robinson (1995b), Sortable silt and fine sediment size/composition slicing: Parameters for paleocurrent speed and paleoceanography, *Paleoceanography, 10*, 593–610.

McCave, I. N., T. Kiefer, D. J. R. Thornalley, and H. Elderfield (2005), Deep flow in the Madagascar-Mascarene Basin over the last 150000 years, *Philos. Trans. R. Soc. London Ser. A, 363*, 81–99.

McManus, J., G. Bond, W. Broecker, S. J. Johnsen, L. Labeyrie, and S. Higgins (1994), High resolution climate records from the North Atlantic during the last interglacial, *Nature, 371*, 326–329.

McManus, J. F., R. Francois, J. M. Gherardi, L. D. Kiegwin, and S. Brown-Leger (2004), Collapse and rapid resumption of Atlantic meridional circulation linked to deglacial climate changes, *Nature, 428*, 834–837.

Michel, E., L. D. Labeyrie, J.-C. Duplessy, N. Gorfti, M. Labracherie, and J.-L. Turon (1995), Could deep subantarctic convection feed the world deep basins during the last glacial maximum?, *Paleoceanography, 10*, 927–942.

Ninnemann, U. S., and C. D. Charles (2002), Changes in the mode of Southern Ocean circulation over the last glacial cycle revealed by foraminiferal stable isotopic variability, *Earth Planet. Sci. Lett., 201*, 383–396.

Nowlin, J. W. D., and J. M. Klinck (1986), The physics of the Antarctic Circumpolar Current, *Rev. Geophys., 24*, 469–491.

Oppo, D. W., and R. G. Fairbanks (1987), Variability in the deep and intermediate water circulation of the Atlantic Ocean during the past 25,000 years: Northern Hemisphere modulation of the Southern Ocean, *Earth Planet. Sci. Lett., 86*, 1–15.

Oppo, D. W., and M. Horowitz (2000), Glacial deep water geometry: South Atlantic benthic foraminiferal Cd/Ca and $\delta^{13}C$ evidence, *Paleoceanography, 15*(2), 147–160.

Orsi, A. H., T. Whitworth III, and J. W. D. Nowlin (1995), On the meridional extent and fronts of the Antarctic Circumpolar Current, *Deep Sea Res. Part I, 42*, 641–673.

Orsi, A. H., G. C. Johnsen, and J. L. Bullister (1999), Circulation mixing and production of Antarctic bottom water, *Prog. Oceanogr., 43*, 55–109.

Pahnke, K., and R. Zahn (2005), Southern Hemisphere water mass conversion linked with North Atlantic climate variability, *Science, 307*, 1741–1746.

Pahnke, K., R. Zahn, H. Elderfield, and M. Schulz (2003), 340,000 year centennial-scale marine record of Southern Hemisphere climate oscillation, *Science, 301*, 948–952.

Peeters, F. J. C., R. Acheson, G.-J. A. Brummer, W. P. M. De Ruijter, R. R. Schneider, G. M. Ganssen, E. Ufkes, and D. Kroon (2004), Vigorous exchange between the Indian and Atlantic oceans at the end of the past five glacial cycles, *Nature, 430*, 661–665.

Petit, J. R., et al. (1999), Climate and atmospheric history of the past 420,000 years from the Vostok ice core, Antarctica, *Nature, 399*, 429–436.

Pfuhl, H. A., and N. J. Shackleton (2004), Two proximal, high resolution records of foraminiferal fragmentation and their implications for changes in dissolution, *Deep Sea Res. Part I, 51*, 809–832.

Piotrowski, A. M., S. L. Goldstein, S. R. Hemming, and R. G. Fairbanks (2004), Intensification and variability of ocean thermohaline circulation through the last deglaciation, *Earth Planet. Sci. Lett., 225*, 205–220.

Piotrowski, A. M., S. L. Goldstein, S. R. Hemming, and R. G. Fairbanks (2005), Temporal relationships of carbon cycling and ocean circulation at glacial boundaries, *Science, 307*, 1933–1938.

Pudsey, C. J., and J. A. Howe (1998), Quaternary history of the Antarctic Circumpolar Current: Evidence from the Scotia Sea, *Mar. Geol., 148*, 83–112.

Reid, J. L. (1989), On the total geostrophic circulation of the South Atlantic Ocean: Flow patterns, tracers, and transports, *Prog. Oceanogr., 23*, 149–244.

Reid, J. L. (2005), On the world-wide circulation of the deep water from the North Atlantic Ocean, *J. Mar. Res., 63*, 187–201.

Richardson, P. L., J. R. E. Lutjeharms, and O. Boebel (2003), Introduction to the "Inter-ocean exchange around southern Africa," *Deep Sea Res. Part II, 50*, 1–12.

Rosenthal, Y., E. A. Boyle, and L. Labeyrie (1997), Last Glacial Maximum paleochemistry and deepwater circulation in the Southern Ocean: Evidence from foraminiferal cadmium, *Paleoceanography, 12*(6), 787–796.

Rutberg, R. L., S. R. Hemming, and S. L. Goldstein (2000), Reduced North Atlantic deep water flux to the glacial Southern Ocean inferred from neodymium isotope ratios, *Nature, 405*, 935–938.

Samthein, M., and R. Tiedemann (1990), Younger Dryas-style cooling events at glacial terminations I-VI: Associated benthic delta13C anomalies ad ODP site 658 constrain meltwater hypothesis, *Paleoceanography, 5*, 1041–1055.

Samthein, M., K. Winn, S. J. A. Jung, J.-C. Duplessy, L. Labeyrie, H. Erlenkeuser, and G. Ganssen (1994), Changes in east Atlantic deepwater circulation over the last 30000 years: Eight time slice reconstructions, *Paleoceanography, 9*, 209–268.

Schlitzer, R. (2000), Electronic atlas of WOCE hydrographic and tracer data, *Eos Trans. AGU, 81*(5), 45.

Schrag, D. P., J. F. Adkins, K. McIntyre, J. L. Alexander, D. A. Hodell, C. D. Charles, and J. F. McManus (2002), The oxygen isotopic composition of seawater during the Last Glacial Maximum, *Quat. Sci. Rev., 21*, 331–342.

Seidov, D., B. J. Haupt, E. J. Barron, and M. Maslin (2001), Ocean bi-polar seesaw and climate: Southern versus northern meltwater impacts, in *The Ocean and Rapid Climate Change: Past, Present and Future, Geophys. Monogr. Ser.*, vol. 126, edited by D. Seidov, B. J. Haput, and M. Maslin, pp. 147–167, AGU, Washington, D. C.

Shackleton, N. J., and M. A. Hall (1997), The late Miocene stable isotope record, site 926, *Proc. Ocean Drill. Program Sci. Results, 154*, 367–373.

Shackleton, N. J., M. A. Hall, and E. Vincent (2000), Phase relationships between millennial-scale events 64,000-24,000 years ago, *Paleoceanography, 15*(6), 565–569.

Siddall, M., E. Bard, E. J. Rohling, and C. Hemleben (2006), Sea-level reversal during termination II, *Geology, 34*, 817–820.

Sigman, D. M., and E. A. Boyle (2000), Glacial/interglacial variations in atmospheric carbon dioxide, *Nature, 407*, 859–869.

Sikes, E. L., C. R. Samson, T. P. Guilderson, and W. R. Howard (2000), Old radiocarbon ages in the southwest Pacific Ocean during the last glacial period and deglaciation, *Nature, 405*, 555–559.

Sloyan, B. M., and R. S. Rintoul (2001), Circulation, modification, and renewal of Antarctic mode and intermediate water, *J. Phys.*, 31,1005–31,1030.

Spero, H. J., and D. W. Lea (2002), The cause of carbon isotope minimum events on glacial terminations, *Science, 296*, 522–525.

Stocker, T. F., and S. J. Johnsen (2003), A minimum thermodynamic model for the bipolar seesaw, *Paleoceanography, 18*(4), 1087, doi:10.1029/2003PA000920.

Streeter, S. S., and N. J. Shackleton (1979), Paleocirculation of the deep North Atlantic: 150,000-year record of benthic foraminifera and oxygen-18, *Science, 203*, 168–171.

Tucholke, B. E., and G. B. Carpenter (1977), Sediment distribution and Cenozoic sedimentation patterns on Agulhas Plateau, *Geol. Soc. Am. Bull., 88*, 1337–1346.

Uenzelmann-Neben, G. (2001), Seismic characteristics of sediment drifts: An example from the Agulhas Plateau, southwest Indian Ocean, *Mar. Geophys. Res., 22*, 323–343.

Uenzelmann-Neben, G. (2002), Contourites on the Agulhas Plateau, SW Indian Ocean: Indications for the evolutions of currents since Paleogene times, in *Deep-water Contourite Systems: Modern Drifts and Ancient Series, Seismic and Sedimentary Characteristics*,

Geol. Soc. Mem., vol. 22, edited by D. Stow et al., pp. 271–288, Geol. Soc. of London, London.

Volbers, A. N. A., and R. Henrich (2004), Calcium carbonate corrosiveness in the South Atlantic during the Last Glacial Maximum as inferred from changes in the preservation of Globigerina bulloides: A proxy to determine deep-water circulation patterns?, *Mar. Geol.*, *204*, 43–57.

Waelbroeck, C., L. Labeyrie, E. Michel, J.-C. Duplessy, J. McManus, K. Lambeck, E. Balbon, and M. Labracherie (2002), Sea-level and deep water temperature changes derived from benthic foraminifera isotopic records, *Quat. Sci. Rev.*, *21*, 295–305.

Weaver, A. J., O. A. Saenko, P. U. Clark, and J. X. Mitrovica (2003), Meltwater pulse 1A from Antarctica as a trigger of the Bolling-Allerod warm interval, *Science*, *299*, 1709–1713.

Weijer, W., W. P. M. de Ruijter, A. Sterl, and S. S. Drijfhout (2002), Response of the Atlantic overturning circulation to South Atlantic sources of buoyancy, *Global Planet. Change*, *34*, 293–311.

Whitworth, T., III, and R. G. Peterson (1985), Volume transport of the Antarctic Circumpolar Current from bottom pressure measurements, *J. Phys. Oceanogr.*, *15*, 810–816.

Yu, E.-F., R. Francois, and M. P. Bacon (1996), Similar rates of modern and last glacial ocean thermohaline circulation inferred from radiochemical data, *Nature*, *379*, 689–694.

P. Diz, I. R. Hall, and E. G. Molyneux, School of Earth, Ocean, and Planetary Sciences, Cardiff University, Main Building, Park Place, Cardiff CF10 3YE, UK. (molyneuxeg@cardiff.ac.uk)

R. Zahn, Institució Catalana de Recerca i Estudis Avançats, Institut de Ciencia i Tecnologia Ambientals, Universitat Autónoma de Barcelona, Edificio Ciències, E-08193 Bellaterra, Spain.